UNIVERSITY OF MARYLAND

National Transportation Center

Project ID: NTC2016-MU-R-02

Impact of Level of Service (LOS) on the Driver's Behavior on Arterials

Final Report

by

Behzad Aghdashi, Ph.D.
Research Associate, ITRE, NC State University
behzad_aghdashi@ncsu.edu

Celeste Chavis, Ph.D.
Assistant Professor, Morgan State University
celeste.chavis@morgan.edu

Nabaruna Karmakar,
Graduate Research Assistant, ITRE, NC State University
nkarmak@ncsu.edu

Mansoureh Jeihani, Ph.D.
Associate Professor, Morgan State University
mansoureh.jeihani@morgan.edu

Justin Babich
Research Assistant, ITRE, NC State University
jebabich@ncsu.edu

for

National Transportation Center at Maryland (NTC@Maryland)
1124 Glenn Martin Hall, University of Maryland, College Park, MD 20742

March, 2018

ACKNOWLEDGEMENTS

This project received funding from the National Transportation Center @ Maryland (NTC@Maryland), one of the five National Centers that were selected in this nationwide competition, by the Office of the Assistant Secretary for Research and Technology (OST-R), U.S. Department of Transportation (US DOT). Many thanks for the support provided by NTC. We would like to acknowledge the research team who helped conducting this research and without their gracious contribution, this effort would not have been successful.

DISCLAIMER

TABLE OF CONTENTS

LIST OF TABLES

LIST OF FIGURES

EXECUTIVE SUMMARY

This research presents a data driven approach to investigate driver behavior as a function of surrounding traffic condition on arterial roads. The driver behavior was characterized by a set of microscopic variables such as speed, longitudinal accelerations, lateral acceleration, jerk, percent throttle position etc., while the traffic condition surrounding drivers was characterized by Level of Service (LOS). For this purpose, the research team utilized two test beds, which were real-world naturalistic tests and experiments using a driver simulator. The real-world analysis used high-resolution trajectory data collected via i2D technology. This massive data set contained more than 40 drivers and four years' worth of vehicle trajectory data, provided at a 1 second resolution. At the time of performing analysis in this project, this data set comprised more than 47 million seconds of microscopic driver behavior data. To measure LOS, the research team used speed data reported by INRIX, which is among one of the most reliable probe vehicle data providers.

The research team identified 15 routes to establish the spatial scope of real-world analysis, each of which included a diverse set of drivers and a large number of trips. The high-resolution trajectory data collected on these routes, merged with INRIX speed records formed the database to perform the real-world analysis. Alongside real-world analysis, a driver simulator at Morgan State University was also used to perform experiments to analyze driver behavior as a response to LOS. A set of drivers were recruited and asked to drive a modeled corridor in Maryland, using the driver simulator. Each driver was asked to drive under different scenarios of the six LOS (A through F). The driver simulator was used to record microscopic driver behavior variables comparable to the real-world data, but with a resolution of 1/10 of a second. The research team assessed these outputs and constructed relationships between driver behavior and LOS from both data sources.

Trends in measures of driver aggressiveness with change in LOS is established in this research, and the performance of a supervised machine learning algorithm, Random Forest Classification, in predicting aggressive driving events is also evaluate. In this report, parallels between the relationships found using real-world data and the driver simulator experiments are drawn and insights into the validity of the driver simulator are provided. It was found that the trends of accelerations and jerk for the driver simulator over different LOS were consistent with that observed in the real-world data. However, measures such as throttle position and RPM readings across different LOS in the driver simulator were quite different from empirical data. The results from the real-world data analysis can be used in the calibration of driver simulators as well.

1.0 INTRODUCTION

1.1 PROBLEM STATEMENT

Conventional freeway analysis has often times focused on mobility improvements. However, by improving mobility performance measures, which results in a better Level of Service (LOS), other types of benefits may emerge (Triber et. al., 2008). Next to travel time, fuel consumption is an important measure for the performance of future Intelligent Transportation Systems. Unal et. al. found that emission rates were highest during acceleration and tend to decrease for cruise, deceleration and idle conditions (2003). Thus, a comprehensive model on predicting the driver's behavior can result in a more accurate estimation regarding benefits of LOS improvement. This research project is aimed at investigating driving behavior as a function of surrounding traffic conditions, which in turn can help estimate benefits from *'fuel cost'* and *'emission'* savings.

As shown in Figure 1, the blue boxes represent the conventional mobility improvement framework which mostly relies on minimizing *'user delay cost'*. By identifying the impacts of traffic condition on the driver's behavior (shown in red section), a more comprehensive analysis can be performed and thus resulting in more accurate planning and operation.

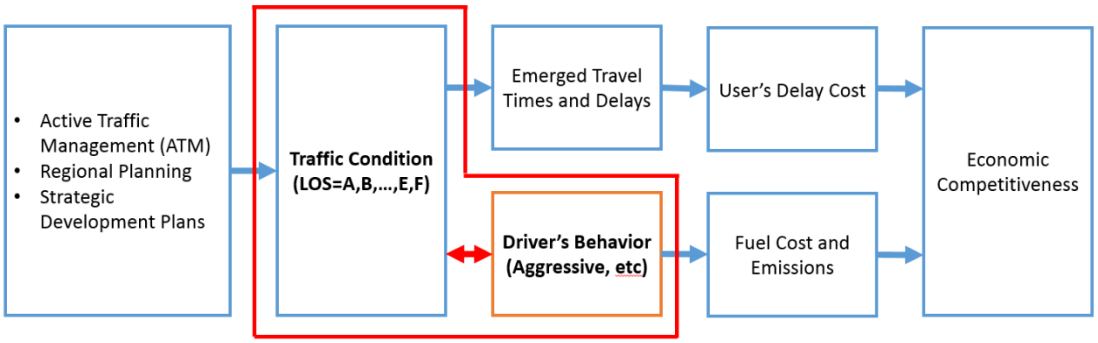

Figure 1 – Scope of research

This study expands the conventional surface streets analysis to include driver aggressiveness in addition to the user delay cost savings. This cost savings not only stems from the traffic state (ex. stop and go traffic) but also due to driver behavior and operations. It is hypothesized that as the LOS deteriorates, drivers become more aggressive. Cobina et. al. found that the optimal level for emissions release in arterial streets is achieved in LOS B and the greatest incremental decrease in emissions was observed between LOS D and C (2009). This is not fully consistent with observations at intersections, where LOS A generates the lowest emissions.

In this research, these savings have been modeled by finding trends in driver aggressiveness with change in LOS. The data collected is via two means: (1) high resolution trajectory data gathered and collected by i2D (intelligent to Drive) devices and (2) a driver simulator with motion console. In addition, this study provides insights into validity of simulated environments by comparing the results from the i2D devices and the traffic simulator.

1.2 OBJECTIVES

The objectives of this project were to:

1. Analyze driver's behavior based on surrounding traffic conditions using 1) field data observations, and 2) driver simulator;
2. Create appropriate model(s) to estimate impact of surrounding traffic condition (Level of Service) on driving behavior, and,
3. Provide insights to the accuracy of driver simulators in replicating real-world driver behavior.

1.3 RESEARCH APPROACH

Figure 2 shows the scope and the methodology adopted to carry out research in this project. The first step was to select a set of appropriate sites for data collection, which were selected in a way to eliminate any possible source of outliers, such as overly aggressive driving behavior or non-standard facility geometric designs, etc. Of course, another main criterion to select these sites was to ensure that high quality of trajectory data is available to the research via i2D devices.

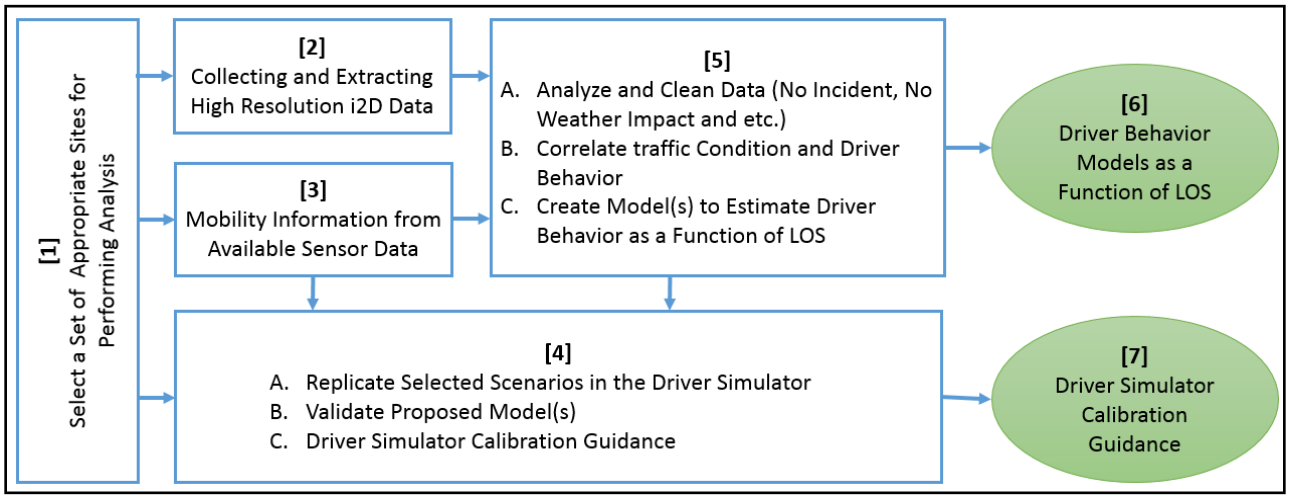

Figure 2 - Scope of project

High resolution vehicle trajectory data for the selected sites was collected by i2D devices available at ITRE/NCSU (Figure 2 box #2). At the time of this research, ITRE had already collected over 47 million seconds of driving data that includes majority of driving behavior parameters such as accelerations, high speeds, etc. The i2D database was updated during the project with more recently collected data to increase the accuracy of any proposed models. At the same time, probe based speed data was downloaded to collect mobility information and calculate LOS for the selected sites (Figure 2 box #3).

After collecting probe data and i2D data, the project team started investigated the correlation between surrounding traffic condition and the driver's behavior (Figure 2 Box #5). The collected data was filtered to exclude any abnormal days, such as days with inclement weather conditions and incidents. Then, trends and relationships between LOS and driver behavior factors, such as acceleration, jerk, throttle position, etc. were established.

Morgan State University owns two advanced computer-based driving simulators with route choice ability. The DS software is UC-Win/Road developed by Forum 8 Co. Ltd. based in Tokyo, Japan. One of the DSs includes motion platform (Forum 8). The software, UC-win/Road Version 10, is the state-of-the-art 3D Virtual Reality applications for different fields. The simulator includes a software development kit in which one can write programs to customize the driving simulator software. Drivers' speed, acceleration, and deceleration in different traffic regimes or LOS is recorded in the simulator environment and then compared to the field data.

Using the driver simulator, experiments were conducted where participants were asked to drive in all six LOS conditions in a virtual environment (Figure 2 box #4). Finally, the results from the i2D data were used to train a machine learning model to estimate driver aggressiveness (Figure 2 box #6) and the results from the driver simulator experiments were compared to the real-world data and the need for calibration was established (Figure 2 box #8).

In the real world, the i2D device was attached to a vehicle and data was recorded as vehicle was driven through different links in the network. Recorded data was collected, and free-flow traffic speed was determined using methods obtained from the Highway Capacity Manual (HCM6). Free-flow traffic speed was utilized in the determination of the Level of Service. Recorded parameters were analyzed for each Level of Service and an investigation was made to determine the validity of the driving simulator.

In this study, an arterial in the simulated environment was built/designed to closely resemble Perring Parkway, located in the northeastern part of Baltimore City, Maryland, near Morgan State University. The simulated network was northbound along Perring Parkway, from 33rd Street to I-695, a 4.4-mile stretch, consisting of six sections (links). Six scenarios with traffic at Levels of Service A, B, C, D, E and F were designed. Each participant was required to drive each scenario. Several parameters were recorded in real time and used in the determination of the number of brakes per mile, number of accelerations per mile, number of lane changes per mile per available lane, average throttle ratio, number of uncomfortable jerks and number of unsafe jerks.

1.4 DATA SOURCES

This section provides descriptions of the data sources used in this research. The data collection mechanism and the different variables measured by the devices are also described.

1.4.1 i2D (intelligent to Drive)

Our approach to collect high-resolution real-world data relies on an existing, functional on-board diagnostic (OBD)-connected, GPS enabled, in-vehicle trajectory data collection tool developed in partnership with the Technical University of Lisbon and Live Drive (Live Drive,

2018). The device, labeled i2D (for **i**ntelligence to **D**rive) does more than collecting trajectory data. It is equipped with an accelerometer that reports three-dimensional accelerations, and when the vehicle is registered it can provide good estimates of instantaneous fuel consumption. More importantly, all data are gathered and archived while the vehicle is in motion at a resolution of 1Hz. Currently, i2D vehicles are equipped to gather trajectory data in four continents including Europe, Asia, North America, and South America. Figure 3 depicts the various components of i2D and their placement in a vehicle. These include an OBD-II connector, the OBU (circled), and the GPS antenna.

Figure 3 - Components and installation of i2D system

Figure 4 depicts how the various components within the i2D system operate. The i2D device includes additional sensors, a memory card, a high-end processor, and a cellular network interface. All OBU raw data are collected at the 1Hz resolution and are transmitted over the mobile network every 23 seconds to a secure server and archived in a standard format for further analysis. Then, processed data is displayed on a secure website for the driver to access trip based information immediately after completing the trip.

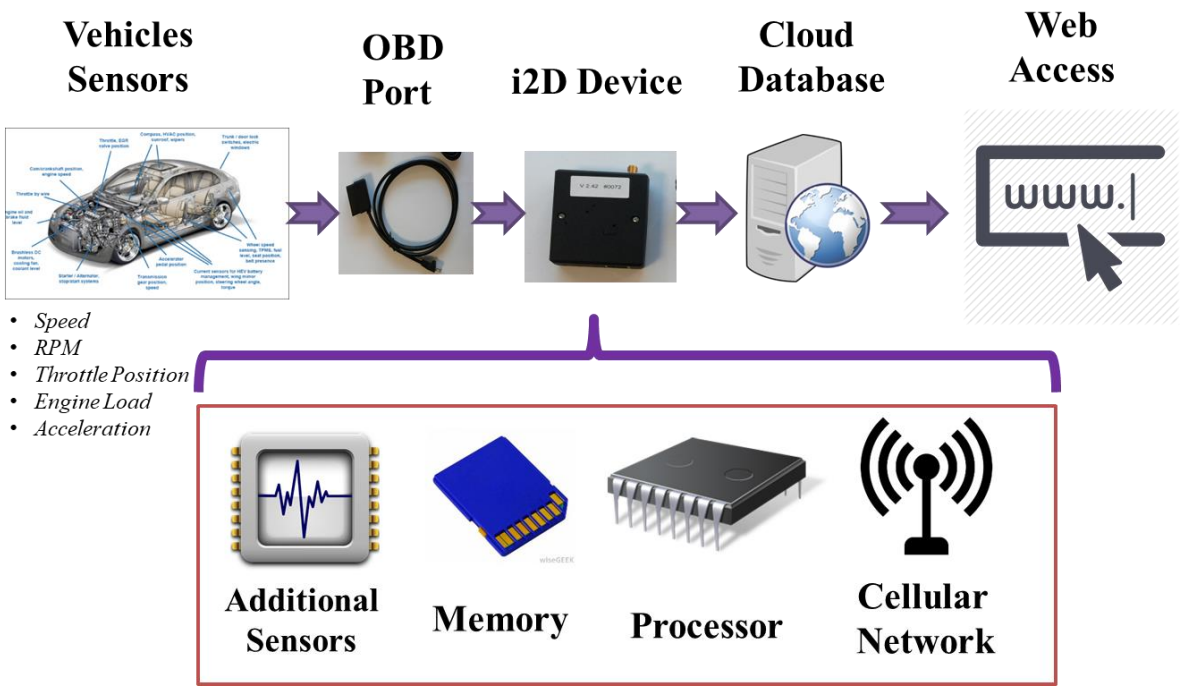

Figure 4 – In-vehicle system data path and routing

Figure 5 shows the current capabilities of the i2D system in generating and visually displaying the micro-scale vehicle data. It shows a screenshot of what the driver accessing his/her private website would observe when clicking on a specific trip and requesting the trip details. In the original screen (not shown), summary trip information such as start and end time, duration, distance traveled, fuel used, etc., is provided. Figure 5 on the right depicts timelines of, from top to bottom: (a) second by second vehicle speed (blue) and engine rpm (green); (b) 3D accelerations in the longitudinal, lateral and vertical dimensions indicated by the various line colors; (c) instantaneous and cumulative fuel consumption for a single trip whose origin, destination and path highlighted on the left side of the graph; and (d) the path elevations as measured by a barometric altimeter.

The trip shown in Figure 5 was made on city streets and an urban freeway in Raleigh, NC. Those data and others not shown on the graph are all archived by trip for the driver (note that a trip begins as the engine is started, and ends when the ignition key is off). This data are used to develop driver-specific reports of fuel use and acceleration profiles. In addition, several icons on the top bar (not displayed here) are used to track specific events on the trip. For example, a displayed X speed icon provides a time stamp and location whenever the vehicle speeds are at or exceeds X mph. The STOP icon will indicate stopped vehicle positions with the engine is still running. Finally, there is a trip simulator feature (circled) that runs the actual trip and depicts the various events as travel is unfolding.

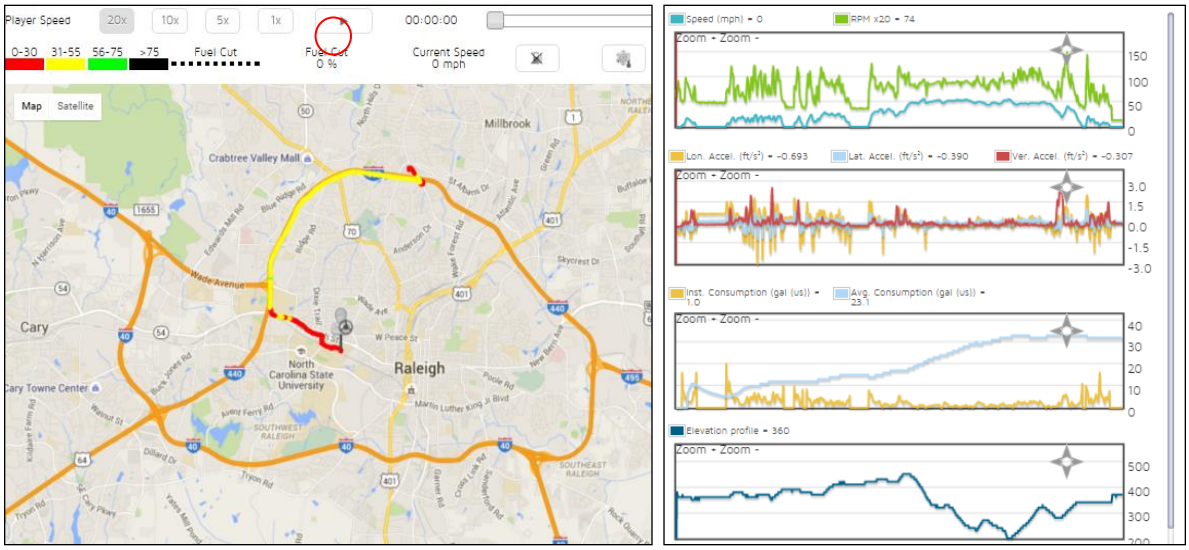

Figure 5 - i2D trip data displays and travel dynamics profiles

The research team downloaded anonymized high-resolution trajectory data from i2D devices and used as the database to conduct this research project. The size of i2D data at the time of this research was about 47 million seconds worth of travel spreading across North Carolina and neighboring states.

1.4.2 ITS Probe Data

In this research, in order to estimate the Level of Service (LOS) on the arterials, we have used probe-based data sources. Probe-based data sources, which primarily rely on cellular devices located within each vehicle can report speeds and travel times. However, they cannot report volumes and demand flow rates. The unit which these system report speeds and travel times are called Traffic Message Channel (TMC) segments. Typically, each TMC segment on the arterial includes one or a few intersections.

There are several providers of probe-based data such as INRIX, Here.com, and etc. NC State University has used INRIX data through Regional Integrated Transportation Information System (RITIS, 2018).

1.4.3 Driver Simulator

A high-fidelity full-scale driving simulator available at the Safety and Behavioral Analysis (SABA) Center, Morgan State University, was utilized for the driving simulation aspect of this study. The driving simulator allows for the creation of different driving environments very similar to real-life driving scenarios. However, unlike many other simulators, the UC-winRoad Driving Simulator (Forum 8) gives the driver the freedom to choose routes, change lanes and perform maneuvers. Data such as driver's route choice, speed, acceleration, steering rotation, offset distance from lane center, offset from road shoulders, yaw/pitch/roll angle and other parameters are recorded by the simulator as drivers navigate through the simulated environment. The hardware

components shown in Figure 6 closely resemble the interior of the driver's side of a real car; it comprises of the driver seat, cockpit, steering wheel, acceleration and brake pedals, ignition key, gear stick, flash lights and three surrounding monitors to provide a 3D view. All parts required for the control of the vehicle are intelligent and respond accordingly when handled by the driver. A virtual reality system developed by FORUM8 Co. (Forum 8); VR-Design Studio software, enables researchers to design and edit different network elements allowing for the creation of a different driving environments composed of different road alignments, cross-sections, traffic signals, road signs and topography settings. VR-Design Studio also allows for real-time presentation or manipulation of traffic flow, weather conditions and objects, both spatial and static, in the simulated environment. A real-world arterial in Baltimore, MD, was created using the VR-Design Studio and different scenarios of a network with varying Levels of Service was simulated using the driving simulator. Participants' speed, acceleration, brake, and other parameters were recorded, every 10th of a second, as they drove through the study corridor. These parameters were utilized in the investigation of the effect of LOS on driver's behavior.

Figure 6 - Driving simulator at the SABA Center, Morgan State University

2.0 LITERATURE REVIEW

2.1 DRIVER BEHAVIOR

Classification and modeling of driver behavior or aggressiveness is an integral aspect of intelligent transport systems and human-vehicle systems. Recent progress in this area has been made both from the perspective of vehicle dynamics applications and human factors research. Traffic safety and energy efficiency of vehicles are also directly related to driver's behavior.

For many years, effect of driving style on fuel consumption and emissions has been a main motivation for studies related to data collection and modeling of driver behavior. For example, De Vlieger (1997) used on-board measuring system to conclude that average fuel emissions were up to four times higher for aggressive drivers. Ericsson (2001) carried out research to investigate which factors describing driving style have a direct impact on emissions and fuel-use, by analyzing 62 driving parameters for each of 19,230 driving patterns collected in real traffic. Four of the main factors identified were associated with power demand and acceleration, three factors related to aspects of gear changing and two describe the effect of certain speed intervals.

Murphey et al. (2009) developed an algorithm that classifies driver's style using jerk profile, with an ultimate aim to control fuel economy as well. Daniel et al. (2009) used different features to develop a drive style analysis toolset, which quantified driving behavior into two drive type and drive style. Drive type referred to the recognition of the road infrastructure, while drive style was determined as an interaction of pedal input and vehicle speed using an aggressive algorithm. They categorized drive style as gentle, normal and aggressive.

Road safety and design of driver assistance systems also provide big motivation for studies related to classification of driving styles. Many insurance agencies use in car devices to collect data and hence determine insurance rates for their customers. Toledo and Lotan (2006) described an in-vehicle data recorder (IVDR) in monitoring and analyzing driver behavior not only for crash events, but also under normal conditions, ultimately to provide feedback to drivers for purposes of education and training. Their study found a connection between driver safety indices as captured by the system and historic crash data, which suggested that these indices could be a good indicator of the risk involvement in car crashes.

Wang et al. (2014) discussed a wide range of mathematical methods for both identification and modeling of driver behavior, based on driving data, such as brake or throttle pedal position and the steering wheel angle, among others. The driver's characteristics derived from the models presented are embedded into advanced driver assistance systems, which are also evaluated and validated.

Vaiana et al. (2014) developed a prototype mobile application to evaluate the safety on the road by measuring of accelerations (longitudinal and lateral) and warn drivers when to correct their driving style. The driver aggressiveness was evaluated by plotting vehicle's acceleration on a g-g diagram and several experimental tests were carried out with different drivers and cars to assess the system accuracy and the usability of the application.

Lee and Öberg (2015) made use of on-board diagnostic (OBD) data, commonly available in modern cars, to develop advanced driver assistance systems (ADAS) for enhancing road safety and drivability. Also, a velocity-based road type classification method is evaluated on measurements collected from real driving conditions and compared to an open-sourced map. Two commonly adopted methods of driving style classification, i.e., acceleration and jerk-based methods were evaluated, which revealed that these methods are only applicable to certain driving conditions, prompting for the need of a more comprehensive classification of driving style.

Carmona et al. (2015) presented a framework for data fusion using in-vehicle sensors, such as Controller Area Network Bus (CAN-BUS), an Inertial Measurement Unit (IMU) and GPS to detect aggressive behavior of drivers. The methodology is based on the use of signal descriptors, which identifies specific patterns in the driver's behavior.

Nowadays, with the high market penetration of smartphones and mobile devices with advanced motion sensors, identifying risky driving maneuvers and to improving driver efficiency has become easier have become useful. This type of data can be useful in fleet management, insurance premium adjustment, fuel consumption optimization or CO2 emission reduction, etc. Castignani et al. (2015) analyzed how smartphone sensors can be used to identify driving maneuvers and proposed a driver profile platform that is able to detect risky driving events and provide a representative score for each driver, using a Fuzzy Inference System.

However, the validity of mobile devices or smartphones are questionable as shown by Paefgen et al. (2012), where an evaluation of a mobile application that assesses driving behavior based on in-vehicle acceleration measurements that found to overestimate critical driving events.

Shabikhani and Gonzales (2013) have used NGSIM trajectory data to validate an emission model which is highly sensitive to acceleration, deceleration, cursing and idling on signalized intersections, however, the NGSIM trajectory data provides a limited access to few sites for validation purposes. Beside fuel cost and emission savings, the understanding of driver's behavior at different facilities operational condition (LOS) can also improve many different models such as breakdown propensity estimations (Kerner, 2010). Treiber et. al. found that traffic congestion typically leads to an increase of fuel consumption of the order of 80% while travelling time increased by a factor of up to 4. They conclude that the influence of congestion on fuel consumption is distinctly lower than that on travel time (2008). However, these findings are based on micro simulation results and a limited set of trajectory data (NGSIM) on freeways in California.

This research focuses on using two different data sources to detect a pattern in driving style or driver aggressiveness, as a direct consequence of LOS on arterial streets. The data collected for this research include real-world vehicle trip data (i2D) and ITS probe vehicle speed data. Also, geometric information about some study sites in the Raleigh-Durham area is used to see if that may have a direct impact on driver's aggressiveness.

2.2 DATA MINING TECHNIQUES

As an undetectable property or feature, driving behavior is hard or in some cases impossible to analyze using regular methodologies. To characterize hidden patterns in driving behavior, data

mining and Machine Learning techniques have often been used to develop models using OBD as well as smartphone data. Mitrovic (2005) developed a method for driving event recognition using hidden Markov models (HMMs) to be used in a framework for a driver warning system. It uses the pattern history of driving events to may predict future driving events, using data from a data acquisition hardware that consists of a number of sensors, a data acquisition card, and a portable computer.

Johnson and Trivedi (2011) proposed a system aiming at recognizing driving style using smartphone sensors. Their method included smartphone based sensor-fusion of accelerometer, gyroscope, magnetometer, GPS and video data, based on the Dynamic Time Warping (DTW) algorithm and the K-Nearest Neighbors (k-NN) algorithm that ultimately recognizes aggressive and non-aggressive driving behaviors and promote driver safety.

Meseguer et al. (2013) developed a new architecture that integrates both data mining techniques and neural networks to identify the type of road in which the trip is made and the degree of aggressiveness of each driver, using parameters such as speed, rpm, etc. The final aim of this work was to assist drivers at improving their driving style and ultimately their fuel economy.

Higgs and Abbas (2015) defined driver behavior as a map function with current traffic state as the argument and driver action as the dependent variable, or state–action clusters that define the driving pattern of drivers.

Qi et al. (2015) employed the clustering method and topic model to extract latent driving states for use in Advanced Driving Assistant Systems (ADAS). They utilized data mining techniques including ensemble clustering method based on the kernel fuzzy C-means algorithm and the modified latent Dirichlet allocation model to handle the large data set and classified driving style as ‘aggressive’, ‘cautious’ and ‘moderate’.

Wu et al. (2016) developed a driving behavior recognition system using a physical model based on the theory of rigid body kinematics and Kalman filter for noise elimination. They asserted that their method having a solid theoretical basis outperforms other behavior recognition systems using machine learning techniques alone.

Kumtepe et al. (2016) proposed a method of detecting driver aggressiveness, based on the fusion of visual features, such as road lines and vehicle images, and sensor features, like vehicle speed and engine speed. These feature vectors are obtained by using a Gaussian Mixture Model and then, finally, a Support Vector Machine (SVM) classifier is utilized to classify the feature vectors in order for aggressive decision. Field tests using real traffic data yielded an aggressive driving detection rate of 93.1%. Another study involving the use of OBD data, such as vehicle speed, engine RPM, throttle position, engine lead, etc. employed the AdaBoost algorithm to create a driver behavior classification model (Chen et al., 2015).

From the literature on data mining techniques, we can see that no model has been developed, keeping in mind the actual LOS experienced by drivers in the real world. This research looks at using the machine learning algorithm, Random Forest Classification, to see if an improved LOS leads to less aggressiveness among drivers.

2.3 DRIVER SIMULATOR

The ease with which the elements (e.g. traffic/weather conditions, road layout) of a virtual environment can be manipulated and tailored to meet specific research requirements (de Winter et al, 2012), the accuracy and efficiency of data collection and the safe environment devoid of the risks associated with real-life driving scenarios, accounts for the increased use of driving simulators in research (Rizzo et al, 2002; Stern et al, 2006).

However, several researchers have argued that the safe environment provided by a driving simulator is, in fact, a disadvantage; Törnros (1998) stated the driving simulator may not provide accurate data. He based his argument on the influence that the lack of risk in the simulated environment may have on speed and driving behavior. Kappler (1993) expressed that a false sense of safety, responsibility or competence may result from the absence of action consequences and real danger.

According to Shechtman (2010) the simulated environment is an abstraction of reality that differs in some ways from a real one as only specific aspects of the real world can be captured and represented in a simulated environment. He stated that drivers' behavior on a driving simulator may differ since they are presented with only a subset of the overall information-processing associated with driving, hence validation is crucial.

The validation of a driving simulator, however, is a multidisciplinary and complicated task (Blana, 1996). The validity of a simulator is its ability to obtain same responses as would be obtained in real-life scenarios (Rolfe et al, 1970). It is a measure of how closely the simulated environment emulates a behavioral environment (Mudd, 1968). The major problem encountered in the determination of the validity of the driving simulator arises from the fact that the driving simulator is a man-in-the-loop device; measurements may be influenced by human as well as system performance (Blana,1996).

Two types of validity were proposed by Blaauw (1982) - physical validity and behavioral validity. Physical validity explains how closely the physical component, configuration and workings of the simulator resemble the real-world counterpart. A driving simulator on a motion-platform is considered to have greater physical validity than one on a fixed base as the earlier has more driving-associated motions; longitudinal jerk fluctuations depending on driver's throttle/brake handling behavior, lateral jerk fluctuations associated with steering, brake and throttle handling behavior and other driving-related movements. Thus, the closer the physical components and the driving experience of a simulator are to real-life driving, the greater the physical validity.

Behavioral validity, on the other hand, "concerns correspondence between the simulator and the real world in the way the human operator behaves" (Godley et al, 2002). It is a measure of the ability of the simulator to elicit the same driving behavior, from a driver, as the real-world driving environment.

According to Blaauw (1982), the most effective way of determining the behavioral validity of a simulator is to design and execute similar tasks in the two environments, simulated and real, and

subsequently compare the results obtained from both environments. The validity observed may be absolute, relative or non-existent. Absolute validity is established if the numerical values obtained from both vehicles are the same. Relative validity results when the numerical values differ but variations in numerical values are similar. Absolute validity is not a required condition for driving simulation study research results to be useful; however, relative validity is essential (Tonros, 1998). This research aims at evaluating the validity of driver simulator environment compared to real world from driver behavior perspective.

3.0 ROUTE SELECTION

In this section, the routes selected to perform research analysis are described. In order to carry out the real-world analysis and observe how LOS can affect driver behavior, suitable routes need to be identified based on a number of criteria, as described below:

- Sample Size: Since the real-world data relies on availability of i2D trajectory data as well as probe-based speed readings, the research team evaluated several arterial streets in Raleigh NC area and gauged the amount of data available for these sites.
- Besides the availability of i2D data for each route, the number of drivers (driver diversity) on each route is also considered, in order to assure unbiased estimations of driver behavior.
- The routes are selected after examining the range of LOS observations over the study segments and the analysis period, using ITS probe data.

Considering these criteria, the research team selected 15 routes, in which the data was available for a diverse range of drivers and covered a wide range of LOS. Details of the selected routes are discussed in the following sections.

3.1 REAL WORLD ROUTE DESCRIPTION

Table 1 shows the summary of the selected 15 routes in Raleigh NC area. These routes are selected based on criteria discussed earlier in this chapter. As shown, majority of the routes selected in this research have two lanes in the direction of the interest and a posted speed limit of 40 or 45 mph. Table 1 also shows calculated Free Flow Speed for each site using HCM6 (Highway Capacity Manual, 2015). Since the analysis also uses ITS probe speed data collected from INRIX reported at TMC segment level spatially, the route selection for this study was done at a TMC aggregation level.

Table 1 - Geometry of selected routes

Route Name	Length (miles)	Distance between intersections (miles)	Number of Lanes	Speed limit	Density of Driveways (per mile)	Free Flow Speed (mph)
Western Blvd WB - Site 1	0.7	0.2 - 0.2 - 0.3	2	45	0	44.1
Western Blvd WB - Site 2	0.6	0.1 - 0.2	2	45	23.33	43.6
Western Blvd EB - Site 1	0.7	0.3 - 0.2 - 0.2	2	45	4.28	42.8
Western Blvd EB - Site 2	0.6	0.2 - 0.1	2	45	30	43.7
Avent Ferry Rd EB - Site 1	1.4	0.9 - 0.2 - 0.3	2	40	10	41.5
Avent Ferry Rd WB - Site 1	1.4	0.3 - 0.2 - 0.9	2	40	11.42	41.6
Glenwood Ave WB - Site 1	1.2	0.5-0.6	2	45	10	43.3
Tryon Rd EB - Site 1	0.4	0.1	2	45	15	43.3
Tryon Rd EB - Site 2	1.8	0.7-0.2-0.9	2	45	10.56	43.6
Tryon Rd EB - Site 3	1.3	0.3-0.9	2	45	14.62	43.7
Tryon Rd EB - Site 4	1.3	0.9-0.3	2	45	11.54	43.3
Tryon Rd WB - Site 1	1.8	0.9-0.7-0.2	2	45	8.33	43.7
Tryon Rd WB - Site 2	0.4	0.3	2	45	12.5	43.6
Tryon Rd WB - Site 3	1.2	0.6-0.5	2	45	7.5	43.8
Tryon Rd WB - Site 4	0.7	0.2 - 0.3 - 0.2	3	45	7.14	43.9

Figure 7 shows the location of these routes on the map. Since, majority of the drivers participated in this research are students and staff members of NC State university (Raleigh, NC), majority of the routes are located close to the Centennial Campus of NC State University.

Figure 7 - Map showing location of all selected routes in Raleigh, NC

The INRIX TMC codes, along with the start and end geographical coordinates for these selected routes can be viewed in Table 2.

Table 2 - TMC codes and start and end coordinates of selected routes

Route Name	INRIX TMC Code	Start Co-ordinates	End Co-ordinates
Western Blvd WB - Site 1	125+14768	35.780889, -78.675385	35.785080, -78.687037
Western Blvd WB - Site 2	125+14769	35.785080, -78.687037	35.783983, -78.695953
Western Blvd EB - Site 1	125-14768	35.784922, -78.687074	35.780675, -78.675562
Western Blvd EB - Site 2	125-14767	35.783857, -78.695906	35.784922, -78.687074
Avent Ferry Rd EB - Site 1	125+14796	35.768378, -78.694026	35.780656, -78.675557
Avent Ferry Rd WB - Site 1	125-14795	35.780870, -78.675432	35.768355, -78.694245
Glenwood Ave WB - Site 1	125+14698	35.743428, -78.762378	35.745596, -78.740770
Tryon Rd EB - Site 1	125+14699	35.745568, -78.740557	35.745925, -78.732934
Tryon Rd EB - Site 2	125+14700	35.745971, -78.732737	35.748487, -78.702051
Tryon Rd EB - Site 3	125+14701	35.748487, -78.702051	35.742871, -78.680679
Tryon Rd EB - Site 4	125-14700	35.742967, -78.680438	35.748592, -78.701756
Tryon Rd WB - Site 1	125-14699	35.748685, -78.702101	35.746116, -78.732861
Tryon Rd WB - Site 2	125-14698	35.746087, -78.732993	35.745745, -78.740304
Tryon Rd WB - Site 3	125-14697	35.745781, -78.741073	35.743604, -78.762402
Tryon Rd WB - Site 4	125+06515	35.836559, -78.671156	35.843015, -78.680174

3.2 DRIVER SIMULATOR ROUTE DESCRIPTION

The study arterial, Perring Parkway, is located north east of Baltimore City, MD near Morgan State University. The simulated segment is northbound along Perring Parkway, from 33rd Street to I-695, a 4.4-mile stretch, consisting of six sections (links) as shown in Figure 8. All sections of the road have three lanes; however, in some periods of time, typically 8 am to 4 pm, the far-right lane is used as on-street parking and thus is not available to the traffic stream. The length, speed limit, and number of available lanes for each level of service are presented in Table 3.

Table 3 - Specifications of the simulated arterial

Section	Length (miles)	Speed Limit (mph)	Number of available lanes for level of service					
			A	B	C	D	E	F
Link-1	0.8	35	3	3	2	2	2	2
Link-2	0.38	35	3	3	2	2	2	2
Link-3	0.81	35	3	3	2	2	2	2
Link-4	1.42	45	3	3	3	3	3	3
Link-5	0.4	45	3	3	3	3	3	3
Link-6	0.39	45	3	3	3	3	3	3

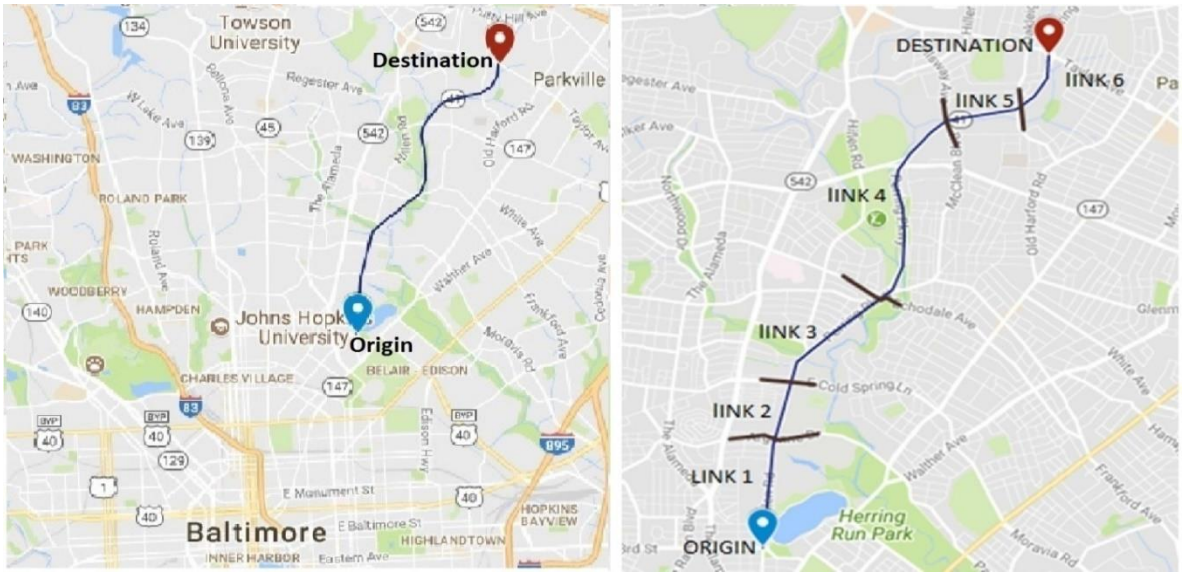

Figure 8 - Driving simulator at the SABA Center, Morgan State University

The simulated road segment and surrounding environment were designed as close as possible to the actual environment to ensure that subjects experience similar conditions and have realistic reactions accordingly. The simulated road segment includes traffic lights, trees, building structures

and other objects as seen in Figure 9. Data such as lane-changing, acceleration, braking, steering control and speed were recorded in real time by the driving simulator software.

Figure 9 - A screenshot of the simulated driving environment

In this study, drivers (henceforth referred to as participants) were asked to drive different scenarios presenting levels of service (LOS) of A to F as defined in the 6th edition of HCM for urban streets. Per HCM, LOS is function of geometric design of the roadway (Highway Capacity Manual, 2015). The scenarios' order was mixed up to be B, E, C, F, A, and D to avoid correlation of driver behavior with learning through the progression of traffic congestion.

4.0 DATA COLLECTION

4.1 I2D DATA COLLECTION

A database containing the vehicle trajectory data collected by the i2D devices described above is maintained and updated on a regular basis. After selecting the study routes, the vehicular trip data for each site was filtered for these routes. A Python tool developed alongside ArcMap was used for this data extraction. The data was filtered by road name, start and end latitude/longitude and date range for the selected routes. Similarly, 15-minute averaged probe-based speed readings were also collected for these routes, from INRIX, to calculate the Level of Service (LOS), prevailing on the road segment at the time the trips were made.

The data collection ranged from April 2014 to April 2017. For the year 2016, data collection was done only between the months of September and December, since the devices were being upgraded at the beginning of the year. A total of 4,479 trips were made during that period of time, by 46 distinct drivers on these selected sites. The number of trips and number of drivers for each selected route for each year of data collection is shown in Table 4.

Table 4 - Aggregate sample size number of drivers and trips

Route Name	# of Drivers				# of Trips			
	2014	2015	2016	2017	2014	2015	2016	2017
Avent Ferry Rd EB - Site 1	10	9	5	2	89	41	7	2
Avent Ferry Rd WB - Site 1	13	10	8	3	122	47	21	4
Glenwood Ave WB - Site 1	12	13	9	6	36	172	58	9
Tryon Rd EB - Site 1	9	11	4	3	27	68	10	5
Tryon Rd EB - Site 2	16	18	12	9	275	262	98	56
Tryon Rd EB - Site 3	8	10	6	4	37	61	42	16
Tryon Rd EB - Site 4	9	10	1	1	23	33	1	1
Tryon Rd WB - Site 1	8	8	2	1	27	28	2	1
Tryon Rd WB - Site 2	9	9	8	6	19	55	37	17
Tryon Rd WB - Site 3	18	14	13	13	298	270	110	61
Tryon Rd WB - Site 4	8	12	6	7	22	67	13	8
Western Blvd EB - Site 1	16	20	11	9	142	188	57	36
Western Blvd EB - Site 2	19	18	15	19	556	161	105	61
Western Blvd WB - Site 1	5	20	11	12	7	216	32	23
Western Blvd WB - Site 2	21	22	14	16	534	447	100	54

The total number of trips made during each LOS in each study route is summarized in Table 5. It can be seen that the number of observations observed in low LOS (E and F) are significantly lower than LOS A through D.

Table 5 - Total number of trips on each route by different LOS

Route Name	LOS A	LOS B	LOS C	LOS D	LOS E	LOS F
Avent Ferry Rd EB - Site 1	3	21	37	57	24	-
Avent Ferry Rd WB - Site 1	10	39	73	61	20	-
Glenwood Ave WB - Site 1	29	75	113	52	23	2
Tryon Rd EB - Site 1	66	43	9	1	1	-
Tryon Rd EB - Site 2	173	292	217	15	5	2
Tryon Rd EB - Site 3	136	25	4	-	-	-
Tryon Rd EB - Site 4	44	11	5	-	1	1
Tryon Rd WB - Site 1	23	22	15	-	-	-
Tryon Rd WB - Site 2	116	12	1	-	-	-
Tryon Rd WB - Site 3	167	343	197	33	13	3
Tryon Rd WB - Site 4	36	56	21	2	-	-
Western Blvd EB - Site 1	43	104	214	72	17	4
Western Blvd EB - Site 2	128	257	418	91	29	16
Western Blvd WB - Site 1	18	69	136	51	13	5
Western Blvd WB - Site 2	104	311	616	109	45	9
Grand Total	**1096**	**1680**	**2076**	**544**	**191**	**42**

The distribution of Level of Service (LOS) across these routes is intuitively displayed in Figure 10. The LOS is represented by the color coding (green to red), where green represents LOS A and it transitions into LOS C, displayed in red.

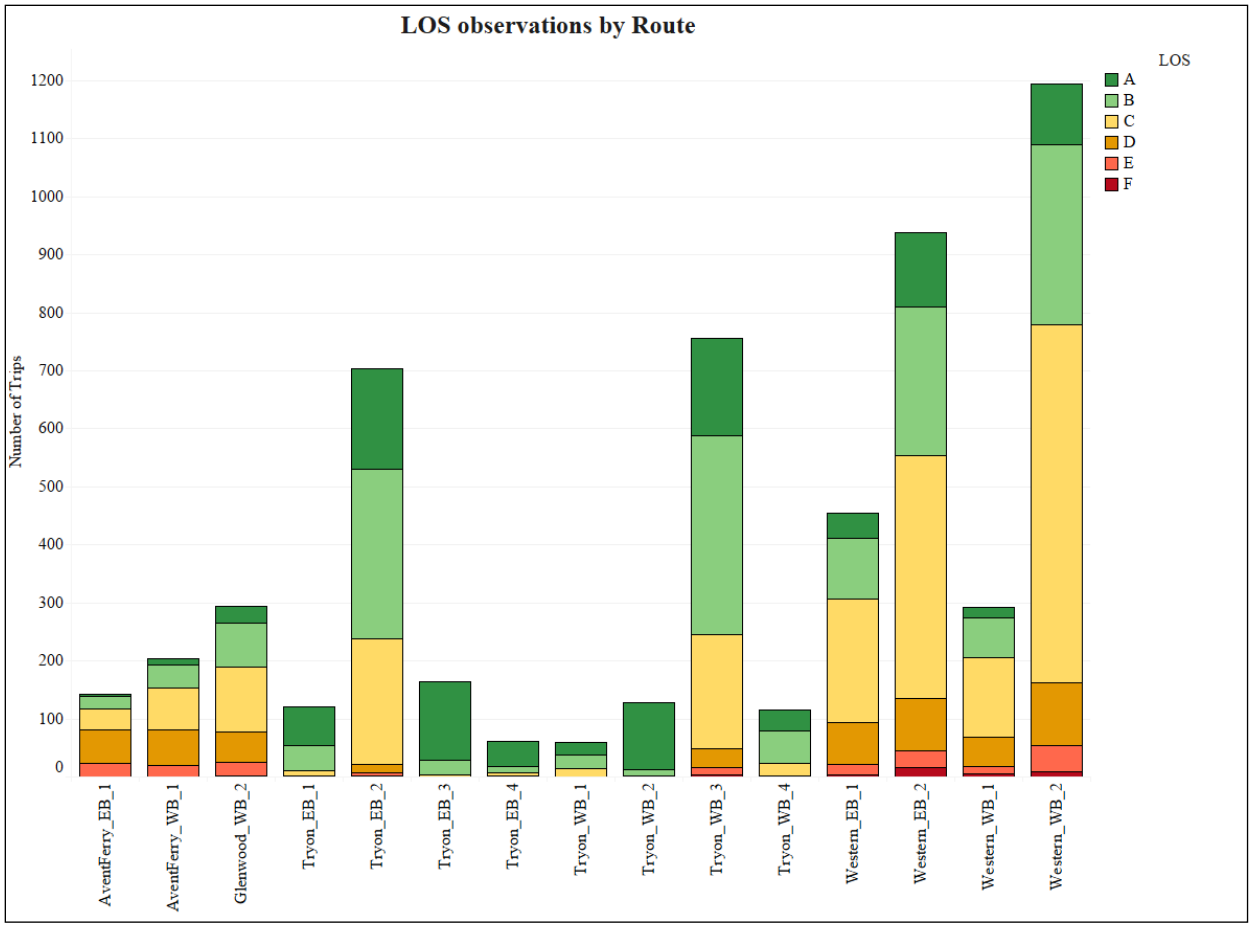

Figure 10 - LOS observations on Selected Routes

Appendices A through D provide detailed information on the characteristics of the collected data. Appendix A shows number of trips driven by each driver in each year for selected routes. Appendix B presents number of data points, trips, and distinct drivers for each route binned into different levels of service. The data collection via i2D devices did not have a constant trend across data collection period. Appendix C shows the monthly distribution of the collected data for each route. Appendix D shows the hourly distribution of the collected data in each route.

4.2 INRIX TRAVEL TIME DATA COLLECTION

The INRIX probe data was collected from RITIS.org website. The website gives the user the ability to select one or more TMC segments, a date range and the aggregation time period for downloading travel time and speed data. The data for this research was collected for the 15 TMC codes mentioned in Table 2 and the date range selected was between April 1, 2014 and April 30, 2017. The aggregation time period was selected to be 15 minutes, since most HCM calculations are based on a 15-minute aggregation period. The data collection takes a few minutes, depending on the number of TMC segments and the date range. The format of the data is a CSV file and contains fields such as Tmc_Code, Measurement_tStamp, Speed and Travel Time.

4.3 DRIVER SIMULATOR

IRB approval was received before human participants were recruited. Fliers were distributed across Morgan State University (MSU), Baltimore County and Baltimore City to recruit participants to drive the simulator. Participants were paid $15 per hour for their involvement in the study. A total of 53 participants were recruited. Despite attempts to have an unbiased sample, majority of volunteers were younger males.

To gather some socio-demographic data, participants were required to fill a pre-simulation survey. A post-simulation survey designed to capture participants' perception of the simulation session(s) and adverse effect(s)-if any-was also completed by Participants.

The study, rules and penalties were explained to the participants and practice sessions were initiated to familiarize participants with the simulator and simulated environment. They were randomly penalized for non-compliance with traffic signs (such as speed limit signs), and for accidents and crashes to ensure driving realism. Table 6 displays the socio-demographic data of Participants enrolled in the driving simulation study:

Table 6 - Socio-demographic characteristics of the participants

Characteristics	States	Percentages
Gender	Female	28
	Male	72
Age	<18	0
	18-25	37.74
	26-35	41.51
	36-45	9.43
	46-55	5.66
	>55	5.66
Education Level	High School or less	32
	College degree	47
	Post-graduate	21
Household income level	<$20k	25
	$20K-$30K	11
	$50-$75K	17
	$75-$100K	4
	>$100K	4

5.0 METHODOLOGY

This section presents a set of methods used to analyze data collected from both real world (via i2D devices) and driver simulator. The LOS calculation along with acceleration computations, which are similar for both data sources, are described. However, for the data collected from real world, additional computations were performed to relate driver behavior with observed LOS in the field.

5.1 RELATIONSHIP BETWEEN DRIVER BEHAVIOR AND LOS

5.1.1 Real World

After selecting the study routes, the data had to be filtered for the selected sites. An internal tool developed within ArcGIS software, is used to filter the trips that have occurred on the selected sites by connecting to the local MySQL database containing all the i2D data. The information regarding the desired corridor can be entered in this tool, such as the latitude and longitude combinations for the start and end of the selected corridor, the date range for the data collection and the road name. The trips that have used the specified corridor is identified using a geo-fencing technique. Meanwhile, the ITS probe data, reported by INRIX, which is used to calculate the LOS on these selected corridors or TMC segments, are also downloaded using the RITIS.org website. The INRIX speed data is downloaded for each of the selected TMC segments for each 15-min aggregation period within the temporal scope of the study and the Level of Service (A through F) is calculated using the free-flow speed of the facility and the method provided in the HCM6 (Highway Capacity Manual, 2015).

After filtering for the selected study corridors, the two datasets are combined or merged. Since the i2D trip data is reported for every second, the corresponding timestamps were rounded to the nearest 15-minute period. Then each observation of the trip data was matched with the INRIX speed provided for the 15-minute period. A sample of the important variable measurements of the i2D trip data used in this research, merged with the corresponding INRIX probe-based travel time data is tabulated in Table 7 and can be visualized for a few rows of observations in Figure 11.

Table 7 - List of variables in the merged i2D and INRIX data

Serial Number	Data Element	Data Source	Unit	Description
1	Trip_ID	i2D Trip Data	N/A	Unique ID assigned to each trip as an identifier
2	Start_Date	i2D Trip Data	N/A	Date when trip was started
3	Seconds	i2D Trip Data	seconds	Seconds elapsed since start of trip
4	Time	i2D Trip Data	timestamp	Second-by-second timestamp of trip event
5	i2D Speed (mph)	i2D Trip Data	mph	Speedometer reading for the current timestamp
6	Engine Load	i2D Trip Data	%	% Engine Load for the current timestamp
7	RPM	i2D Trip Data	revolutions per minute	Engine RPM for the current timestamp
8	Throttle position	i2D Trip Data	%	% Throttle pressed for the current timestamp
9	Acceleration_X (m/s2)	i2D Trip Data	m/s2	3-D accelerometer reading in x-direction
10	Acceleration_X (m/s2)	i2D Trip Data	m/s2	3-D accelerometer reading in y-direction
11	Acceleration_Z (m/s2)	i2D Trip Data	m/s2	3-D accelerometer reading in z-direction
12	Driver_ID	i2D Trip Data	N/A	Unique ID assigned to each driver as an identifier
13	Tmc_Code	INRIX Probe Data	N/A	TMC code of the segment for which the travel time is reported
14	Measurement_tStamp	INRIX Probe Data	timestamp	15-minute timestamp for which the travel time is reported
15	INRIX Speed (mph)	INRIX Probe Data	mph	Travel time averaged for the 15-minute interval in which it is reported
16	INRIX Travel Time (sec)	INRIX Probe Data	seconds	Speed averaged for the 15-minute interval in which it is reported

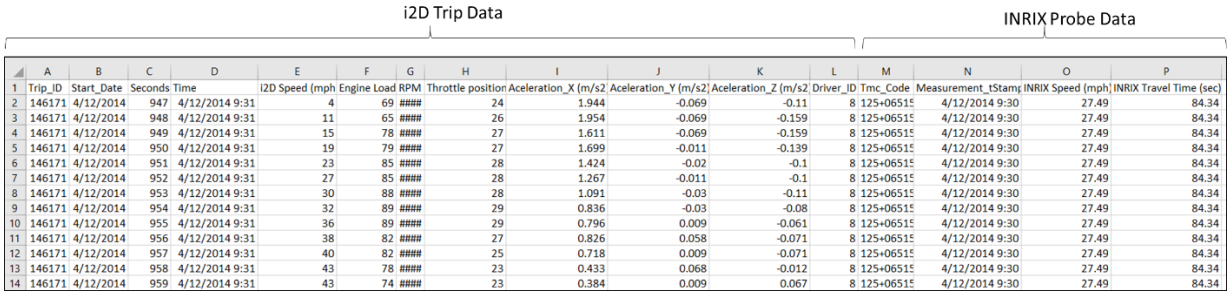

	A	B	C	D	E	F	G	H	I	J	K	L	M	N	O	P
1	Trip_ID	Start_Date	Seconds	Time	i2D Speed (mph	Engine Load	RPM	Throttle position	Aceleration_X (m/s2	Aceleration_Y (m/s2	Aceleration_Z (m/s2	Driver_ID	Tmc_Code	Measurement_tStamp	INRIX Speed (mph)	INRIX Travel Time (sec)
2	146171	4/12/2014	947	4/12/2014 9:31	4	69	####	24	1.944	-0.069	-0.11	8	125+06515	4/12/2014 9:30	27.49	84.34
3	146171	4/12/2014	948	4/12/2014 9:31	11	65	####	26	1.954	-0.069	-0.159	8	125+06515	4/12/2014 9:30	27.49	84.34
4	146171	4/12/2014	949	4/12/2014 9:31	15	78	####	27	1.611	-0.069	-0.159	8	125+06515	4/12/2014 9:30	27.49	84.34
5	146171	4/12/2014	950	4/12/2014 9:31	19	79	####	27	1.699	-0.011	-0.139	8	125+06515	4/12/2014 9:30	27.49	84.34
6	146171	4/12/2014	951	4/12/2014 9:31	23	85	####	28	1.424	-0.02	-0.1	8	125+06515	4/12/2014 9:30	27.49	84.34
7	146171	4/12/2014	952	4/12/2014 9:31	27	85	####	28	1.267	-0.011	-0.1	8	125+06515	4/12/2014 9:30	27.49	84.34
8	146171	4/12/2014	953	4/12/2014 9:31	30	88	####	28	1.091	-0.03	-0.11	8	125+06515	4/12/2014 9:30	27.49	84.34
9	146171	4/12/2014	954	4/12/2014 9:31	32	89	####	29	0.836	-0.03	-0.08	8	125+06515	4/12/2014 9:30	27.49	84.34
10	146171	4/12/2014	955	4/12/2014 9:31	36	89	####	29	0.796	0.009	-0.061	8	125+06515	4/12/2014 9:30	27.49	84.34
11	146171	4/12/2014	956	4/12/2014 9:31	38	82	####	27	0.826	0.058	-0.071	8	125+06515	4/12/2014 9:30	27.49	84.34
12	146171	4/12/2014	957	4/12/2014 9:31	40	82	####	25	0.718	0.009	-0.071	8	125+06515	4/12/2014 9:30	27.49	84.34
13	146171	4/12/2014	958	4/12/2014 9:31	43	78	####	23	0.433	0.068	-0.012	8	125+06515	4/12/2014 9:30	27.49	84.34
14	146171	4/12/2014	959	4/12/2014 9:31	43	74	####	23	0.384	0.009	0.067	8	125+06515	4/12/2014 9:30	27.49	84.34

Figure 11 - Sample of merged i2D and INRIX data

After the data collected from the two sources are integrated, some additional MOE's are calculated to aid in analysis and subsequently the LOS is calculated based on the Free Flow Speed of each route and the speed reported by the INRIX speed data. This process was conducted using scripts written in the R programming environment and for each of the 15 selected sites. Exploratory data exploration, data visualization and predictive modeling is done after the cleaned and integrated data tables are created.

5.1.2 Driver Simulator

The LOS along arterials is a function of traffic volume, average speed of the traffic stream, travel time as well as the extent to which drivers can maneuver between vehicles. Six scenarios of various traffic volumes were designed to match traffic speed of LOS A, B, C, D, E and F. The driving simulator software recorded participant's speed, acceleration, brake, and so on for about every 10^{th} of a second as they drive through the corridor. We aggregated the data into per-second intervals and extracted speeds, acceleration readings, the number of acceleration, brake, and lane changes per mile per available lane, as well as throttle-use.

5.2 ADDITIONAL MOE CALCULATIONS

5.2.1 Longitudinal Acceleration

One thing to be noted is that the second-by-second acceleration readings collected by these devices from the vehicle sensors are reported in three axes (x, y and z). These axes can vary between vehicle to vehicle depending on the way these devices are attached in the car. In order to analyze driver aggressiveness, positional acceleration is an important variable that should be considered.

In order to ensure homogeneity in the subsequent analyses, the measured OBD speed was used as the true indicator of acceleration in the direction of travel (x axis) and calculated for the i^{th} row of observations, using the following equation:

$$Acc\_x\_est_i = (OBD\_Speed_i - OBD\_Speed_{i-1}) * 0.44704 \quad (1)$$

Where,

$Acc\_x\_est_i$ = the estimated longitudinal acceleration (m/s^2) in direction of travel for i^{th} observation

OBD_Speed_i = the measured OBD speed (mph) for i^{th} observation

OBD_Speed_{i-1}= the measured OBD speed (mph) for $(i-1)^{th}$ observation

0.44704 = conversion factor from mph to m/s

5.2.2 3-D Combined Acceleration

The total acceleration was calculated for every observation using the following formula:

$$Acc_{3D\_Combined} = \sqrt{(Acc\_x\_obs)^2 + (Acc\_y\_obs)^2 + (Acc\_z\_obs)^2} \quad (2)$$

Where,

$Acc_{3D\ Combined}$ = the resultant total acceleration (m/s^2)

Acc_x_obs = Accelerometer reading (m/s^2) in x direction of travel from OBD

Acc_y_obs = Accelerometer reading (m/s^2) in y direction of travel from OBD

Acc_z_obs = Accelerometer reading (m/s^2) in z direction of travel from OBD

5.2.3 Lateral Acceleration

The lateral acceleration was calculated for every observation using the following formula:

$$Acc\_y\_est = \sqrt{abs[(Acc_{3D\ Combined})^2 - (Acc\_x\_est)^2\ ]} \quad (3)$$

Where,

Acc_y_est = the resultant lateral acceleration (m/s^2)

Acc_x_est Acc_x_obsAcc_y_est= the estimated lateral acceleration (m/s^2) in direction of travel

$Acc_{3D\ Combined}$ = the resultant total 3-dimensional acceleration (m/s^2)

5.2.4 Jerk

Jerk is defined as the rate of change of longitudinal acceleration in the direction of travel and is calculated using the following equation:

$$Jerk_i = (Acc\_x\_est_i - Acc\_x\_est_{i-1}) \quad (4)$$

Where,

$Jerk_i$ = the estimated jerk (m/s^3) for ith observation

$Acc\_x\_est_i$ = the estimated acceleration (m/s^2) in direction of travel for ith observation

$Acc\_x\_est_{i-1}$ = the estimated acceleration (m/s^2) in direction of travel for (i-1)th observation

5.3 LOS CALCULATION FOR STUDY ROUTES

The methodology for calculation of Level of Service (LOS) for urban street facilities is described in Chapter 16 of the 6th edition of Highway Capacity Manual. It specifies that LOS for motorized-vehicle-mode is estimated using criteria based on performance measures that can be measured in field, i.e., the through vehicle speed. The base free-flow speed on a facility is used to calculate the threshold values that determines the operating Level of Service. These threshold values are summarized from HCM Chapter 16 in Table 8.

Table 8 - Criteria for determing Level of Service (LOS) for motorized vehicle mode

LOS	Range of Travel Speed	Volume/Capacity Ratio
A	> 0.8* FFS	<=1.0
B	>0.67*FFS and <0.8* FFS	<=1.0
C	>0.5*FFS and <0.67* FFS	<=1.0
D	>0.4*FFS and <0.5* FFS	<=1.0
E	>0.3*FFS and <0.4* FFS	<=1.0
F	<0.3* FFS	<=1.0

Free-flow speed represents the average running speed of through vehicles traveling along a segment under low-volume conditions and not delayed by traffic control devices or other vehicles. The “base free-flow speed” is defined to be the free-flow speed on longer segments.

Since the routes selected for this study has the same spatial scope as TMC segments, each route may consist of one of many HCM segments. The procedure for calculating the free-flow speed for an HCM segment uses the formula, presented by Equation 18-3 in Chapter 18 (Urban Street Segments) of the HCM. The formula takes into account, the influence of speed limit, access point density, median type, curb presence, and on-street parking presence. Then the base free-flow speed for the whole facility or study route is calculated using a length-based average of the free-flow speed for each HCM segment, provided by Equation 16-2 in Chapter 16 (Urban Street Facilities) of the HCM. The FFS for the routes selected in this research has been presented in Table 1.

6.0 OBSERVATIONS AND RESULTS

This section presents the results and observations from analysis of the cleaned real-world data as well as driver simulator data. These observations are made on the selected routes, described in section 3 of this final report. The calculation procedures presented in chapter 5 of this report has been carried out on the collected data. This section is divided into two sub-sections to discuss observations from real world and driver simulator in detail separately.

6.1 REAL WORLD OBSERVATIONS

6.1.1 Summary of the Impact of LOS on Driver Behavior Observations

This section summarizes the impact of LOS on the observed driver behavior. Driver behavior is characterized by the set of variables collected from i2D data such as acceleration, jerk, etc. Details of observations are reported in the appendices. As discussed in earlier sections, each i2D device is equipped with a 3-dimensional accelerometer that is capable of recording acceleration in the direction of travel as well as vertical and lateral directions.

To record the three components of the accelerometer readings correctly, the i2D device needs to be installed as directed by fleet manager. Thus, it can identify longitudinal and lateral directions appropriately. Based on the observations, not all fleet drivers had their devices installed in the right orientation, to correctly measure the accelerations. As such, in this research we developed two methods to compute the longitudinal and lateral accelerations correctly (discussed in section 5).

Figure 12 shows the 3-dimensional combined acceleration (or total acceleration) observations from real world data across different LOS (A through F) for all the selected routes. These readings have been categorized by LOS and the minimum, maximum and average values were calculated by grouping the average acceleration by routes. The blue band shown in the figure indicates the inner range between 25^{th} and 75^{th} percentile readings for each LOS. As seen in Figure 12, the average 3D acceleration by shows a slight increase with deterioration in LOS. However, the range between minimum and maximum observations shows a significant increase as LOS deteriorates. Appendix E provides detailed information on 3D acceleration observation categorized by each route.

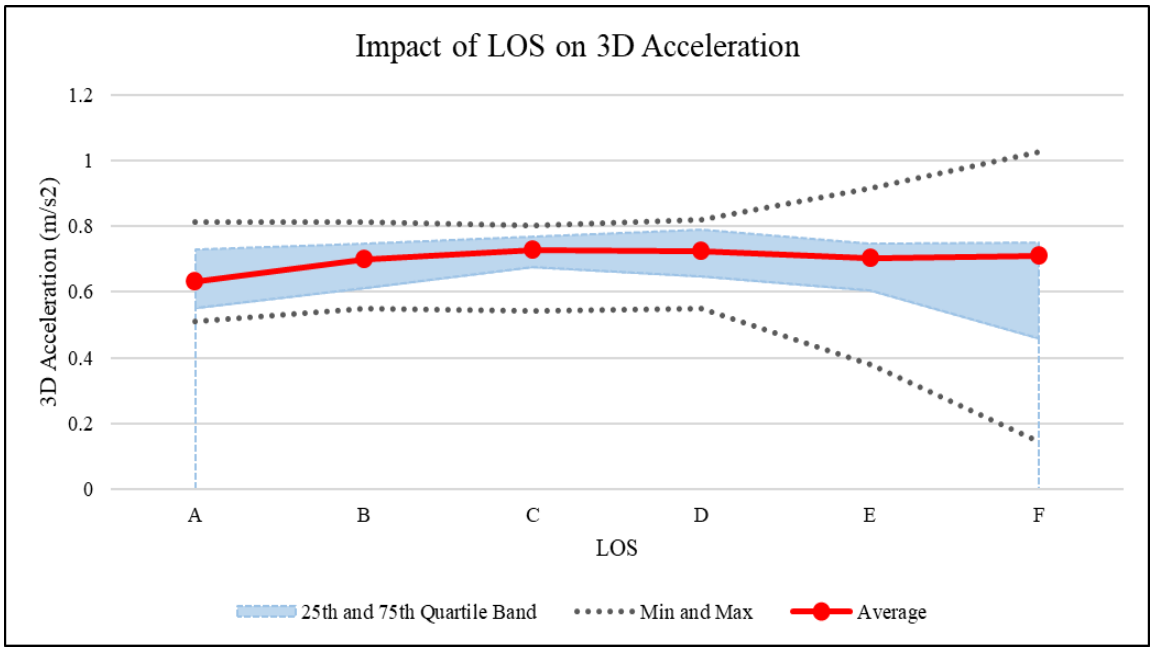

Figure 12 - Impact of LOS on 3D Acceleration

Figure 13 and Figure 14 below show the breakdown of the 3D acceleration readings into longitudinal and lateral components, the calculations for which have been presented in Section 5 earlier. As seen, the bigger part of the 3D acceleration is the lateral piece, and shows a trend similar to that shown by 3D acceleration.

On the other hand, the average longitudinal acceleration shows higher values for LOS B and C. The higher longitudinal acceleration in LOS B and C, compared to LOS A could be due to cruising at desirable speed in LOS A, which may not happen in LOS B or C. On the other hand, a lower average longitudinal acceleration for LOS D, E and F could be due to lack of spacing between the vehicles, which makes it harder to increase and decrease speeds. Appendices F and G present detailed information on average and standard deviation of acceleration and deceleration readings for each individual route. Appendix H and I show the average and boxplot of lateral acceleration readings in each route binned by LOS.

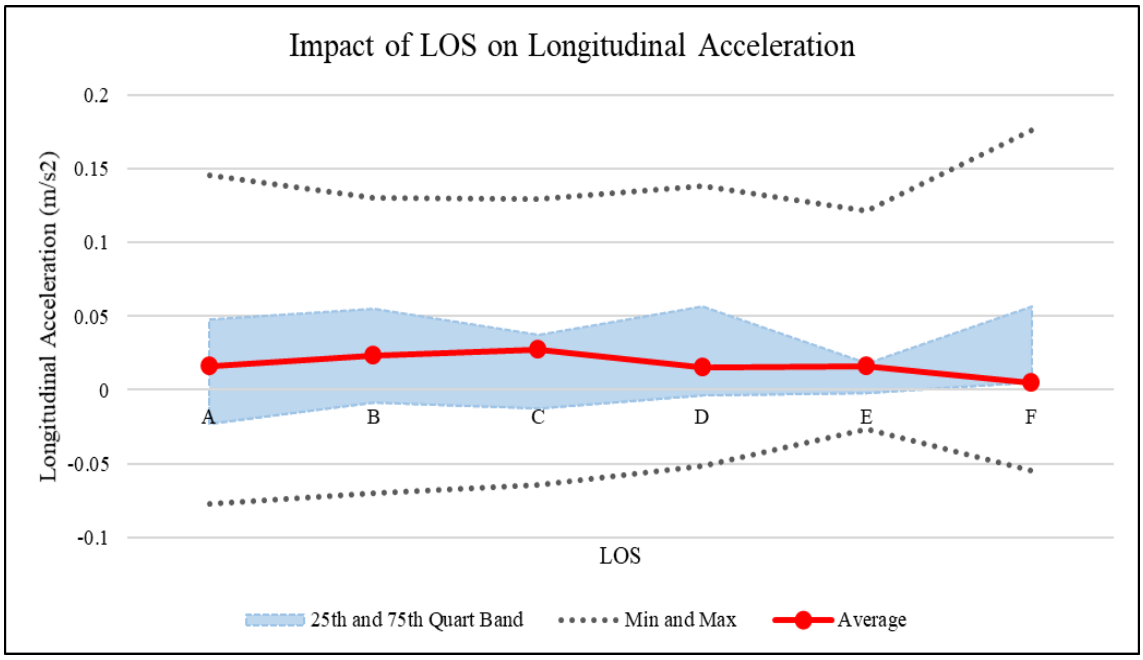

Figure 13 - Impact of LOS on Longitudinal Acceleration

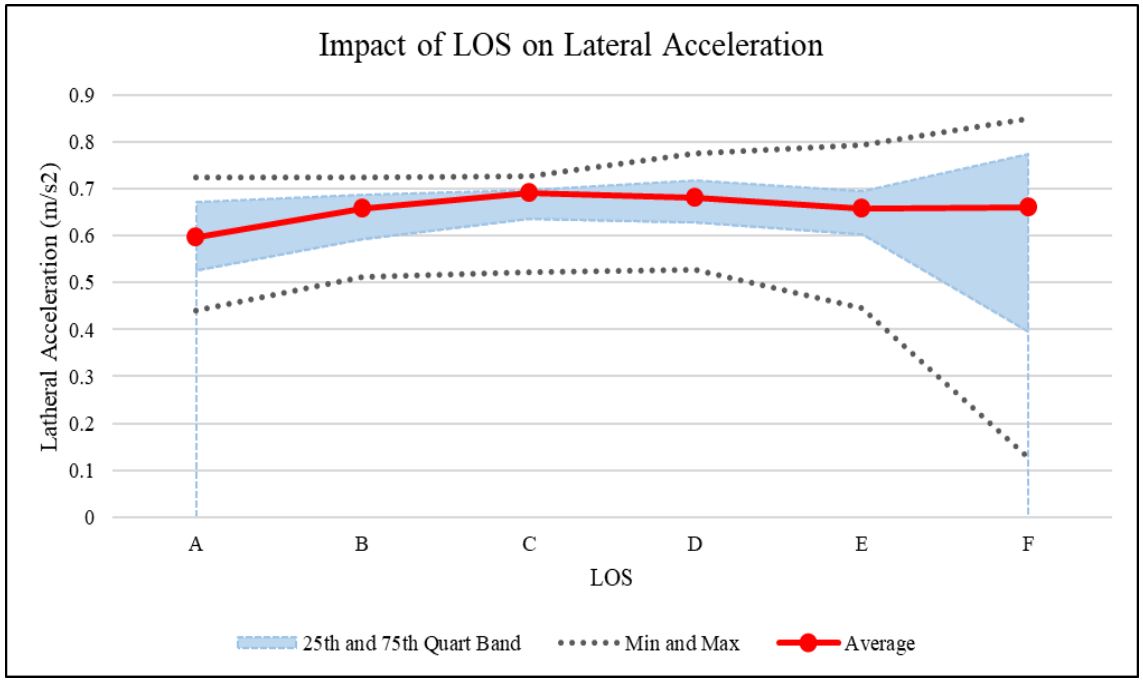

Figure 14 - Impact of LOS on Lateral Acceleration

Figure 15 and Figure 16 show the distribution of maximum observed acceleration and deceleration readings in the 15 selected sites. Appendix J shows details of maximum acceleration and deceleration observations for each analysis route. Appendices K and L present details of observed acceleration and deceleration readings binned for LOS.

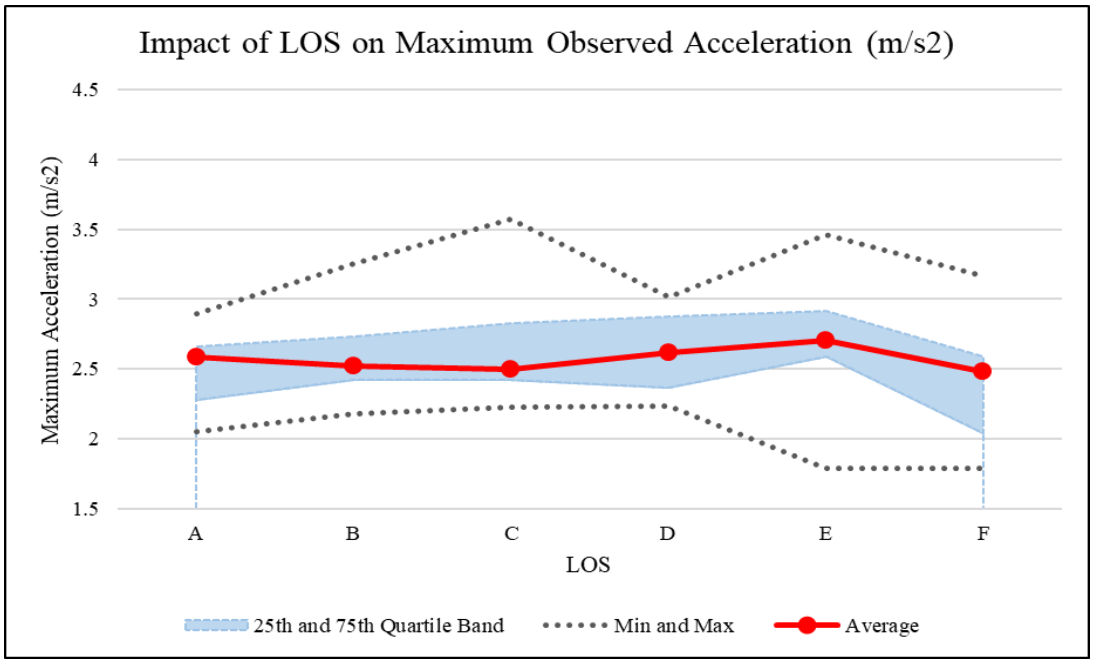

Figure 15 - Impact of LOS on Maximum Observed Acceleration

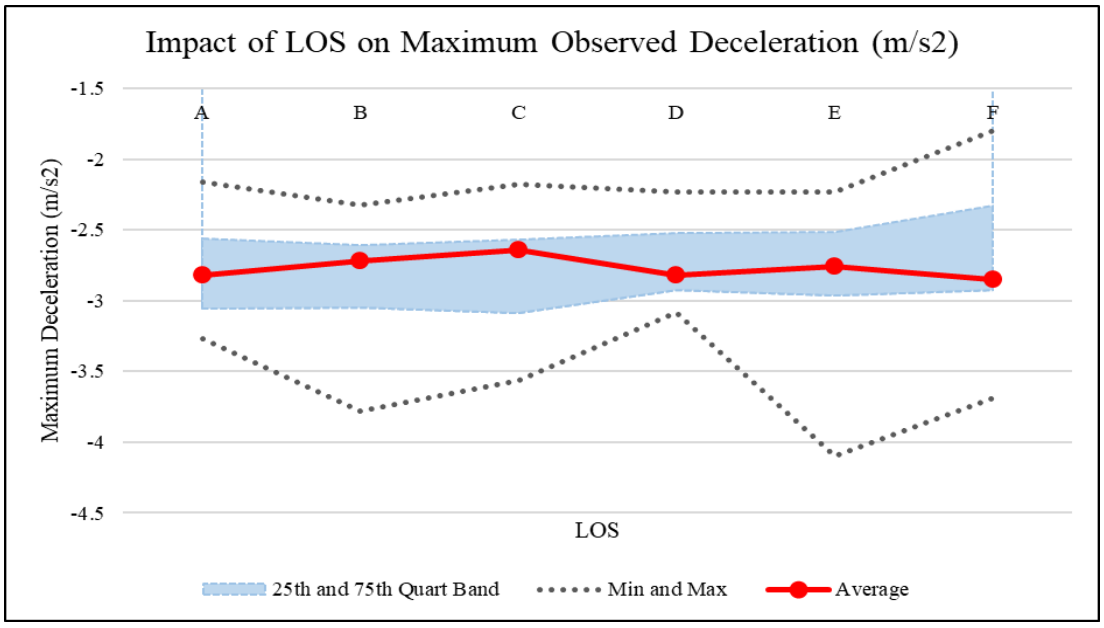

Figure 16 - Impact of LOS on Maximum Observed Deceleration

Figure 17 shows the distribution of rate of change of acceleration or jerk observed across all selected routes, across different LOS. The lower the LOS, the lesser is the variation in the range of jerk. This finding shows that drivers have more opportunity in less traffic condition to change the rate of acceleration or deceleration. This observation is significant in LOS A and in other ranges of LOS, a consistent pattern is observed.

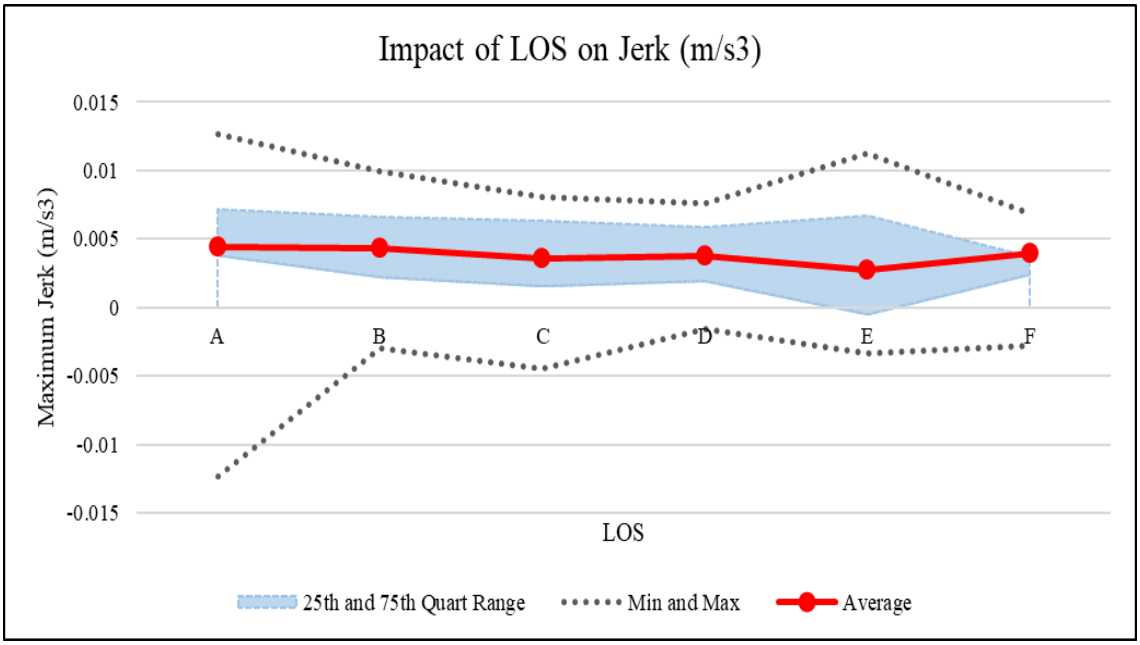

Figure 17 - Impact of LOS on Jerk

Figure 18, Figure 19 and Figure 20 show the impact of LOS on RPM, throttle position, and engine load respectively. These three metrics show a consistent decreasing pattern with LOS deterioration. Appendices M and N present a detailed summary of the RPM and throttle readings for each of the selected routes.

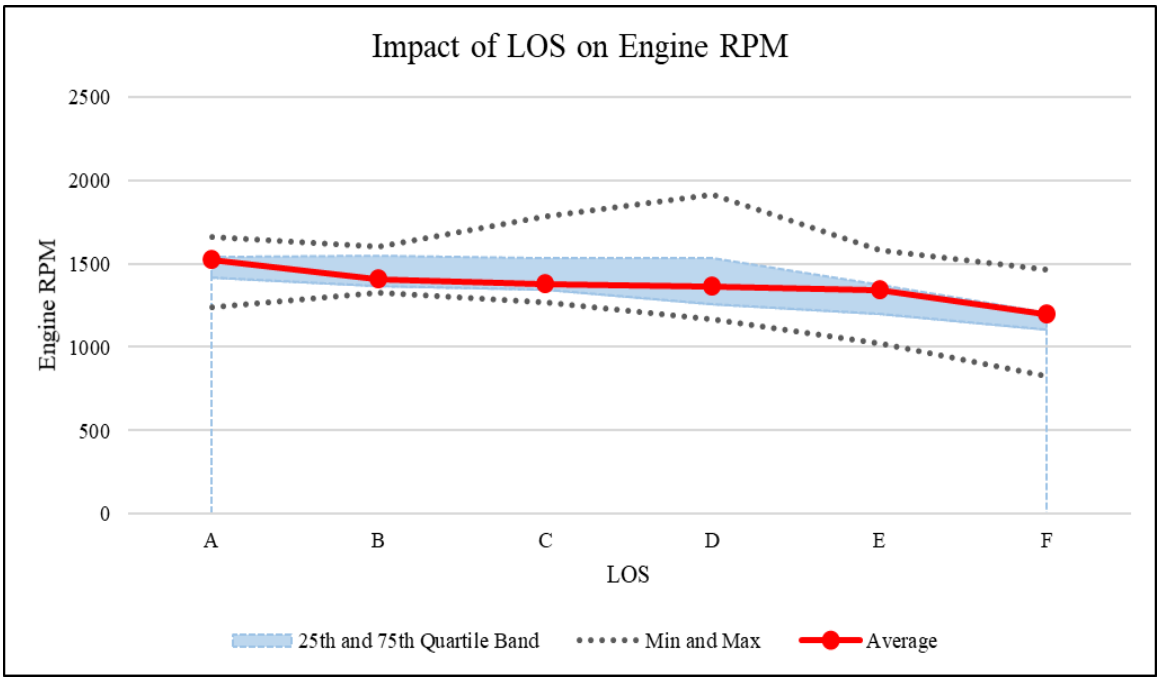

Figure 18 - Impact of LOS on Engine RPM

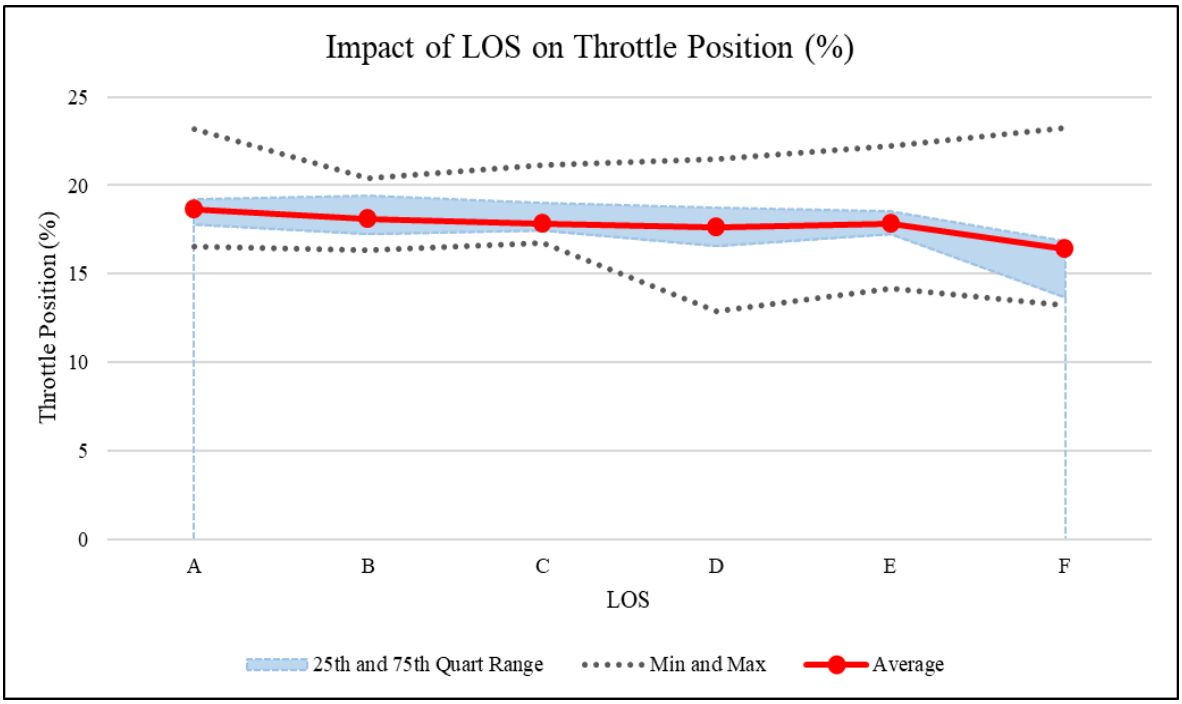

Figure 19 - Impact of LOS on Throttle Position

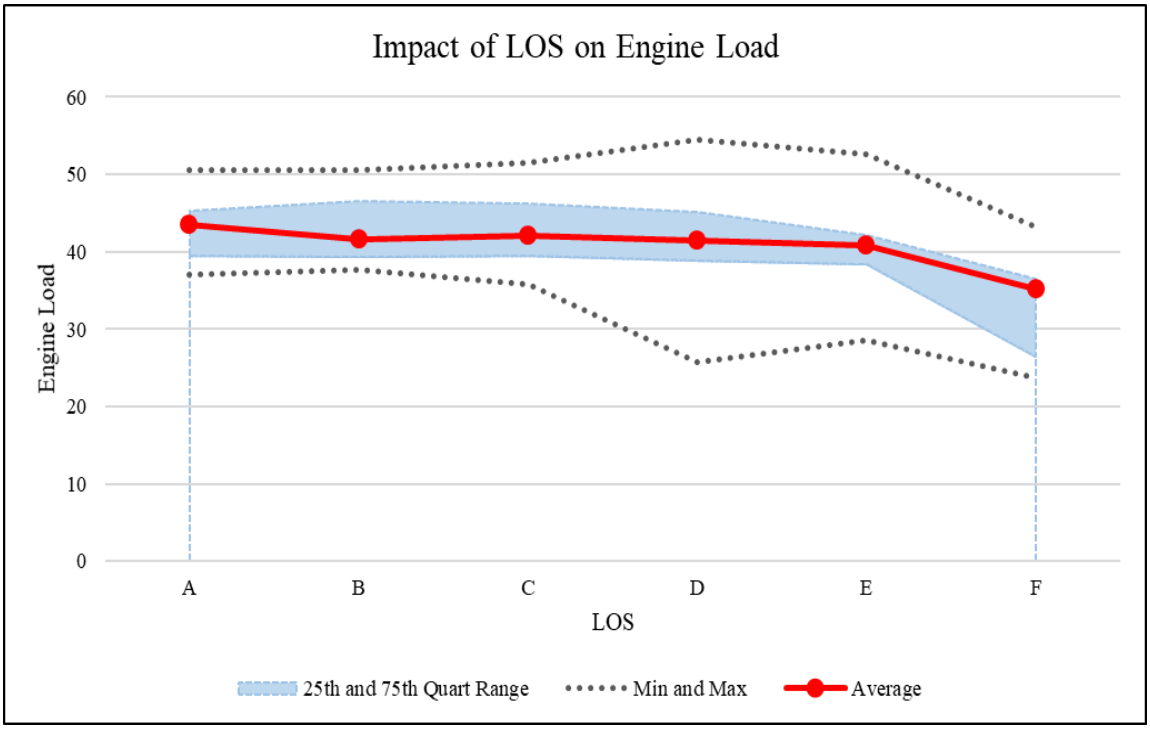

Figure 20 - Impact of LOS on Engine Load

6.1.2 Correlation Plot

The i2D devices report measurement of a total of 64 variables, collected from a vehicle's sensor readings and their in-built GPS systems. However, since not all 64 variables are directly related to the scope of the project, the set of variables to be analyzed was reduced to include ones that can be directly used to measure driver aggressiveness. These include:

- Speed (mph)
- Engine Load (%)
- Revolutions per minute (RPM)
- Throttle Position (%)
- Level of Service (LOS)
- Linear Acceleration (m/s2)
- Jerk (m/s3)
- Total Acceleration (m/s2)
- Longitudinal Acceleration (m/s2)

The following figure represents a correlation plot between these variables. Positive correlations are displayed in blue and negative correlations in red color. Color intensity and the size of the

ellipses are proportional to the correlation coefficients. From Figure 21, we can see that RPM and Speed are positively correlated with each other, as are Engine Load and Throttle Position. An even stronger correlation is shown between total acceleration and lateral acceleration, suggesting the use of only one of these pairs in any regression or statistical models. However, the LOS does not show any correlation with any of the measured variables.

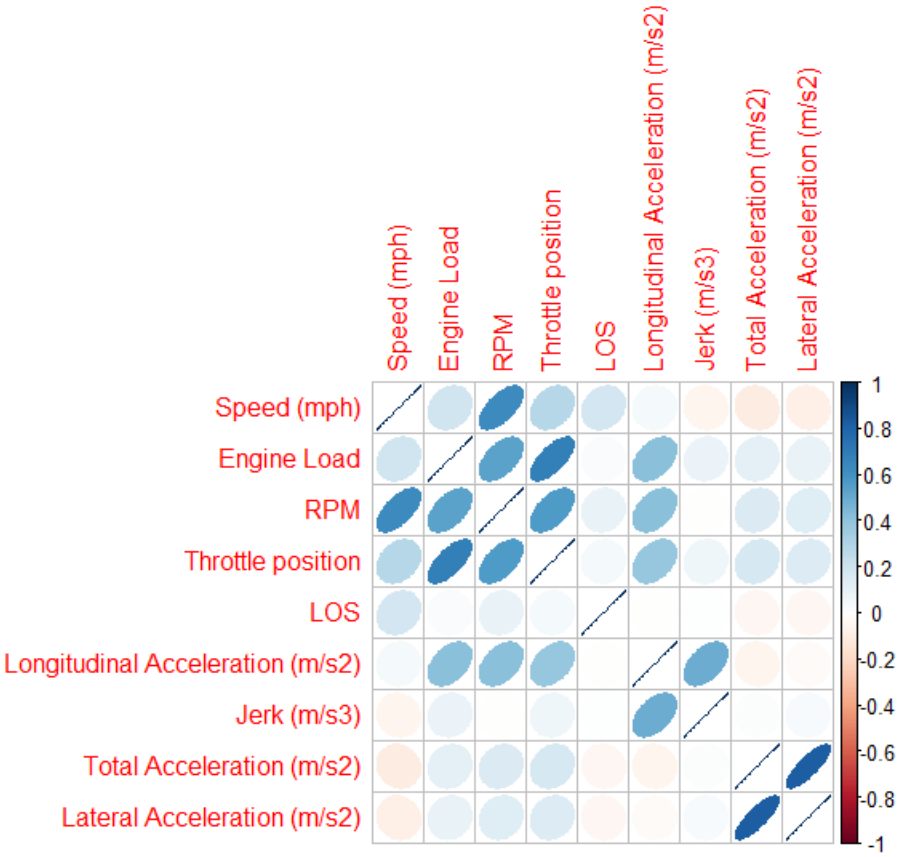

Figure 21 - Correlation Plot for i2D Data Variables and LOS

6.1.3 One Way ANOVA Results

6.1.3.1 Revolutions per minute (RPM)

The results for one-way ANOVA test with RPM as the response variable and LOS as the categorical predictor variable is shown in Table 9 below. The F test for LOS is significant, indicating that the means for RPM across different LOS are statistically significant from each other.

Table 9 - Results of one-way ANOVA test for LOS on RPM

Source	DF	Sum of Squares	Mean Square	F Value	Pr > F
Model	5	2101613848.1	420322769.61	1185.41	<.0001
Error	544498	193067362565	354578.64412		
Corrected Total	544503	195168976413			

The Means comparison table for RPM over different Level of Service (LOS) in Table 10 shows that RPM decreases with a decrease in LOS.

Table 10 - Means Comparison table for RPM over different LOS

Level of LOS	Sample Size (N)	RPM	
		Mean	Std Dev
A	113522	1523.53908	564.445901
B	146037	1409.48049	588.981248
C	191657	1379.03078	605.037975
D	65103	1364.73081	630.836948
E	23748	1339.64915	609.649507
F	4437	1194.26842	550.934058

6.1.3.2 Throttle Position

The results for one-way ANOVA test with Throttle Position as the response variable and LOS as the categorical predictor variable is shown in Table 11 below. The F test for LOS is significant, indicating that the means for Throttle Position across different LOS are statistically significant from each other.

Table 11 - Results of one-way ANOVA test for LOS on Throttle Position

Source	DF	Sum of Squares	Mean Square	F Value	Pr > F
Model	5	79472.93	15894.59	306.74	<.0001
Error	544498	28214596.04	51.82		
Corrected Total	544503	28294068.97			

The Means comparison table for Throttle Position over different Level of Service (LOS) in Table 12 shows that Throttle Position decreases with a decrease in LOS.

Table 12 - Means comparison table for Throttle Position over different LOS

Level of LOS	Sample Size (N)	Throttle position	
		Mean	Std Dev
A	113522	18.6704956	8.02088218
B	146037	18.0946199	7.10807743
C	191657	17.8213110	6.84548266
D	65103	17.6171144	6.95860038
E	23748	17.8527034	6.78214606
F	4437	16.3768312	8.31955796

6.1.3.3 Engine Load

The results for one-way ANOVA test with Engine Load as the response variable and LOS as the categorical predictor variable is shown in Table 13 below. The F test for LOS is significant, indicating that the means for Engine Load across different LOS are statistically significant from each other.

Table 13 - Results of one-way ANOVA test for LOS on Engine Load

Source	DF	Sum of Squares	Mean Square	F Value	Pr > F
Model	5	534886.4	106977.3	204.61	<.0001
Error	544498	284682628.8	522.8		
Corrected Total	544503	285217515.2			

The Means comparison table for Engine Load over different Level of Service (LOS) in Table 14 also shows a generally decreasing trend for Engine Load with decrease in LOS.

Table 14 - Means comparison table for Engine Load over different LOS

Level of LOS	Sample Size (N)	Engine Load	
		Mean	Std Dev
A	113522	43.5194235	23.4333642
B	146037	41.6427481	22.9932495
C	191657	42.0479920	22.7463728
D	65103	41.5089320	22.2758727
E	23748	40.8362388	22.3102633
F	4437	35.1413117	20.4275667

6.1.3.4 3-D Combined Acceleration

The results for one-way ANOVA test with Total Acceleration or the 3-D Combined Acceleration as the response variable and six levels of LOS as the categorical predictor variable is shown in Table 15 below. The F test for LOS is significant, indicating that the means for Total Acceleration across different LOS are statistically significant from each other.

Table 15 - Results of one-way ANOVA test for LOS on 3-D Combined Acceleration

Source	DF	Sum of Squares	Mean Square	F Value	Pr > F
Model	5	703.1267	140.6253	332.17	<.0001
Error	544498	230513.6015	0.4234		
Corrected Total	544503	231216.7281			

The Means comparison table for 3-D Combined Acceleration over different Level of Service (LOS) in Table 16 also shows a generally decreasing trend for Engine Load with decrease in LOS.

Table 16 - Means Comparison table for 3-D Combined Acceleration over different LOS

Level of LOS	Sample Size (N)	3-D Combined Acceleration	
		Mean	Std Dev
A	113522	0.63293422	0.62084345
B	146037	0.69801317	0.63018370
C	191657	0.72896569	0.68093429
D	65103	0.72214182	0.67079712
E	23748	0.70139415	0.60481640
F	4437	0.71013550	0.65717380

6.1.4 Random Forest Predictive Model

In this section, the performance of a Supervised Machine Learning algorithm, Random Forests, in classifying driving events as aggressive or normal is explained.

6.1.4.1 Algorithm Description - Random Forest Classification

Random forests or random decision forests are an ensemble learning method for classification, regression and other tasks, that operate by constructing a multitude of decision trees at training time and outputting the class that is the mode of the classes (classification) or mean prediction (regression) of the individual trees (Ho, 1995). Random decision forests correct for decision trees' habit of overfitting to their training set. The method constructs multiple decision trees and applies bootstrap aggregating (bagging) to the trees, i.e., it selects a random sample with replacement of the training set and fits trees to these samples. In the original implementation of the random forest algorithm, each tree is trained on about 2/3 of the total training data and as the forest is built, each tree can thus be tested on the samples not used in building that tree. This is also known as the out-of-bag error estimate and is an internal error estimate of a random forest as it is being constructed. This estimate is also an indication of how well the algorithm performs.

All the properties described above makes Random Forrest Classification algorithm unexcelled in accuracy among current algorithms and run efficiently on large dataset. It can handle thousands of input variables without variable deletion, and also provides the importance of different predictor variables. Random forests are non-parametric, i.e., they make no distributional assumptions, and

can thus handle skewed and multi-modal data as well as categorical data that are ordinal or non-ordinal. Figure 22 displays a diagram that explains the working of the algorithm in a simplified manner.

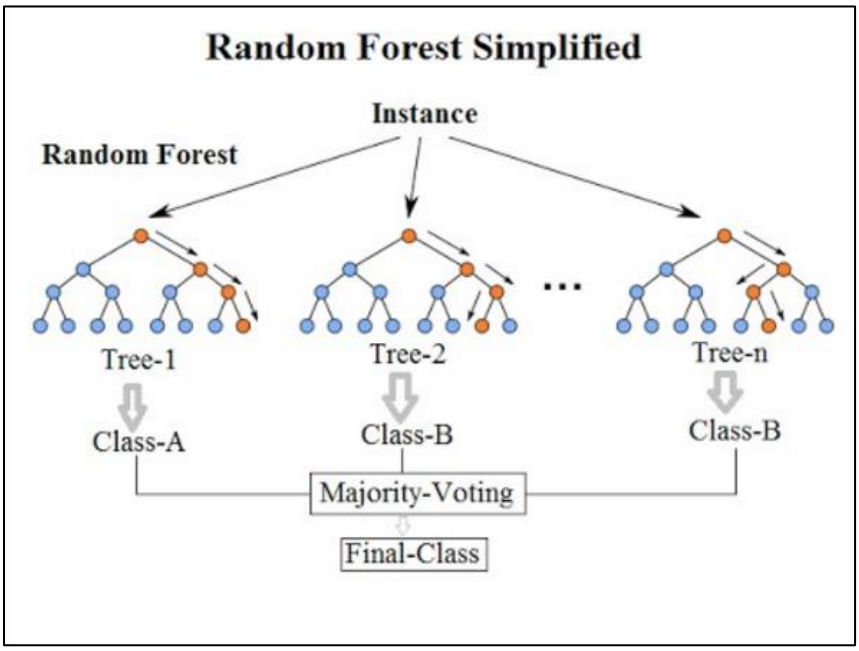

Figure 22 - Summarizing the working of Random Forest Classification Technique

6.1.4.2 Labeling and Creating Training and Test Datasets

In order to train the model, each row of observation of the collected data was labeled as "Aggressive" vs "Normal". Two different measures for aggressiveness was calculated, based on literature (Chen et al., 2015). These measures were selected since they normalize the measures of aggressiveness by the RPM, which helps account for the differences between vehicles. The measures were calculated for each row of observations.

1. R1 – ratio of change in speed to change in RPM

$$R_1 = \frac{\Delta\, Speed\ of\ the\ vehicle}{\Delta\, RPM} \tag{5}$$

Where,

$\Delta\, Speed\ of\ the\ vehicle$ = change in speed of the vehicle

$\Delta\, RPM$ = Change in RPM of the vehicle

2. R2 – ratio of change in throttle position to change in RPM

$$R_2 = \frac{\Delta\, Throttle\ Position}{\Delta\, RPM} \tag{6}$$

Where,

$\Delta\, Throttle\ Position$ = change in % Throttle Position of the vehicle

$\Delta\, RPM$ = Change in RPM of the vehicle

A record was labeled as 'Aggressive' if R1 and R2 was found below the 15th percentile or above 70th percentile value, otherwise 'Normal'. After labeling the data, it was found that 67% of the driving events were labeled as 'Normal' and the rest were aggressive driving events. The distribution of these driving events is shown in Figure 23.

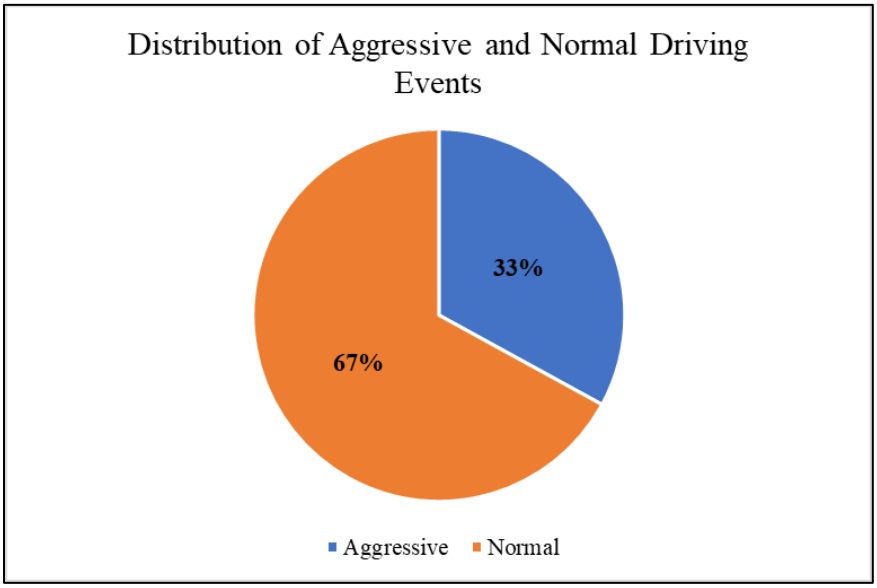

Figure 23 - Distribution of 'Normal' and 'Aggressive' driving labels in collected data

A 10% training sample was used to train the Random Forest Model and tested against the rest of the data for accuracy. The model was trained and programmed in R environment.

6.1.4.3 Results

The error in classification for each class and the out-of-bag error is displayed in Figure 24, along the number of decision trees constructed in the forest, which is usually specified as an input parameter. This is one way to visualize the error convergence or the fit of the algorithm.

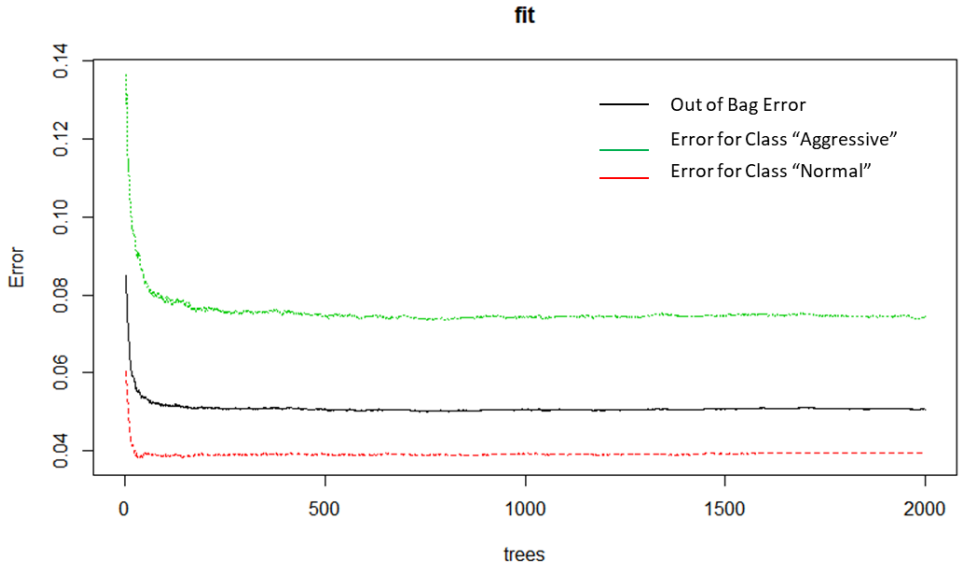

Figure 24 - Random Forest Error Plot

The ratio of correctly predicted observation to the total observations or the overall accuracy of the model was 94.9%. Table 17 below shows the total number of "Normal" and "Aggressive" driving events predicted and the recall rate for each class. Recall is defined as the percentage of accurate predictions for each class.

Table 17 - Number of actual and predicted "Normal" and "Aggressive" data points

	Predicted "Normal"	**Predicted "Aggressive"**	**Recall Rate (%)**
Actual "Normal"	24827	1019	96.05%
Actual "Aggressive"	915	11391	92.57%

Figure 25 below shows the percentage prediction for each class. The darker shaded region represents the actual "Aggressive" data points and the lighter shade represents the actual "Normal" data points.

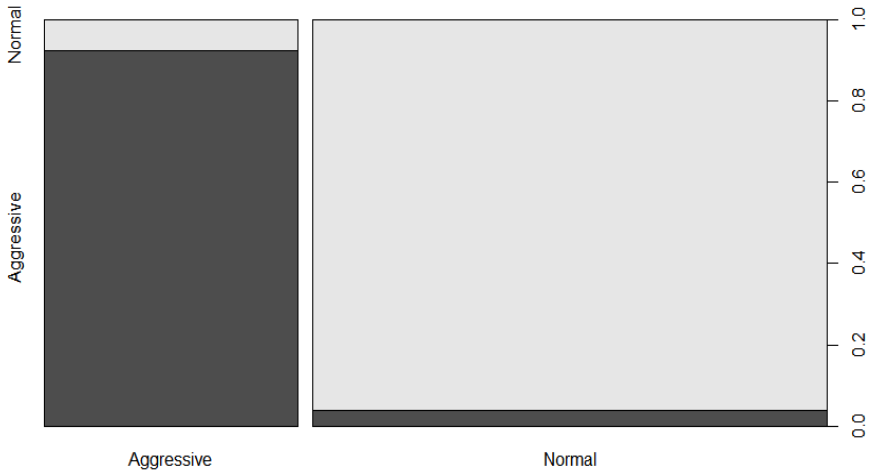

Figure 25 - Random Forest class prediction

Figure 26 shows the percentage of data points, both predicted (in blue) and actual (in orange) for "Aggressive" driving events on the left and "Normal" driving events on the right, over different LOS. This graph shows that the random forest predicts more "Aggressive" driving for LOS F than actual and more "Normal" driving is predicted for LOS A than actual.

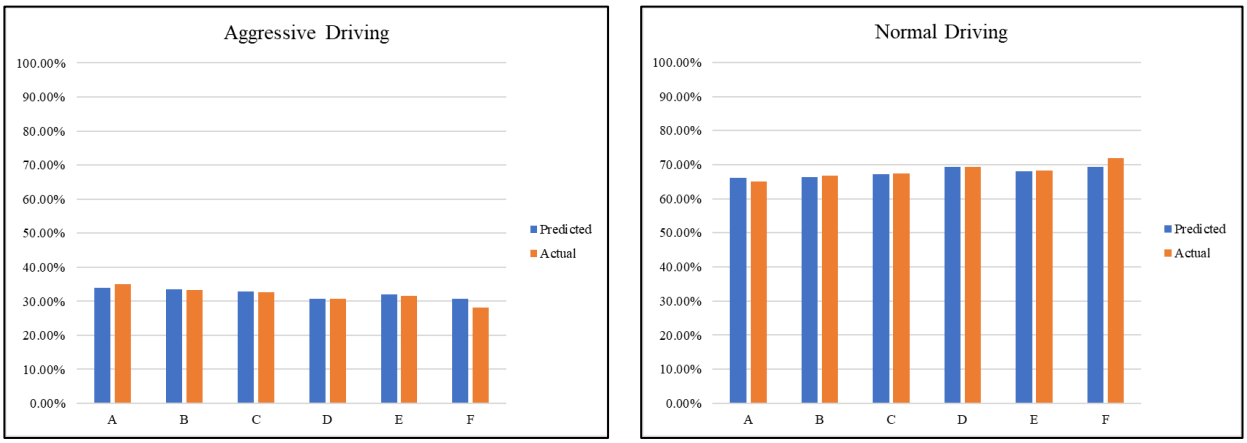

(a) (b)

Figure 26 - Percentage of (a) "Aggressive" and (b) "Normal" driving events, predicted by Random Forest Classification by Level of Service against actual

6.2 DRIVER SIMULATOR

6.2.1 Summary of the Impact of LOS on Driver Behavior Observations

In this section, observations obtained from driver simulator test are processed the driver behavior is analyzed in terms of different LOS experienced. The following four figures show the acceleration, jerk, RPM and throttle position observations in driver simulator. In order to compare to the real-world observations, similar data points for real-world observations from previous sub-sections are drawn in red, while the observations from the driver simulator experiments are displayed using the purple line.

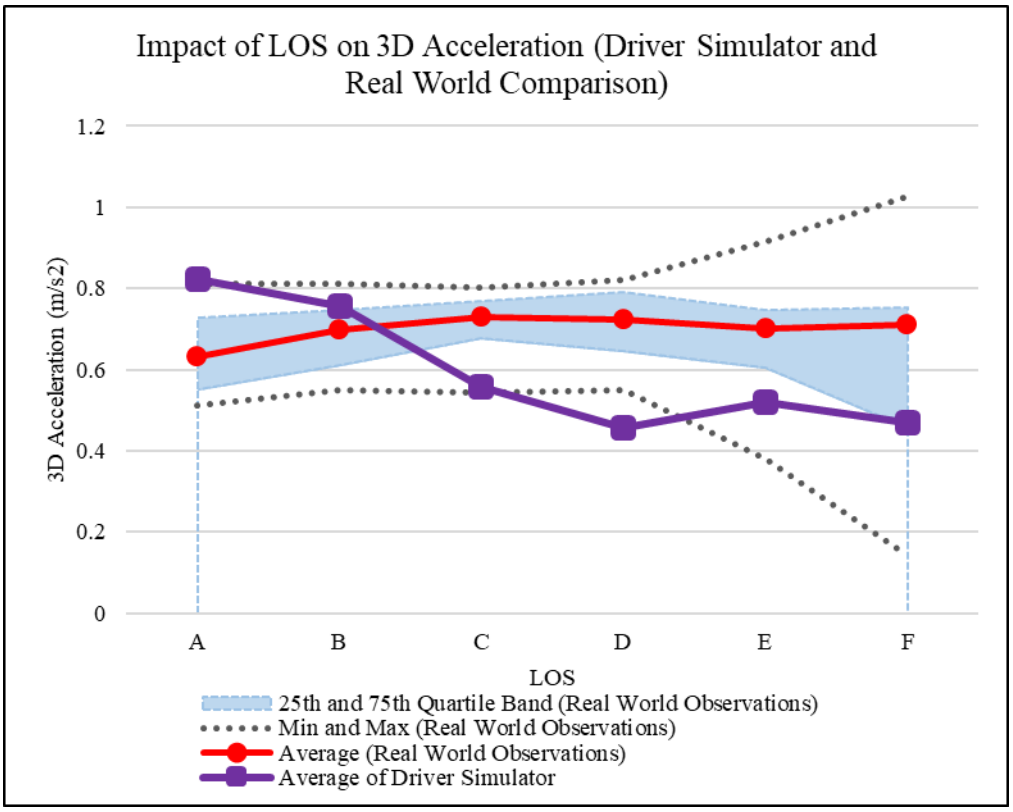

Figure 27 – 3D acceleration of driver simulator for different LOS compared with real world observations

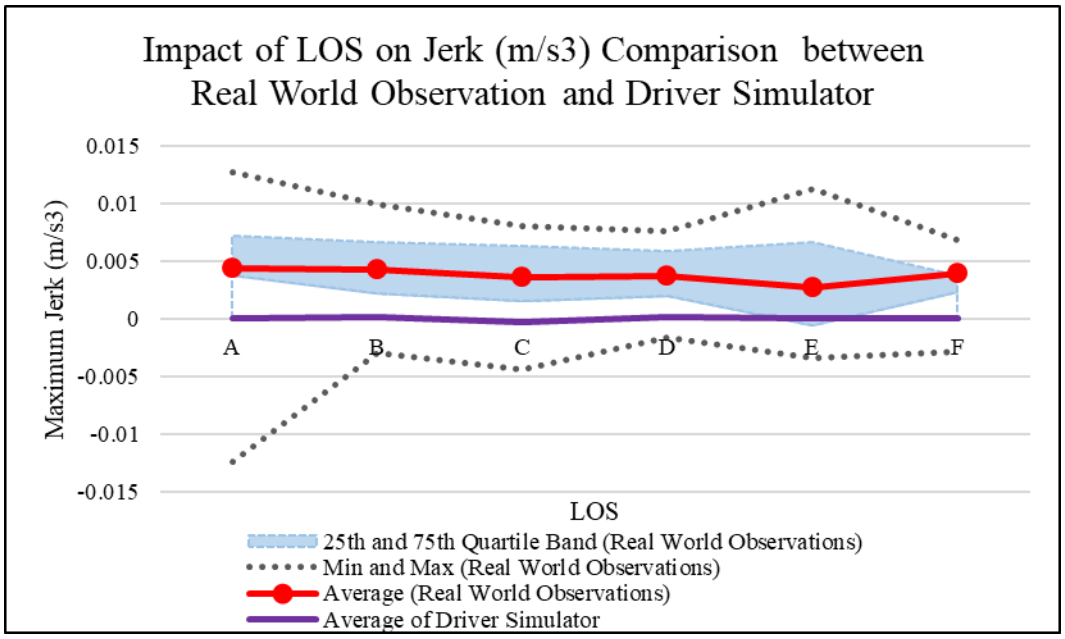

Figure 28 Amount of experienced jerk for driver simulator for different LOS compared with real world observations

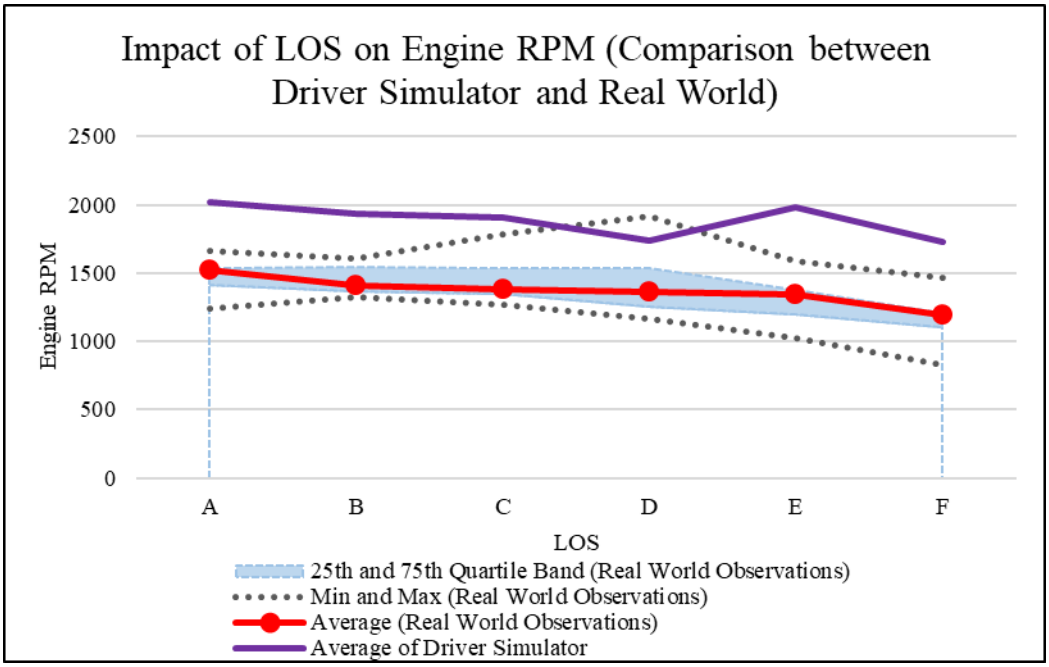

Figure 29 – Engine RPM of driver simulator compared with real world observations

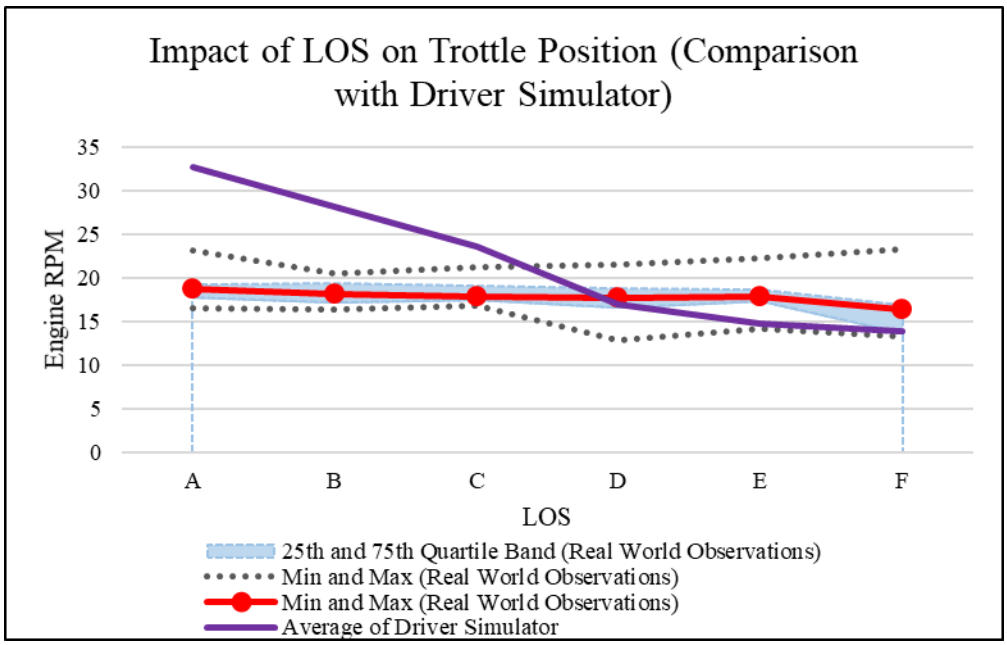

Figure 30 – Trottle Position of driver simulator for different LOS compared with real world observations

The number of accelerations per mile for a given level of service (LOS) was defined as the number of times the gas pedal was pushed down, for each mile travelled, by each participant that drove through the network with that LOS in effect. Figure 31 shows a box-plot of the normalized number of acceleration of participants as they drove through scenarios of Level of Service A to F. The figure shows a general increase in number of accelerations per mile and standard deviation of observed data as Level of Service deteriorates. The increase in standard deviation is an indication of an increase in the variety of driving behavioral response to deterioration of Level of Service. In conclusion, the analysis shows that even though drivers respond to deteriorating Level of Service in different ways, generally the number of times drivers push down on the gas pedal increases with deterioration of Level of Service.

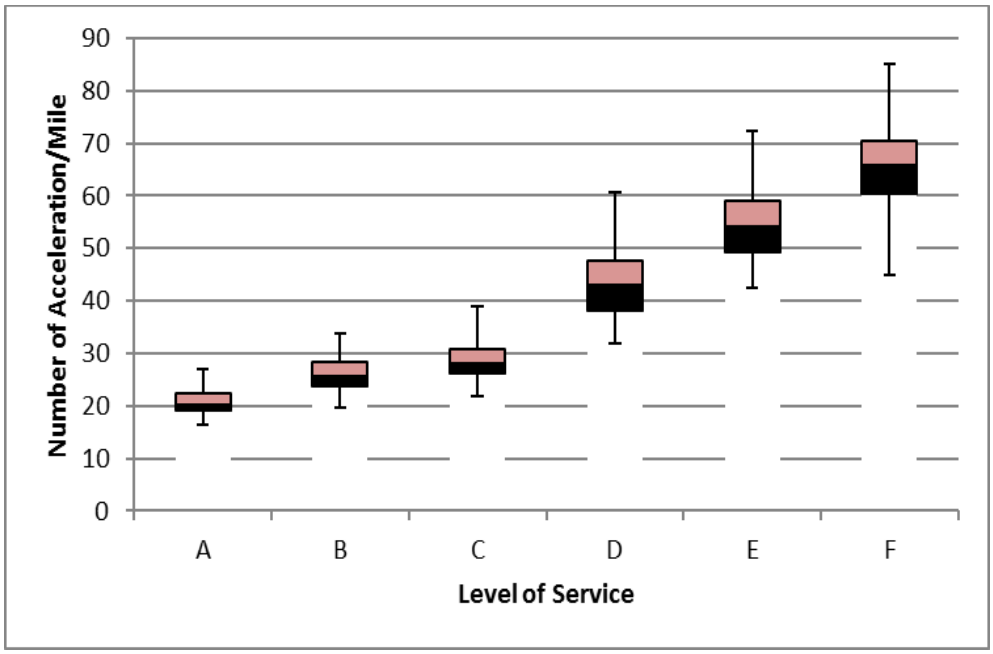

Figure 31 - The number of accelerations per mile over LOS

The number of brakes per mile, for a given Level of Service, is the number of times the brake light turned-on for each mile travelled by each participant that drove through the network with that LOS in effect. It is an indication of the extent to which the driver stepped on the brake pedal for every mile traveled. As seen in Figure 32, the number of brake per mile was lowest in LOS A, and with the exception of LOS B and C, where similar values were observed, the number of brake per mile increased as the LOS progressed from A to F. Also, as observed with the normalized number of acceleration, the standard deviation of the observed data increased with deterioration with LOS.

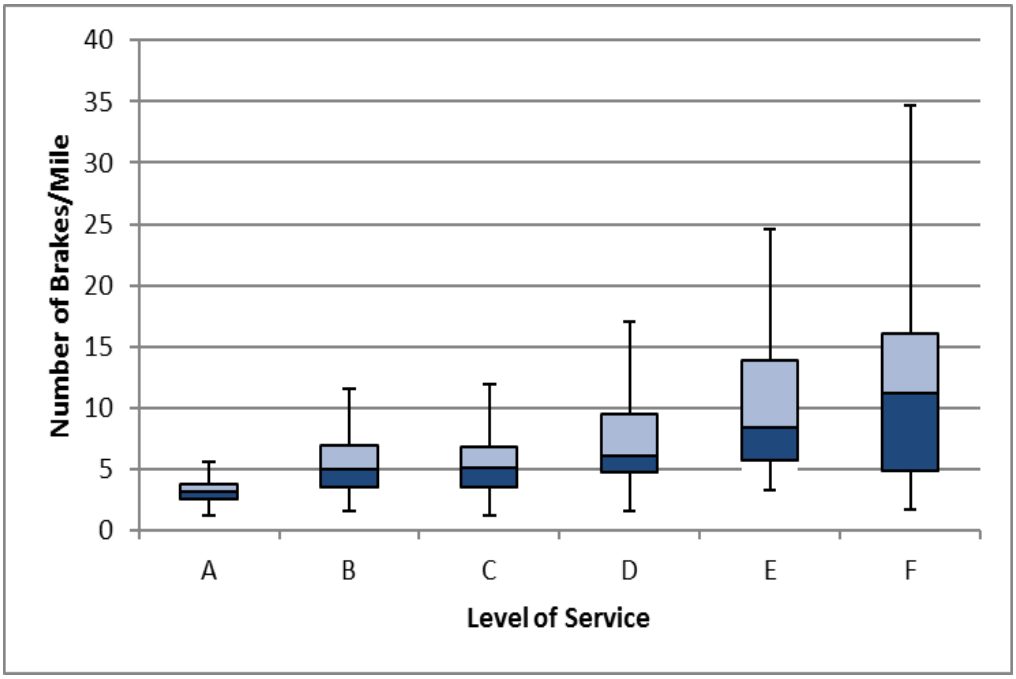

Figure 32 - The number of brakes per mile over LOS

The number of lane changes per mile per available lane (lanes with no parked vehicles) is the number of times a participant changed lanes in each mile and each available lane. Figure 33 presents the results of the analysis of this parameter for all participants. As seen in Figure 33 below, little variation in driving behavior, between Participants, was observed in LOS A. As a result, the first and second quartiles coincide, and the standard deviation was relatively small. However, as traffic volume increased, and LOS deteriorated, the standard deviation increased, *indicating* an increase in variety lane-changing behavior. In addition, with exception of the progression from LOS C to D, the observed number of lane changes per mile per available lane increased implying that, generally, the tendency of drivers to change lanes increased as LOS degenerates from A to F.

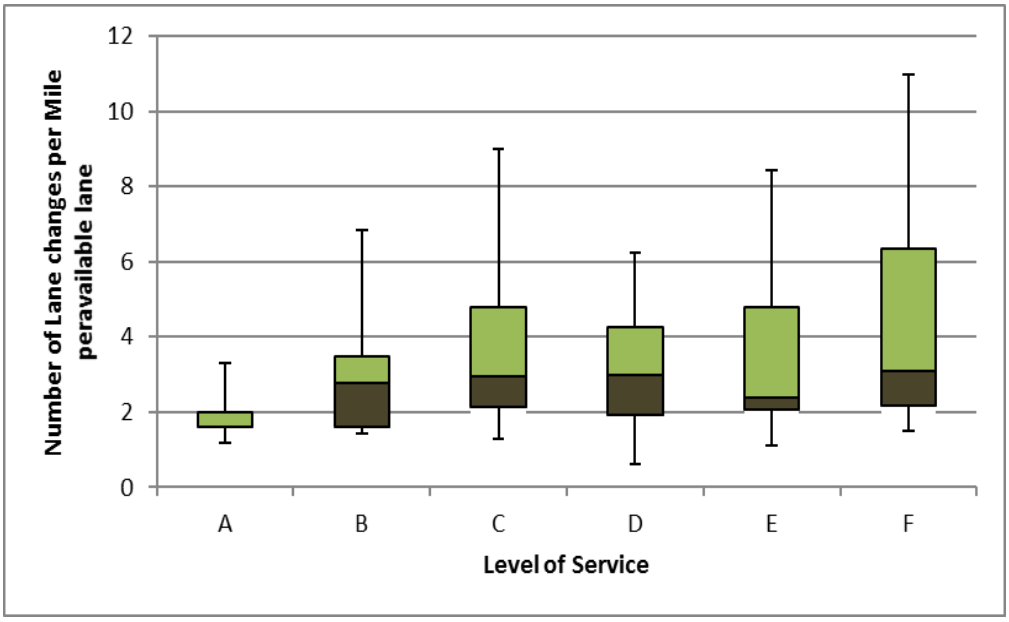

Figure 33 - Number of lane changes per mile per available lane over LOS

The average throttle ratio shows the extent to which the participant stepped on the throttle. The greater the extent to which the throttle is depressed, the higher the throttle ratio and velocity of the vehicle. The box-plot displayed in Figure 34 shows that drivers tend to push down harder on the throttle when the speed of the traffic stream is high and traffic density is low as seen above in LOS A, B and C. However, as the speed decreases and traffic density of the network increases, the extent to which the throttle is depressed reduces hence the throttle ratio decreases.

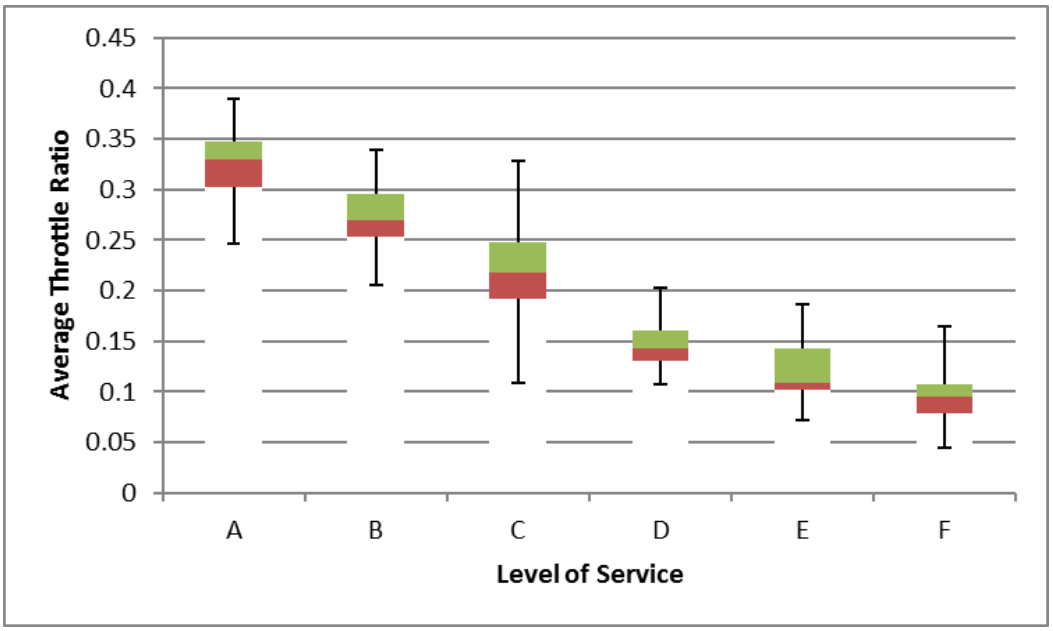

Figure 34 - Average throttle ratio over LOS

Jerk is the rate of change of acceleration or deceleration. Longitudinal jerk can be negative, associated with an abrupt depression of the brake pedal resulting in a plunge forward due to inertia, or positive, caused by an abrupt depression of the gas pedal resulting in a backward plunge.

According to Wei and Rizzoni (4), the boundaries for comfortable jerk is $\pm 1 m/s^3$. This is shown in the jerk profile Figure 35 as "minimum Jc" and "maximum Jc" respectively. Wei and Rizzoni also defined the acceptable limit for jerk to be is $\pm 2 m/s^3$. This is also shown on the jerk profile as "max. allowable" and "min. allowable". Given these limits, depending on Jerk magnitudes, Jerk may be comfortable, uncomfortable (negative or positive) or unsafe as shown in Table 18 below:

Table 18 - Comfortable, uncomfortable, and unsafe jerk

$-1 m/s^3 \leq$ Jerk $\leq 1 m/s^3$	→	**Comfortable jerk**
$-2 m/s^3 \leq$ Jerk $\leq -1 m/s^3$	→	Uncomfortable negative jerk
$1 m/s^3 \leq$ Jerk $\leq 2 m/s^3$	→	Uncomfortable positive jerk
Jerk $\geq 2 m/s^3$ or Jerk $\leq -2 m/s^3$	→	Unsafe jerk values (beyond allowed jerk values)

Figure 35 below is a 30-s window showing the vehicle jerk profile and the associated brake and gas pedal movements of a randomly selected participant. The top, middle and bottom graphs show the longitudinal acceleration, Jerk profile and Pedal (Gas and Brake) ratios respectively.

At t=1s, the brake was almost completely depressed, between t=1s and t = 2s, brake pedal was gradually released, the driver then lifted foot completely off the brake pedal and abruptly stepped

on the gas pedal at 2s≤t≤3s. This results in the unsafe positive Jerk value shown on the jerk profile at t=3. The longitudinal acceleration profile shows a constant longitudinal acceleration at 1s ≤ t < 2s and a sudden increase, corresponding with the depression of the gas pedal, between at 2s≤t < 3s. All unsafe and uncomfortable positive jerk values are associated with abrupt release of the brake pedal and sudden depression of the gas pedal. The extent to which the brake was gradually released before being abruptly released, the abruptness with which the gas pedal was stepped-on and depression-rate of the gas pedal (throttle velocity) determines the magnitude of positive jerk.

Beginning at t=9s, the driver starts gradually releasing the gas pedal but suddenly releases the gas pedal and abruptly depresses the brake pedal at t=10s to t=11s, resulting in the unsafe negative Jerk value shown on the Jerk profile at t=11s. The longitudinal acceleration profile shows a decrease in acceleration at 9s ≤ t < 10s, at 10s ≤ t < 11s the rate of deceleration increases as shown by the steeper curve, this corresponds with the depression of the brake pedal.

Negative jerk values are generally associated with an abrupt release of the gas pedal and an abrupt depression of the brake pedal. The magnitude of the negative jerk depends on the extent to which the gas pedal was gradually released before being abruptly released, the abruptness with which the brake pedal was stepped-on and the depression-rate of the brake pedal determines the magnitude of negative Jerk.

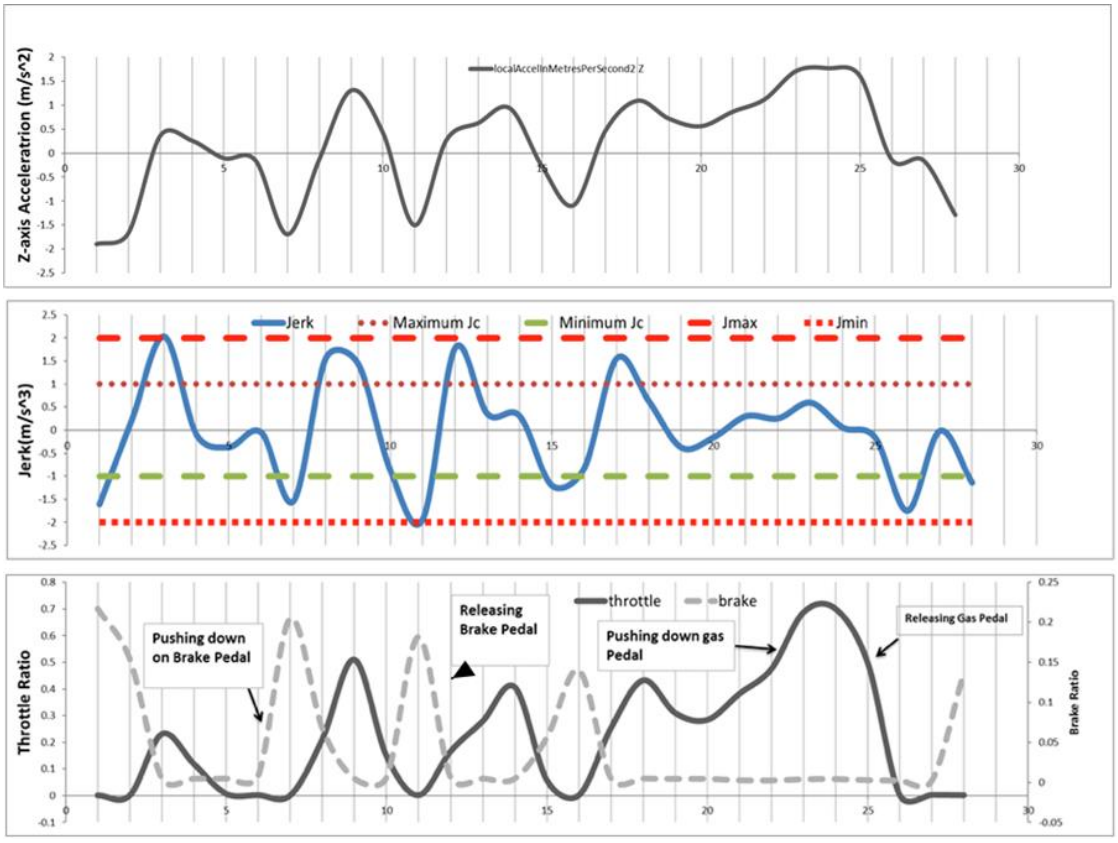

Figure 35 - Number of longitudinal jerks over LOS

Results from correlation analysis shows a negative relationship between Jerk and Brake Velocity (R^2= -0.67254). The greater the velocity with which the brake is depressed, the larger the negative jerk experienced. No significant relationship was seen between Jerk and Brake Travel. Additional correlation analysis showed a positive correlation (R^2=0.12573) between jerk and throttle travel however a much stronger positive correlation (R^2=0.587517) was observed between Jerk and throttle velocity. This implies an increase in positive jerk values with increase in velocity with which the gas pedal is pressed.

Figure 36 shows that number of uncomfortable longitudinal jerk increases as LOS deteriorates from C to E. This parameter, however, dropped slightly in LOS F. The variation in number of Longitudinal Jerks, between drivers, increases from LOS C to F. Figure 37 shows no significant trend in number of Unsafe Jerks as LOS deteriorates from A to F.

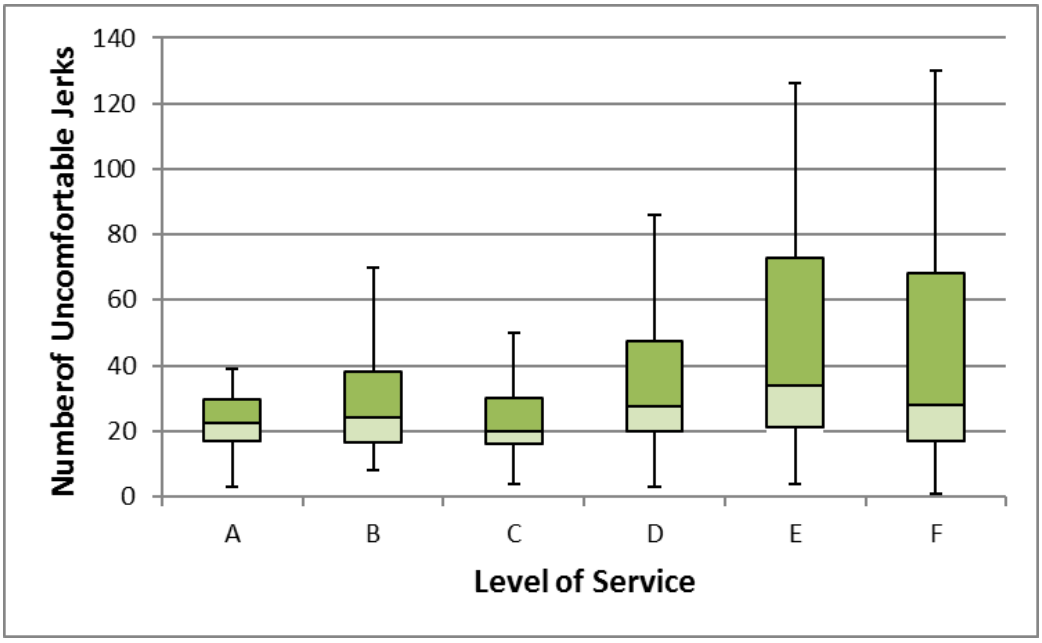

Figure 36 - Number of uncomfortable jerks over LOS

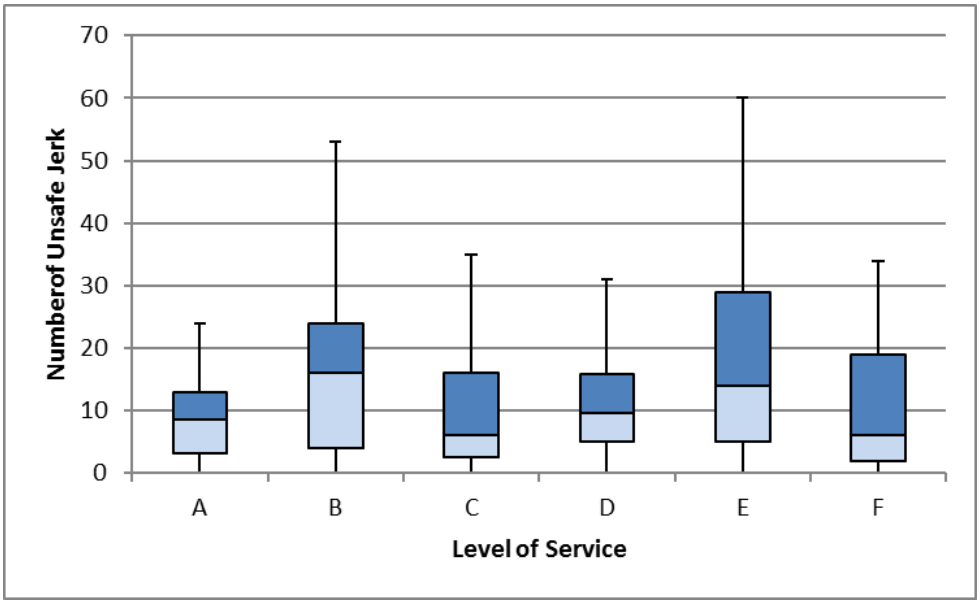

Figure 37 - Number of unsafe jerks over LOS

7.0 CONCLUSIONS & FUTURE WORK

This research presented data-driven insights into the response in driver behavior or aggressiveness as a function of surrounding traffic condition or Level of Service (LOS). The driver behavior is described using a set of microscopic variables such as speed, longitudinal accelerations, lateral acceleration, jerk, percent throttle pushed etc. The traffic condition surrounding drivers was characterized by Level of Service (LOS), which is an established measure provided in the Highway Capacity Manual (HCM). This research focused on arterial streets within urban areas, and other surface streets such as freeways, remain a scope for future research.

The research team utilized two test beds to assess driver behavior's correlation to the level of service, which were real-world naturalistic tests, and a driver simulator. The real-world analysis used high-resolution trajectory data collected via i2D technology. This massive data set contained more than 40 drivers and four years' worth of driving information. At the time of performing analysis in this project, this data set contained more than 47 million seconds of microscopic driver behavior data. The research team used INRIX, one of the main probe-based speed data providers to measure the LOS. LOS on the arterials depend on the average operational speed of the vehicles, and was calculated based on calculation steps provided in the HCM using the probe-based speed data.

Fifteen real-world routes were identified for the purpose of establishing the spatial scope of analysis, which were diverse in terms of number of distinct drivers as well as the total number of trips driven on them. The high-resolution vehicle trajectory data and the LOS calculated from 15-minute averaged INRIX speeds were integrated to form a final data table, which were analyzed to show the relationships and trends between different microscopic driver behavior variables and LOS (A through F). An implementation of a machine learning algorithm in predicting aggressive and normal driving events is also described, which showed an accuracy of 94.9%. These findings were summarized in Chapter 6 and details are presented in the appendices.

Alongside real-world analysis, the research team also performed experiments using a driver simulator at Morgan State University, where a set of drivers were asked to drive in a modeled corridor. Scenarios representing all six LOS (A through F) were simulated to each driver to see how their behavior changed. The driver simulator was able to record high-resolution microscopic driver behavior as an output. The research team analyzed these outputs and constructed relationships between driver behavior and LOS within driver simulator.

The major findings of this research project as well as recommendations for future work is provided in the sections below.

7.1 MAJOR FINDINGS

Some of the major findings of this research effort are listed below:

1. Through this study, we found that the driver simulator experiences similar accelerations and jerks for different LOS consistent with real world routes. However, throttle position and RPM readings and their behavior in different LOS are quite different from empirical data.

2. The 15 selected real-world sites, used for analysis in this research, are located in Raleigh, North Carolina. The research team selected this region to enable access to high quality of i2D data, since most of the volunteer drivers are employees or students of North Carolina State University. However, this area does not experience heavy traffic congestion, especially on arterial streets and also have more tolerant drivers than other cities. This can be seen from the charts in the several Appendices, which show that the arterial routes operate at LOS A through D most of the time. This unbalanced sample size introduces bias and reduces confidence on any observations for LOS E and F.

3. The trends shown by similar variables in the real-world and driver simulation showed some cases of consistency as well as some cases of inconsistency. The similarities between driver simulation and real-world analysis validates the use of driver simulator in future transportation project analysis. However, the inconsistencies may be caused by the unrealistic environment of the driver simulator, where the drivers are not worried about crashes and other safety issue, or the lack of calibration of the driver simulator. Also, the lack vibrational cues in this particular simulator takes away from the turns, jerks, swerves and other driving-related motions. In addition, only a subset of the variables in a real-world driving scenario can be captured by the driving simulator.

4. The LOS is a simple indication of the condition of surrounding traffic and only represent six stages of traffic condition. Despite simplifying the analysis, it only looks at speed and does not consider other factors such as traffic volume, sun glare, weather, etc. More details and accurate measures for categorizing traffic conditions may help increase the quality of emerged models and relationships.

5. The implementation of a supervised machine learning algorithm, the Random Forest Classification technique, showed an accuracy of 94.9%. The method used some measures found in literature to label the data points as “Normal” and “Aggressive”. However, the error for “Aggressive” class was significantly higher than that for the “Normal” class. This can be attributed to the fact that there was lesser number of observations for “Aggressive” driving events than “Normal”.

7.2 RECOMMENDATIONS FOR FUTURE RESEARCH

A list of recommendation for future research is provided below:

1. The research team was limited to Raleigh area in North Carolina, which does not experience many LOS F observations and does not see a lot of aggressive driving. It is recommended that this research be extended to include data collection in other metropolitan areas, such that the LOS distribution is more even and the sample size is higher for lower LOS.

2. Due to lack of funding, the research team was unable to calibrate the driver simulators parameters, based on the findings of the real world and rerun the experiments to see how a calibration process can help make the simulator results more consistent with the real world. Further research is needed to investigate the calibration process and methodology for driver simulators.

3. Majority of the routes selected in this research had similar characteristics (e.g. speed limit, number of lanes etc.). Future work should involve selecting routes that are more diverse in terms of geometry, speed limit, etc. and hence help characterize the contribution of roadway geometry into driver behavior. Such a diverse selection would also pave way for a more refined machine learning model for predicting driver behavior as a function of LOS and road geometry.

4. Overall, a larger data collection is recommended to eliminate the noise/error sources. Looking into driver behavior for each of 15 real world routes, a considerable amount of variance is observed. This variation within the data is expected to decrease the accuracy of the emerged relationships. A better data collection plan may help in the implementation of unsupervised machine learning algorithms, which would not rely on labeling driver aggressiveness.

8.0 REFERENCES

Blaauw, G.J. (1982) Driving experience and task demands in simulator and instrumented car: a validation study. Human Factors 24(4), 473–486

Blana, E. (1996) Driving simulator validation studies: A literature review.p.3

Carmona, J., García, F., Martín, D., Escalera, A. D. L., & Armingol, J. M. (2015). Data fusion for driver behaviour analysis. Sensors, 15(10), 25968-25991.

Castignani, G., Derrmann, T., Frank, R., & Engel, T. (2015). Driver behavior profiling using smartphones: A low-cost platform for driver monitoring. IEEE Intelligent Transportation Systems Magazine, 7(1), 91-102.

Chen, S. H., Pan, J. S., & Lu, K. (2015, March). Driving behavior analysis based on vehicle OBD information and adaboost algorithms. In Proceedings of the International MultiConference of Engineers and Computer Scientists (Vol. 1, pp. 18-20).

Cobina, R., Henderson, T., Mitra, S., Nuworsoo, C., & Sullivan, E. (2009). Vehicle emissions and level of service standards: exploratory analysis of the effects of traffic flow on vehicle greenhouse gas emissions. City and Regional Planning, 45.

Daniel, R., Brooks, T., & Pates, D. (2009). Analysis of US and EU Drive Styles to Improve Understanding of Market Usage and the Effects on OBD Monitor IUMPR (No. 2009-01-0236). SAE Technical Paper.

De Vlieger, I. (1997). On board emission and fuel consumption measurement campaign on petrol-driven passenger cars. Atmospheric Environment, 31(22), 3753-3761.

de Winter, J.C.F., van Leeuwen, P. M., & Happee, R. (2012). Advantages and Disadvantages of Driving Simulators: A Discussion. Department of Bio-Mechanical Engineering, Faculty of Mechanical, Maritime and Materials Engineering, Delft University of Technology.

Dutta A., D. L. Fisher, A. A. Noyce (2004). Use of a driving simulator to evaluate and optimize factors affecting understandability of variable message signs. Transportation Research Part F, Vol. 7, pp. 209–227.

Ericsson, E., “Independent driving pattern factors and their influence on fuel-use and exhaust emission factors,” Transportation Research Part D: Transport and Environment 6(5), 325-345, 2001.

Forum 8 (2013), UC-win/Road New Features, http://www.forum8.co.jp/english/uc-win/ucwin-road-e1.htm, Accessed on September 20, 2015.

Godley, S.T, T.J. Triggs, B.N. Fildes, Driving simulator validation for speed research, Accident Analysis & Prevention 34, p 589-600, 2002

Higgs, B., & Abbas, M. (2015). Segmentation and clustering of car-following behavior: Recognition of driving patterns. IEEE Transactions on Intelligent Transportation Systems, 16(1), 81-90.

Highway Capacity Manual (HCM). (2016). Sixth Edition: A Guide for Multimodal Mobility Analysis, Transportation Research Board, The National Academies of Science, Engineering, and Medicine.

Ho, T. K. (1995, August). Random decision forests. In Document analysis and recognition, 1995., proceedings of the third international conference on (Vol. 1, pp. 278-282). IEEE.

Johnson, D. A., & Trivedi, M. M. (2011, October). Driving style recognition using a smartphone as a sensor platform. In Intelligent Transportation Systems (ITSC), 2011 14th International IEEE Conference on (pp. 1609-1615). IEEE.

Kappler, W.D. (1993) 'Views on the Role of Simulation in Driver Training' in Proceedings of the XII European Annual Conference on Human Decision Making and Manual Control. Kassel, Germany, June 22-24.

Kerner, B. S. (2010). Effect of driver behavior on spatiotemporal congested traffic patterns at highway bottlenecks in the framework of three-phase traffic theory. arXiv preprint arXiv:1012.5159.

Kumtepe, O., Akar, G. B., & Yuncu, E. (2016). Driver aggressiveness detection via multisensory data fusion. EURASIP Journal on Image and Video Processing, 2016(1), 5.

Lee, C. F., & Öberg, P. (2015). Classification of road type and driving style using OBD data (No. 2015-01-0979). SAE Technical Paper, doi:10.4271/2015-01-0979.

Lee, J. D., et al. Exploratory Advanced Research: Making Driving Simulators More Useful for Behavioral Research–Simulator Characteristics Comparison and Model-Based Transformation. No. N2013-016. 2013.

Live Drive (2018), http://www.livedrive.pt/xportal/xmain?xpid=livedrive&xpgid=home&xlang=pt

Meseguer, J. E., Calafate, C. T., Cano, J. C., & Manzoni, P. (2013, July). Drivingstyles: A smartphone application to assess driver behavior. In Computers and Communications (ISCC), 2013 IEEE Symposium on (pp. 000535-000540). IEEE.

Mitrovic, D. (2005). Reliable method for driving events recognition. IEEE transactions on intelligent transportation systems, 6(2), 198-205.

Mudd, S. (1968) Assessment of the fidelity of dynamic flight simulators. Human Factors.

Murphey, Y. L., Milton, R., & Kiliaris, L. (2009). Driver's style classification using jerk analysis. In Computational Intelligence in Vehicles and Vehicular Systems, 2009. CIVVS'09. IEEE Workshop on (pp. 23-28). IEEE.

Paefgen, J., Kehr, F., Zhai, Y., & Michahelles, F. (2012, December). Driving behavior analysis with smartphones: insights from a controlled field study. In Proceedings of the 11th International Conference on mobile and ubiquitous multimedia (p. 36). ACM.

Qi, G., Du, Y., Wu, J., & Xu, M. (2015). Leveraging longitudinal driving behavior data with data mining techniques for driving style analysis. IET intelligent transport systems, 9(8), 792-801.

RITIS: Regional Integrated Transportation Information System. 2018. www.ritis.org.

Rizzo, M., J. Jermeland, and J. (2002) Severson, Instrumented vehicles and driving simulators. Geron-technology, 1(4): p. 291-296.

Rolfe, J.M., Hammerton-Frase, A.M., Poulter, R.F., And Smith, E.M.B. (1970) Pilot response in flight and simulated flight. Ergonomics 13, pp 761-68.

Shechtman, O. Classen, S., Awadzi, K., & Mann, W. (2009) Comparison of Driving Errors Between On-the-Road and Simulated Driving Assessment: A Validation Study. Traffic Injury Prevention, 10: 379-382.

Stern, E., Schold Davis, E. (2006) Driving Simulators, in Driver Rehabilitation and Community Mobility: Principles and Practice, J.M. Pellirito, Editor, Elsevier MOSBY: St Louis. p. 223-235.

Toledo, T., & Lotan, T. (2006). In-vehicle data recorder for evaluation of driving behavior and safety. Transportation Research Record: Journal of the Transportation Research Board, (1953), 112-119.

Treiber, M., Kesting, A., & Thiemann, C. (2008). How much does traffic congestion increase fuel consumption and emissions? Applying a fuel consumption model to the NGSIM trajectory data. In 87th Annual Meeting of the Transportation Research Board, Washington, DC.

Törnros, J. (1998) Driving behaviour in a real and a simulated road tunnel—a validation study. Accident Analysis & Prevention, 30(4), 497-503. doi:http://dx.doi.org/10.1016/S0001-4575(97)00099-7

Unal, A., Rouphail, N., & Frey, H. (2003). Effect of arterial signalization and level of service on measured vehicle emissions. Transportation Research Record: Journal of the Transportation Research Board, (1842), 47-56.

Vaiana, R., Iuele, T., Astarita, V., Caruso, M. V., Tassitani, A., Zaffino, C., & Giofrè, V. P. (2014). Driving behavior and traffic safety: an acceleration-based safety evaluation procedure for smartphones. Modern Applied Science, 8(1), 88.

Wang, W., Xi, J., & Chen, H. (2014). Modeling and recognizing driver behavior based on driving data: A survey. Mathematical Problems in Engineering, 2014.

Wu, M., Zhang, S., & Dong, Y. (2016). A novel model-based driving behavior recognition system using motion sensors. Sensors, 16(10), 1746.

Yan, X., M. Abdel-Aty, E. Radwan, X. Wang, P. Chilakapati, Validating a driving simulator using surrogate safety measures, Accident Analysis & Prevention 40, p 274-288, 2007

APPENDIX A - NUMBER OF TRIPS PER DRIVER IN EACH YEAR

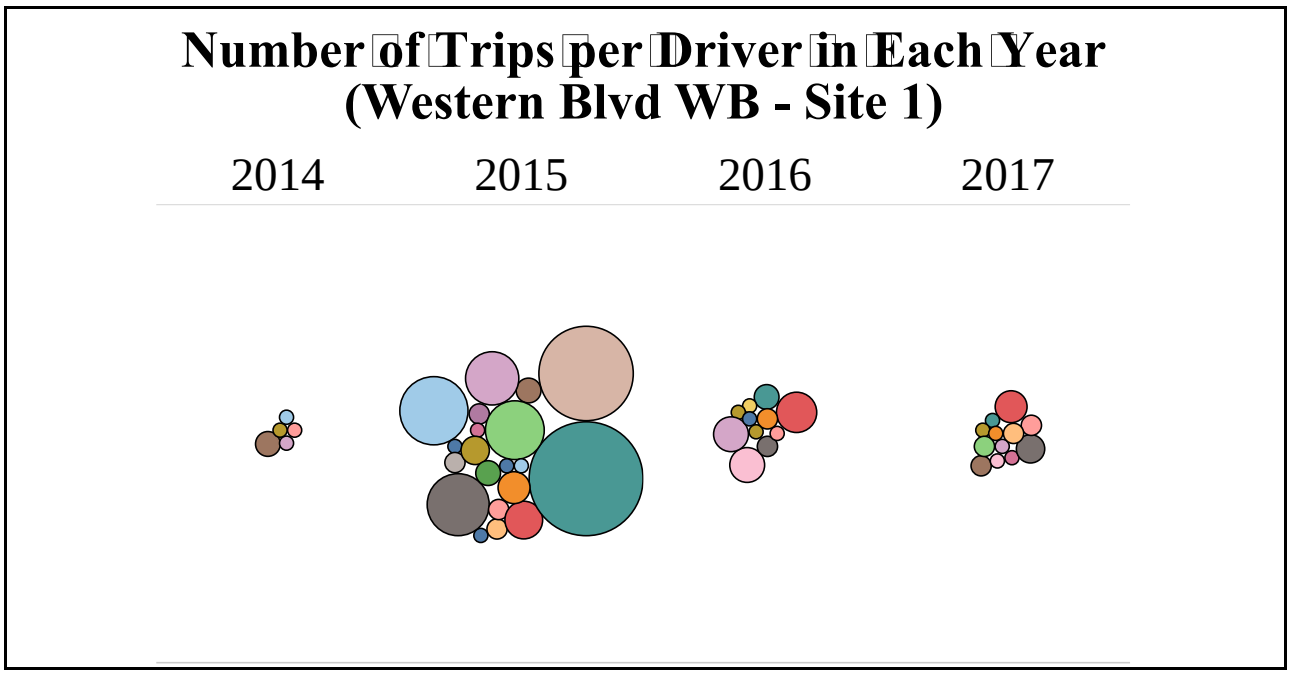

Figure A-1 – Number of Trips per Driver in Each Year (Western Blvd WB – Site 1)

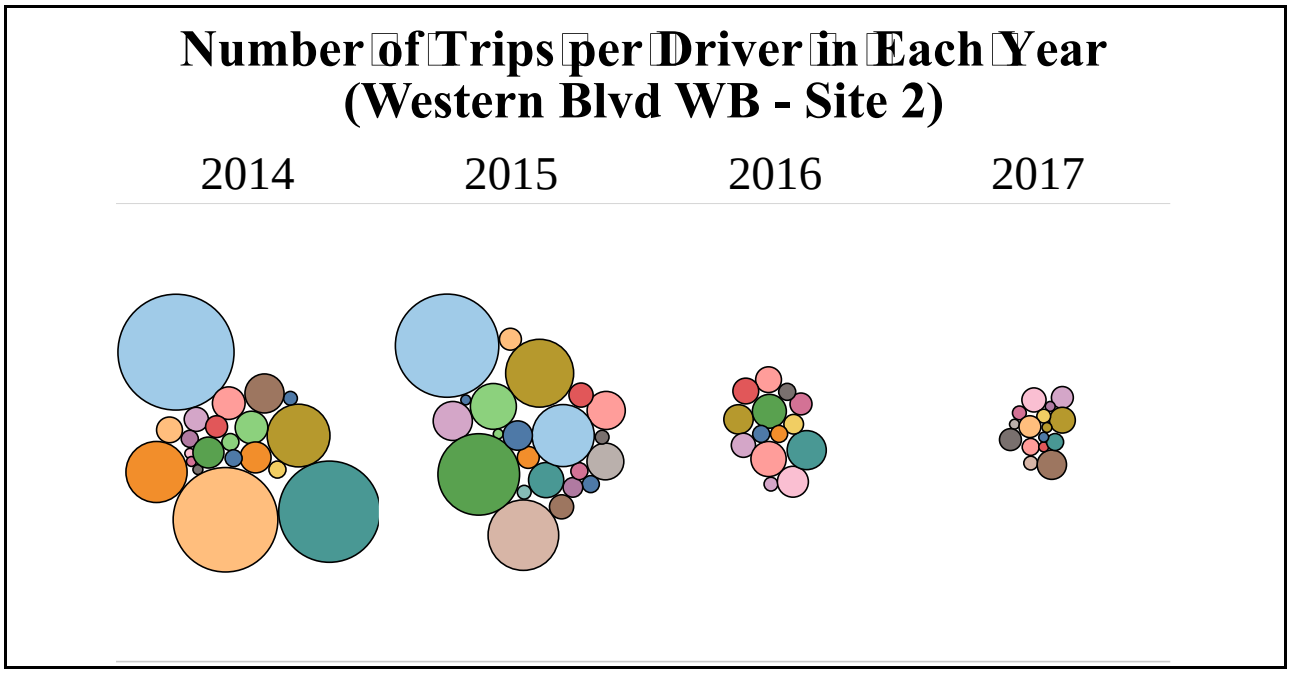

Figure A-2 – Number of Trips per Driver in Each Year
(Western Blvd WB – Site 2)

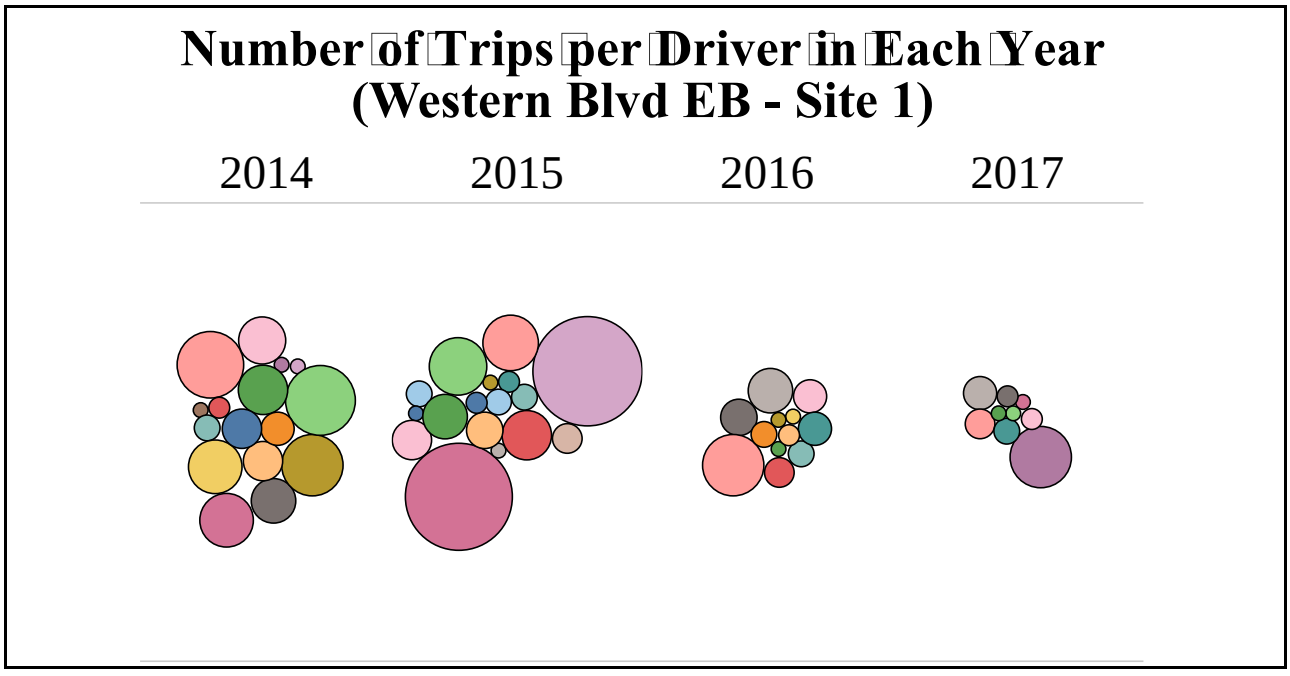

Figure A-3 – Number of Trips per Driver in Each Year
(Western Blvd EB – Site 1)

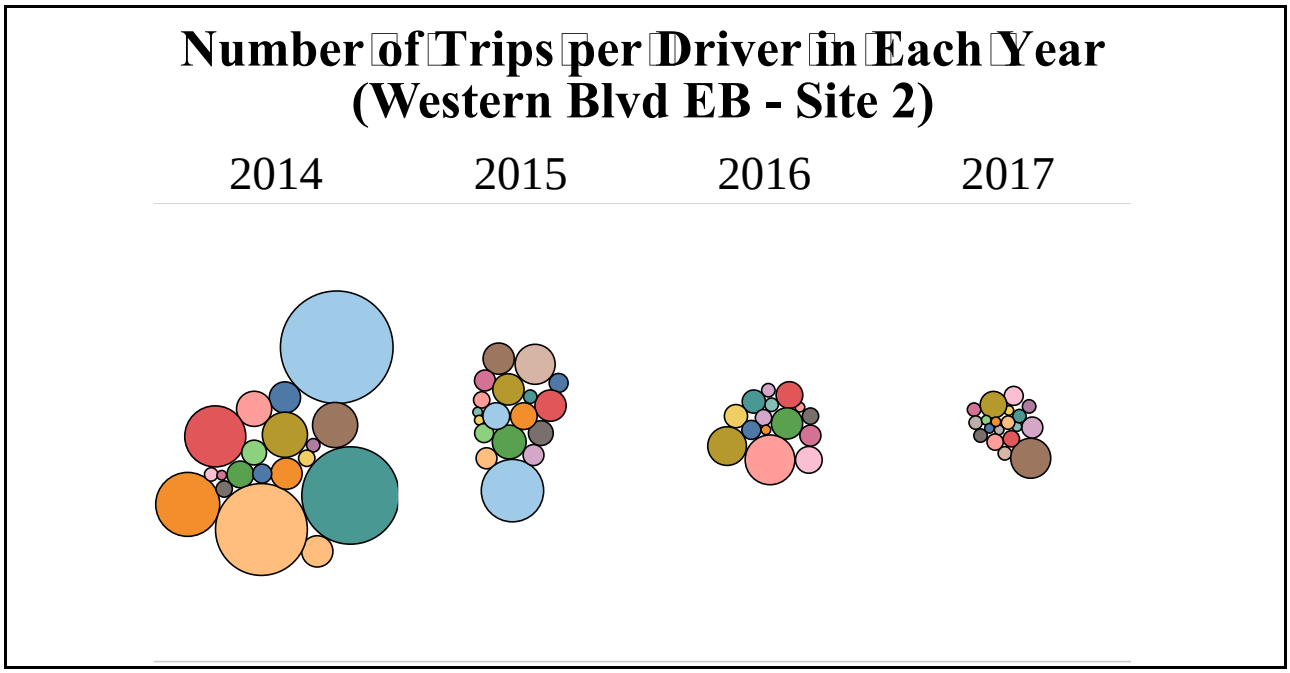

Figure A-4 – Number of Trips per Driver in Each Year (Western Blvd EB – Site 2)

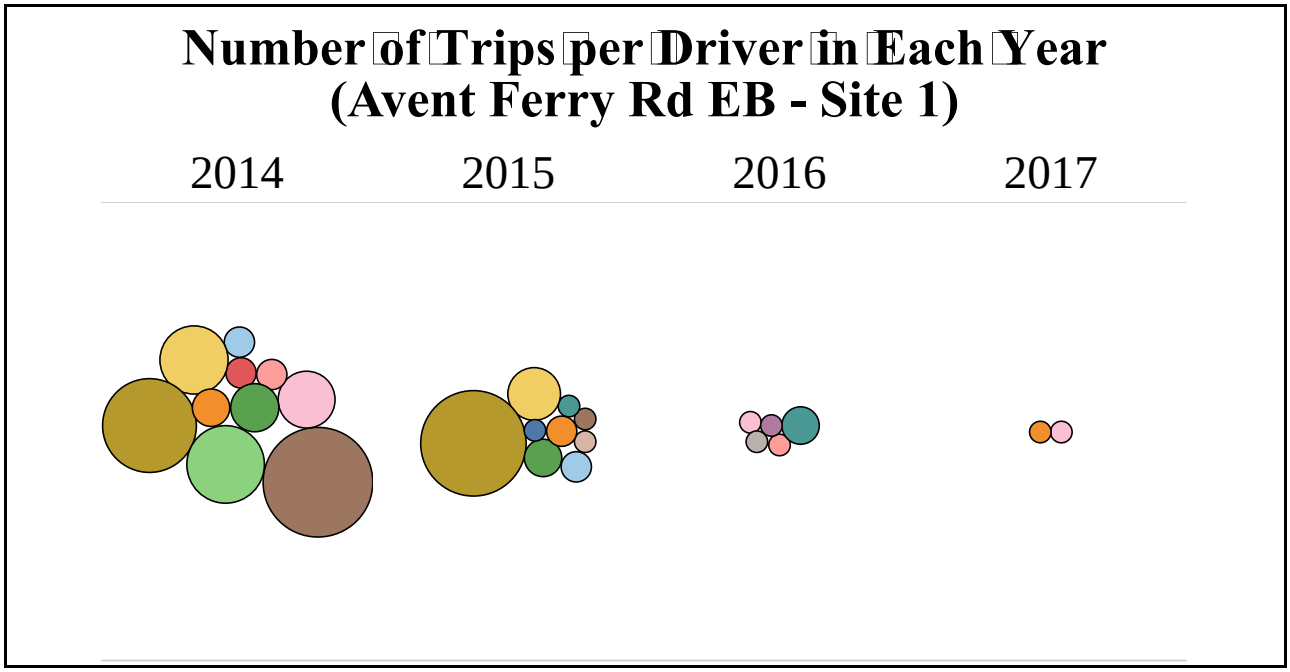

Figure A-5 – Number of Trips per Driver in Each Year (Avent Ferry Rd EB – Site 1)

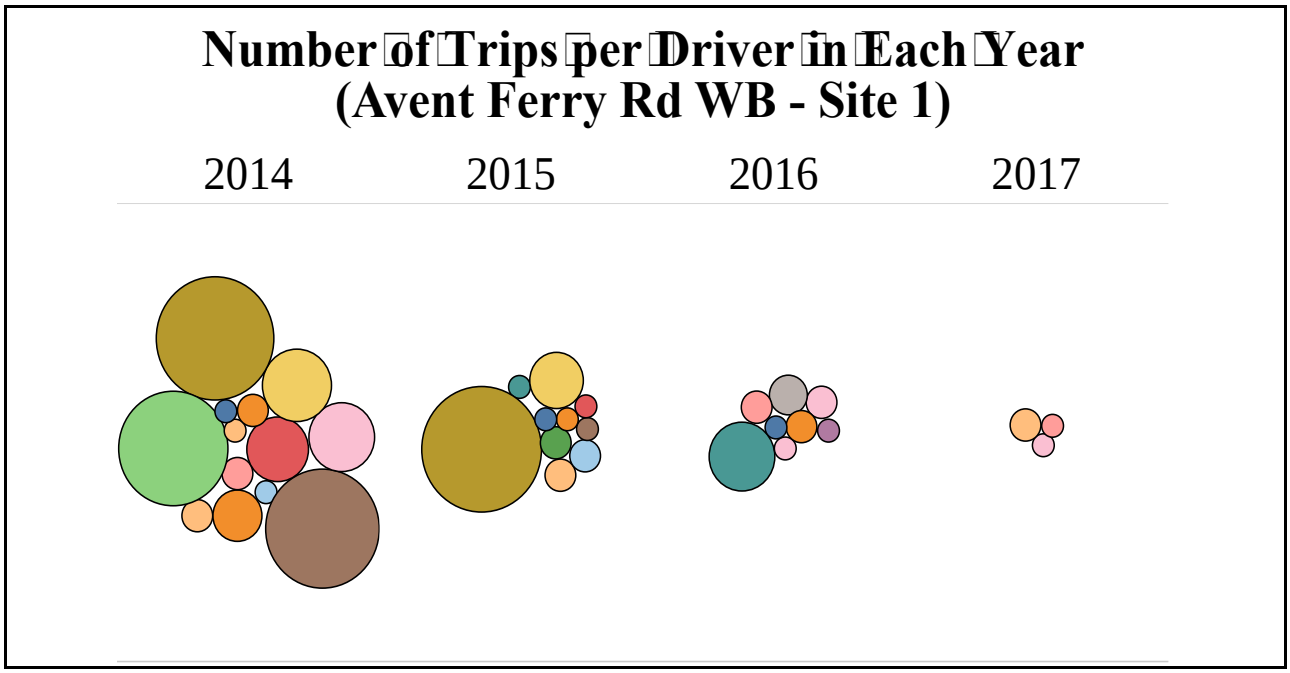

Figure A-6 – Number of Trips per Driver in Each Year (Avent Ferry Rd WB – Site 1)

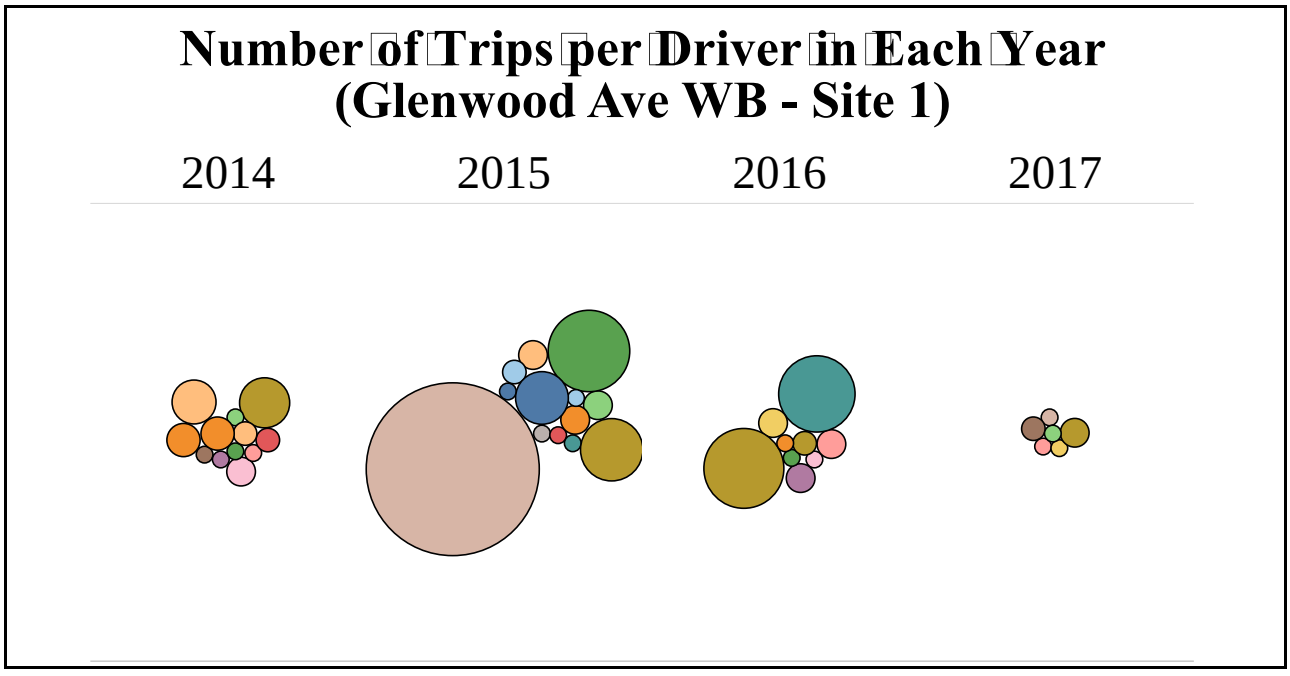

Figure A-7 – Number of Trips per Driver in Each Year (Glenwood Ave WB – Site 1)

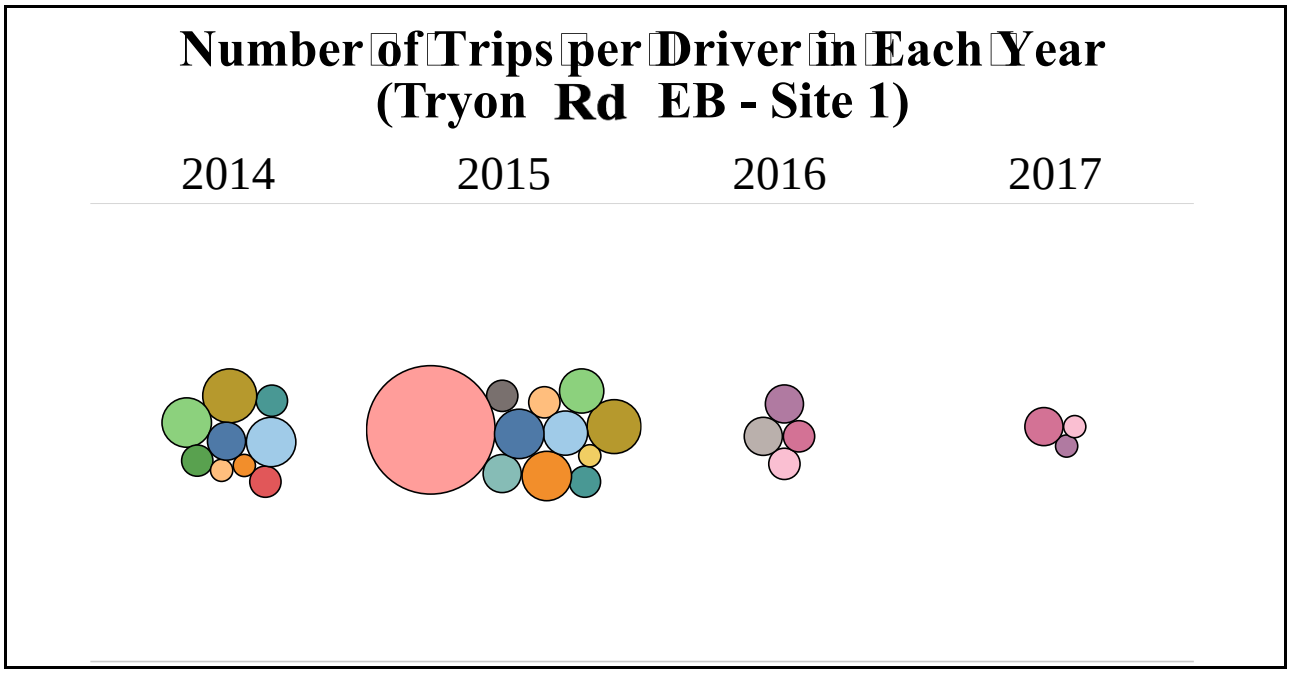

Figure A-8 – Number of Trips per Driver in Each Year
(Tryon Rd EB – Site 1)

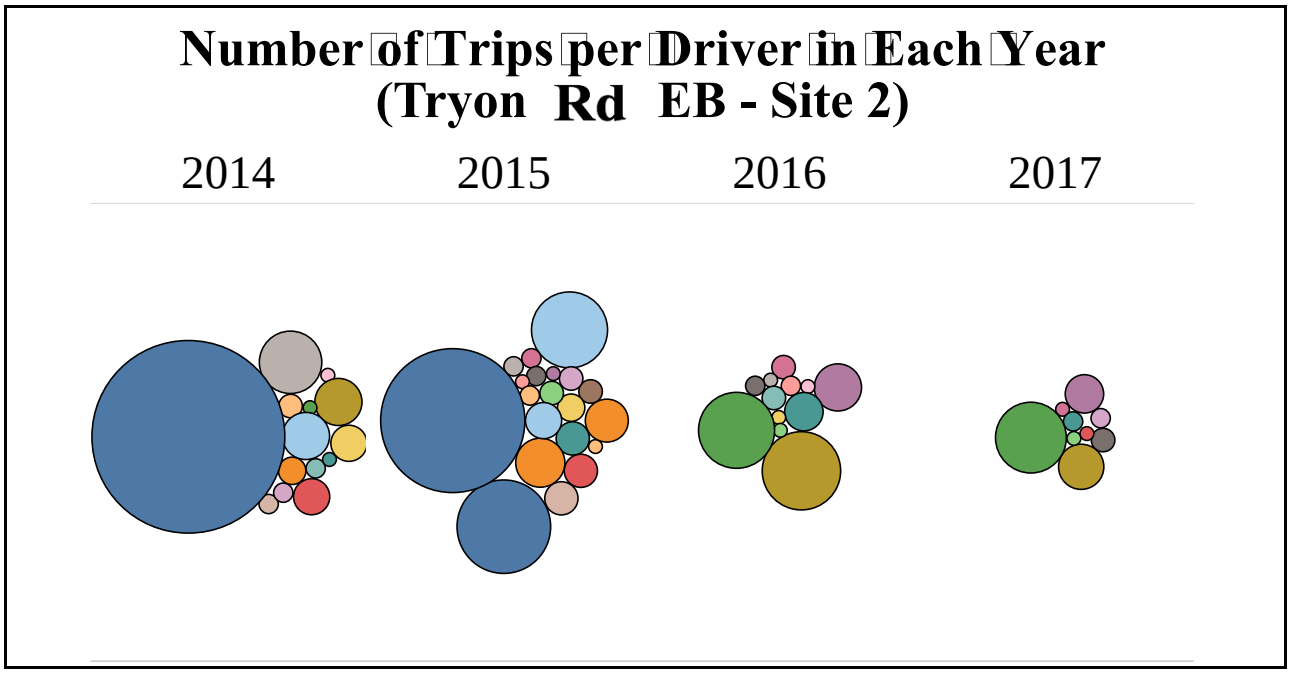

Figure A-9 – Number of Trips per Driver in Each Year
(Tryon Rd EB – Site 2)

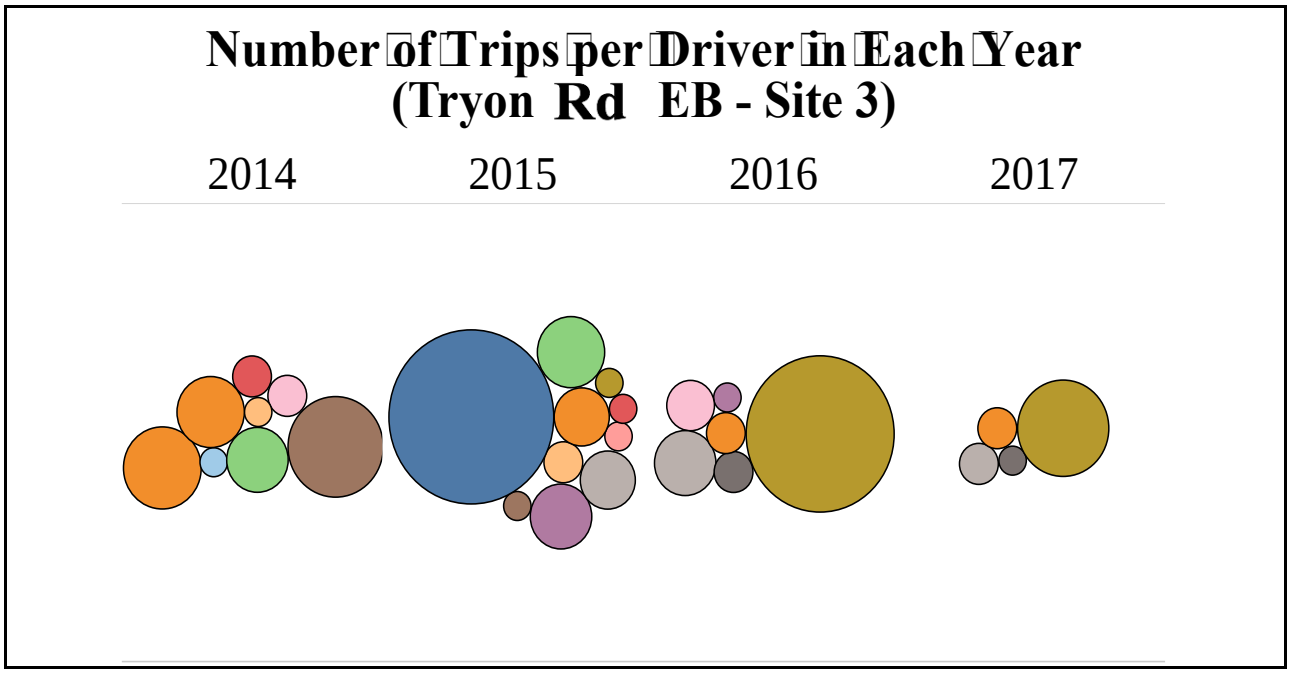

Figure A-10 – Number of Trips per Driver in Each Year (Tryon Rd EB – Site 3)

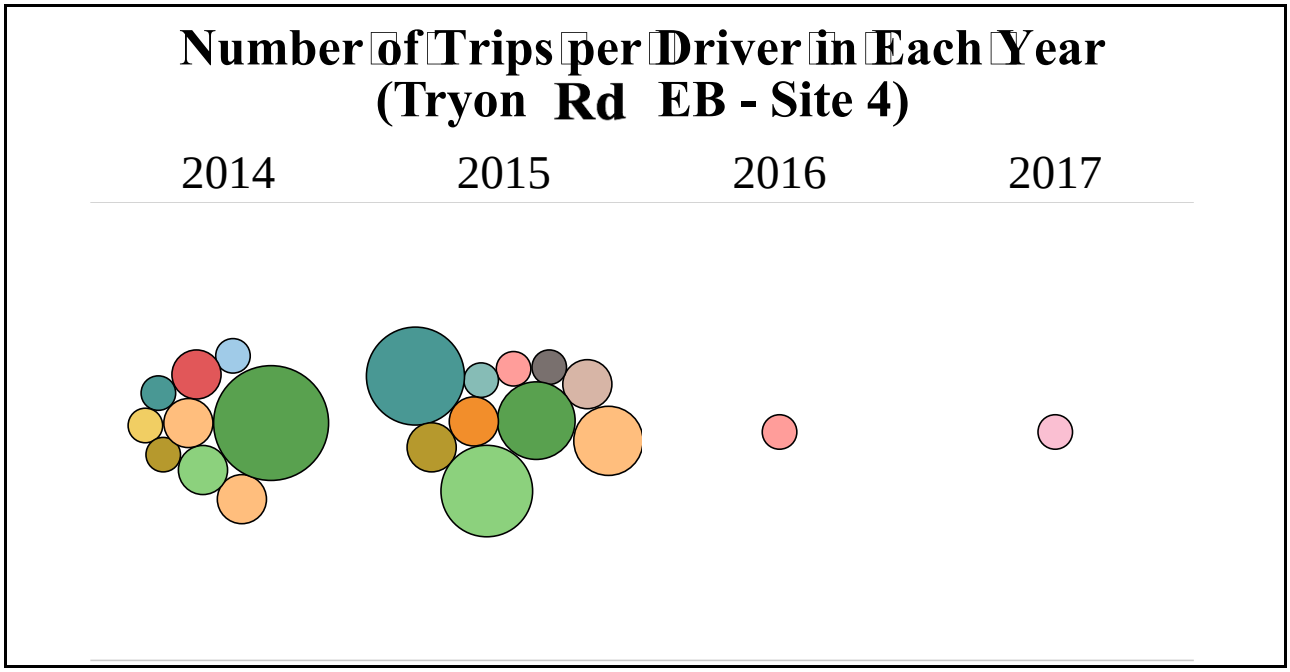

Figure A-11 – Number of Trips per Driver in Each Year (Tryon Rd EB – Site 4)

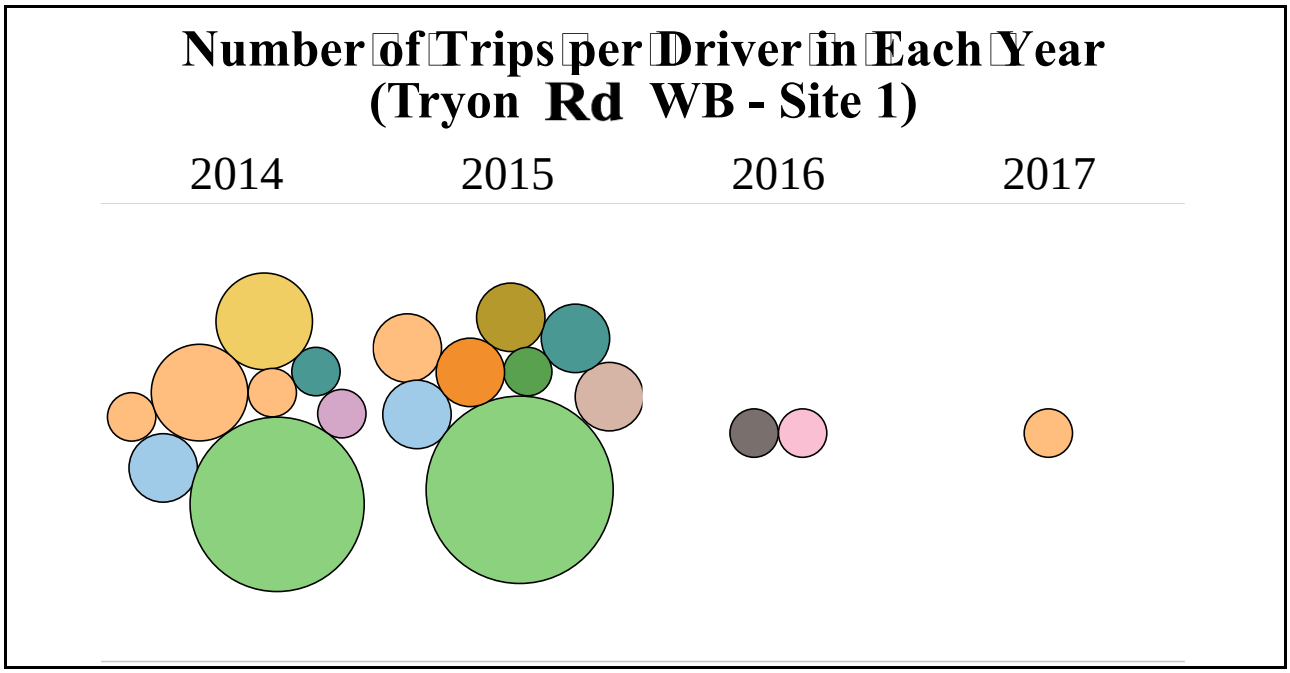

Figure A-12 – Number of Trips per Driver in Each Year (Tryon Rd WB – Site 1)

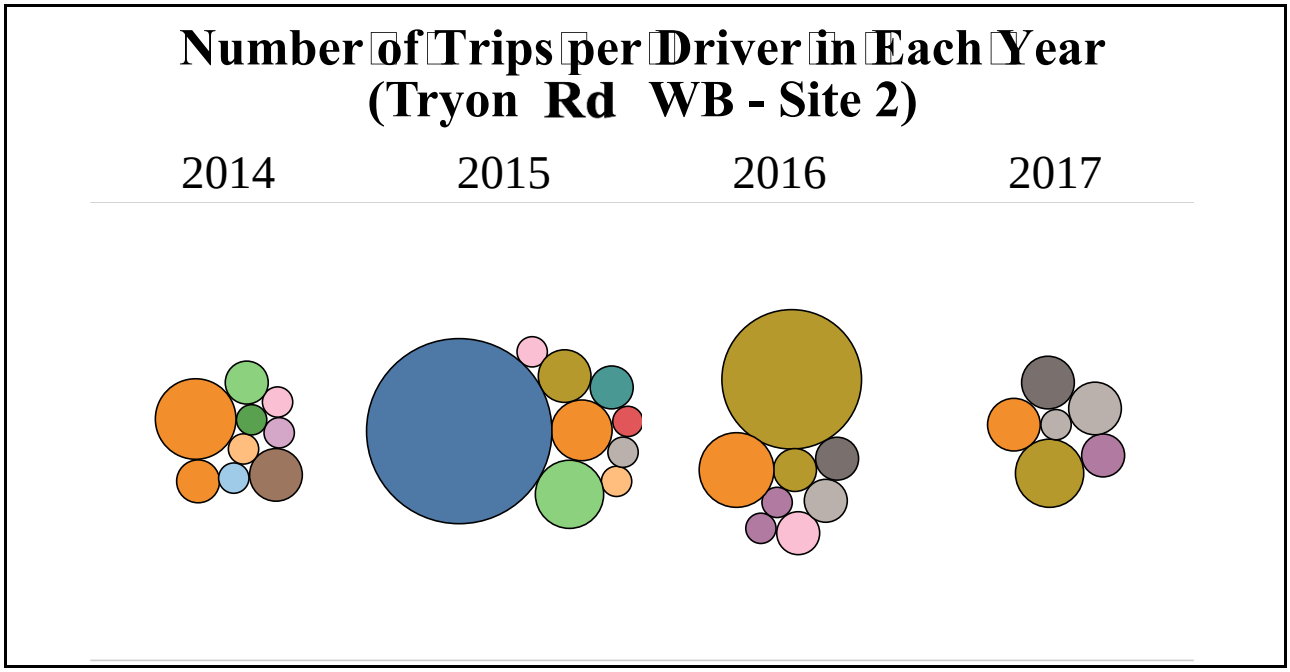

Figure A-13 – Number of Trips per Driver in Each Year (Tryon Rd WB – Site 2)

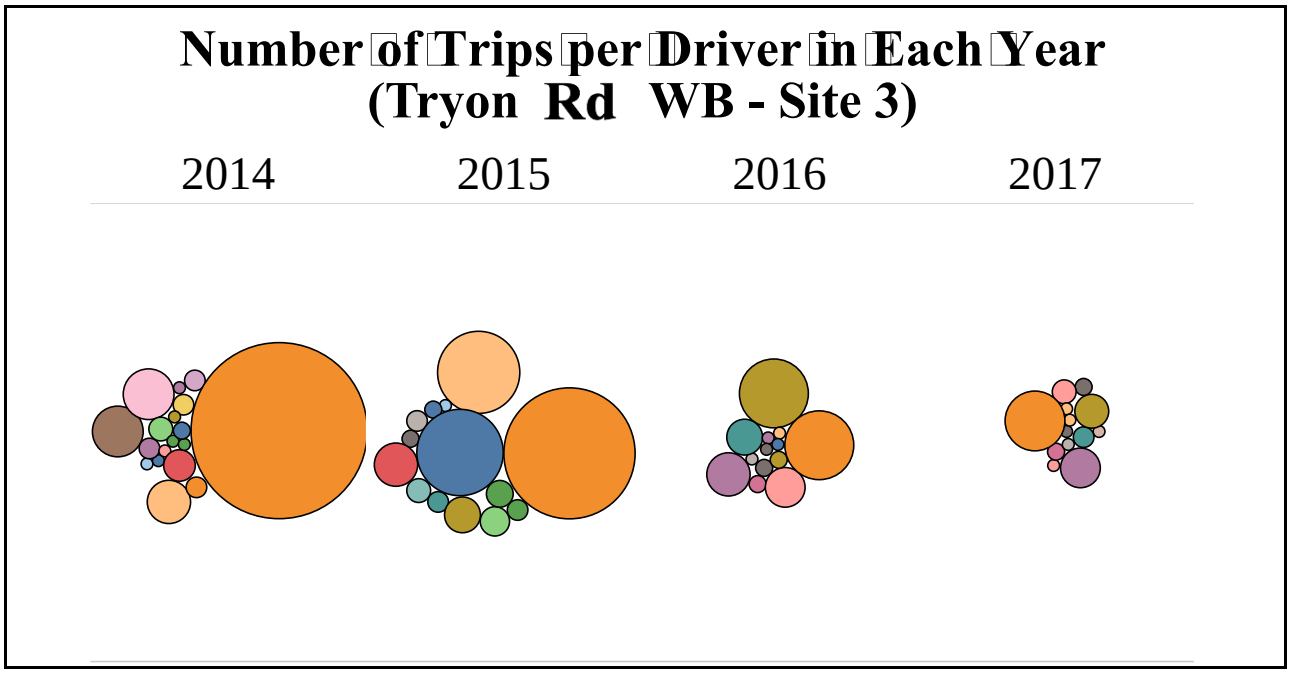

Figure A-14 – Number of Trips per Driver in Each Year
(Tryon Rd WB – Site 3)

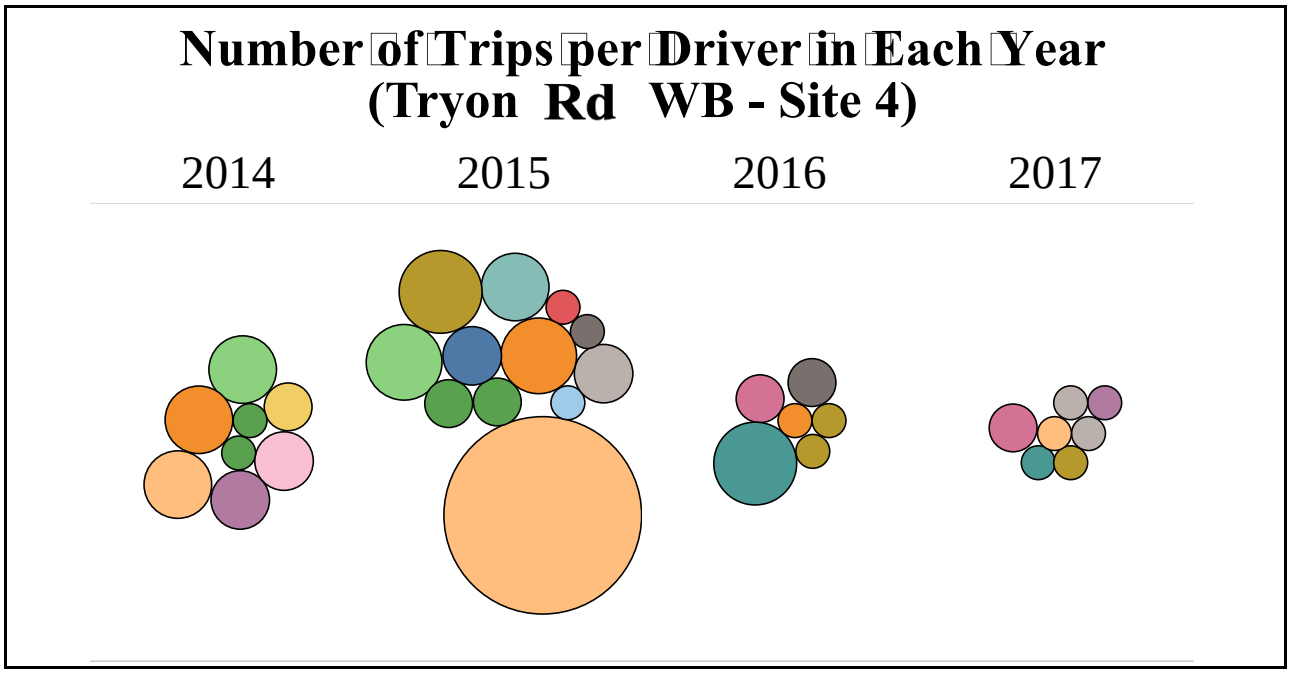

Figure A-15 – Number of Trips per Driver in Each Year
(Tryon Rd WB – Site 4)

APPENDIX C - MONTHLY DISTRIBUTION OF NUMBER OF TRIPS AND DRIVERS

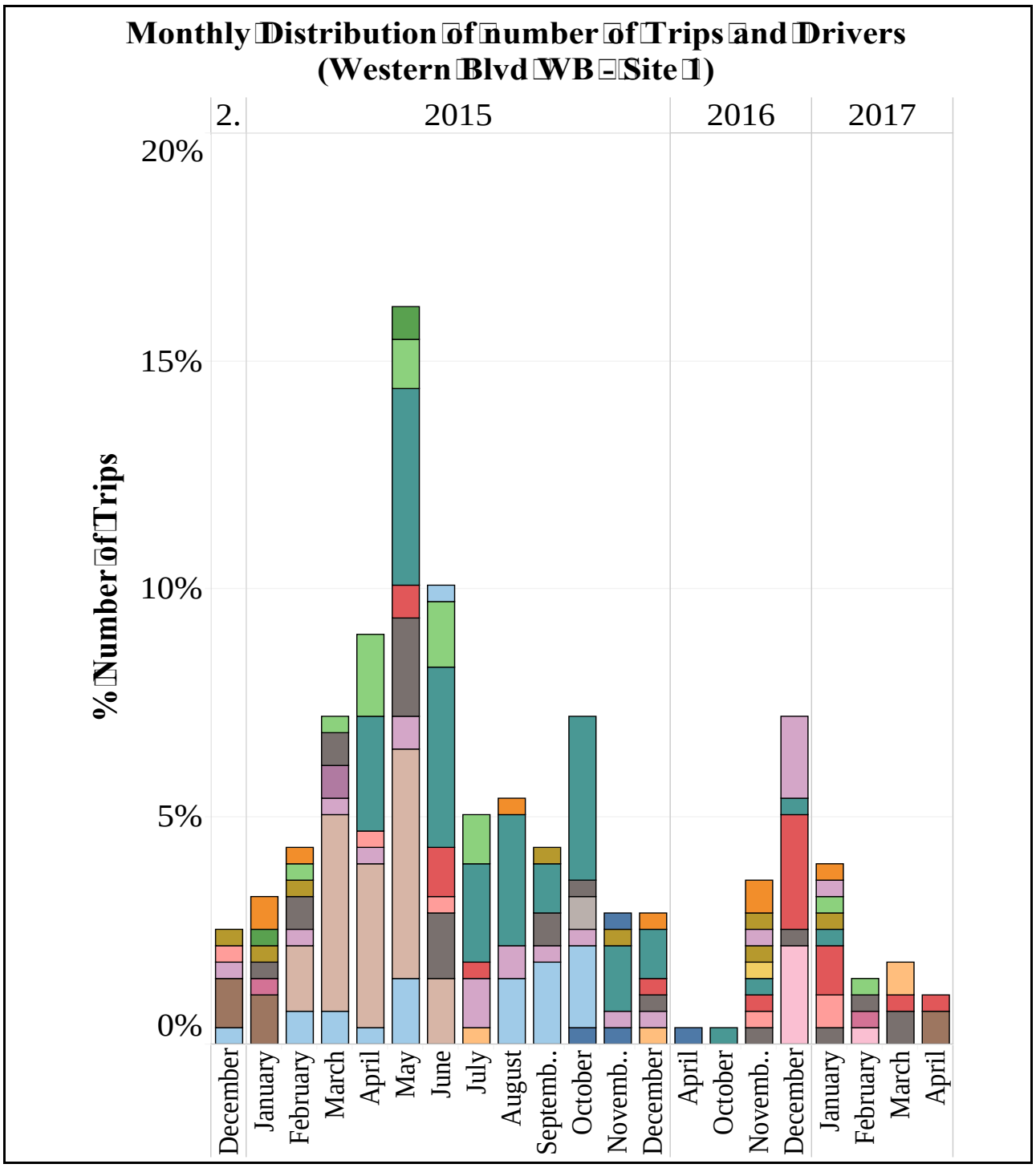

Figure C-1 – Monthly Distribution of number of Trips and Drivers (Western Blvd WB – Site 1)

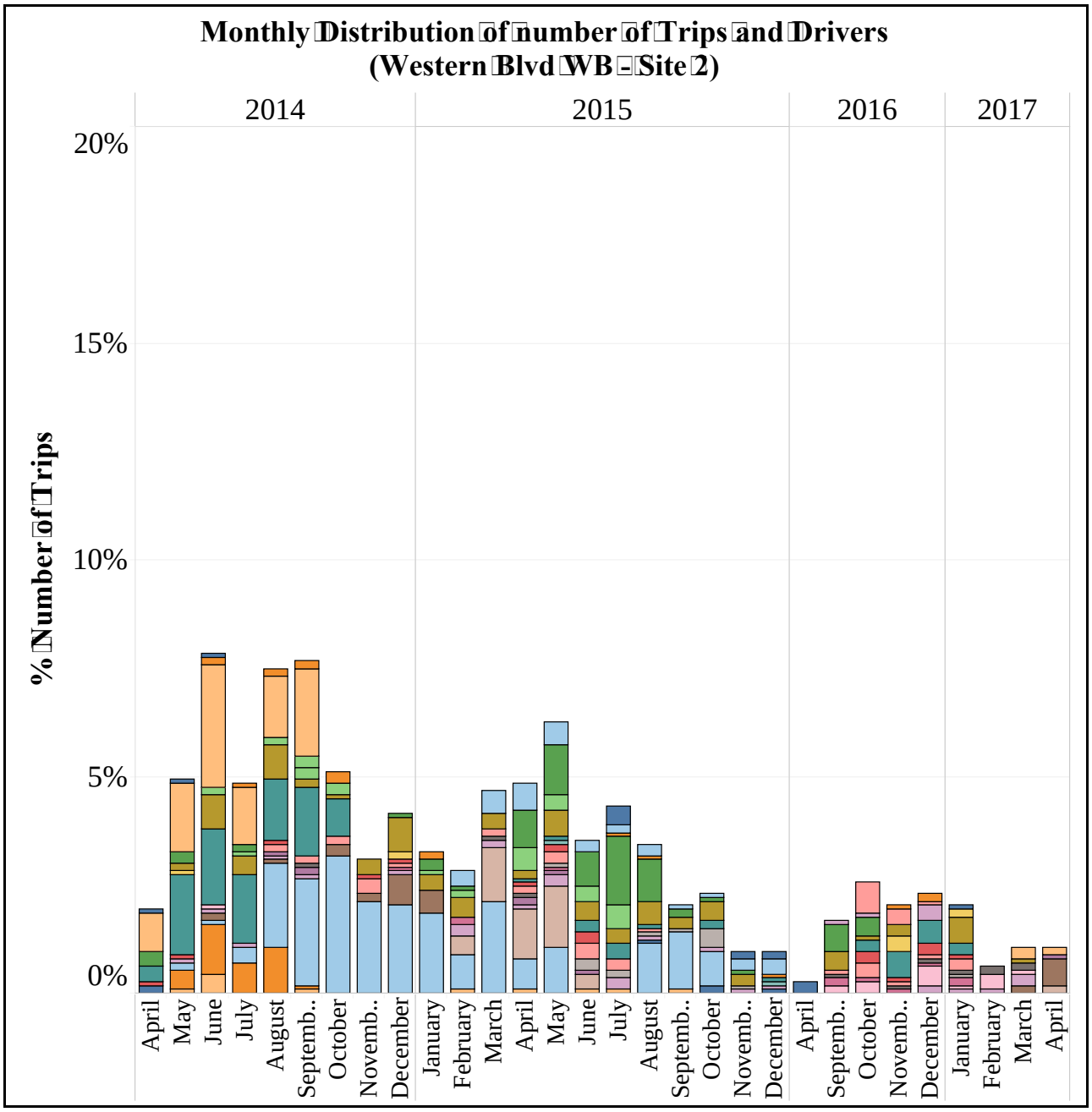

Figure C-2 – Monthly Distribution of number of Trips and Drivers (Western Blvd WB – Site 2)

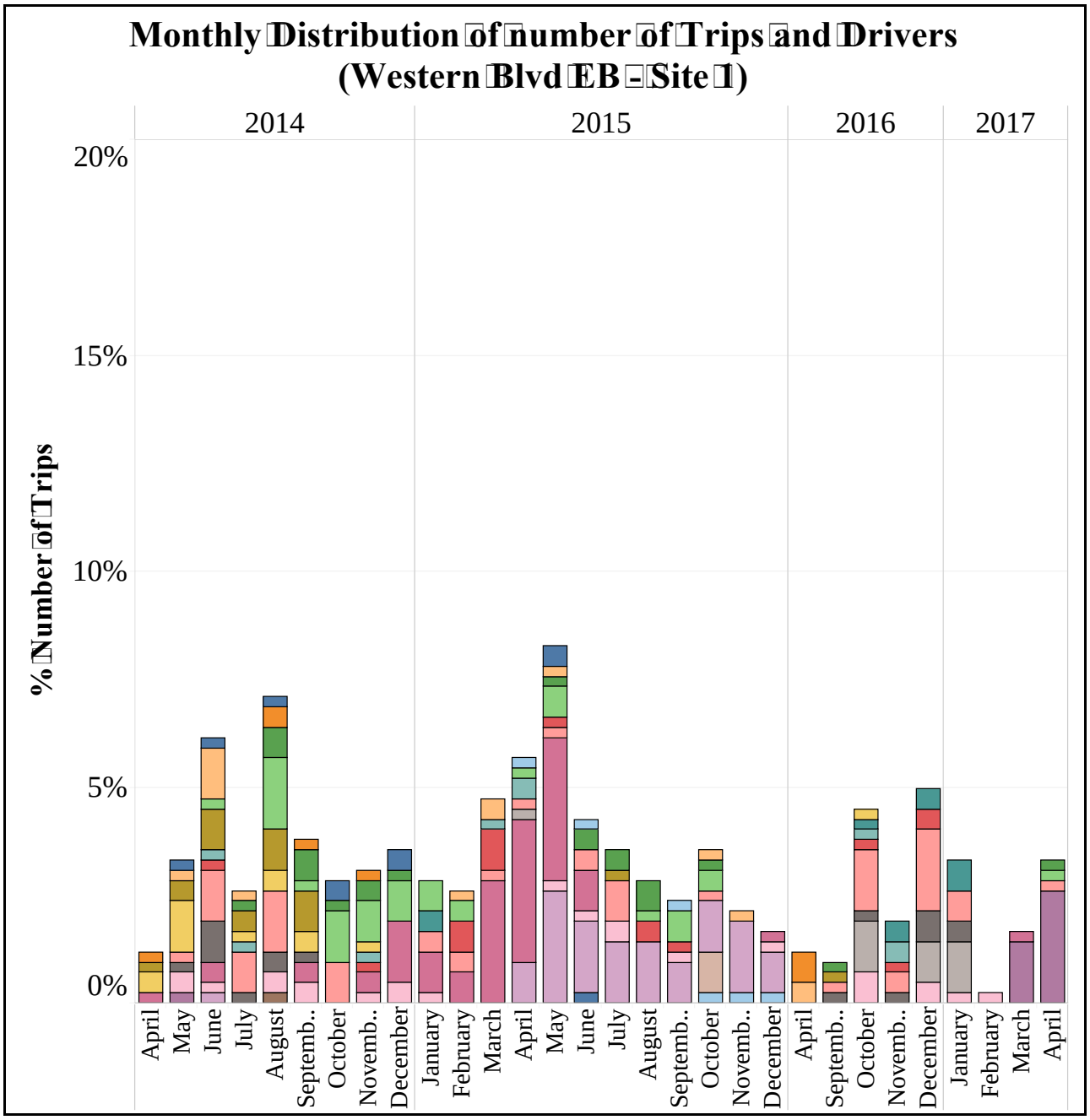

Figure C-3 – Monthly Distribution of number of Trips and Drivers (Western Blvd EB – Site 1)

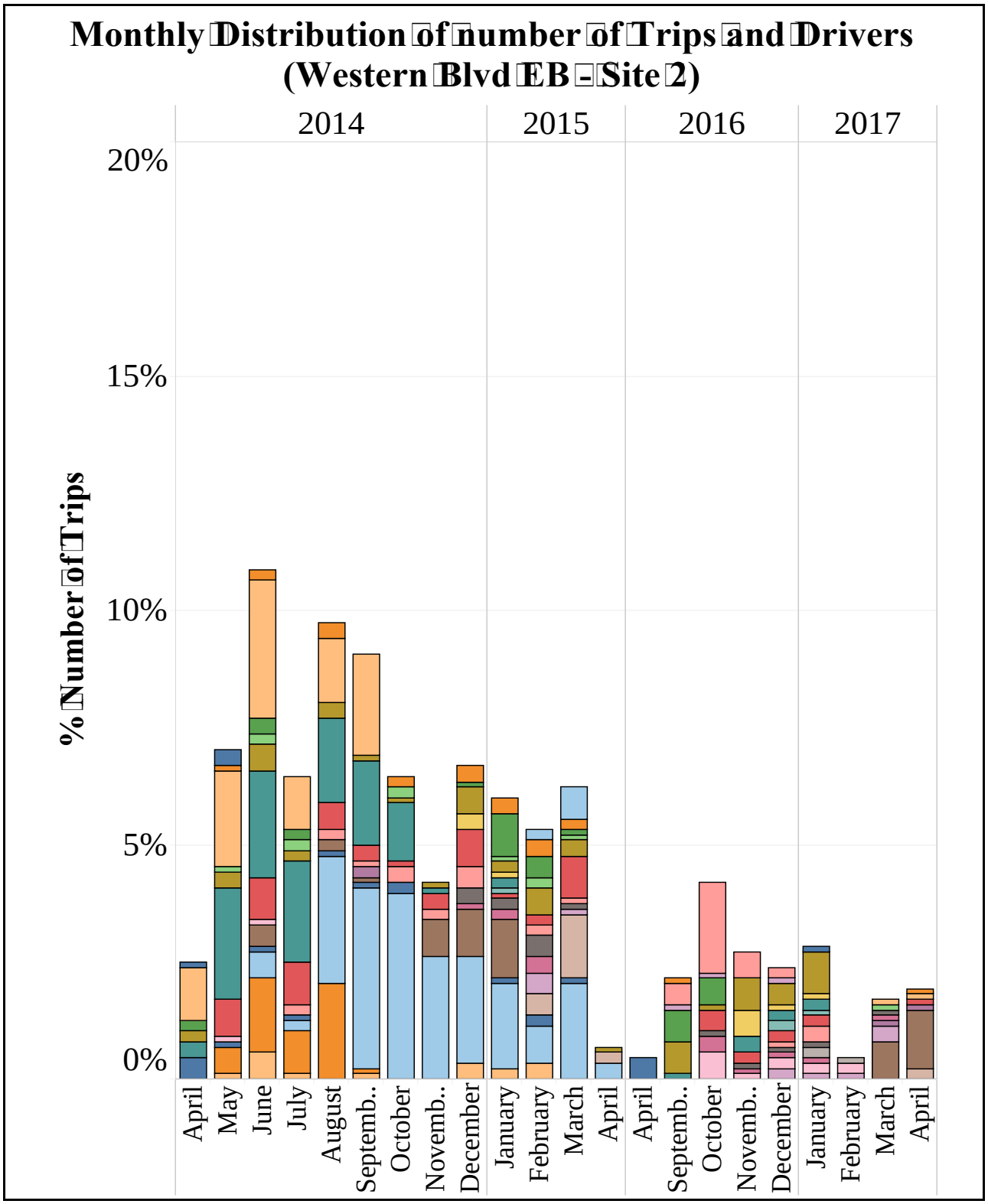

Figure C-4 – Monthly Distribution of number of Trips and Drivers (Western Blvd EB – Site 2)

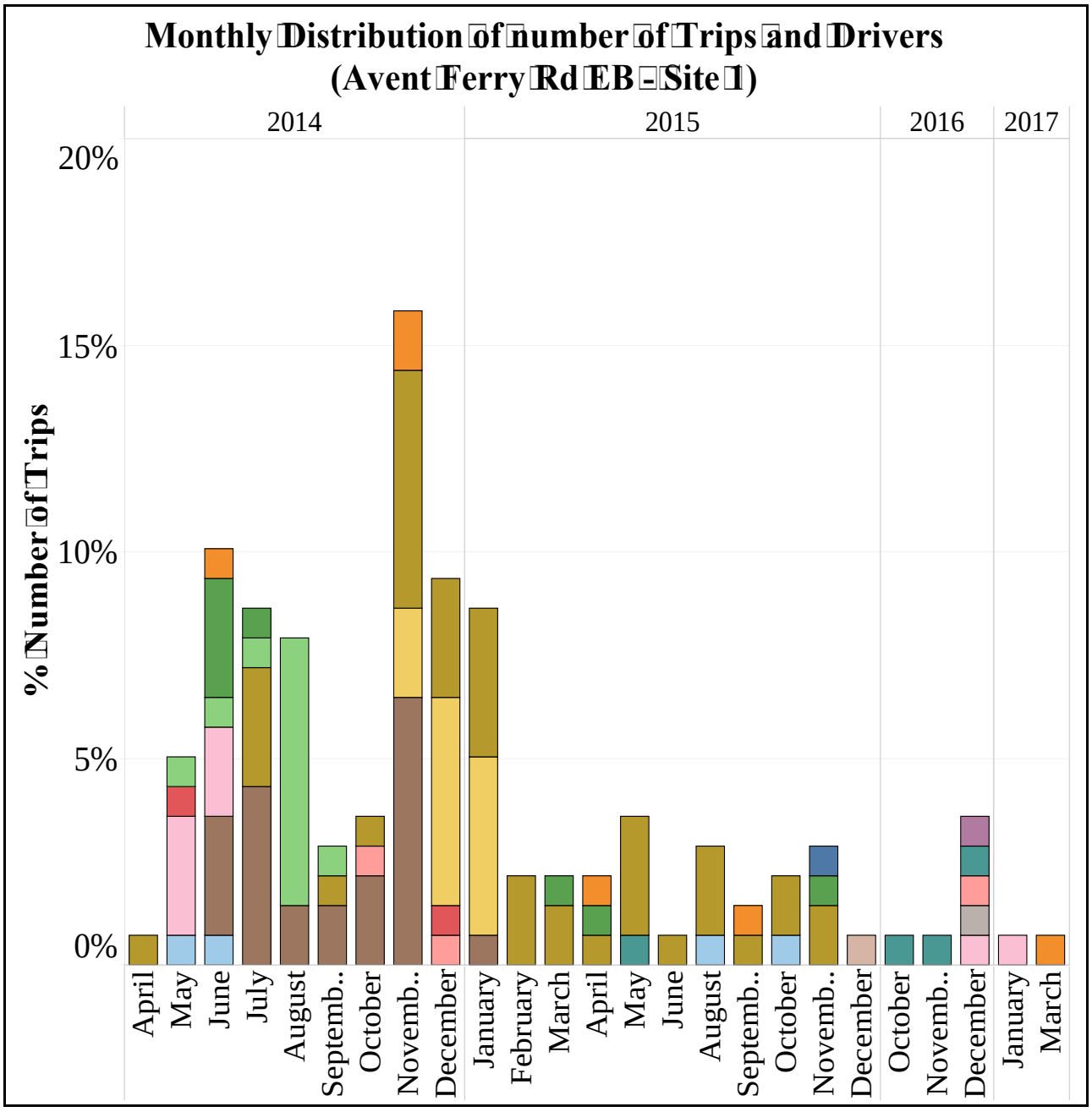

Figure C-5 – Monthly Distribution of number of Trips and Drivers (Avent Ferry Rd EB – Site 1)

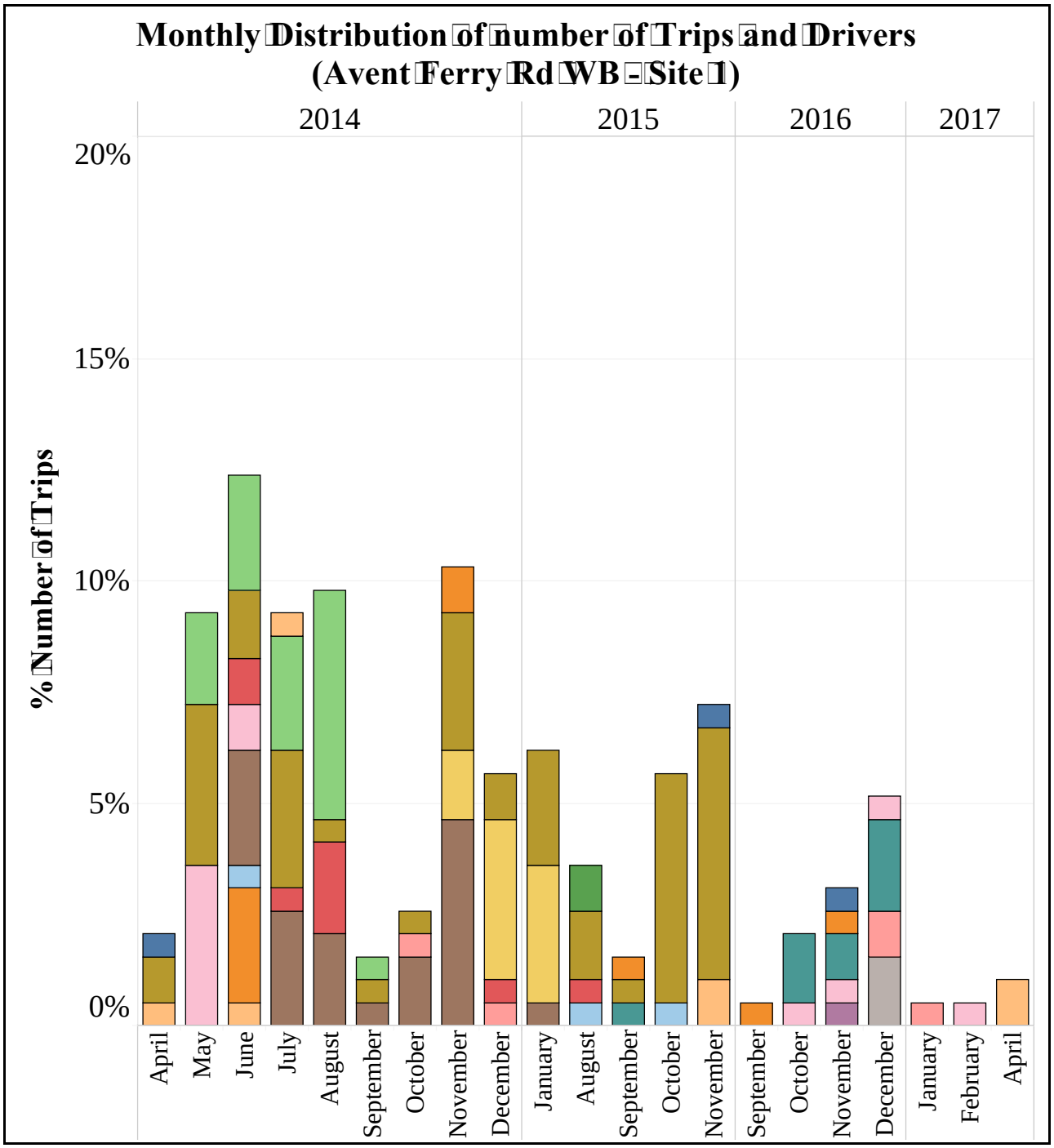

Figure C-6 – Monthly Distribution of number of Trips and Drivers (Avent Ferry Rd WB – Site 1)

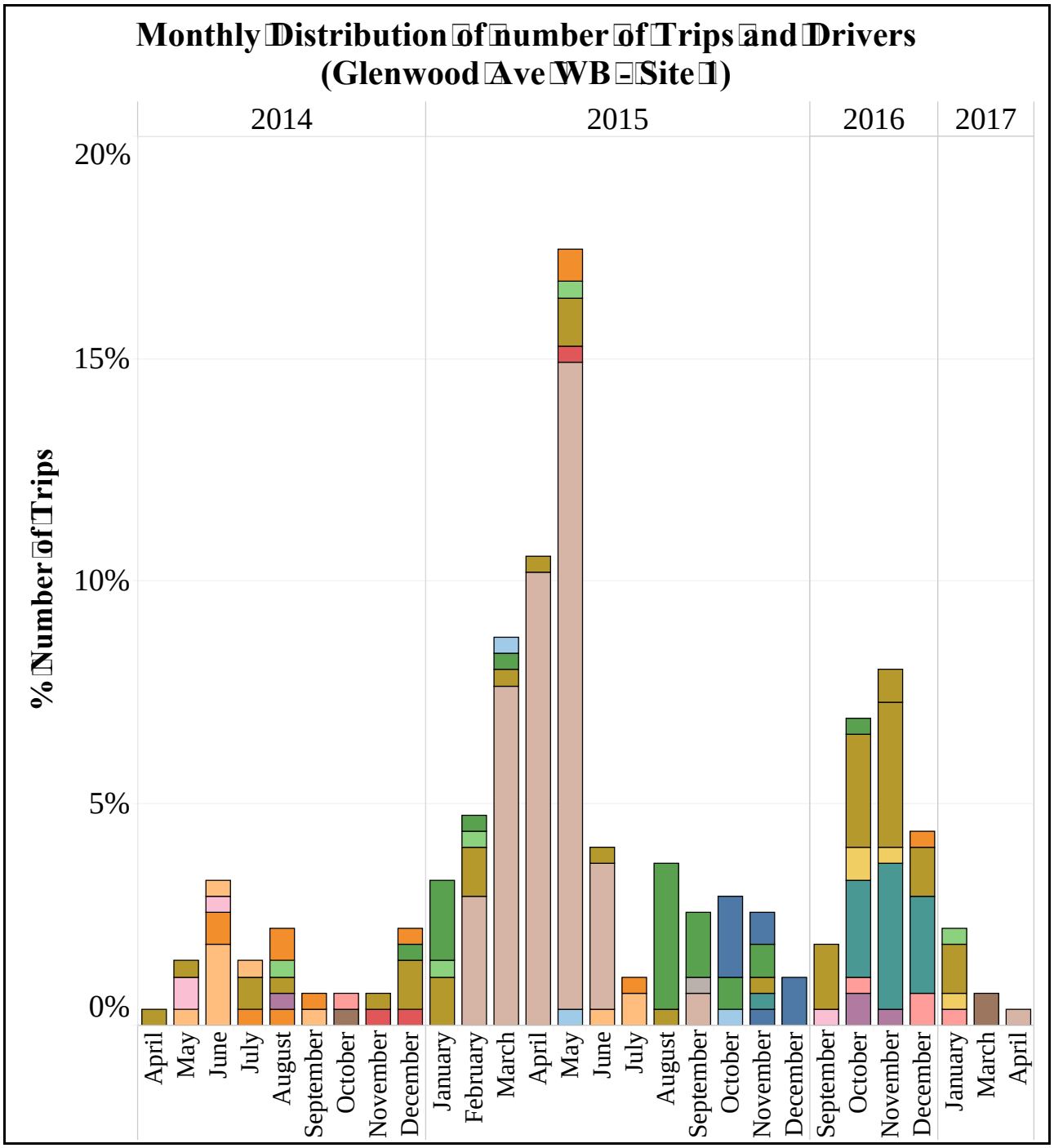

Figure C-7 – Monthly Distribution of number of Trips and Drivers (Glenwood Ave WB – Site 1)

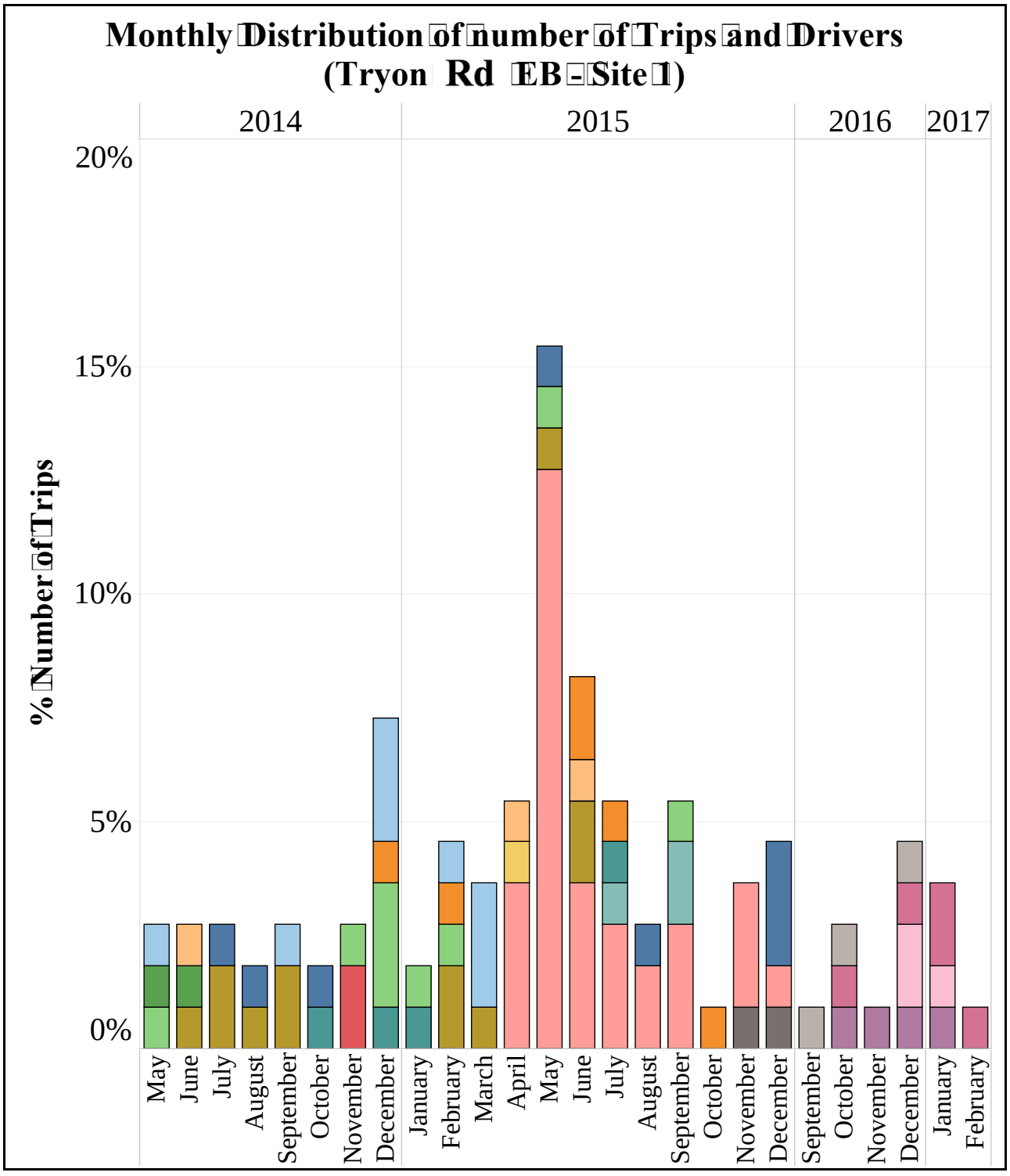

Figure C-8 – Monthly Distribution of number of Trips and Drivers (Western Blvd EB – Site 1)

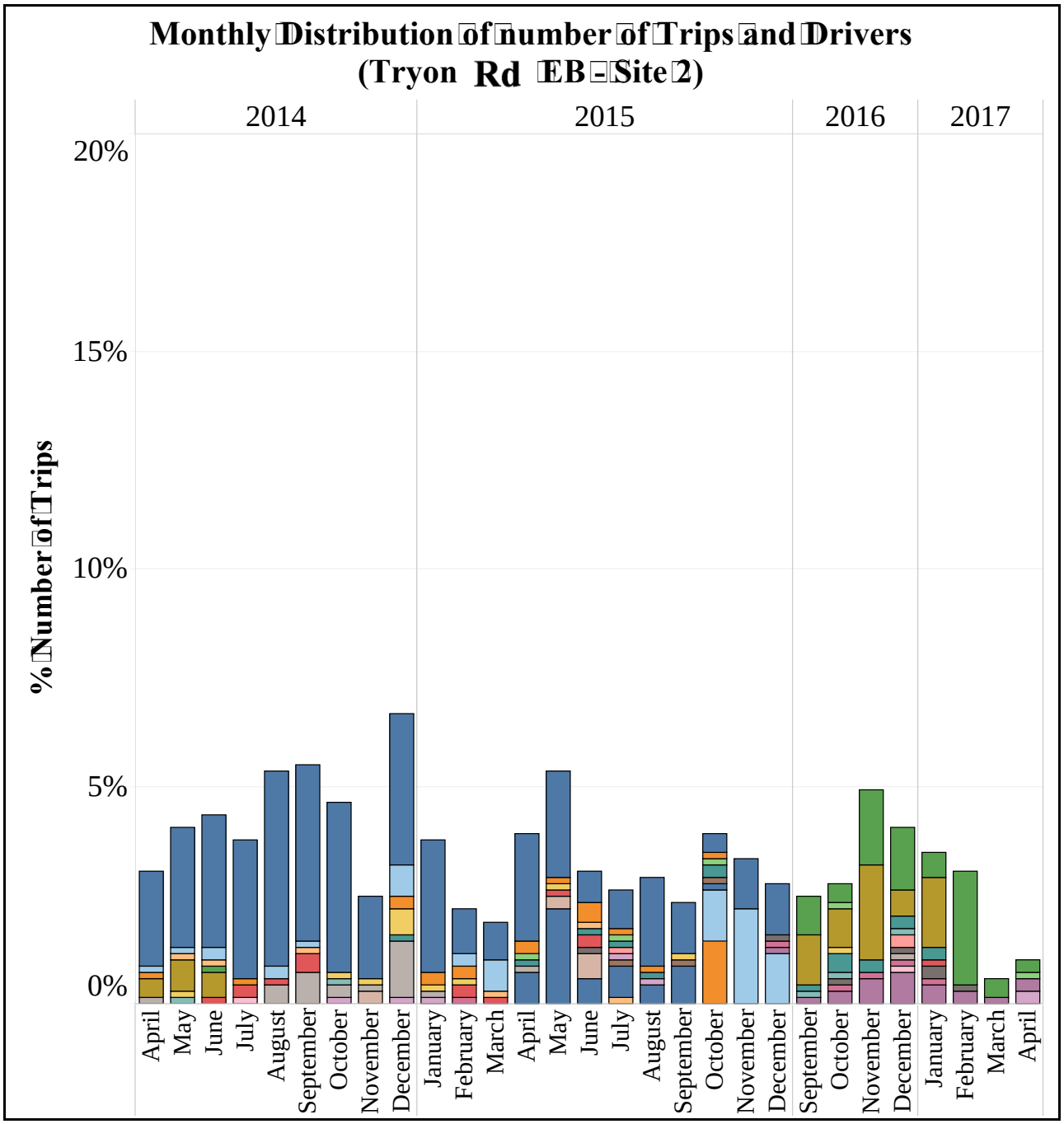

Figure C-9 – Monthly Distribution of number of Trips and Drivers (Tryon Rd EB – Site 2)

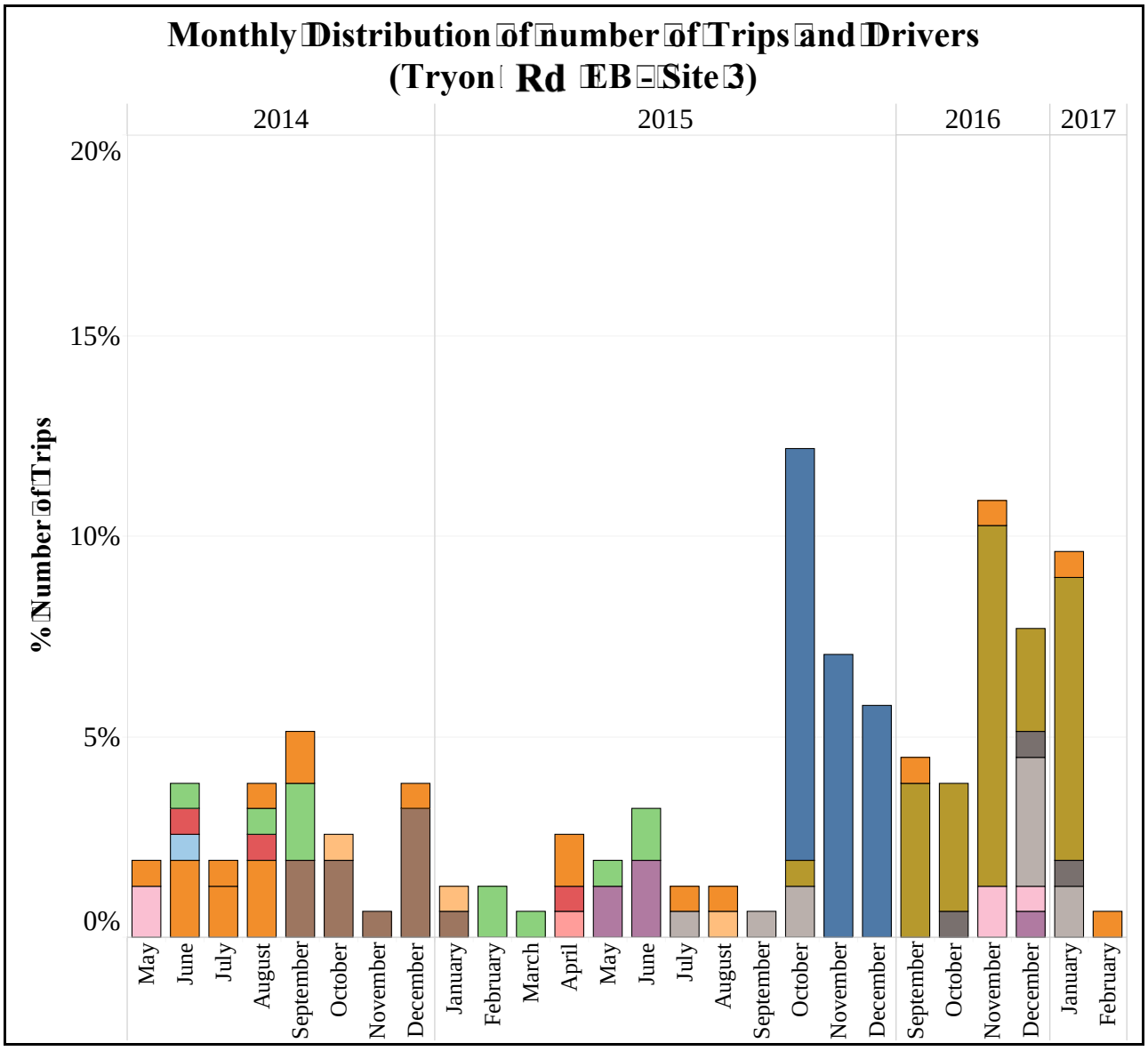

Figure C-10 – Monthly Distribution of number of Trips and Drivers (Tryon Rd EB – Site 3)

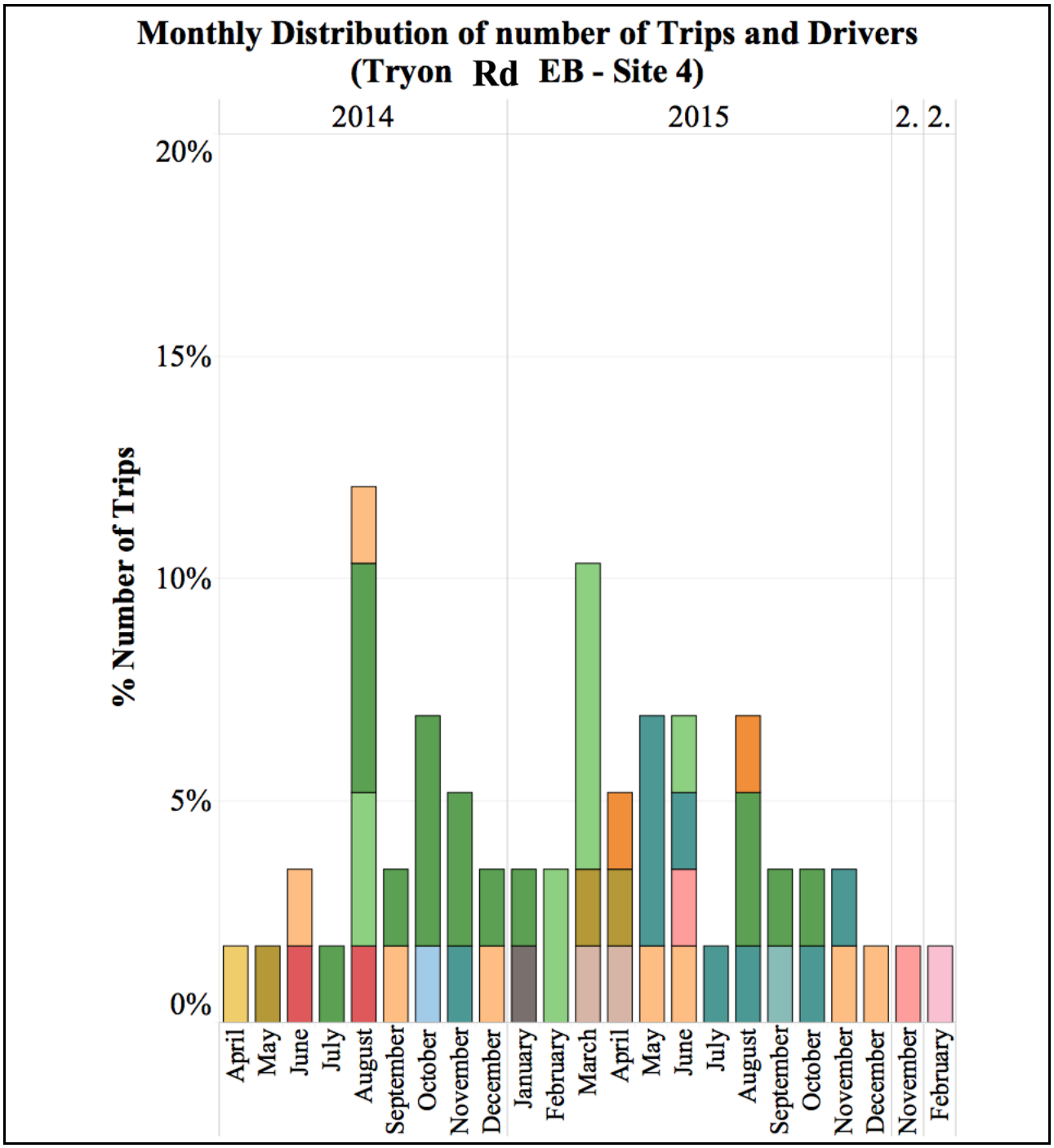

Figure C-11 – Monthly Distribution of number of Trips and Drivers (Tryon Rd EB – Site 4)

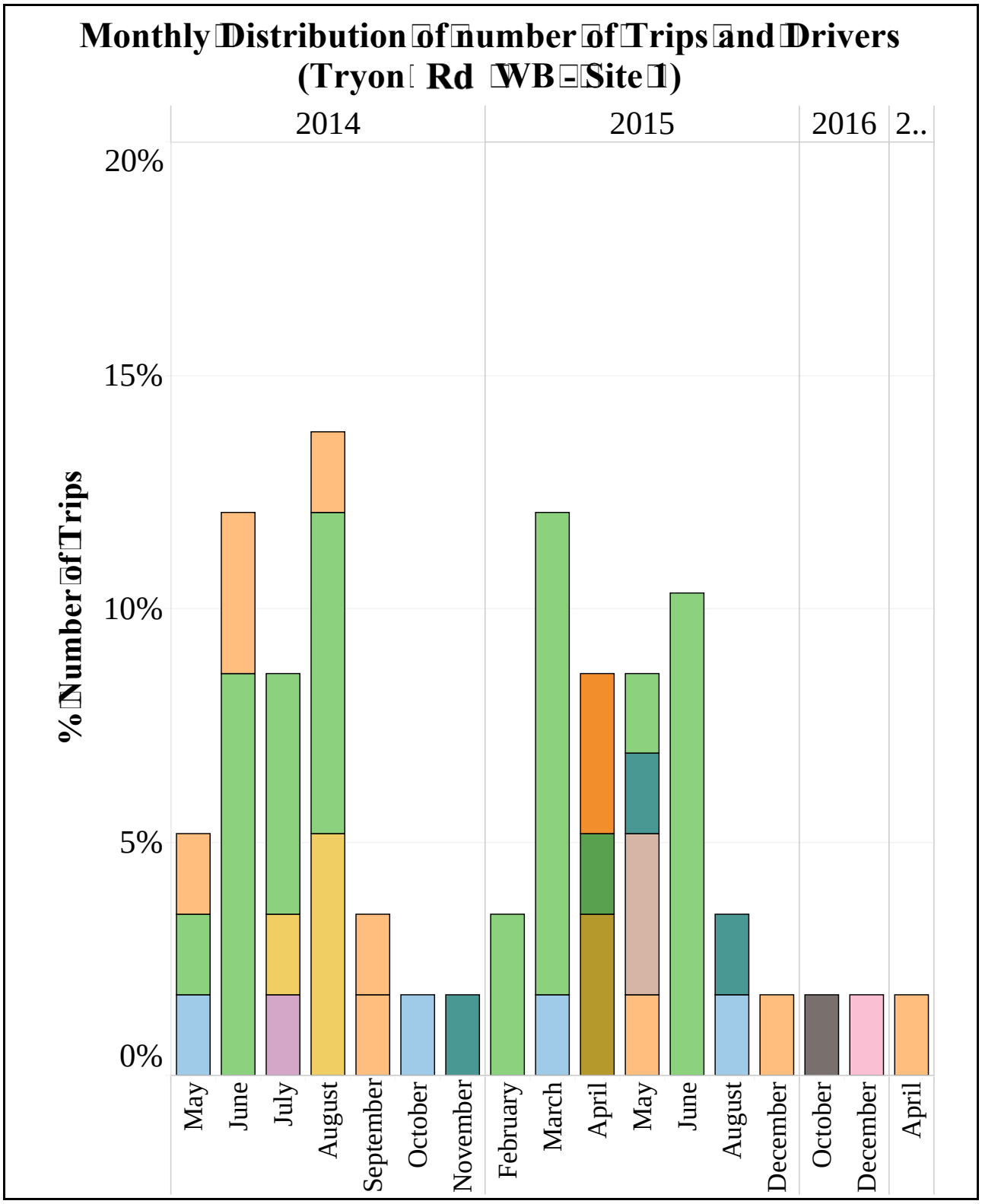

Figure C-12 – Monthly Distribution of number of Trips and Drivers (Tryon Rd WB – Site 1)

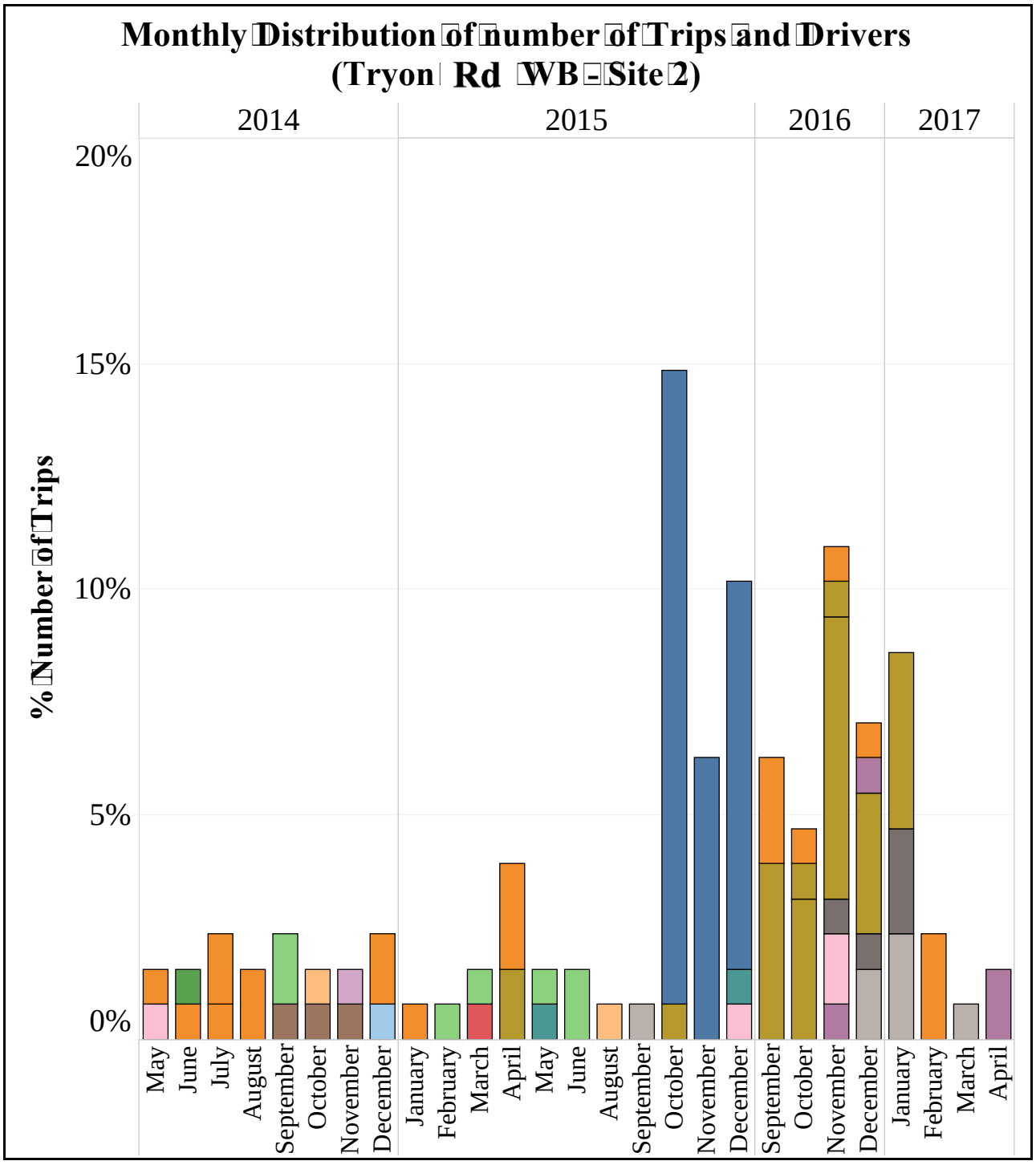

Figure C-13 – Monthly Distribution of number of Trips and Drivers (Tryon Rd WB – Site 2)

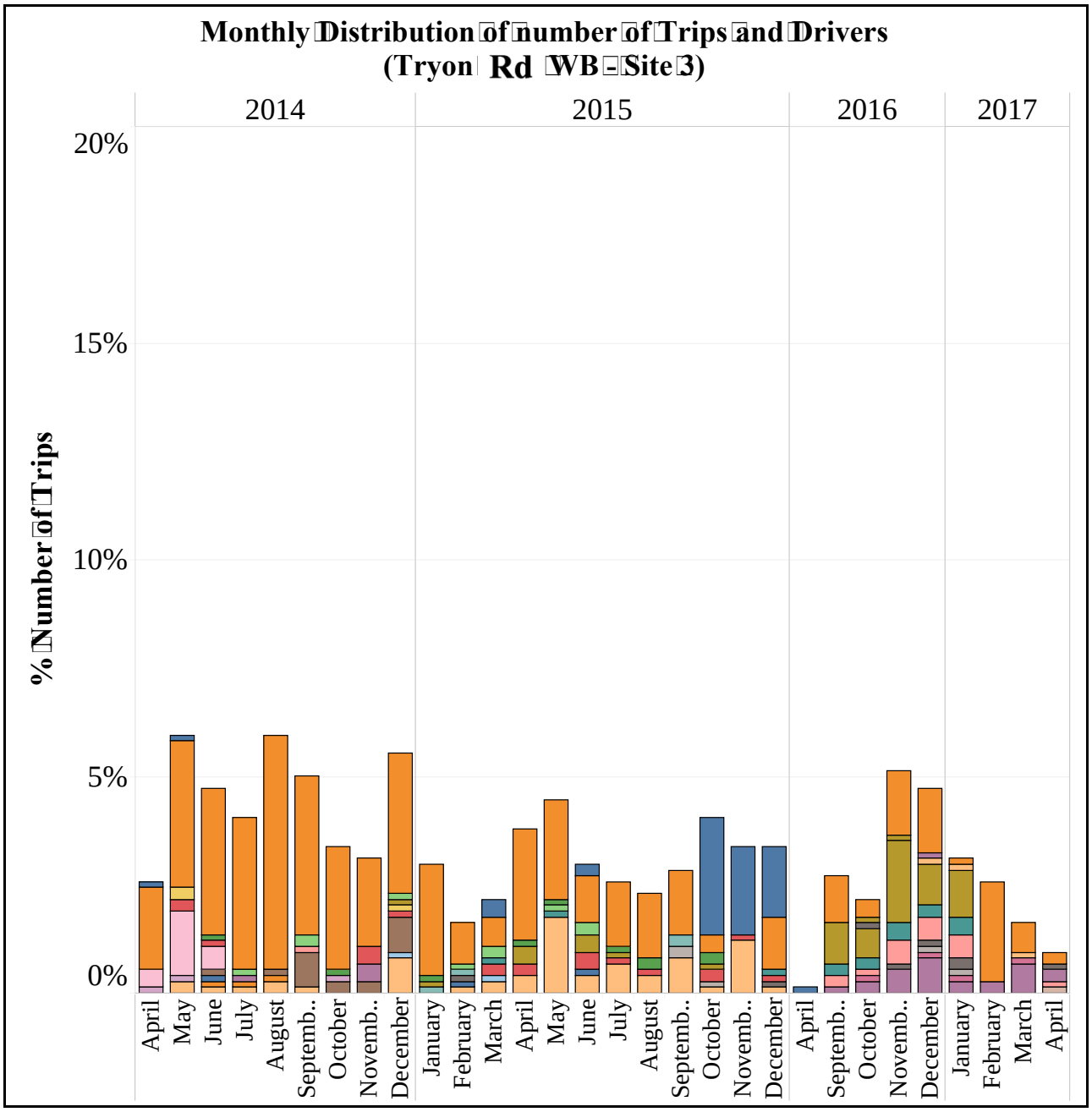

Figure C-14 – Monthly Distribution of number of Trips and Drivers (Tryon Rd WB – Site 3)

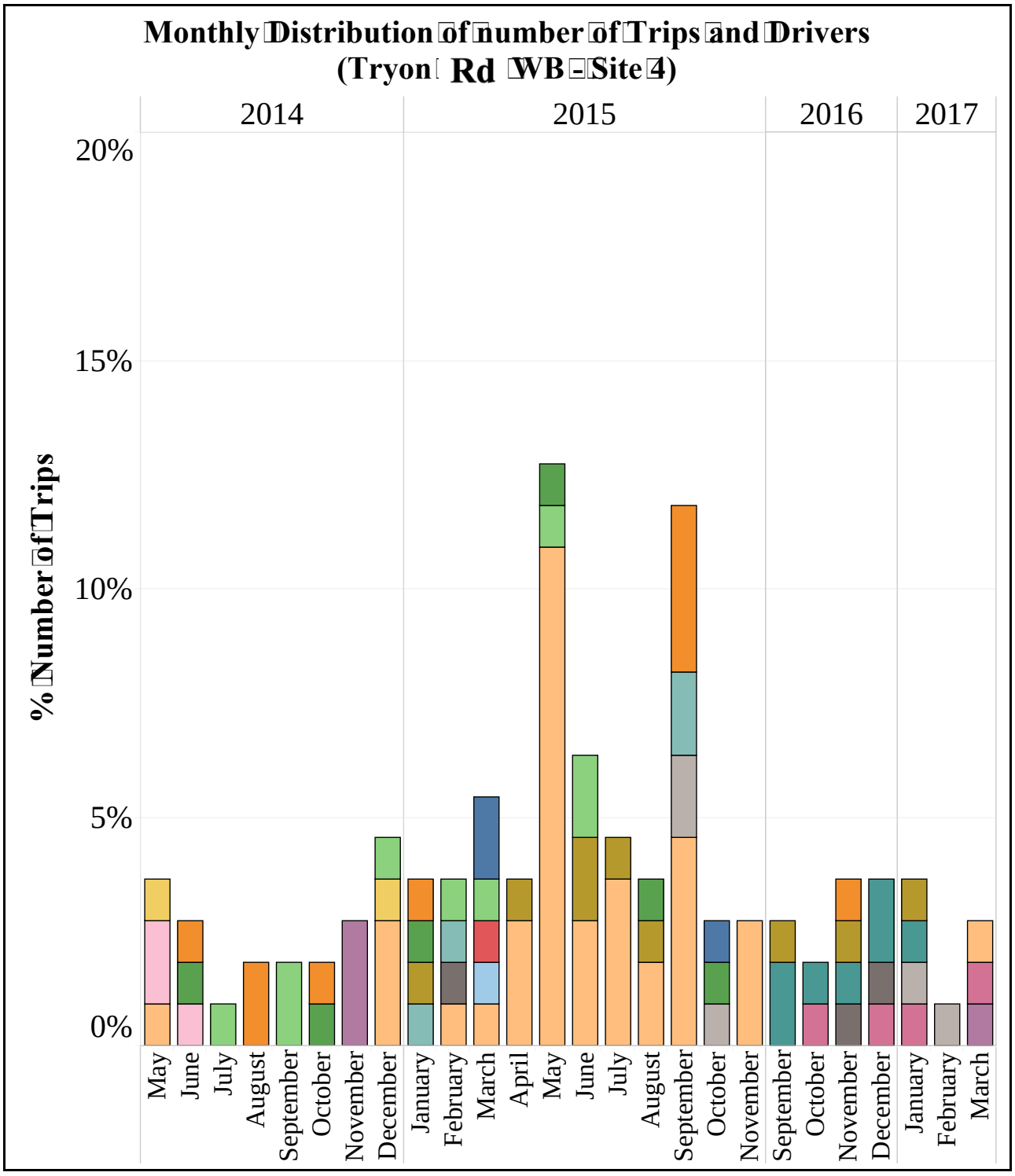

Figure C-15 – Monthly Distribution of number of Trips and Drivers (Tryon Rd WB – Site 4)

APPENDIX B - DISTRIBUTION OF SECOND-BY-SECOND DATA POINTS AND NUMBER OF DRIVERS OVER DIFFERENT LOS

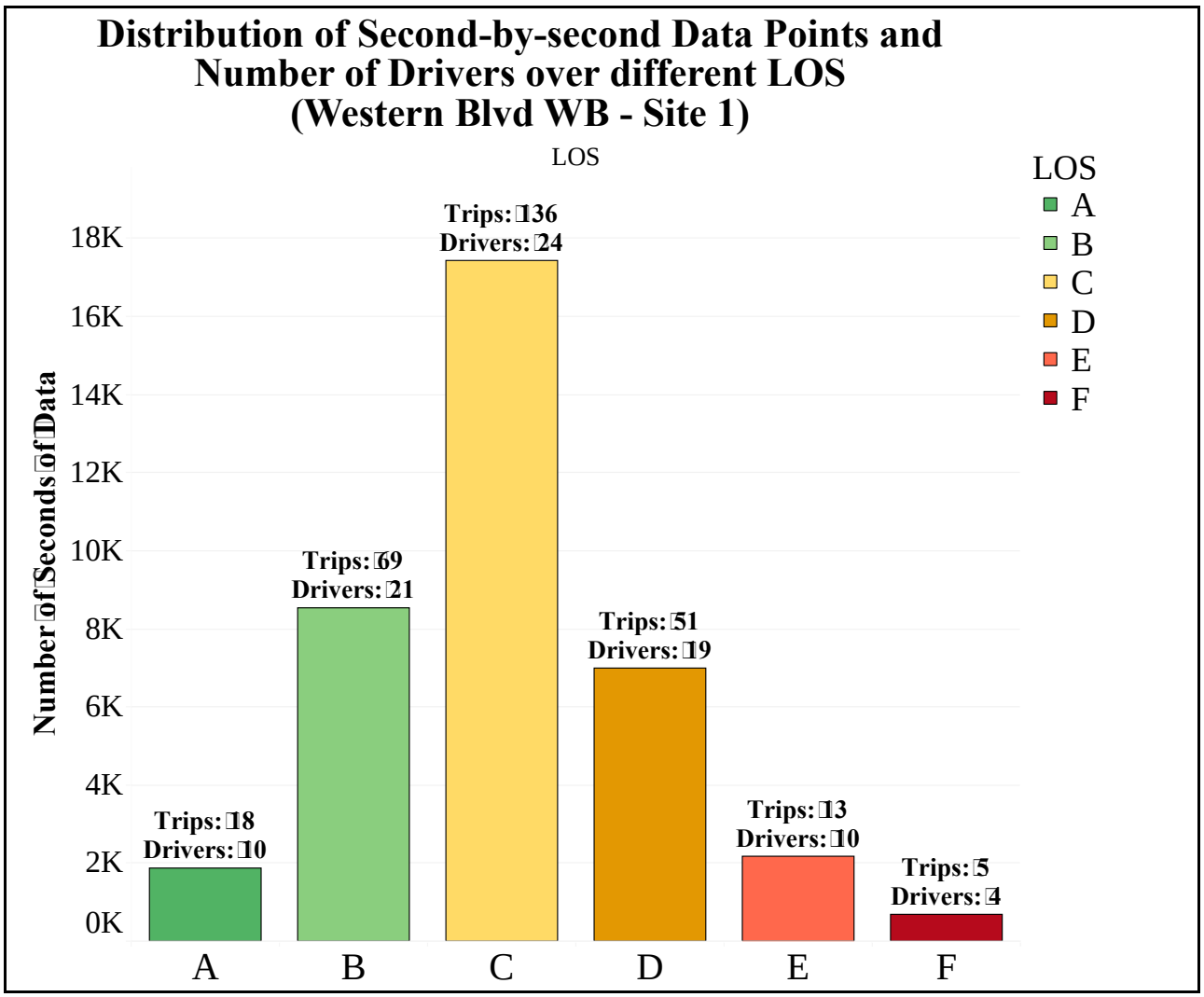

Figure B-1 – Distribution of Second-by-second Data Points and Number of Drivers over Different LOS (Western Blvd WB – Site 1)

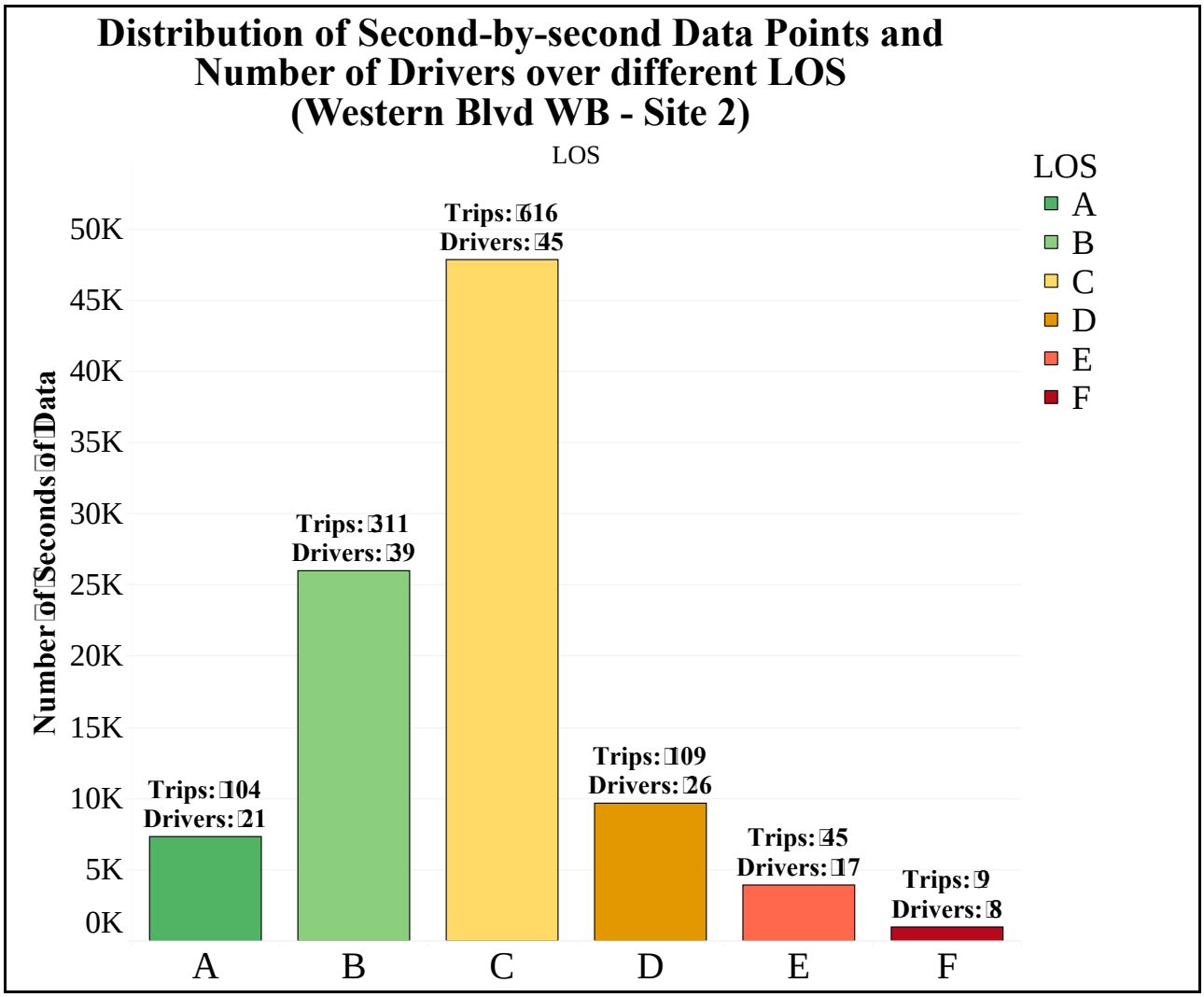

Figure B-2 – Distribution of Second-by-second Data Points and Number of Drivers over Different LOS (Western Blvd WB – Site 2)

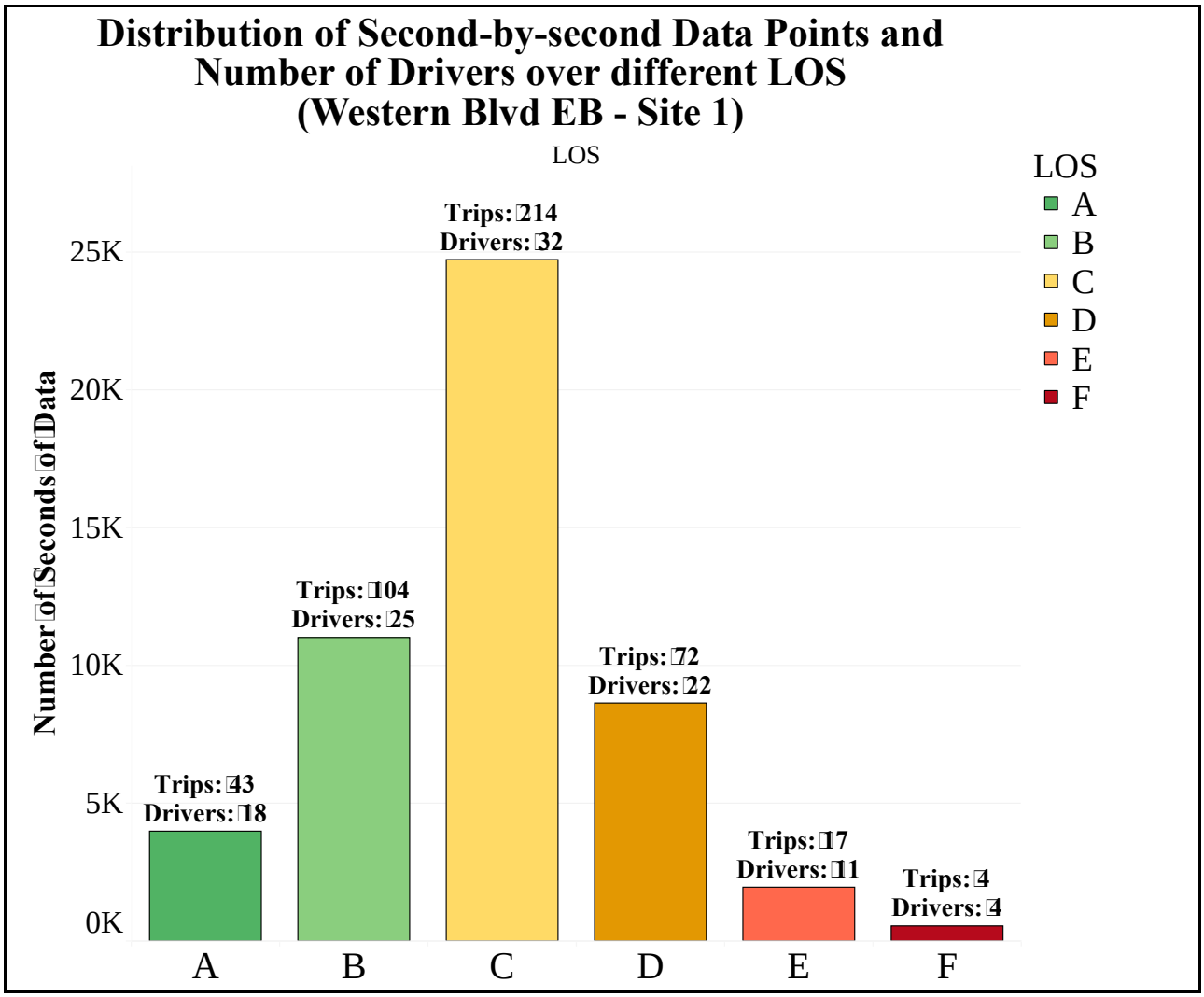

Figure B-3 – Distribution of Second-by-second Data Points and Number of Drivers over Different LOS (Western Blvd EB – Site 1)

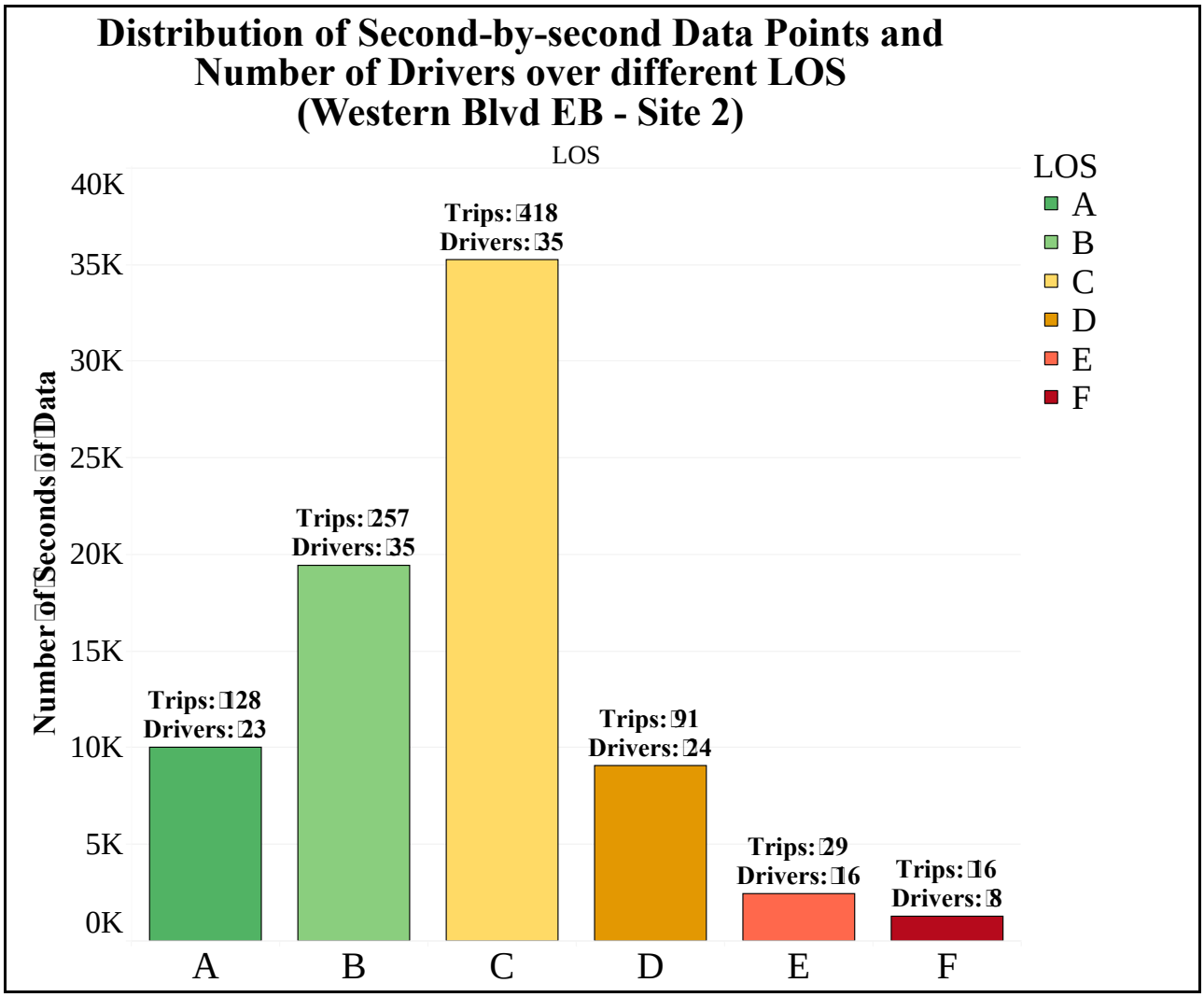

Figure B-4 – Distribution of Second-by-second Data Points and Number of Drivers over Different LOS (Western Blvd EB – Site 2)

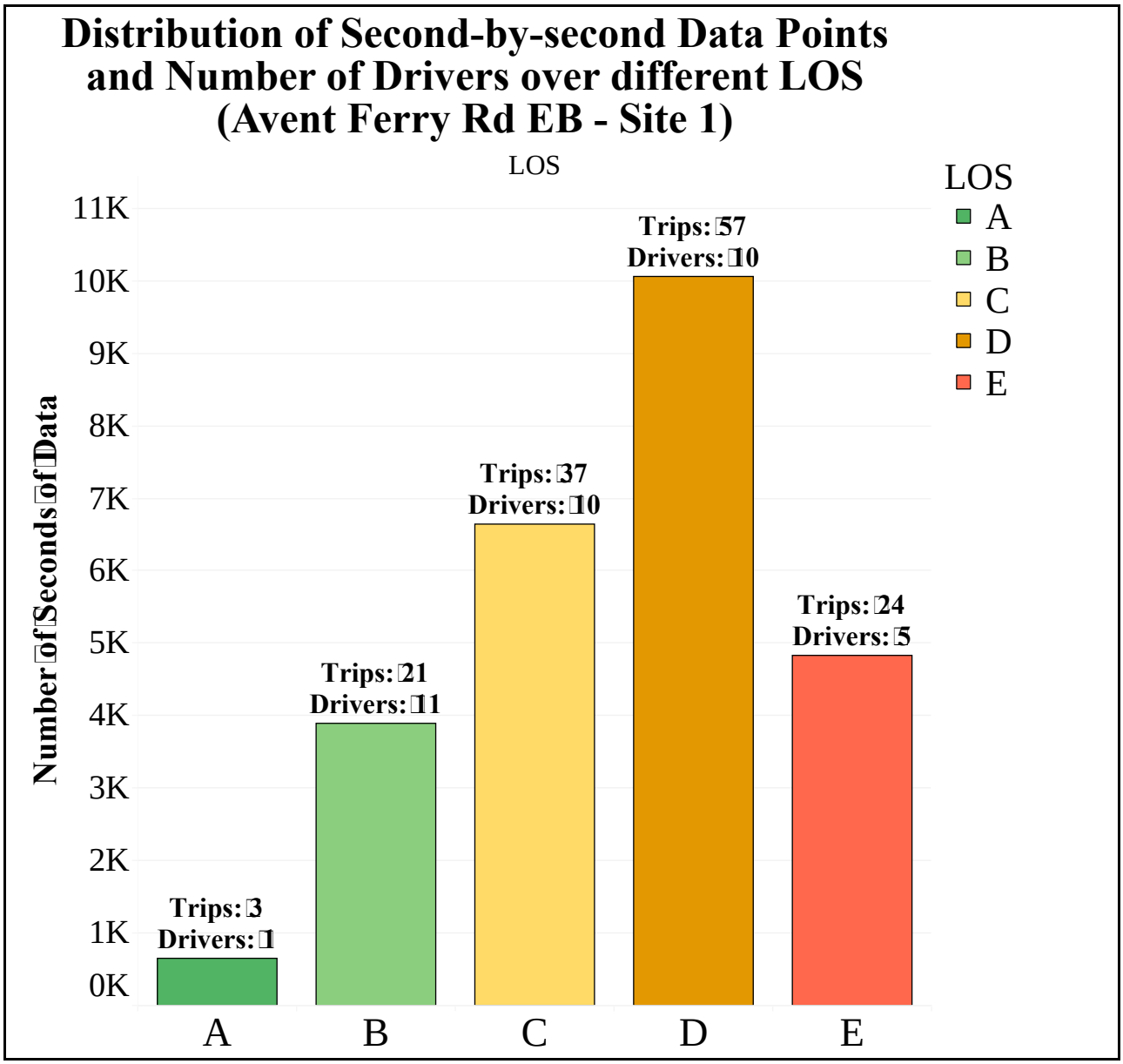

Figure B-5 – Distribution of Second-by-second Data Points and Number of Drivers over Different LOS (Avent Ferry EB – Site 1)

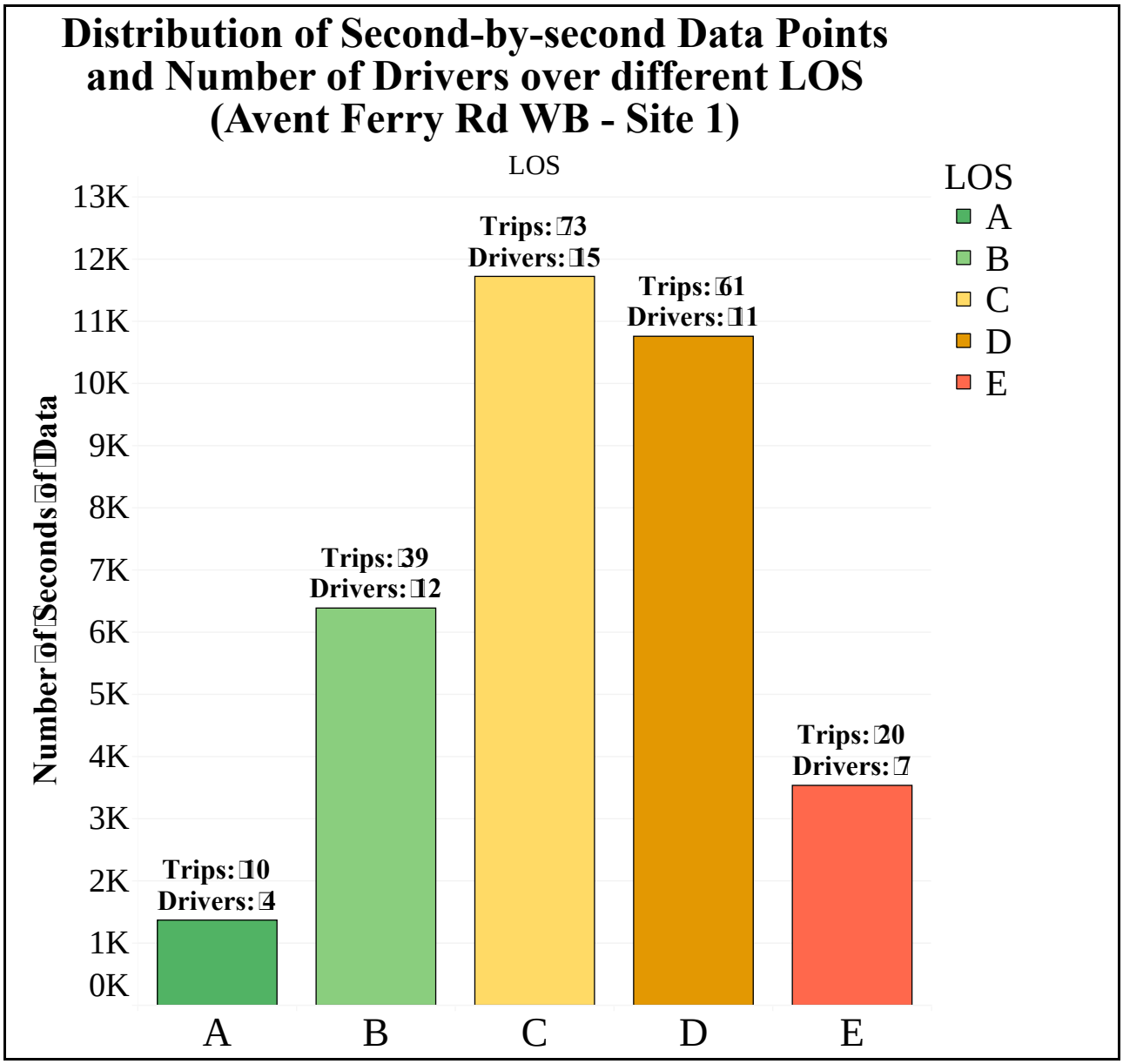

Figure B-6 – Distribution of Second-by-second Data Points and Number of Drivers over Different LOS (Avent Ferry WB – Site 1)

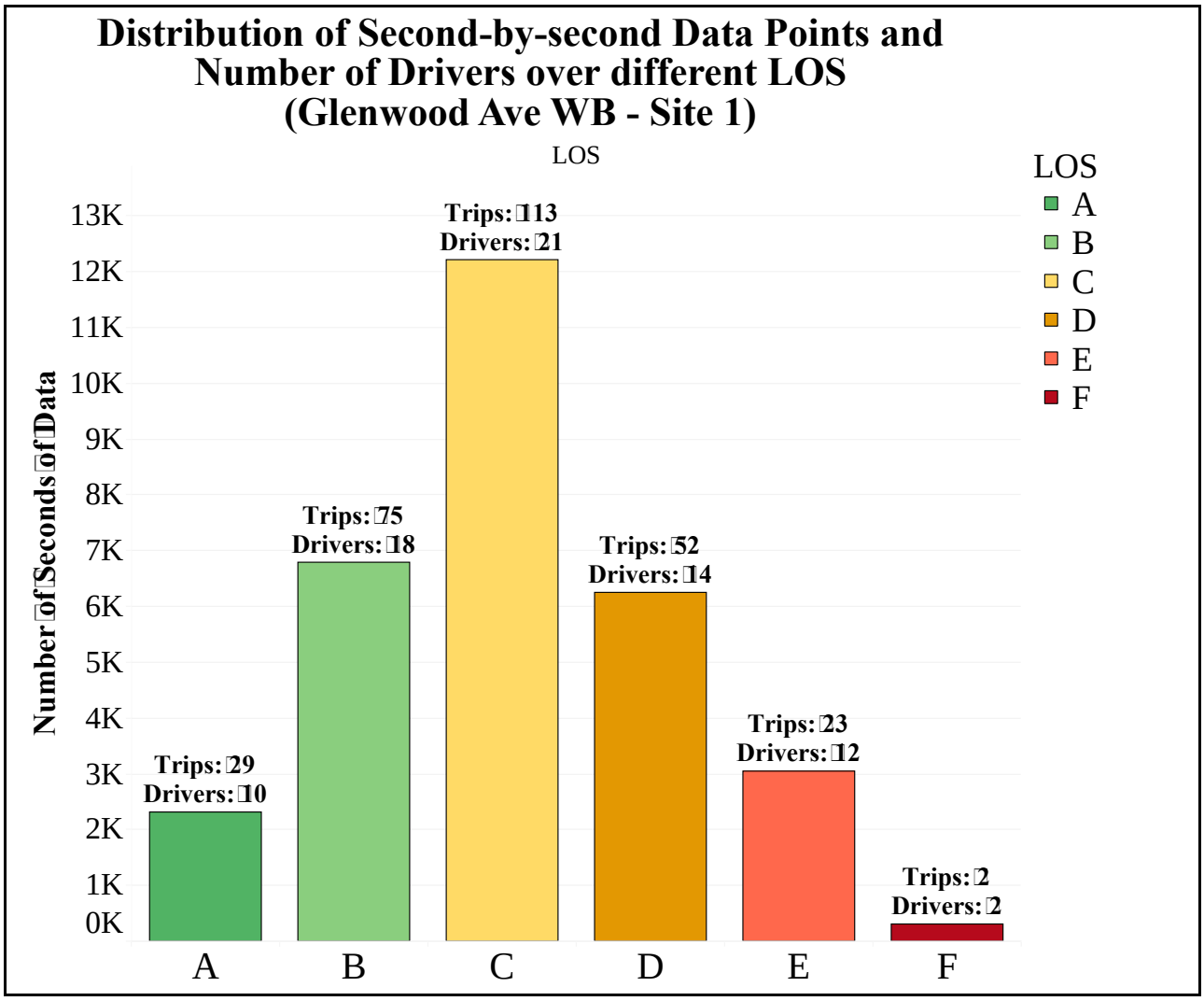

Figure B-7 – Distribution of Second-by-second Data Points and Number of Drivers over Different LOS (Glenwood Ave WB – Site 1)

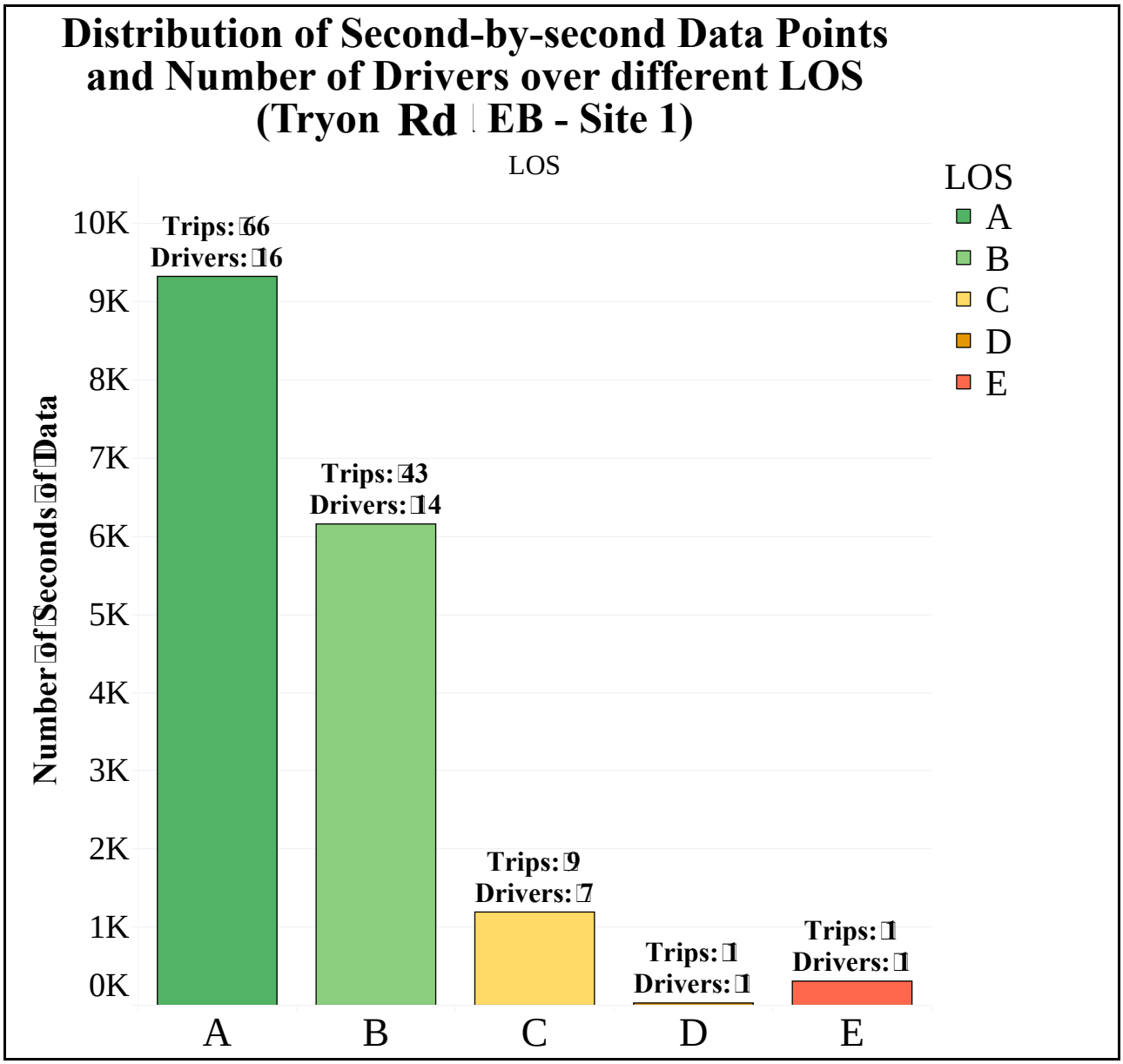

Figure B-8 – Distribution of Second-by-second Data Points and Number of Drivers over Different LOS (Tryon Rd EB – Site 1)

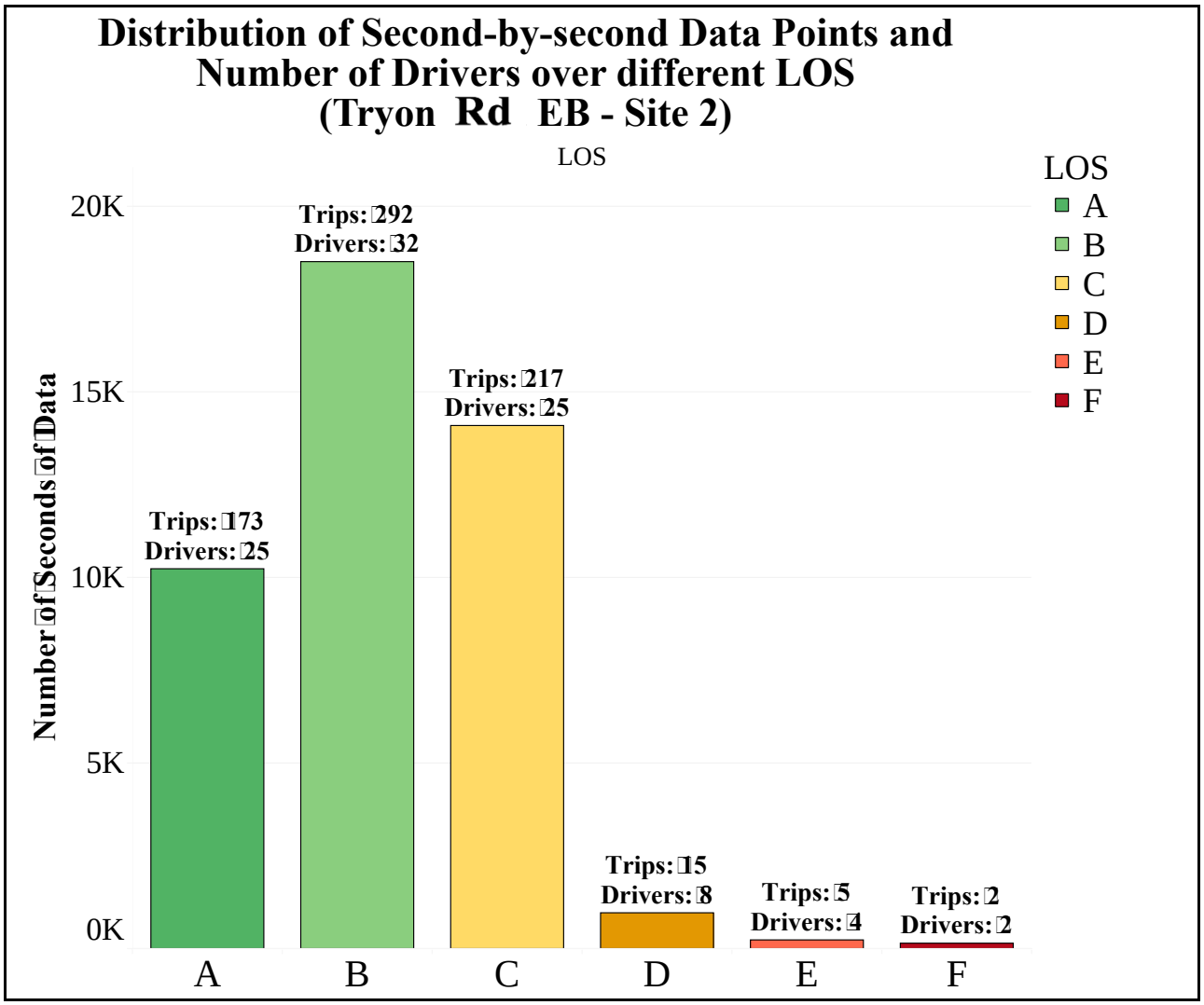

Figure B-9 – Distribution of Second-by-second Data Points and Number of Drivers over Different LOS (Tryon Rd EB – Site 2)

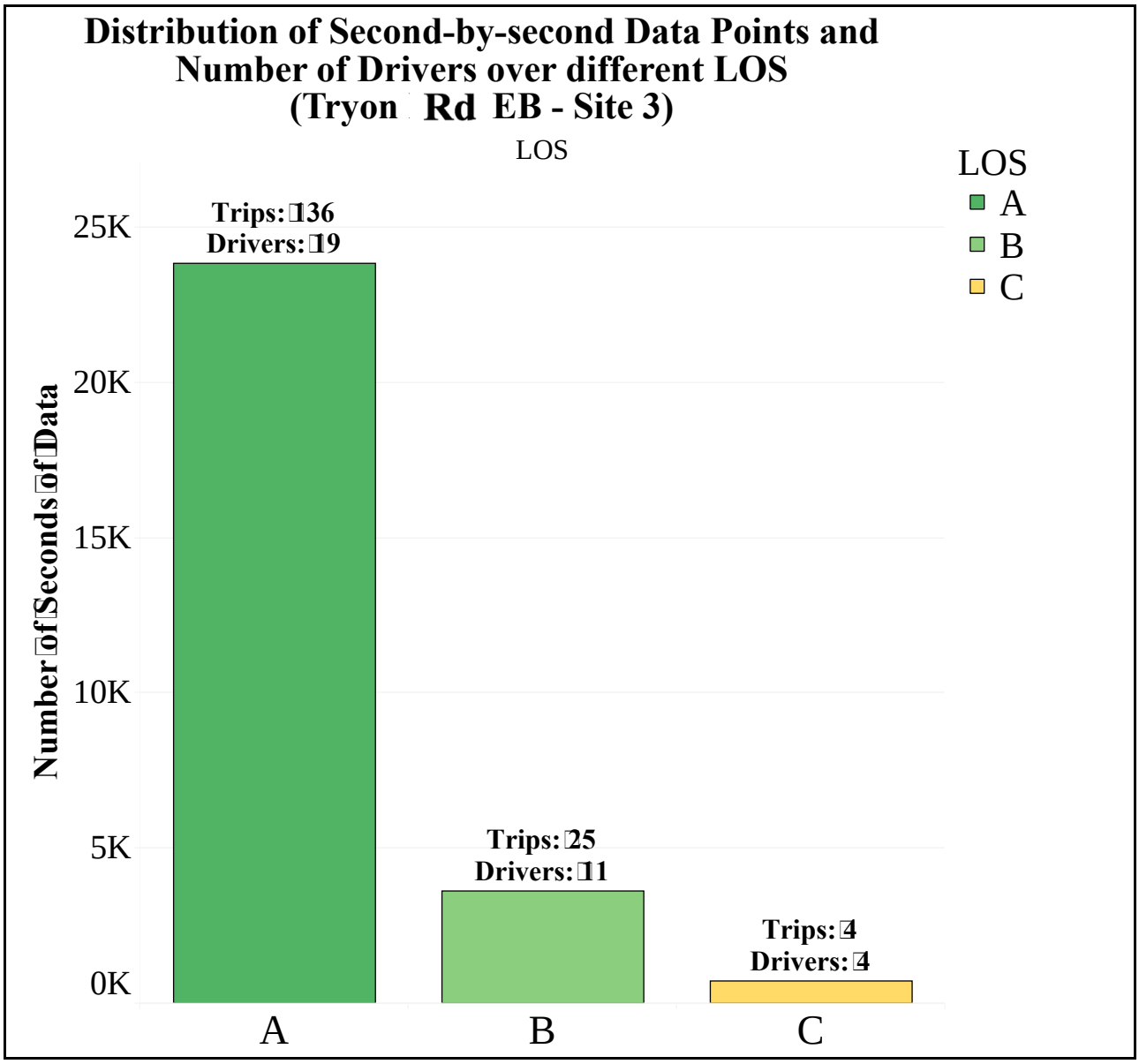

Figure B-10 – Distribution of Second-by-second Data Points and Number of Drivers over Different LOS (Tryon Rd EB – Site 3)

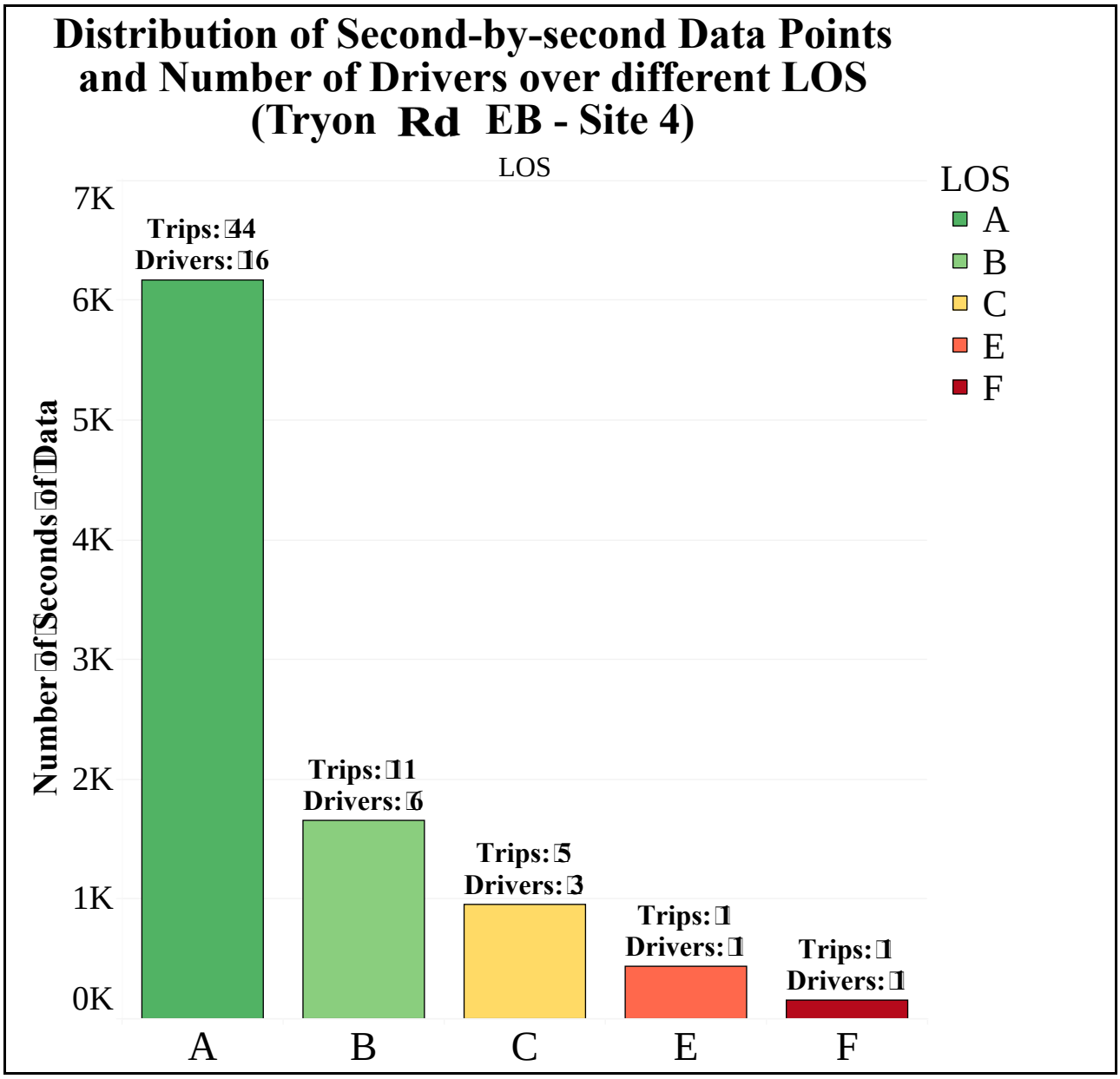

Figure B-11 – Distribution of Second-by-second Data Points and Number of Drivers over Different LOS (Tryon Rd EB – Site 4)

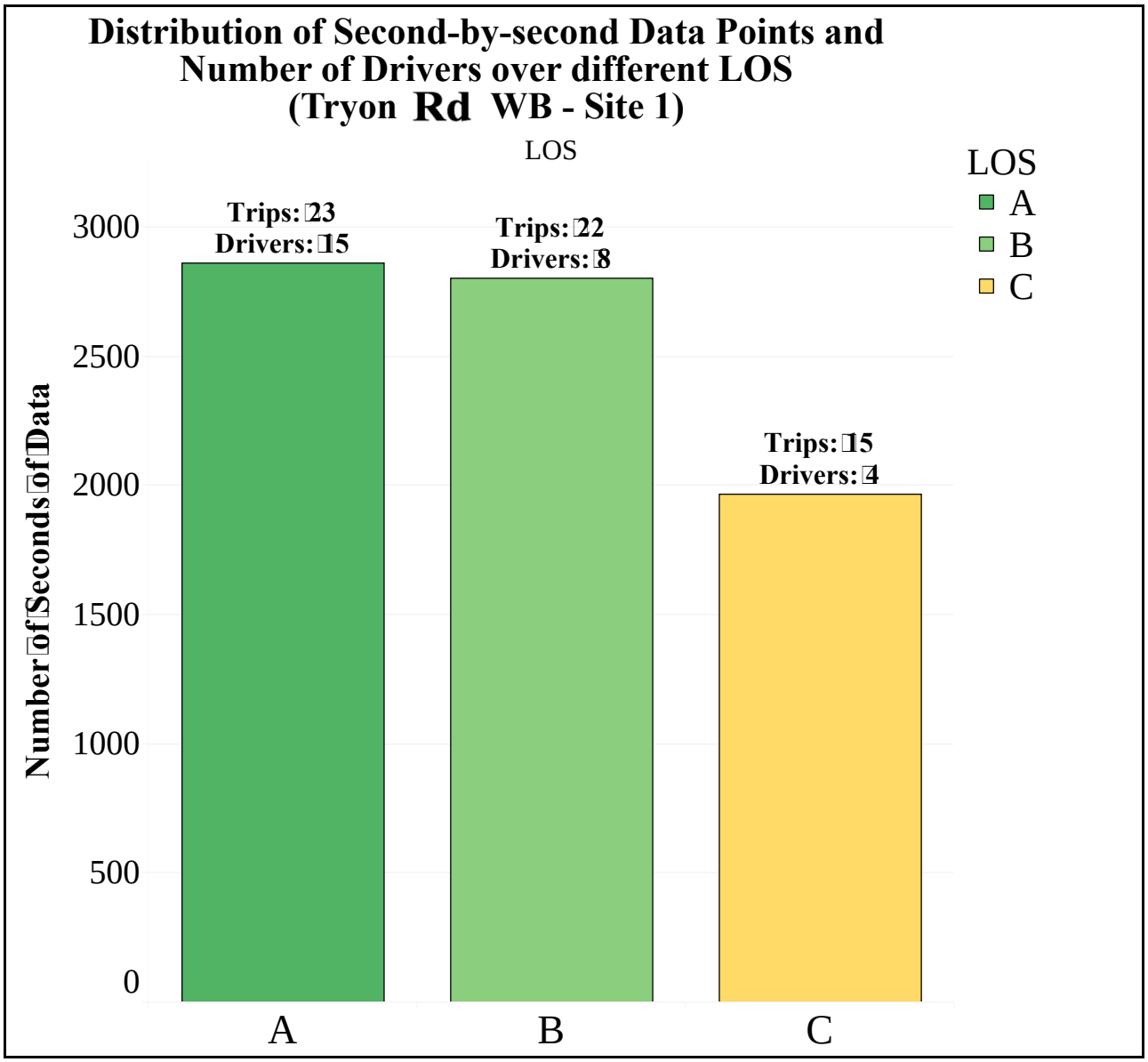

Figure B-12 – Distribution of Second-by-second Data Points and Number of Drivers over Different LOS (Tryon Rd WB – Site 1)

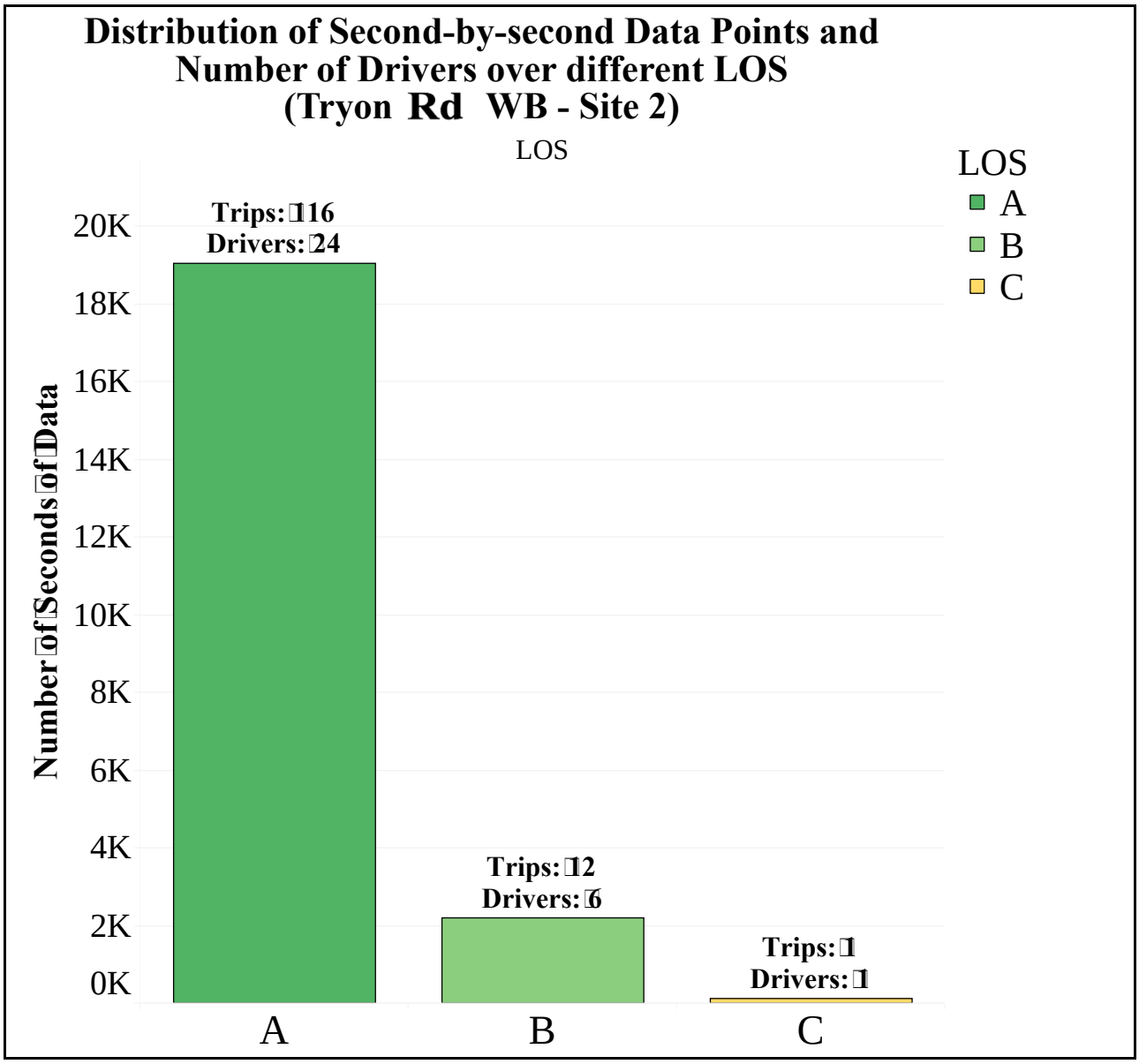

Figure B-13 – Distribution of Second-by-second Data Points and Number of Drivers over Different LOS (Tryon Rd WB – Site 2)

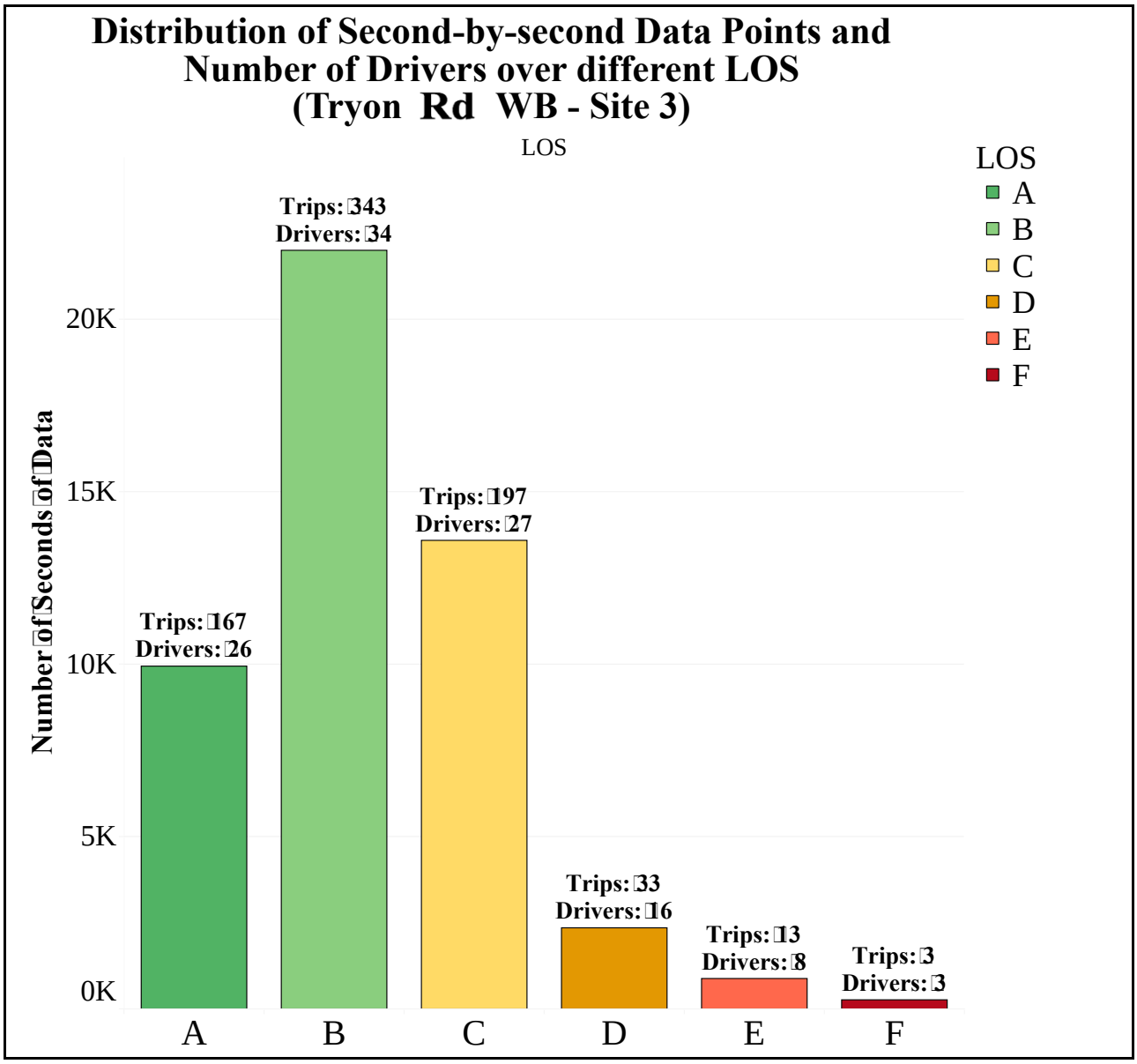

Figure B-14 – Distribution of Second-by-second Data Points and Number of Drivers over Different LOS (Tryon Rd WB – Site 3)

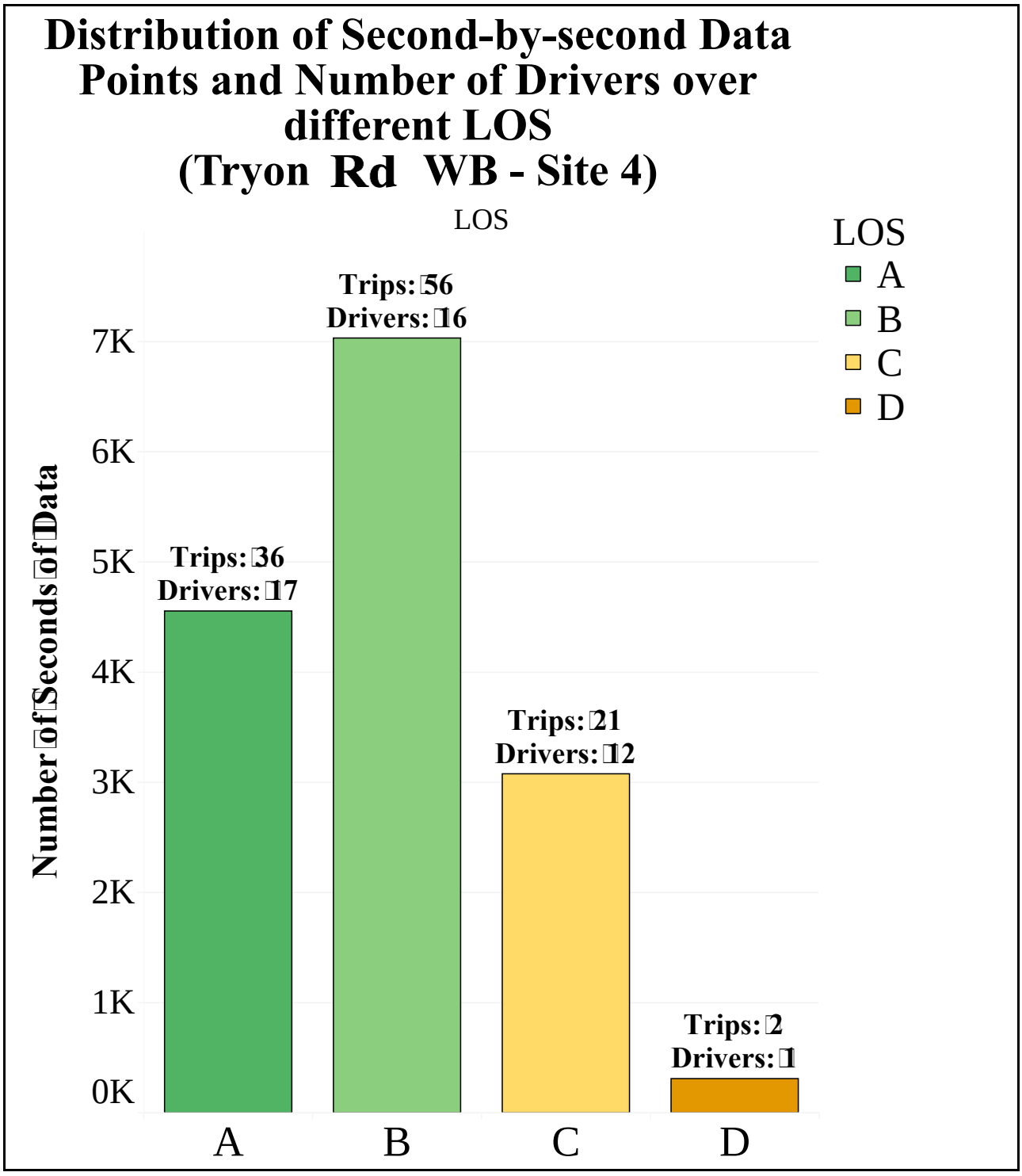

Figure B-15 – Distribution of Second-by-second Data Points and Number of Drivers over Different LOS (Tryon Rd WB – Site 4)

APPENDIX D - DISTRIBUTION OF TRIPS AND LOS OVER HOUR OF DAY

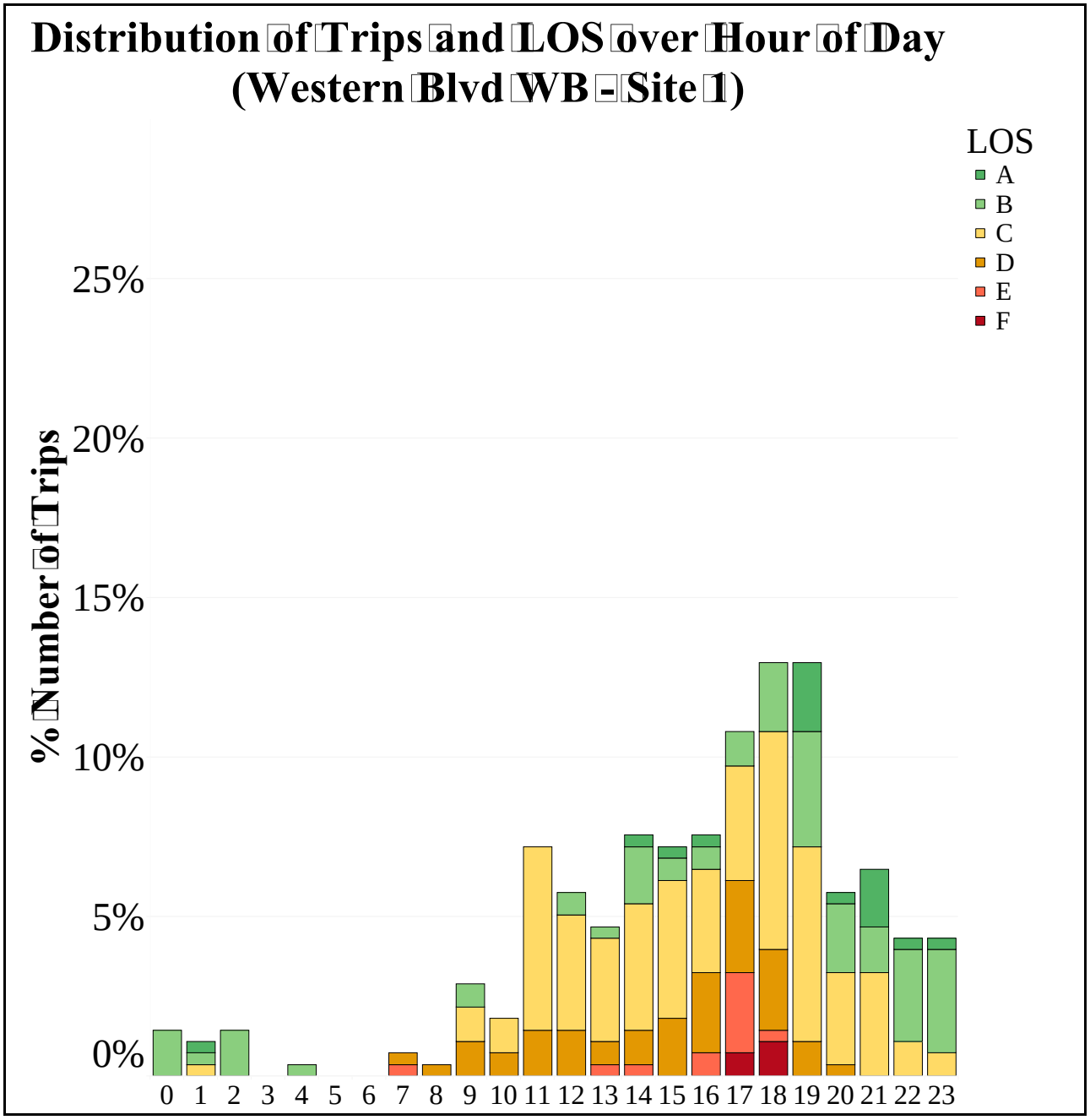

Figure D-1 – Distribution of Trips and LOS over Hour of Day (Western Blvd WB – Site 1)

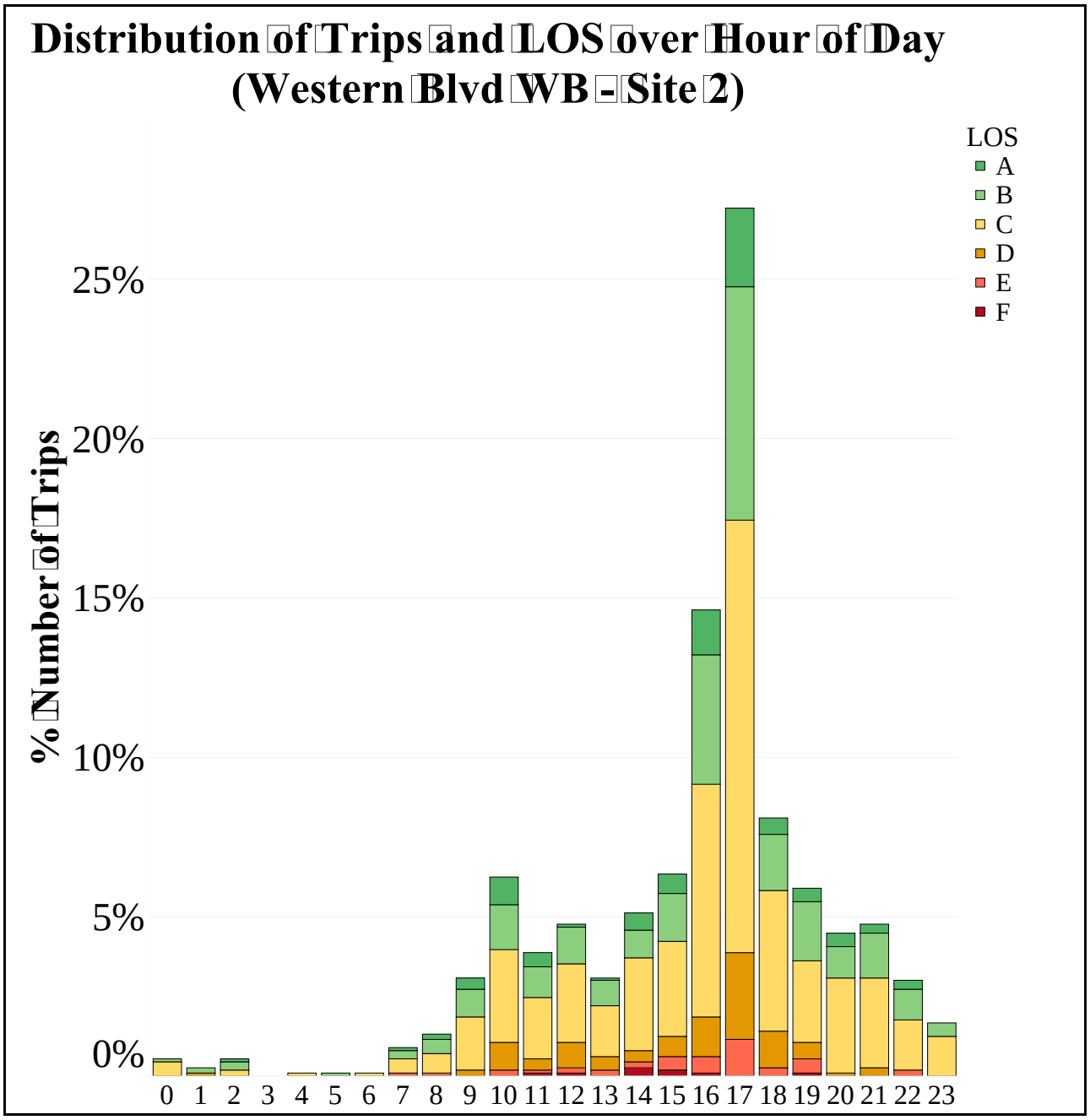

Figure D-2 – Distribution of Trips and LOS over Hour of Day (Western Blvd WB – Site 2)

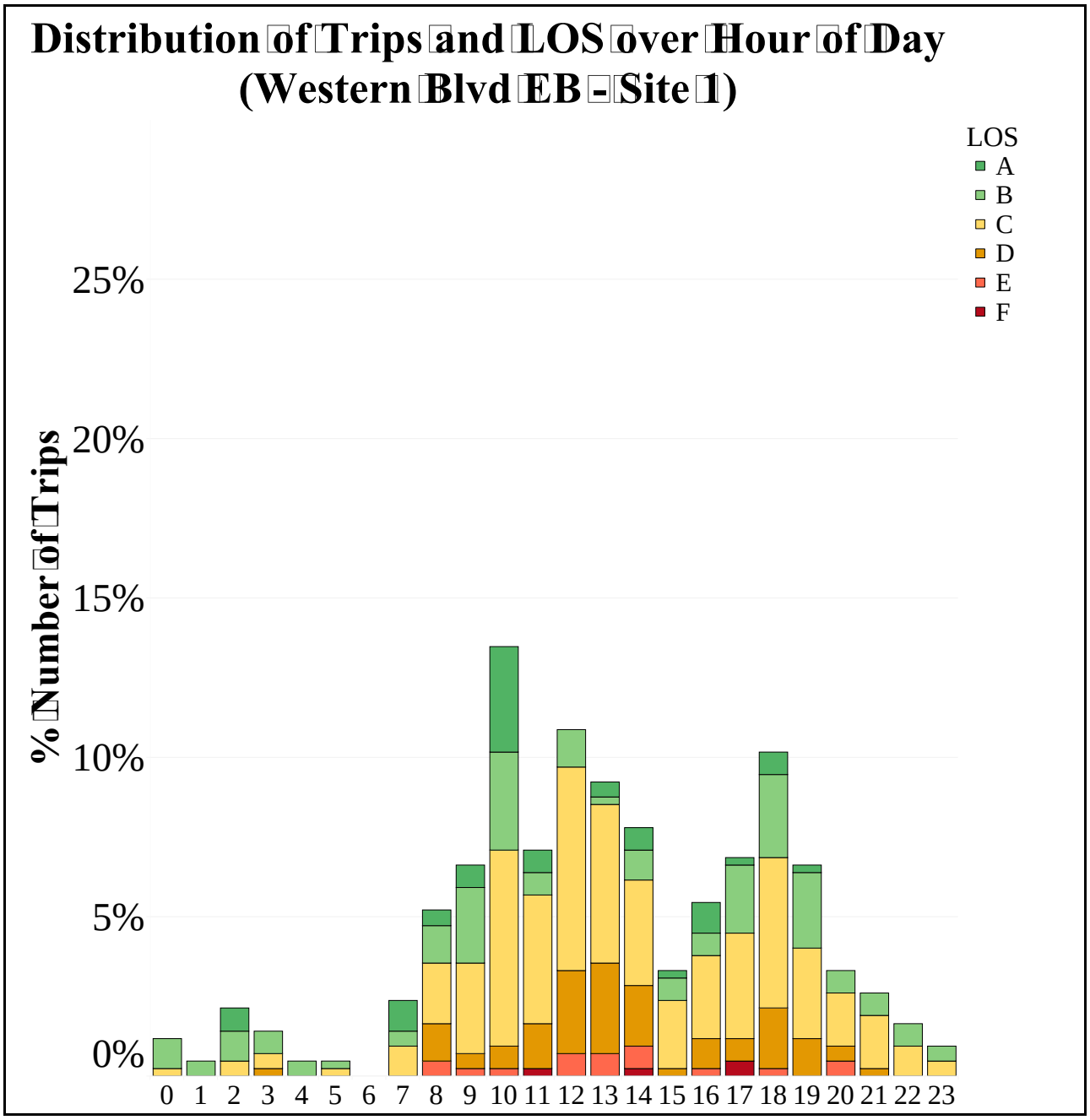

Figure D-3 – Distribution of Trips and LOS over Hour of Day (Western Blvd EB – Site 1)

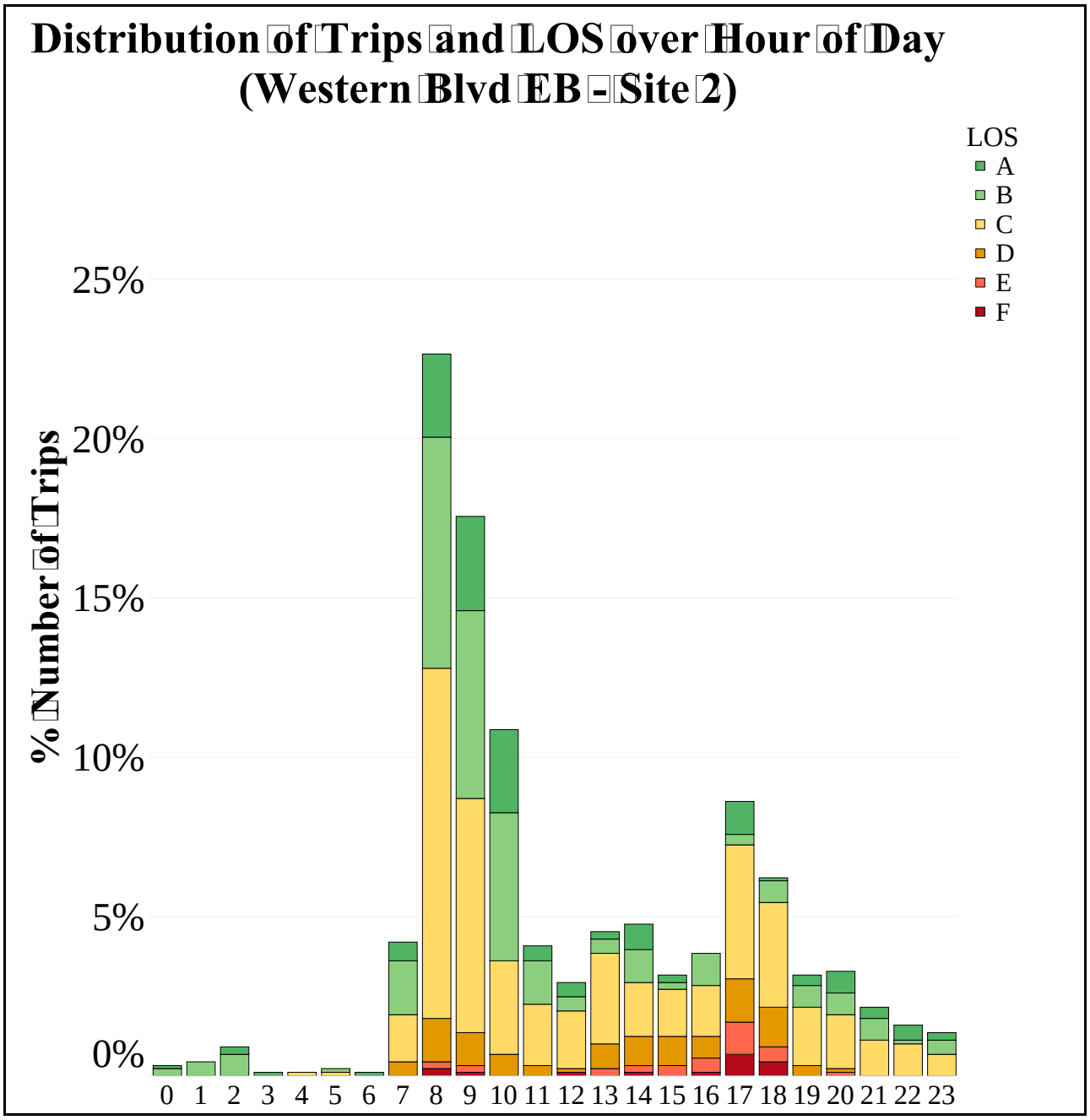

Figure D-4 – Distribution of Trips and LOS over Hour of Day (Western Blvd EB – Site 2)

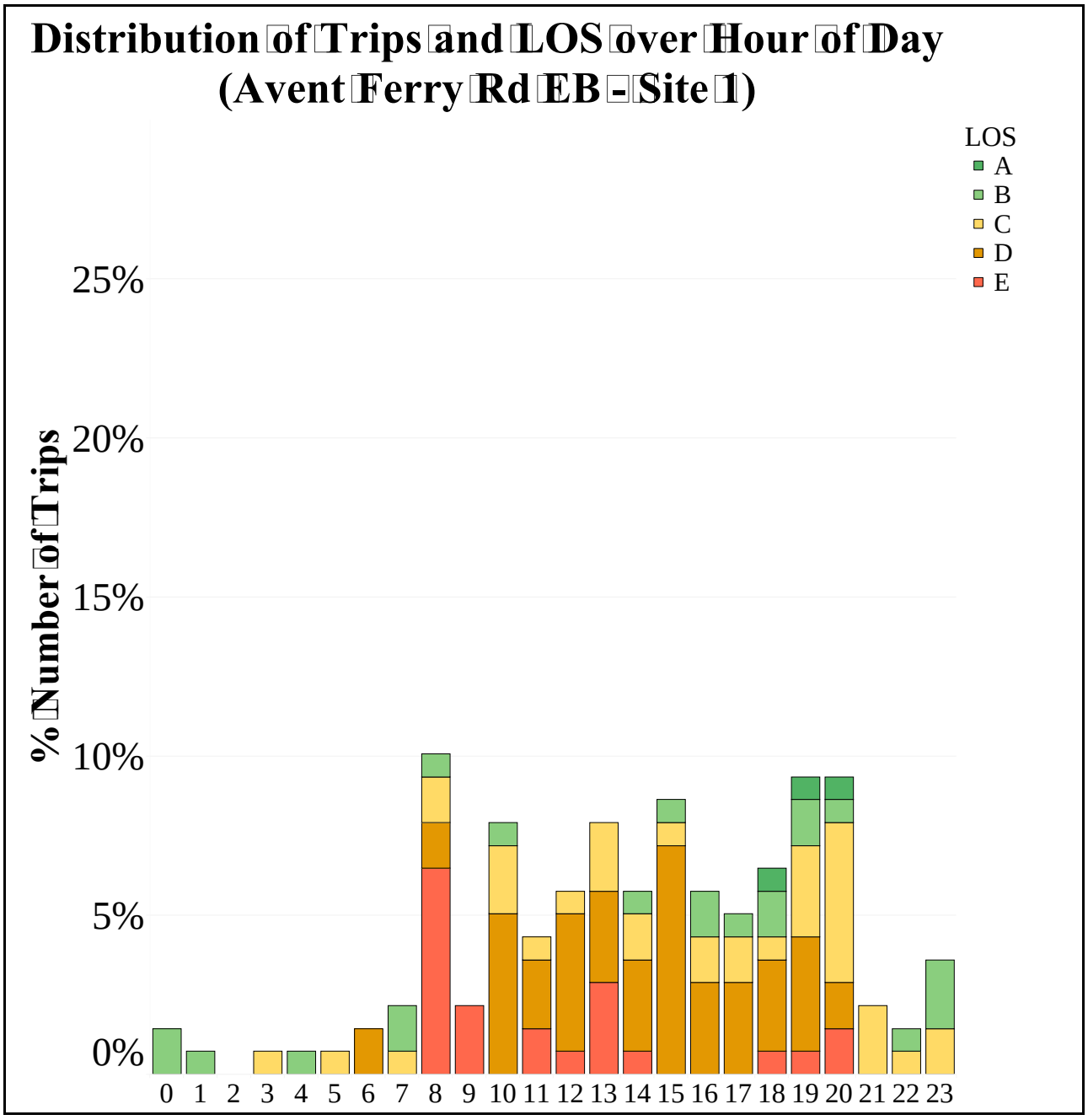

Figure D-5 – Distribution of Trips and LOS over Hour of Day (Avent Ferry Rd EB – Site 1)

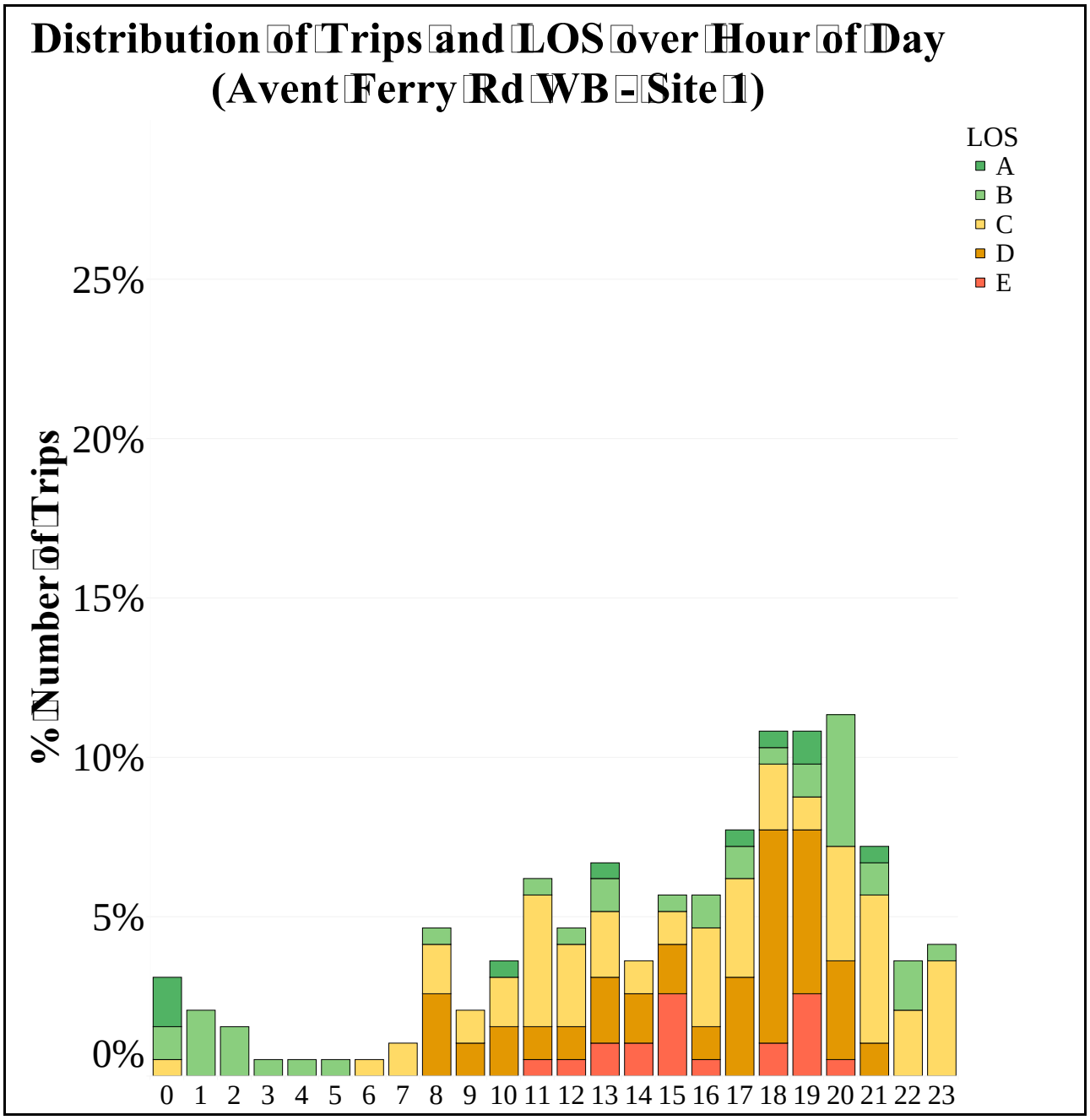

Figure D-6 – Distribution of Trips and LOS over Hour of Day (Avent Ferry Rd WB – Site 1)

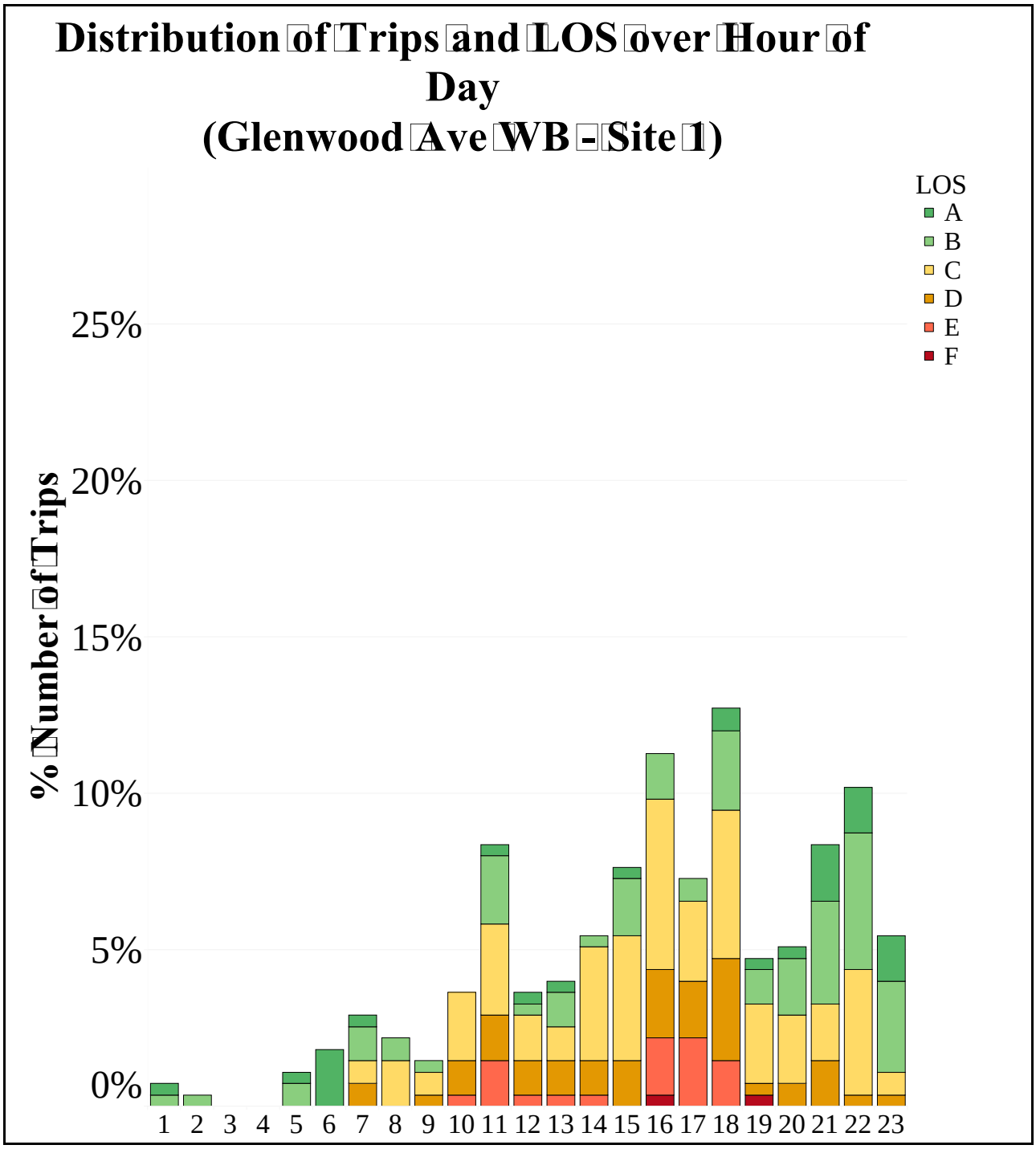

Figure D-7 – Distribution of Trips and LOS over Hour of Day (Glenwood Ave WB – Site 1)

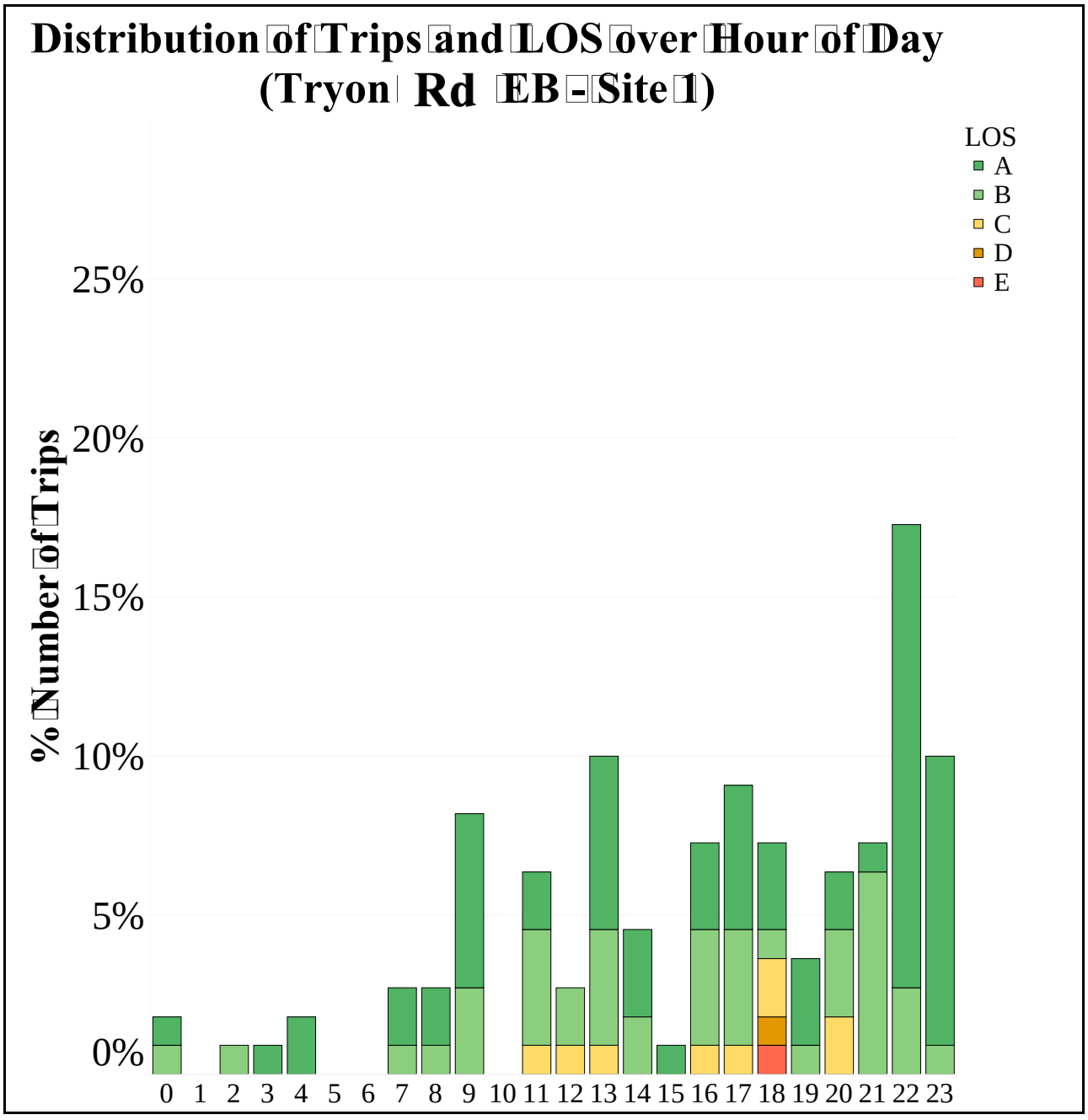

Figure D-8 – Distribution of Trips and LOS over Hour of Day (Tryon Rd EB – Site 1)

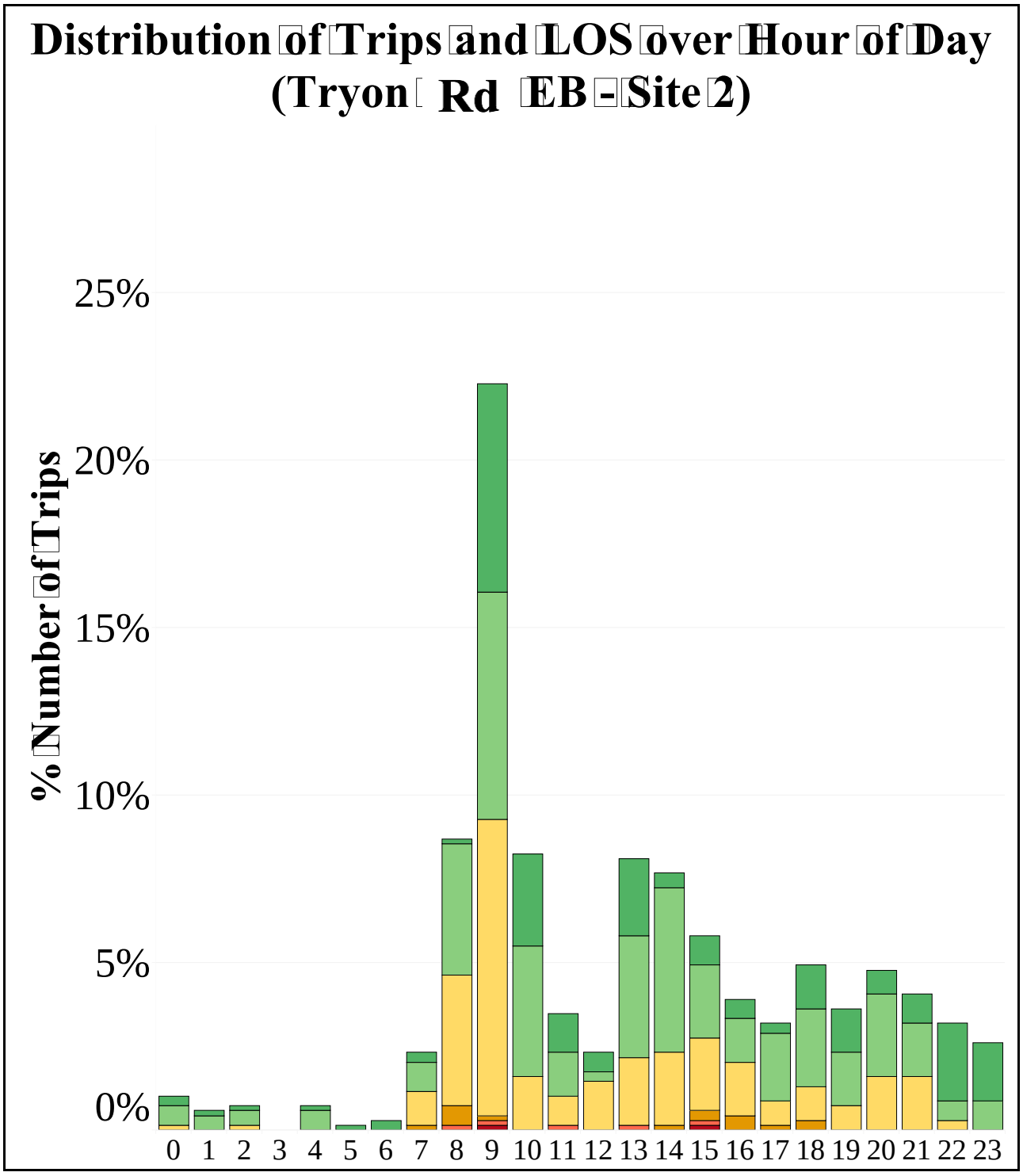

Figure D-9 – Distribution of Trips and LOS over Hour of Day
(Tryon Rd EB – Site 2)

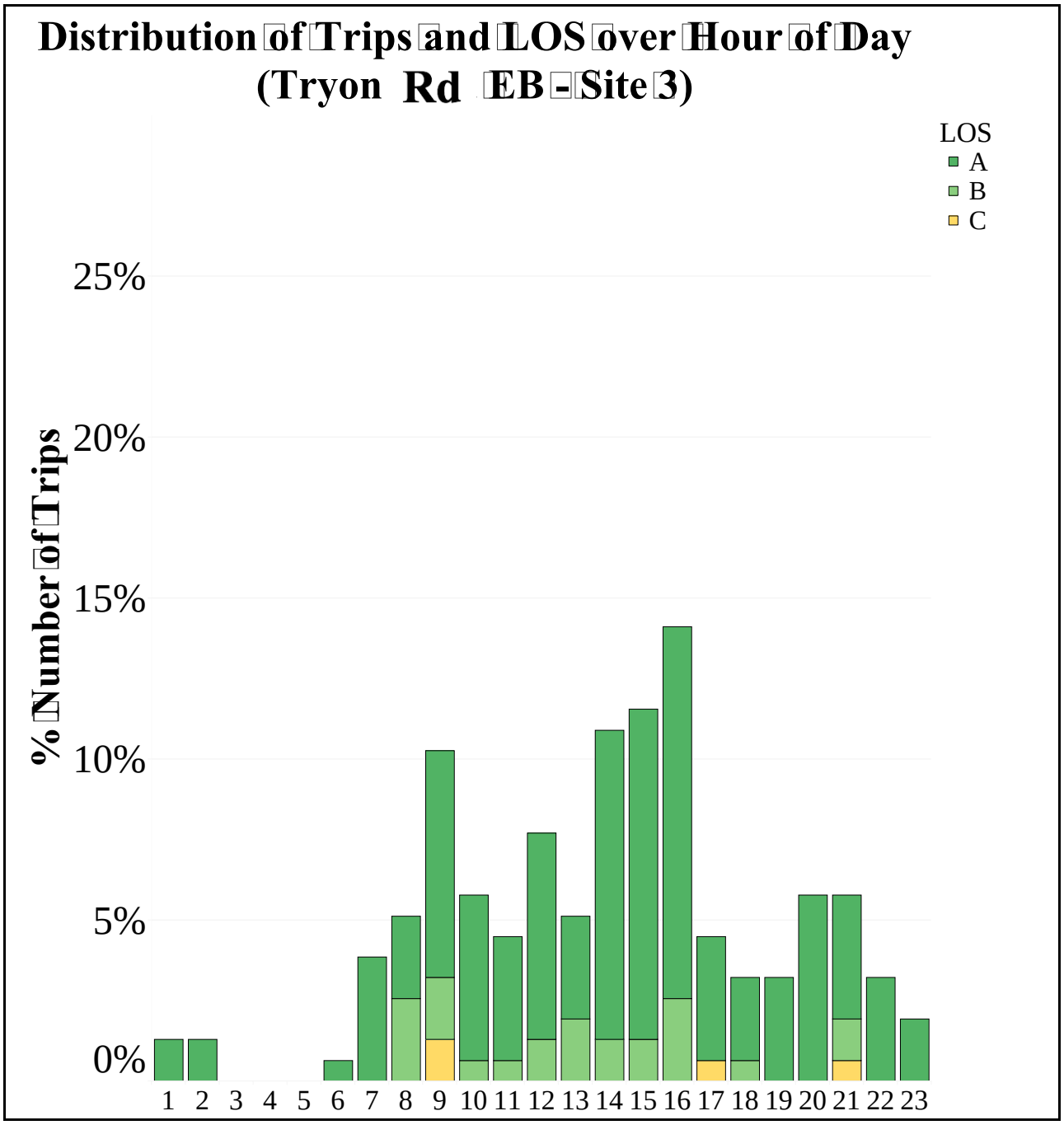

Figure D-10 – Distribution of Trips and LOS over Hour of Day (Tryon Rd EB – Site 3)

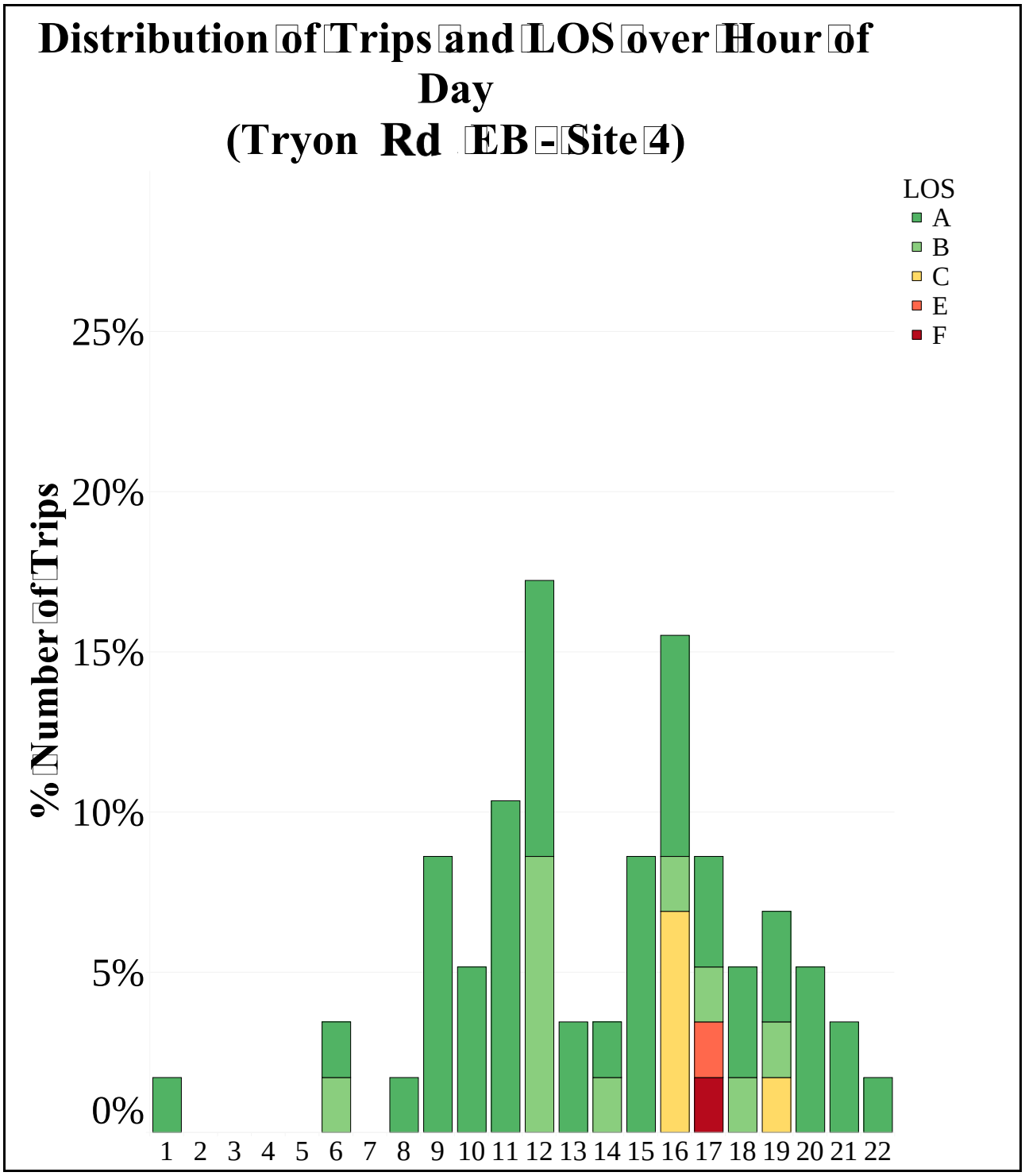

Figure D-11 – Distribution of Trips and LOS over Hour of Day (Tryon Rd EB – Site 4)

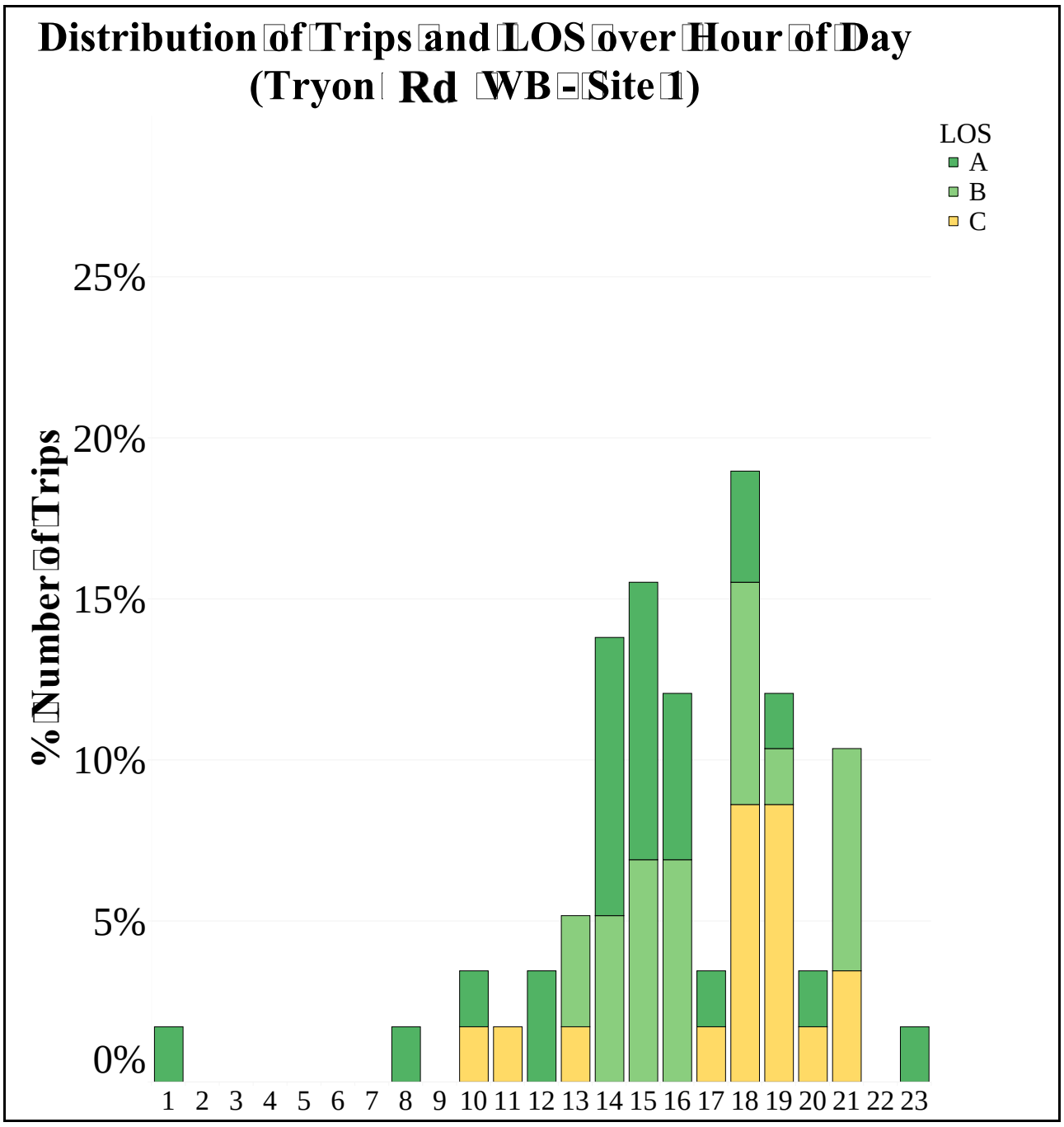

Figure D-12 – Distribution of Trips and LOS over Hour of Day (Tryon Rd WB – Site 1)

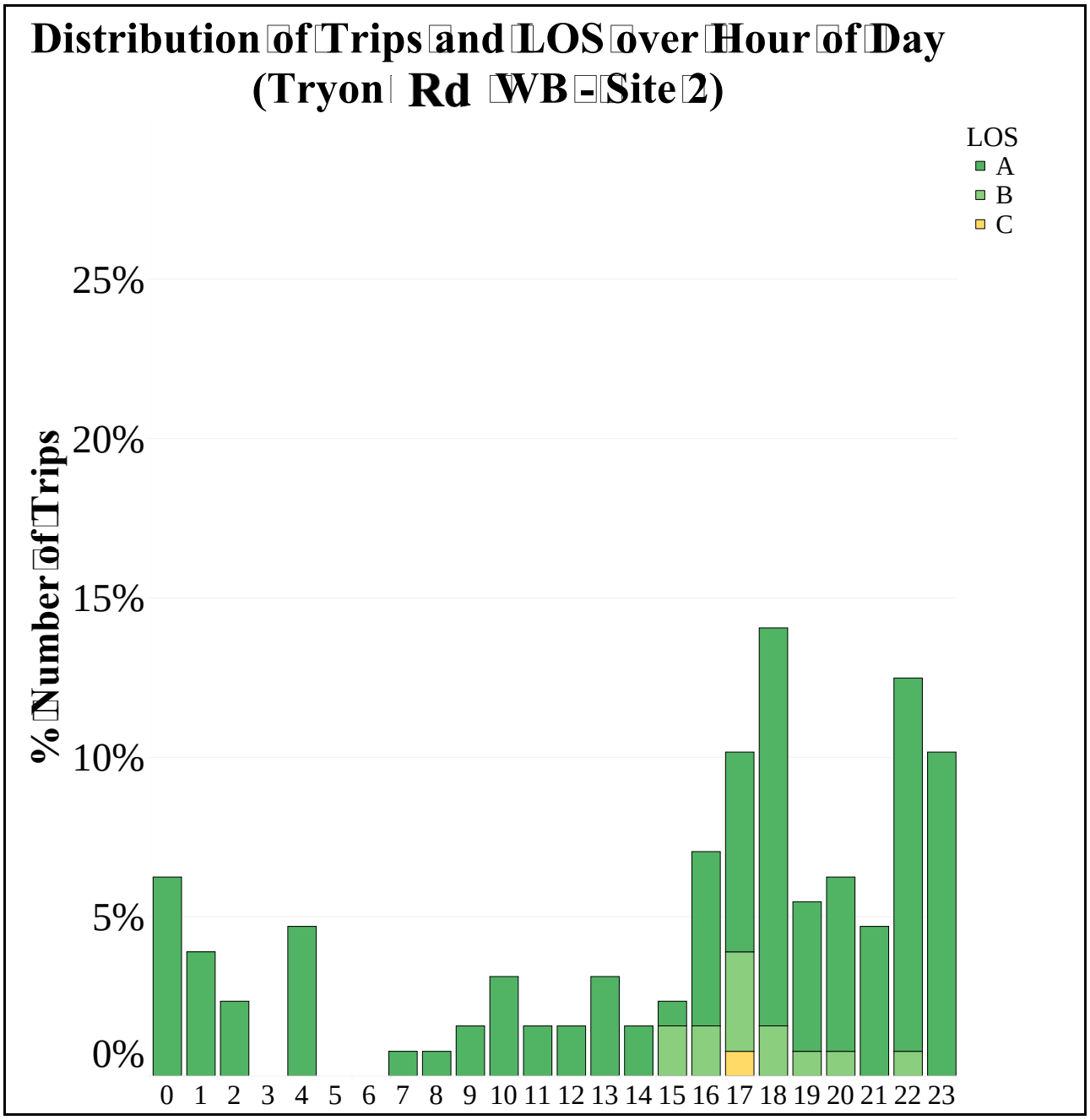

Figure D-13 – Distribution of Trips and LOS over Hour of Day (Tryon Rd WB – Site 2)

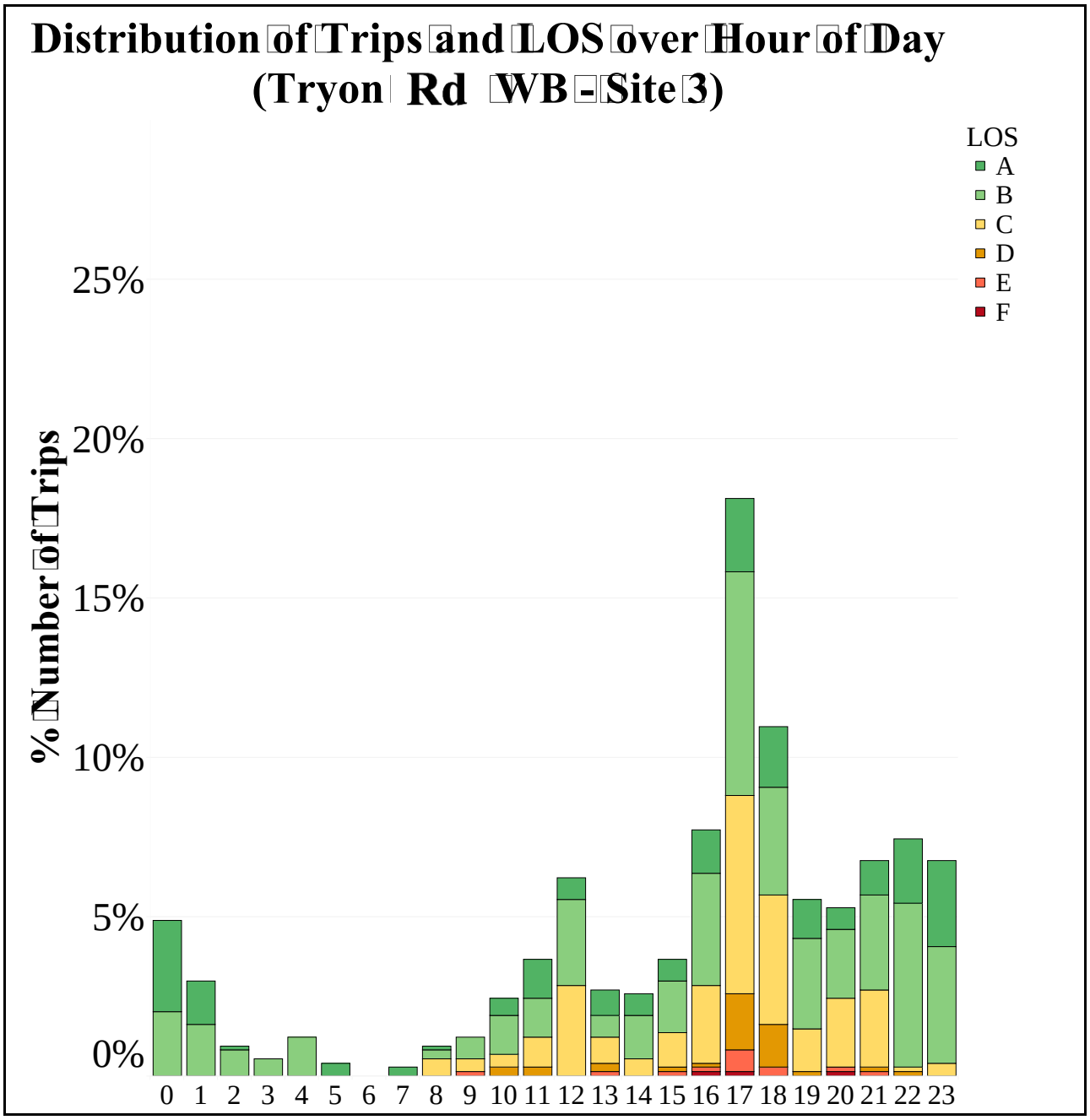

Figure D-14 – Distribution of Trips and LOS over Hour of Day (Tryon Rd WB – Site 3)

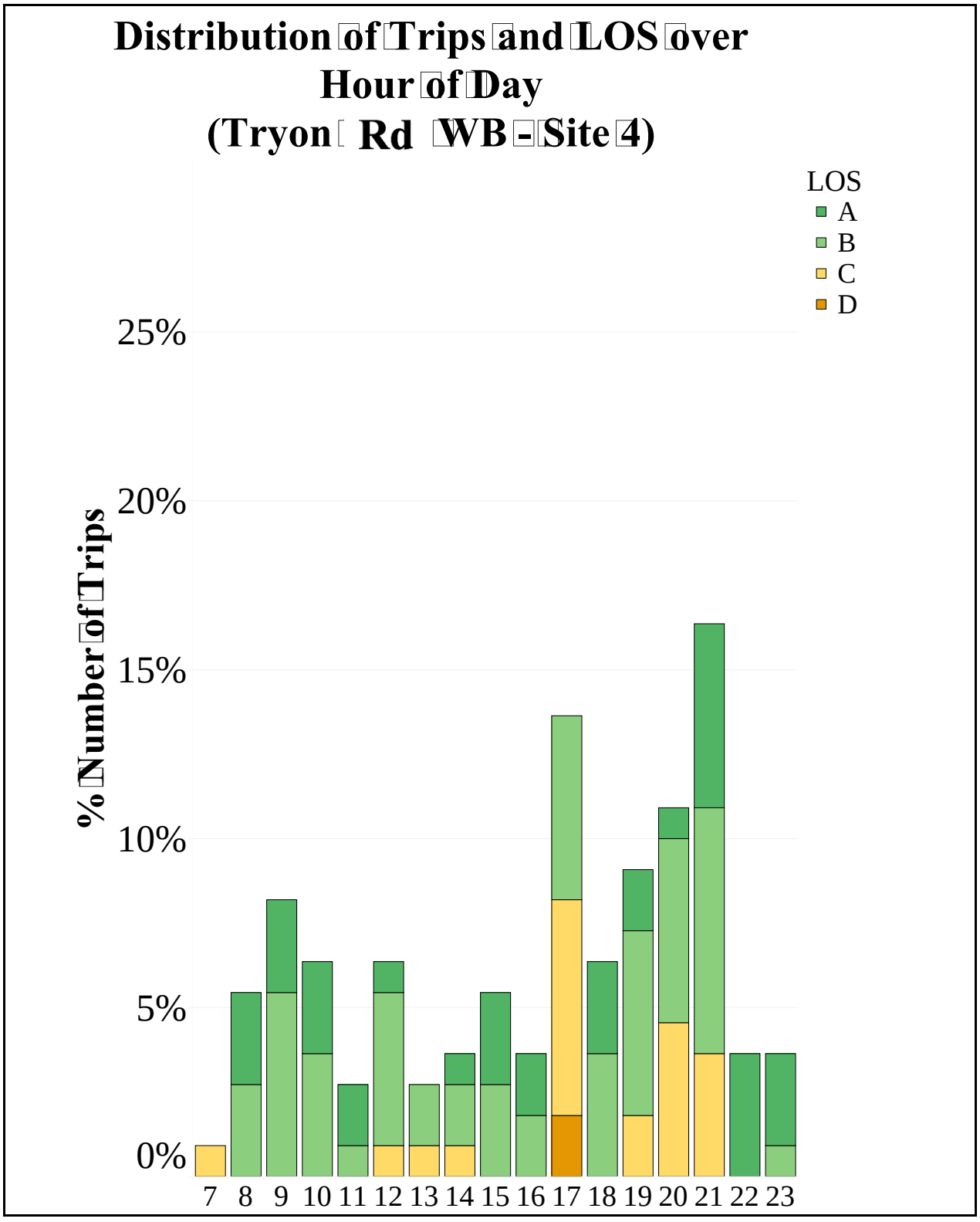

Figure D-15 – Distribution of Trips and LOS over Hour of Day (Tryon Rd WB – Site 4)

APPENDIX E - BOXPLOT OF 3 D COMBINED ACCELERATION OVER DIFFERENT LOS

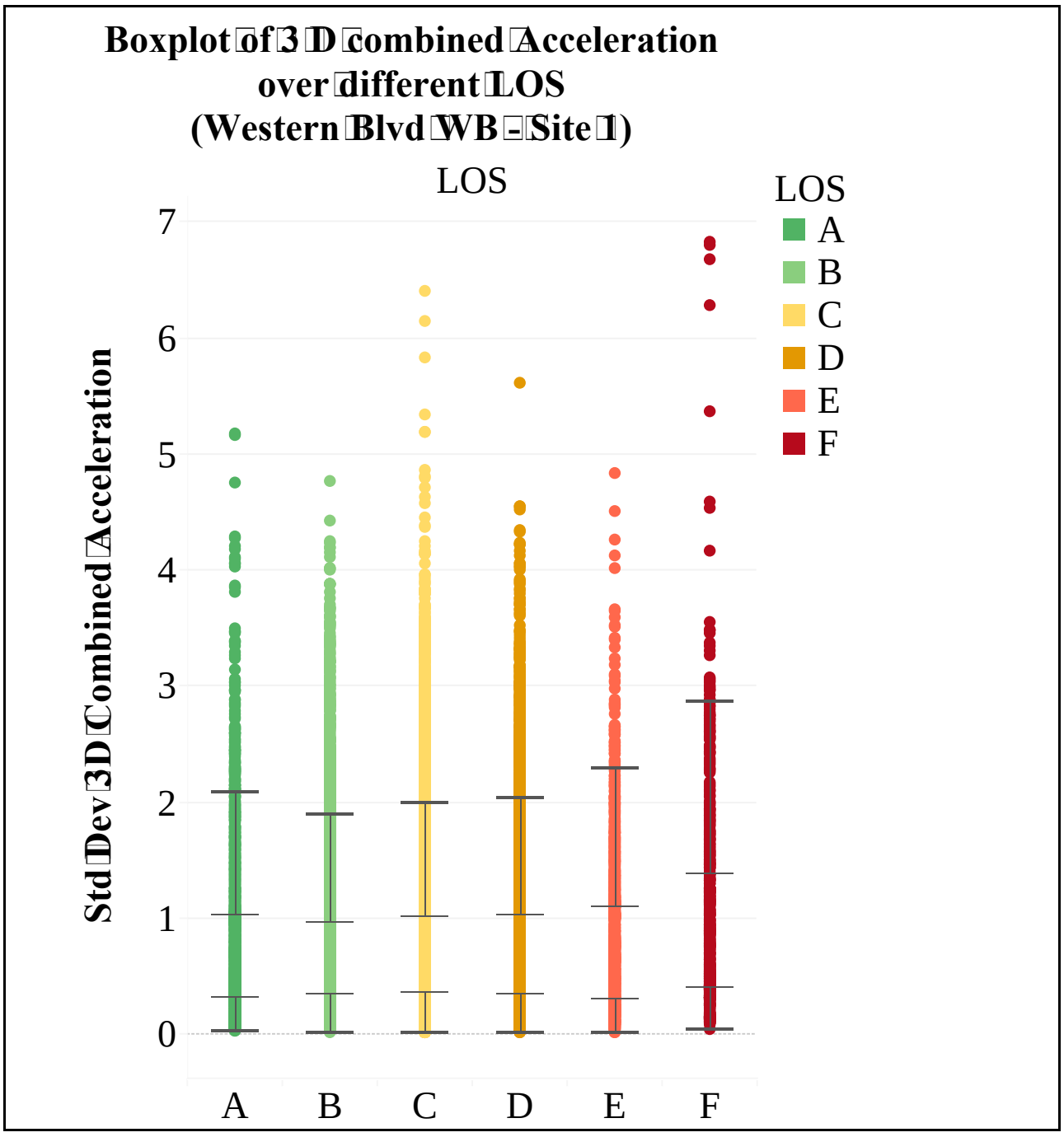

Figure E-1 – Boxplot of 3-D Combined Acceleration over different LOS (Western Blvd WB – Site 1)

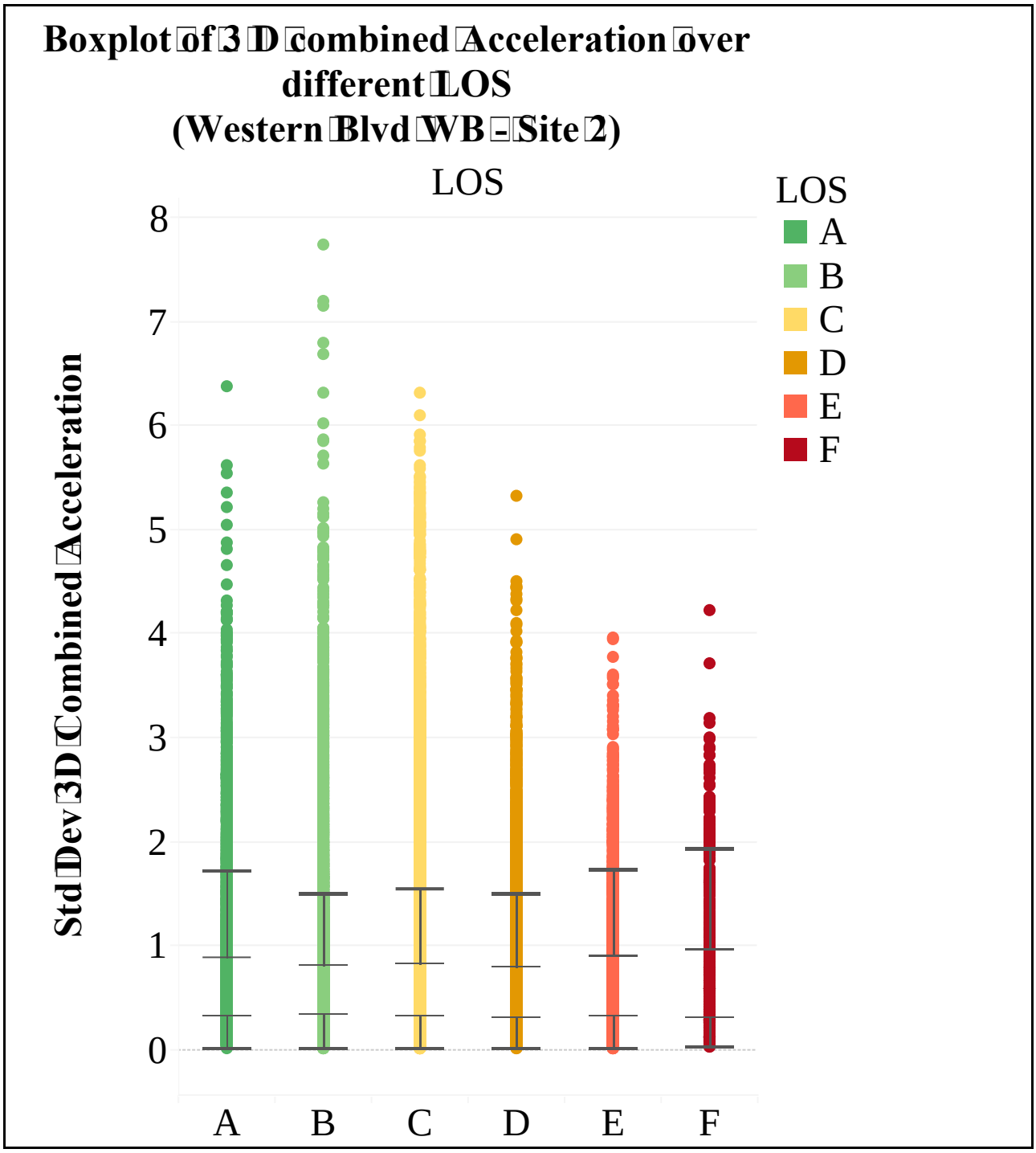

Figure E-2 – Boxplot of 3-D Combined Acceleration over different LOS (Western Blvd WB – Site 2)

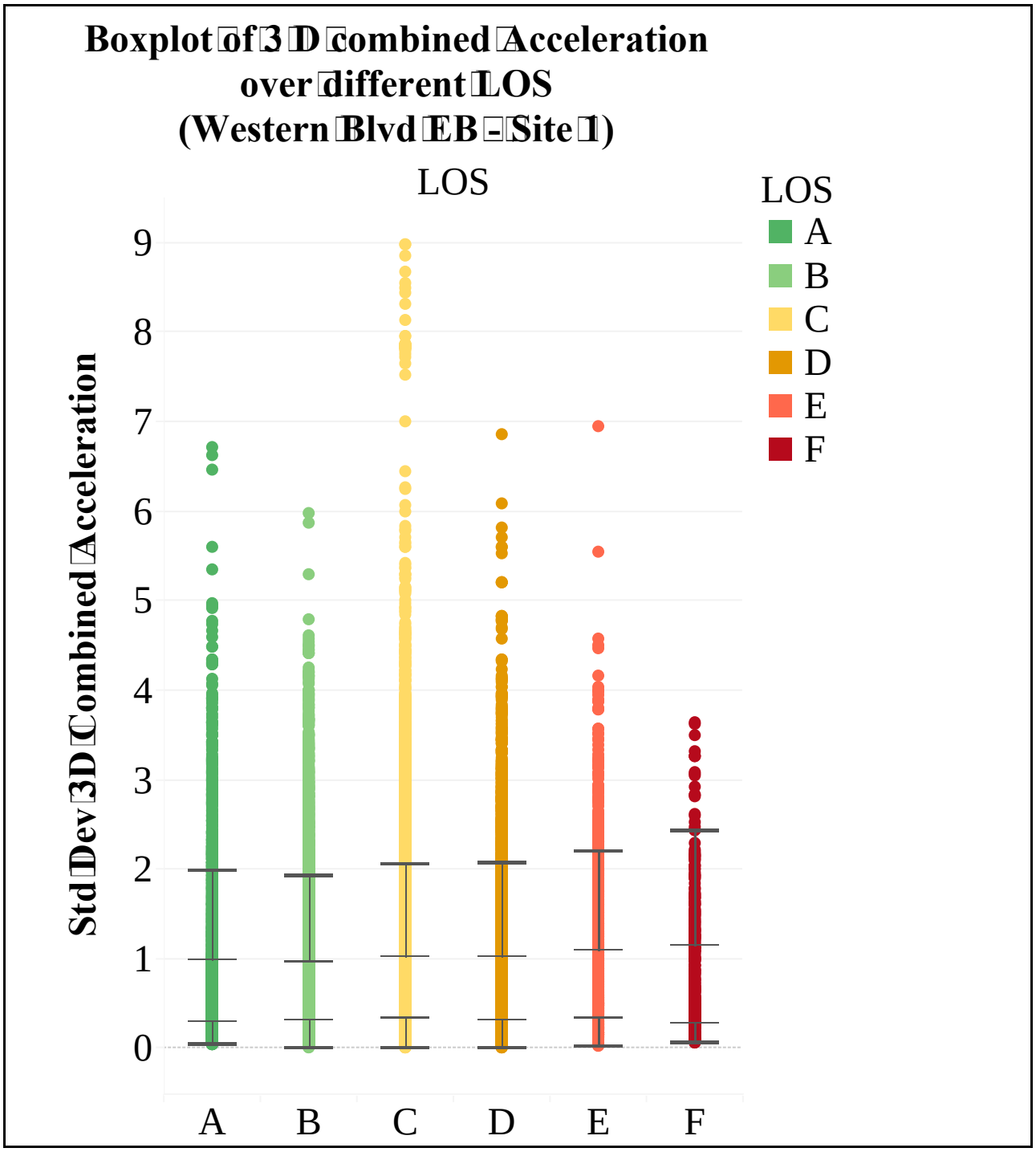

Figure E-3 – Boxplot of 3-D Combined Acceleration over different LOS (Western Blvd EB – Site 1)

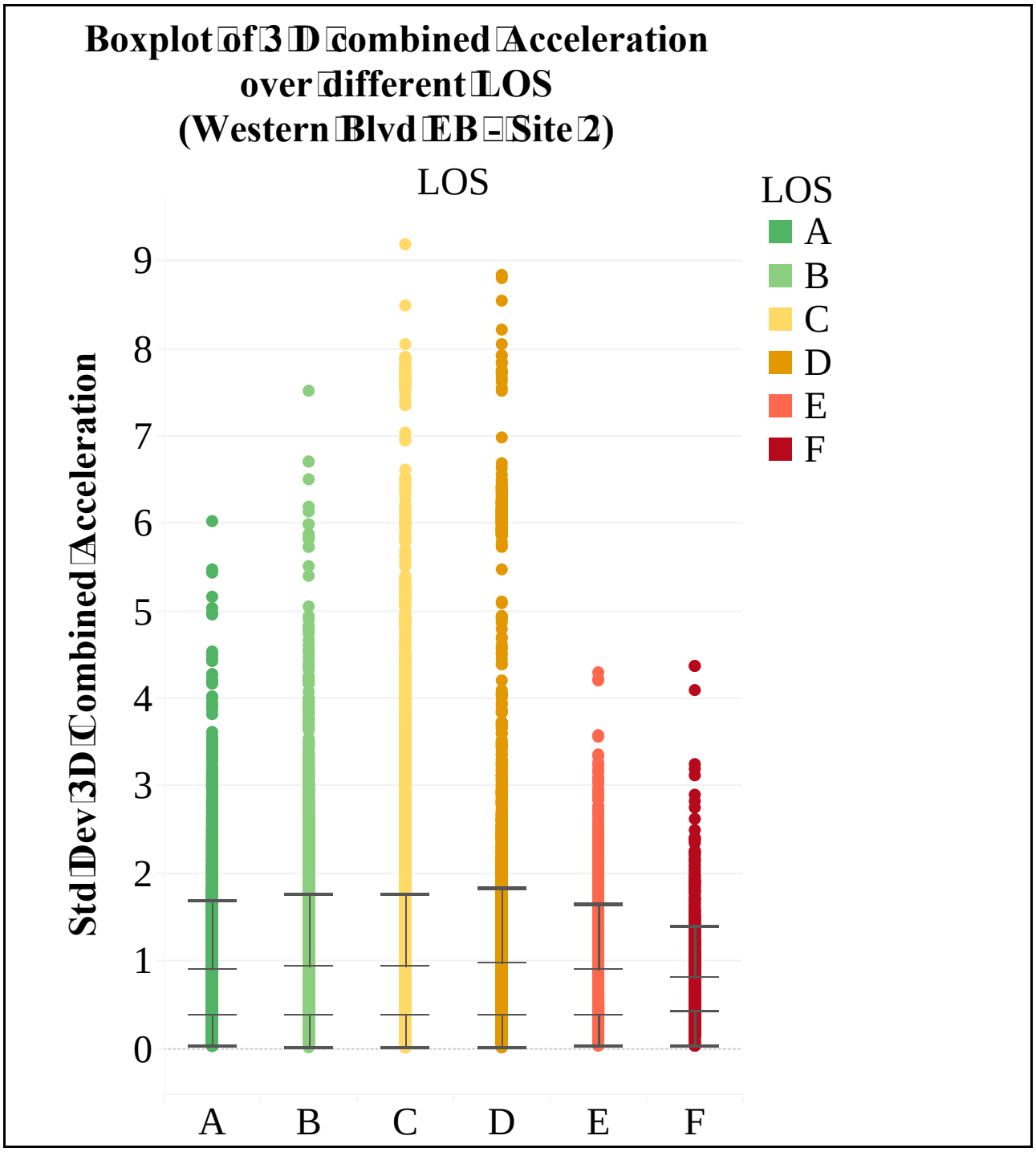

Figure E-4 – Boxplot of 3-D Combined Acceleration over different LOS (Western Blvd EB – Site 2)

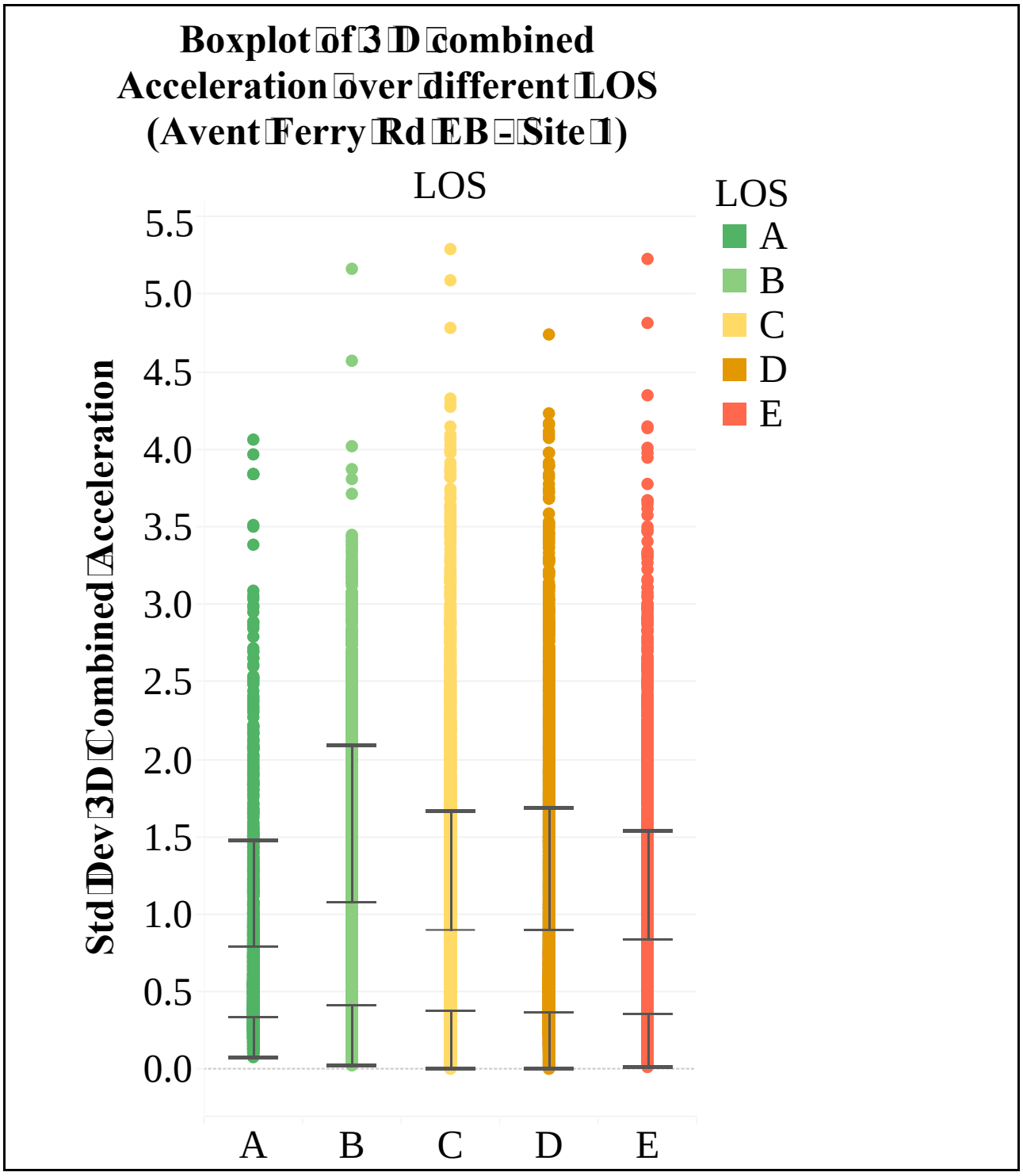

Figure E-5 – Boxplot of 3-D Combined Acceleration over different LOS (Avent Ferry Rd EB – Site 1)

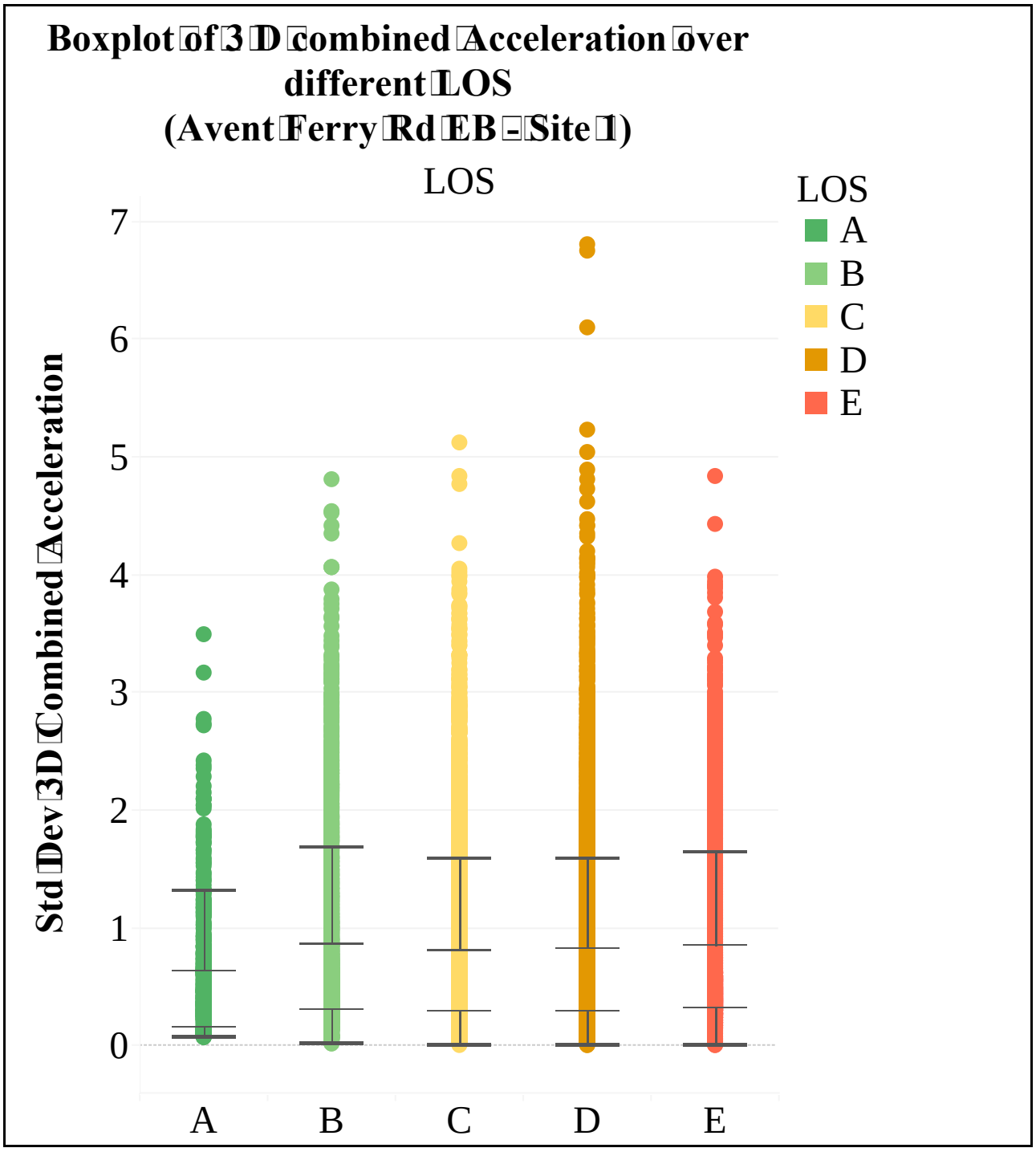

Figure E-6 – Boxplot of 3-D Combined Acceleration over different LOS (Avent Ferry Rd WB – Site 1)

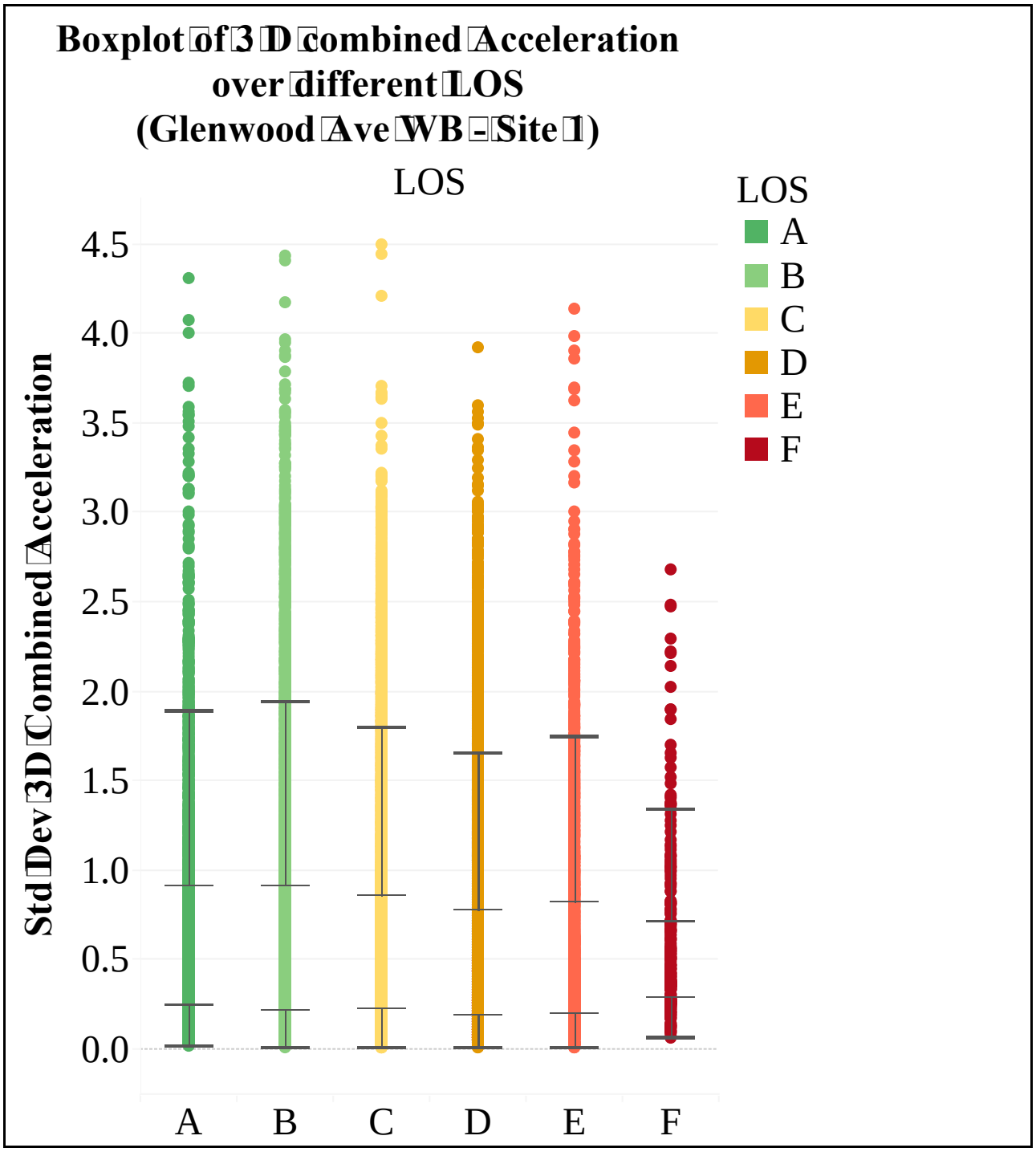

Figure Error! No text of specified style in document.**-7 – Boxplot of 3-D Combined Acceleration over different LOS (Glenwood Ave WB – Site 1)**

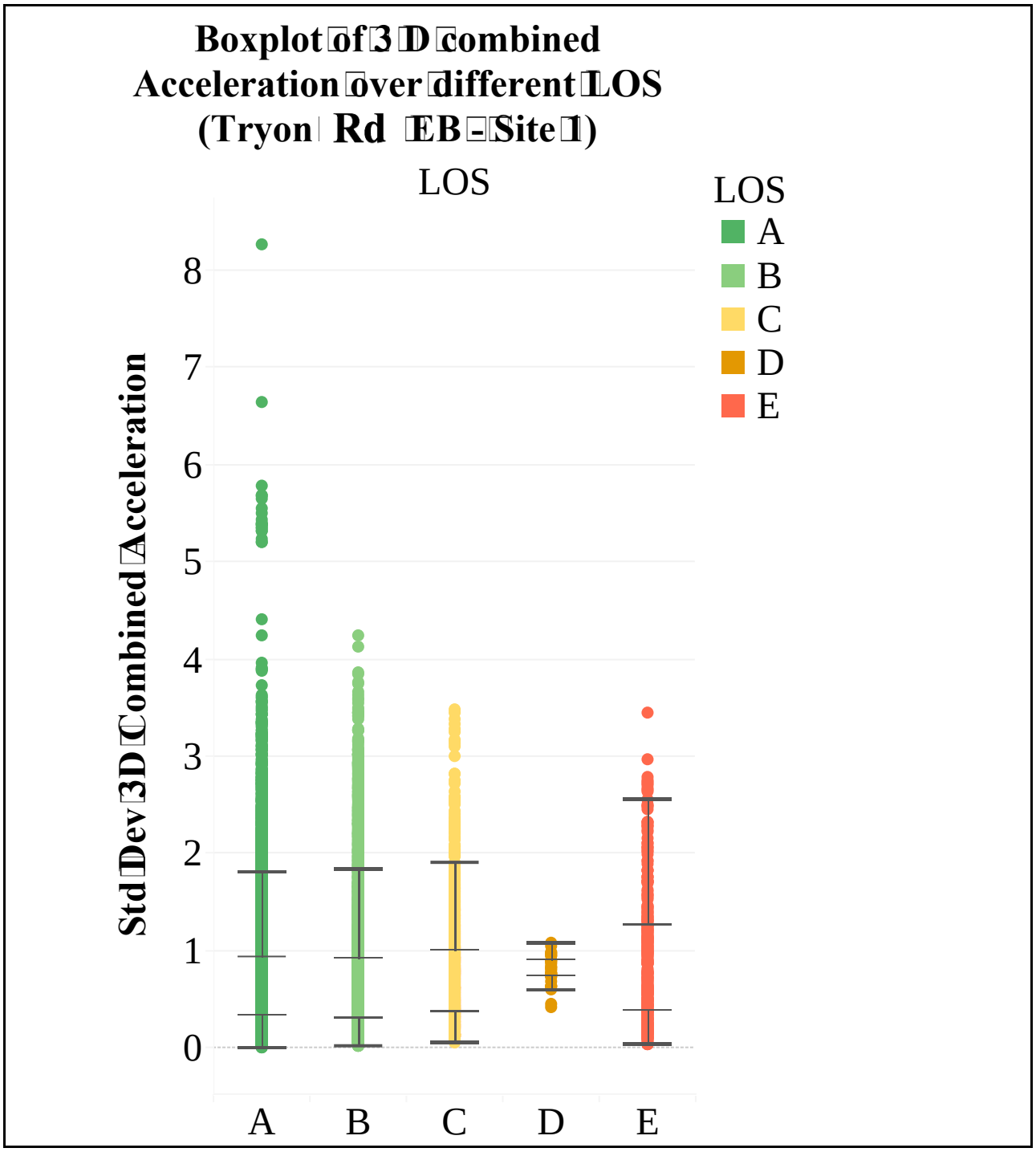

Figure E-8 – Boxplot of 3-D Combined Acceleration over different LOS (Tryon Rd EB – Site 1)

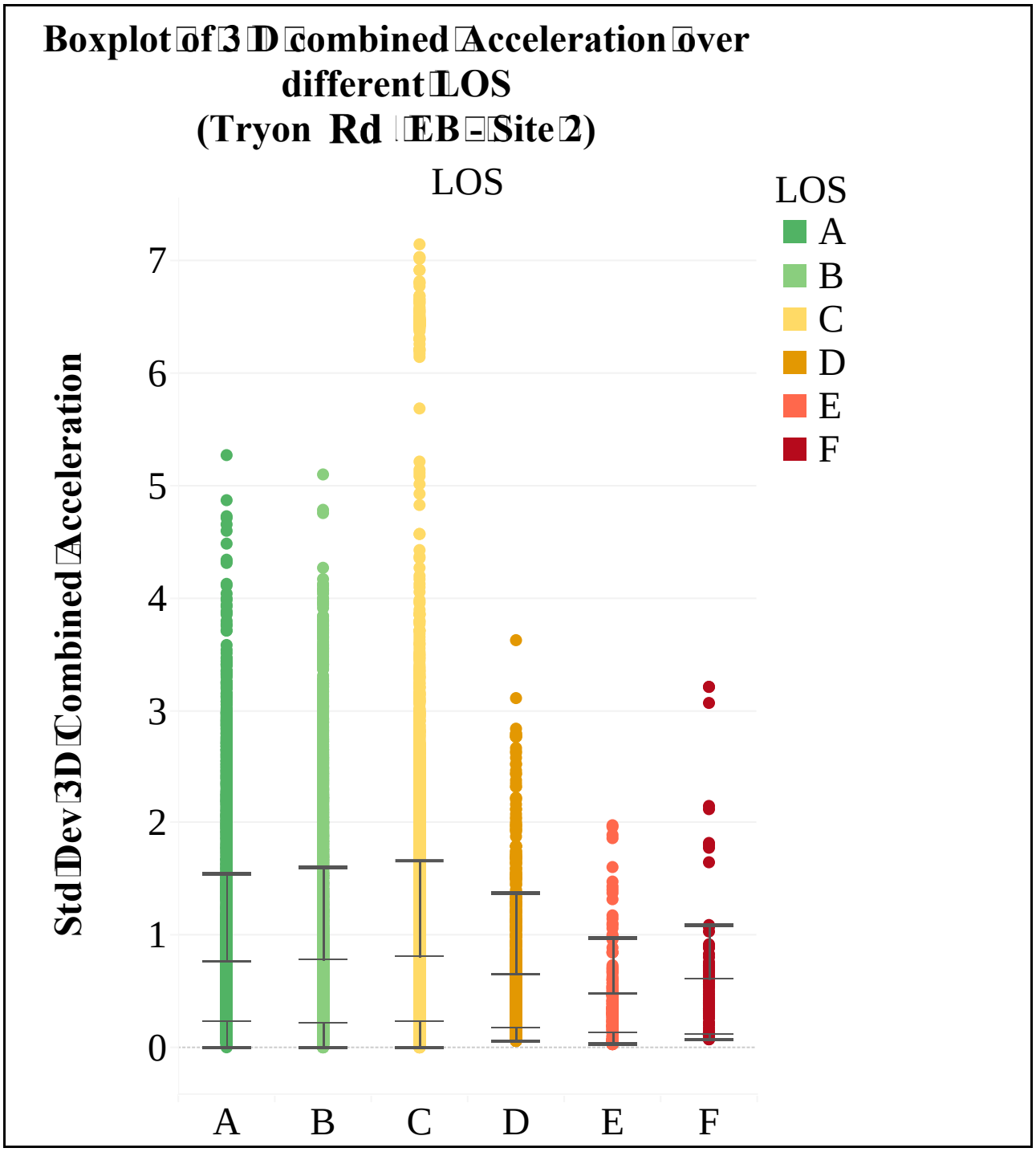

Figure E-9 – Boxplot of 3-D Combined Acceleration over different LOS (Tryon Rd EB – Site 2)

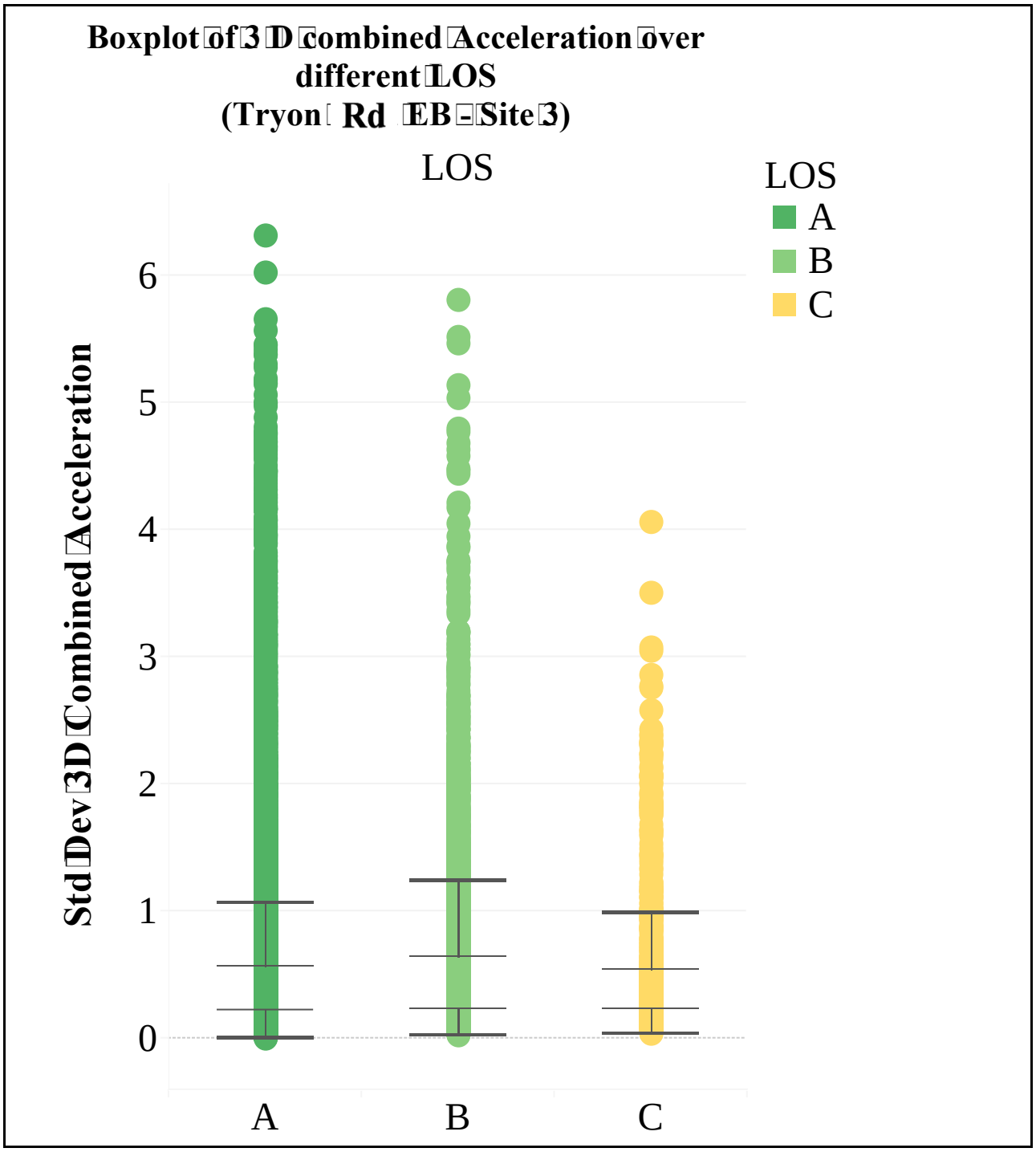

Figure E-10 – Boxplot of 3-D Combined Acceleration over different LOS (Tryon Rd EB – Site 3)

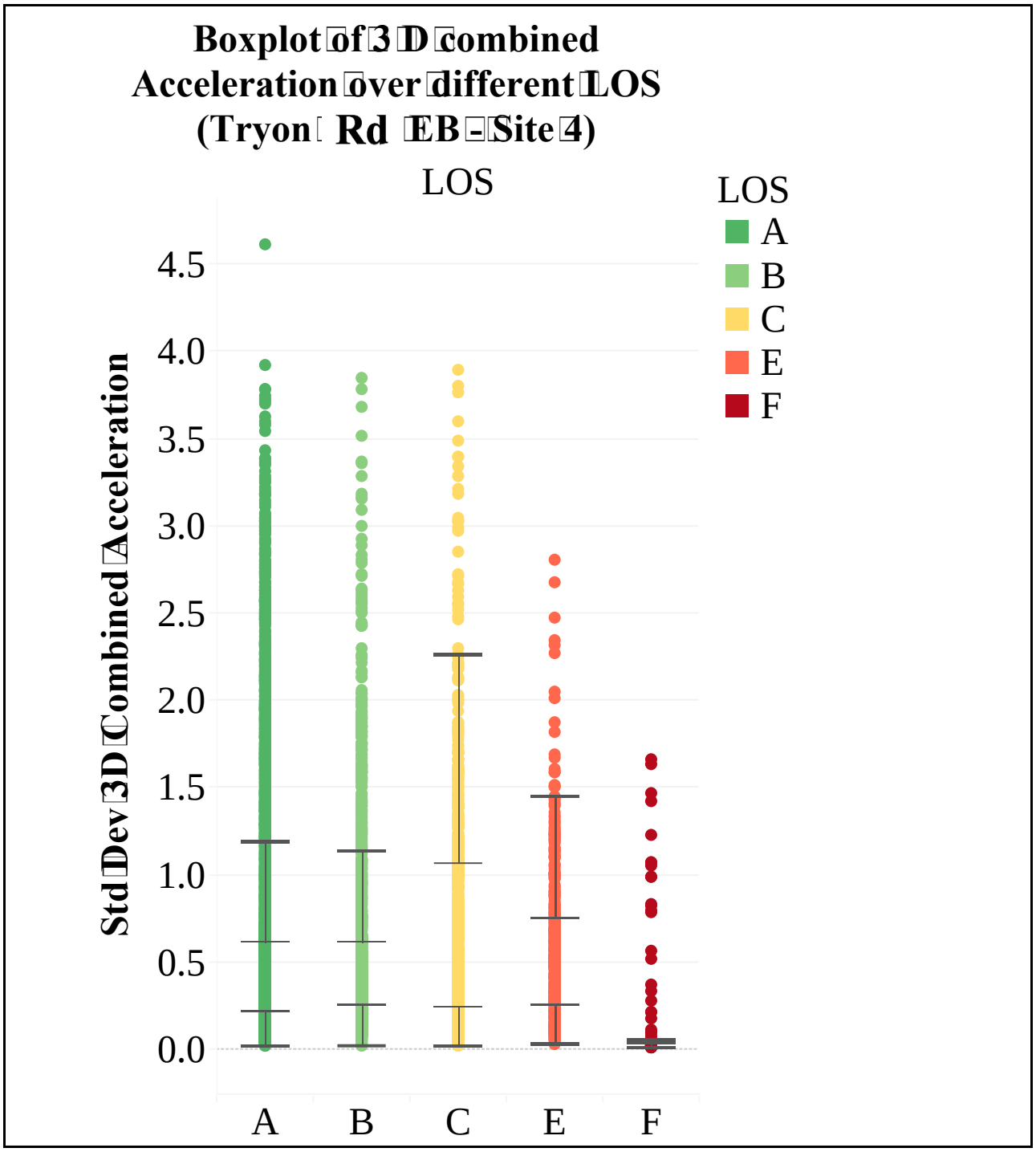

Figure E-11 – Boxplot of 3-D Combined Acceleration over different LOS (Tryon Rd EB – Site 4)

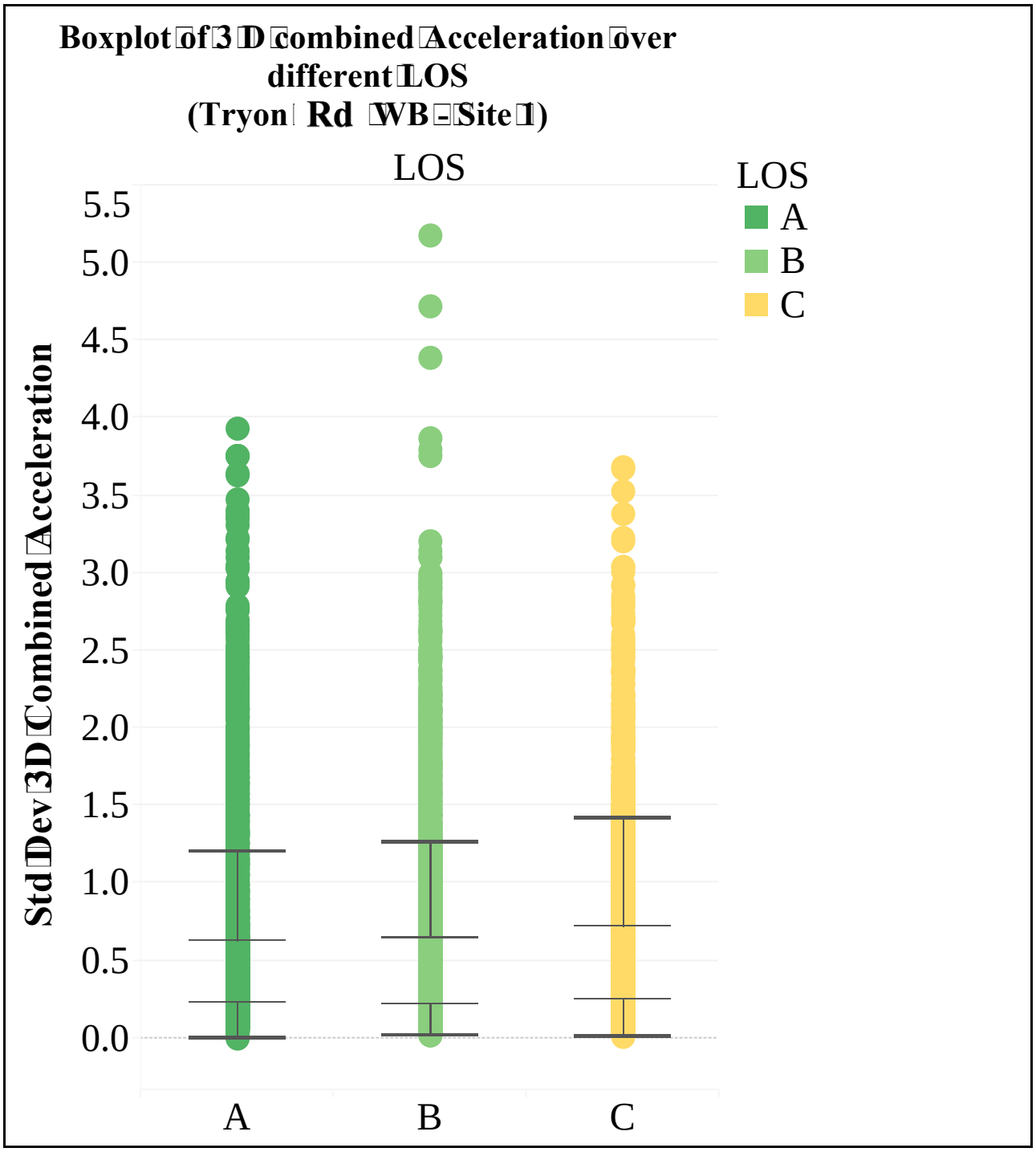

Figure E-12 – Boxplot of 3-D Combined Acceleration over different LOS (Tryon Rd WB – Site 1)

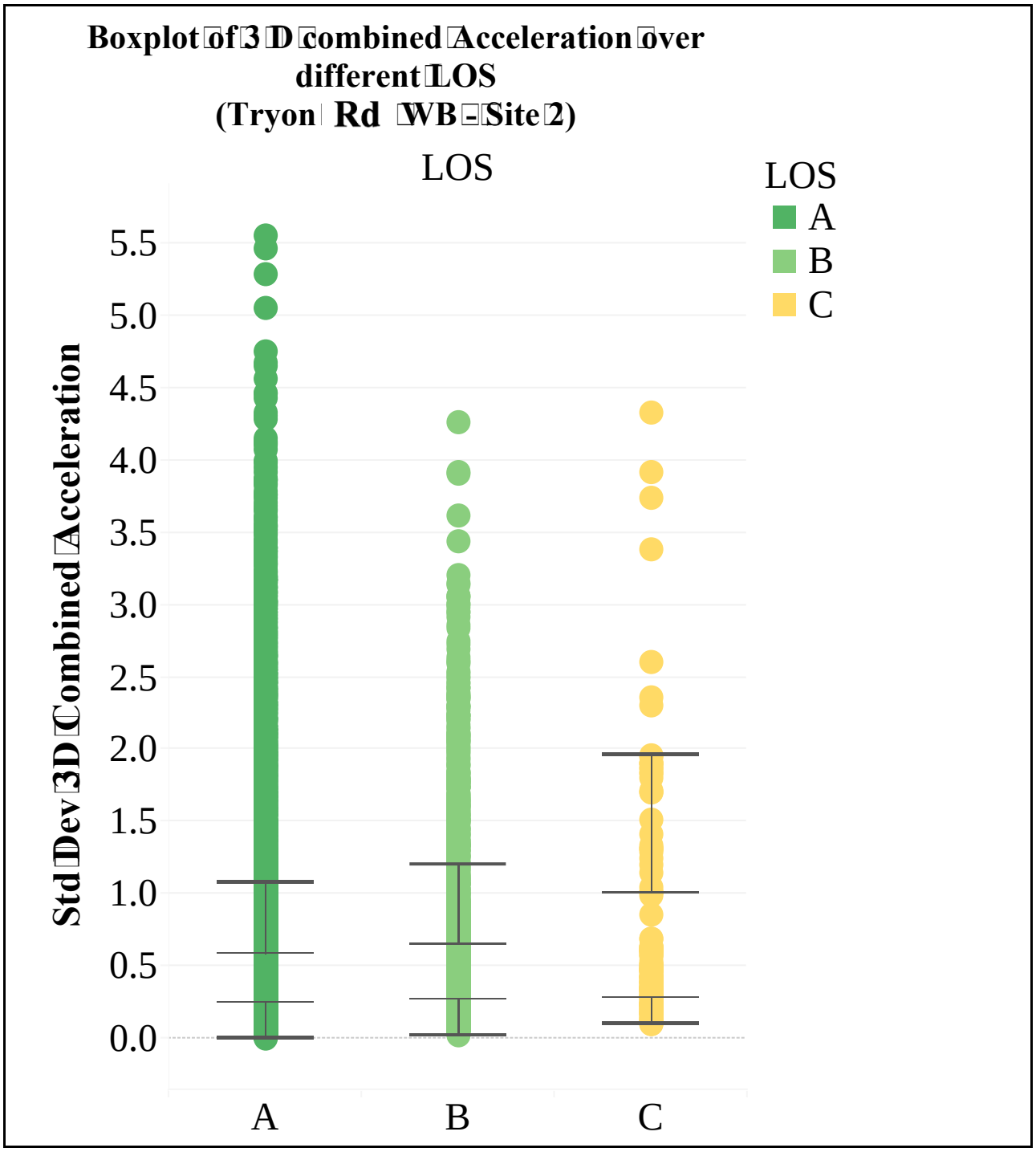

Figure E-13 – Boxplot of 3-D Combined Acceleration over different LOS (Tryon Rd WB – Site 2)

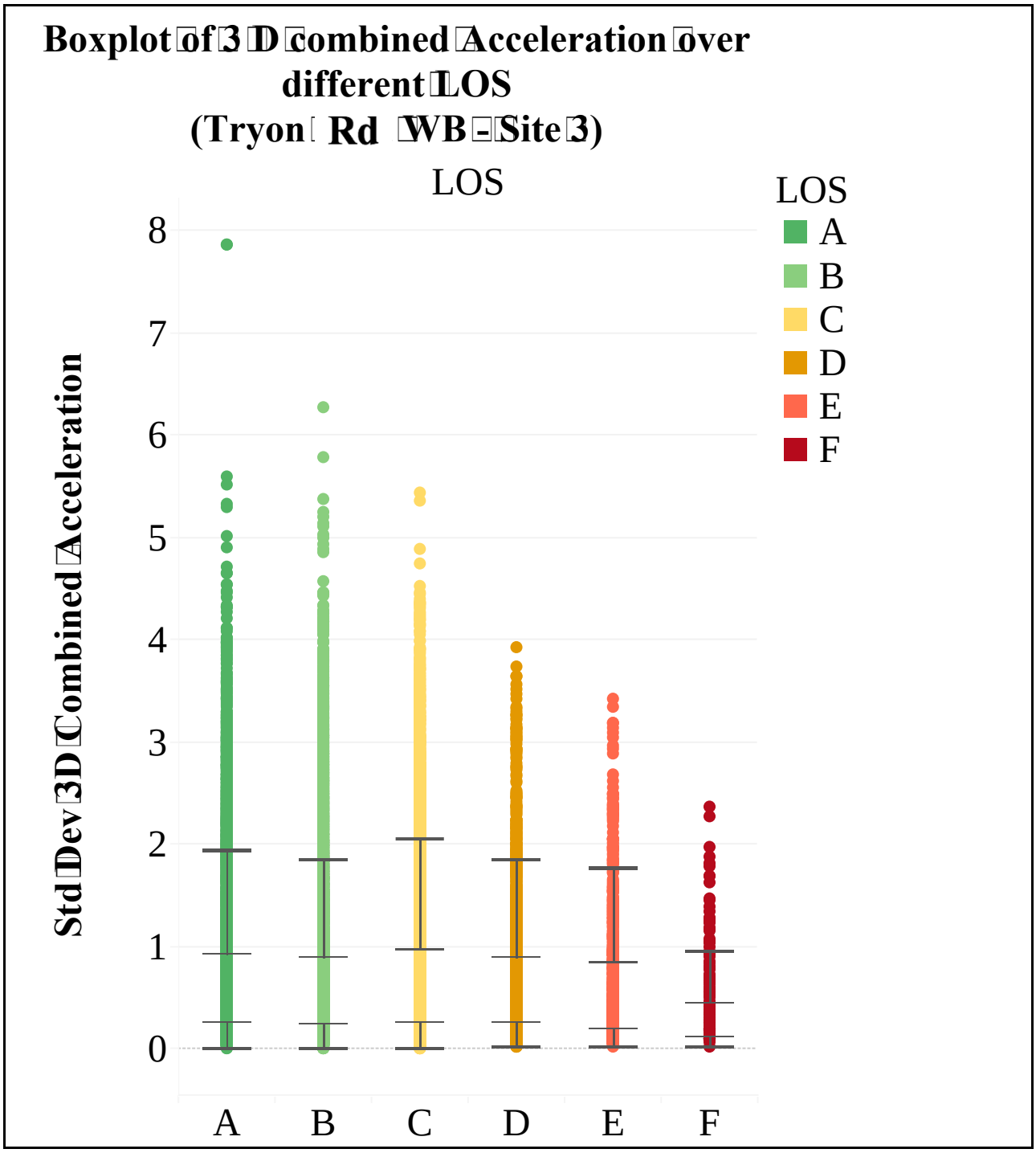

Figure E-14 – Boxplot of 3-D Combined Acceleration over different LOS (Tryon Rd WB – Site 3)

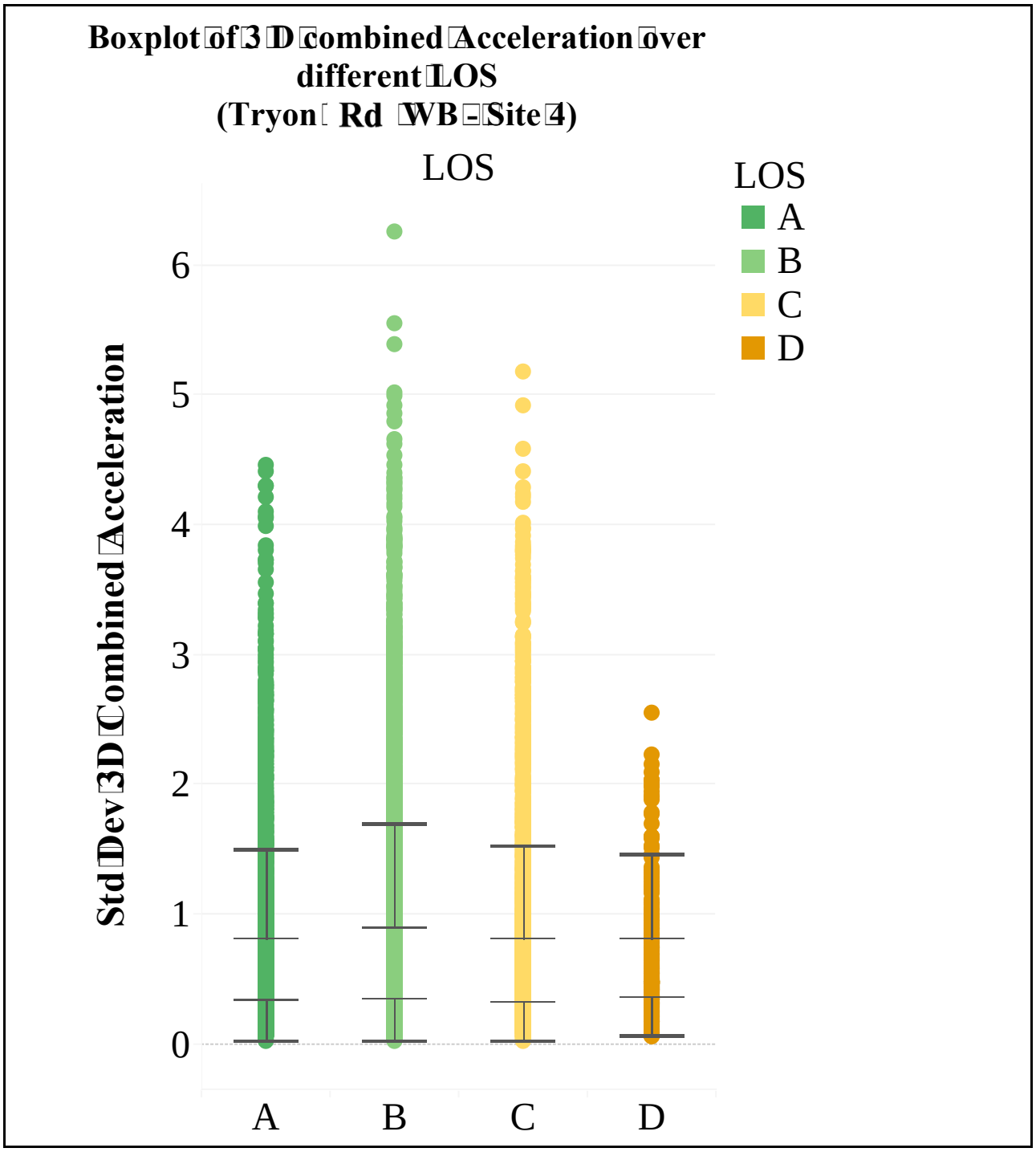

Figure E-15 – Boxplot of 3-D Combined Acceleration over different LOS (Tryon Rd WB – Site 4)

APPENDIX F - AVERAGE AND STD DEV OF ACCELERATION OVER DIFFERENT LOS

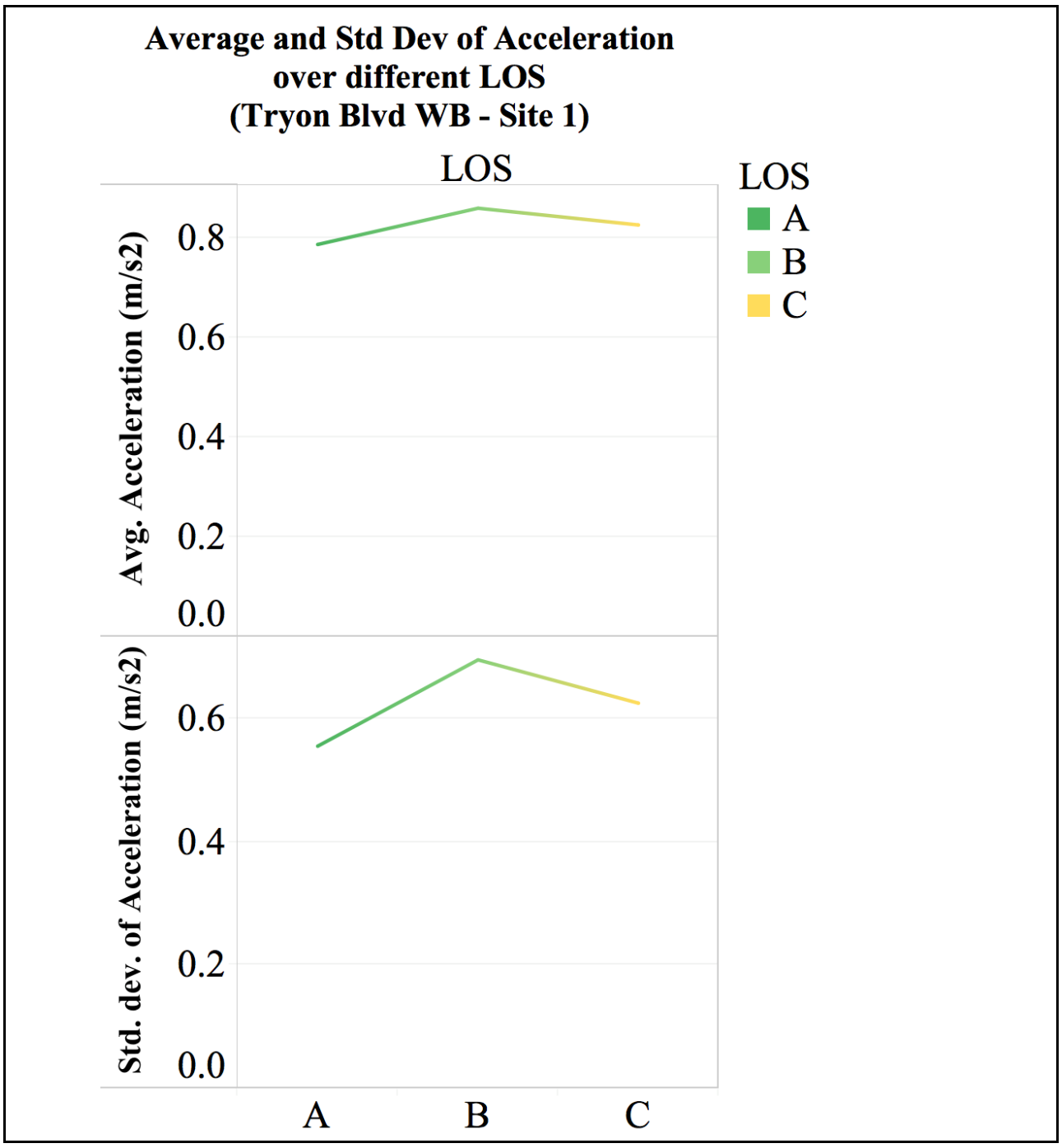

Figure F-1 – Average and Std Dev of Acceleration over different LOS (Western Blvd WB – Site 1)

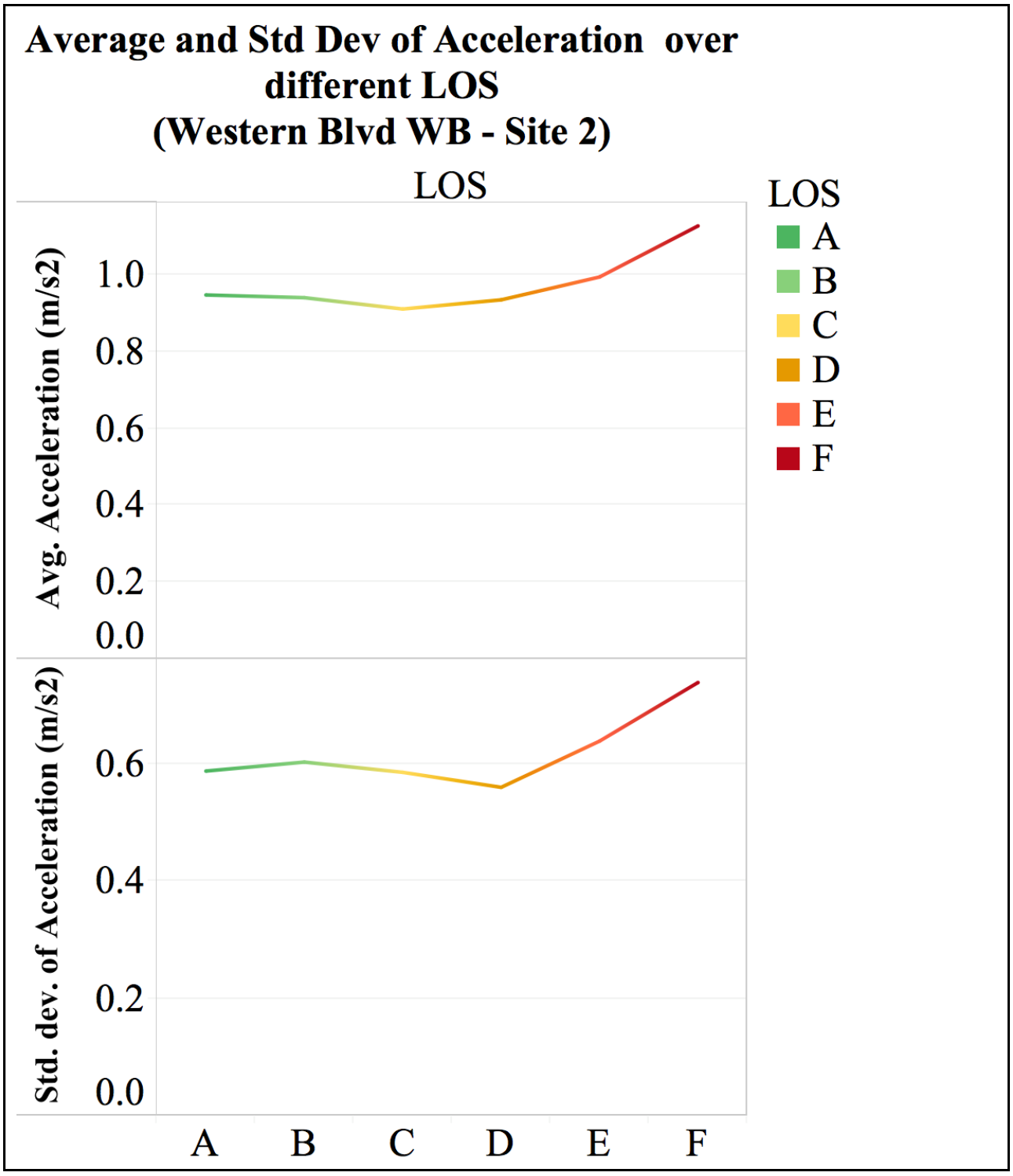

Figure F-2 – Average and Std Dev of Deceleration over different LOS (Western Blvd WB – Site 2)

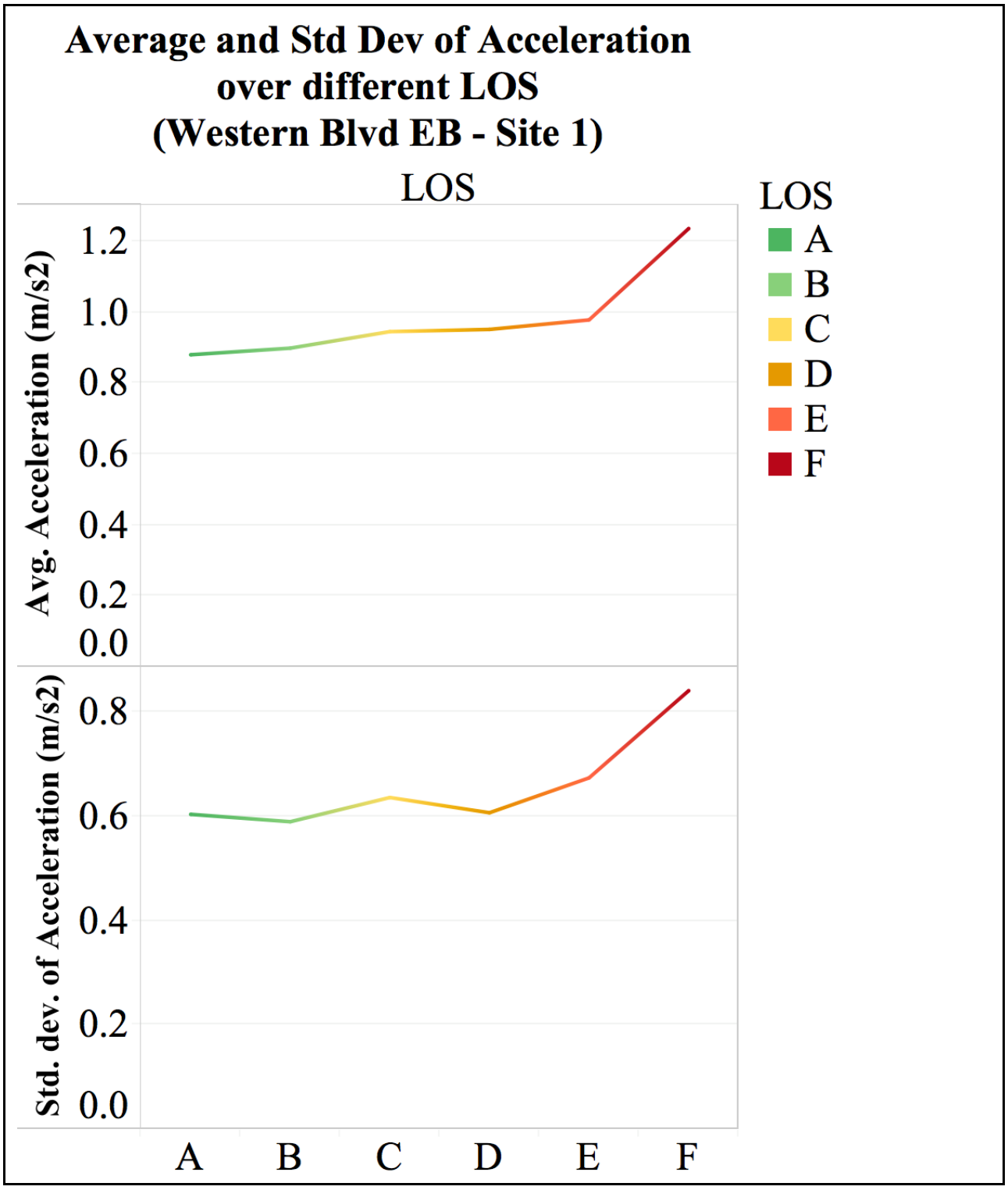

Figure F-3 – Average and Std Dev of Deceleration over different LOS (Western Blvd EB – Site 1)

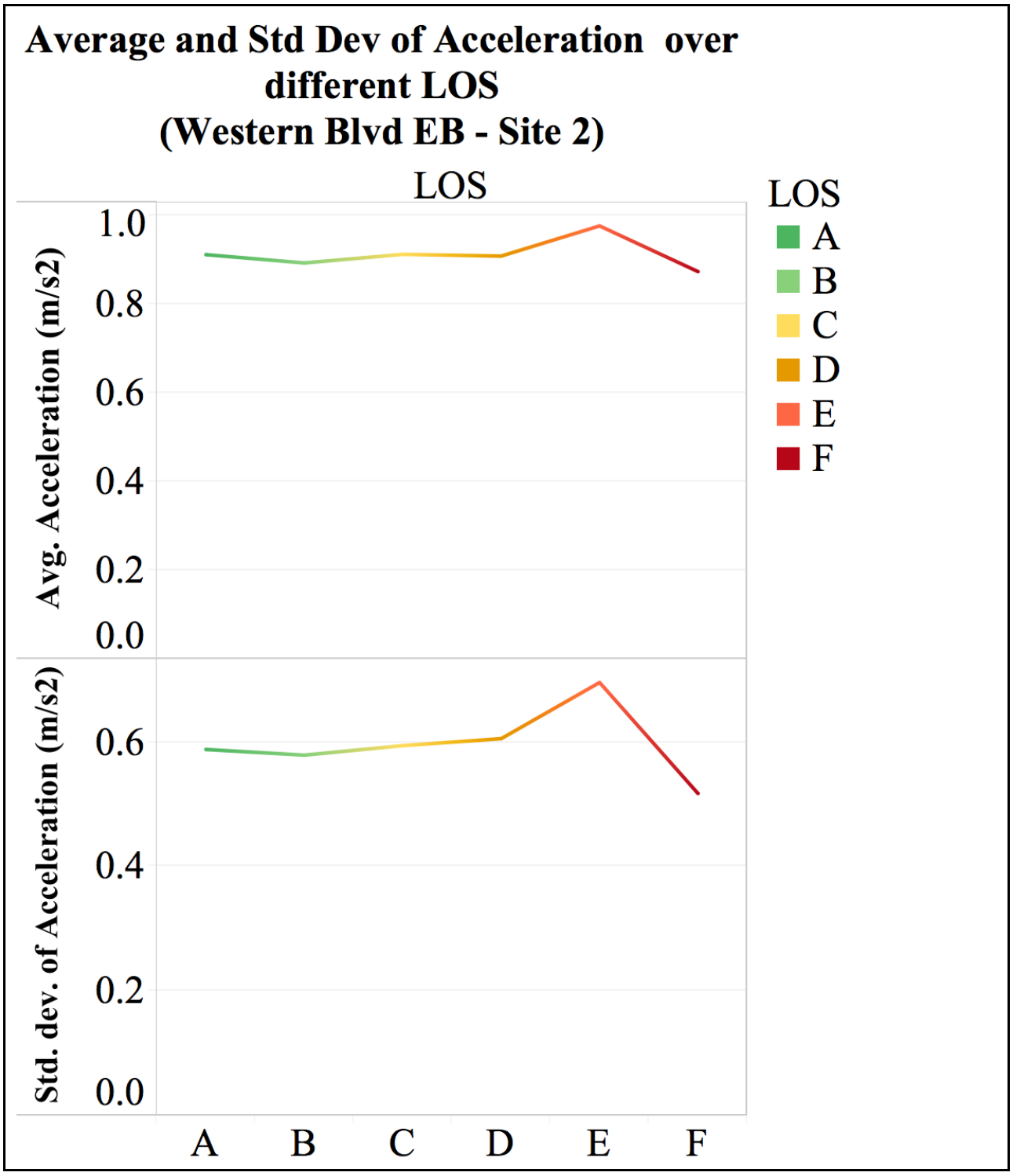

Figure F-4 – Average and Std Dev of Deceleration over different LOS (Western Blvd EB – Site 2)

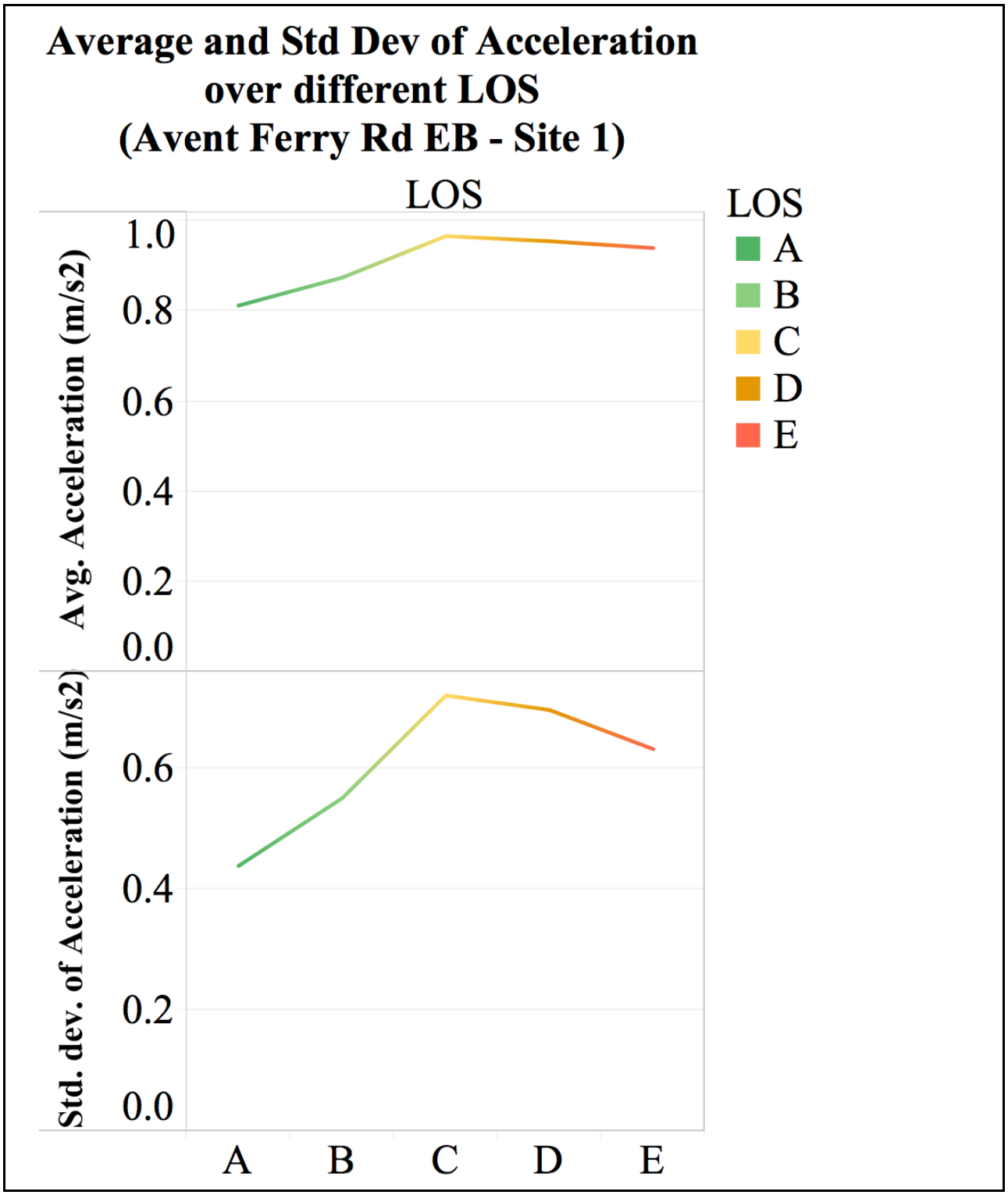

Figure F-5 – Average and Std Dev of Deceleration over different LOS (Avent Ferry Rd EB – Site 1)

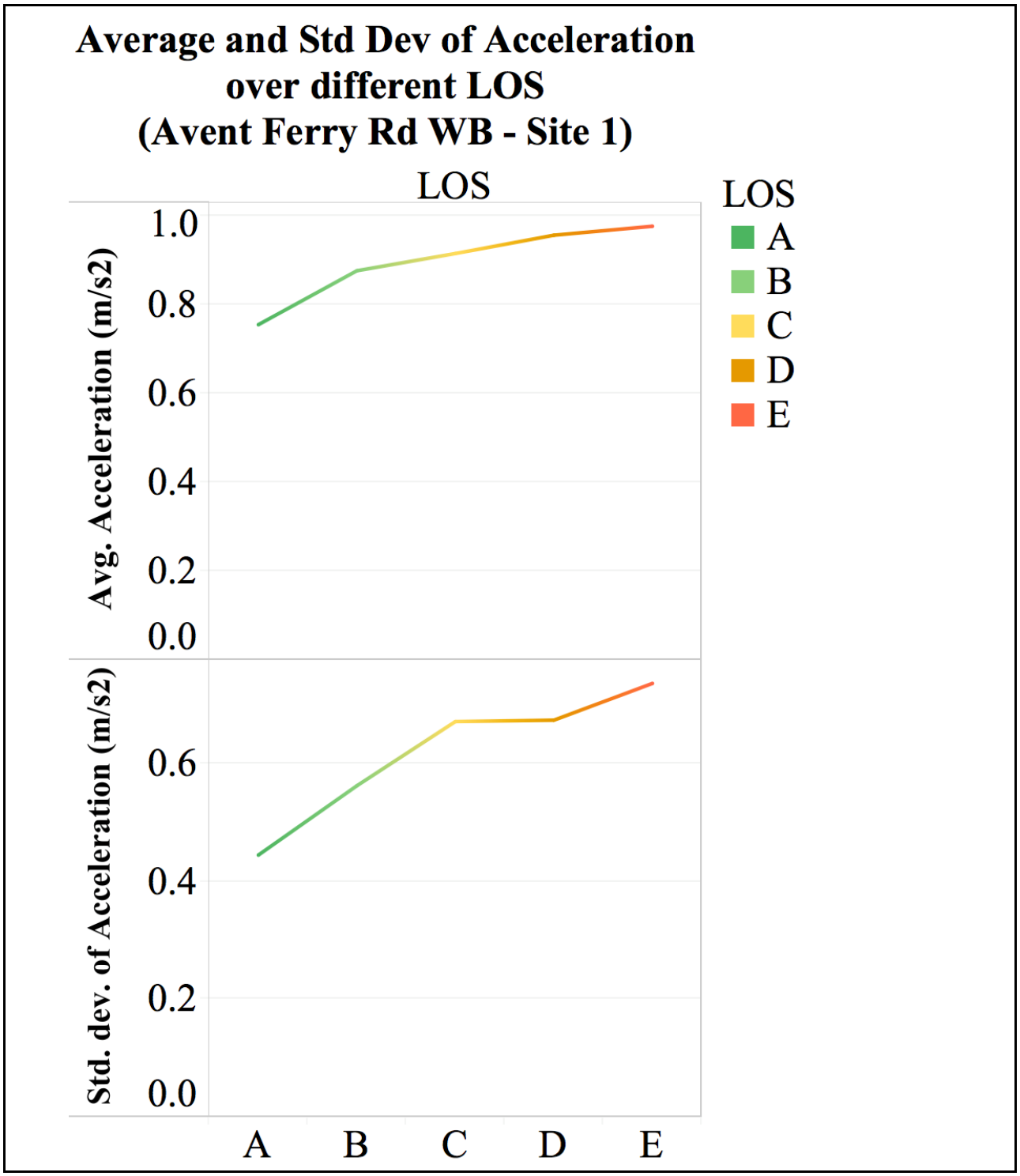

Figure F-6 – Average and Std Dev of Deceleration over different LOS (Avent Ferry Rd WB – Site 1)

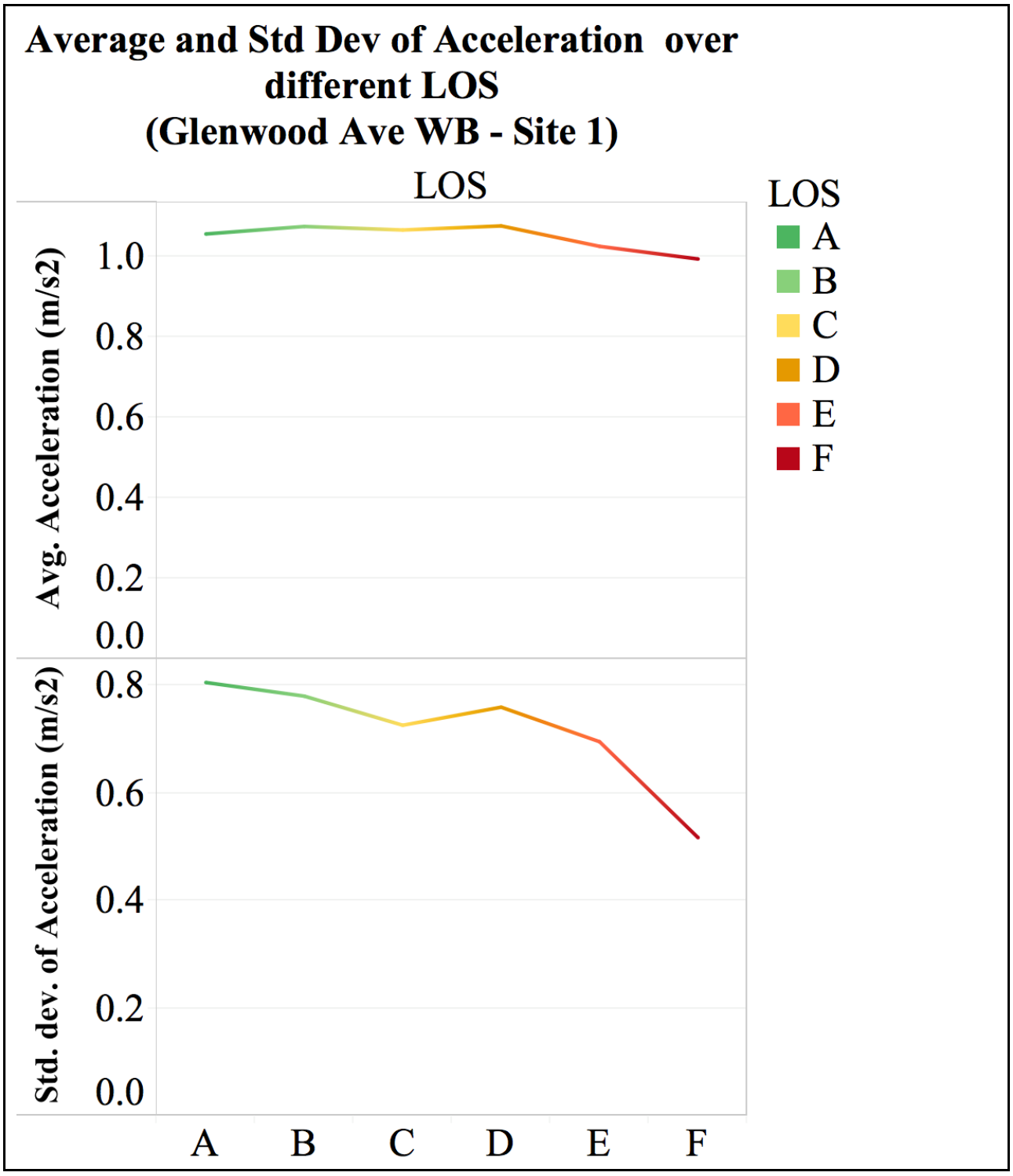

Figure F-7 – Average and Std Dev of Acceleration over different LOS (Glenwood Ave WB – Site 1)

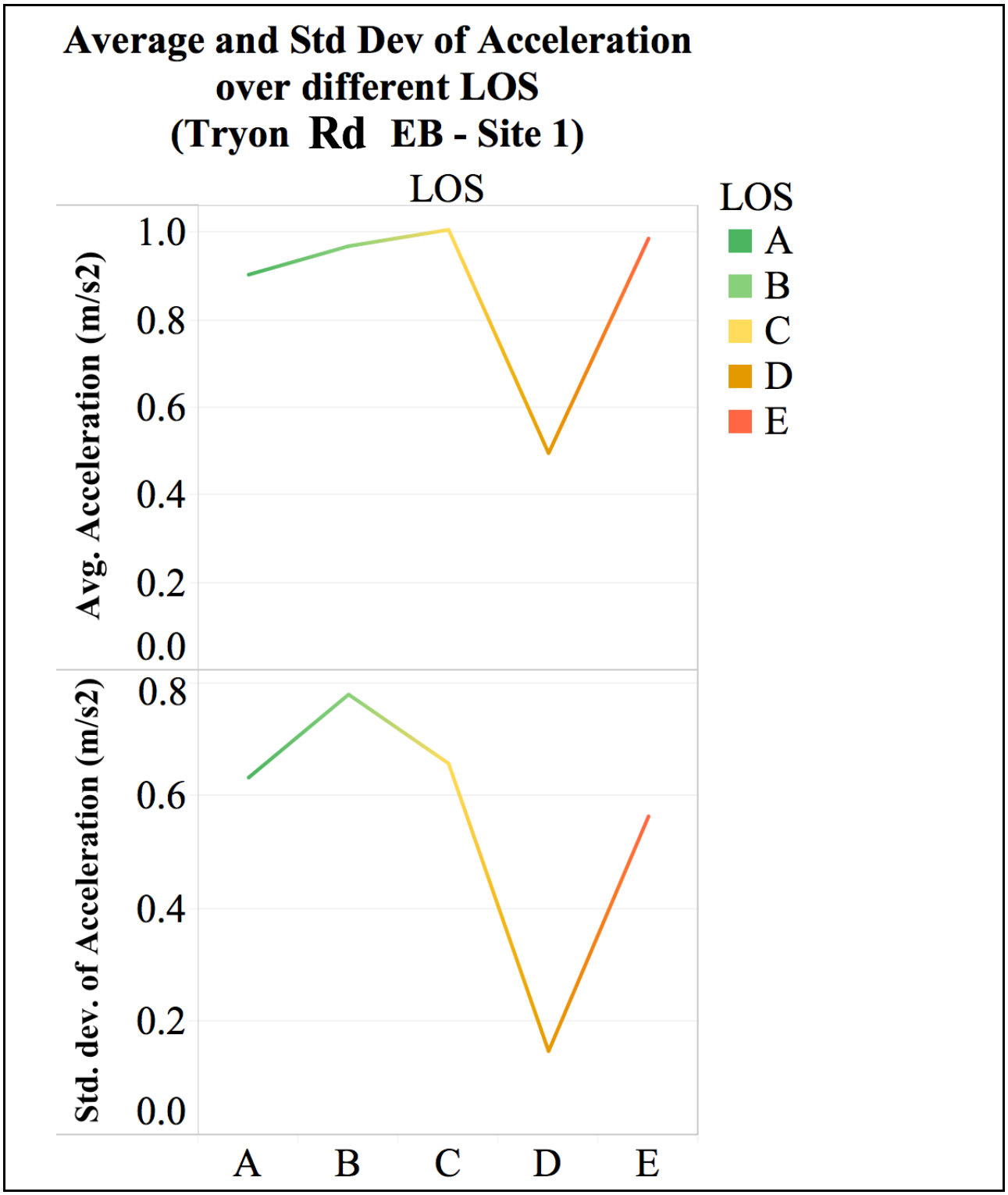

Figure F-8 – Average and Std Dev of Deceleration over different LOS (Tryon Rd EB – Site 1)

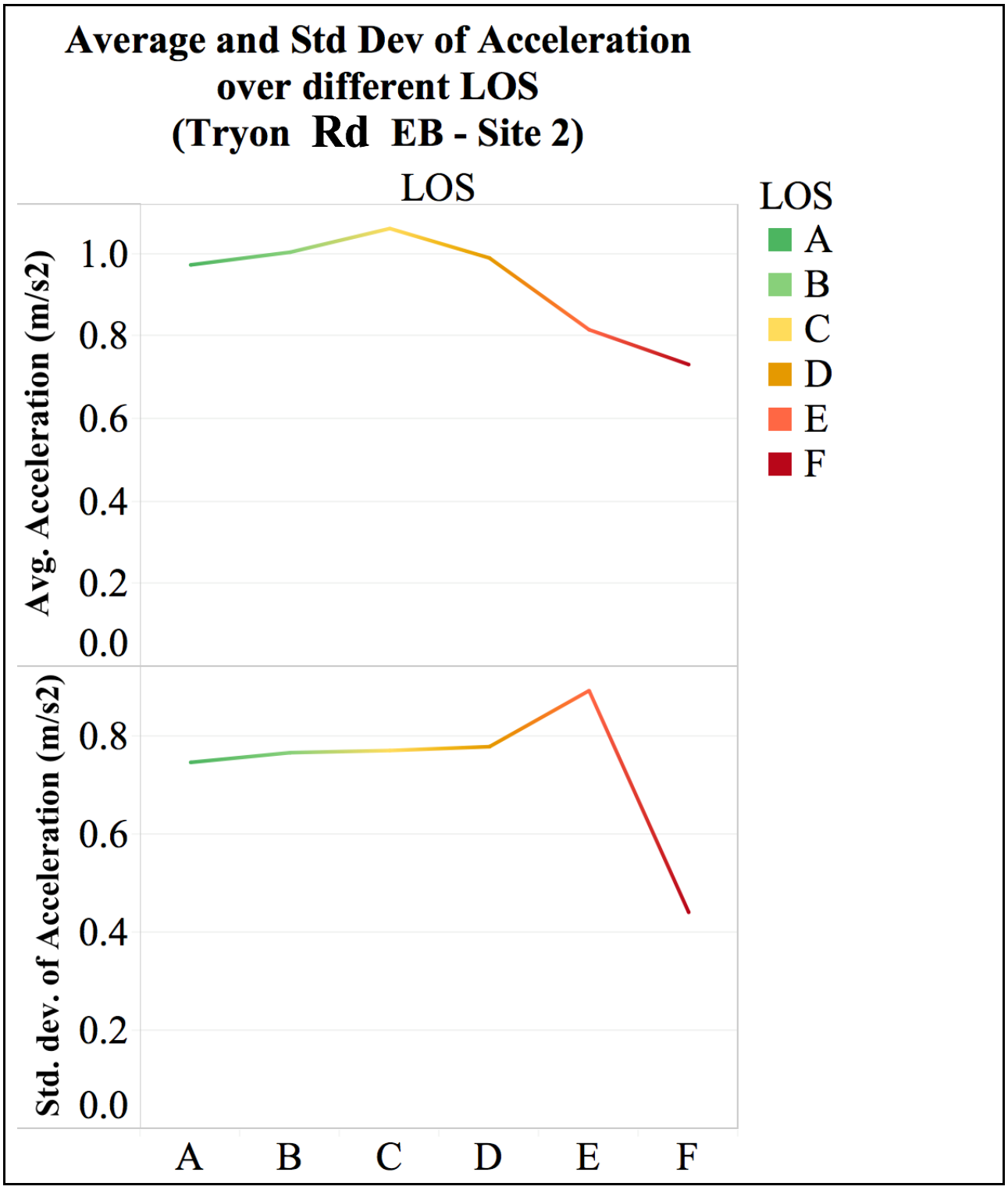

Figure F-9 – Average and Std Dev of Deceleration over different LOS (Tryon Rd EB – Site 2)

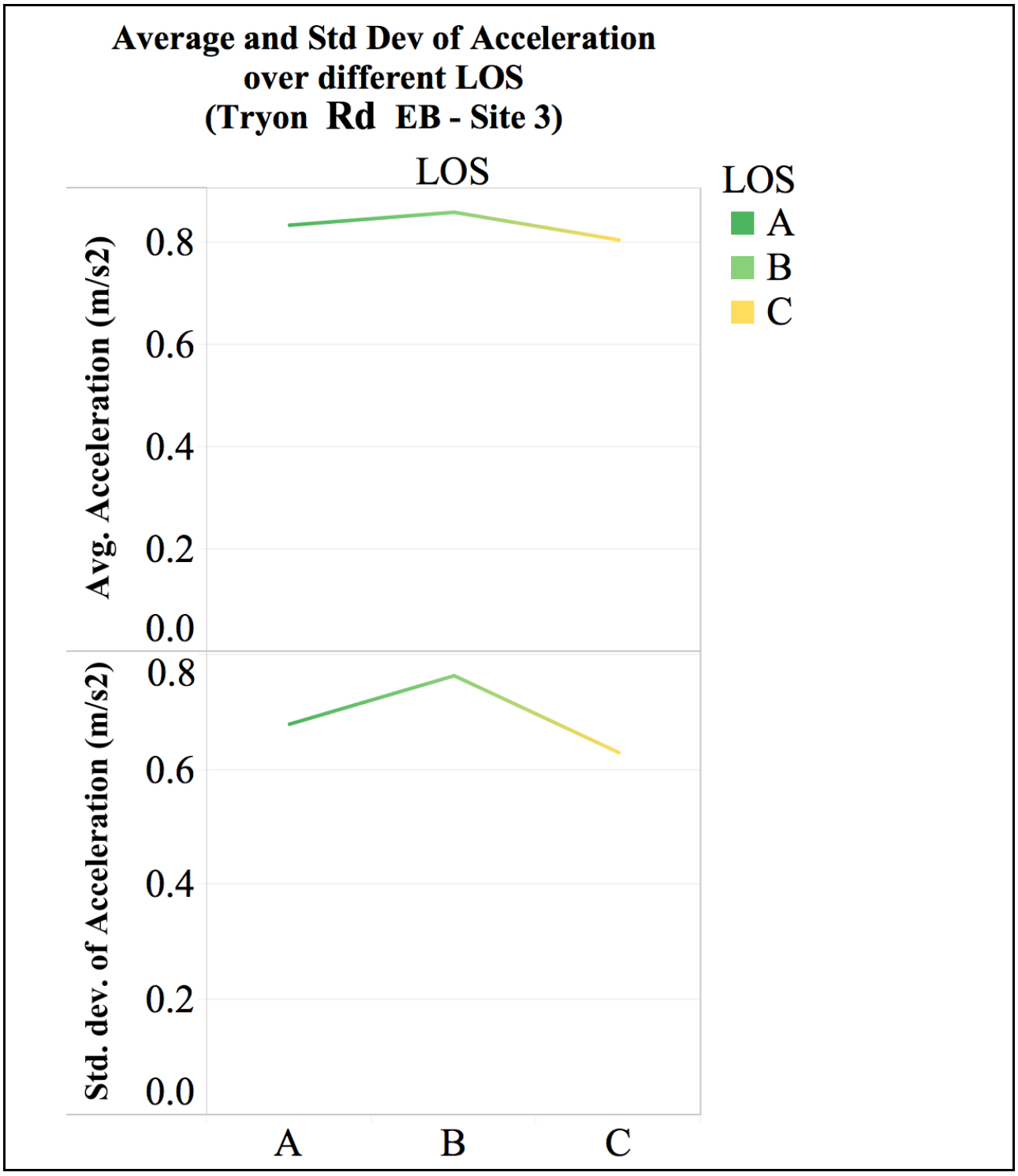

Figure F-10 – Average and Std Dev of Deceleration over different LOS (Tryon Rd EB – Site 3)

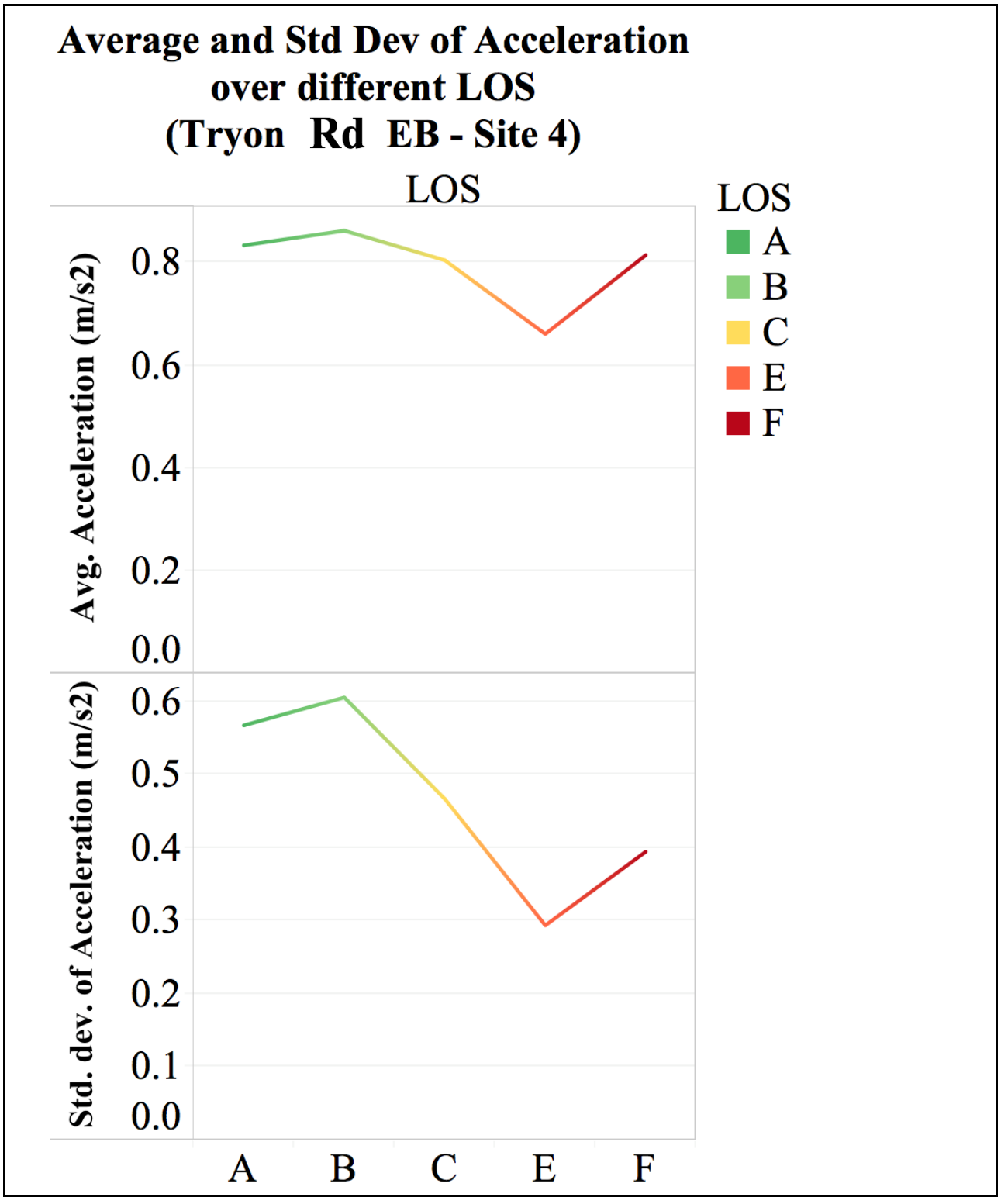

Figure F-11 – Average and Std Dev of Acceleration over different LOS (Tryon Rd EB – Site 4)

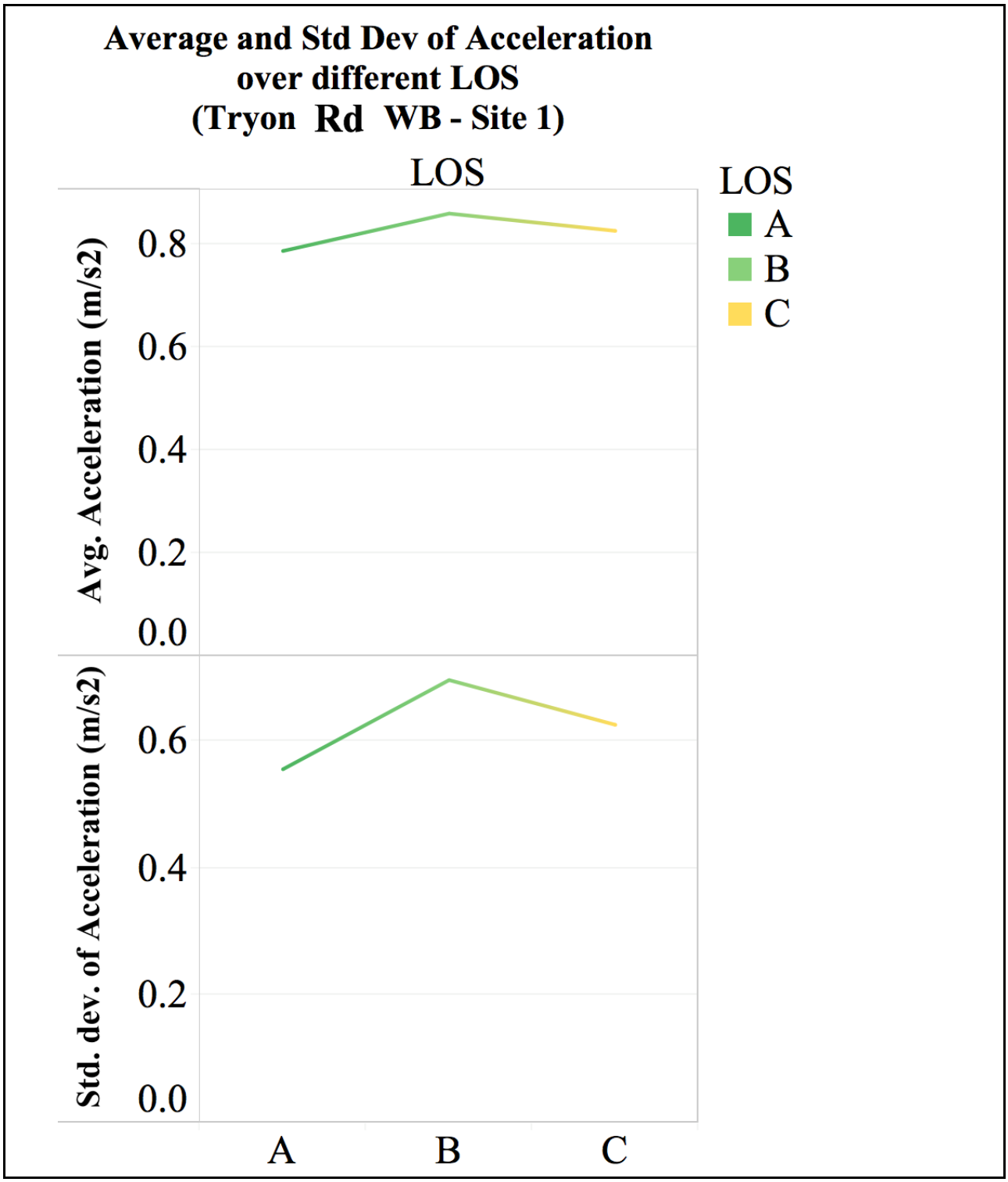

Figure F-12 – Average and Std Dev of Acceleration over different LOS (Tryon Rd WB – Site 1)

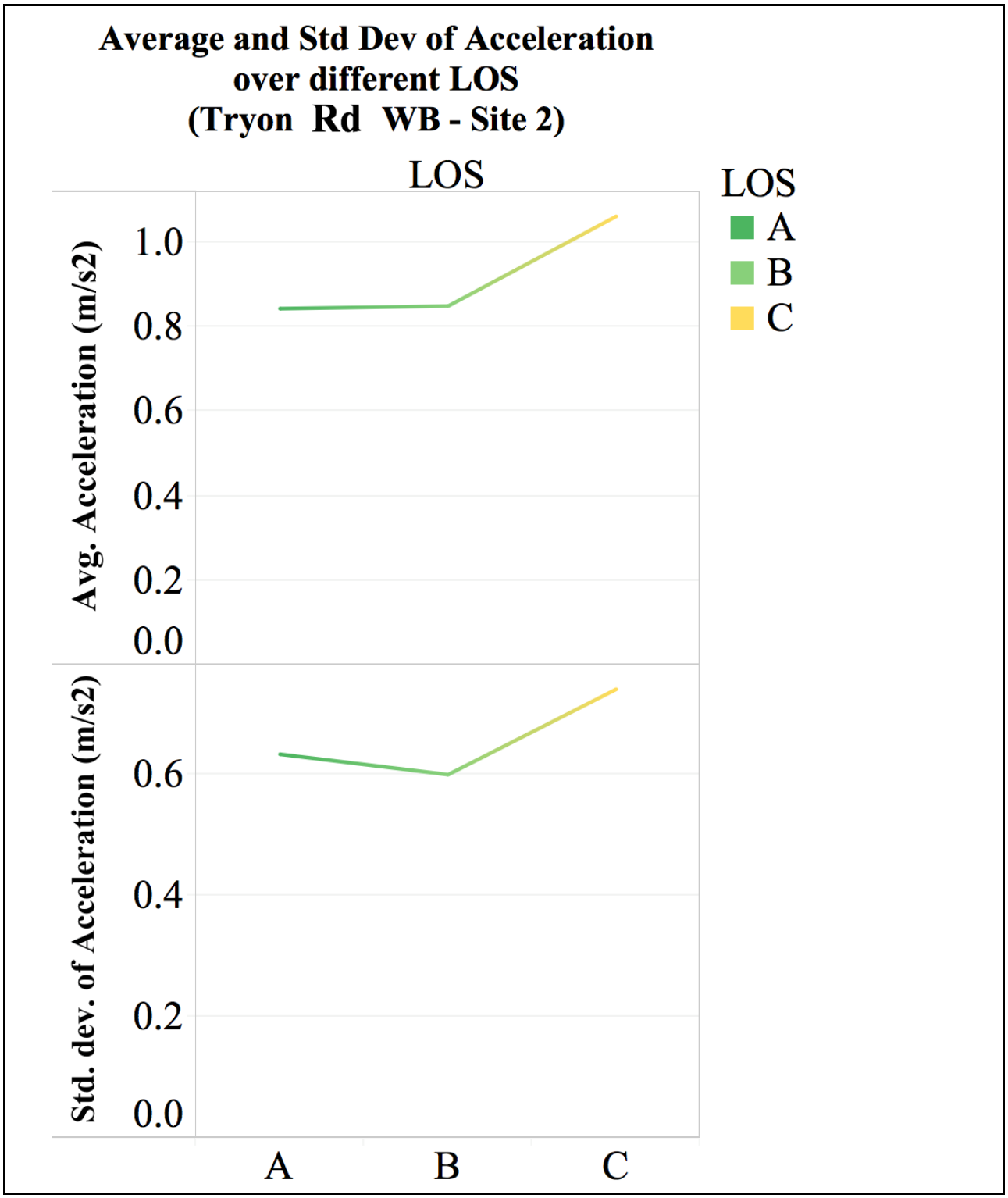

Figure F-13 – Average and Std Dev of Acceleration over different LOS (Tryon Rd WB – Site 2)

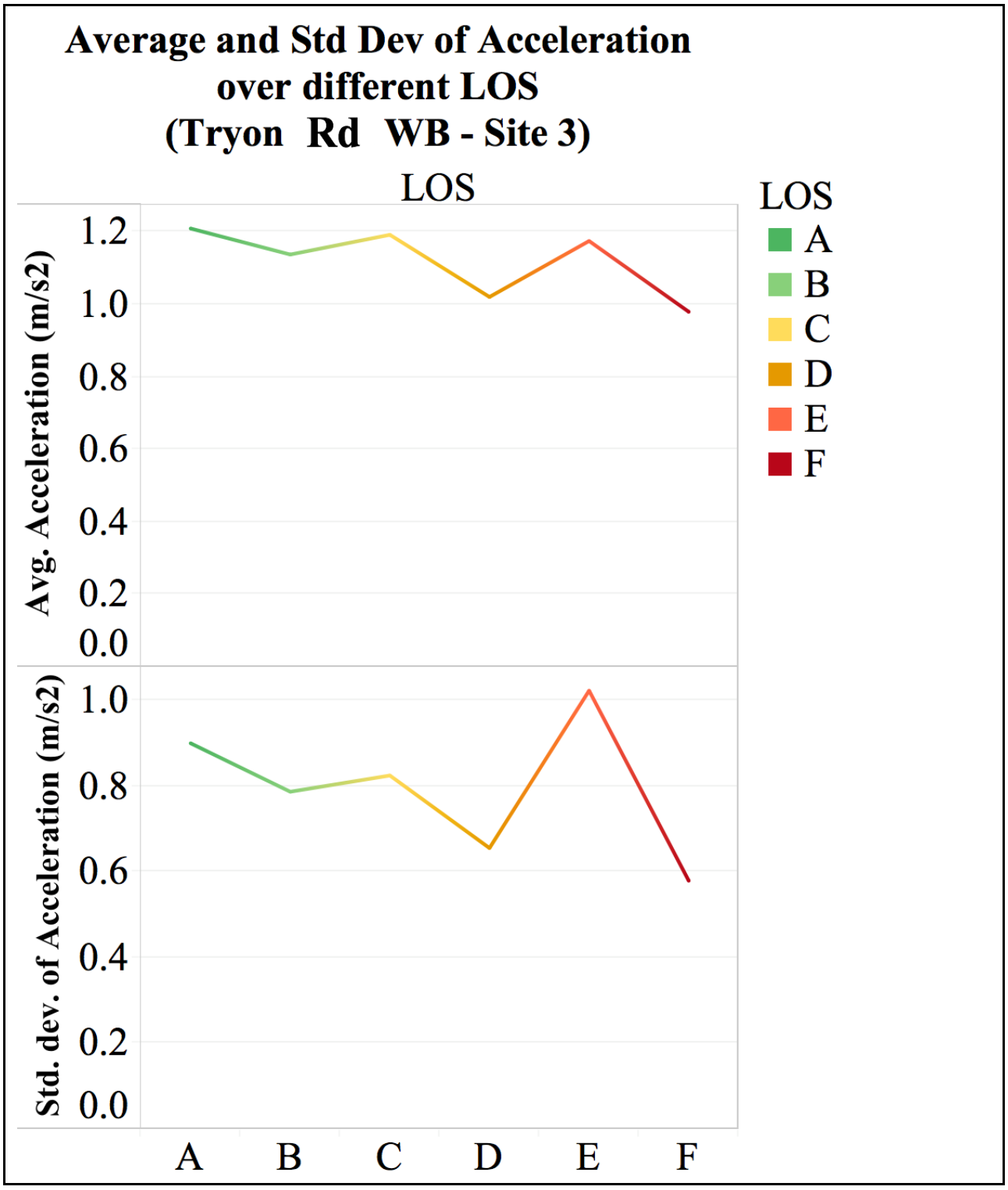

Figure F-14 – Average and Std Dev of Acceleration over different LOS (Tryon Rd WB – Site 3)

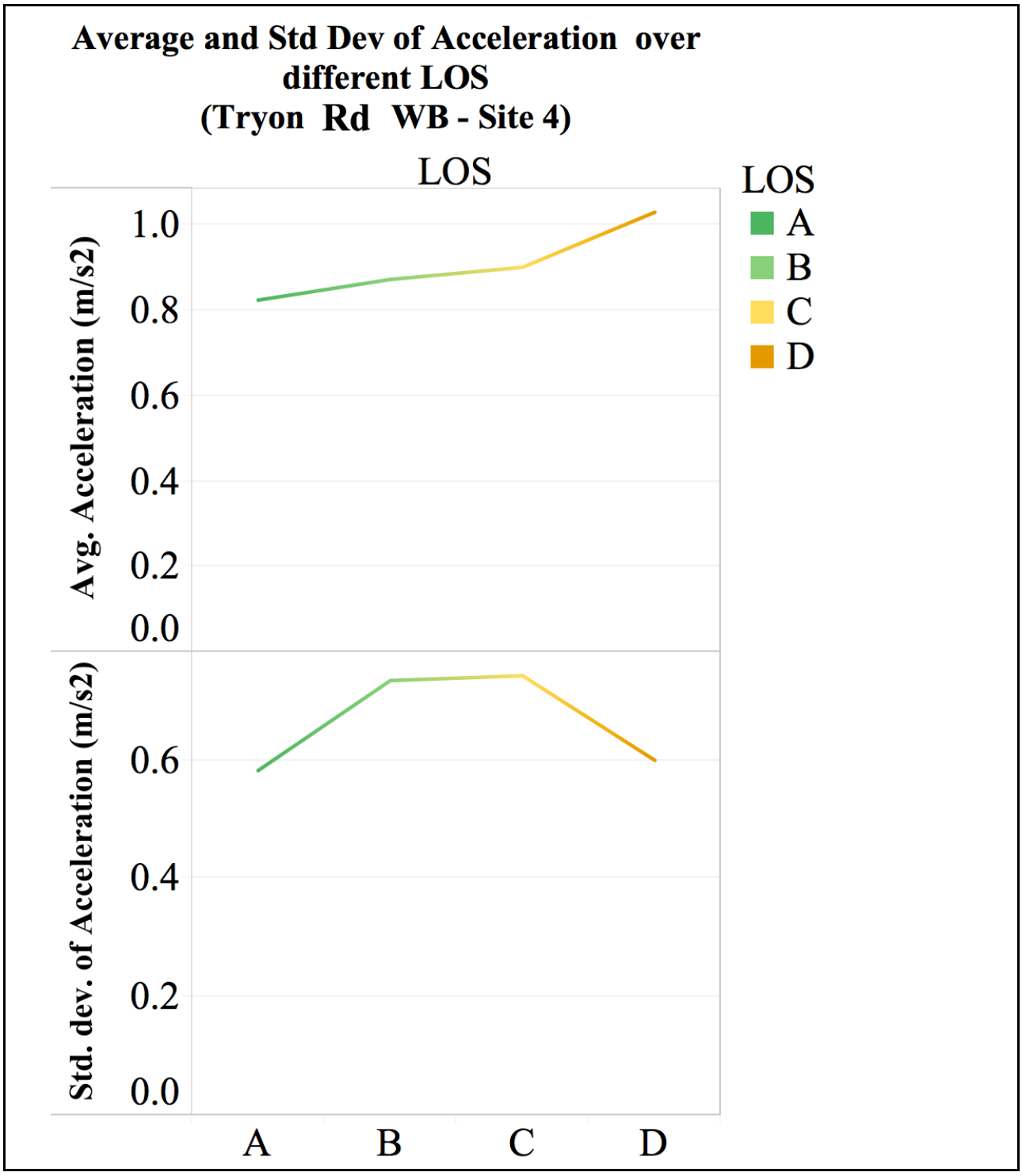

Figure F-15 – Average and Std Dev of Acceleration over different LOS (Tryon Rd WB – Site 4)

APPENDIX G - AVERAGE AND STD DEV OF DECELERATION OVER DIFFERENT LOS

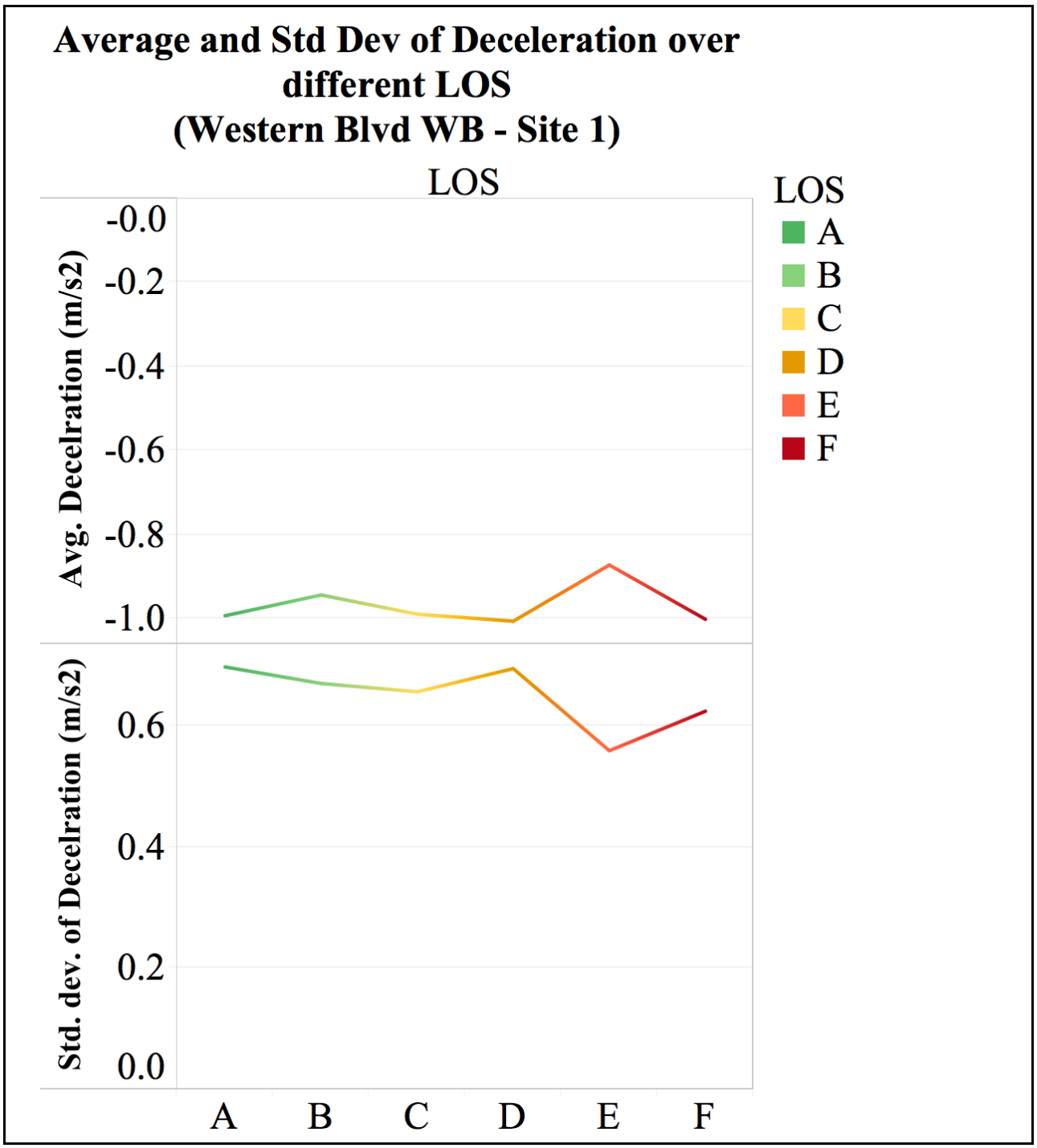

Figure G-1 – Average and Std Dev of Deceleration over different LOS (Western Blvd WB – Site 1)

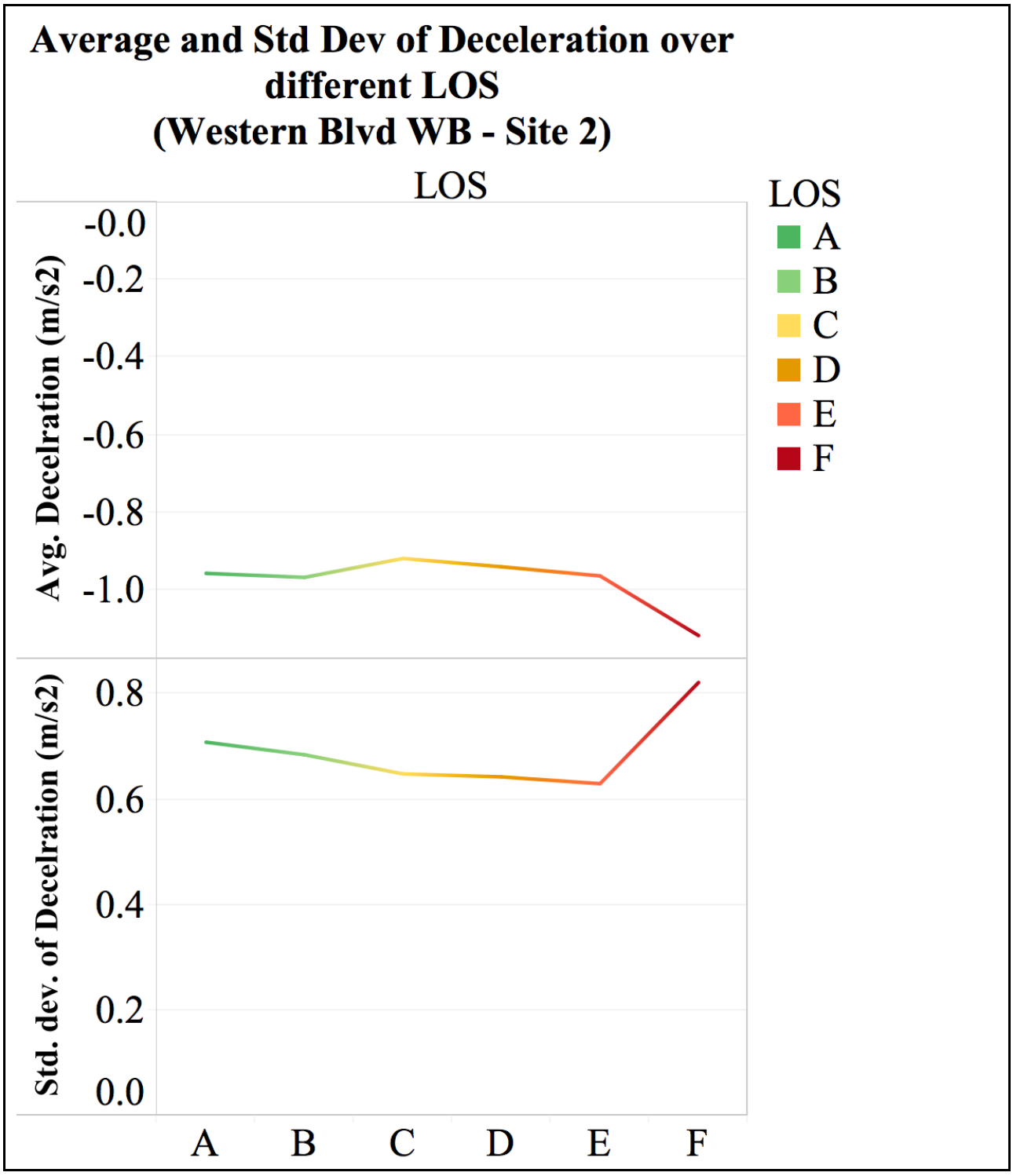

Figure G-2 – Average and Std Dev of Deceleration over different LOS (Western Blvd WB – Site 2)

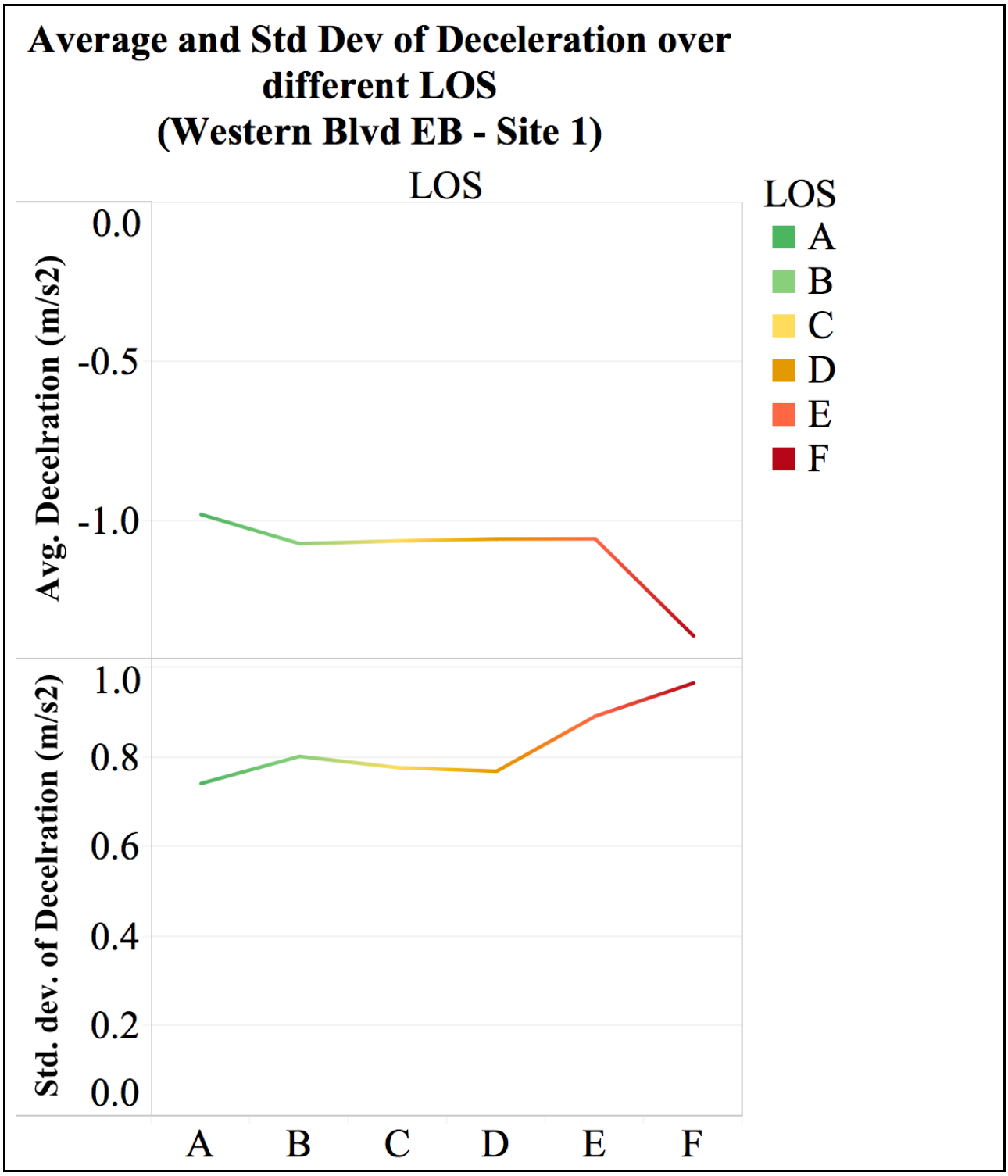

Figure G-3 – Average and Std Dev of Deceleration over different LOS (Western Blvd EB – Site 1)

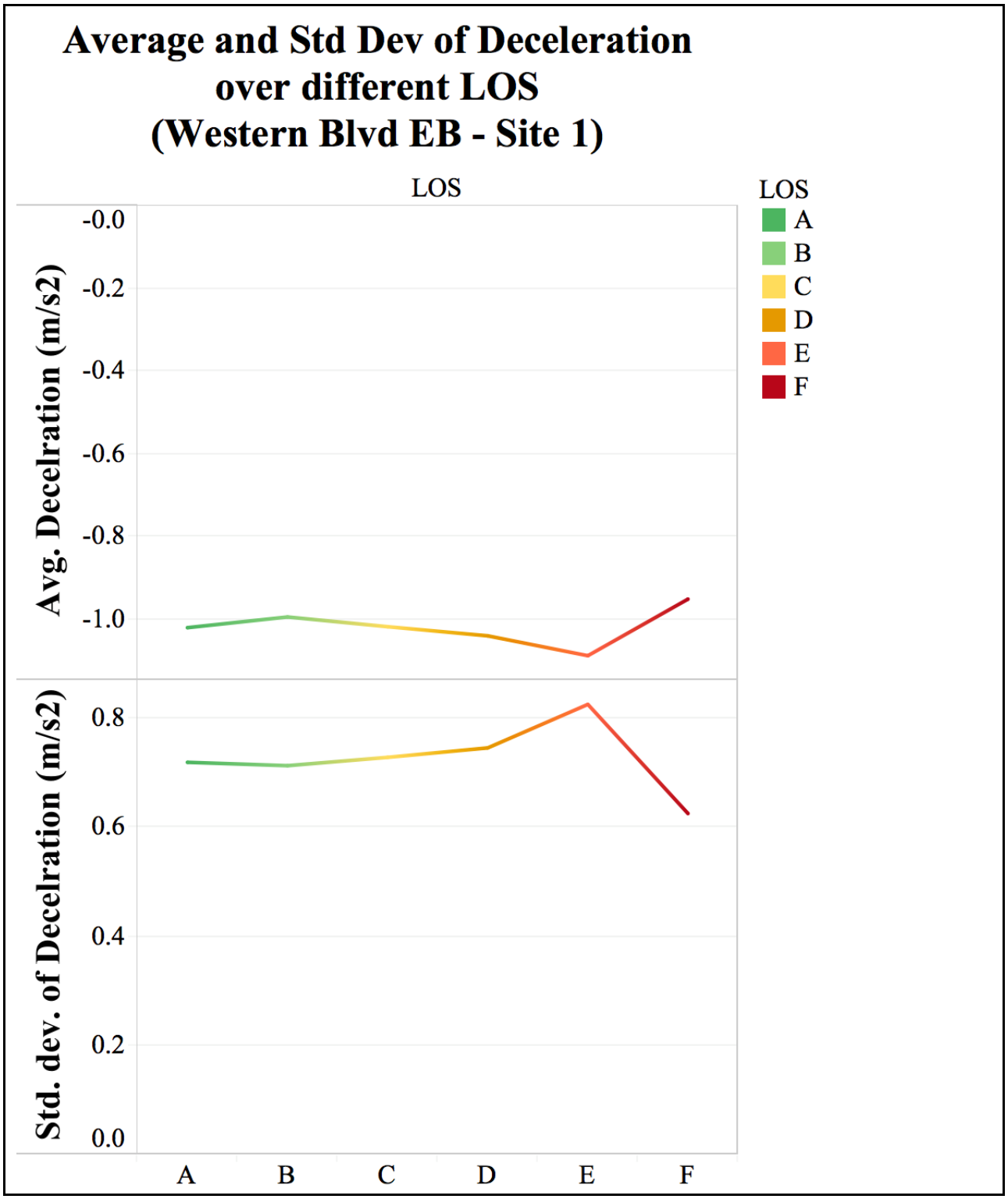

Figure G-4 – Average and Std Dev of Deceleration over different LOS (Western Blvd EB – Site 1)

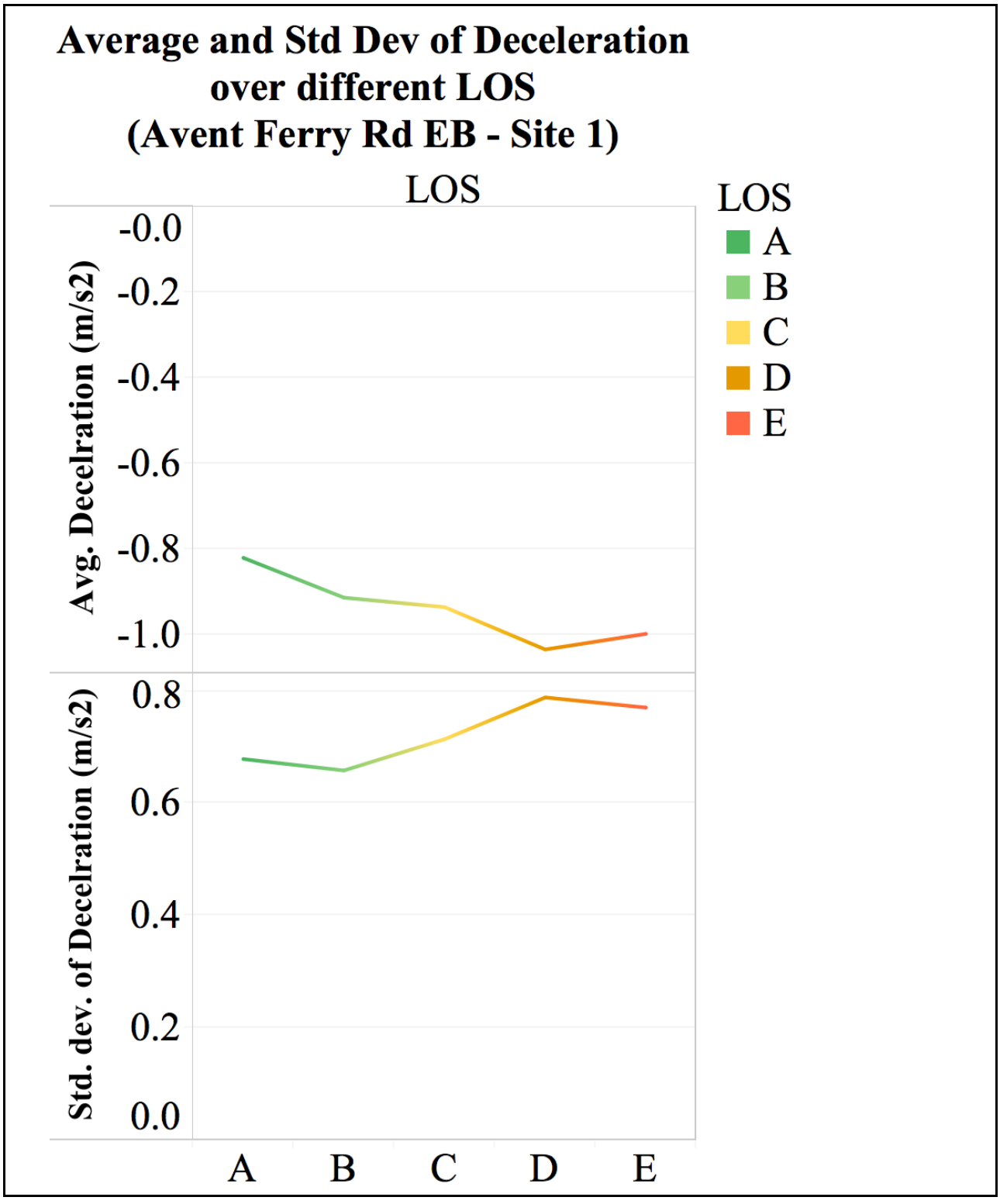

Figure G-5 – Average and Std Dev of Deceleration over different LOS (Avent Ferry Rd EB – Site 1)

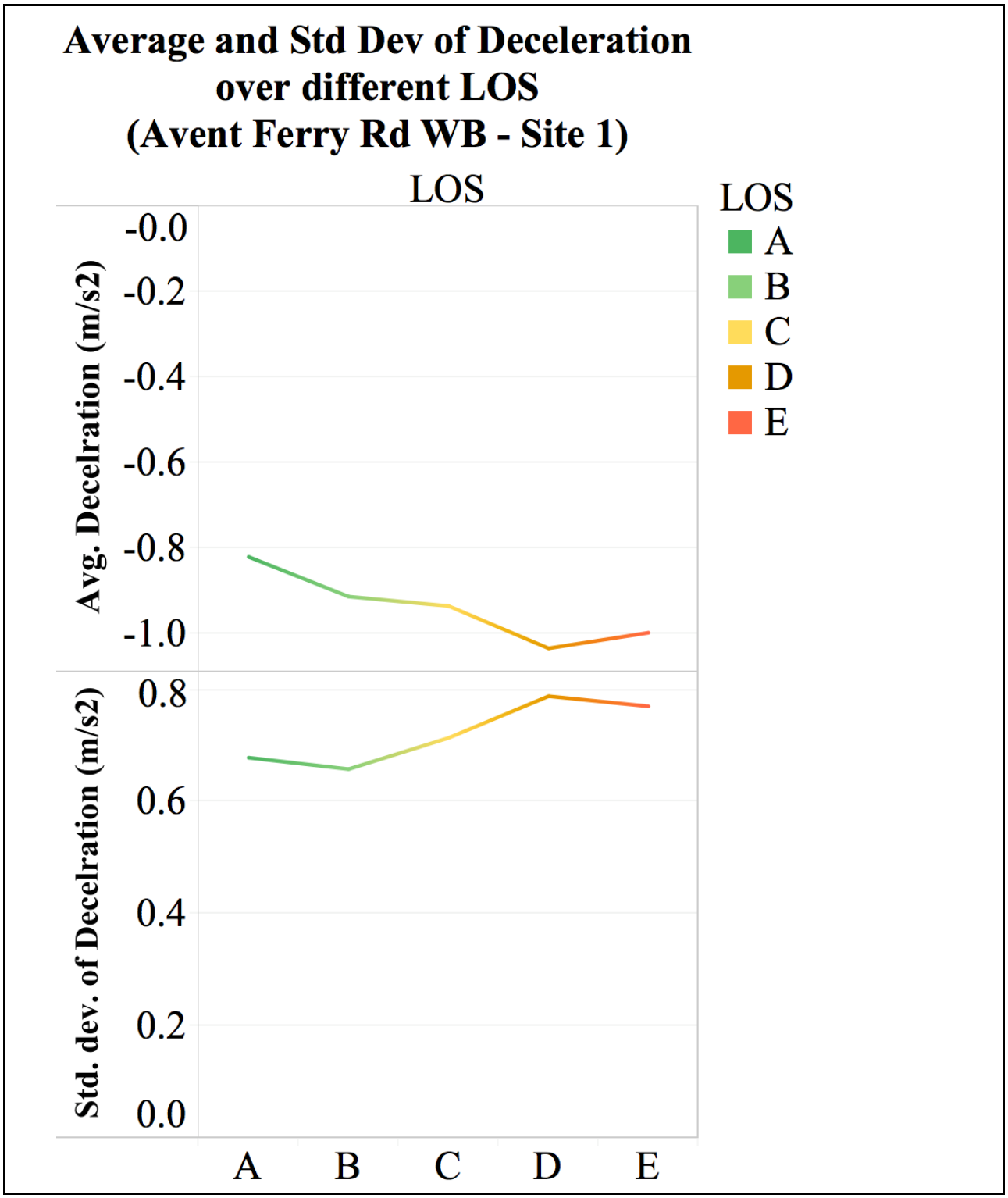

Figure G-6 – Average and Std Dev of Deceleration over different LOS (Avent Ferry Rd WB – Site 1)

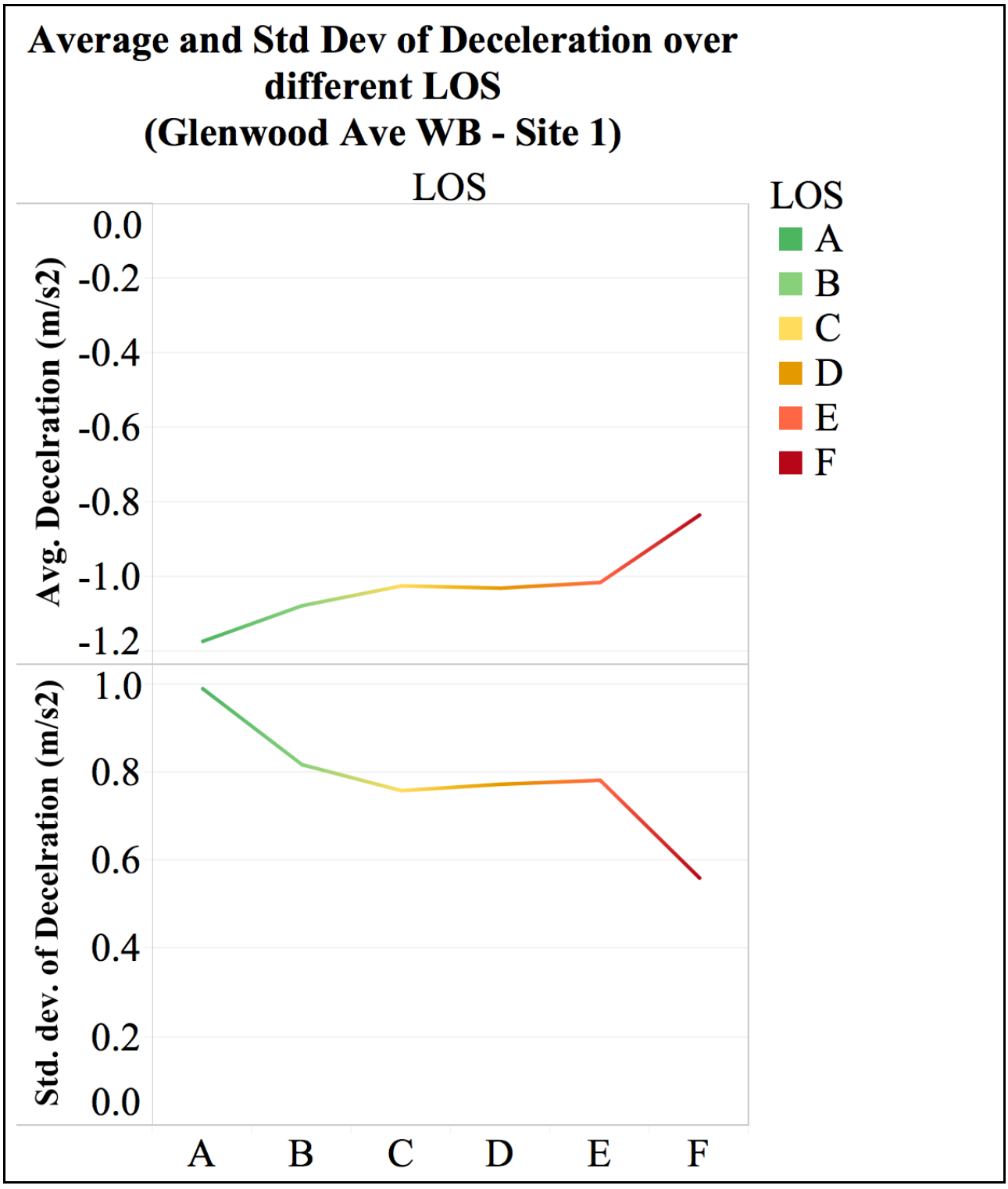

Figure G-7 – Average and Std Dev of Deceleration over different LOS (Glenwood Ave WB – Site 1)

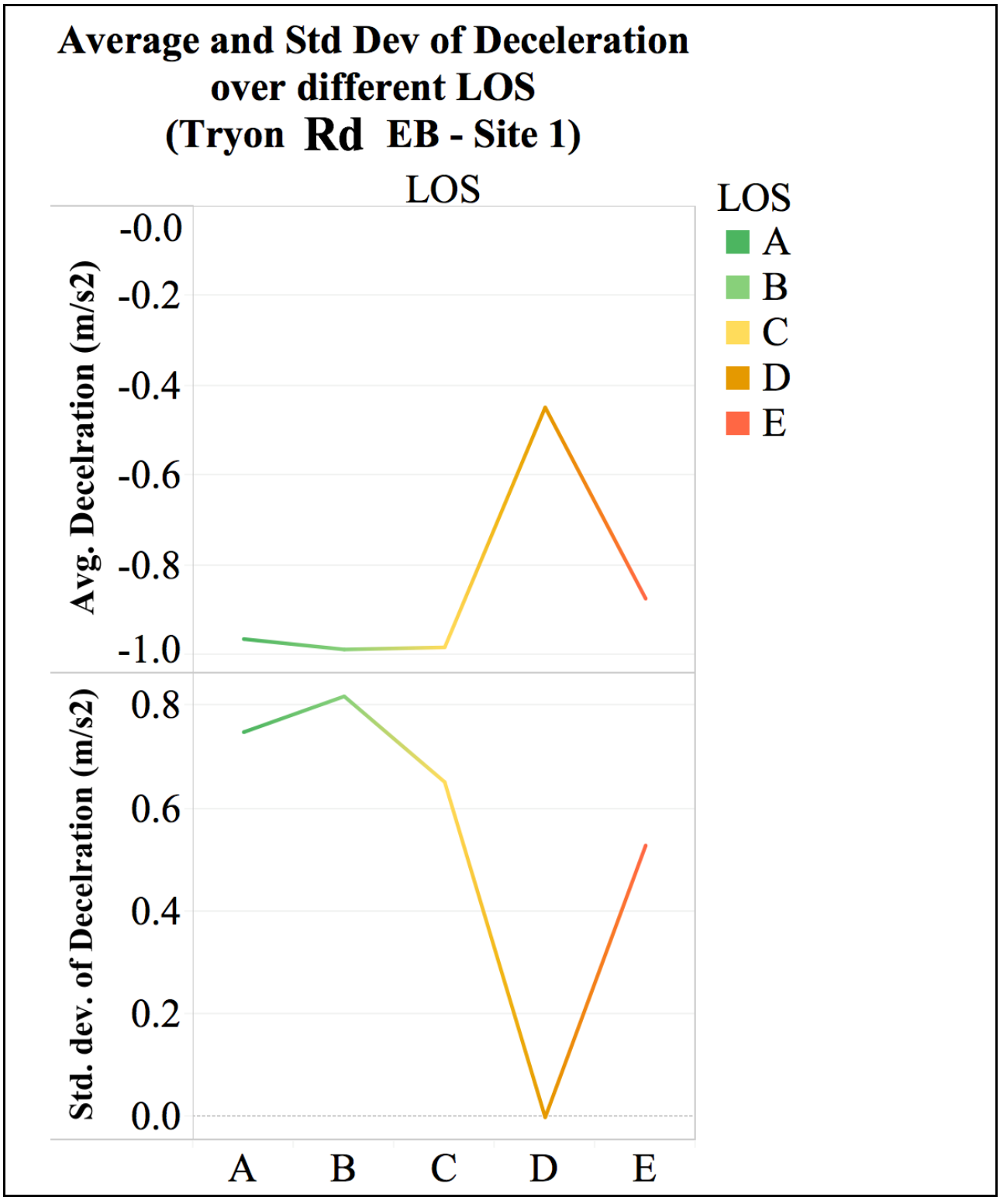

Figure G-8 – Average and Std Dev of Deceleration over different LOS (Tryon Rd EB – Site 1)

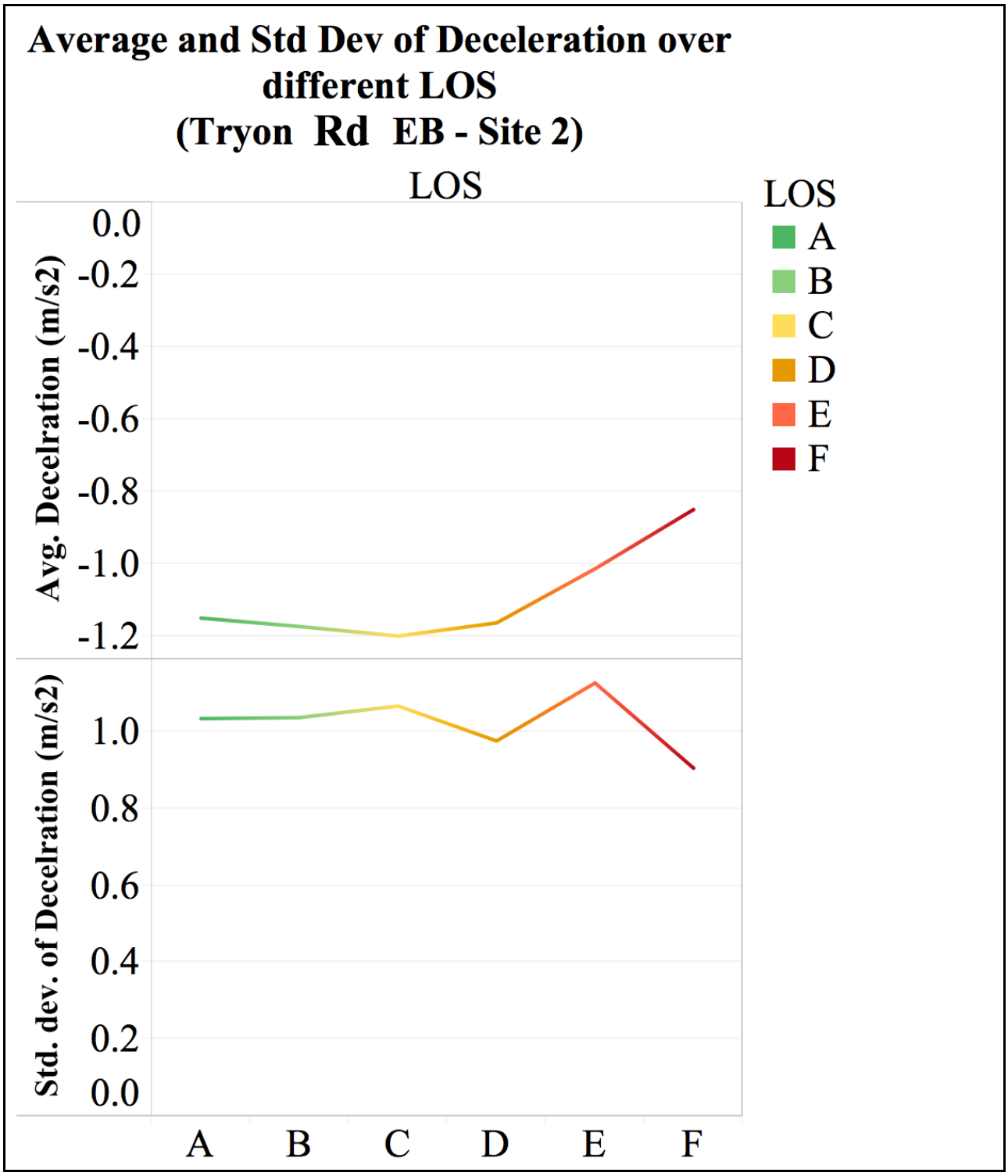

Figure G-9 – Average and Std Dev of Deceleration over different LOS (Tryon Rd EB – Site 2)

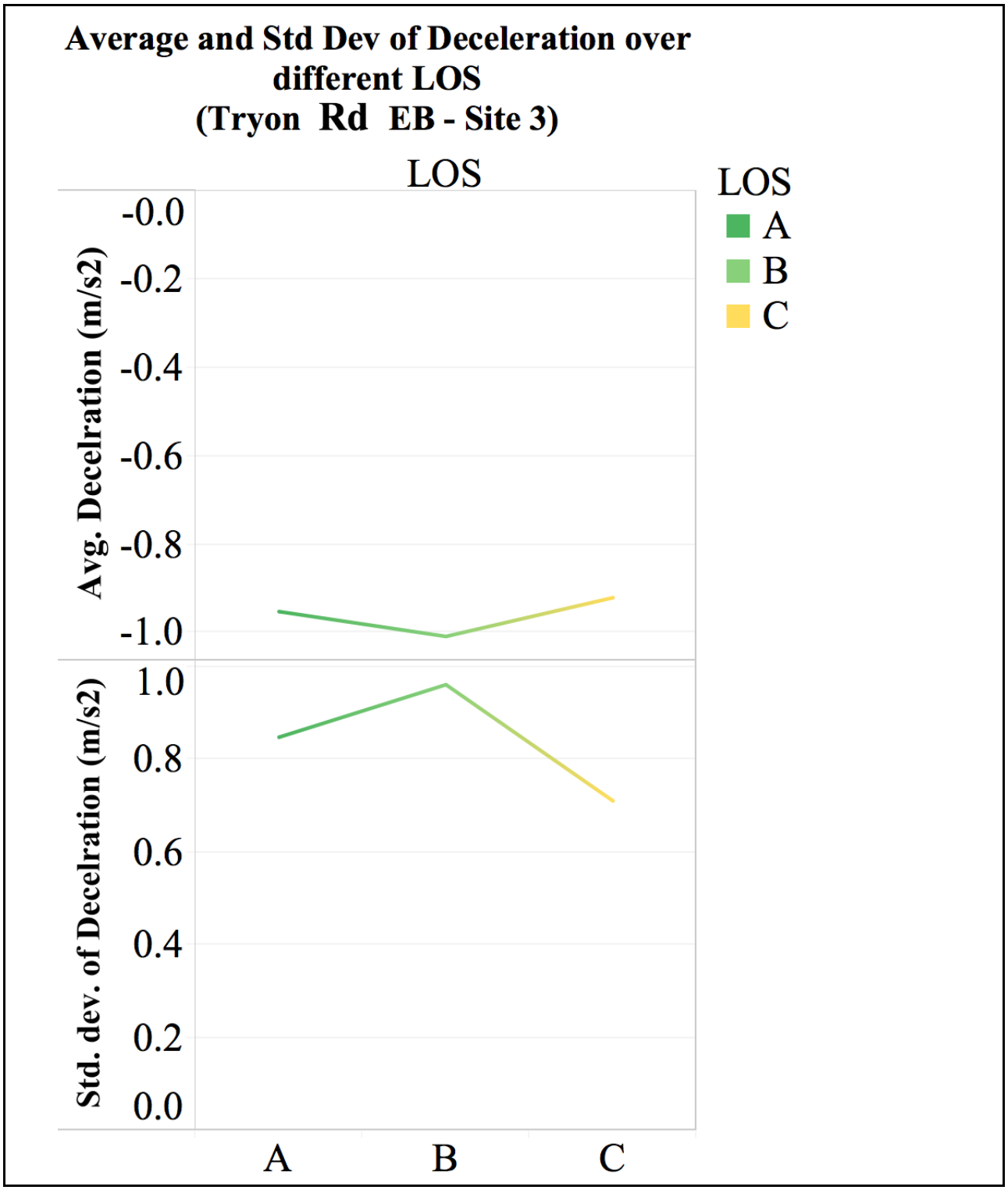

Figure G-10 – Average and Std Dev of Deceleration over different LOS (Tryon Rd EB – Site 3)

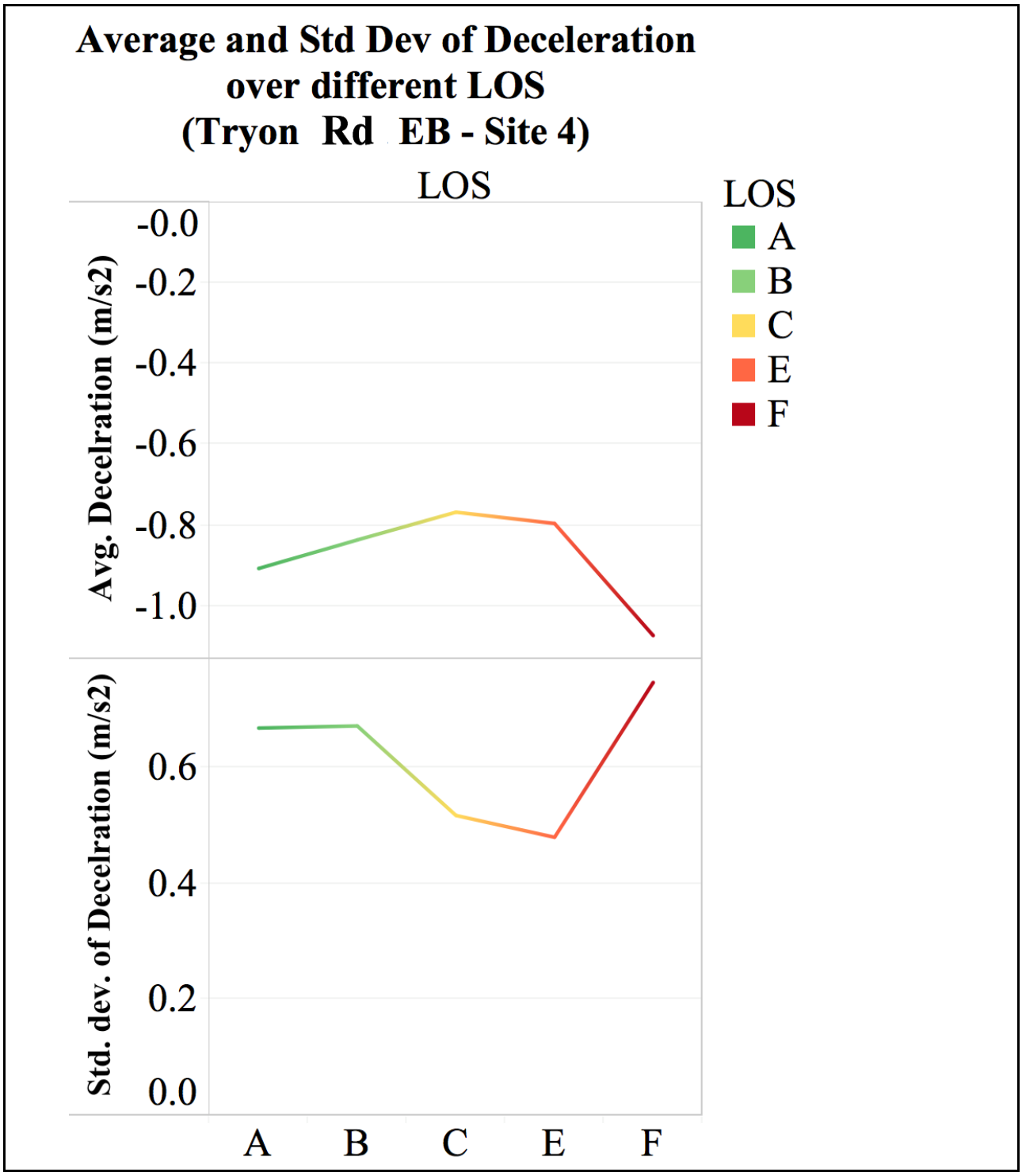

Figure G-11 – Average and Std Dev of Deceleration over different LOS (Tryon Rd EB – Site 4)

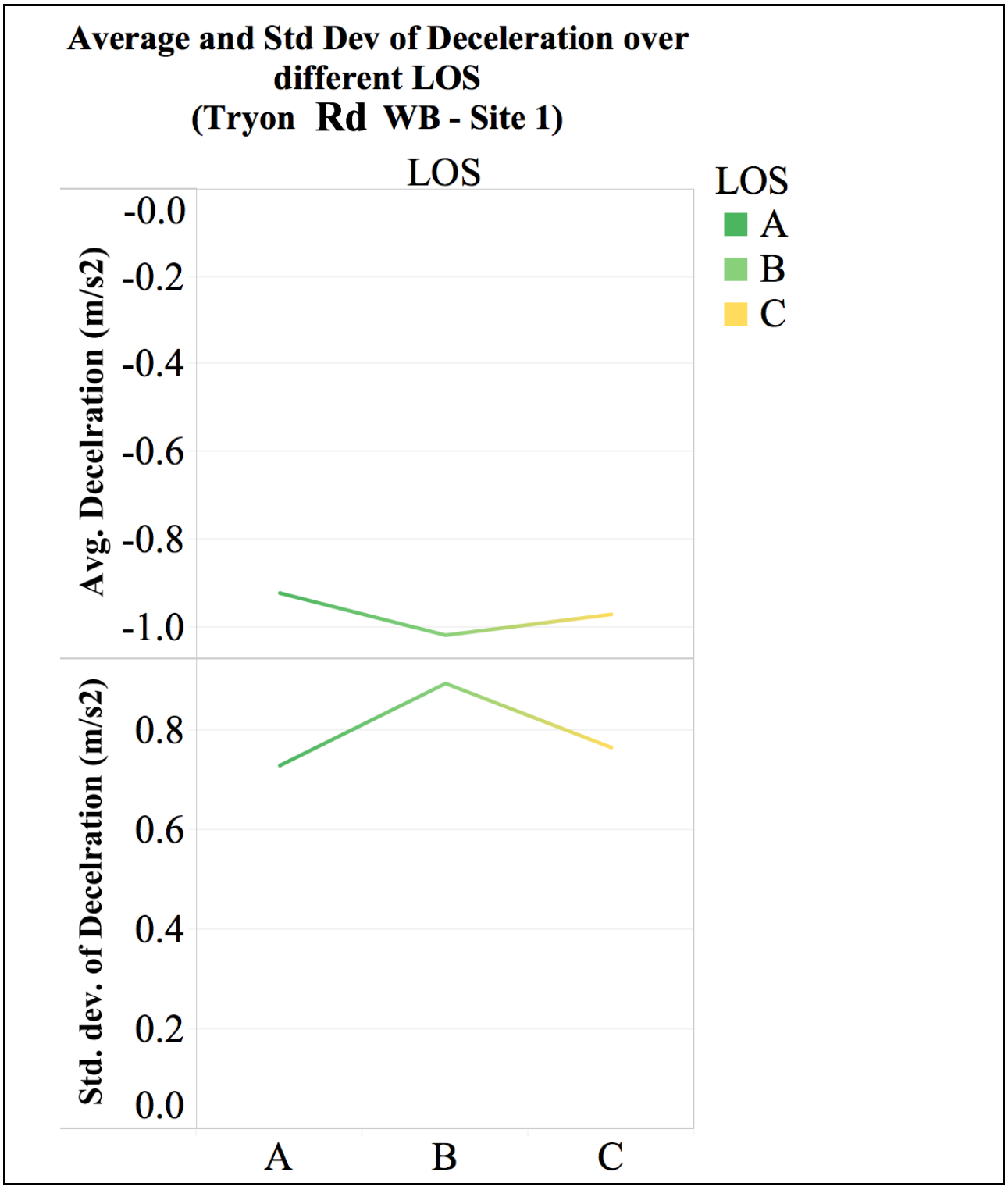

Figure G-12 – Average and Std Dev of Deceleration over different LOS (Tryon Rd WB – Site 1)

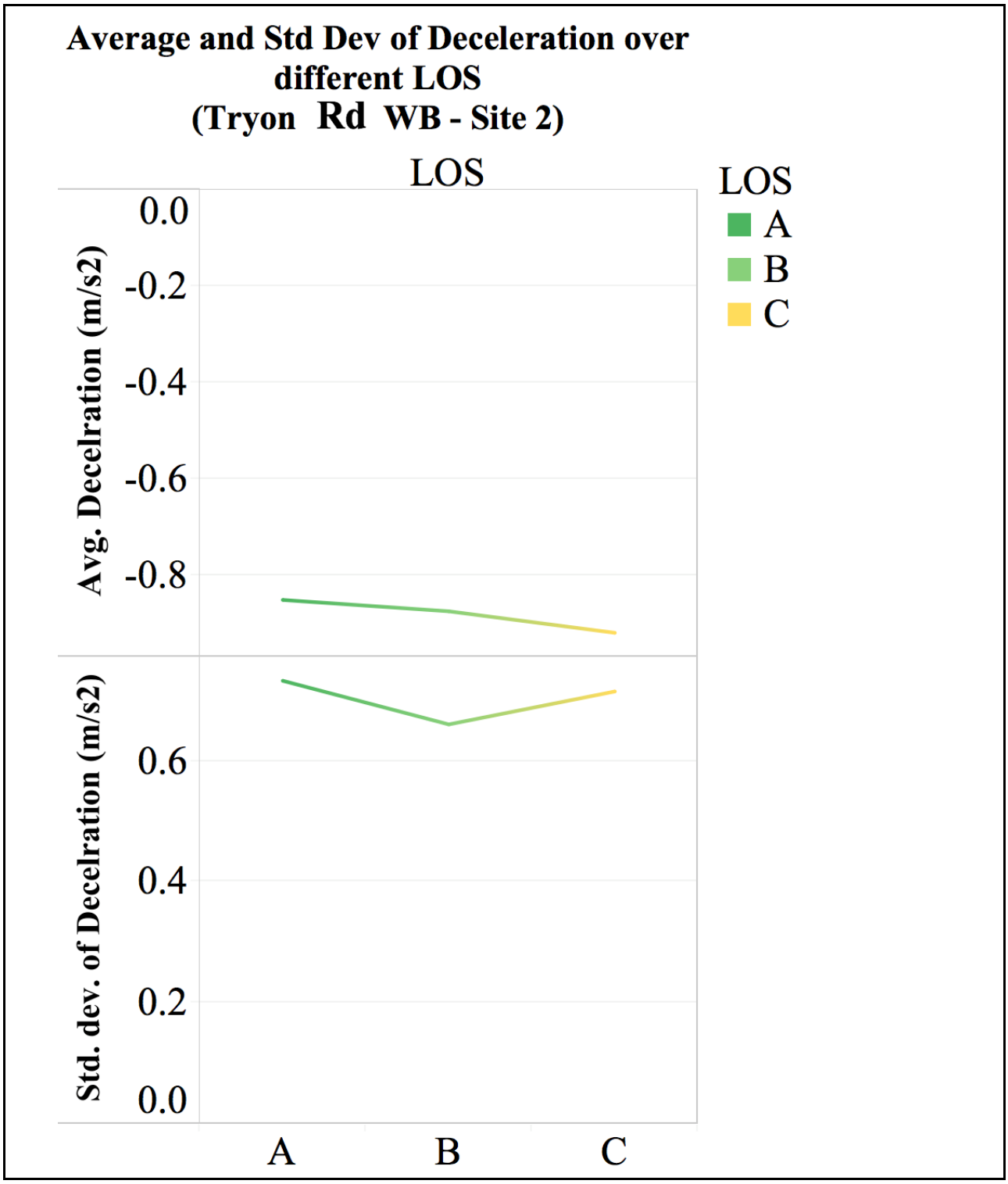

Figure G-13 – Average and Std Dev of Deceleration over different LOS (Tryon Rd WB – Site 2)

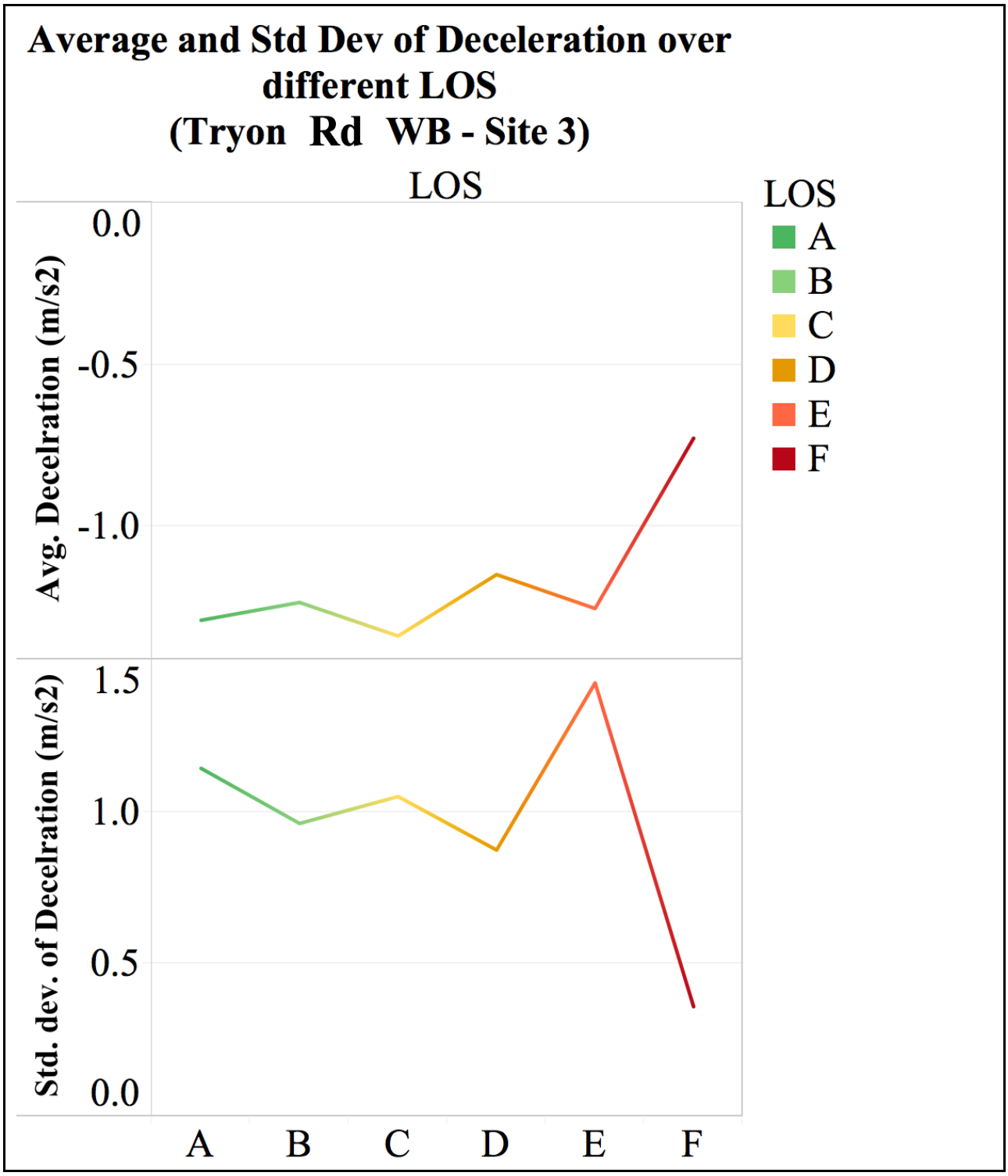

Figure G-14 – Average and Std Dev of Deceleration over different LOS (Tryon Rd WB – Site 3)

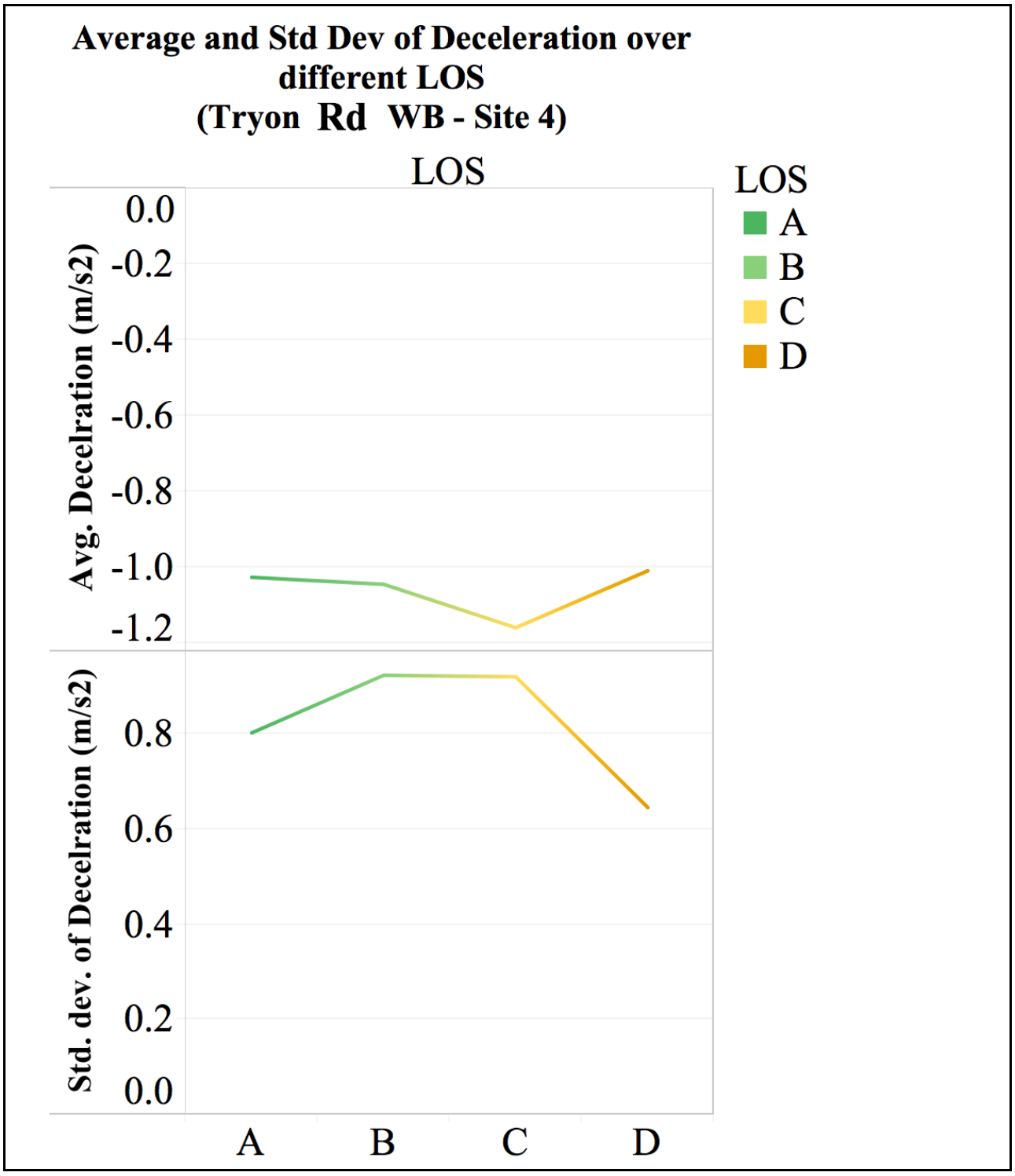

Figure G-15 – Average and Std Dev of Deceleration over different LOS (Tryon Rd WB – Site 4)

APPENDIX H - AVERAGE LATERAL ACCELERATION OVER DIFFERENT LOS

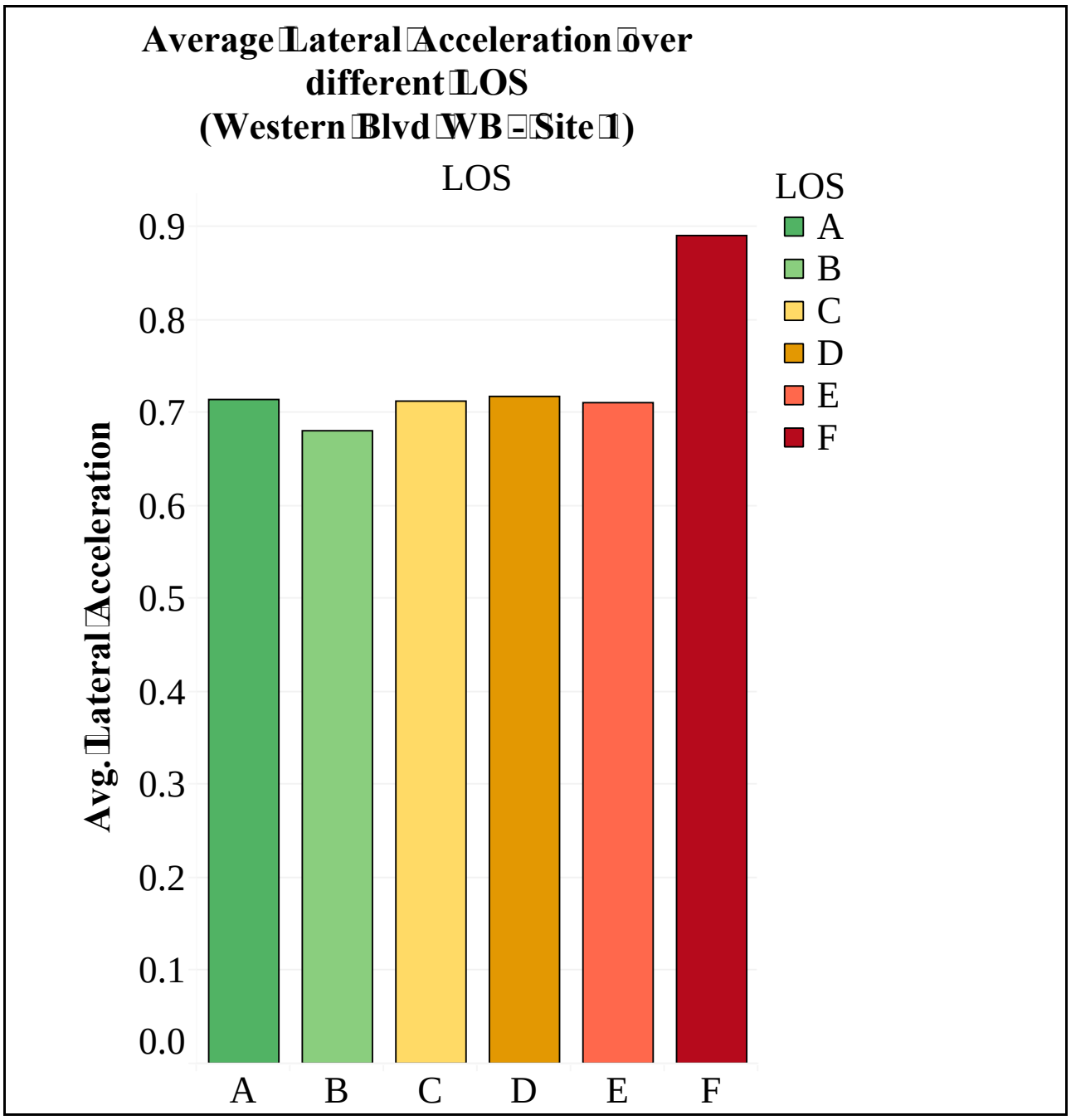

Figure H-1 – Average Lateral Acceleration over different LOS (Western Blvd WB – Site 1)

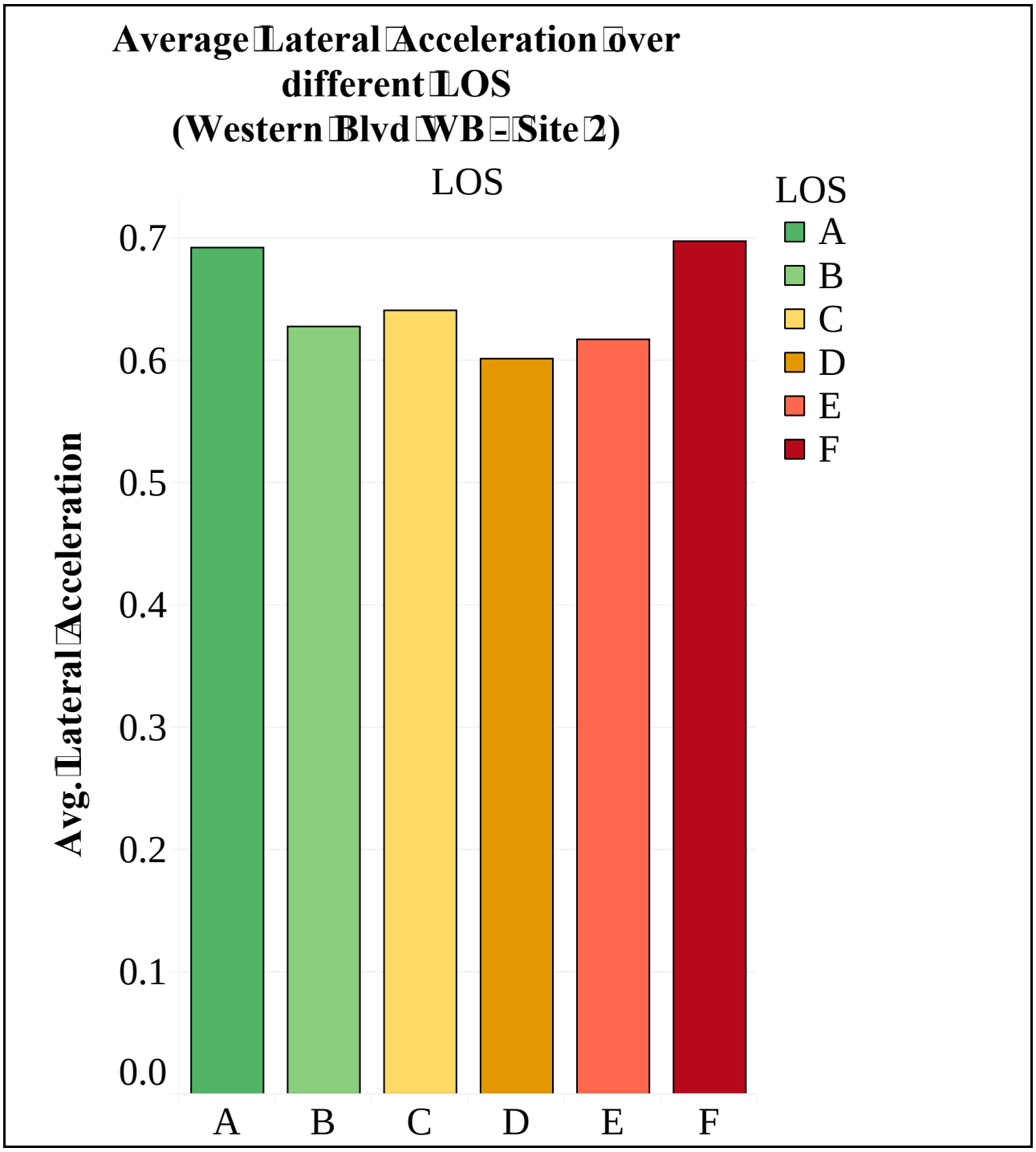

Figure H-2 – Average Lateral Acceleration over different LOS (Western Blvd WB – Site 2)

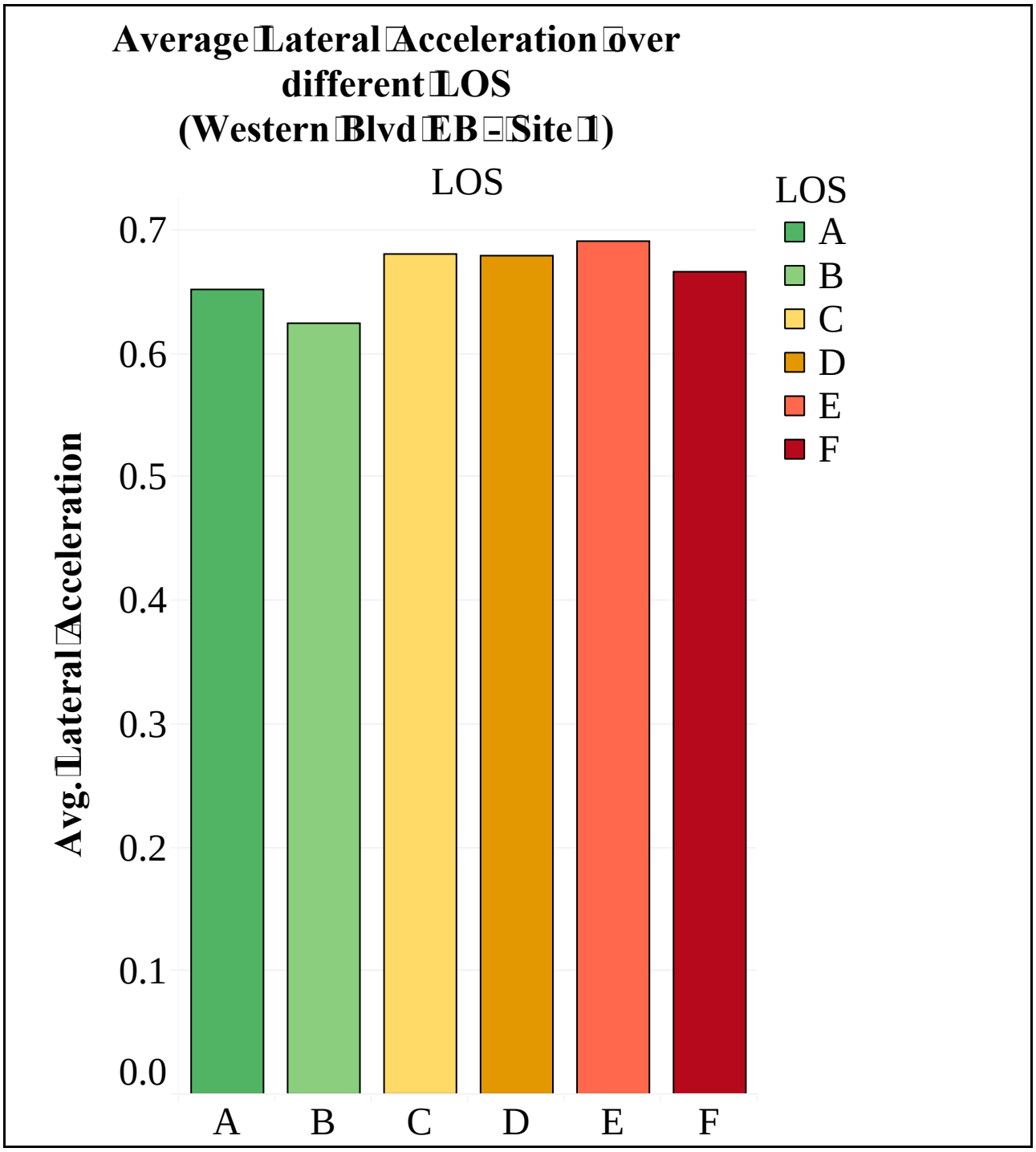

Figure H-3 – Average Lateral Acceleration over different LOS (Western Blvd EB – Site 1)

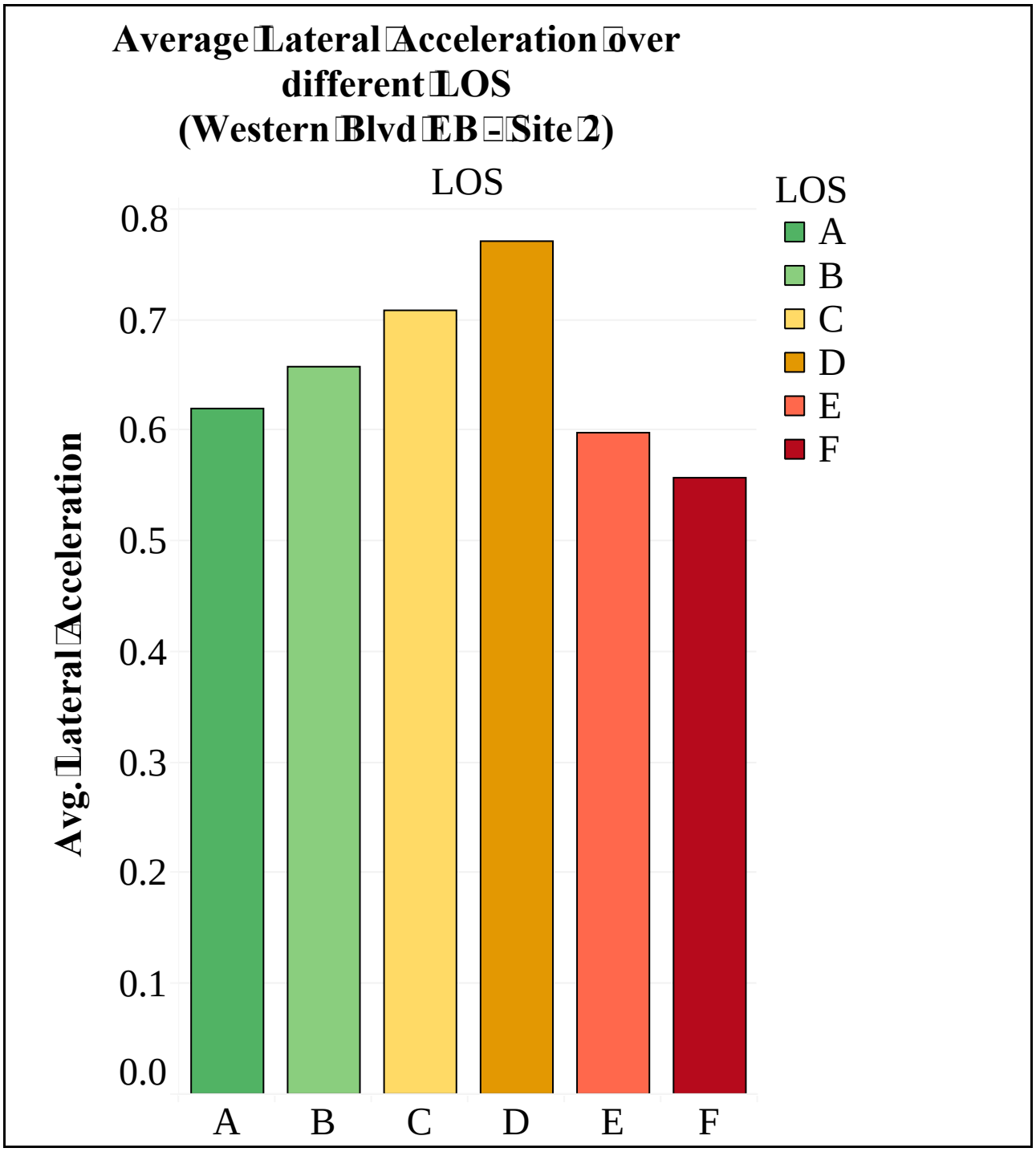

Figure H-4 – Average Lateral Acceleration over different LOS (Western Blvd EB – Site 2)

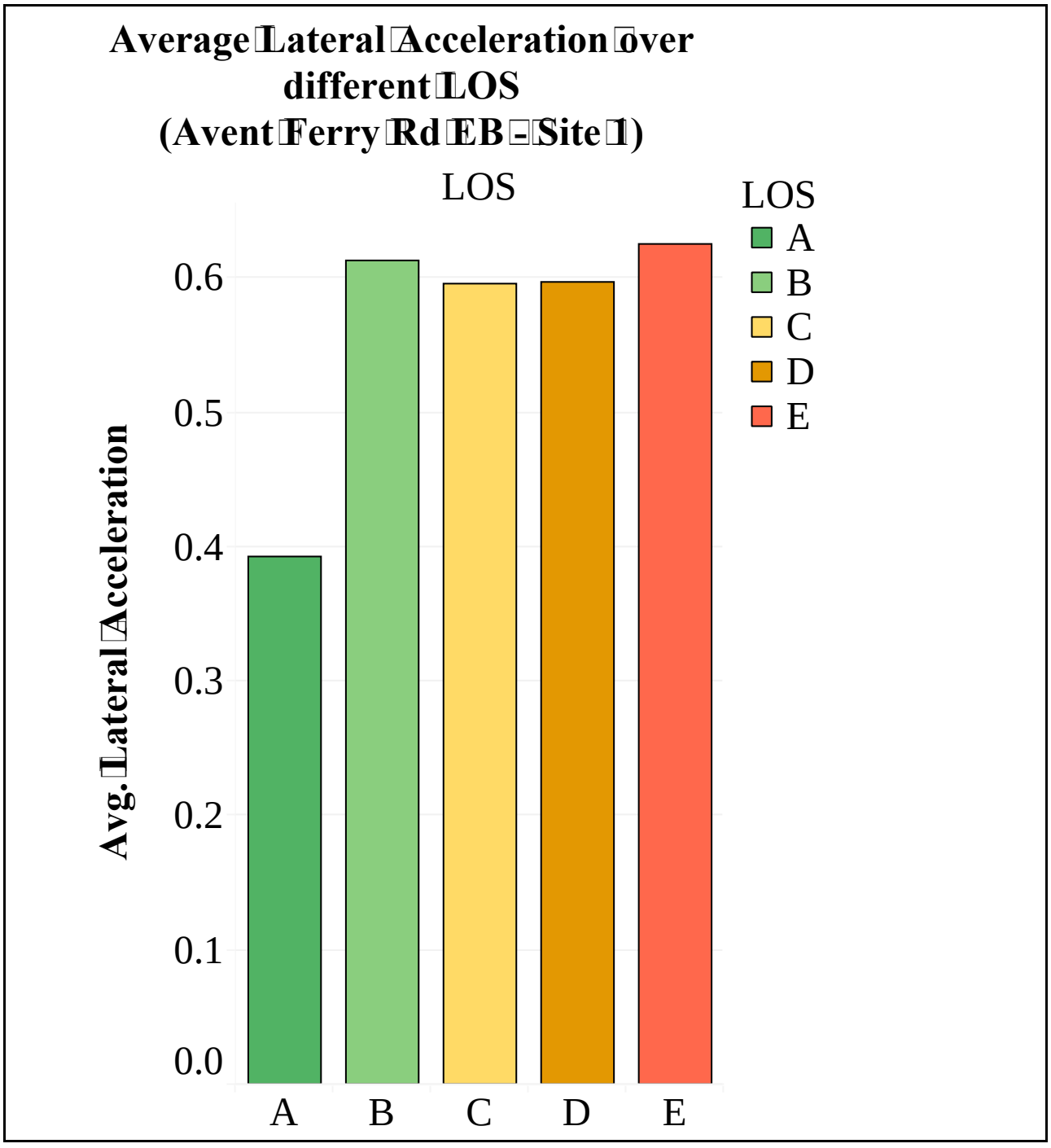

Figure H-5 – Average Lateral Acceleration over different LOS (Avent Ferry Rd EB – Site 1)

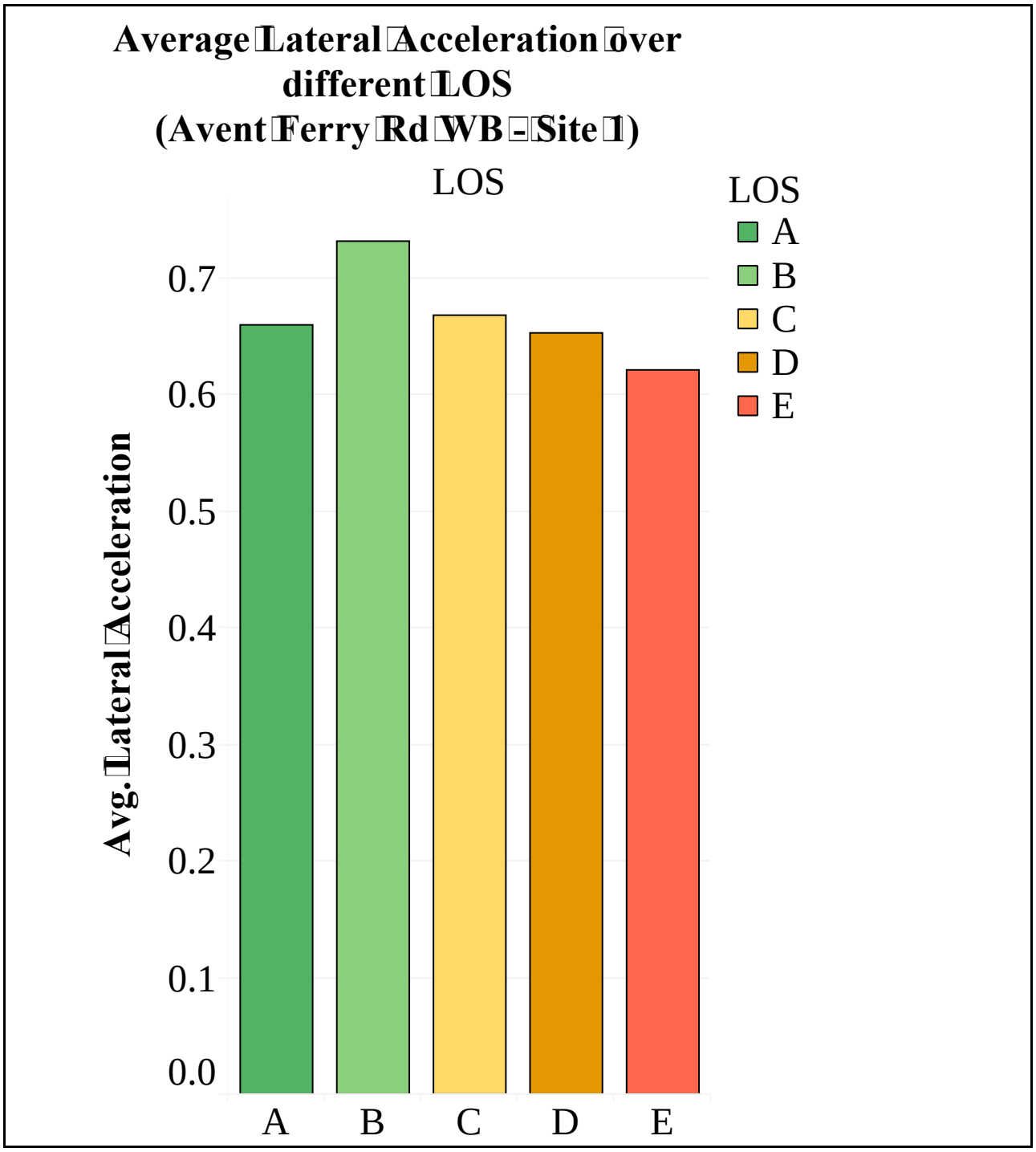

Figure H-6 – Average Lateral Acceleration over different LOS (Avent Ferry Rd WB – Site 1)

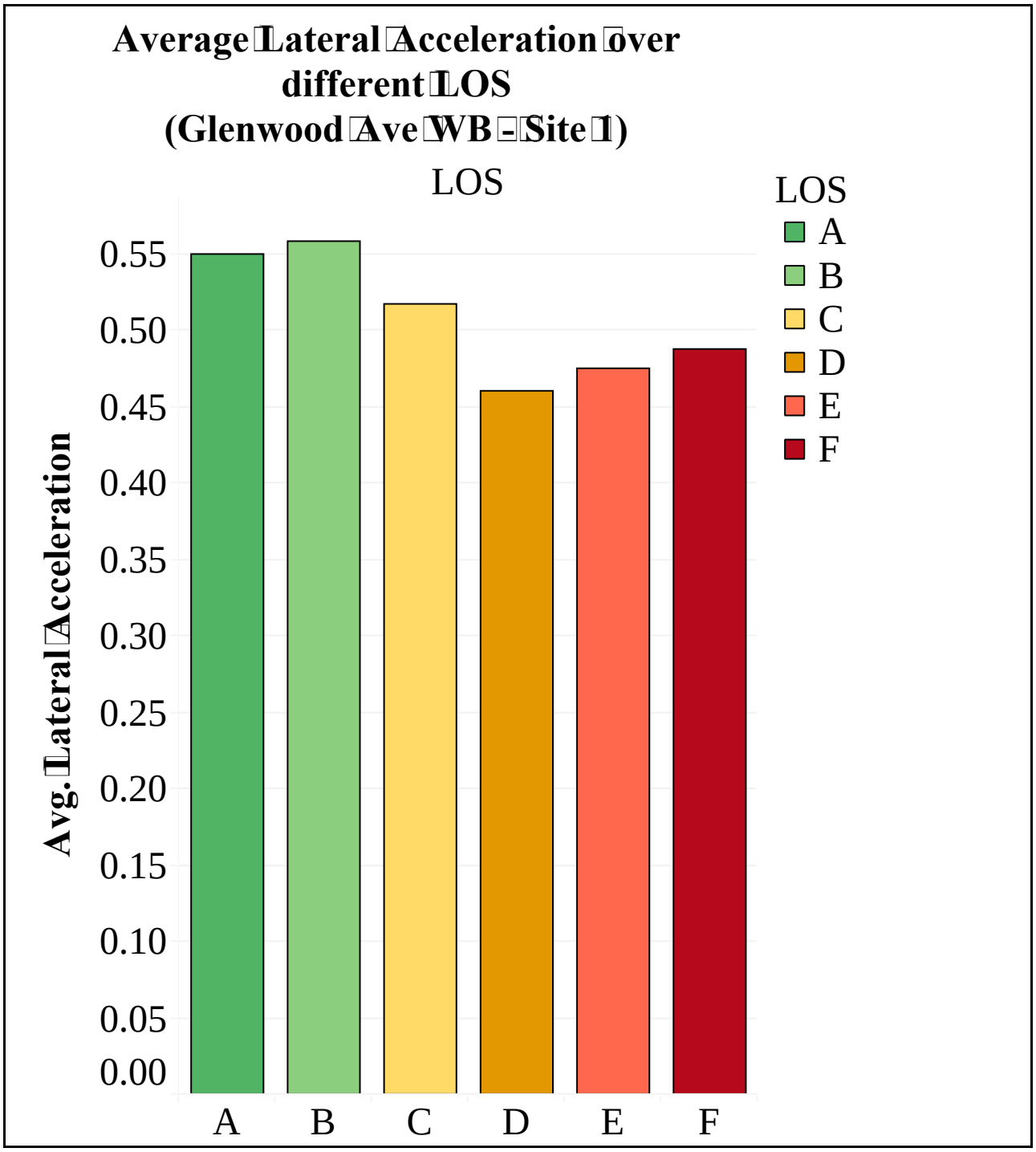

Figure H-7 – Average Lateral Acceleration over different LOS (Glenwood Ave WB – Site 1)

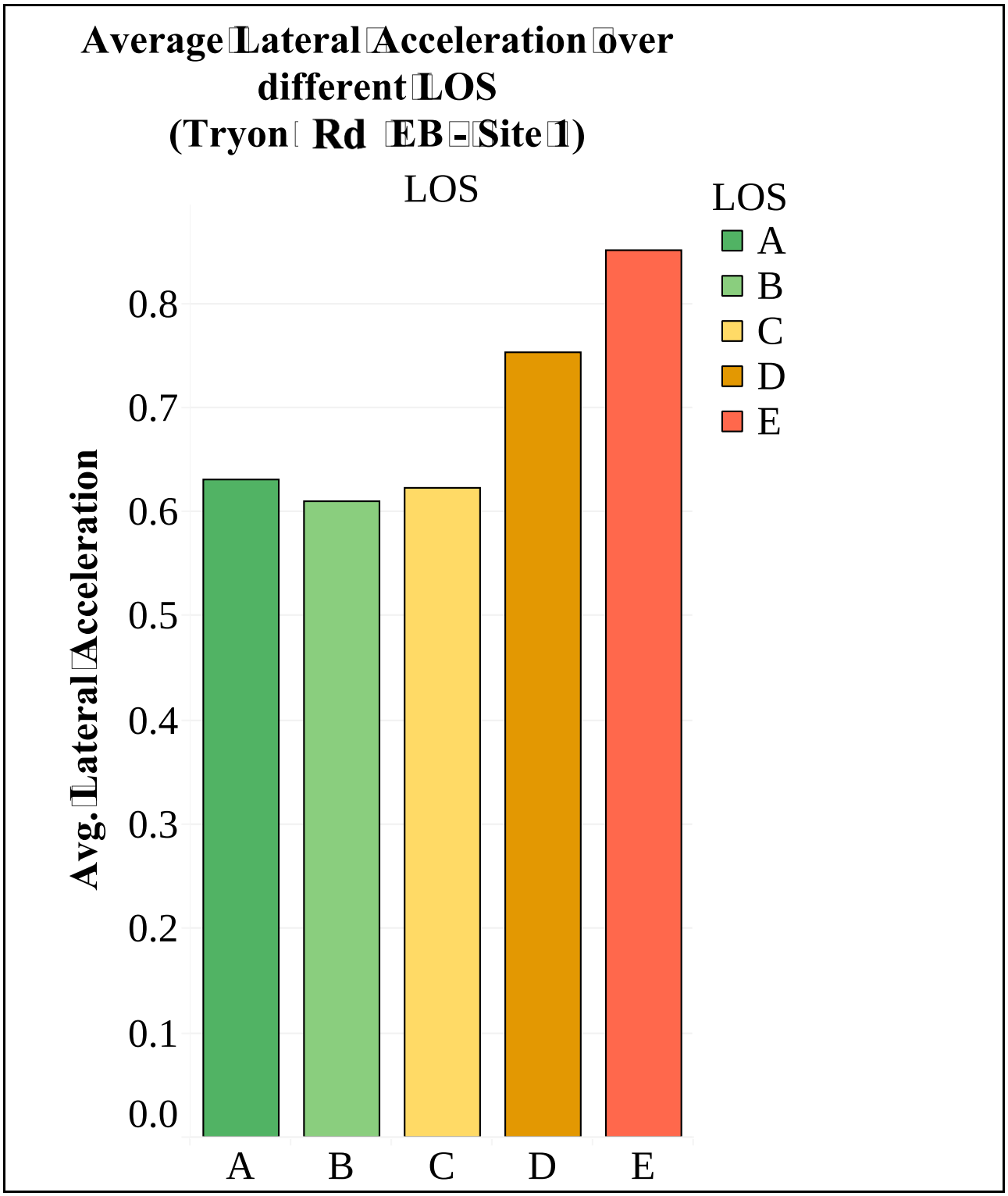

Figure H-8 – Average Lateral Acceleration over different LOS (Tryon Rd EB – Site 1)

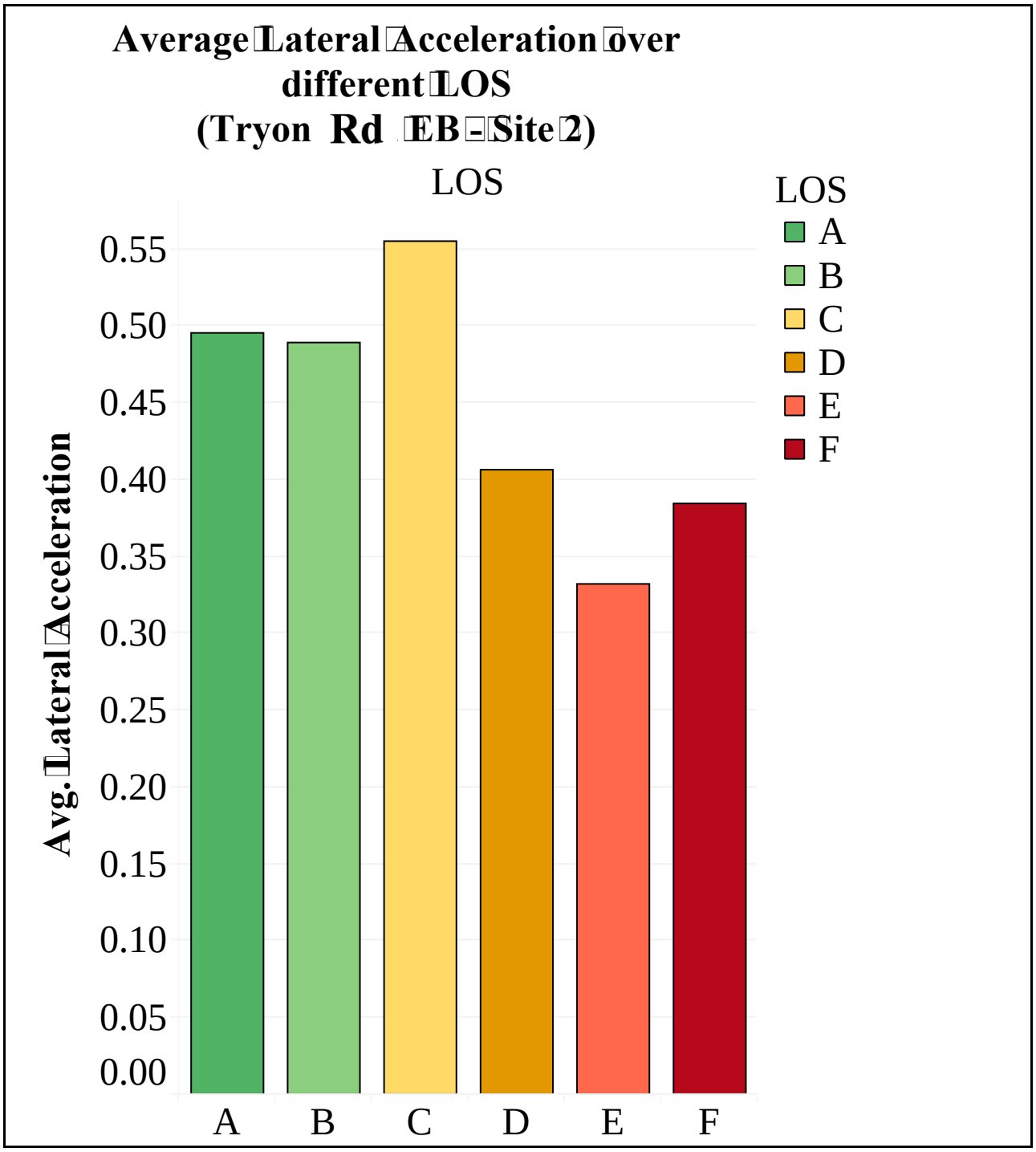

Figure H-9 – Average Lateral Acceleration over different LOS (Tryon Rd EB – Site 2)

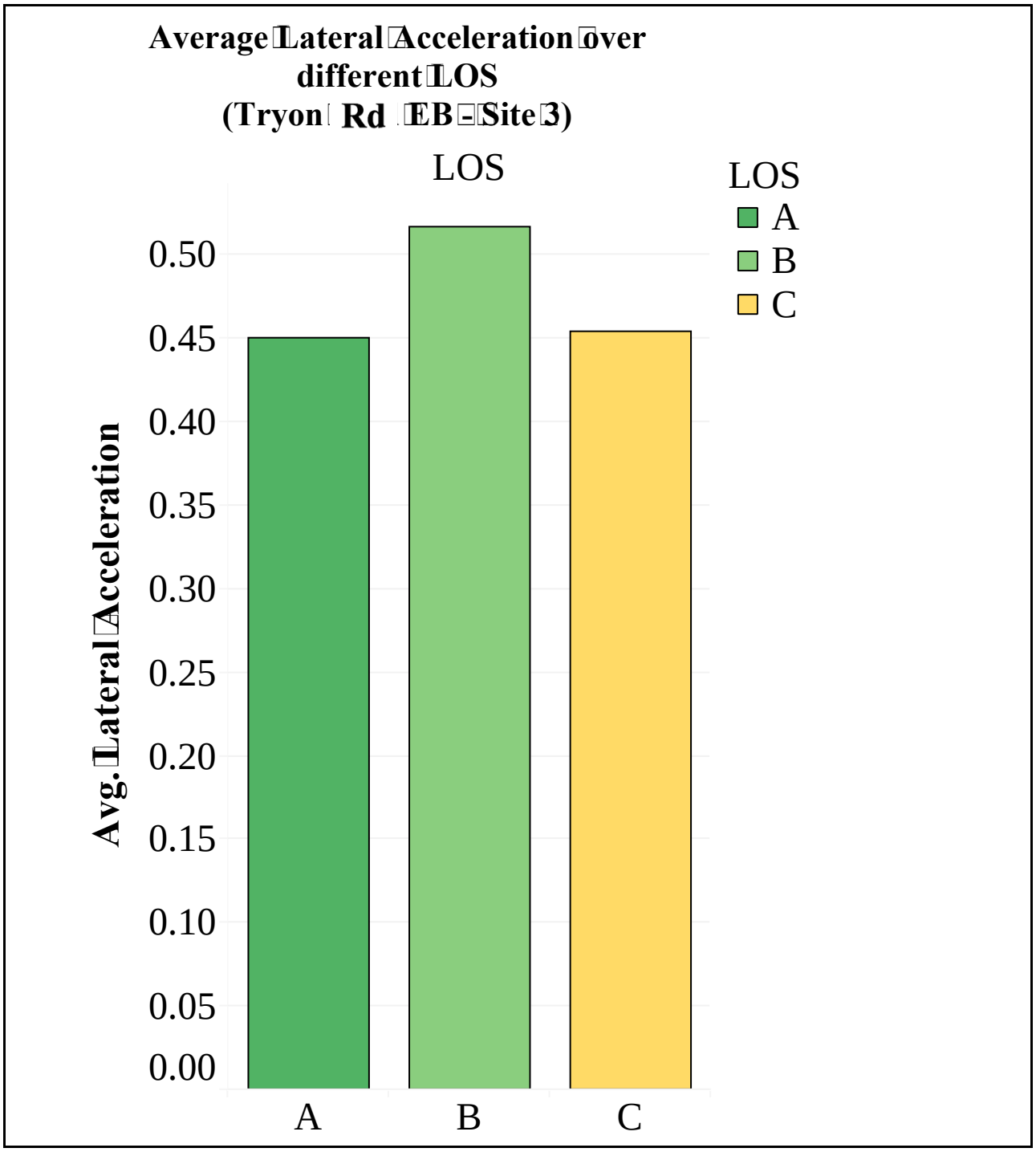

Figure H-10 – Average Lateral Acceleration over different LOS (Tryon Rd EB – Site 3)

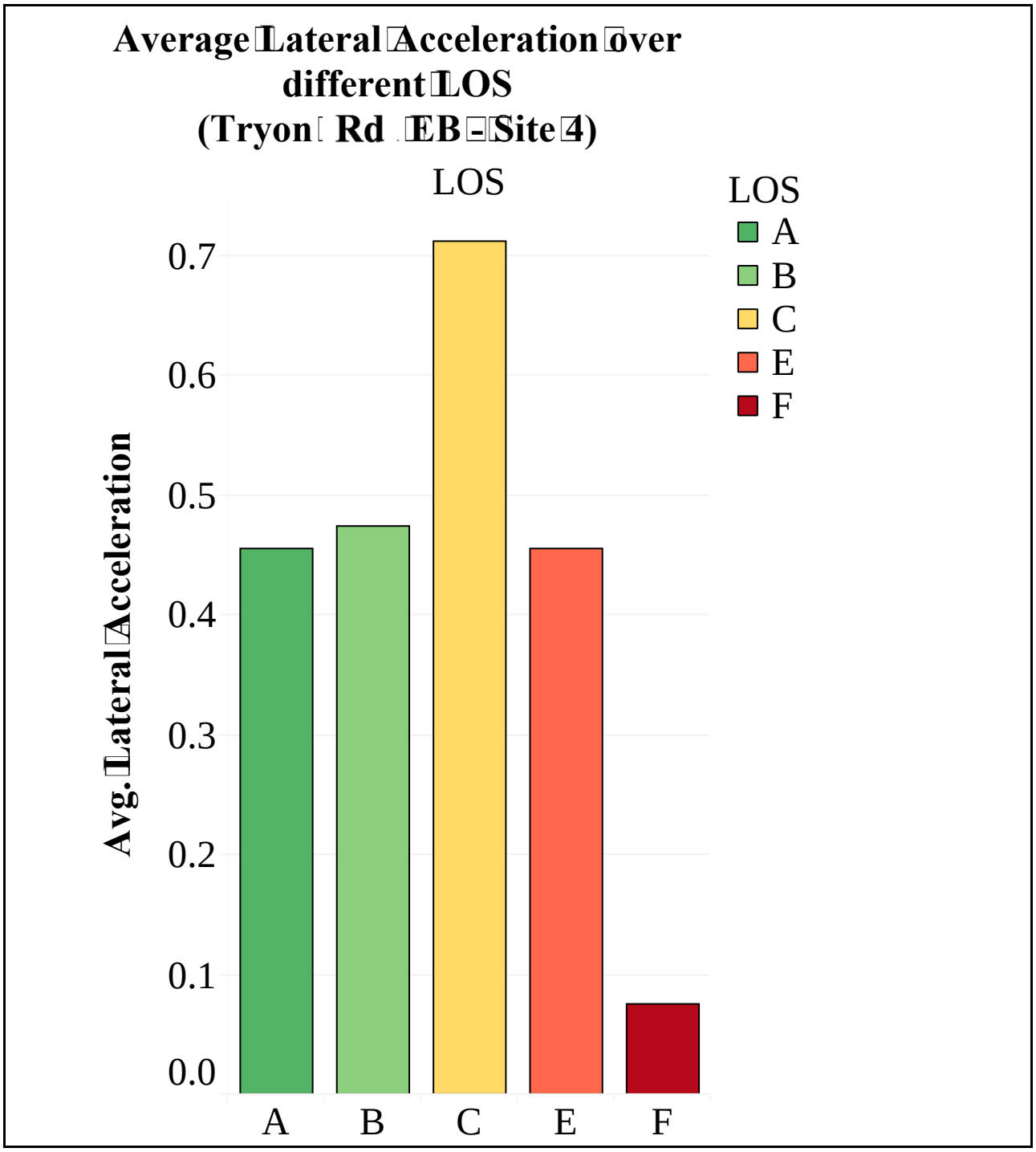

Figure H-11– Average Lateral Acceleration over different LOS (Tryon Rd EB – Site 4)

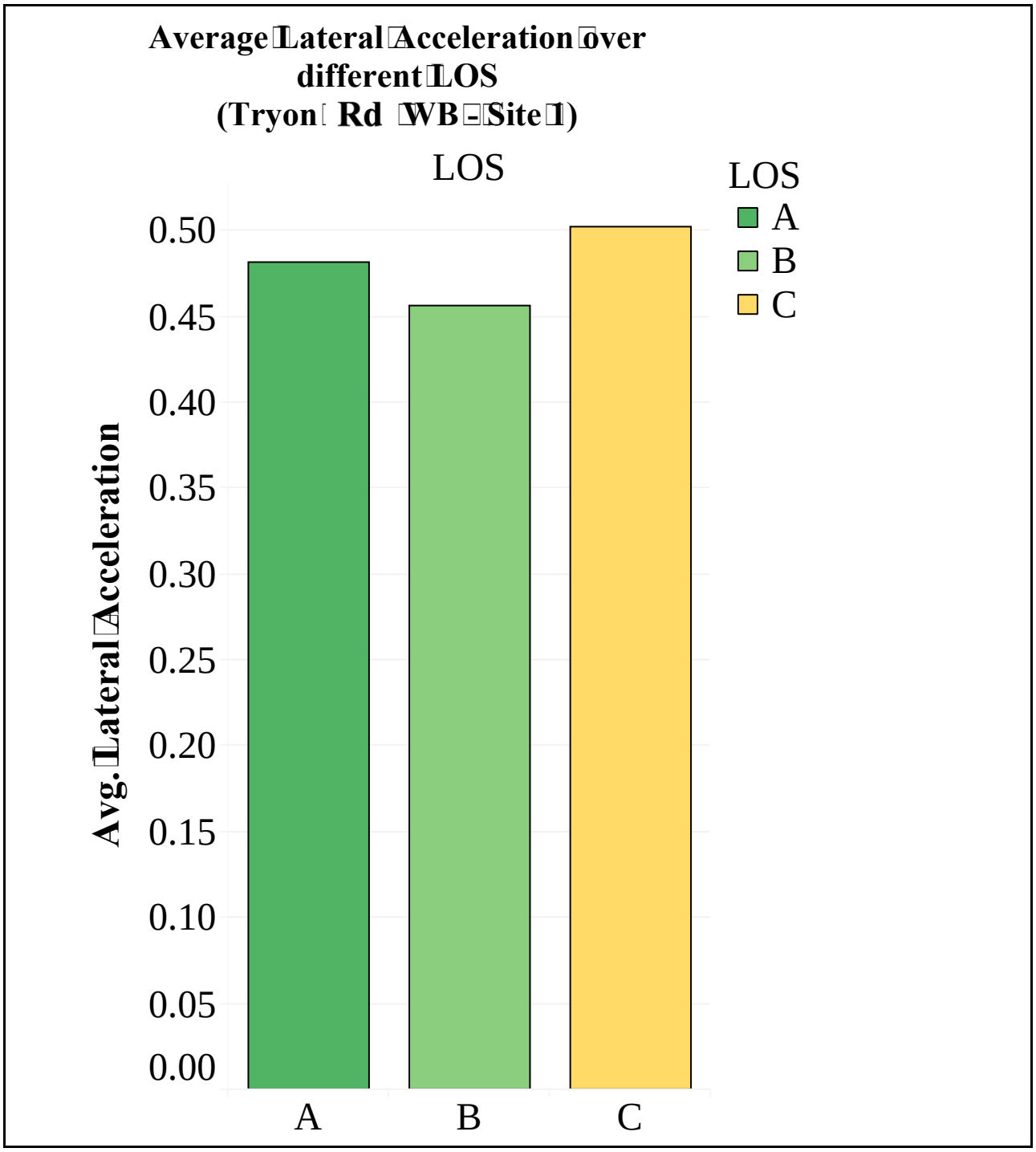

Figure H-12 – Average Lateral Acceleration over different LOS (Tryon Rd WB – Site 1)

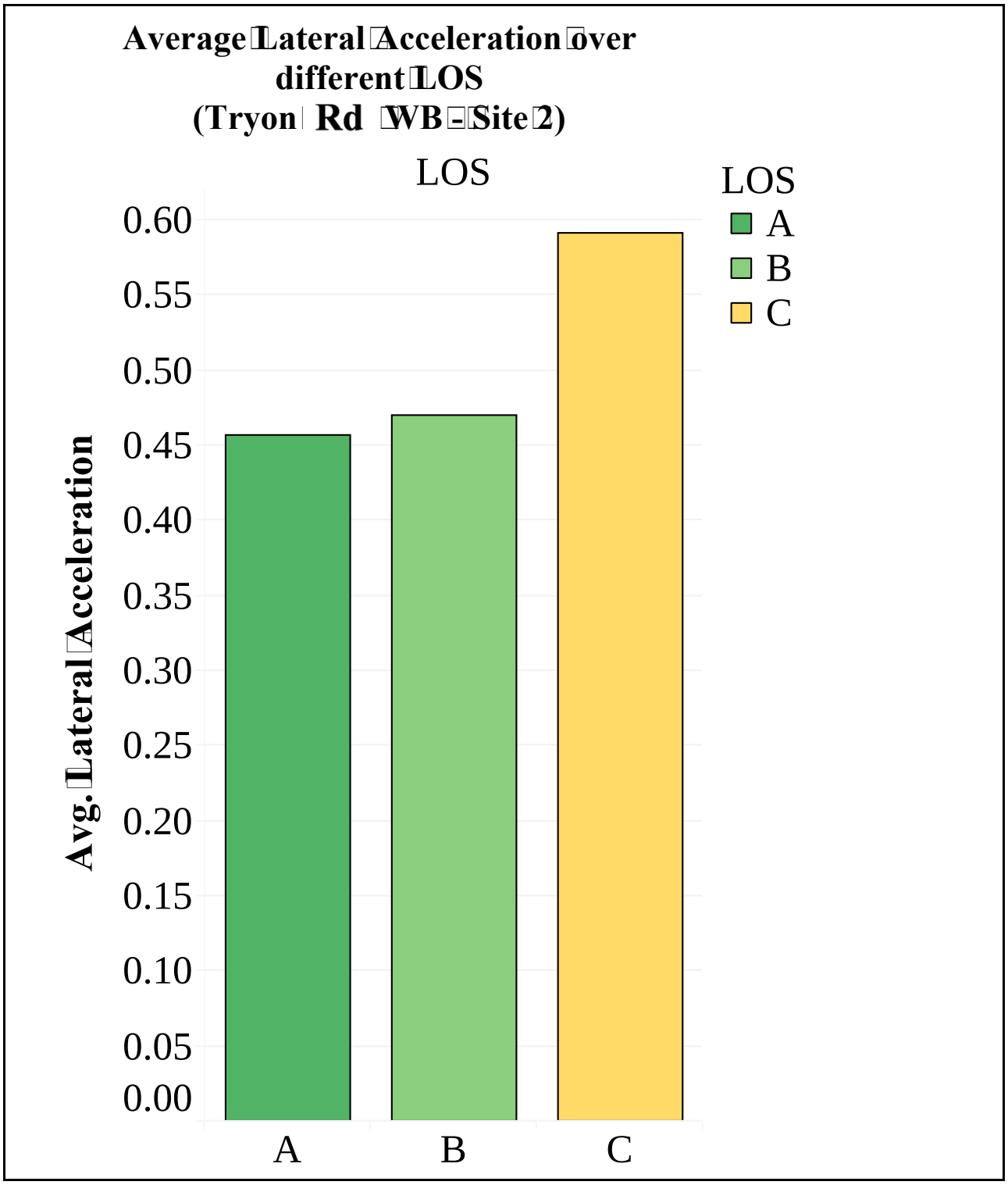

Figure H-13 – Average Lateral Acceleration over different LOS (Tryon Rd WB – Site 2)

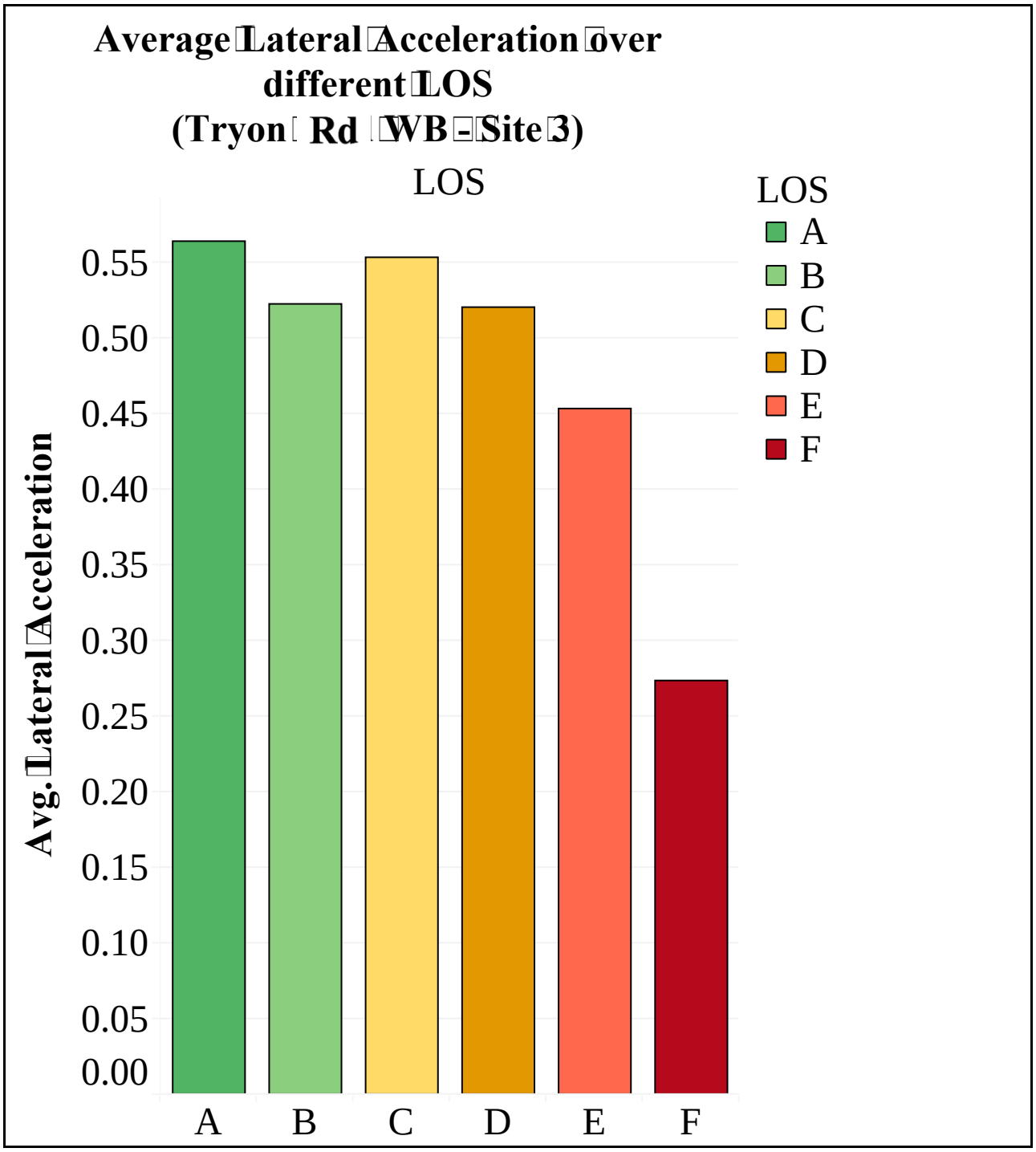

Figure H-14 – Average Lateral Acceleration over different LOS (Tryon Rd WB – Site 3)

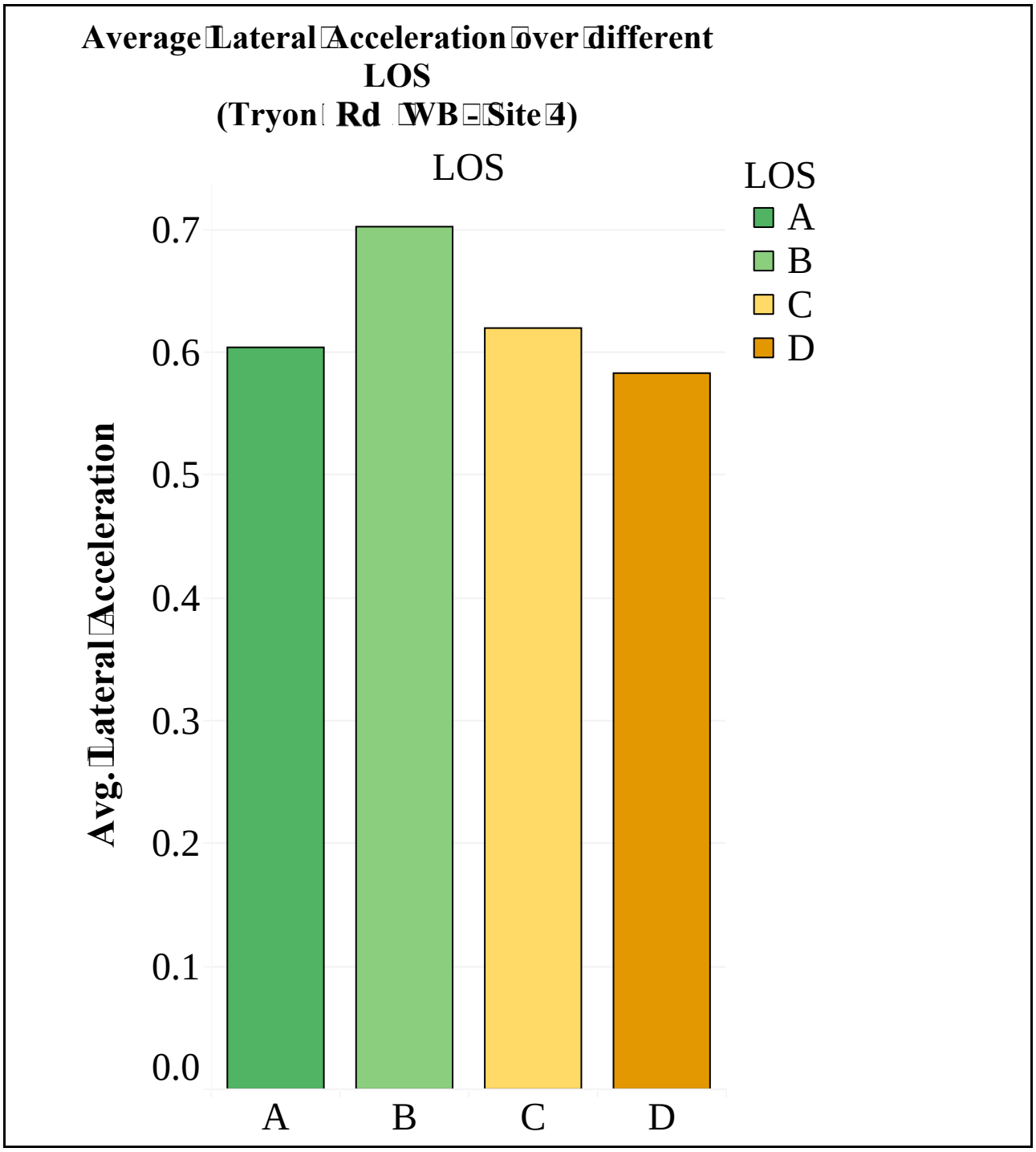

Figure H-15 – Average Lateral Acceleration over different LOS (Tryon Rd WB – Site 4)

APPENDIX I - BOXPLOT OF SECOND-BY-SECOND LATERAL ACCELERATION OVER DIFFERENT LOS

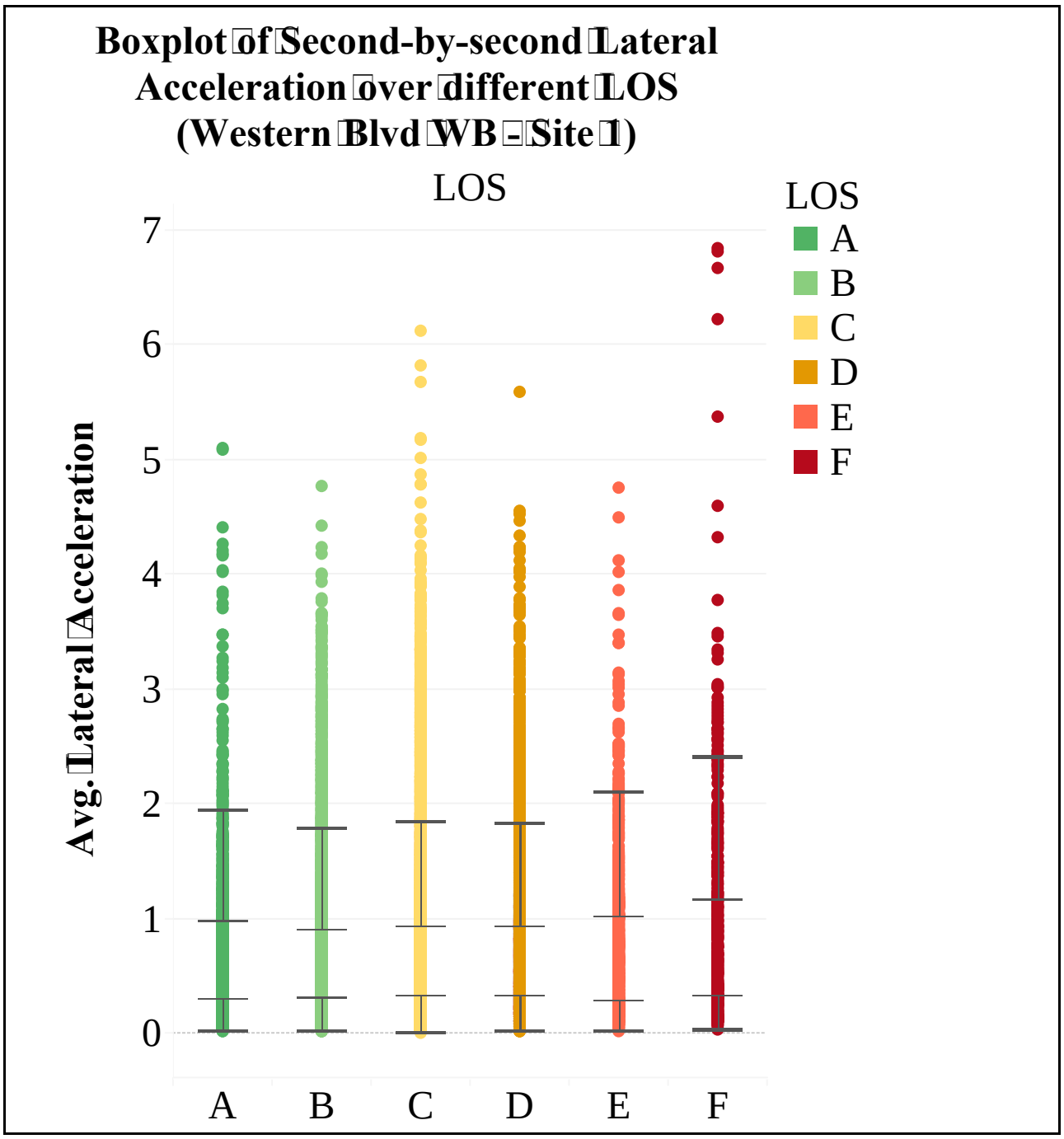

Figure I-1 – Boxplot of Second-by-second Lateral Acceleration over different LOS (Western Blvd WB – Site 1)

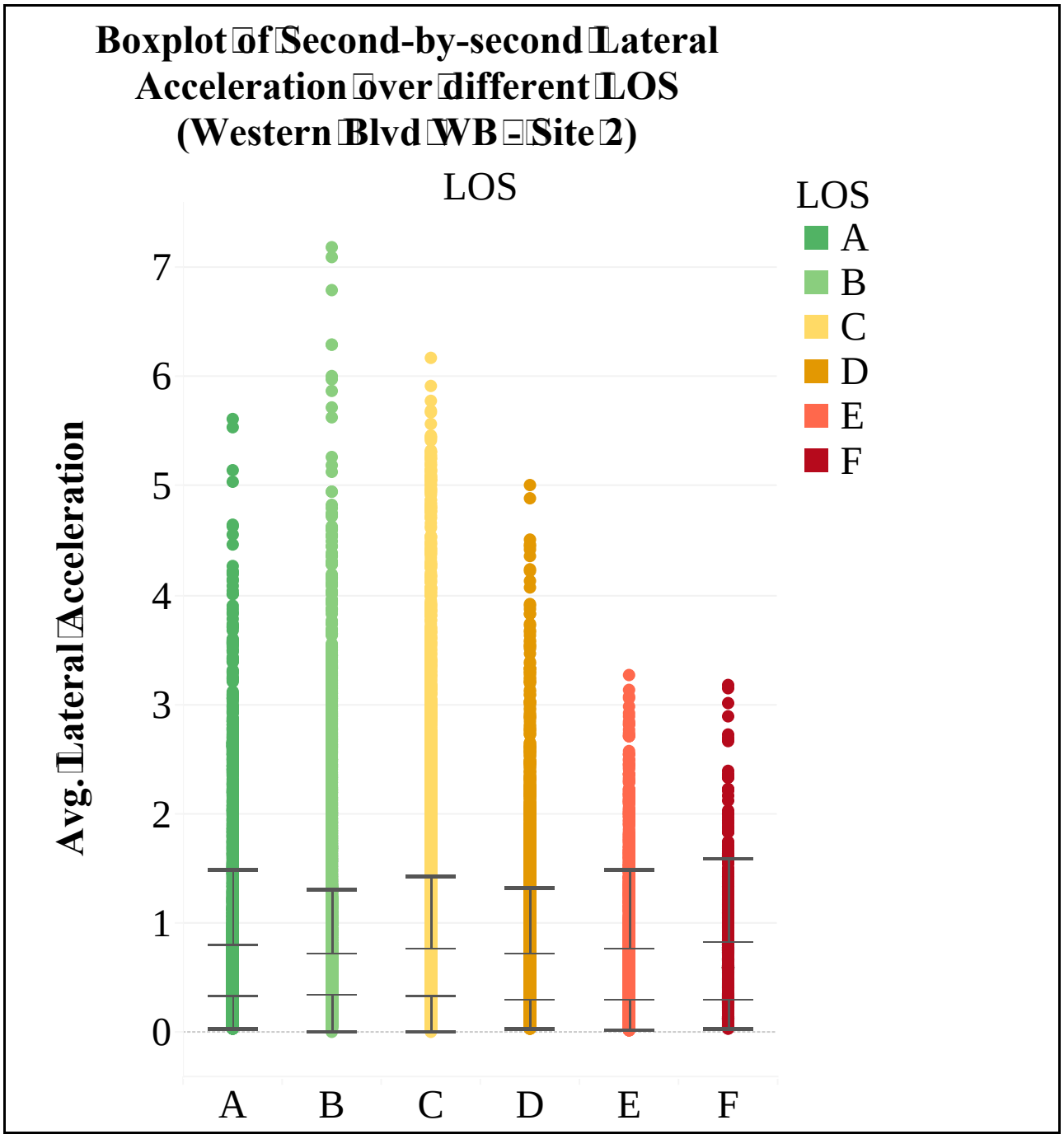

Figure I-2 – Boxplot of Second-by-second Lateral Acceleration over different LOS (Western Blvd WB – Site 2)

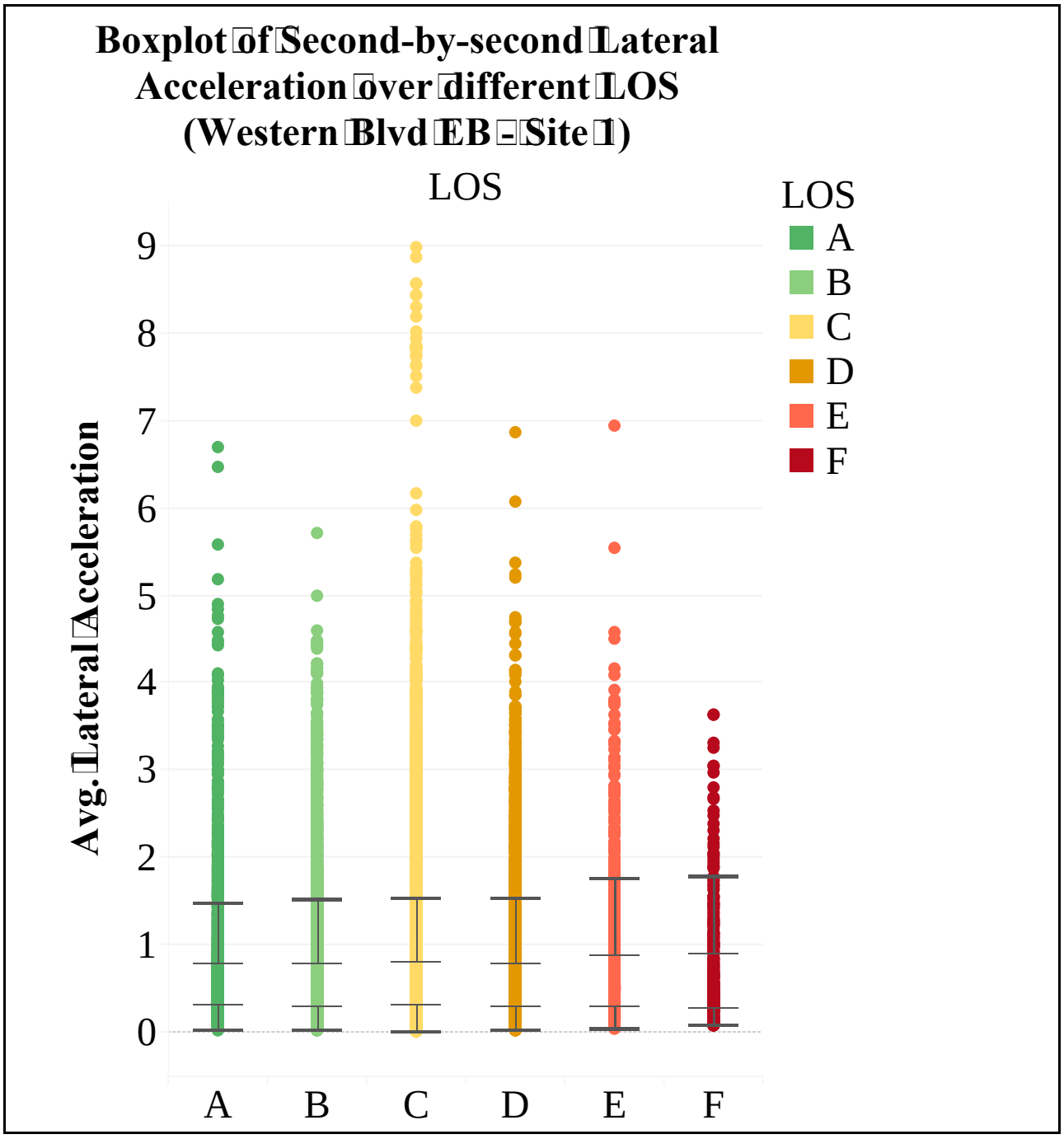

Figure I-3 – Boxplot of Second-by-second Lateral Acceleration over different LOS (Western Blvd EB – Site 1)

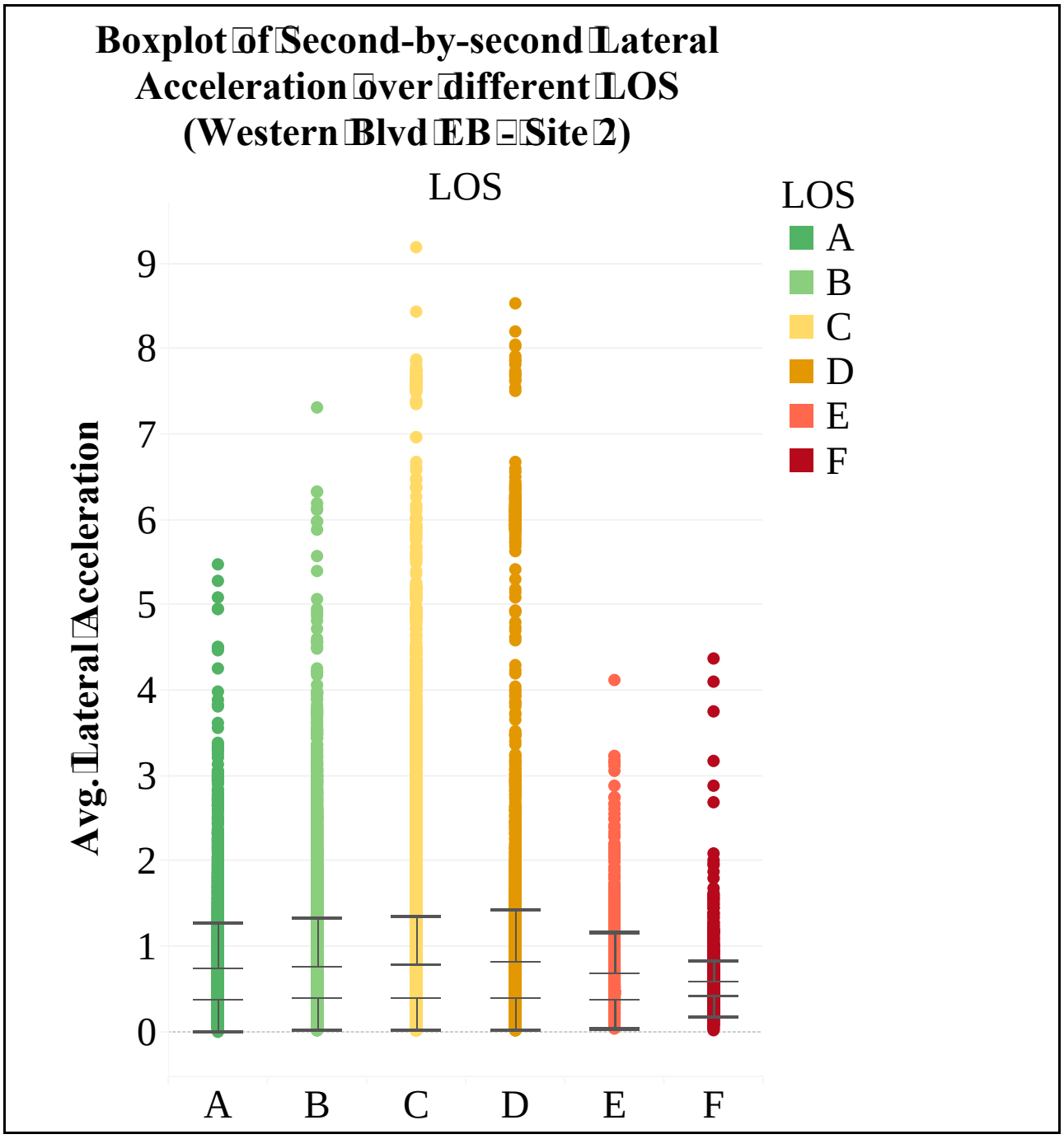

Figure I-4 – Boxplot of Second-by-second Lateral Acceleration over different LOS (Western Blvd EB – Site 2)

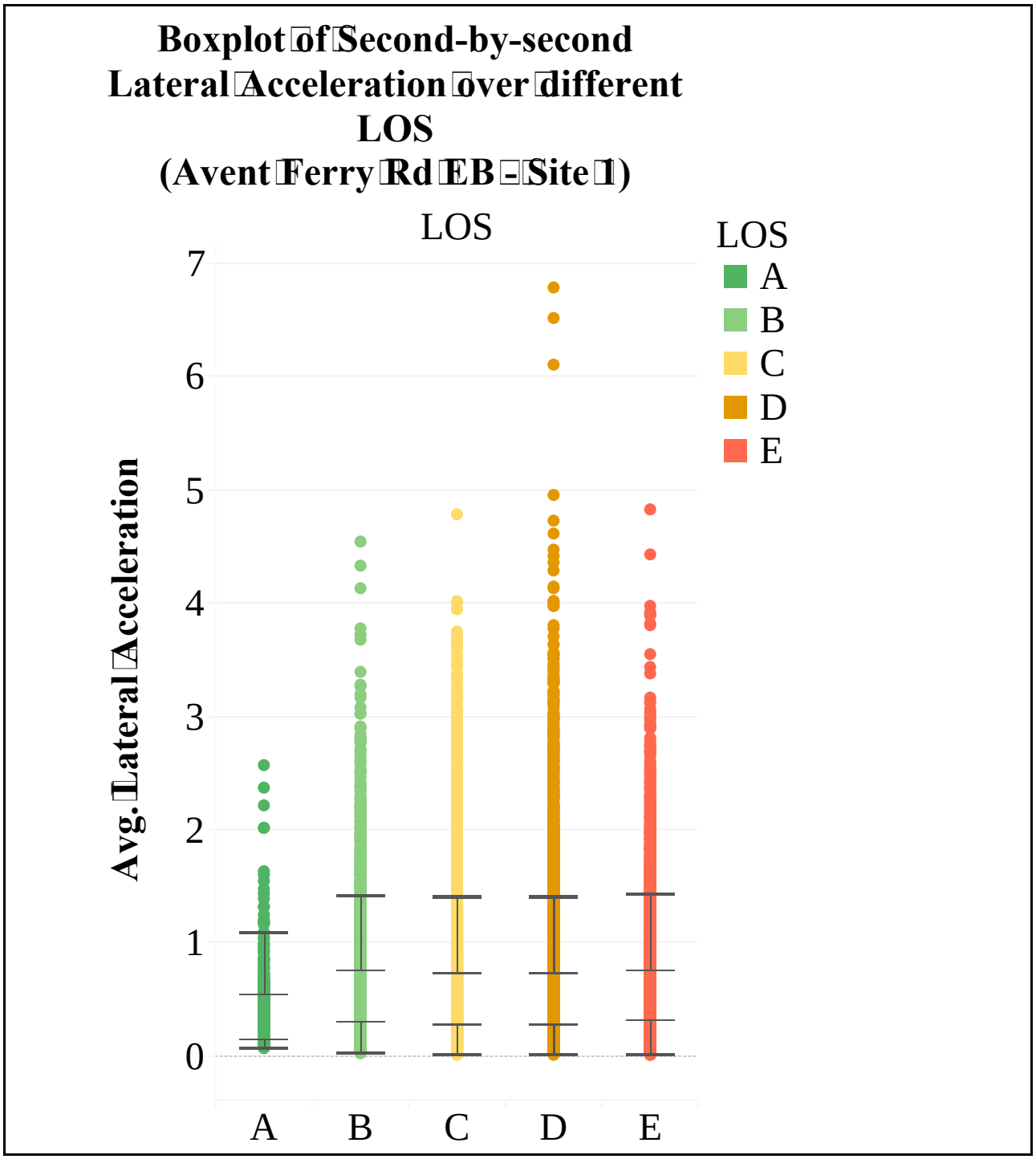

Figure I-5 – Boxplot of Second-by-second Lateral Acceleration over different LOS (Avent Ferry Rd EB – Site 1)

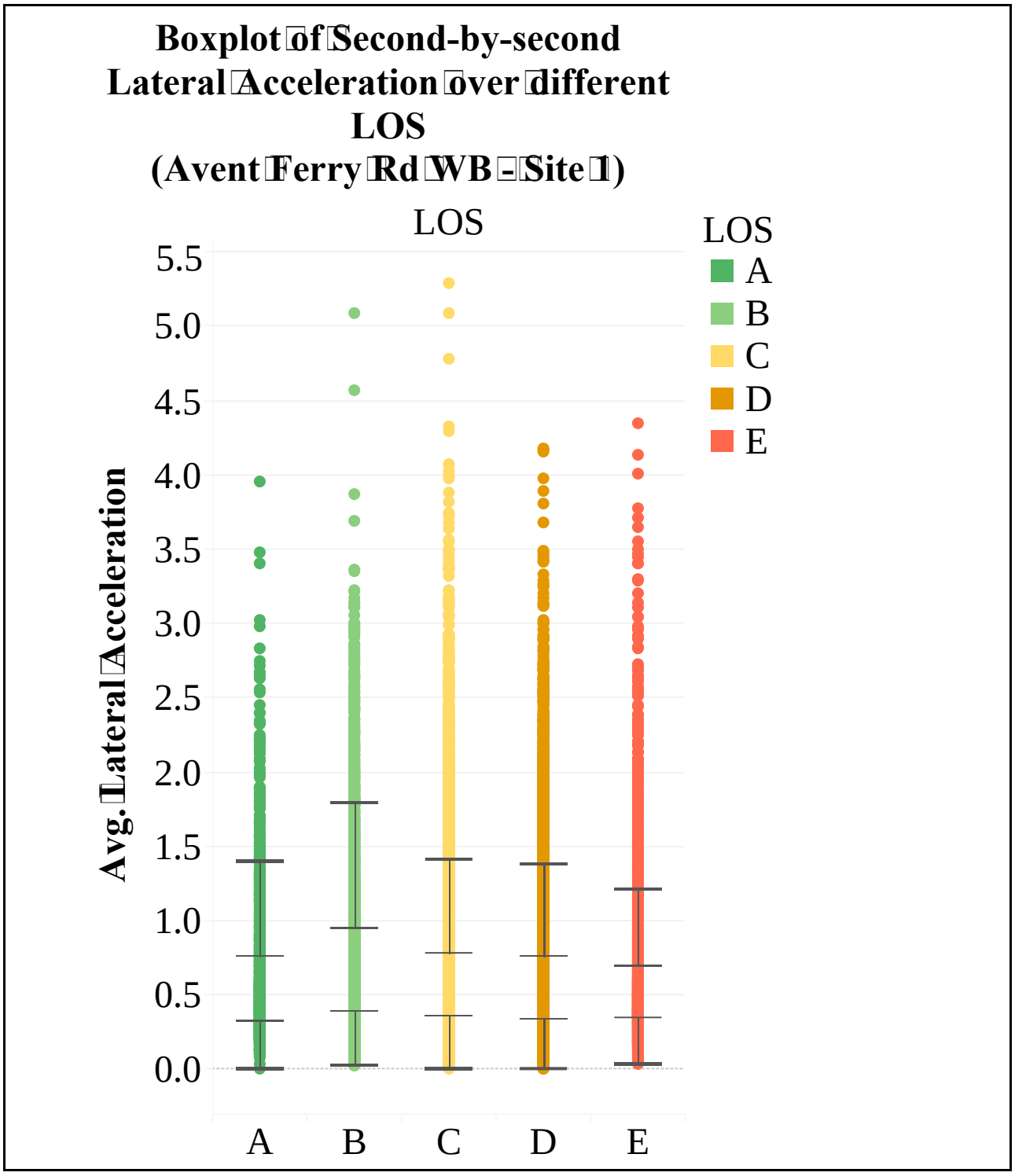

Figure I-6 – Boxplot of Second-by-second Lateral Acceleration over different LOS (Avent Ferry Rd WB – Site 1)

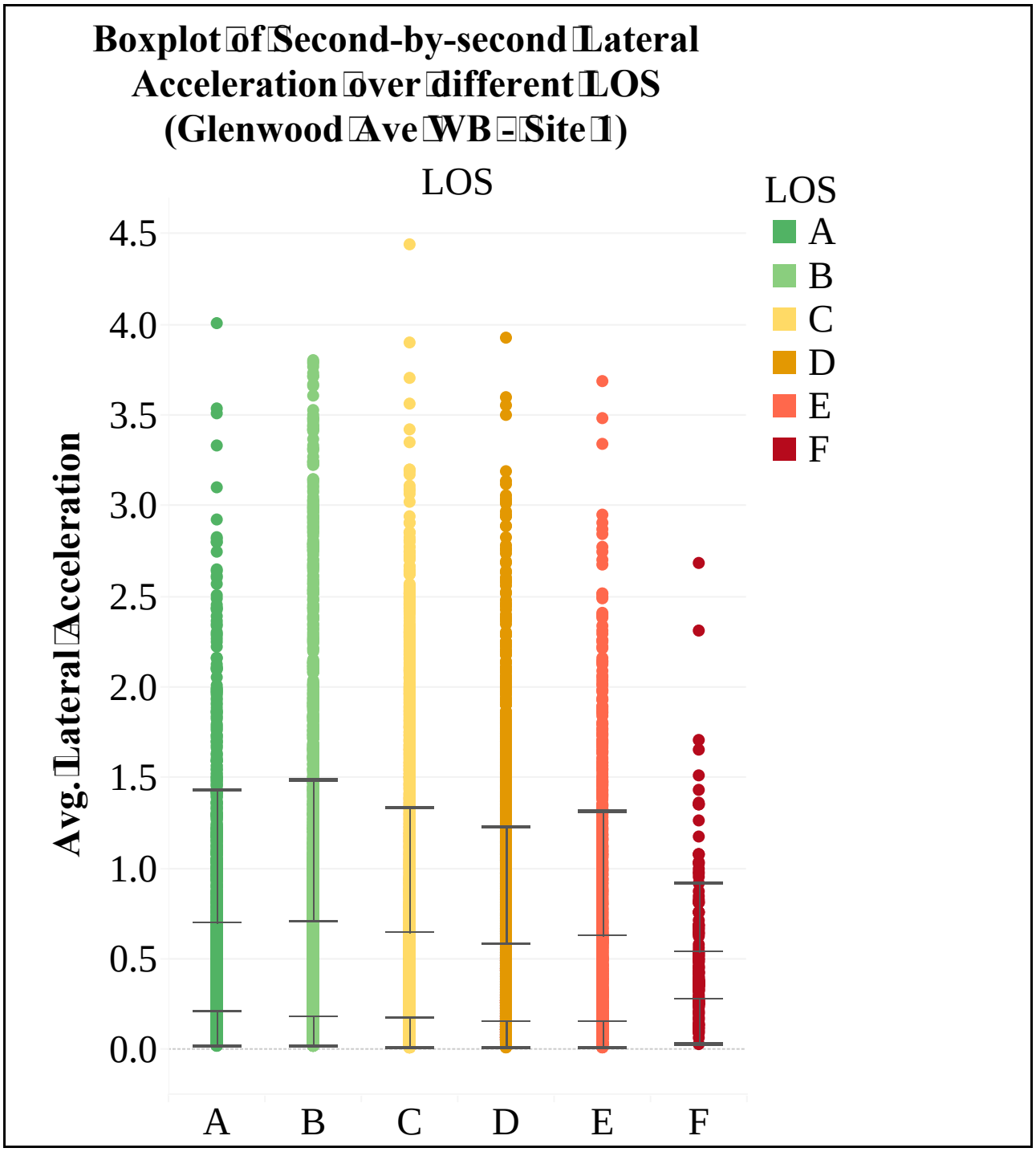

Figure I-7 – Boxplot of Second-by-second Lateral Acceleration over different LOS (Glenwood Ave WB – Site 1)

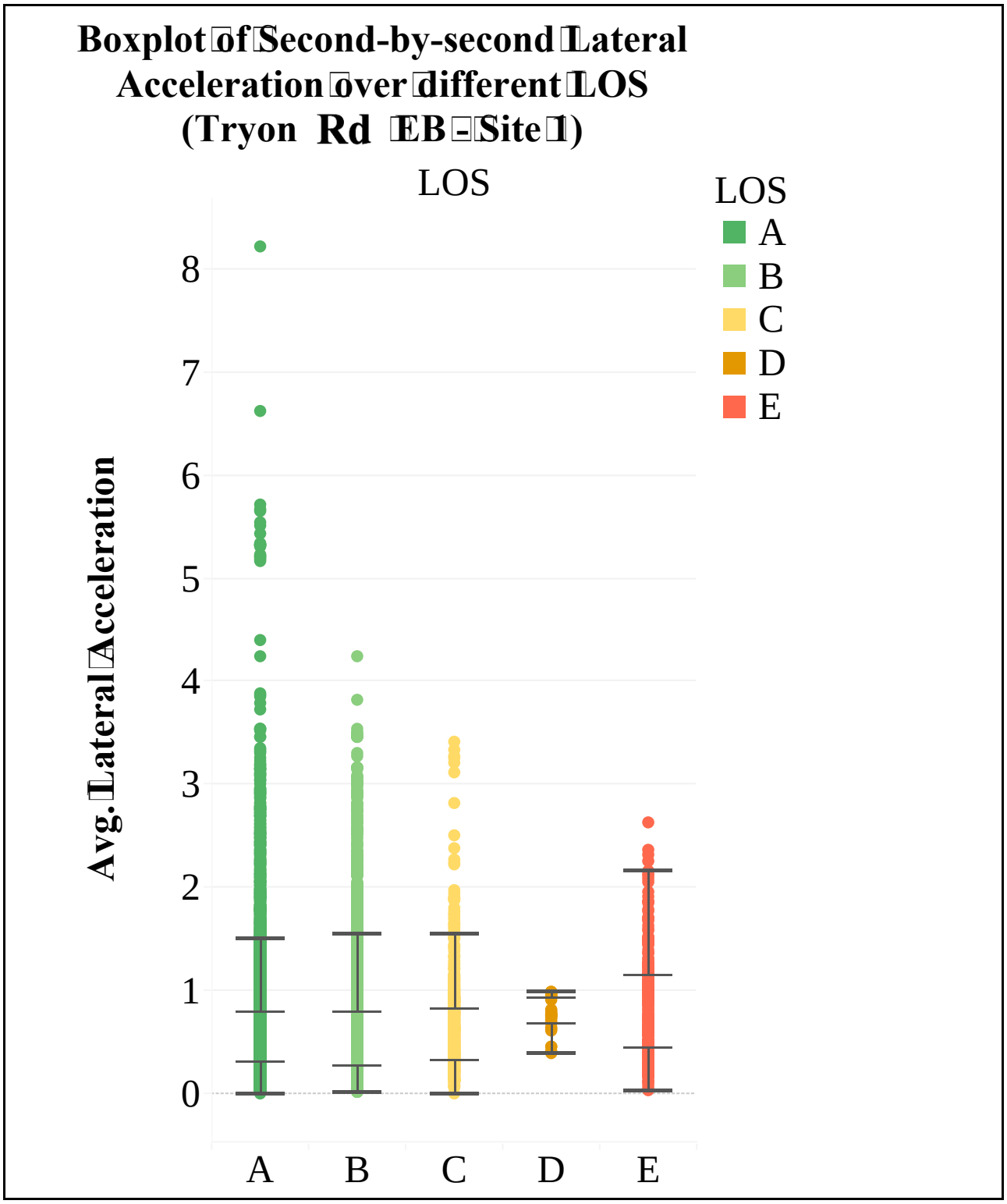

Figure I-8 – Boxplot of Second-by-second Lateral Acceleration over different LOS (Tryon Rd EB – Site 1)

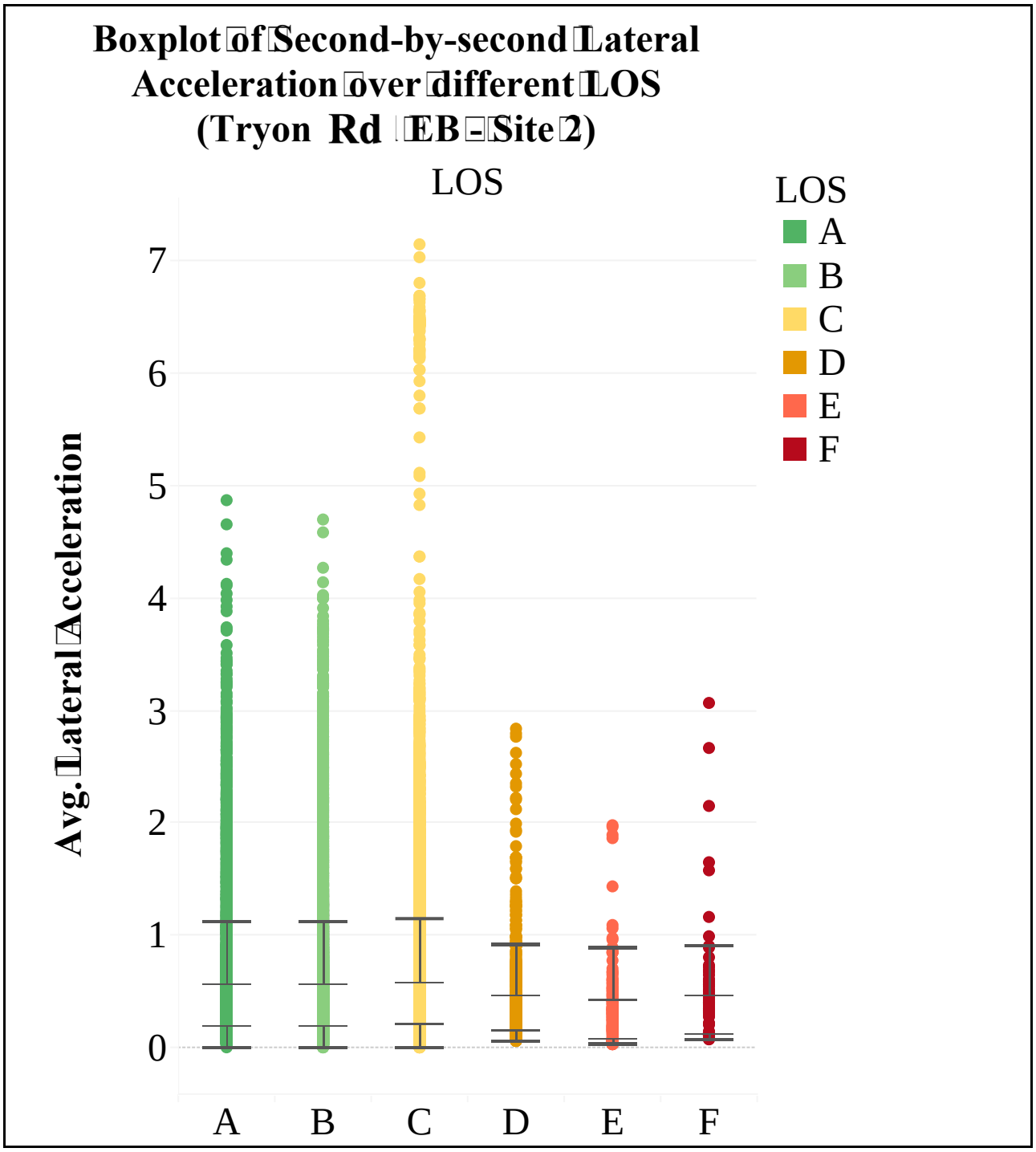

Figure I-9 – Boxplot of Second-by-second Lateral Acceleration over different LOS (Tryon Rd EB – Site 2)

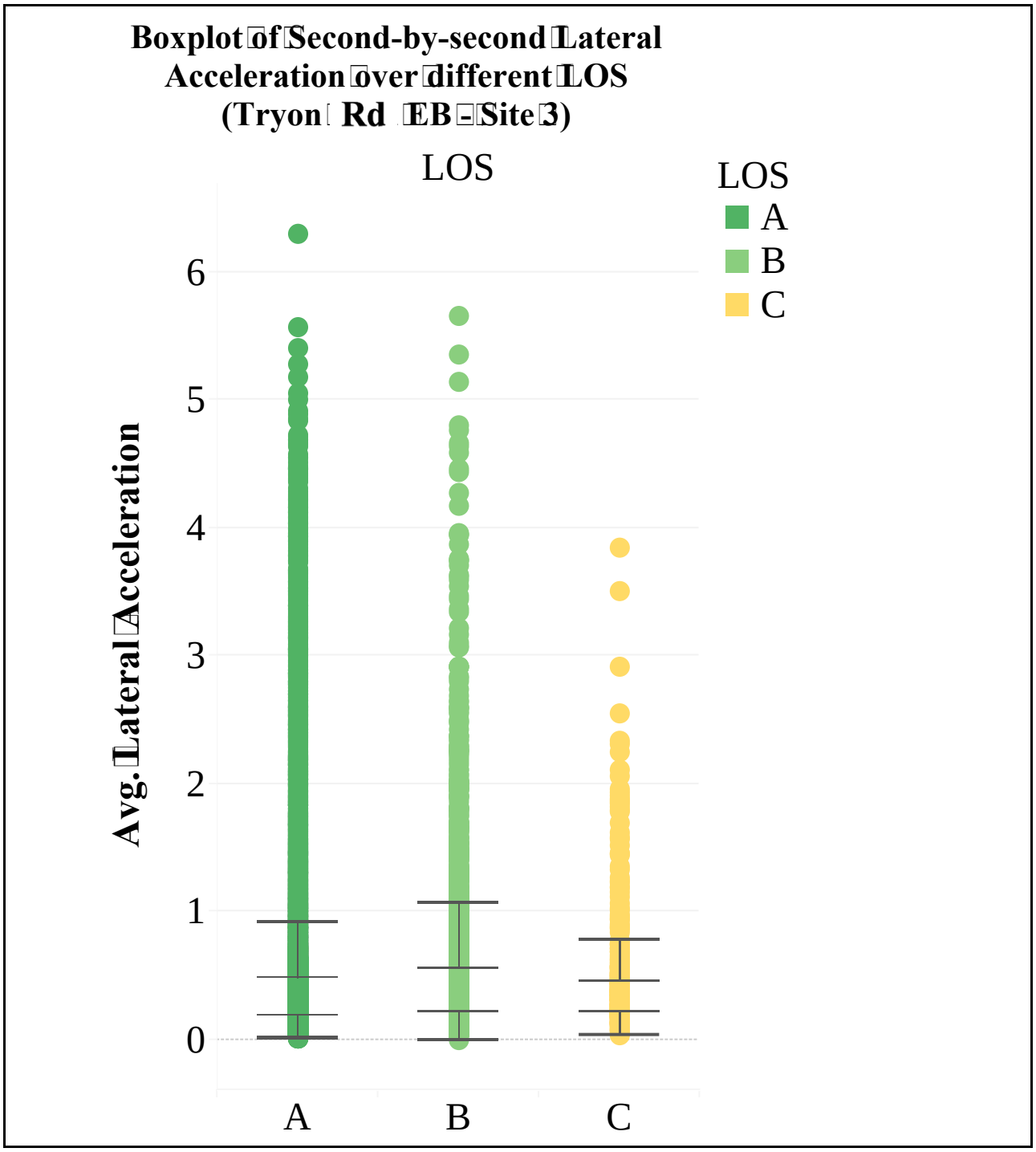

Figure I-10 – Boxplot of Second-by-second Lateral Acceleration over different LOS (Tryon Rd EB – Site 3)

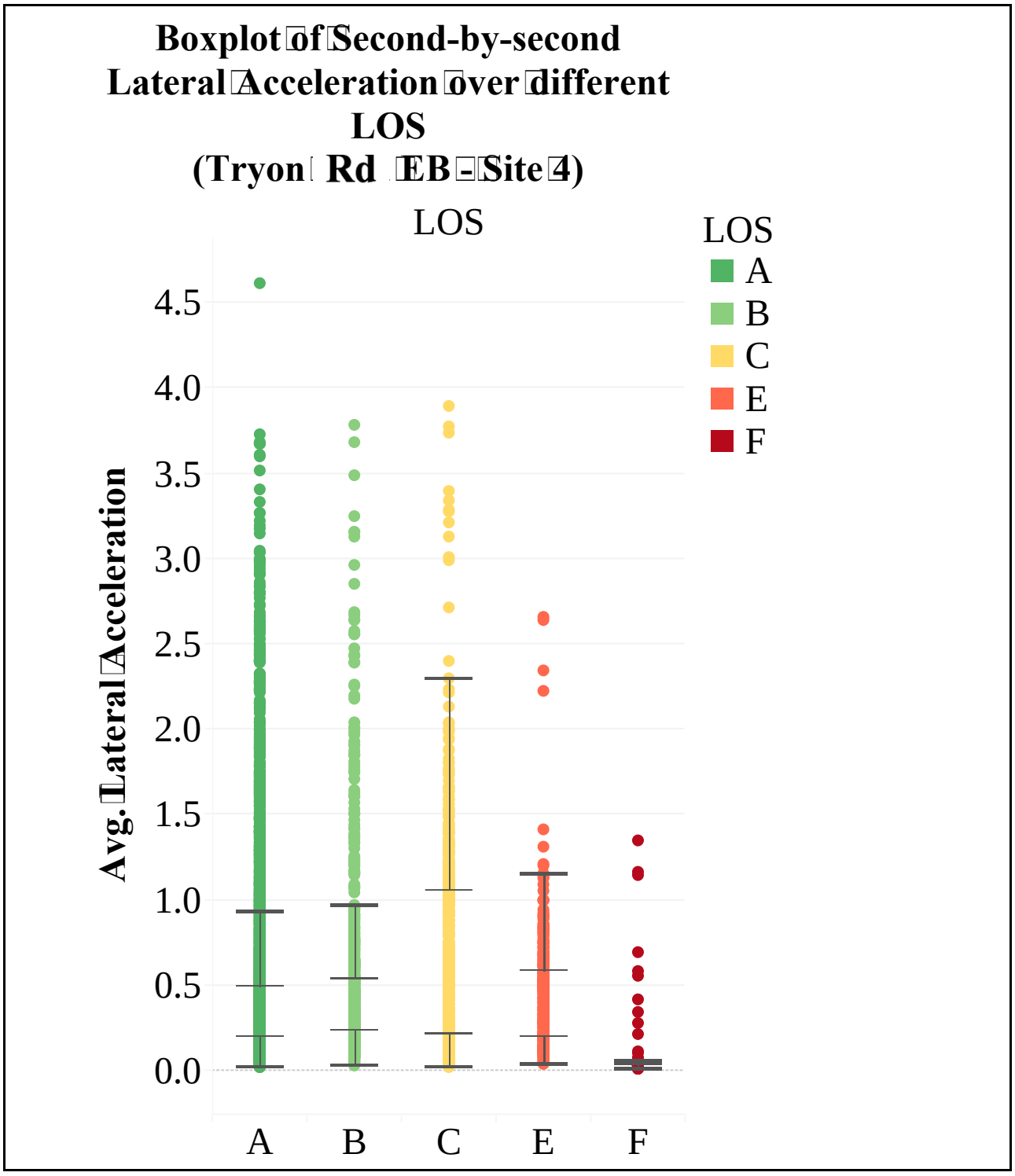

Figure I-11 – Boxplot of Second-by-second Lateral Acceleration over different LOS (Tryon Rd EB – Site 4)

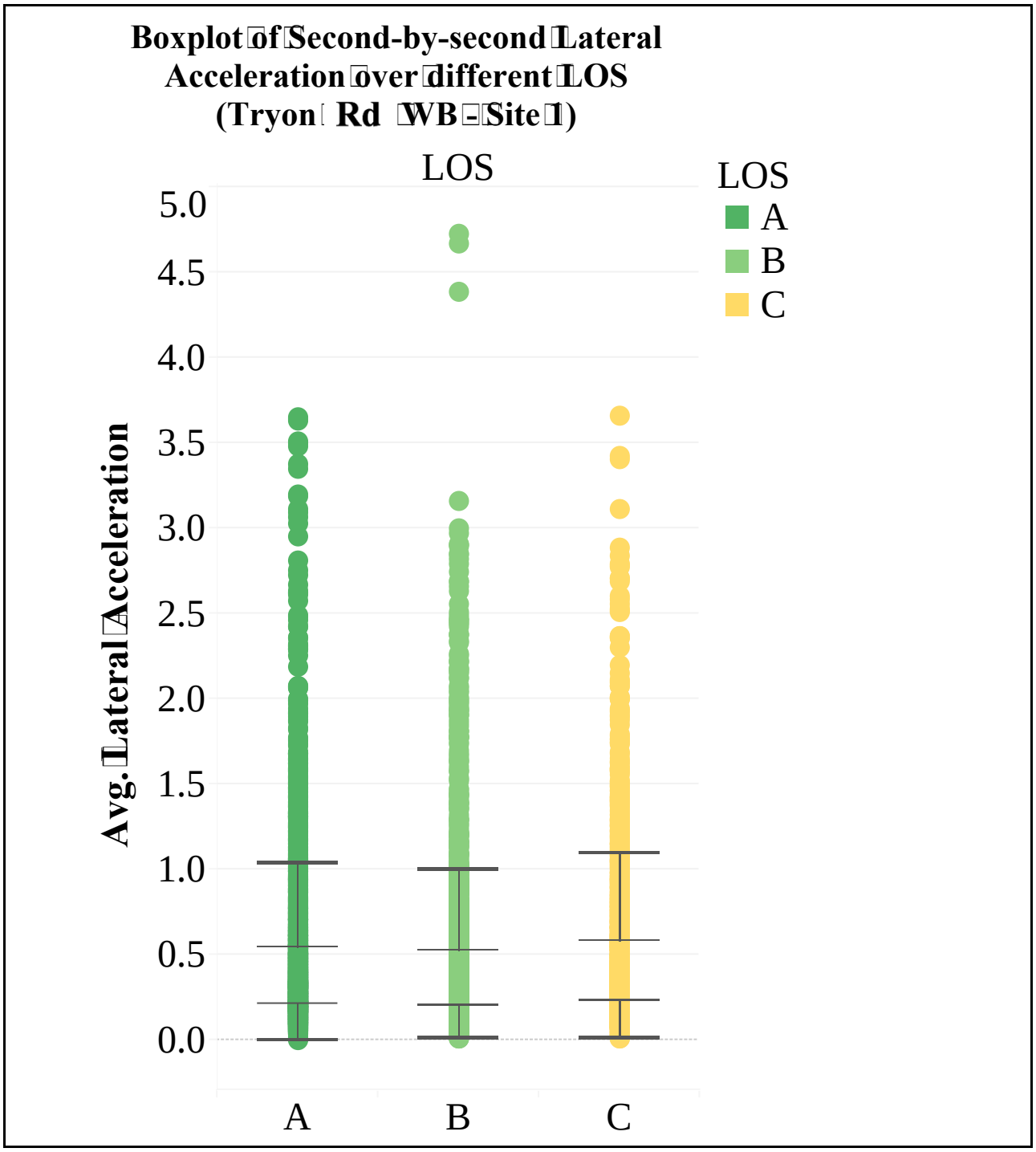

Figure I-12 – Boxplot of Second-by-second Lateral Acceleration over different LOS (Tryon Rd WB – Site 1)

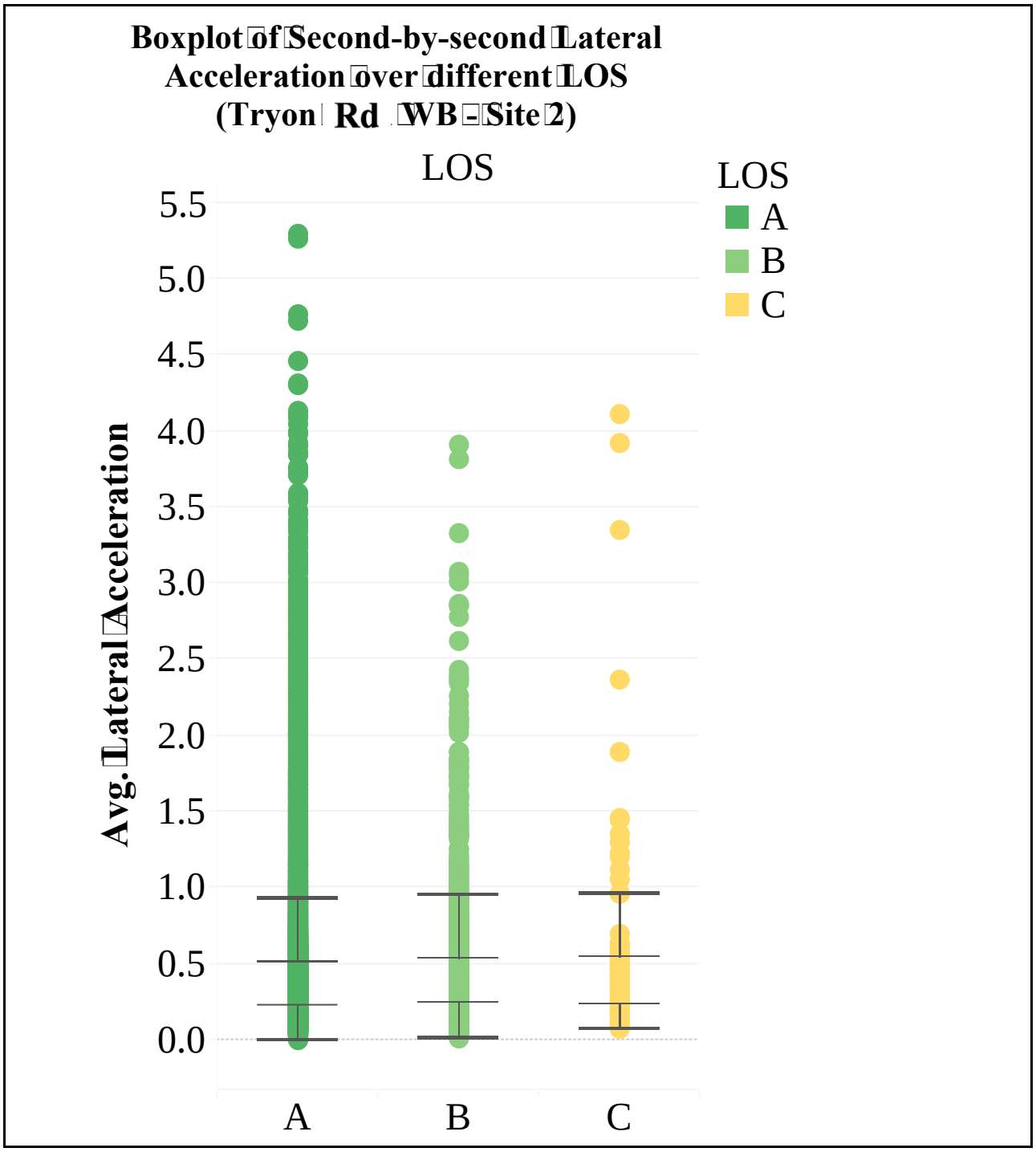

Figure I-13 – Boxplot of Second-by-second Lateral Acceleration over different LOS (Tryon Rd WB – Site 2)

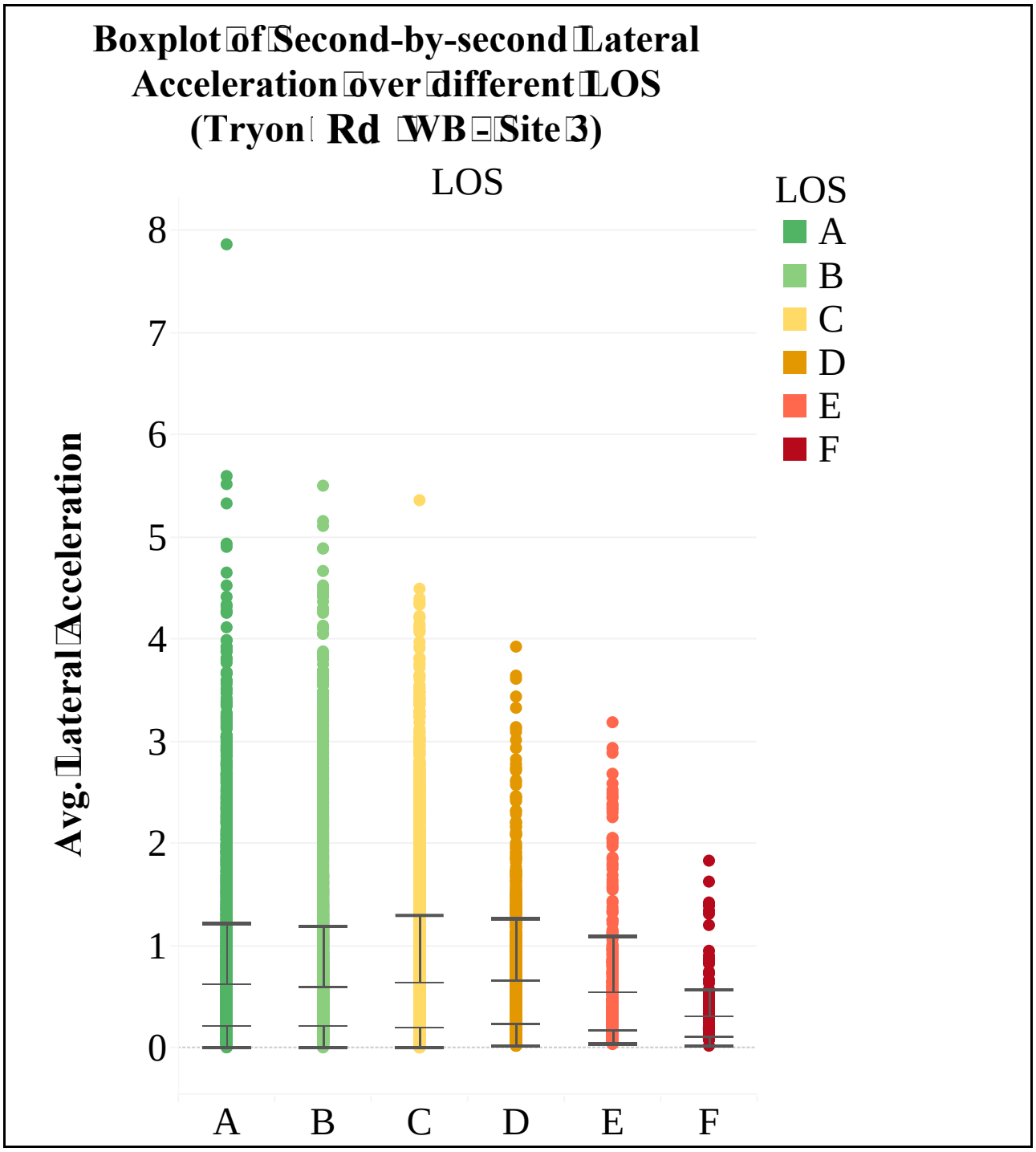

Figure I-14 – Boxplot of Second-by-second Lateral Acceleration over different LOS (Tryon Rd WB – Site 3)

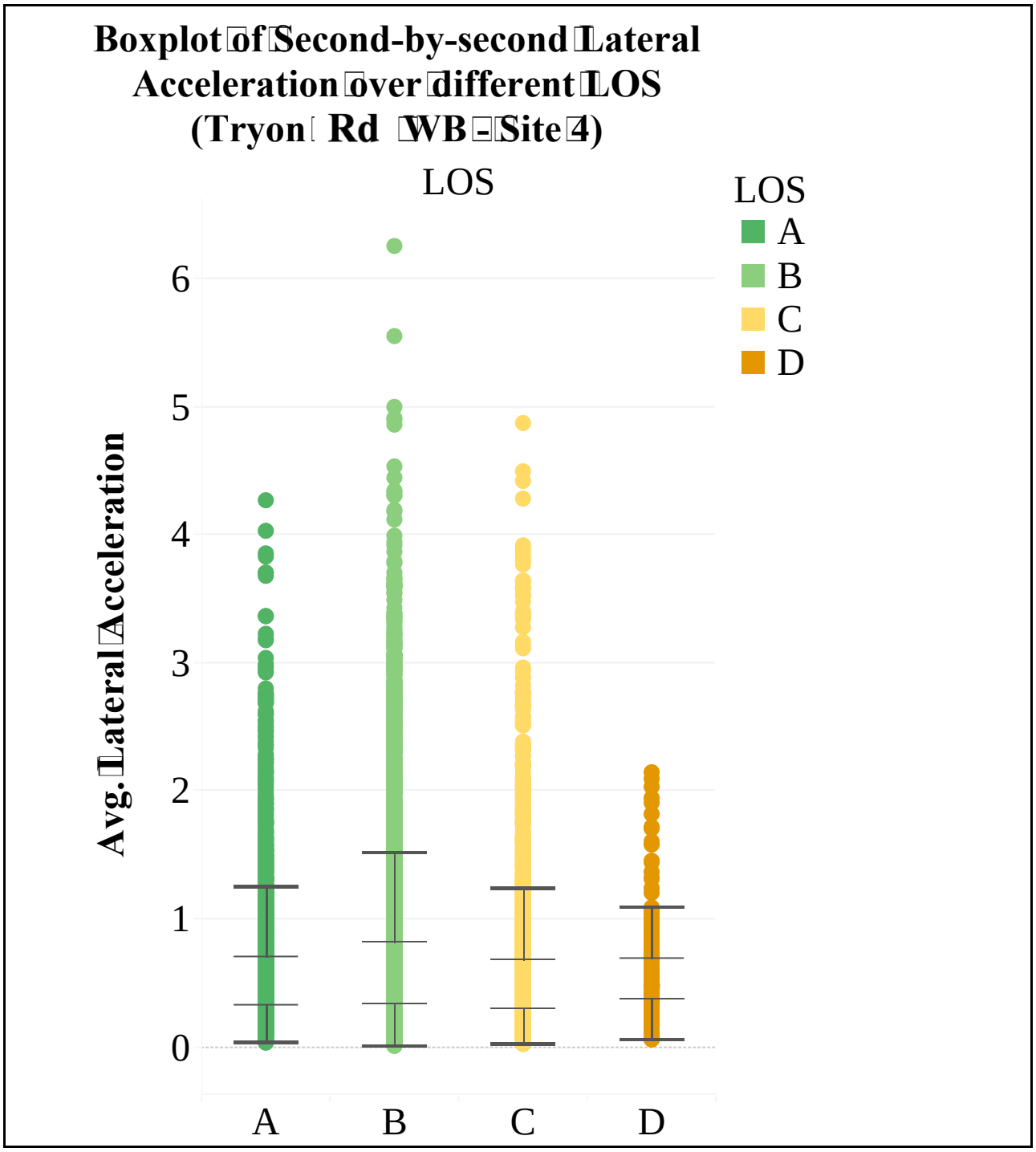

Figure I-15 – Boxplot of Second-by-second Lateral Acceleration over different LOS (Tryon Rd WB – Site 4)

APPENDIX J - AVERAGE MAXIMUM ACCELERATION AND DECELERATION ACROSS TRIPS OVER DIFFERENT LOS

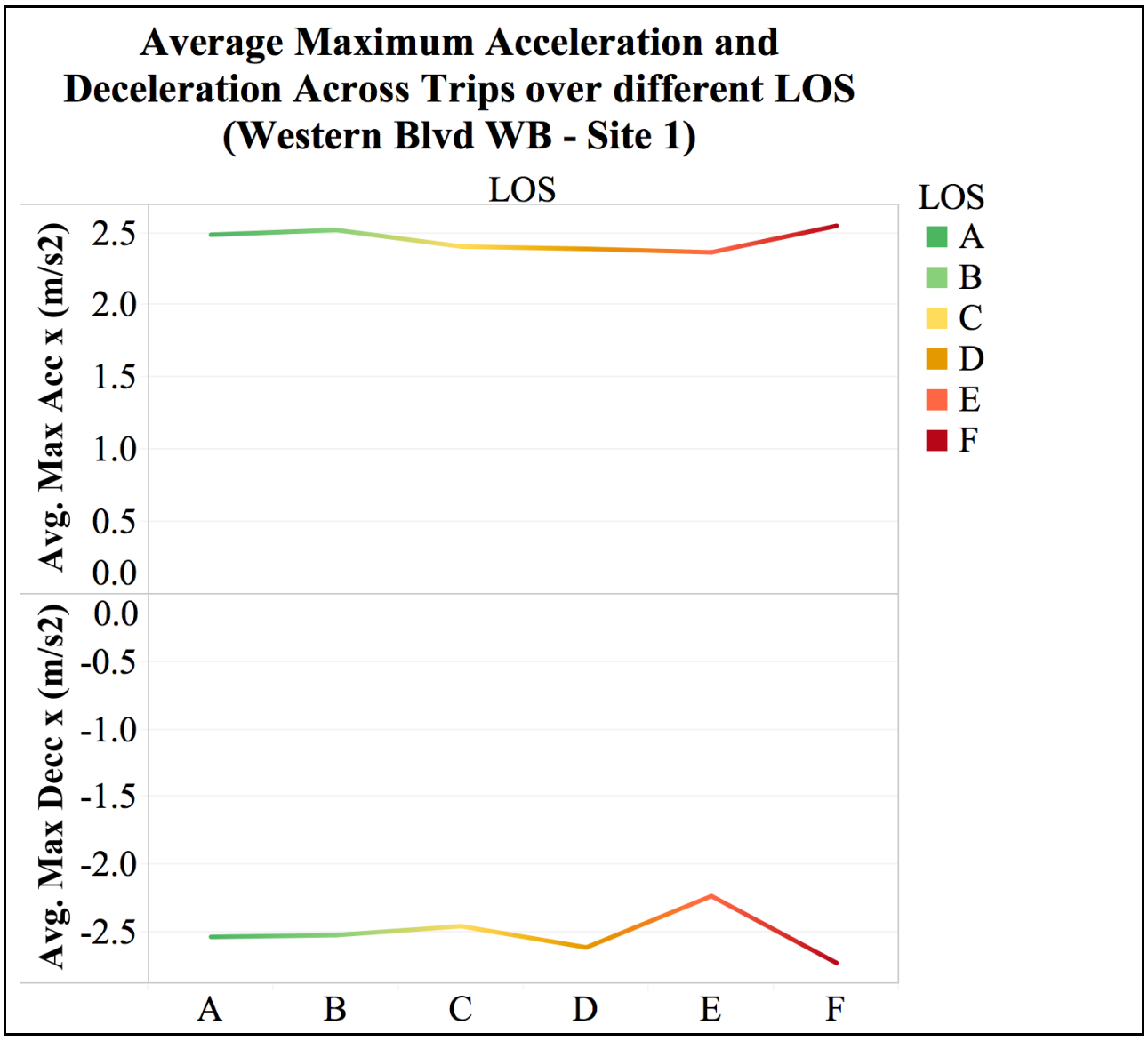

Figure J-1 – Average Maximum Acceleration and Deceleration Across Trips observations over different LOS (Western Blvd WB – Site 1)

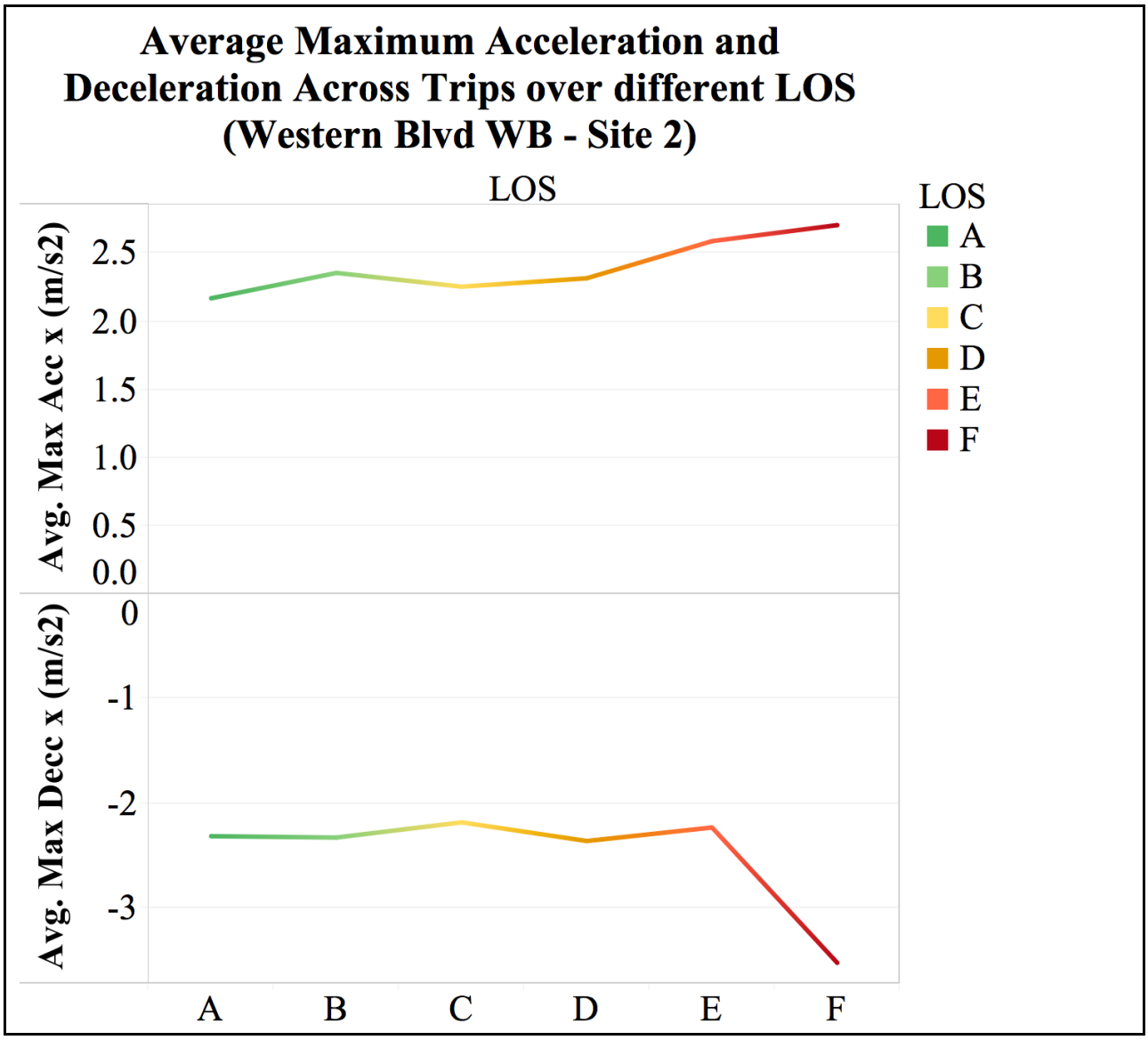

Figure J-2 – Average Maximum Acceleration and Deceleration Across Trips observations over different LOS (Western Blvd WB – Site 2)

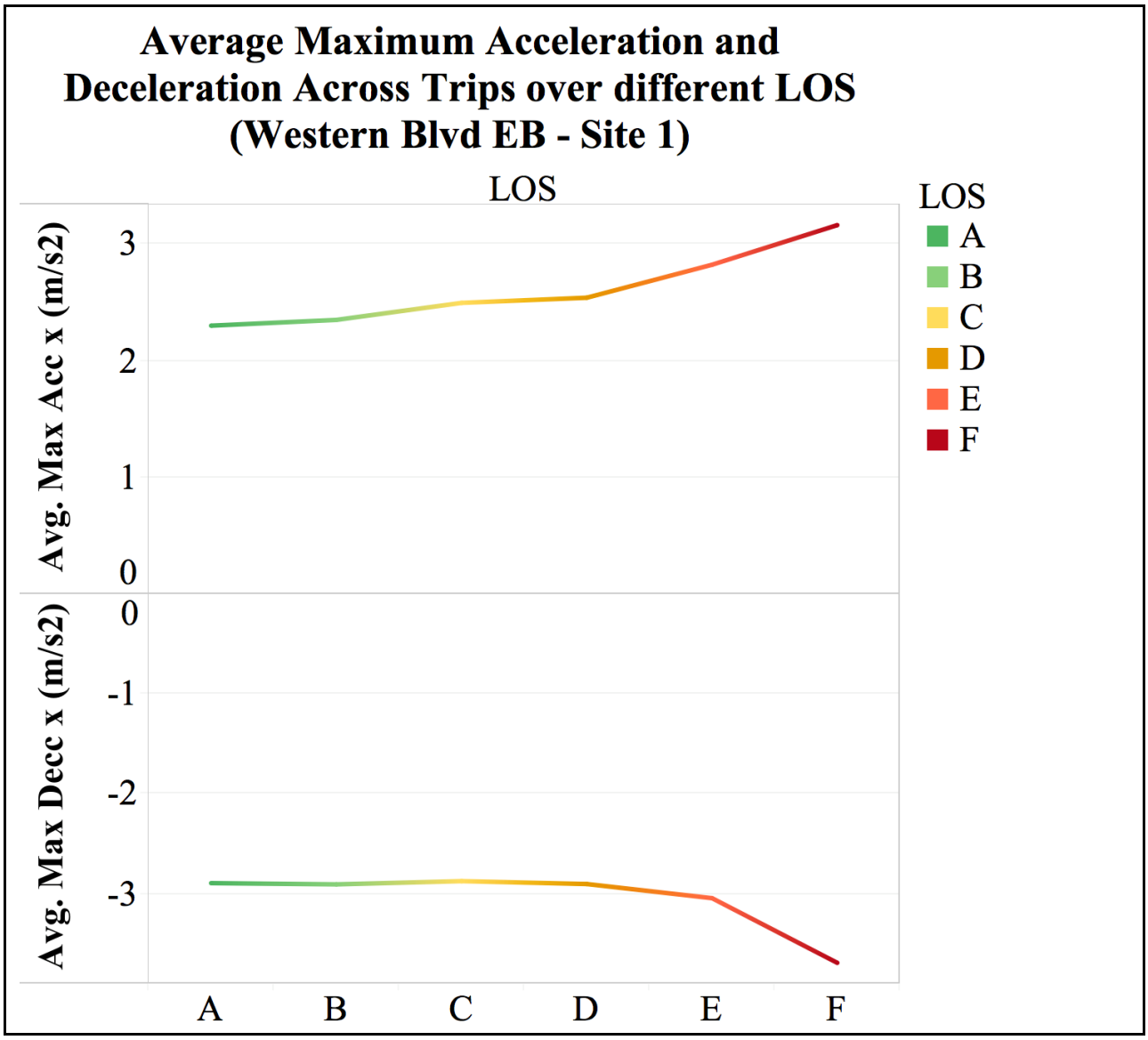

Figure J-3 – Average Maximum Acceleration and Deceleration Across Trips observations over different LOS (Western Blvd EB – Site 1)

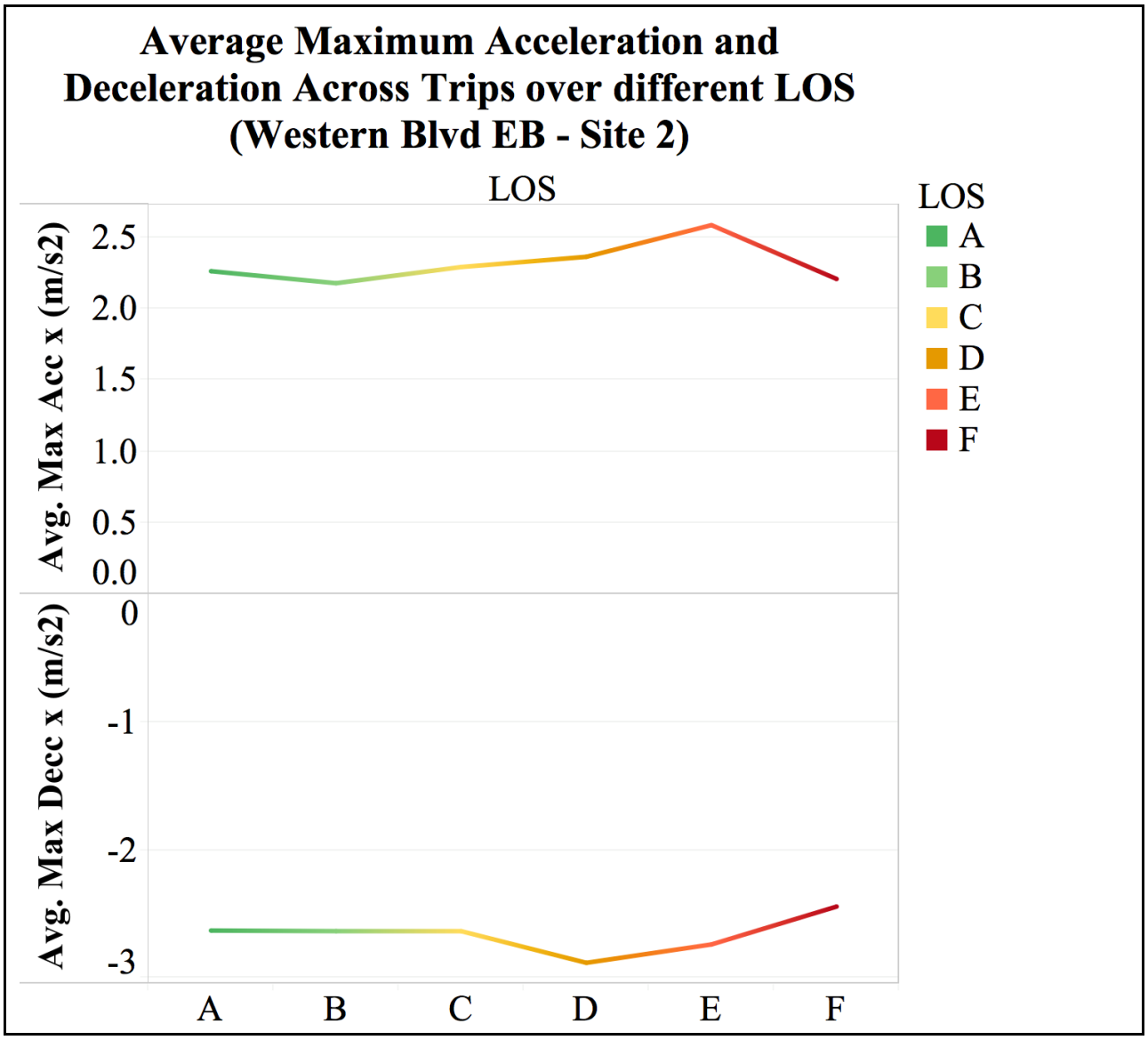

Figure J-4 – Average Maximum Acceleration and Deceleration Across Trips observations over different LOS (Western Blvd EB – Site 2)

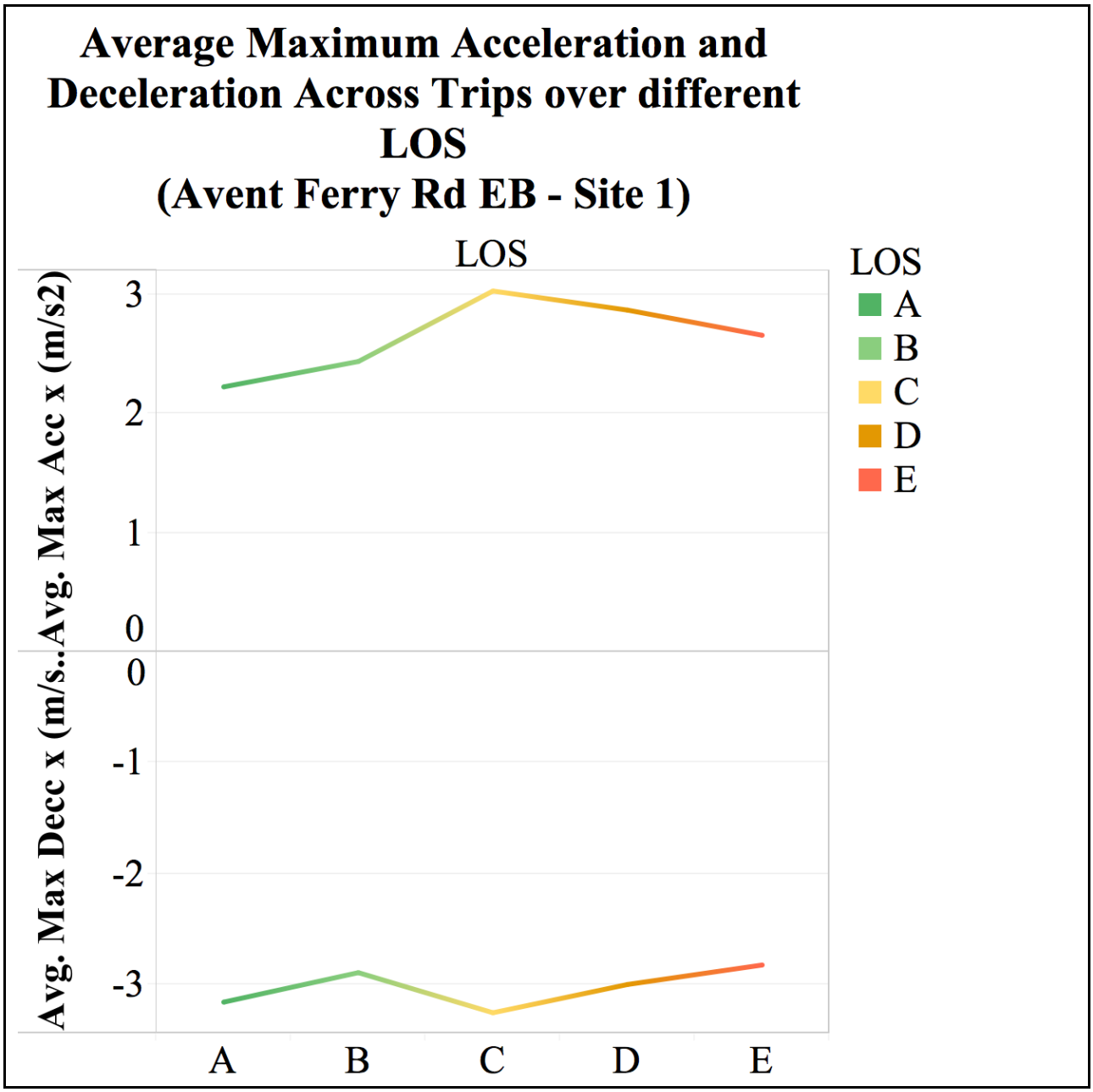

Figure J-5 – Average Maximum Acceleration and Deceleration Across Trips observations over different LOS (Avent Ferry Rd EB – Site 1)

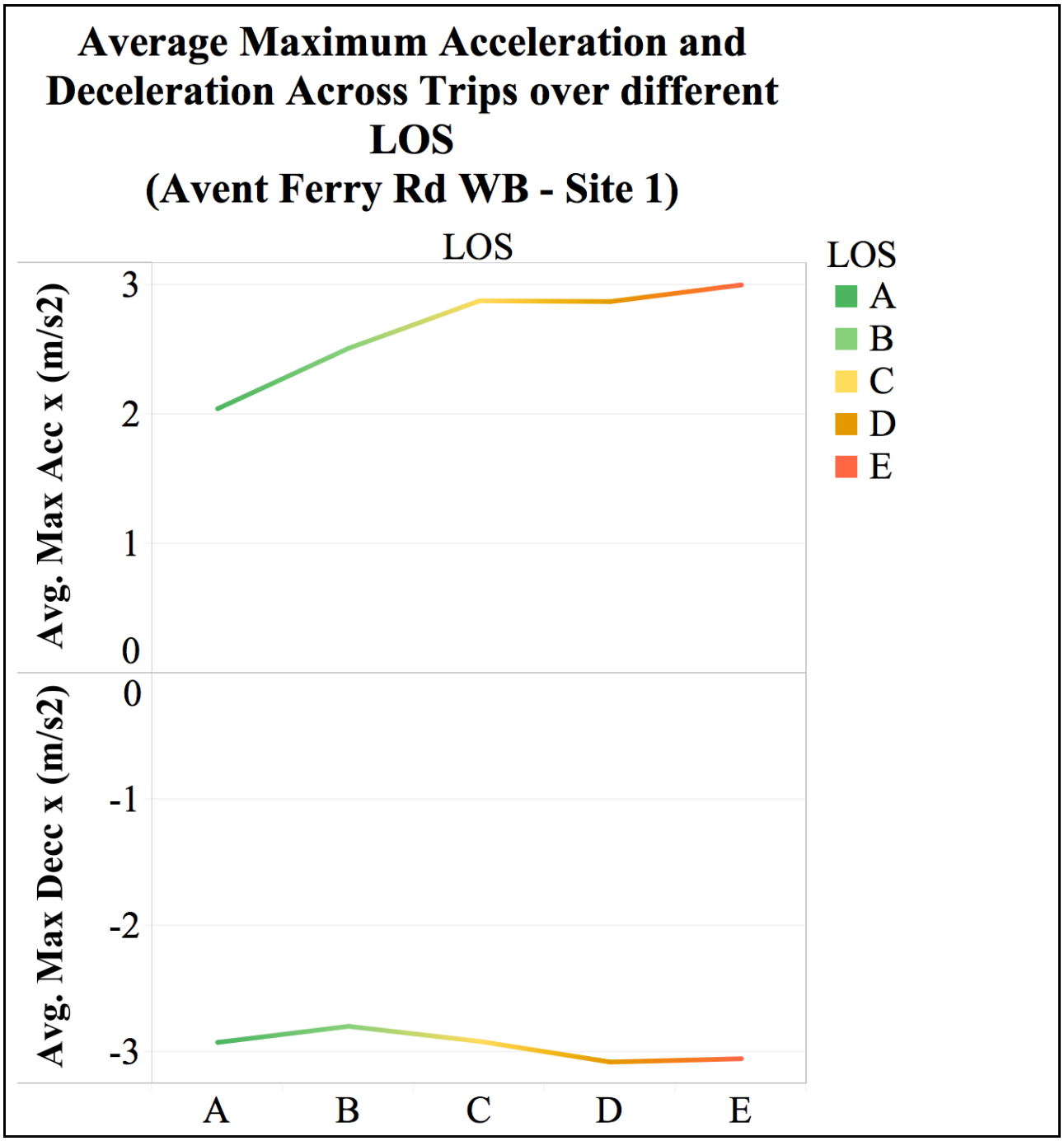

Figure J-6 – Average Maximum Acceleration and Deceleration Across Trips observations over different LOS (Avent Ferry Rd WB – Site 1)

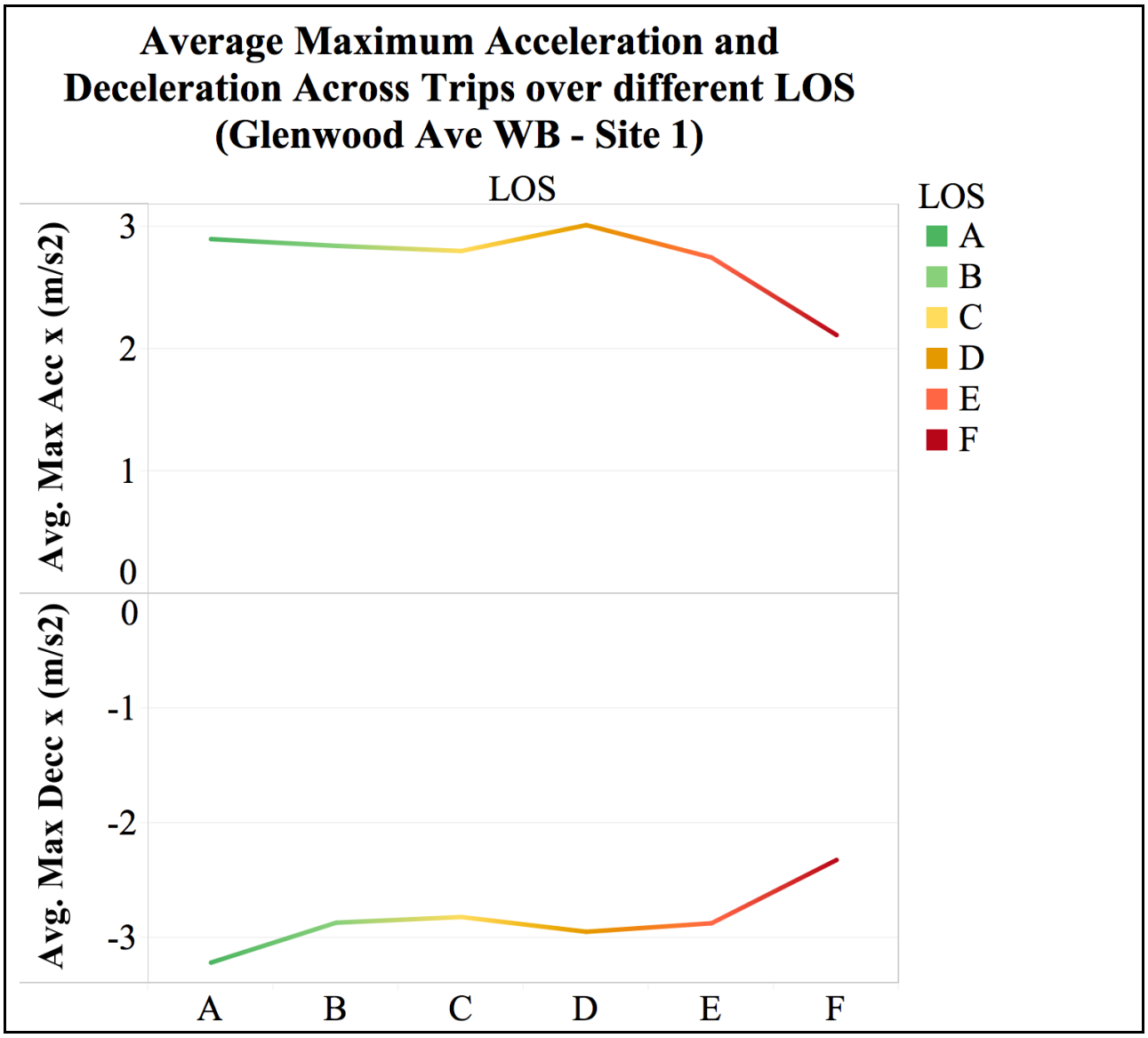

Figure J-7 – Average Maximum Acceleration and Deceleration Across Trips observations over different LOS (Glenwood Ave WB – Site 1)

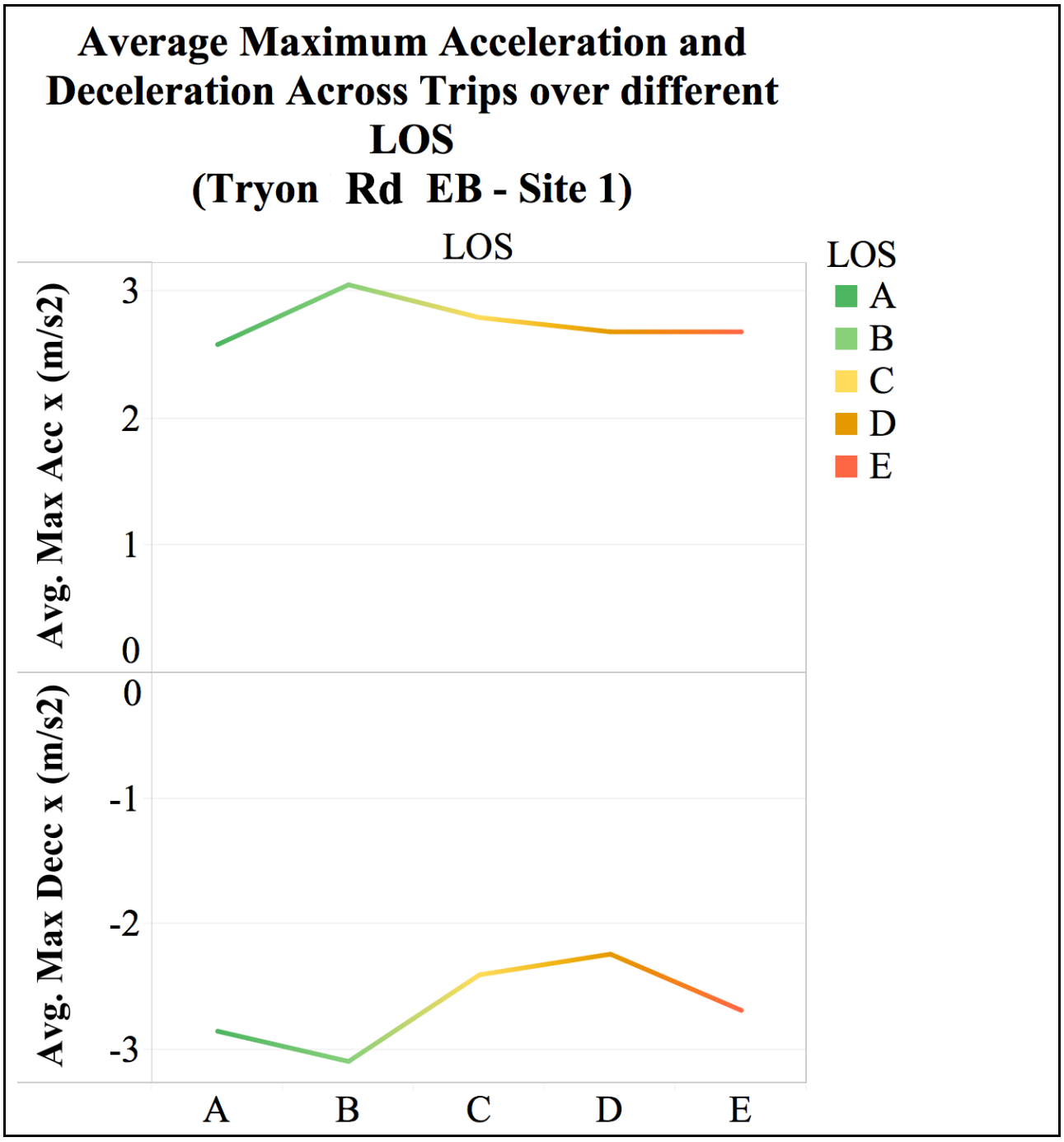

Figure J-8 – Average Maximum Acceleration and Deceleration Across Trips observations over different LOS (Tryon Rd EB – Site 1)

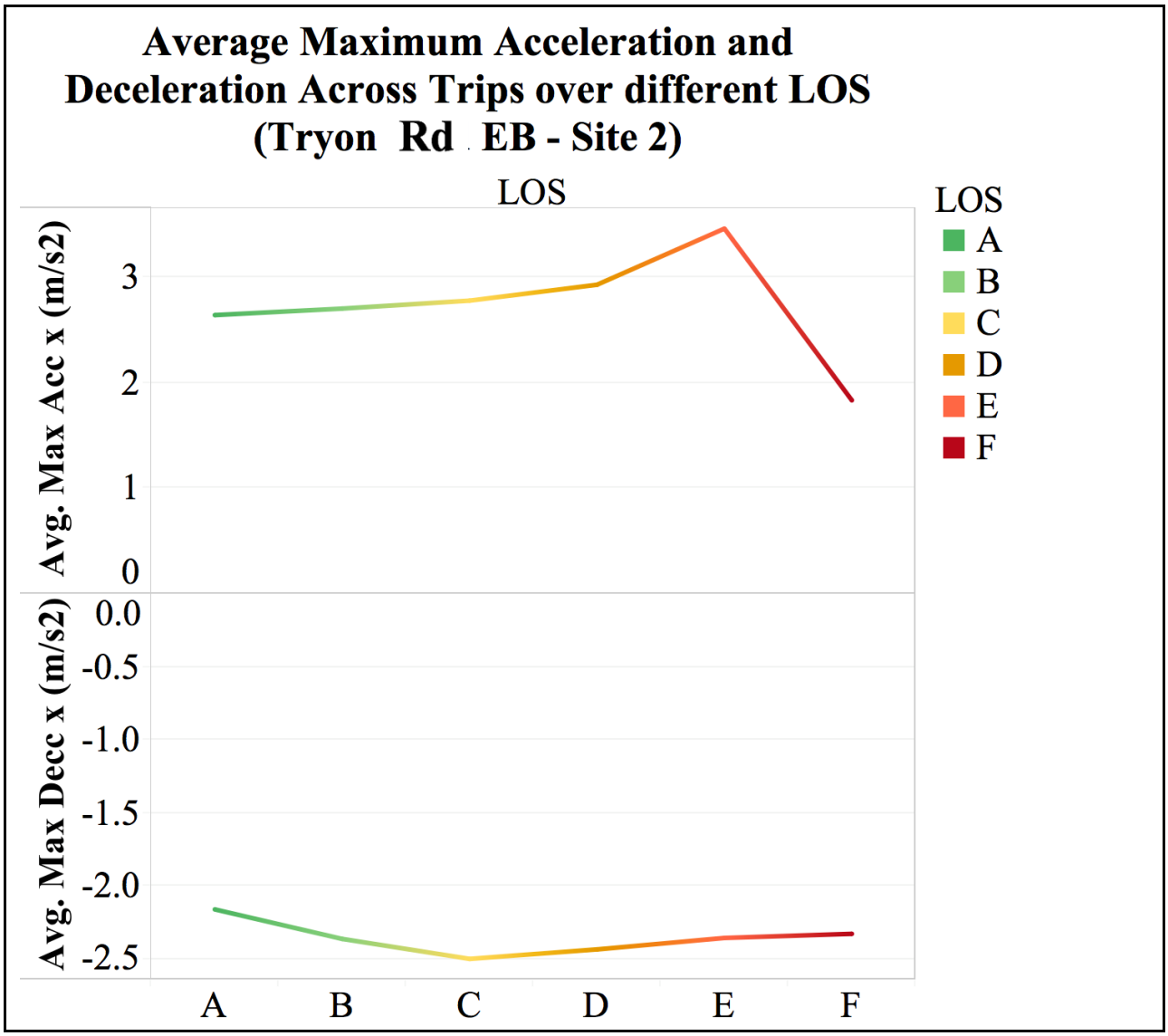

Figure J-9 – Average Maximum Acceleration and Deceleration Across Trips observations over different LOS (Tryon Rd EB – Site 2)

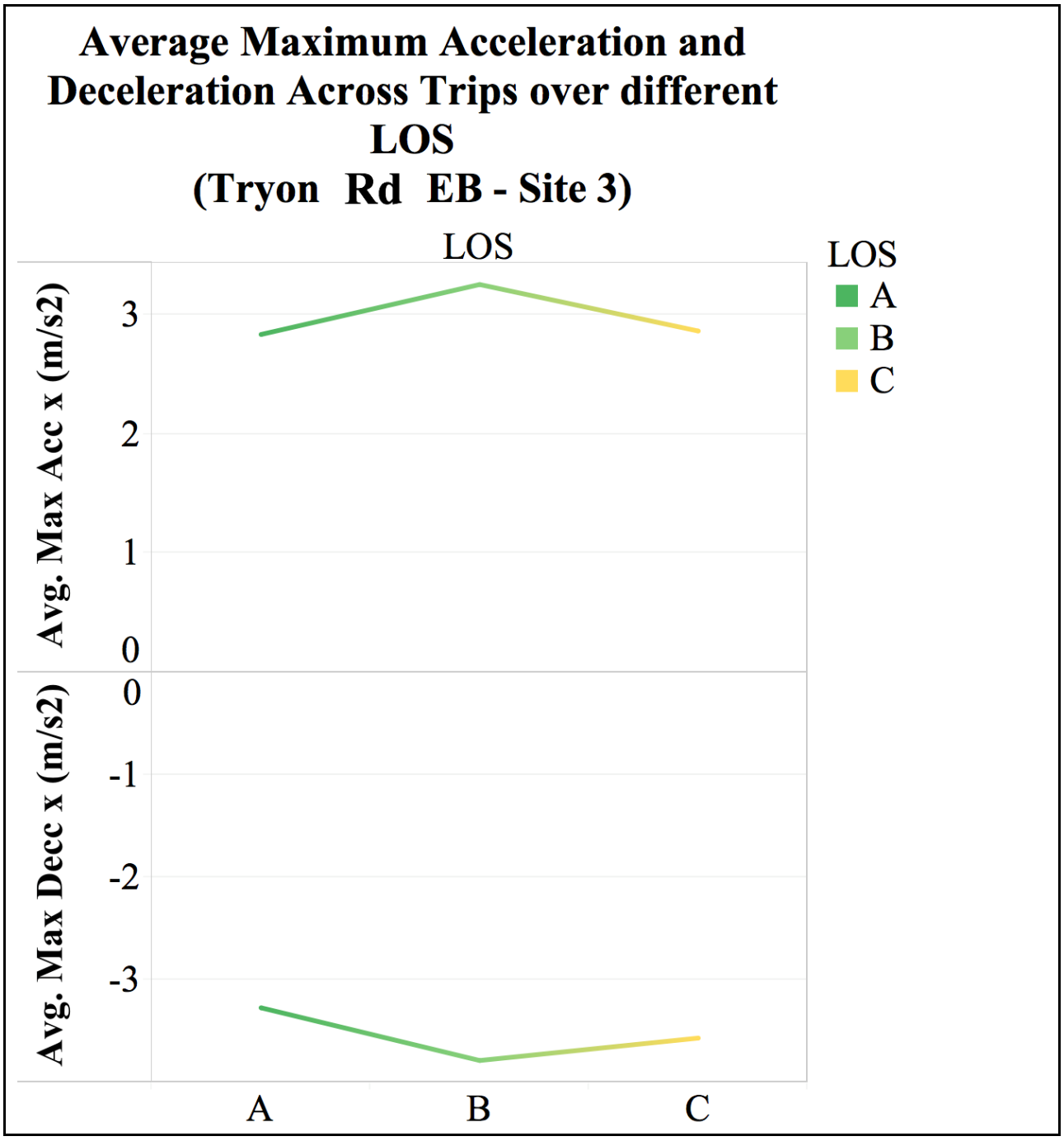

Figure J-10 – Average Maximum Acceleration and Deceleration Across Trips observations over different LOS (Tryon Rd EB – Site 3)

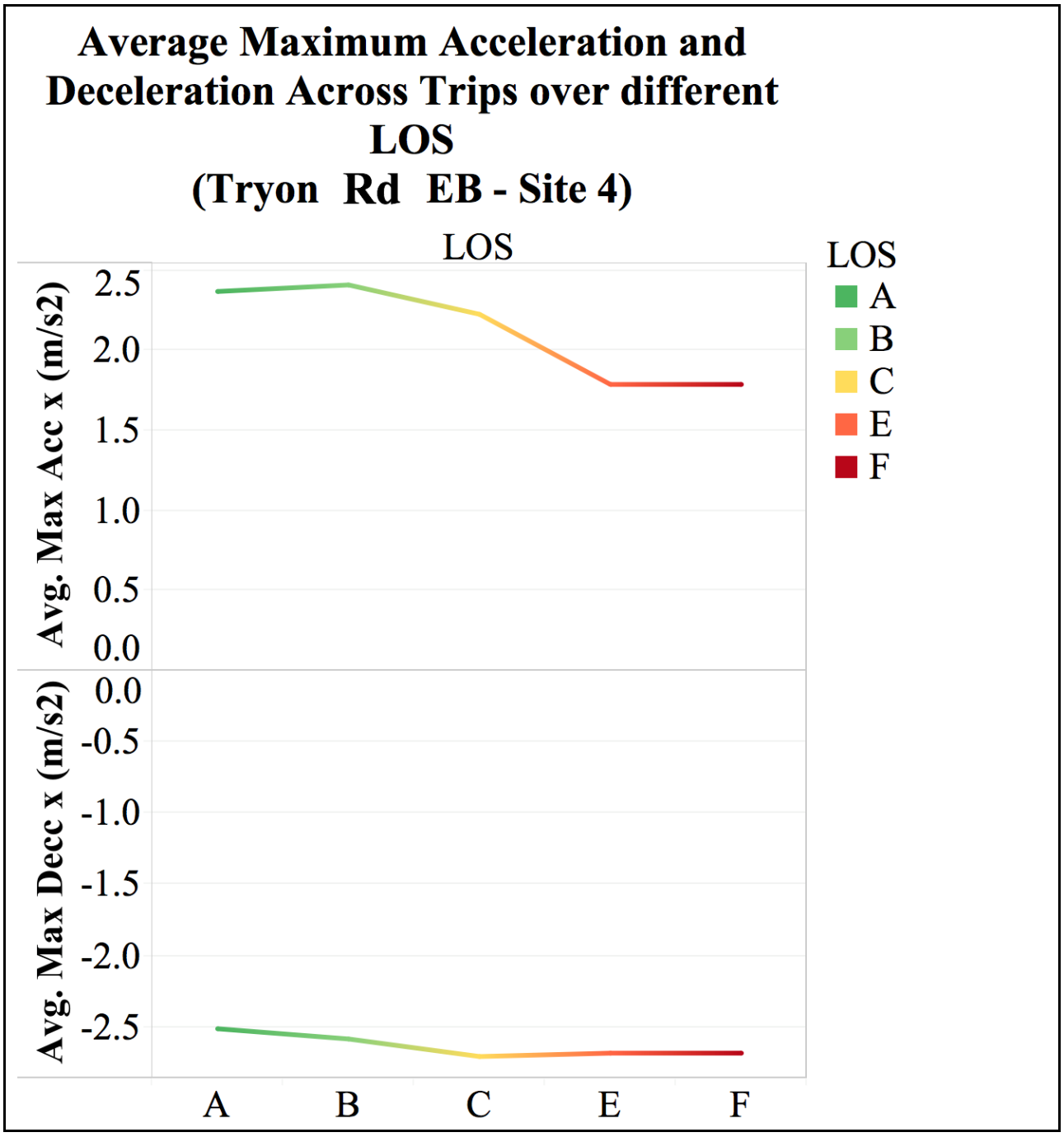

Figure J-11 – Average Maximum Acceleration and Deceleration Across Trips observations over different LOS (Tryon Rd EB – Site 4)

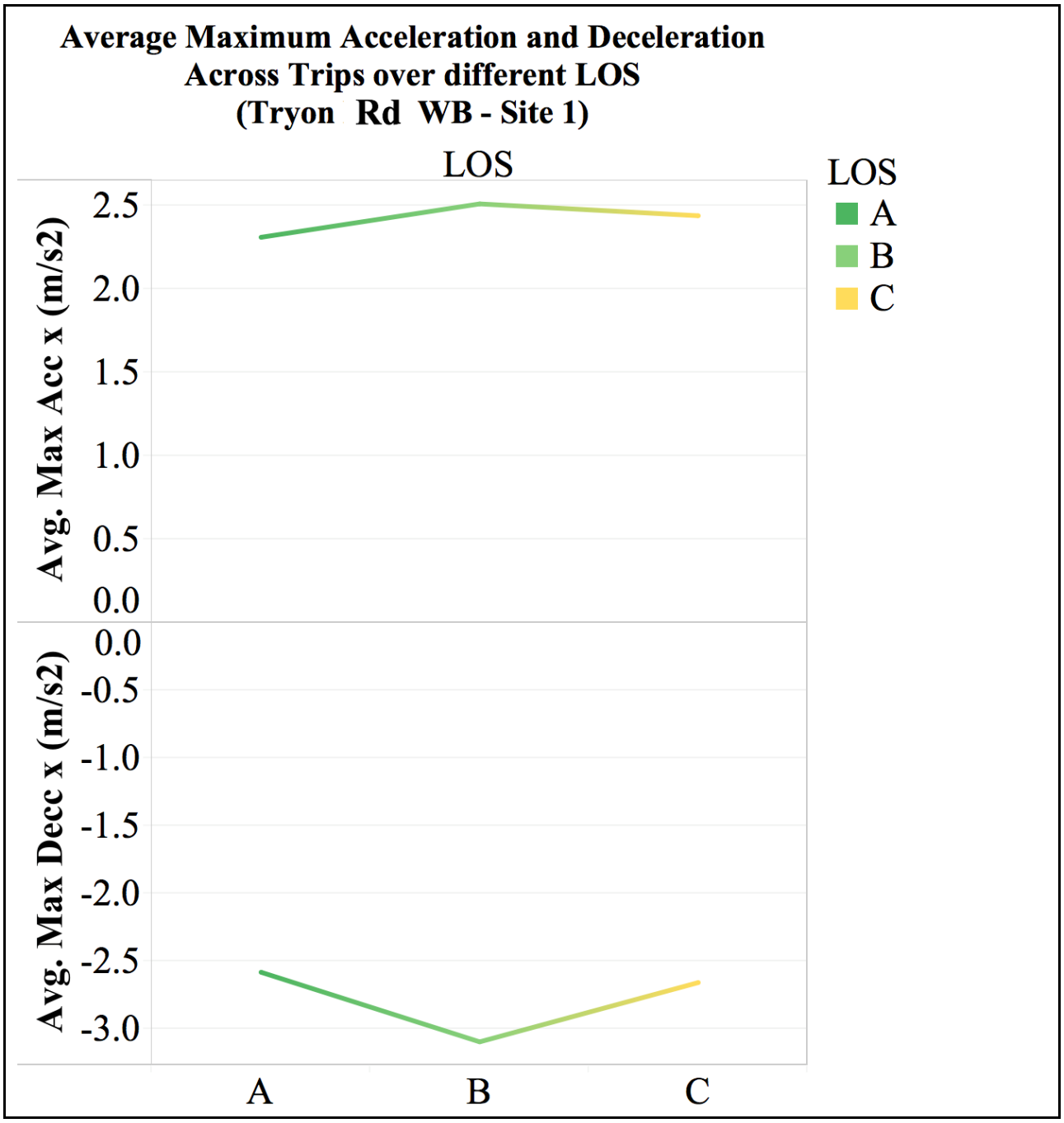

Figure J-12 – Average Maximum Acceleration and Deceleration Across Trips observations over different LOS (Tryon Rd WB – Site 1)

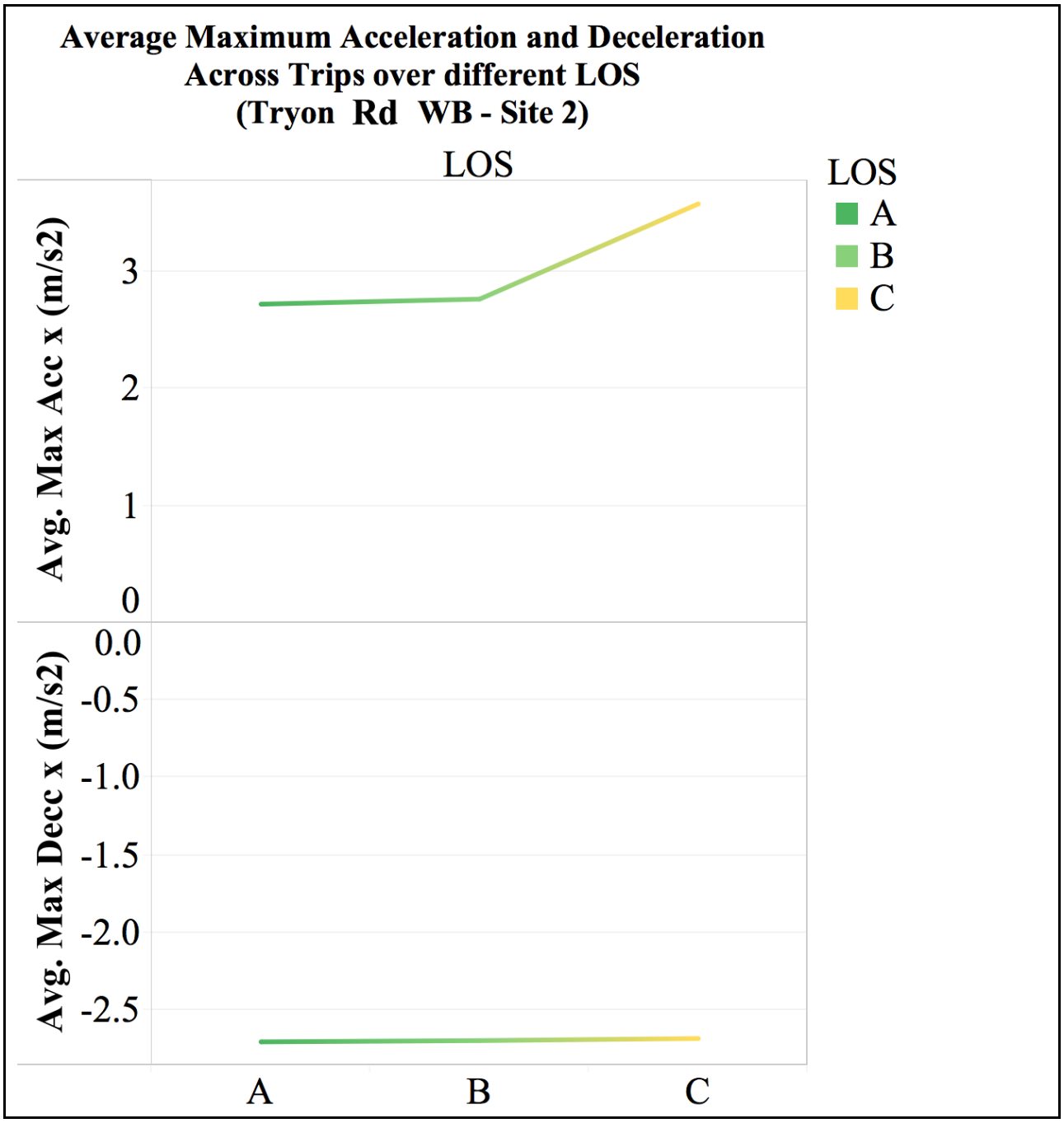

Figure J-13 – Average Maximum Acceleration and Deceleration Across Trips observations over different LOS (Tryon Rd WB – Site 2)

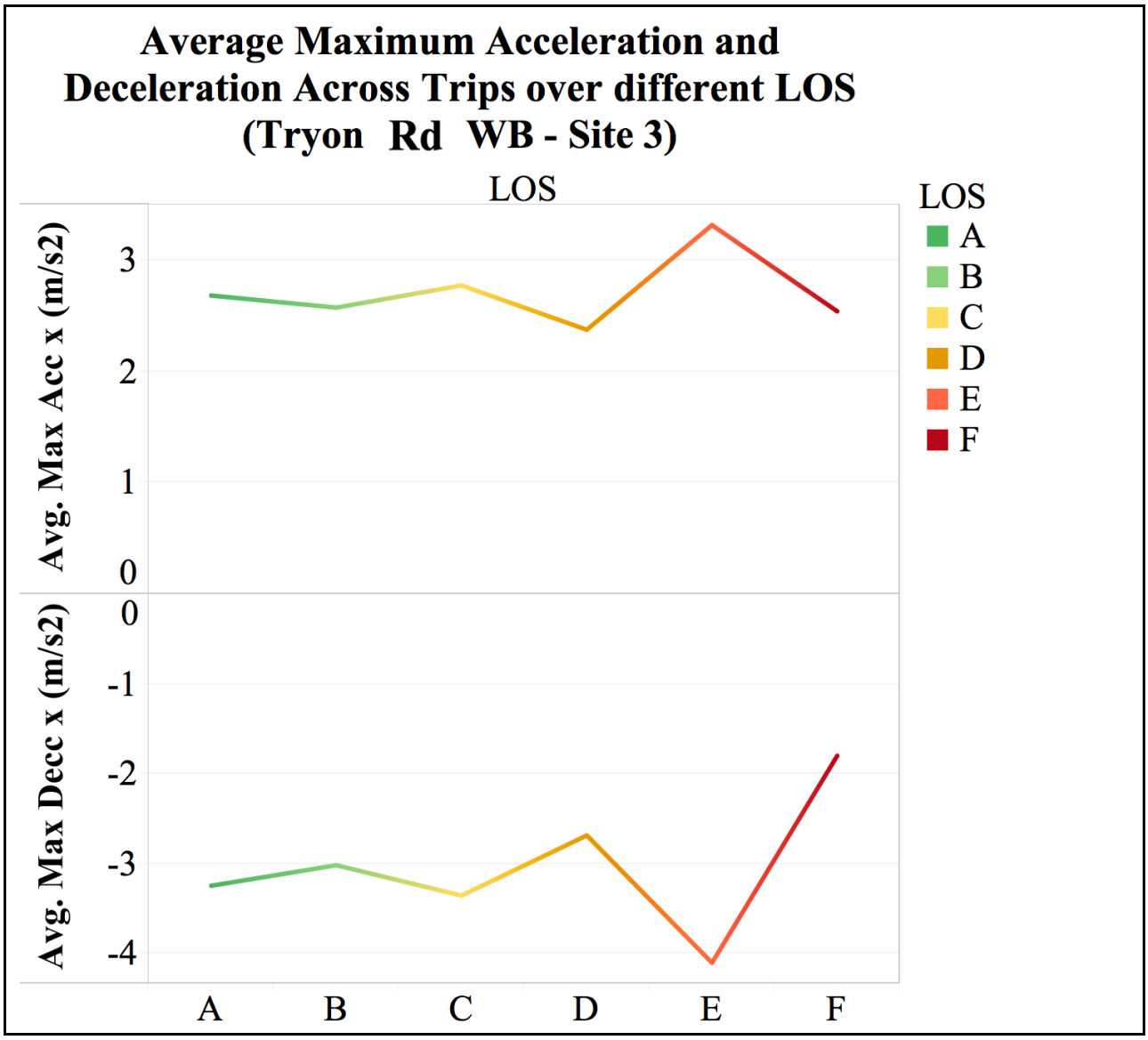

Figure J-14 – Average Maximum Acceleration and Deceleration Across Trips observations over different LOS (Tryon Rd WB – Site 3)

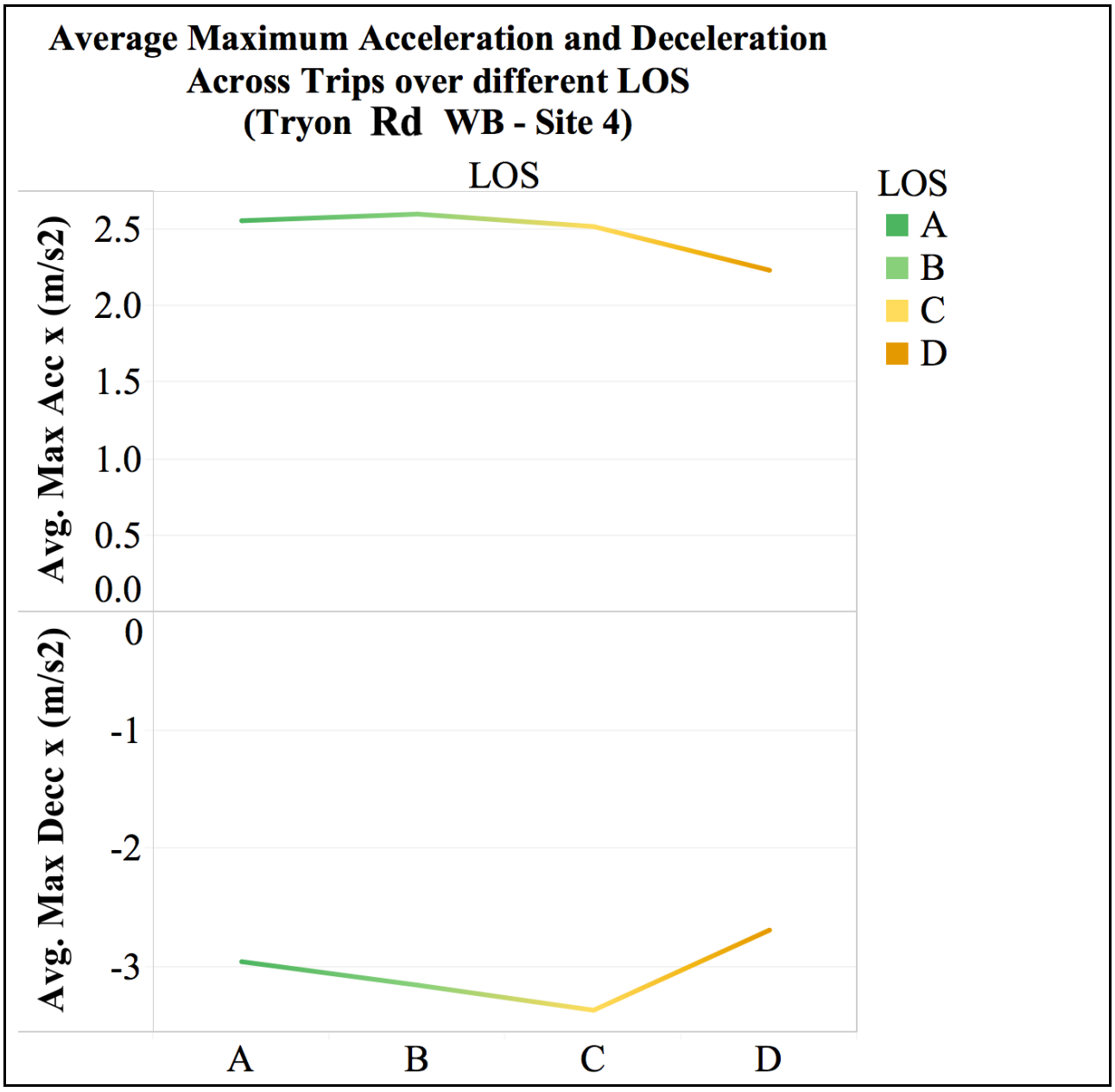

Figure J-15 – Average Maximum Acceleration and Deceleration Across Trips observations over different LOS (Tryon Rd WB – Site 4)

APPENDIX K - BOXPLOT OF SECOND-BY-SECOND ACCELERATION OBSERVATIONS OVER DIFFERENT LOS

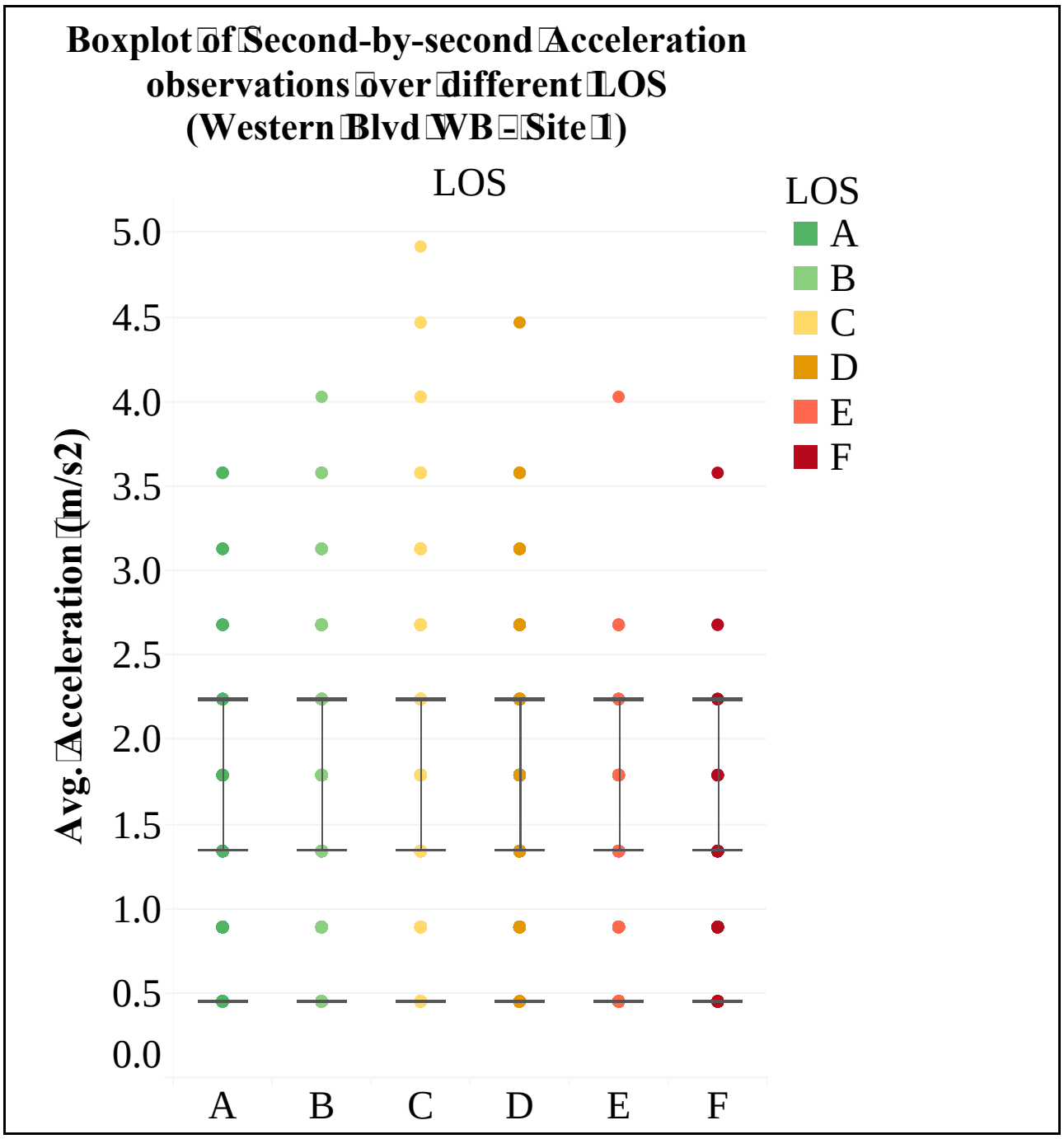

Figure K-1 – Boxplot of Second-by-second Acceleration observations over different LOS (Western Blvd WB – Site 1)

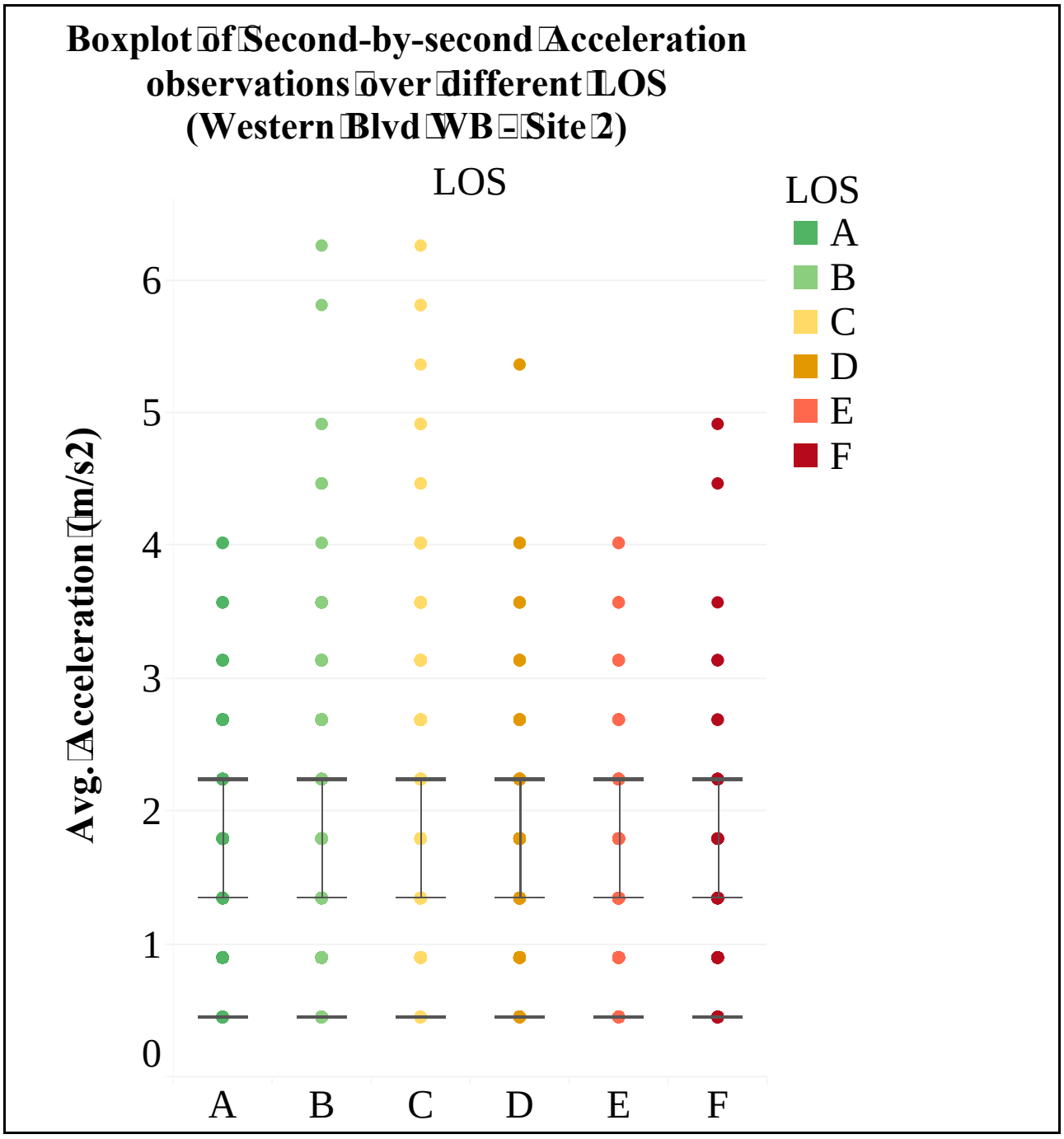

Figure K-2 – Boxplot of Second-by-second Acceleration observations over different LOS (Western Blvd WB – Site 2)

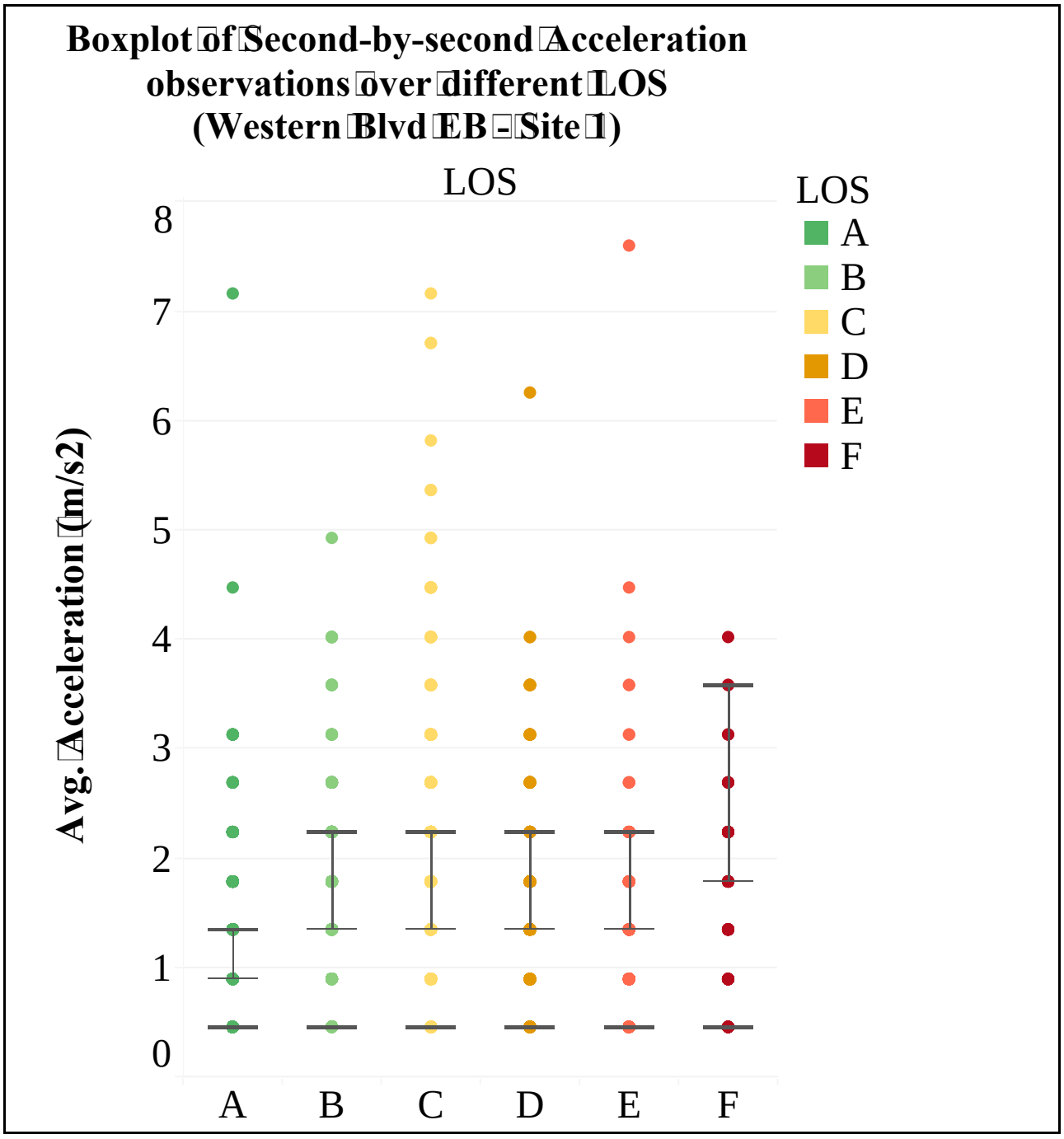

Figure K-3 – Boxplot of Second-by-second Acceleration observations over different LOS (Western Blvd EB – Site 1)

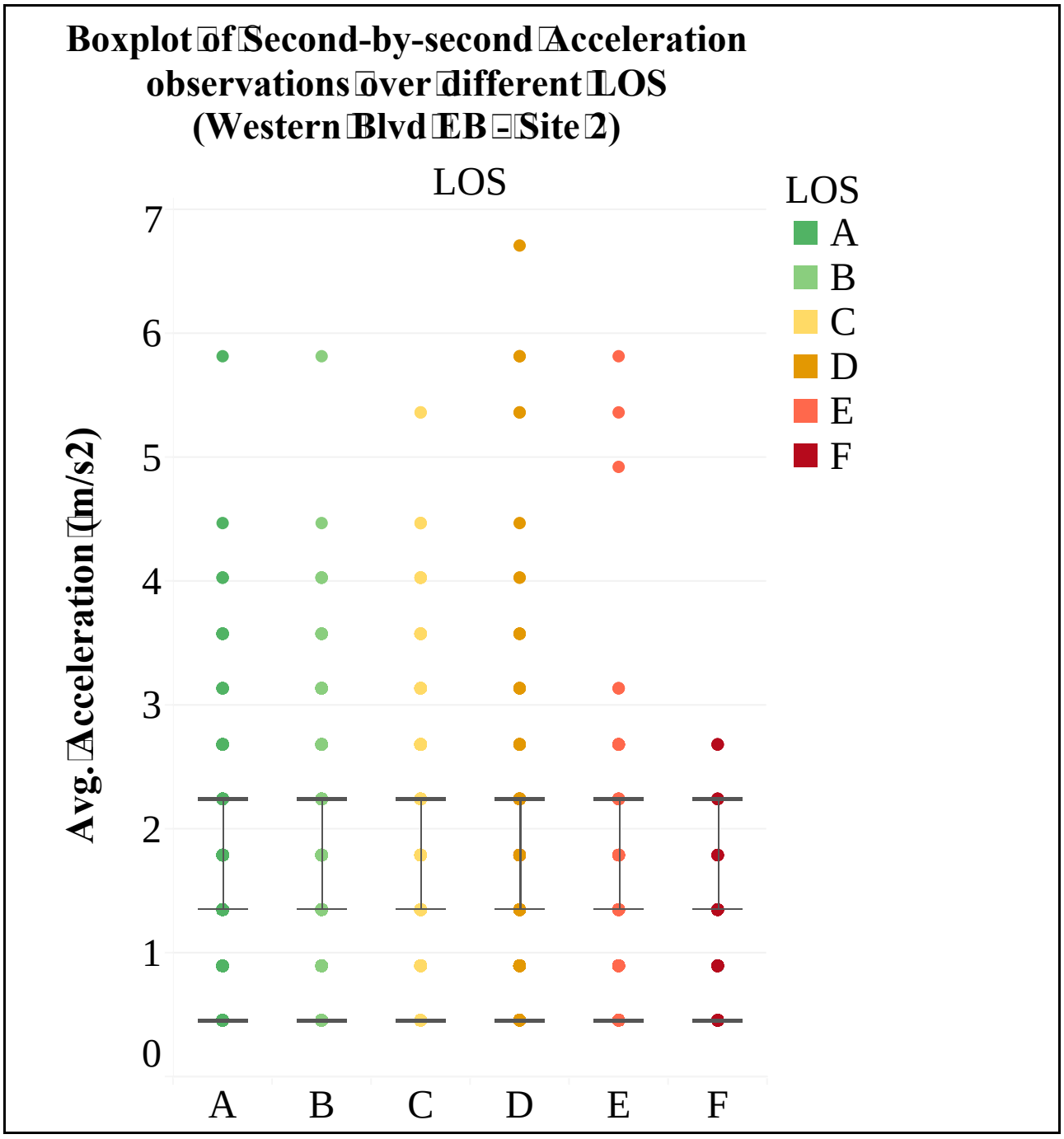

Figure K-4 – Boxplot of Second-by-second Acceleration observations over different LOS (Western Blvd EB – Site 2)

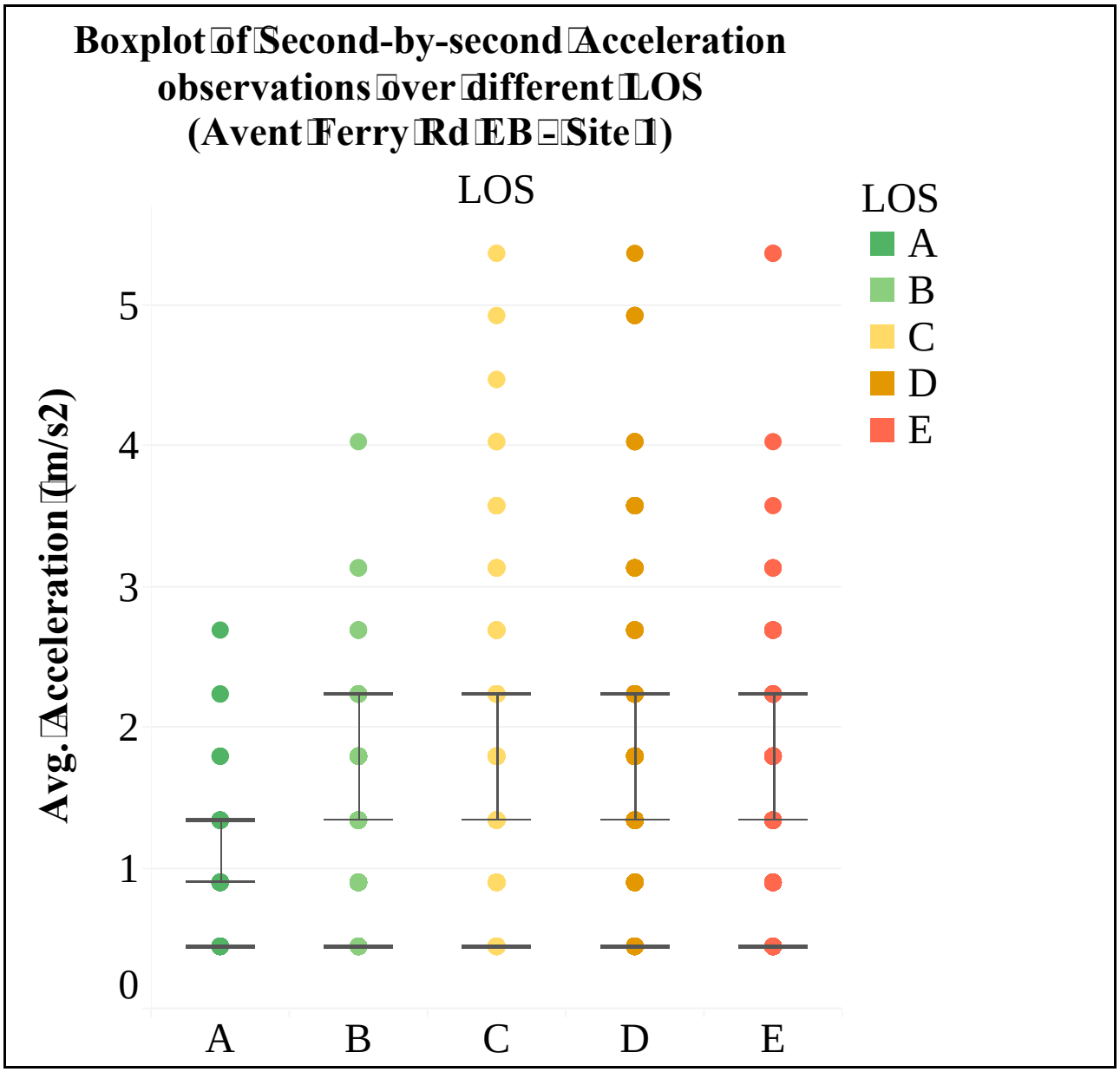

Figure K-5 – Boxplot of Second-by-second Acceleration observations over different LOS (Avent Ferry Rd EB – Site 1)

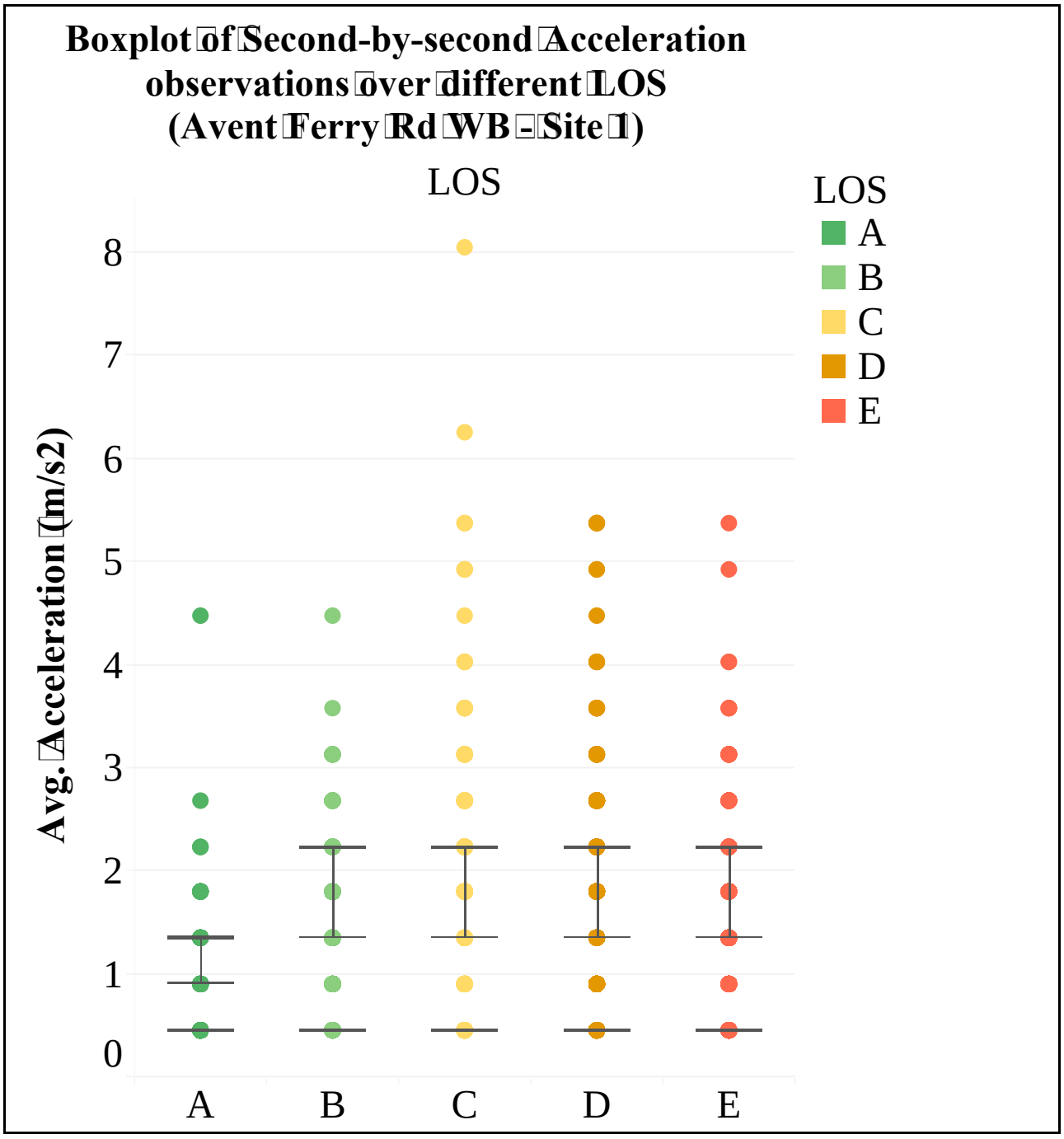

Figure K-6 – Boxplot of Second-by-second Acceleration observations over different LOS (Avent Ferry Rd WB – Site 1)

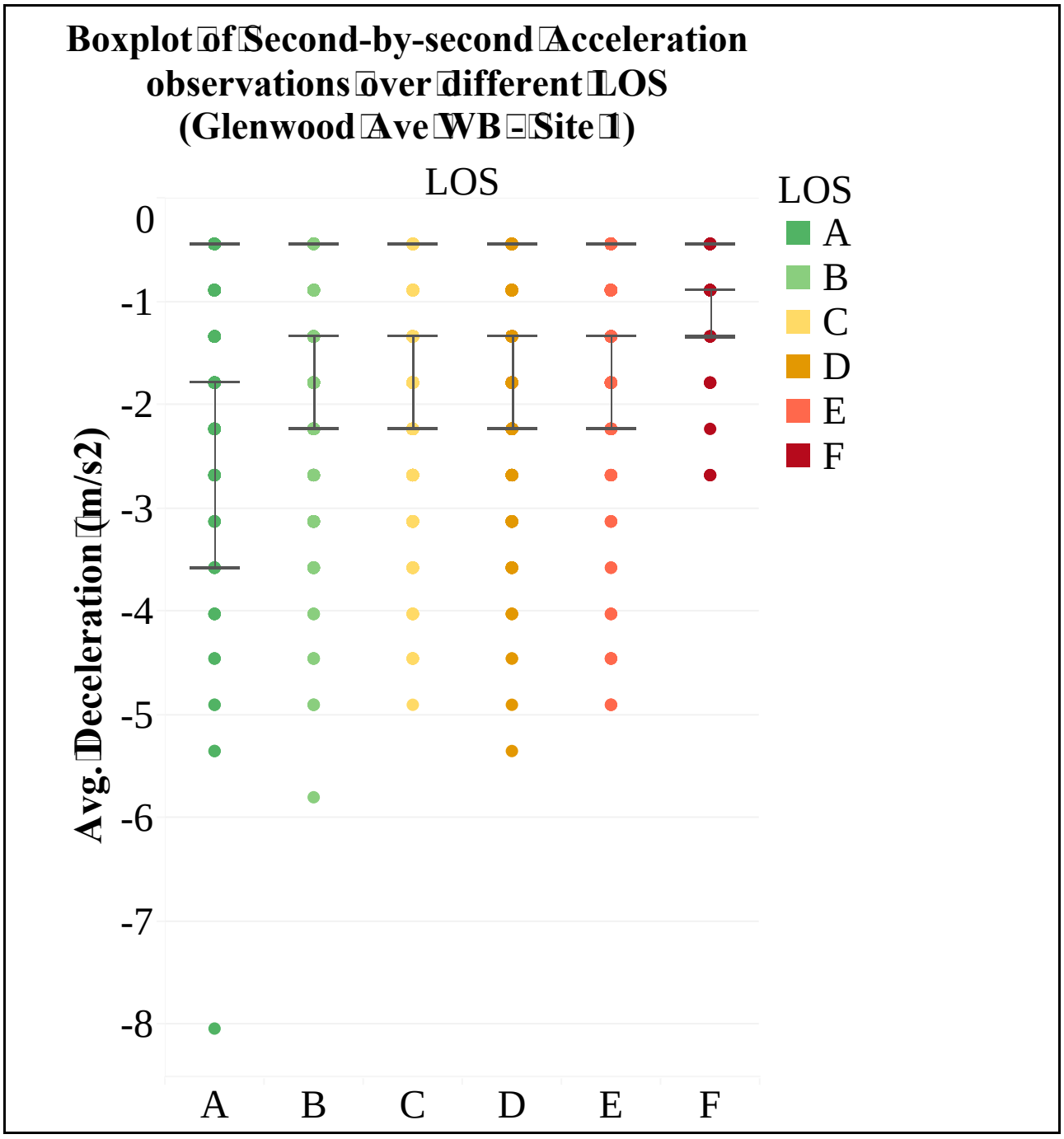

Figure K-7 – Boxplot of Second-by-second Acceleration observations over different LOS (Glenwood Ave WB – Site 1)

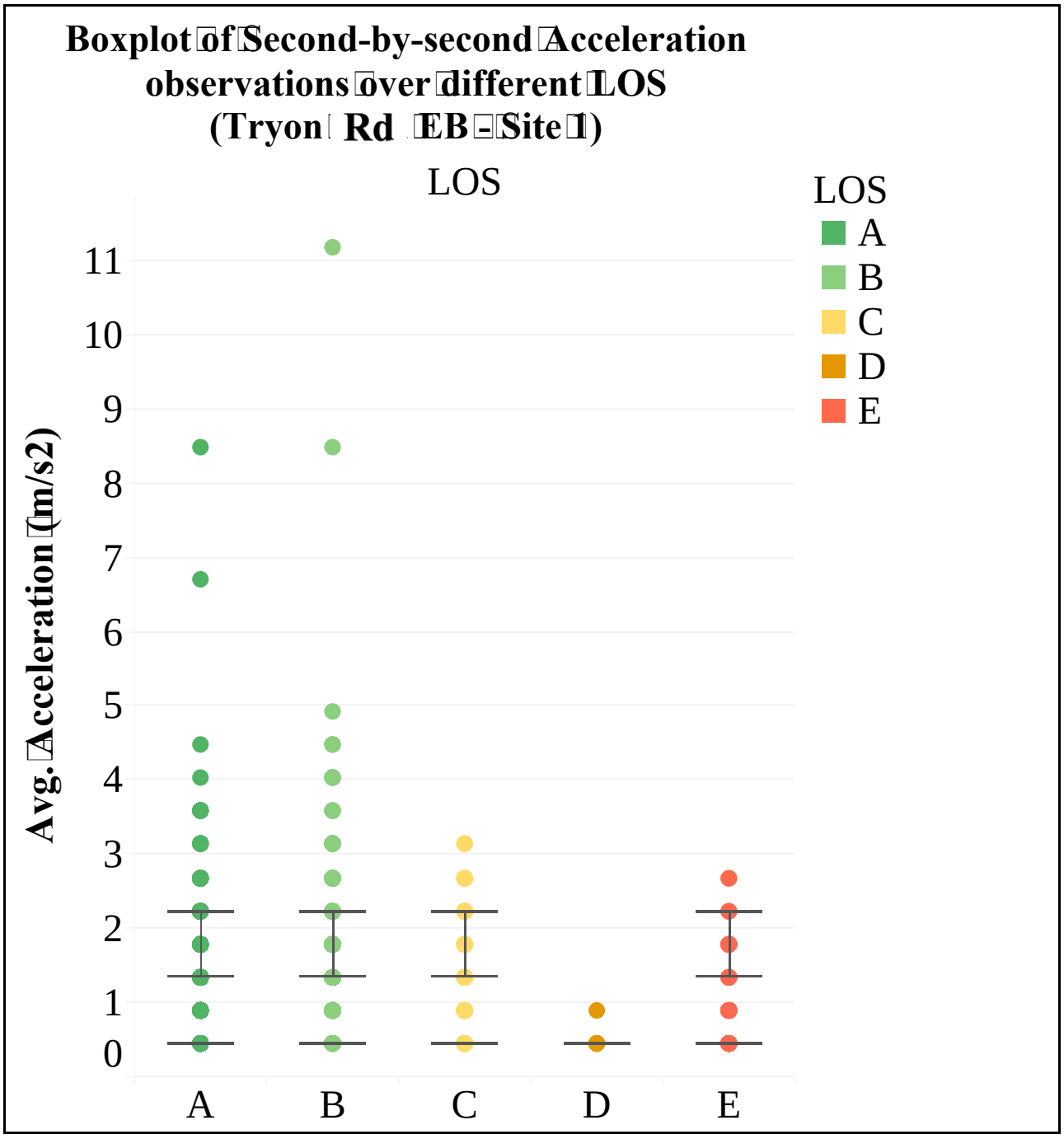

Figure K-8 – Boxplot of Second-by-second Acceleration observations over different LOS (Tryon Rd EB – Site 1)

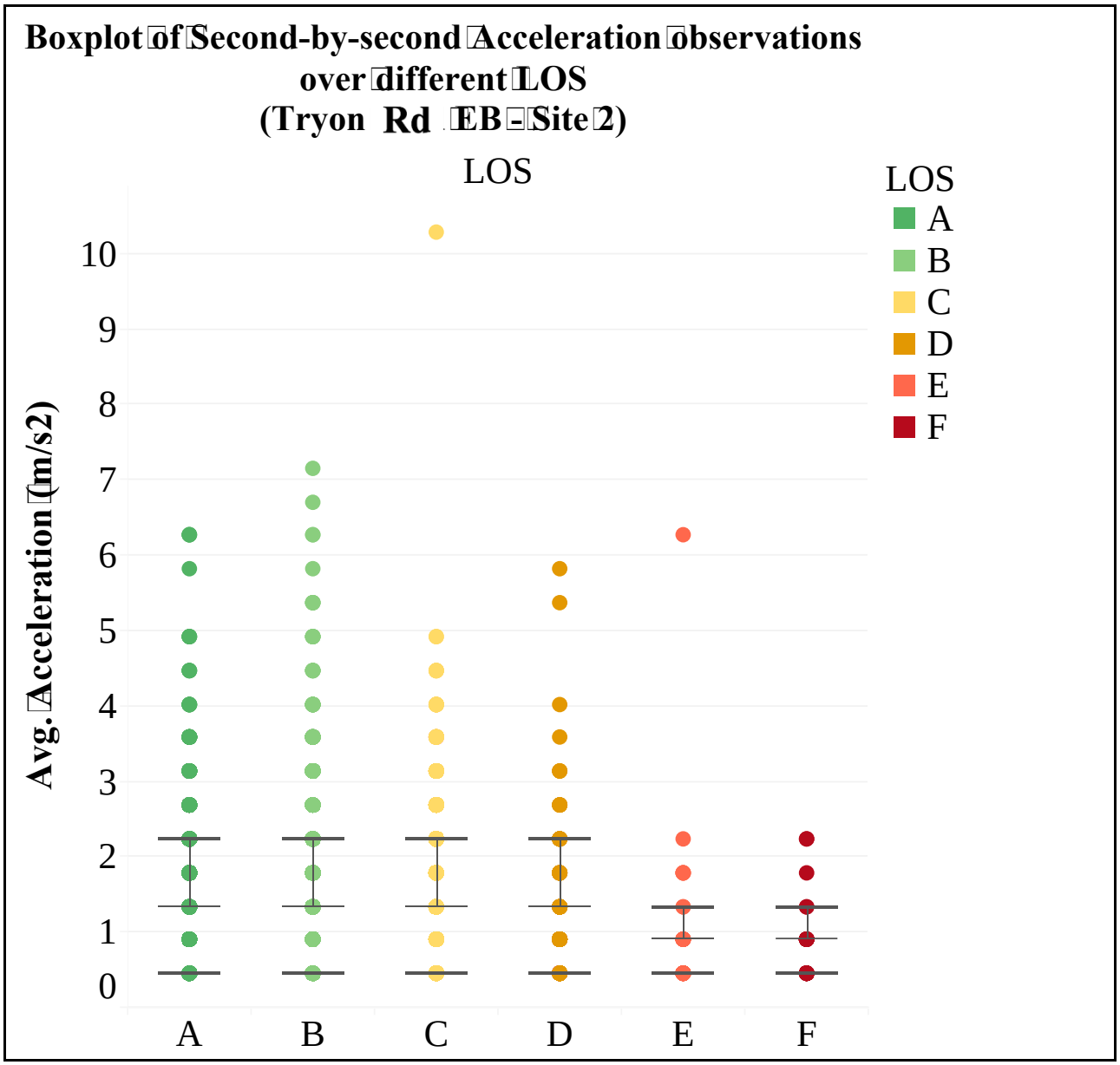

Figure K-9 – Boxplot of Second-by-second Acceleration observations over different LOS (Tryon Rd EB – Site 2)

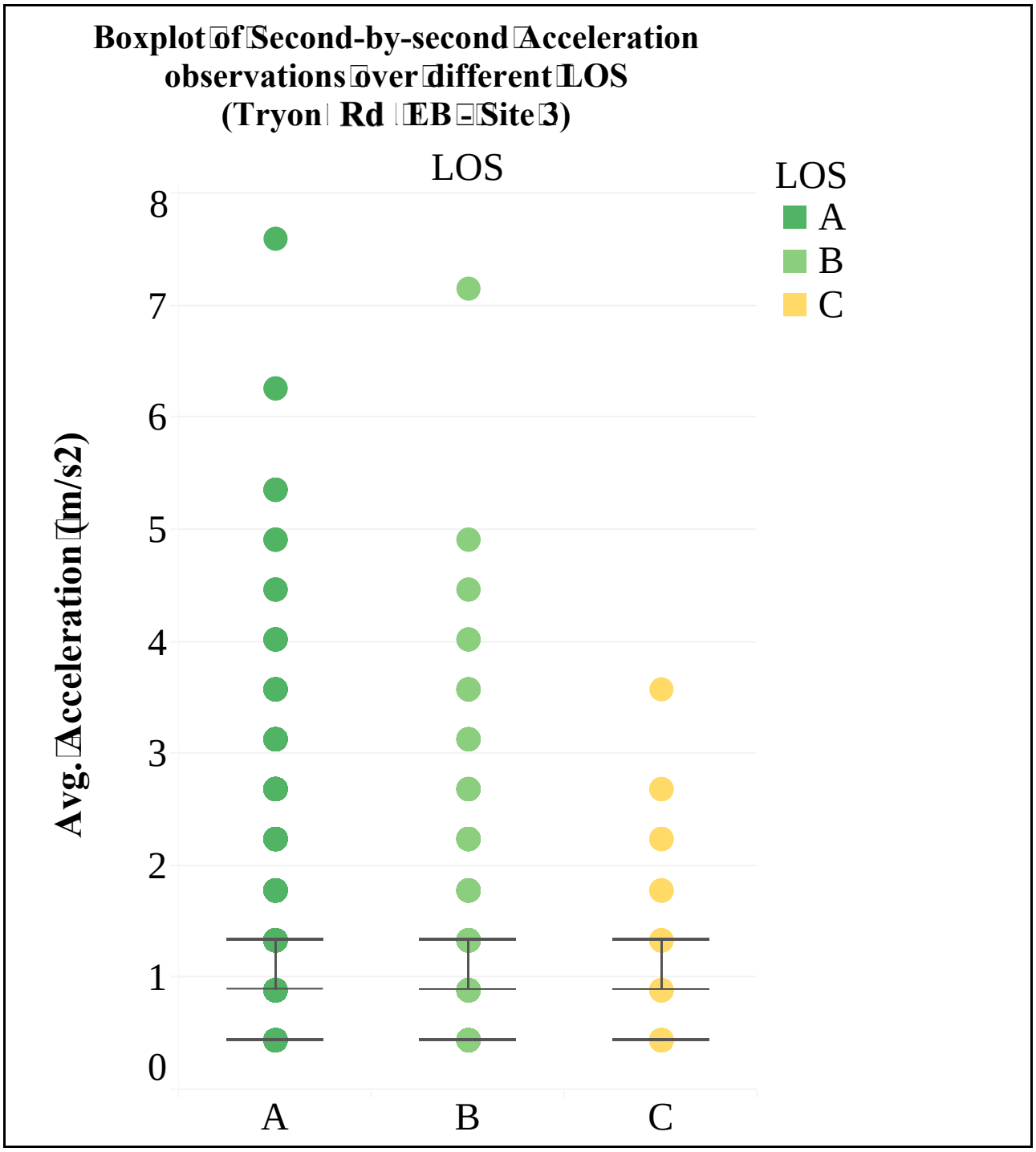

Figure K-10 – Boxplot of Second-by-second Acceleration observations over different LOS (Tryon Rd EB – Site 3)

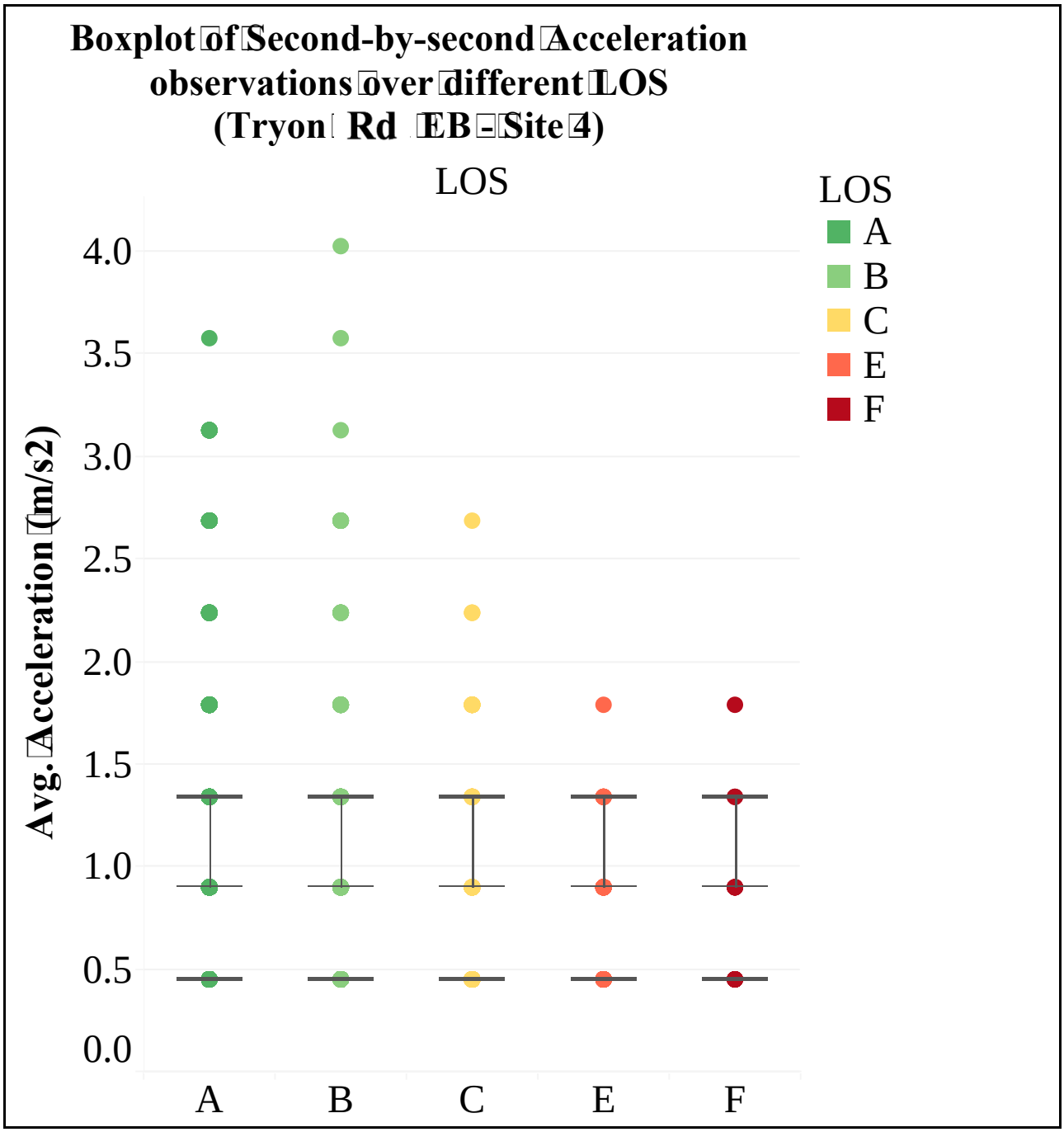

Figure K-11 – Boxplot of Second-by-second Acceleration observations over different LOS (Tryon Rd EB – Site 4)

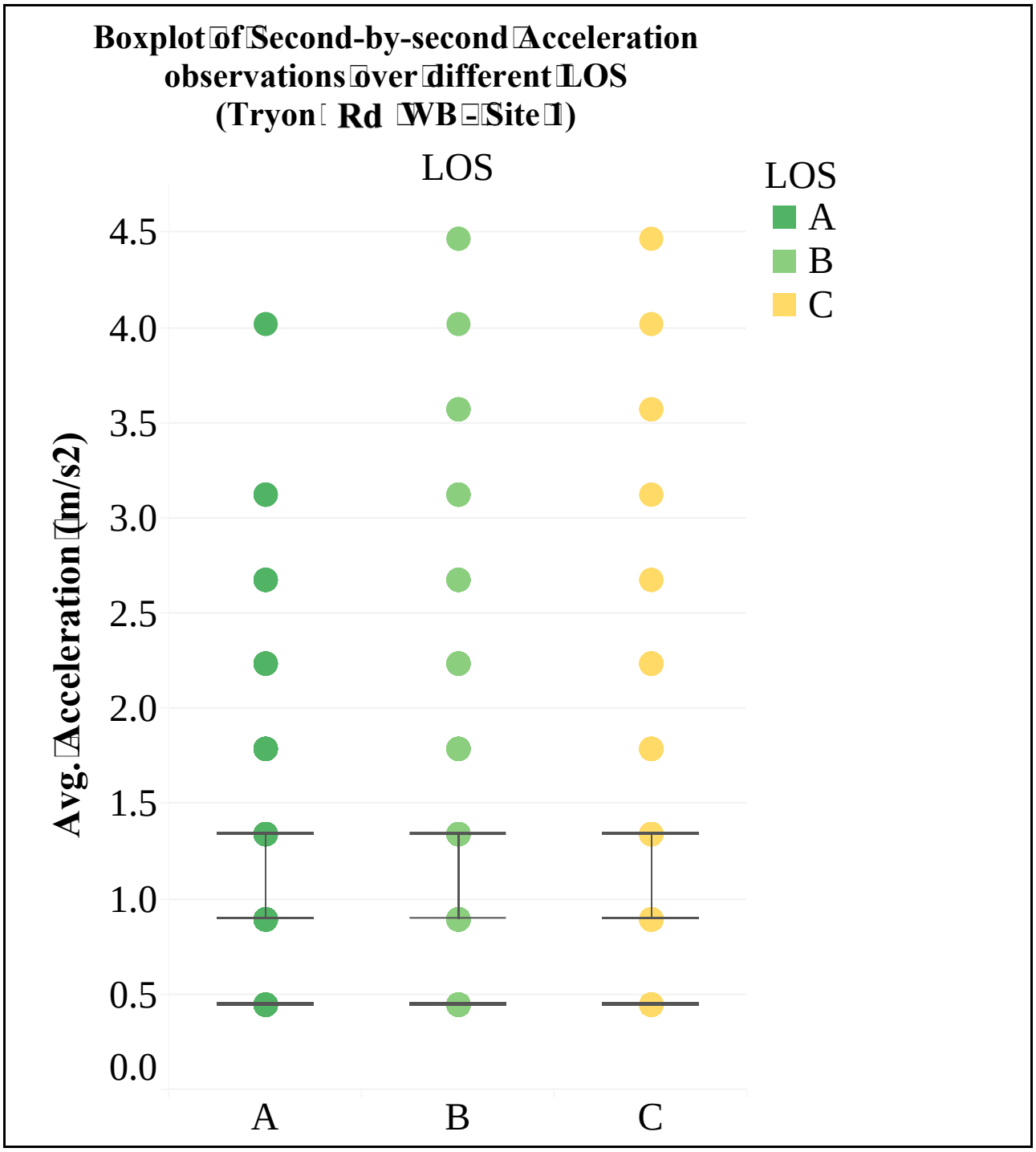

Figure K-12 – Boxplot of Second-by-second Acceleration observations over different LOS (Tryon Rd WB – Site 1)

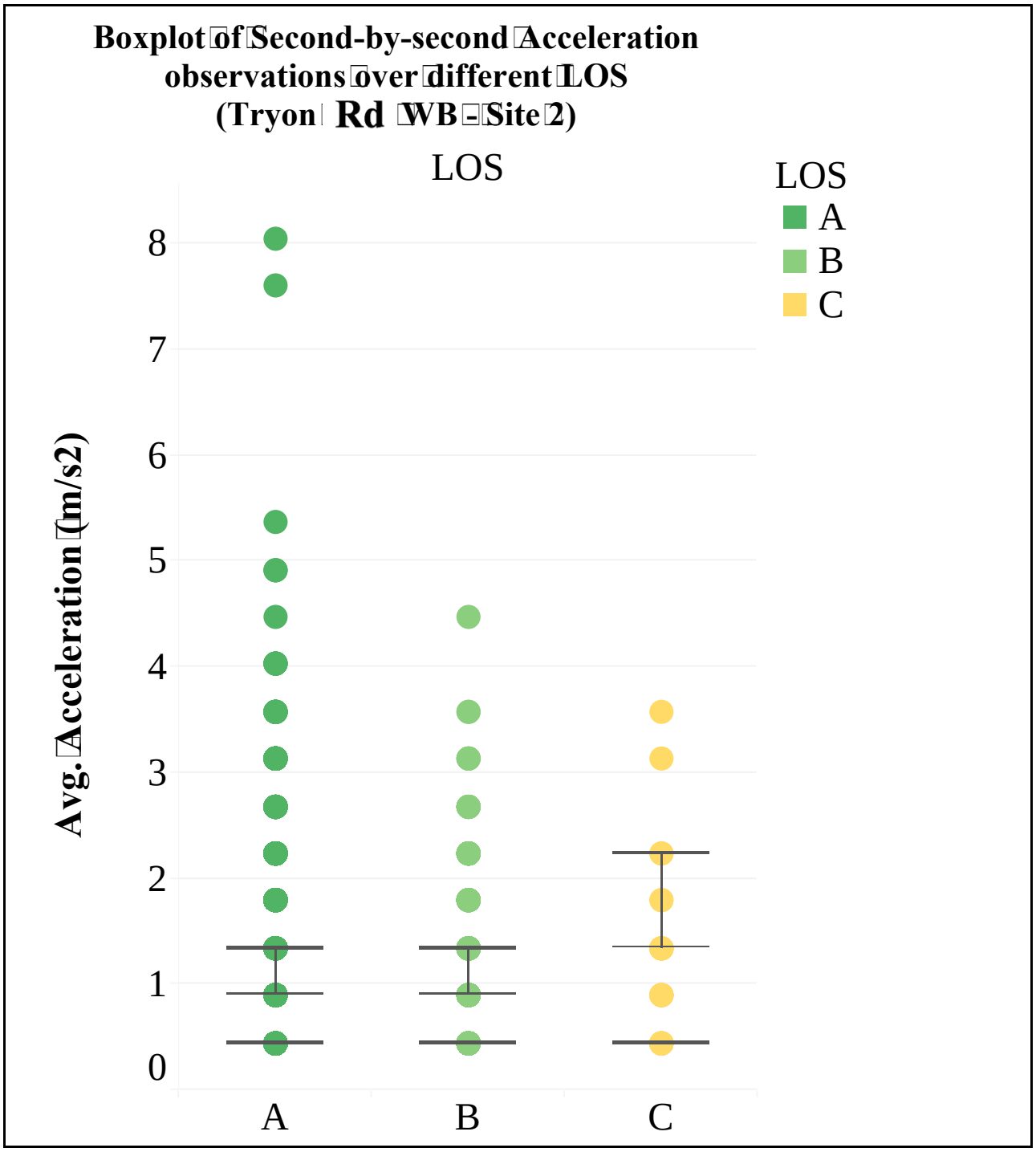

Figure K-13 – Boxplot of Second-by-second Acceleration observations over different LOS (Tryon Rd WB – Site 2)

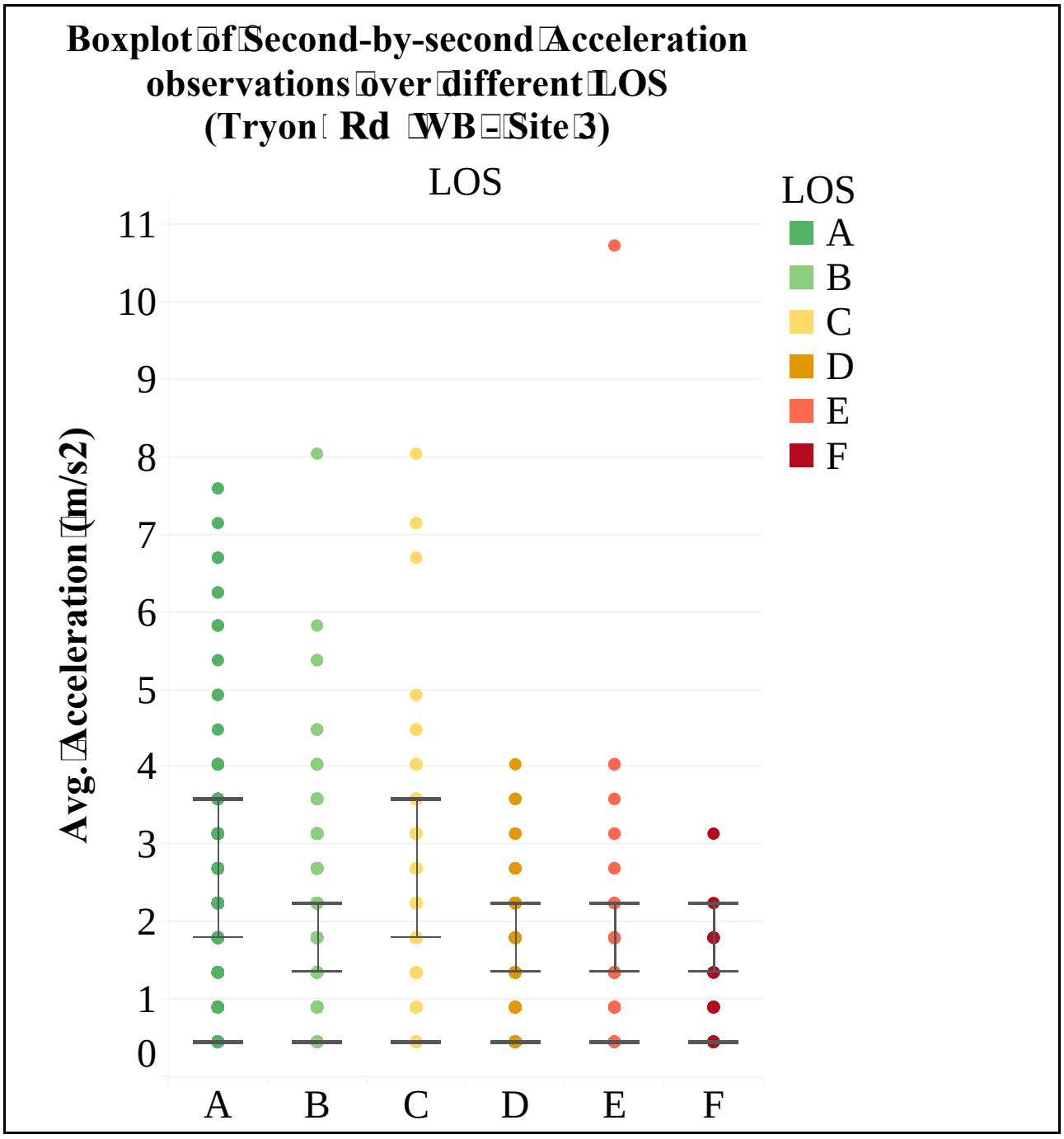

Figure K-14 – Boxplot of Second-by-second Acceleration observations over different LOS (Tryon Rd WB – Site 3)

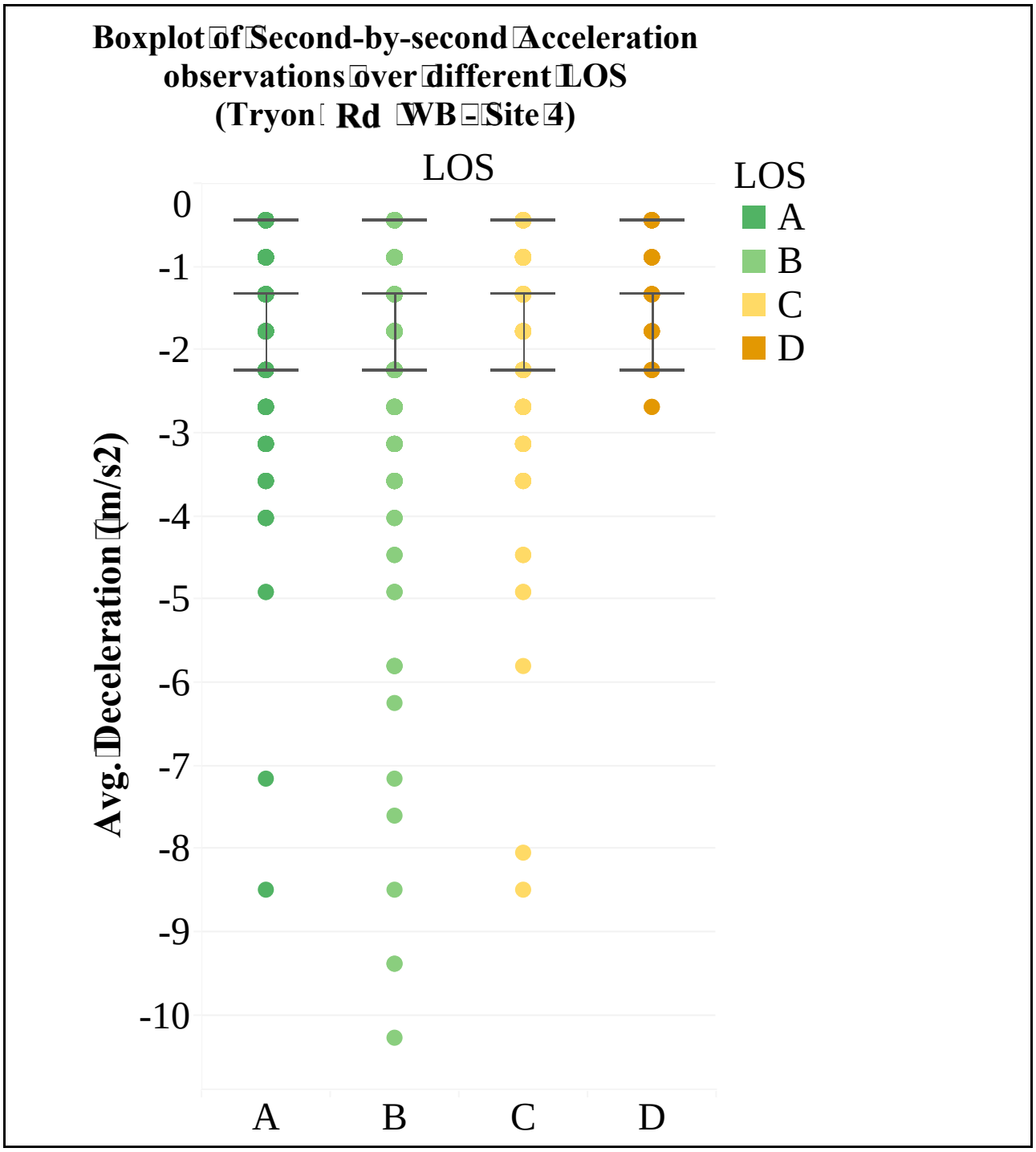

Figure K-15 – Boxplot of Second-by-second Acceleration observations over different LOS (Tryon Rd WB – Site 4)

APPENDIX M - PERCENTAGE OF SECOND-BY-SECOND DECELERATION OBSERVATIONS OVER DIFFERENT LOS

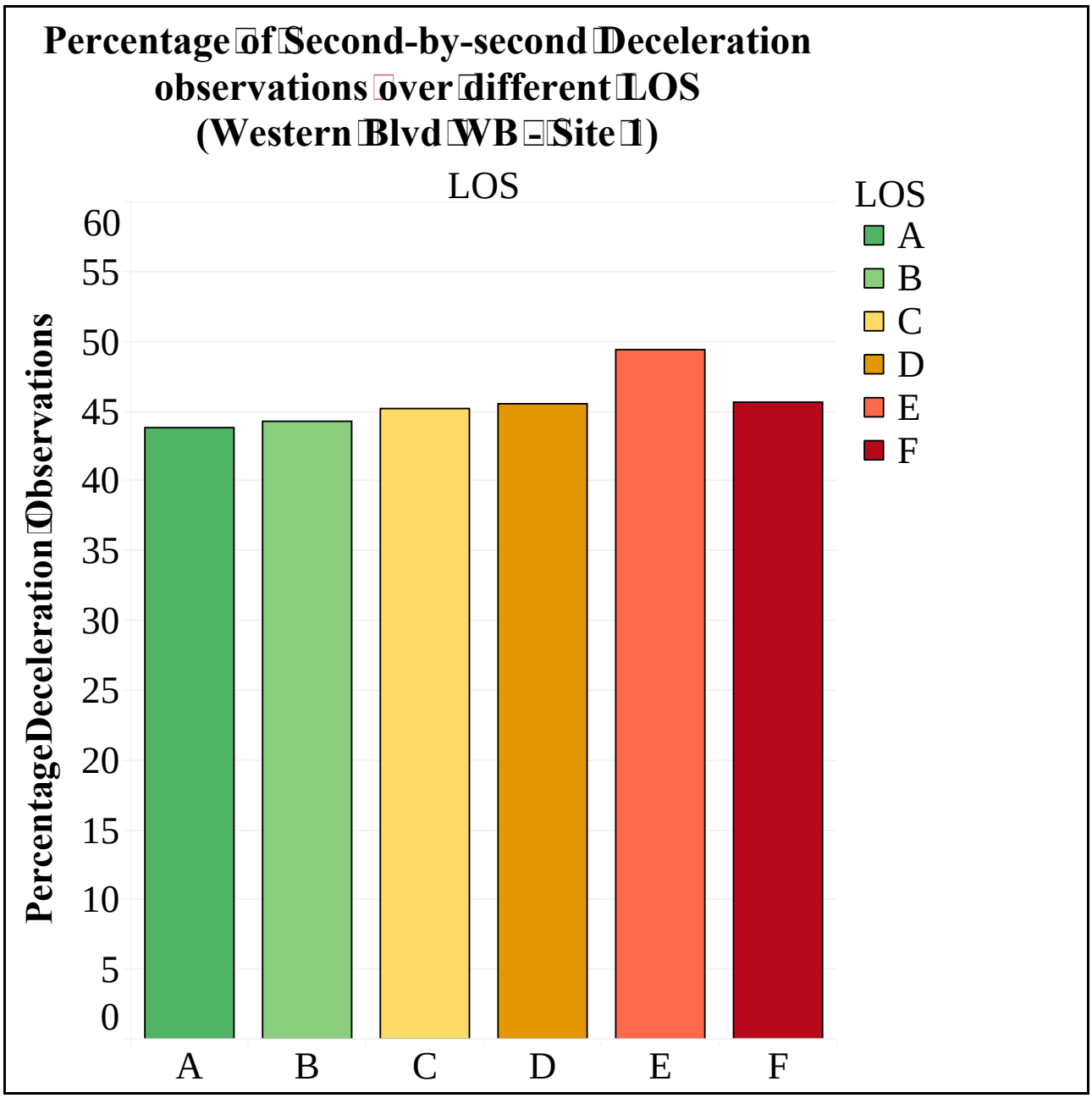

Figure L-1 – Percentage of Second-by-second Deceleration observations over different LOS (Western Blvd WB – Site 1)

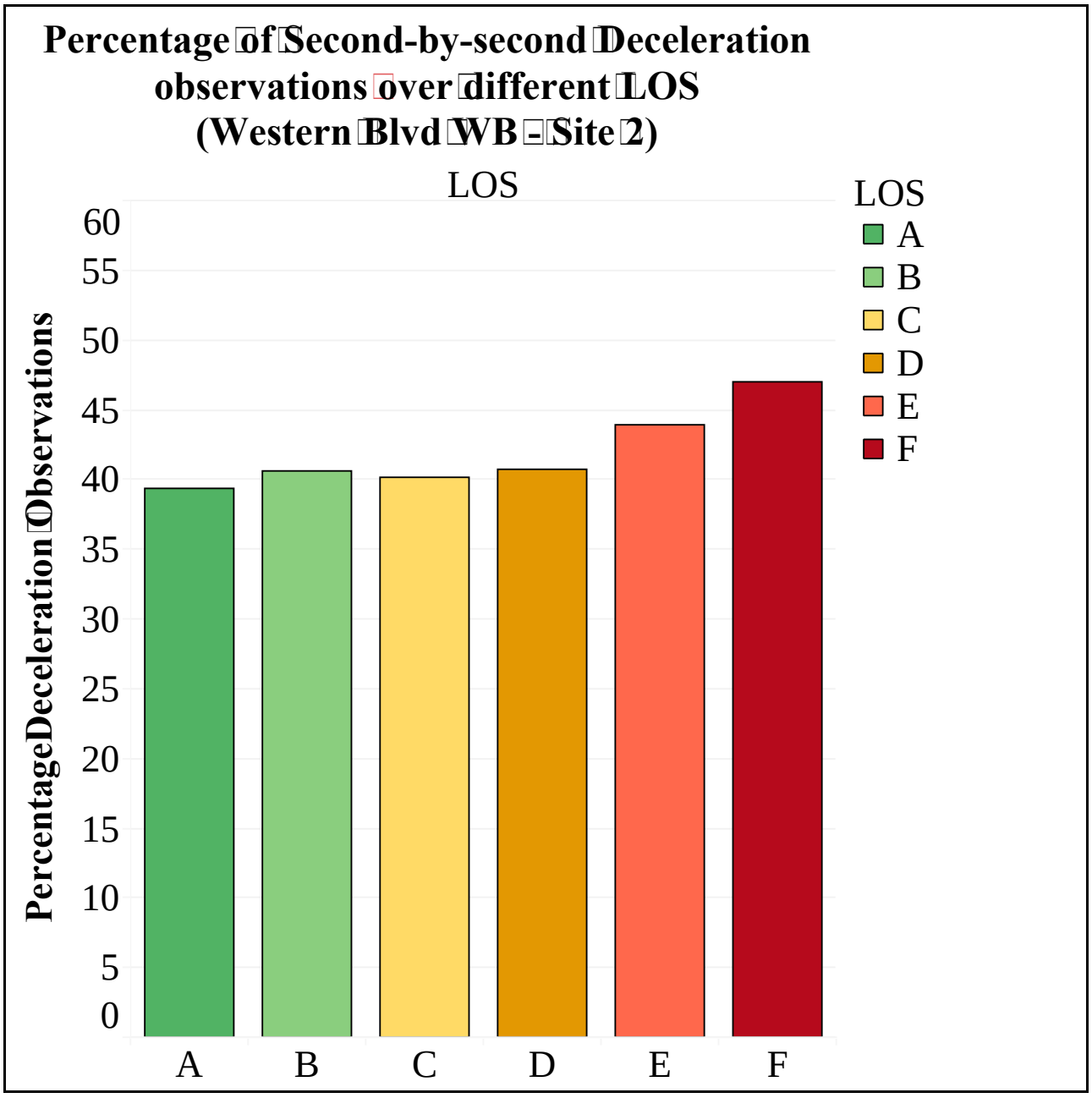

Figure L-2 – Percentage of Second-by-second Deceleration observations over different LOS (Western Blvd WB – Site 2)

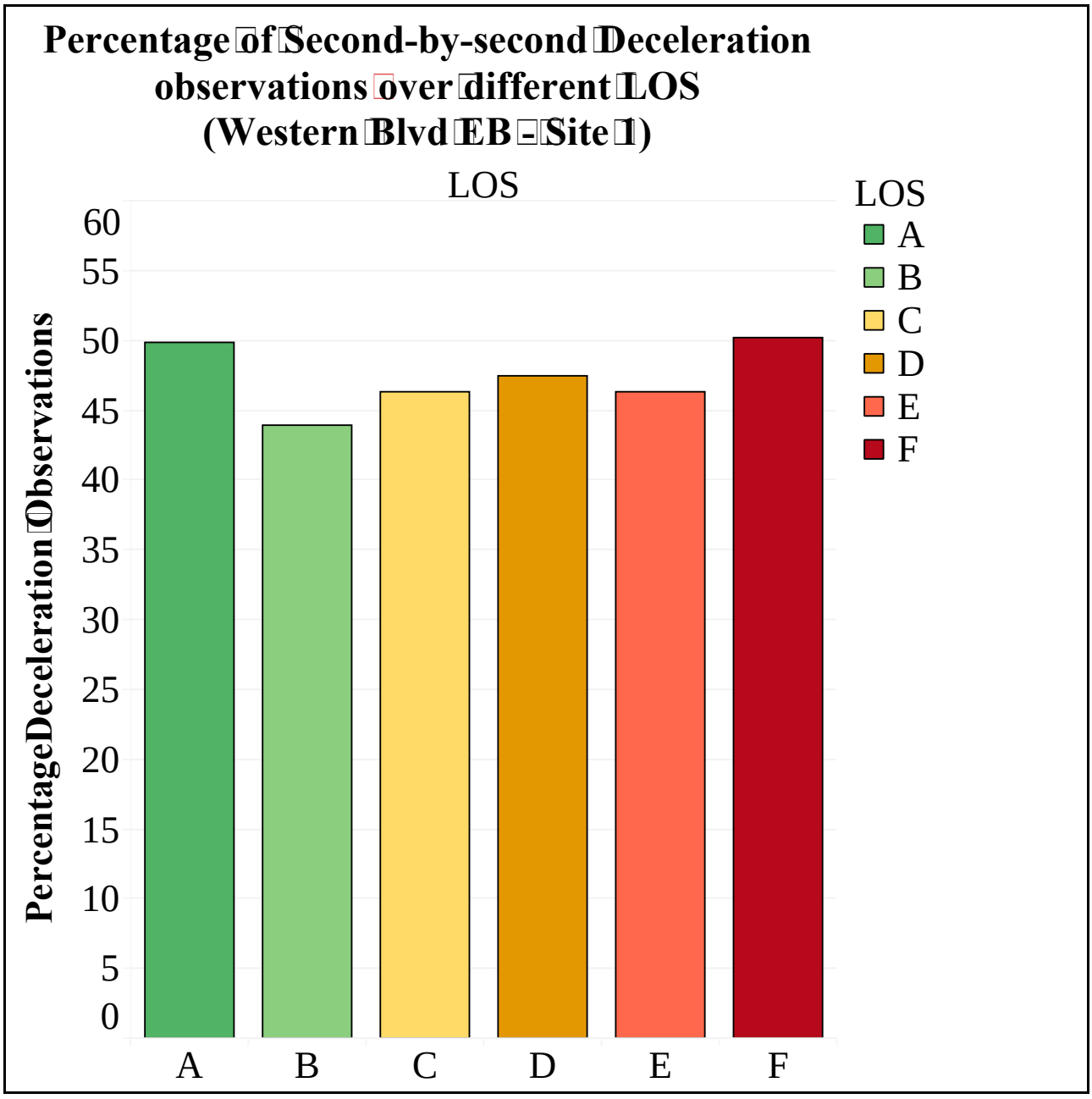

Figure L-3 – Percentage of Second-by-second Deceleration observations over different LOS (Western Blvd EB – Site 1)

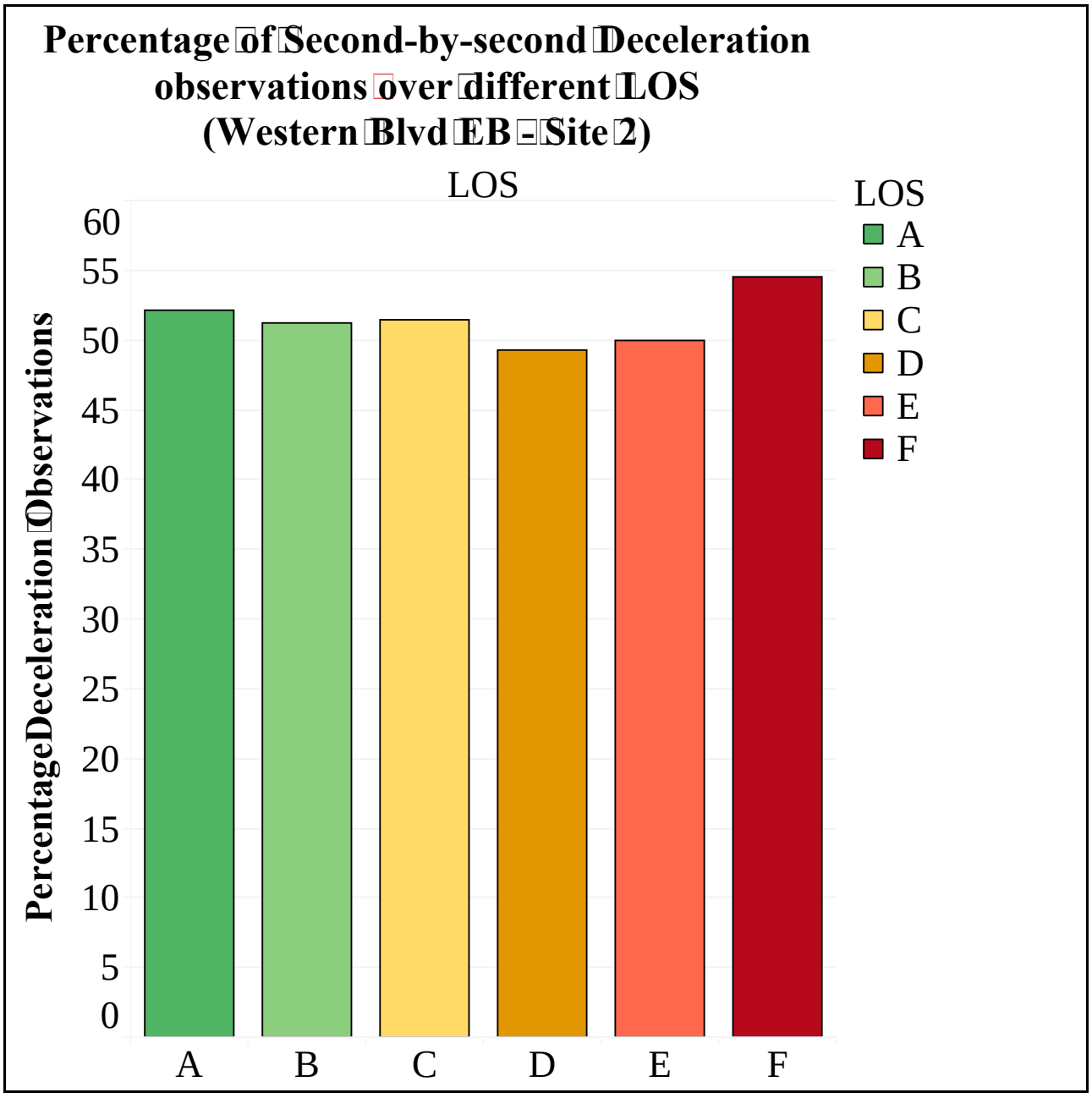

Figure L-4 – Percentage of Second-by-second Deceleration observations over different LOS (Western Blvd EB – Site 2)

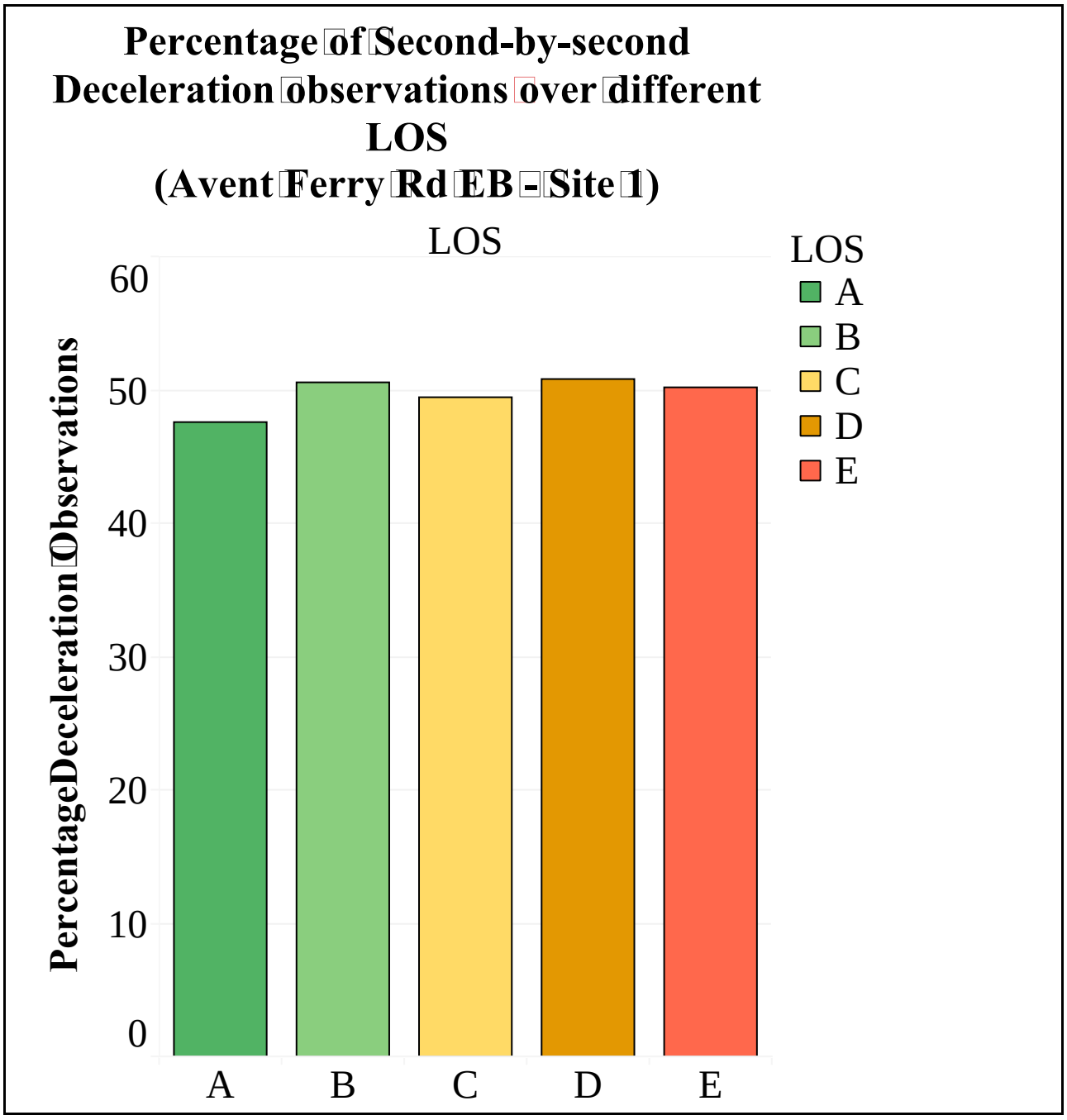

Figure L-5 – Percentage of Second-by-second Deceleration observations over different LOS (Avent Ferry Rd EB – Site 1)

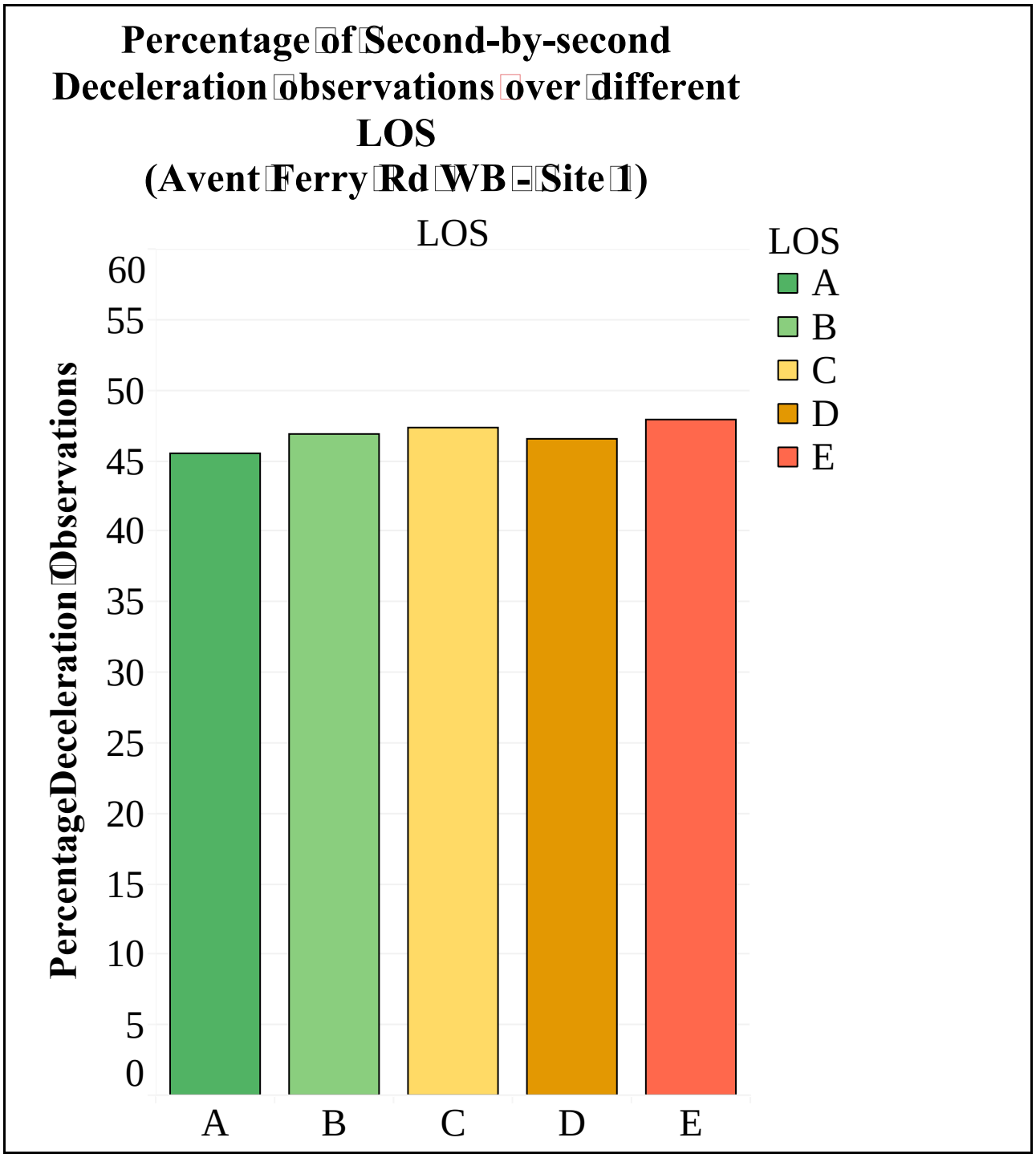

Figure L-6 – Percentage of Second-by-second Deceleration observations over different LOS (Avent Ferry Rd WB – Site 1)

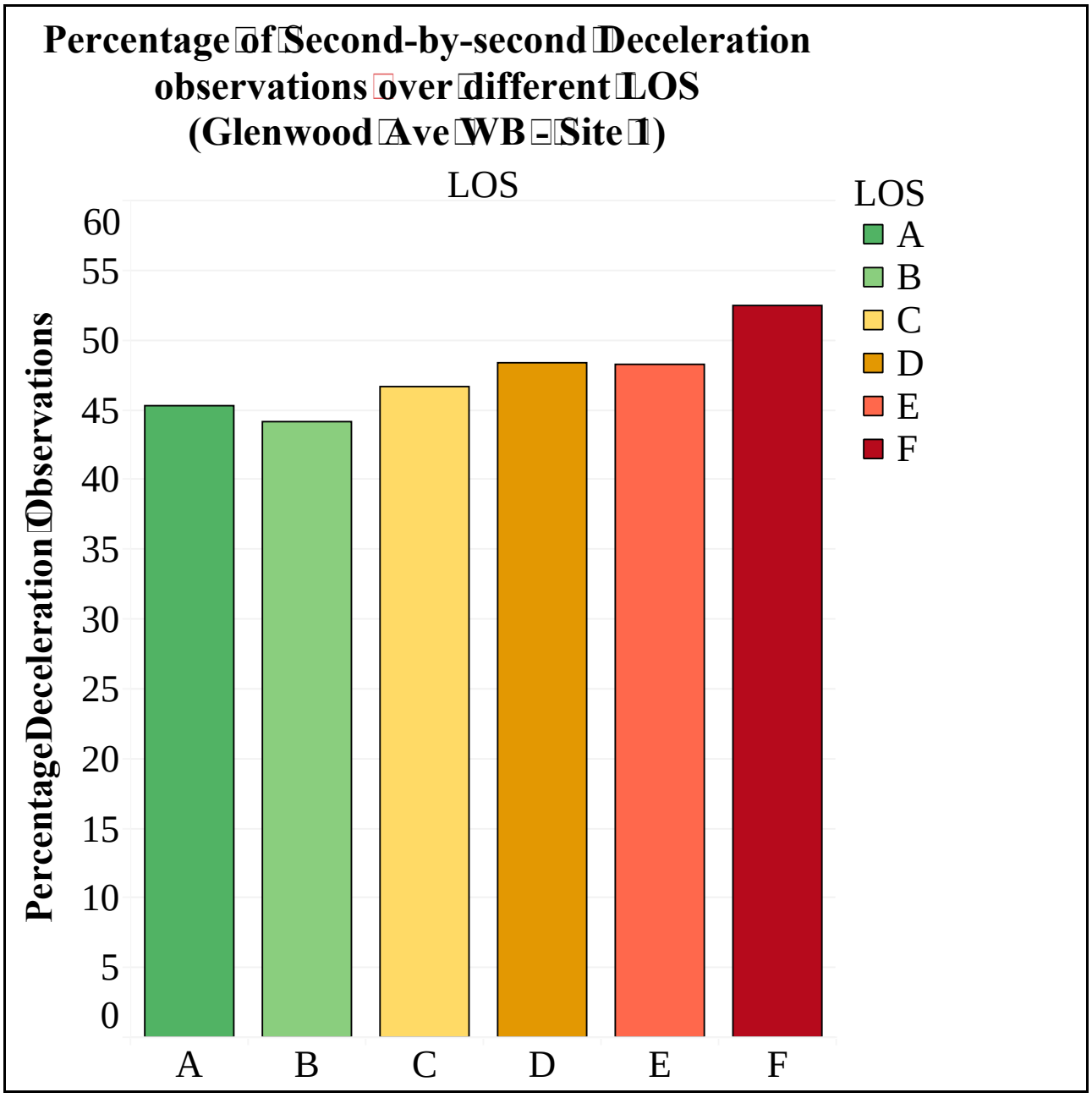

Figure L-7 – Percentage of Second-by-second Deceleration observations over different LOS (Glenwood Ave WB – Site 1)

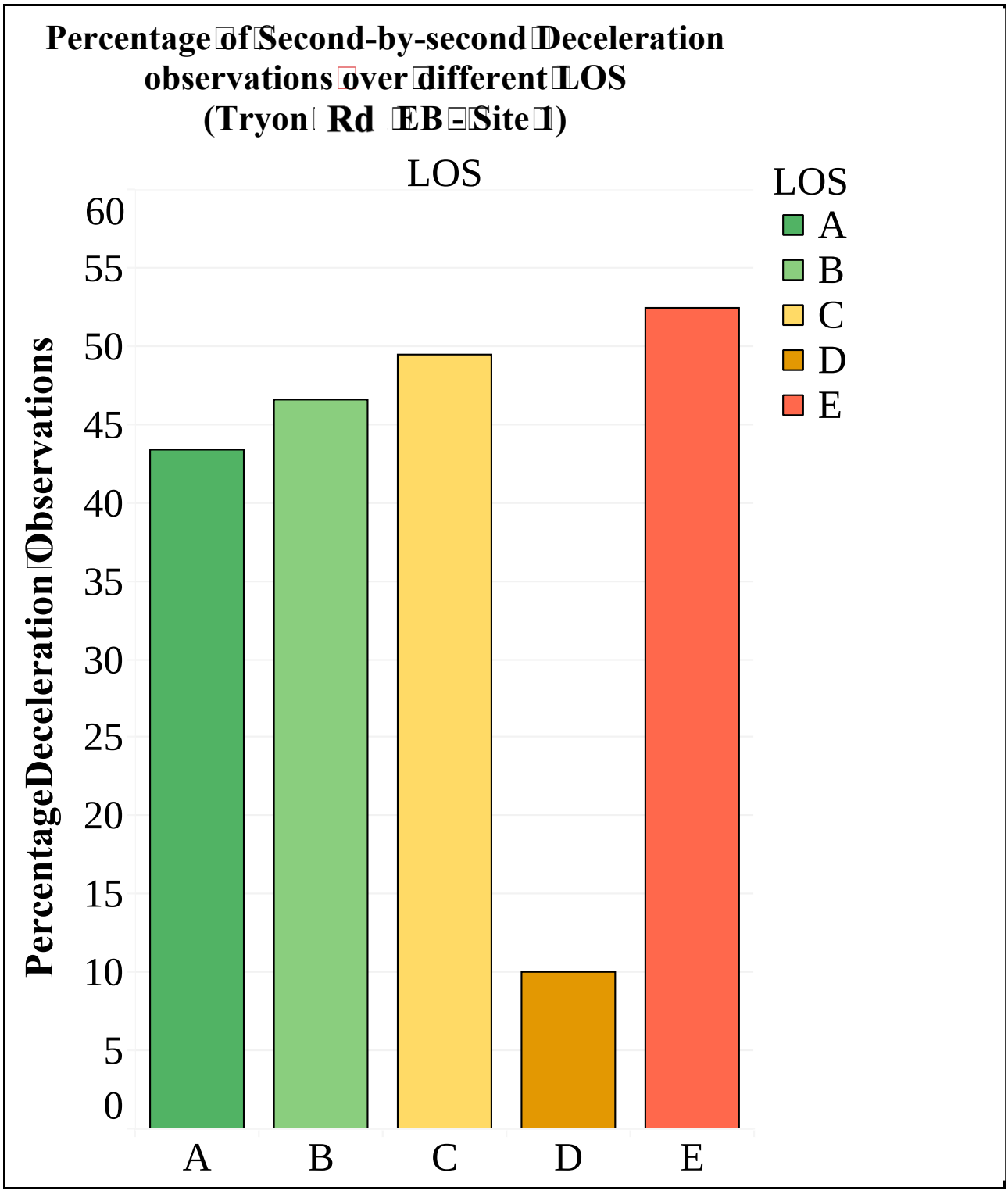

Figure L-8 – Percentage of Second-by-second Deceleration observations over different LOS (Tryon Rd EB – Site 1)

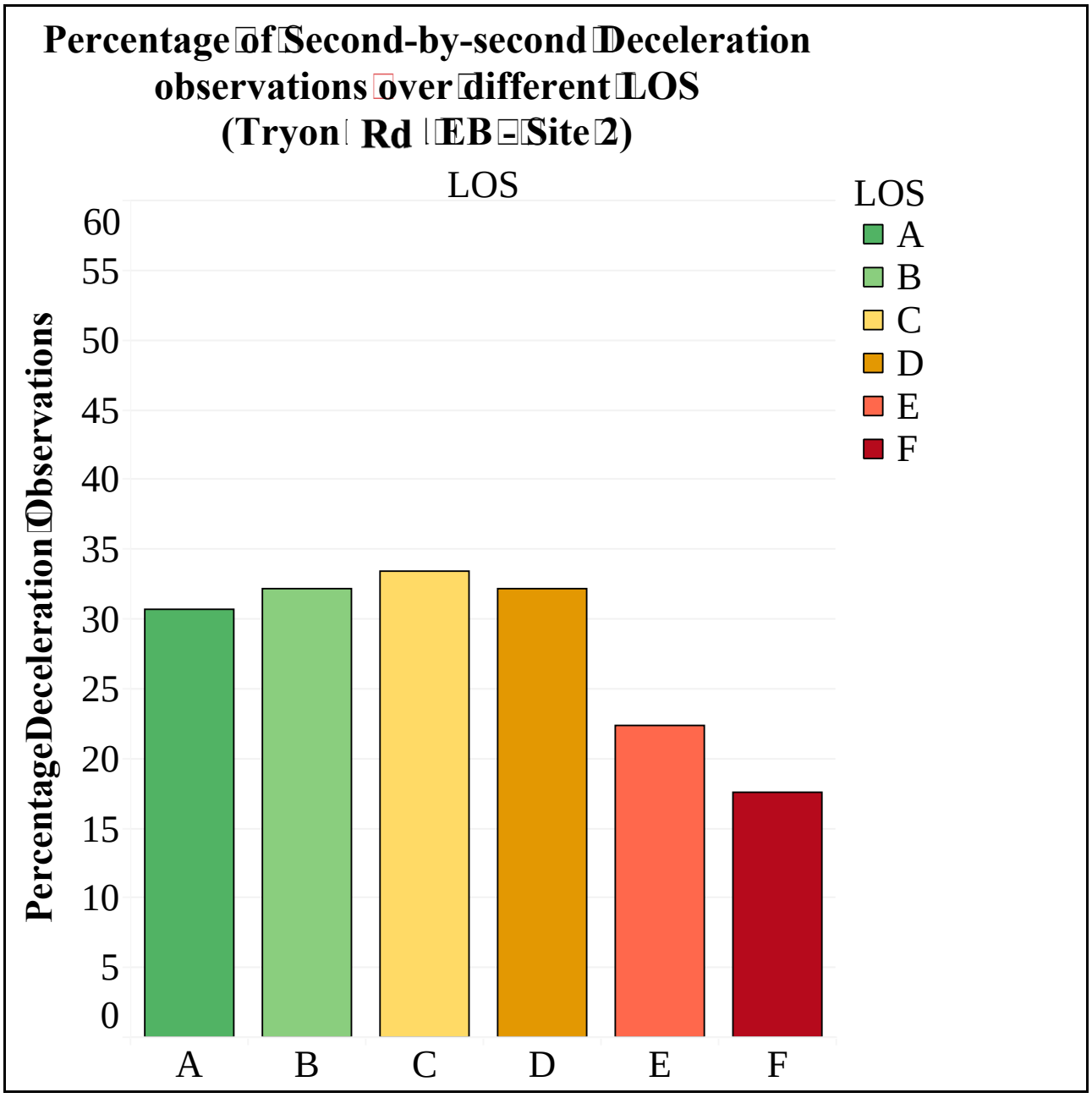

Figure L-9 – Percentage of Second-by-second Deceleration observations over different LOS (Tryon Rd EB – Site 2)

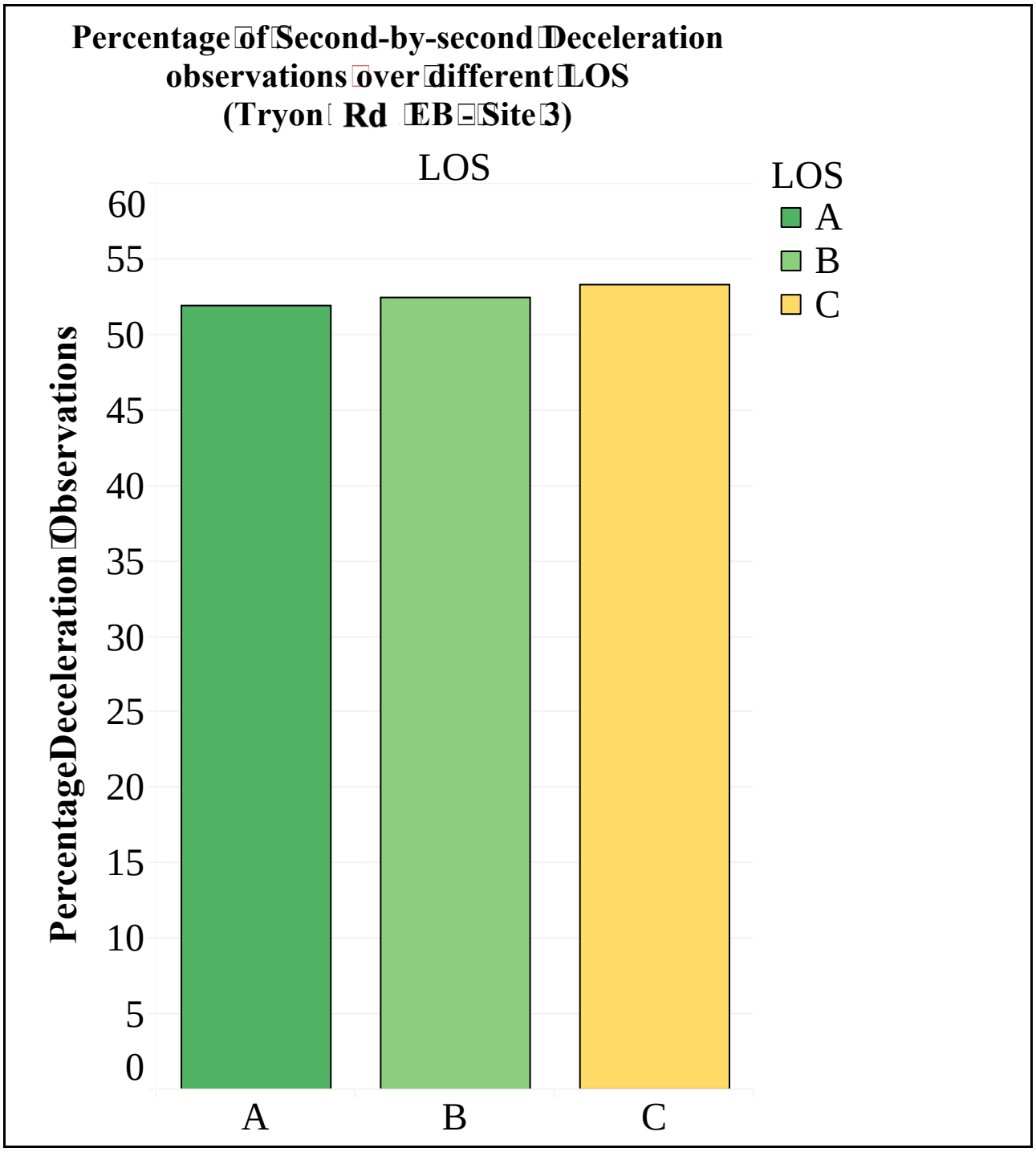

Figure L-10 – Percentage of Second-by-second Deceleration observations over different LOS (Tryon Rd EB – Site 3)

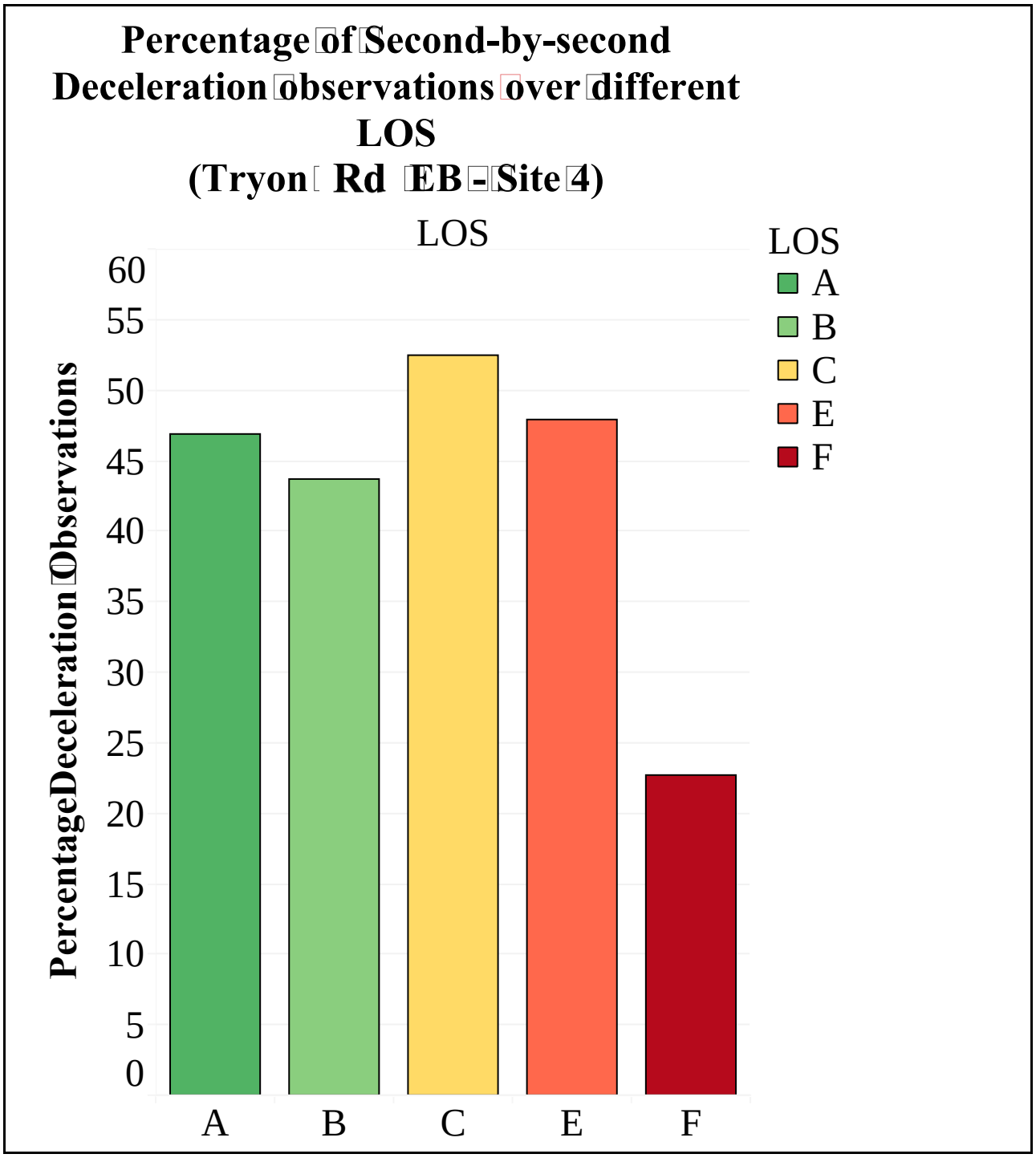

Figure L-11 – Percentage of Second-by-second Deceleration observations over different LOS (Tryon Rd EB – Site 4)

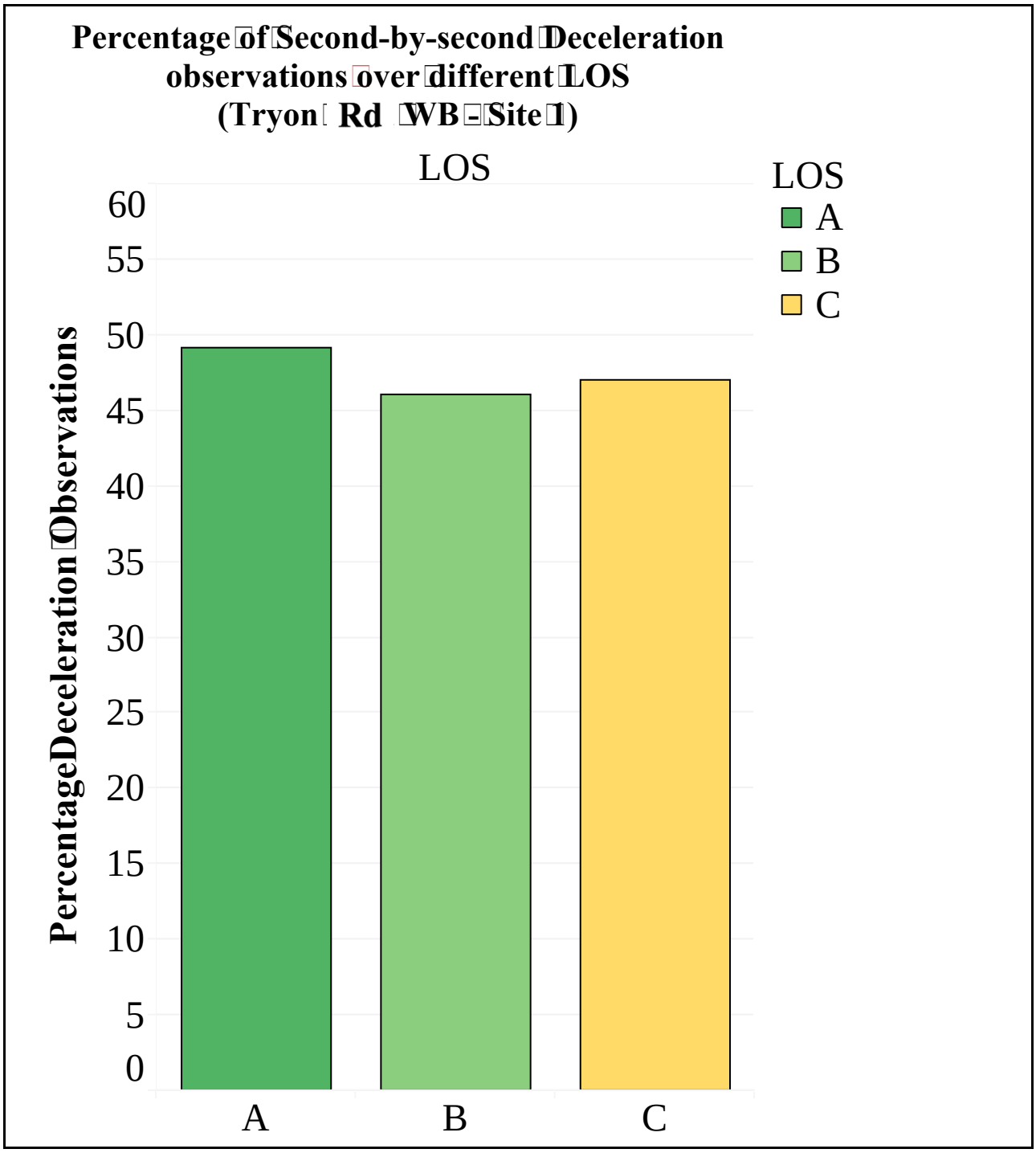

Figure L-12 – Percentage of Second-by-second Deceleration observations over different LOS (Tryon Rd WB – Site 1)

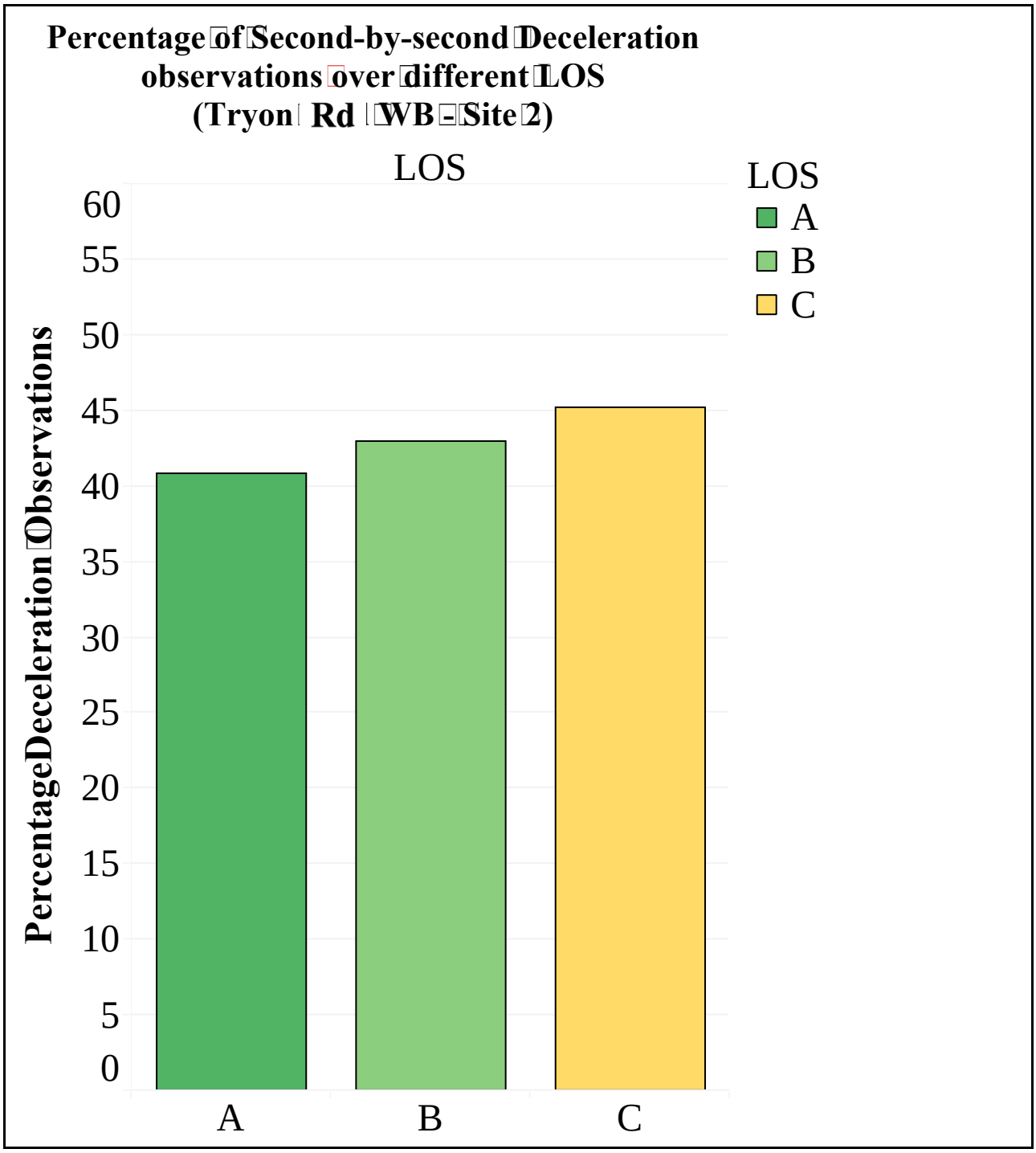

Figure L-13 – Percentage of Second-by-second Deceleration observations over different LOS (Tryon Rd WB – Site 2)

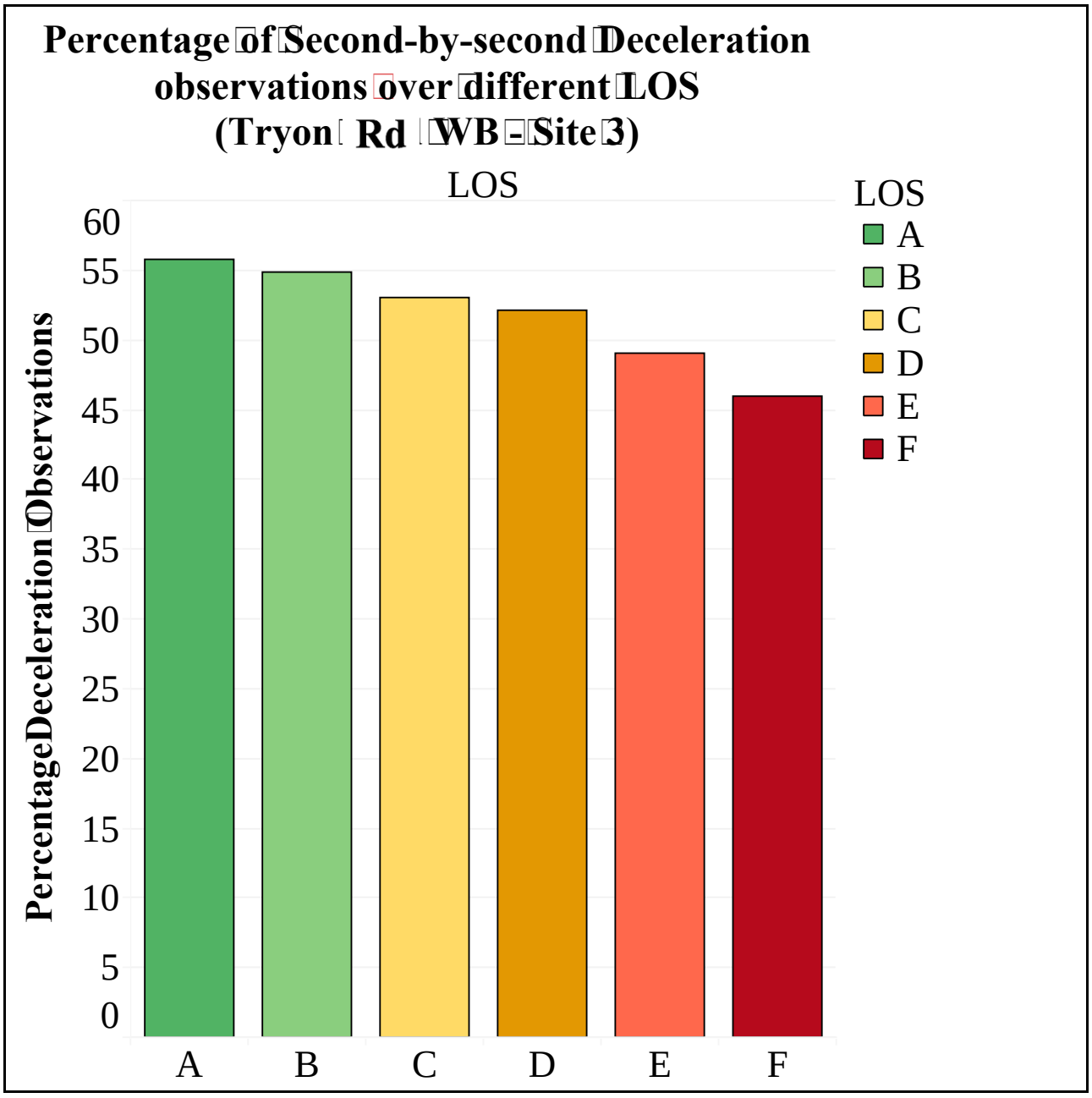

Figure L-14 – Percentage of Second-by-second Deceleration observations over different LOS (Tryon Rd WB – Site 3)

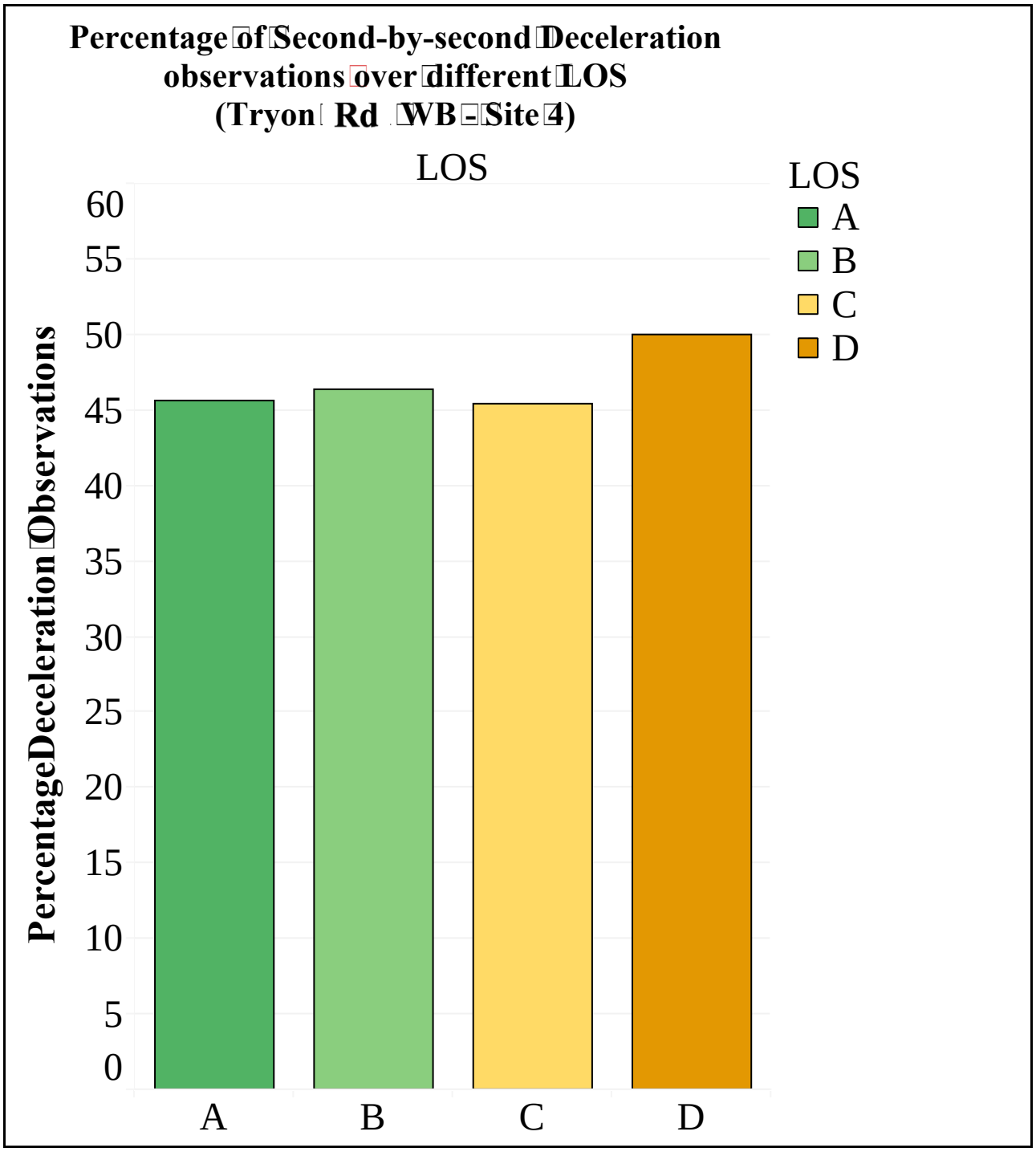

Figure L-15 – Percentage of Second-by-second Deceleration observations over different LOS (Tryon Rd WB – Site 4)

APPENDIX N - BOXPLOT OF SECOND-BY-SECOND READINGS OF RPM OVER DIFFERENT LOS

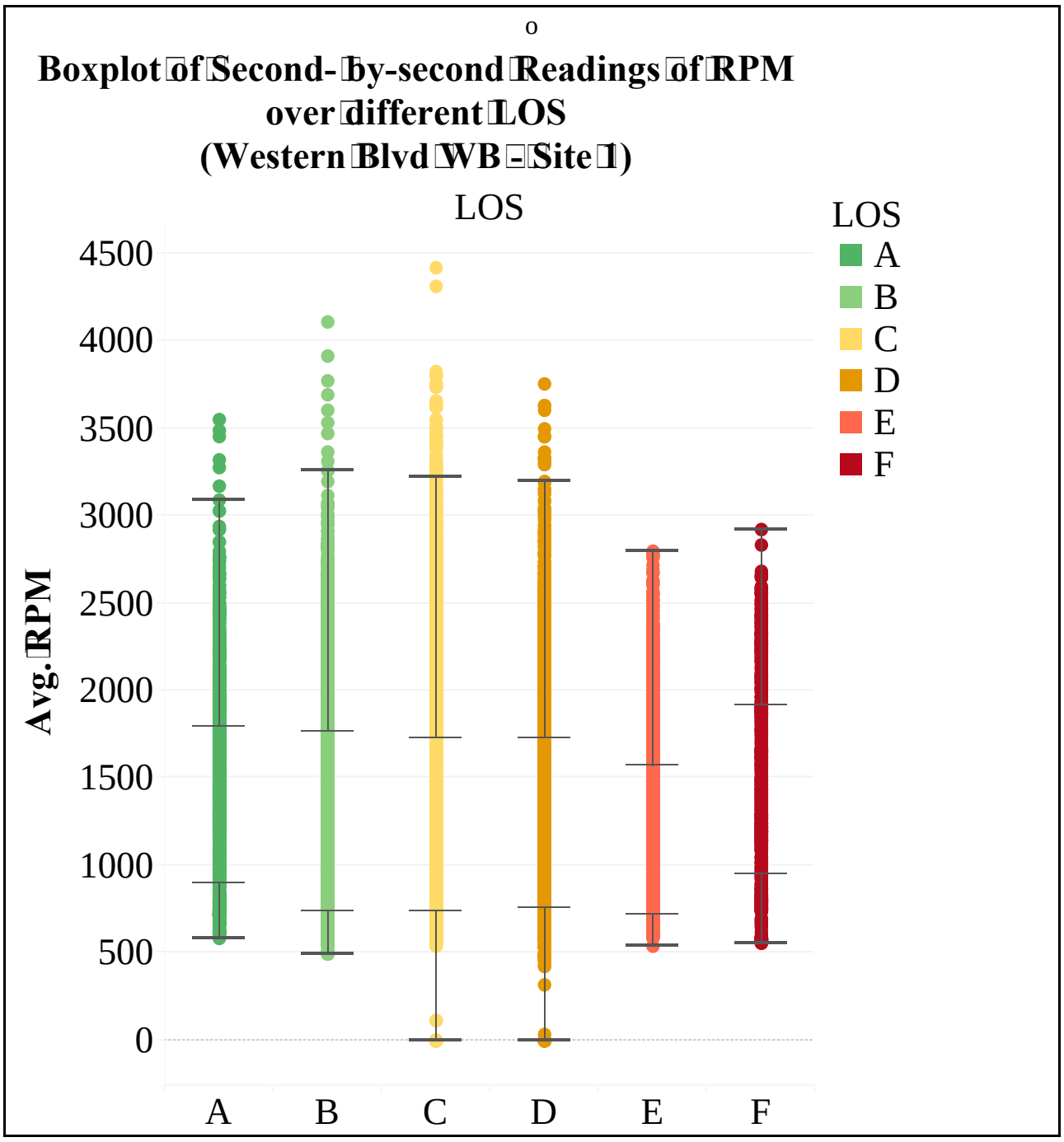

Figure M-1 – Boxplot of Second-by-second Readings of RPM over different LOS (Western Blvd WB – Site 1)

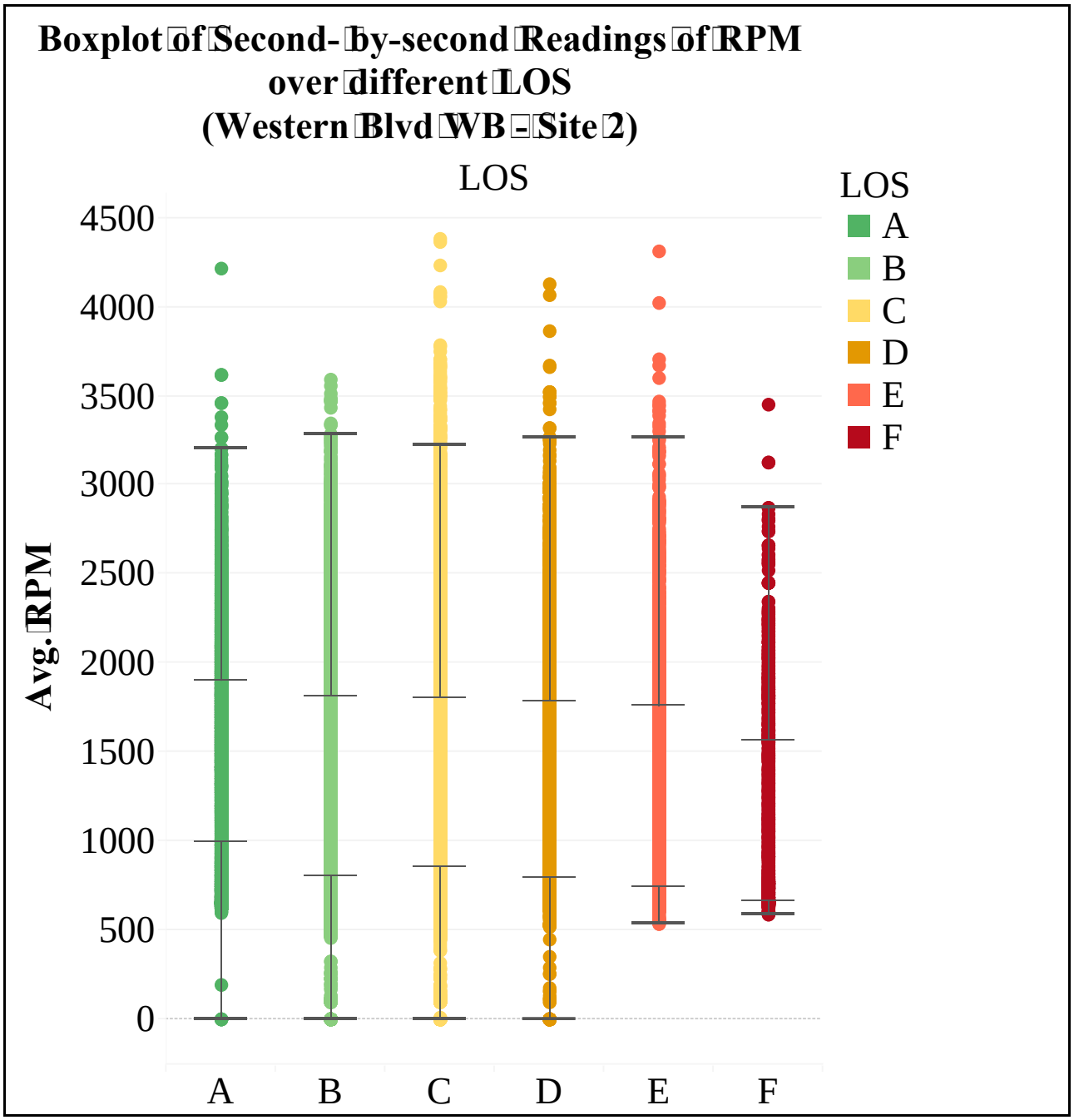

Figure M-2 – Boxplot of Second-by-second Readings of RPM over different LOS (Western Blvd WB – Site 2)

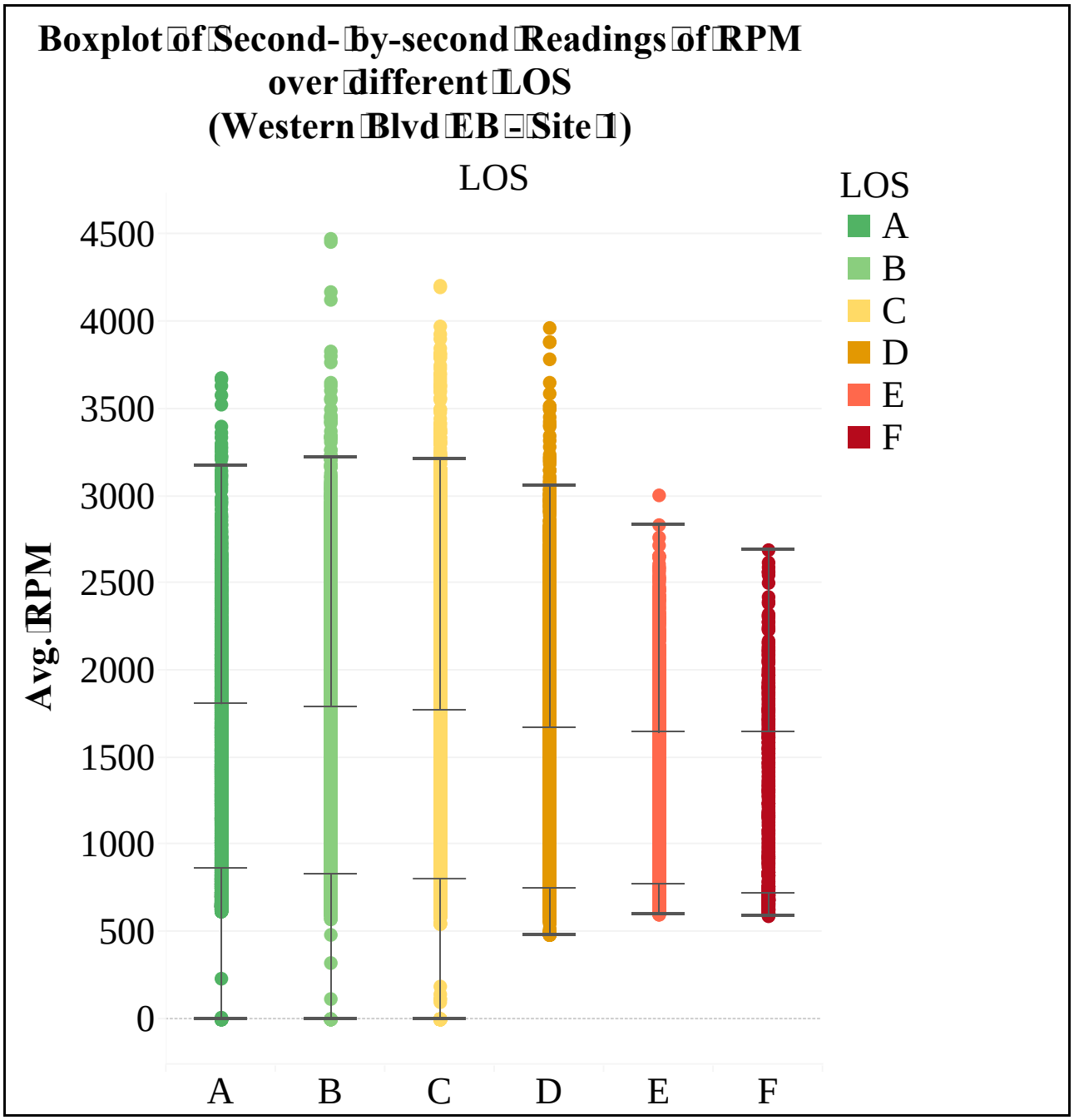

Figure M-3 – Boxplot of Second-by-second Readings of RPM over different LOS (Western Blvd EB – Site 1)

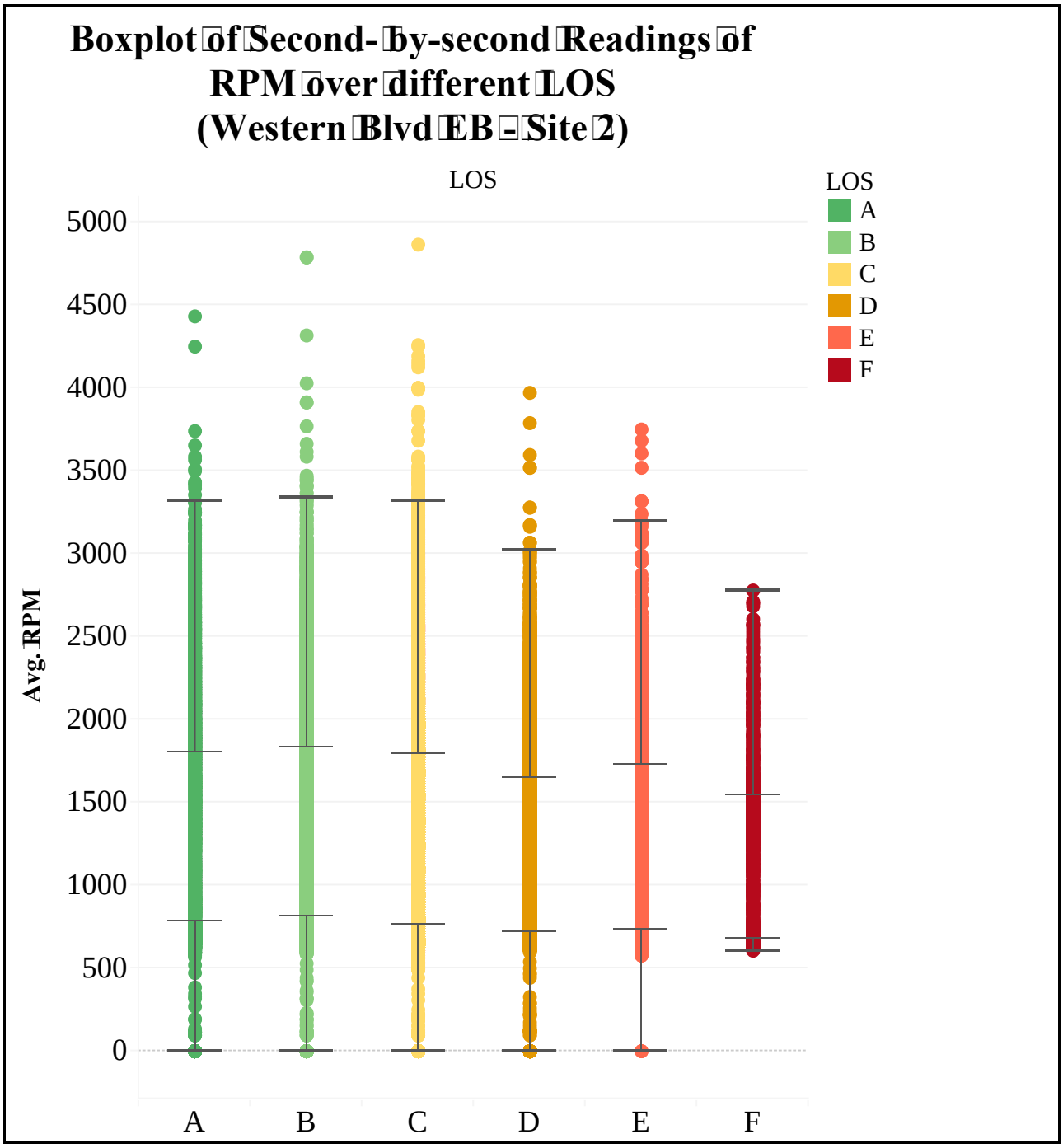

Figure M-4 – Boxplot of Second-by-second Readings of RPM over different LOS (Western Blvd EB – Site 2)

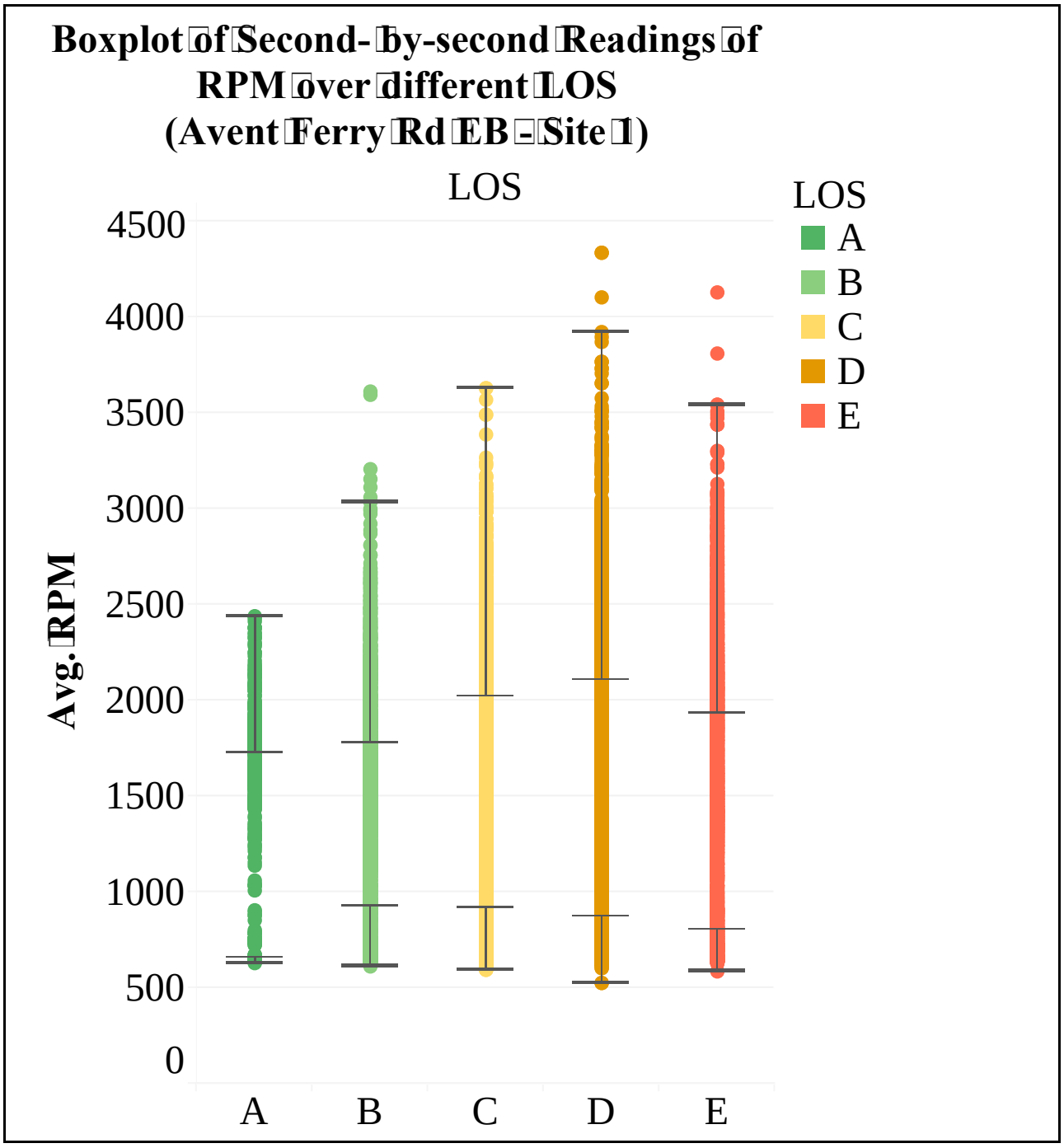

Figure M-5 – Boxplot of Second-by-second Readings of RPM over different LOS (Avent Ferry Rd EB – Site 1)

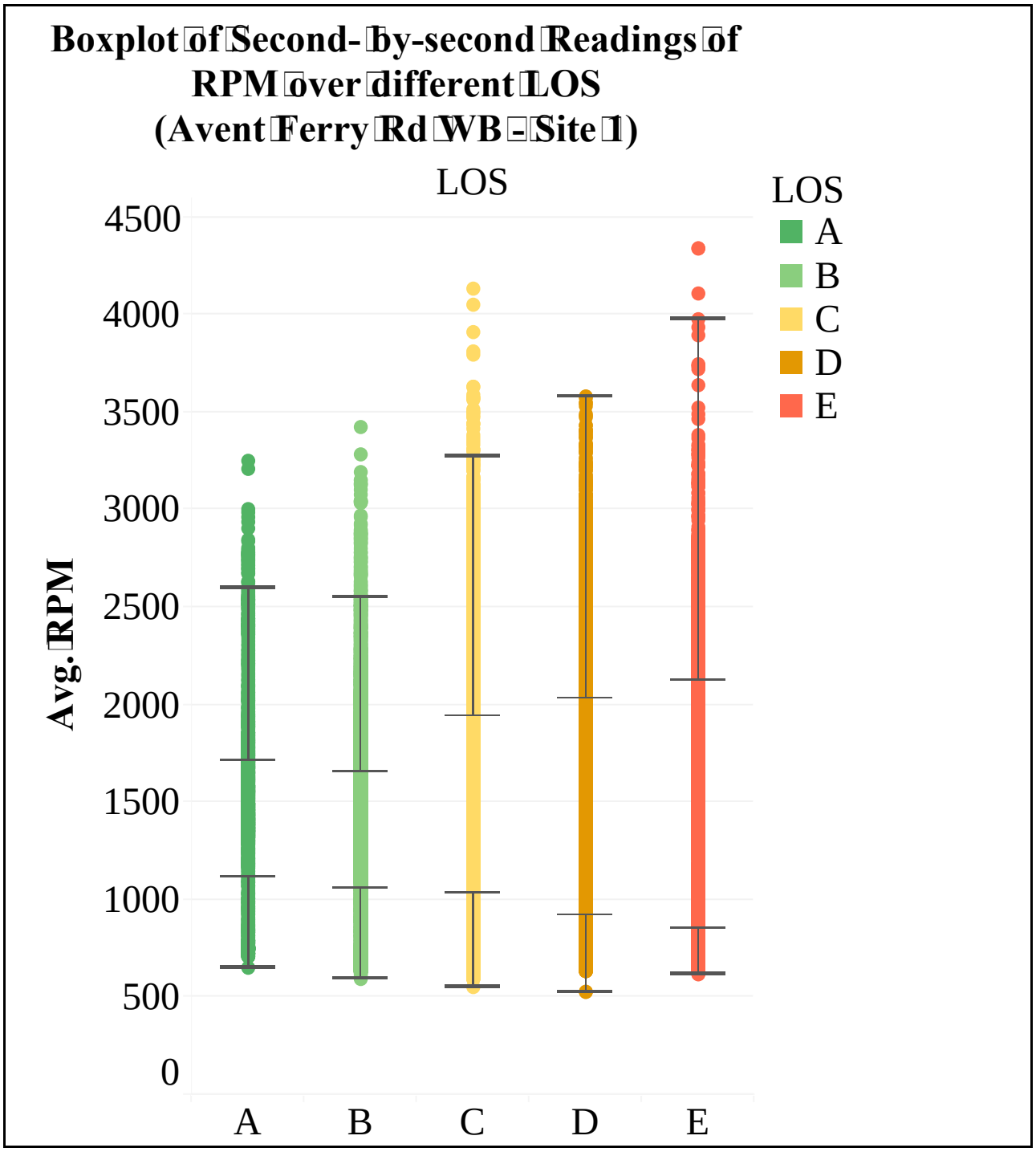

Figure M-6 – Boxplot of Second-by-second Readings of RPM over different LOS (Avent Ferry Rd WB – Site 1)

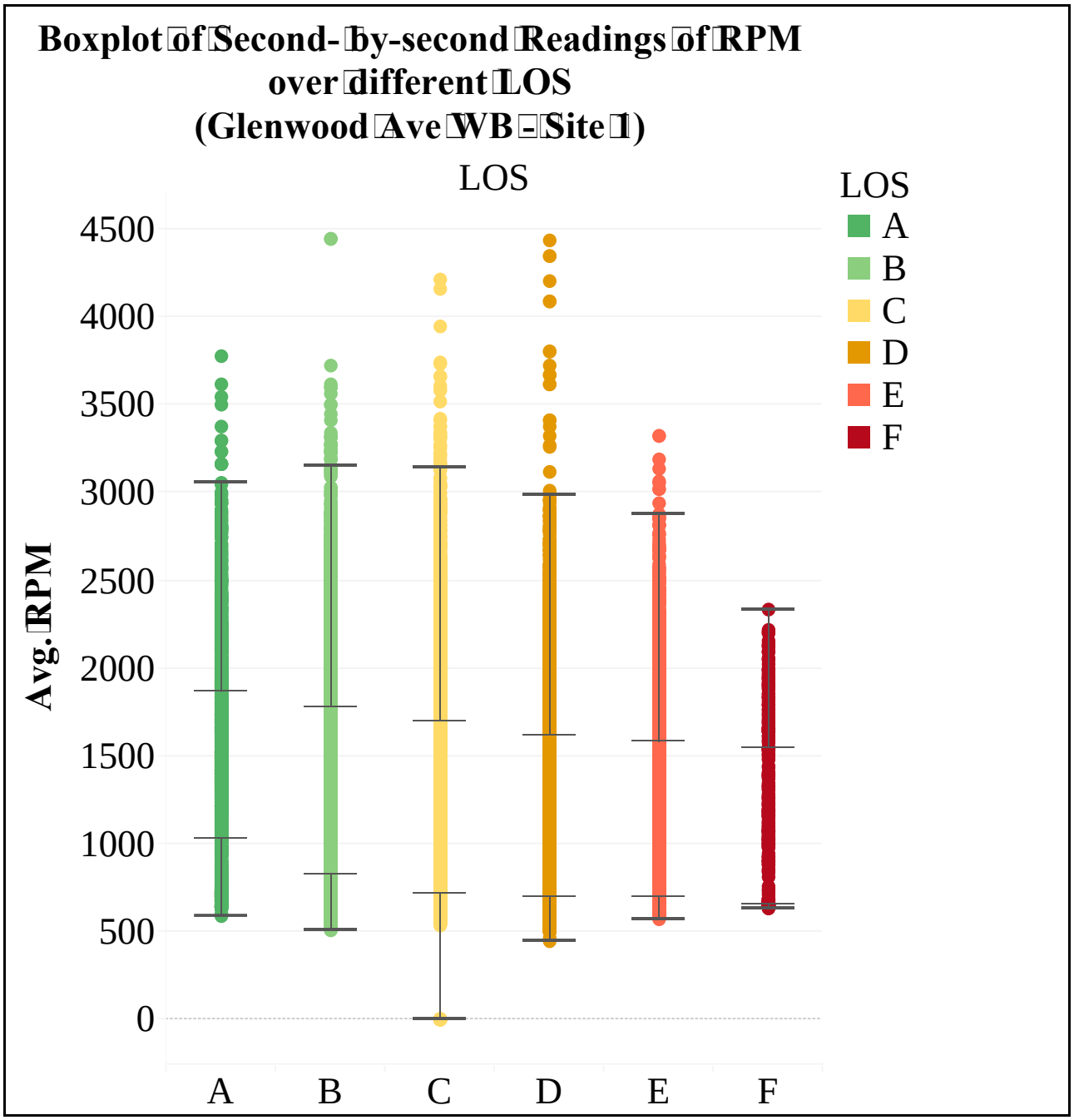

Figure M-7 – Boxplot of Second-by-second Readings of RPM over different LOS (Glenwood Ave WB – Site 1)

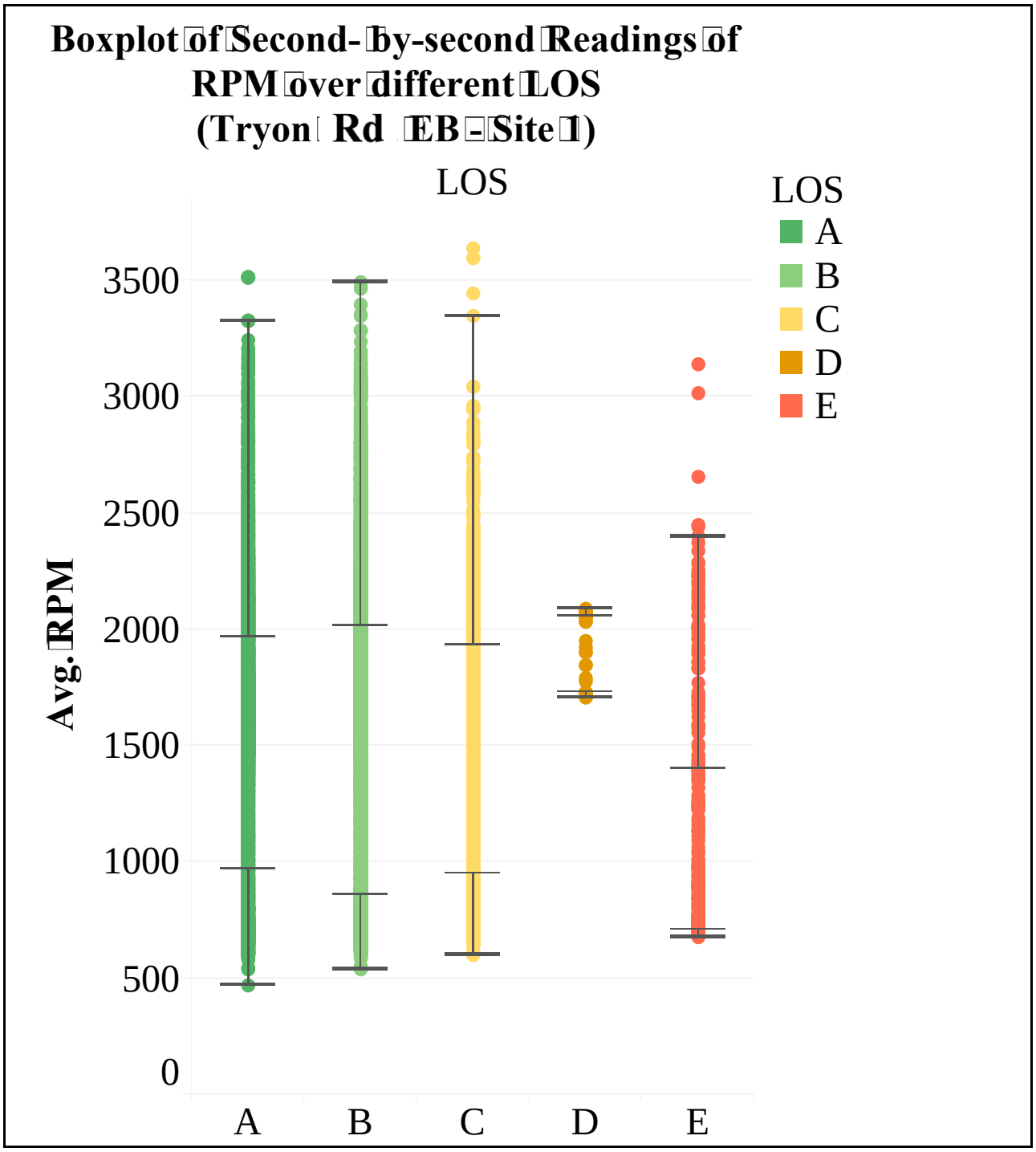

Figure M-8 – Boxplot of Second-by-second Readings of RPM over different LOS (Tryon Rd EB – Site 1)

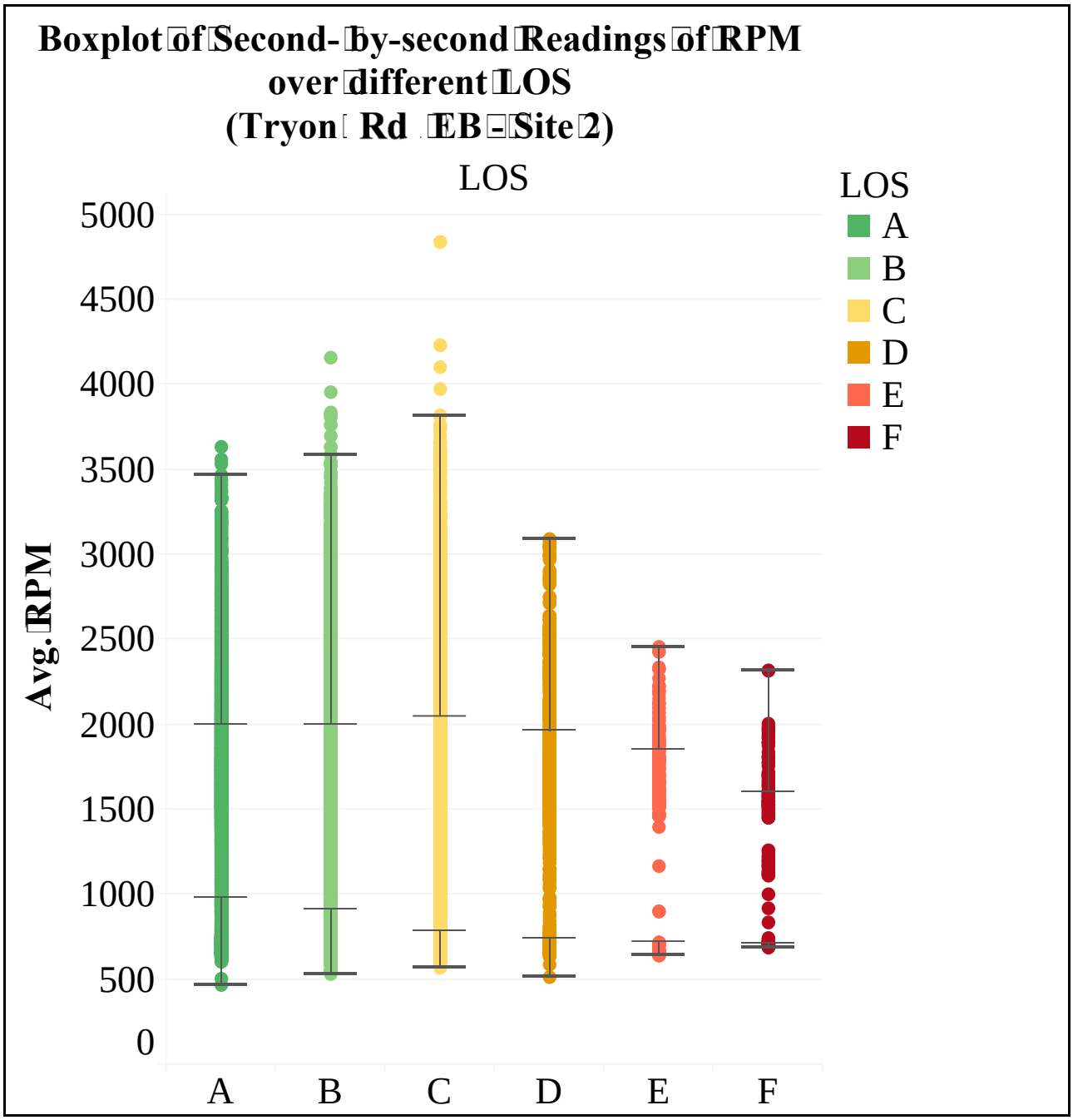

Figure M-9 – Boxplot of Second-by-second Readings of RPM over different LOS (Tryon Rd EB – Site 2)

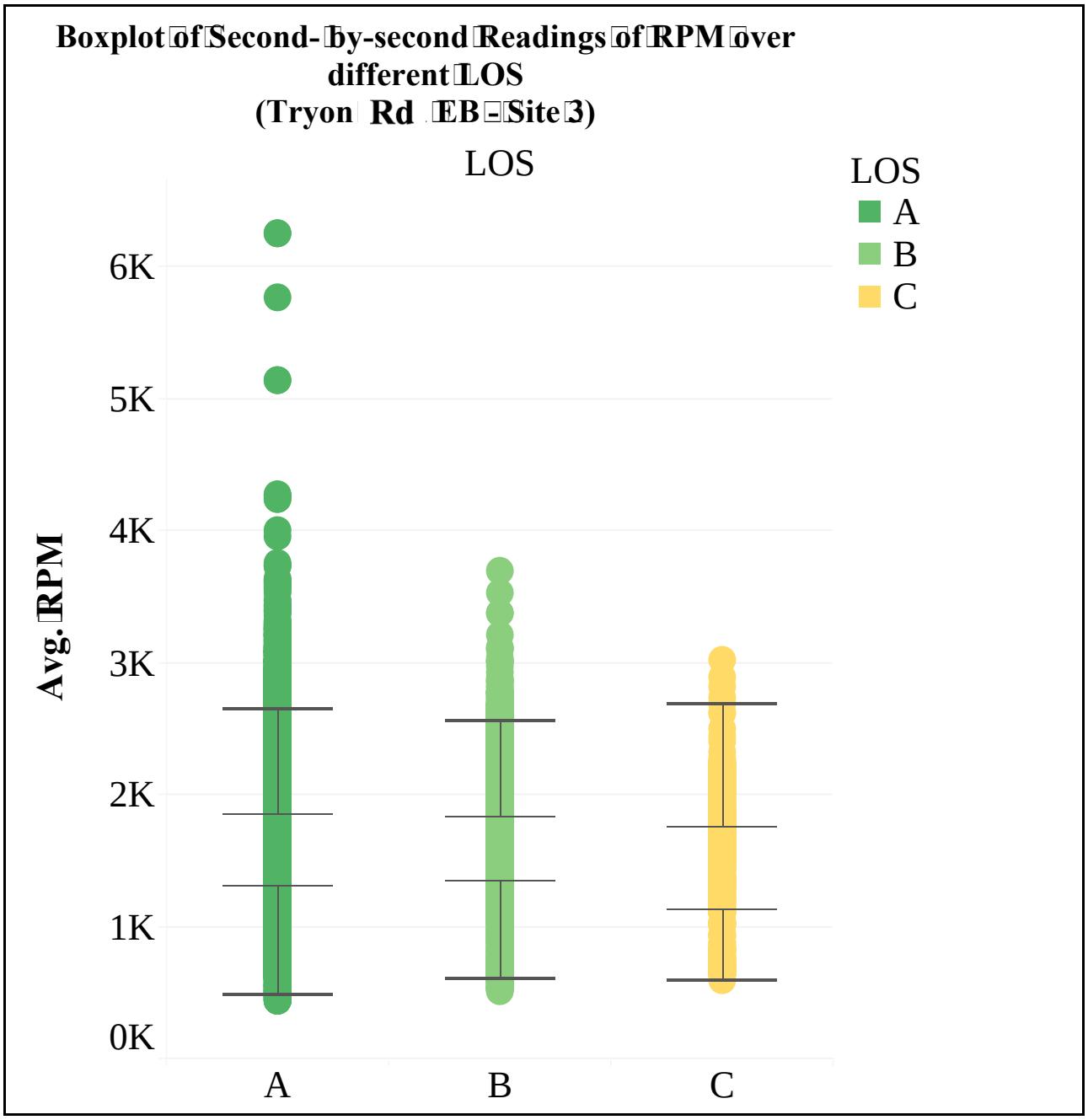

Figure M-10 – Boxplot of Second-by-second Readings of RPM over different LOS (Tryon Rd EB – Site 3)

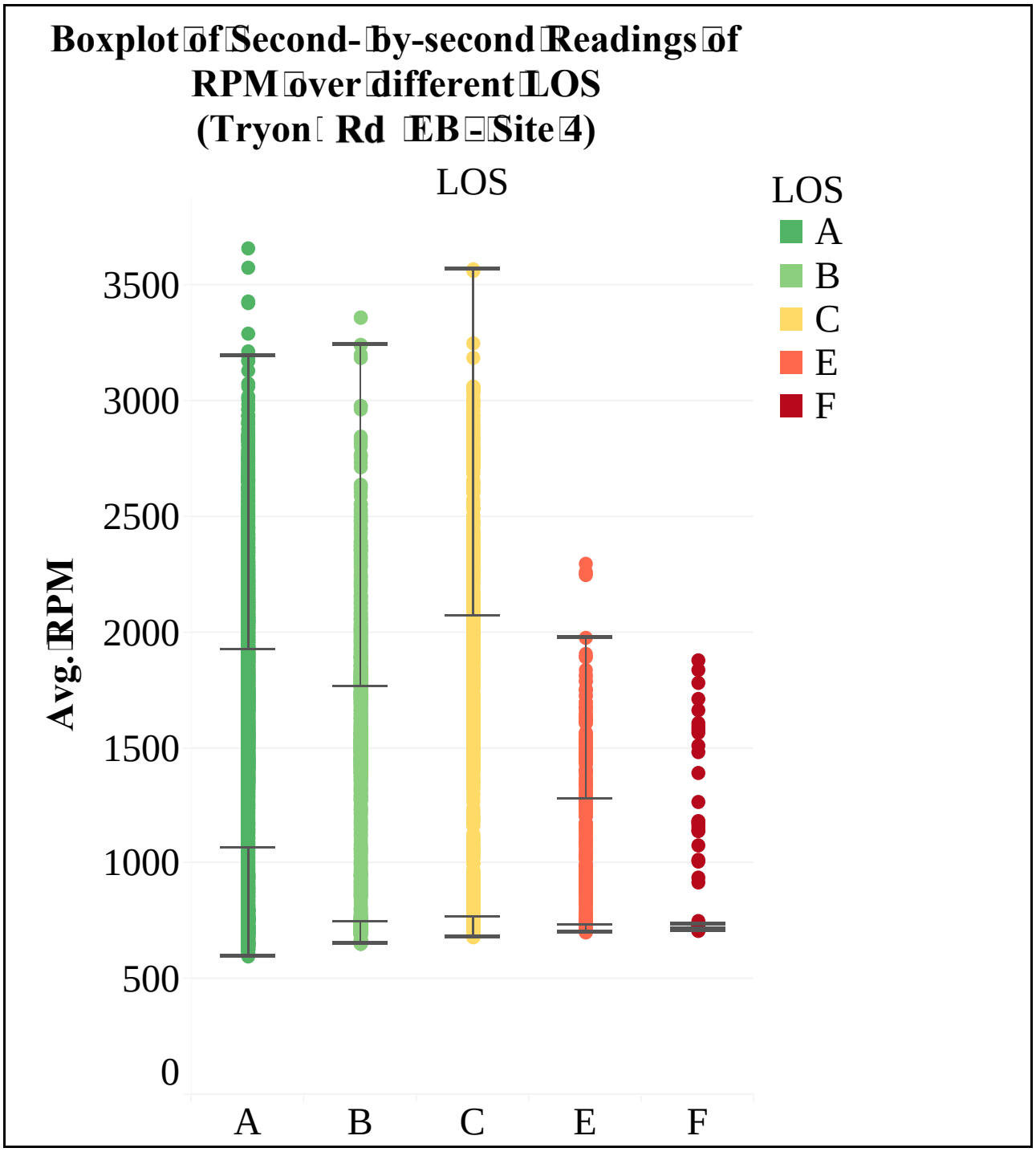

Figure M-11 – Boxplot of Second-by-second Readings of RPM over different LOS (Tryon Rd EB – Site 4)

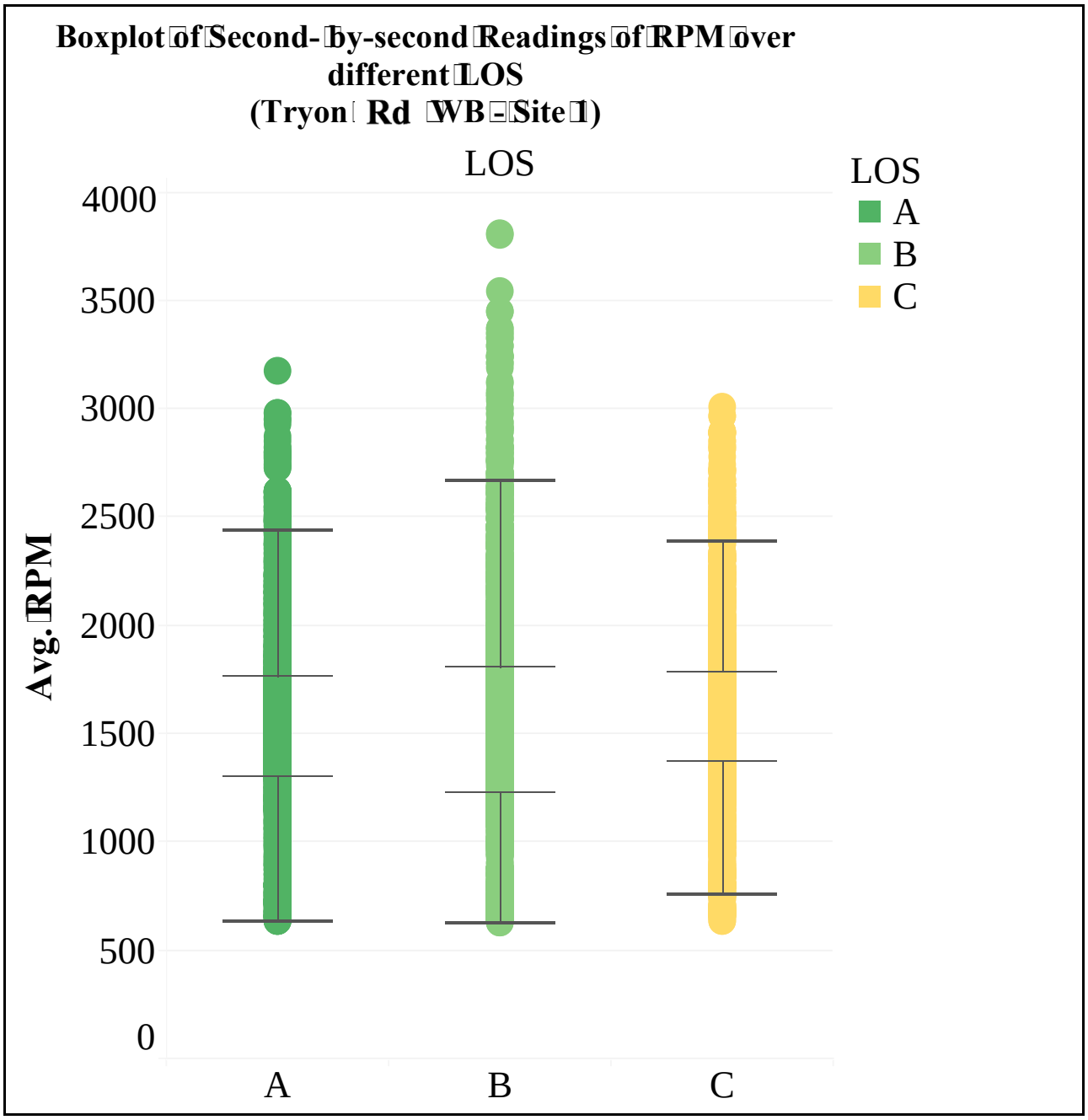

Figure M-12 – Boxplot of Second-by-second Readings of RPM over different LOS (Tryon Rd WB – Site 1)

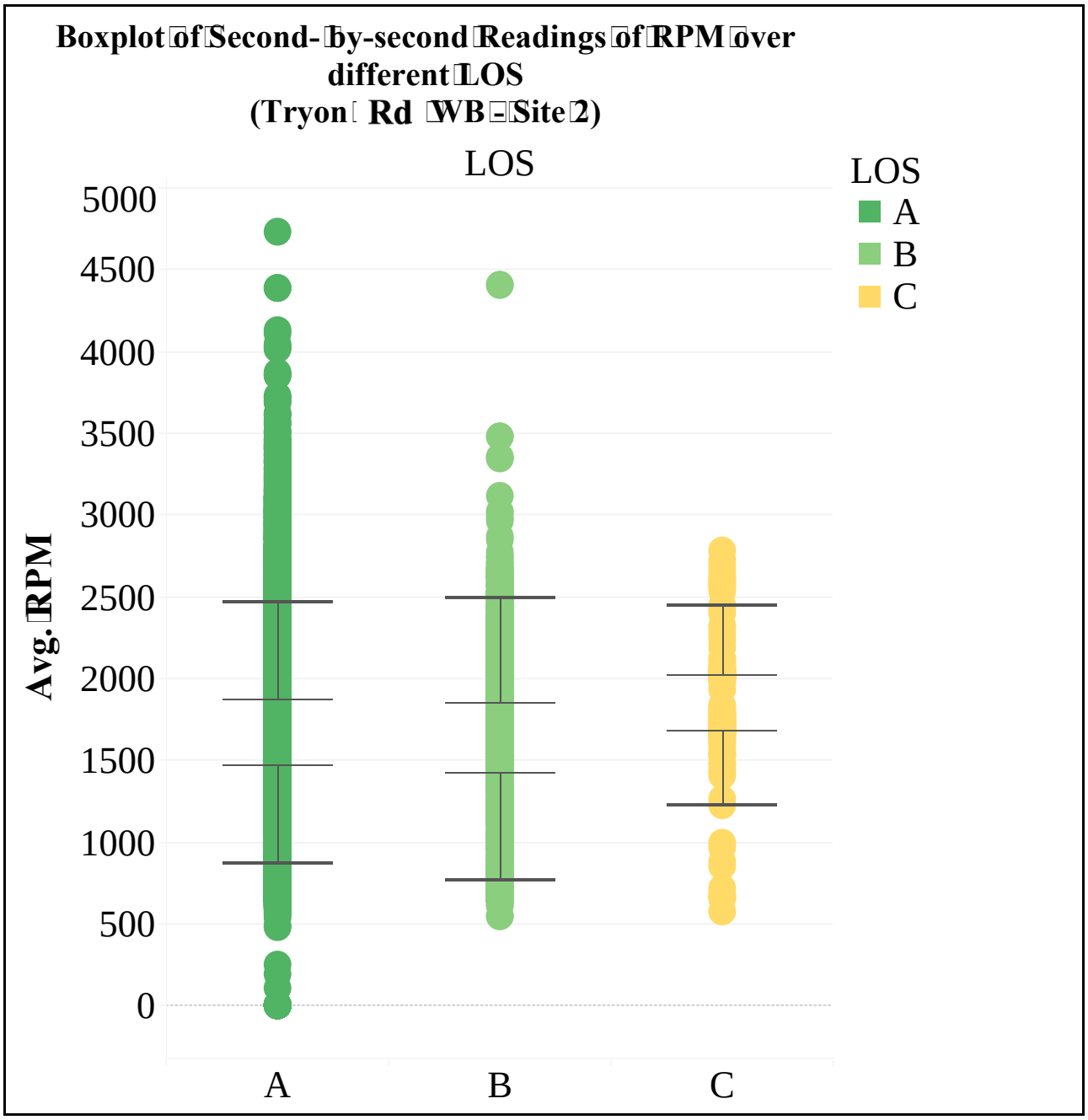

Figure M-13 – Boxplot of Second-by-second Readings of RPM over different LOS (Tryon Rd WB – Site 2)

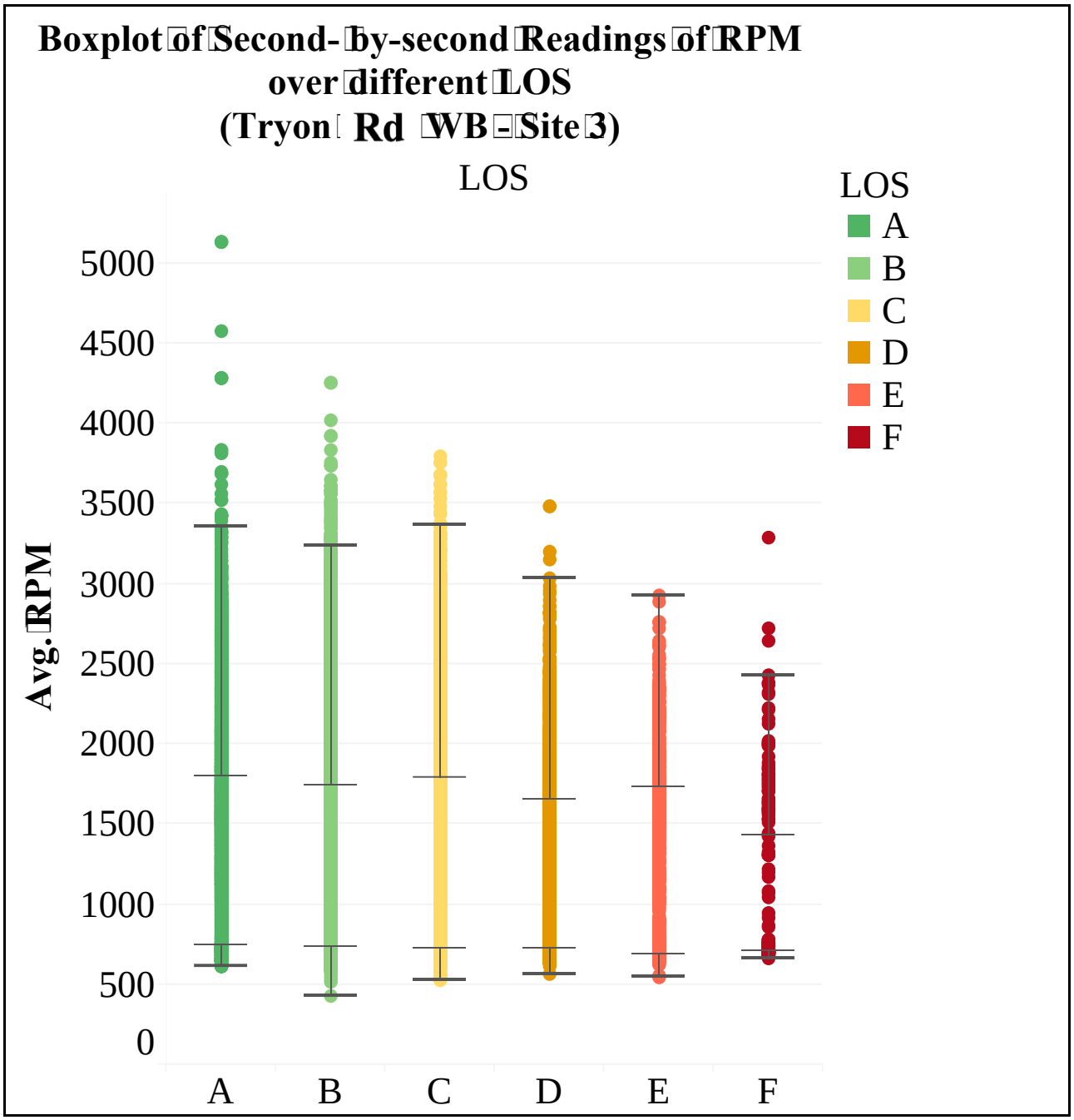

Figure M-14 – Boxplot of Second-by-second Readings of RPM over different LOS (Tryon Rd WB – Site 3)

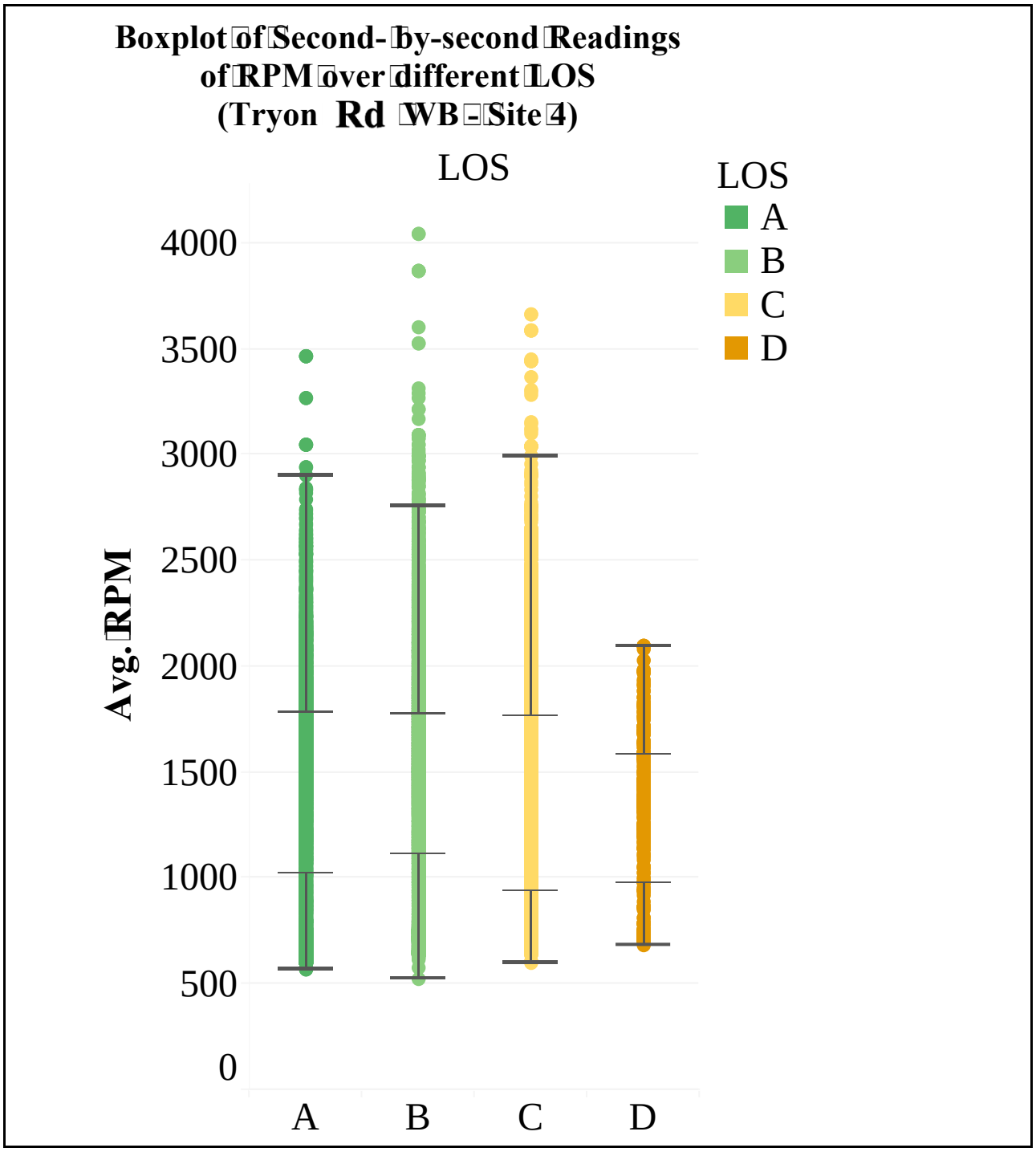

Figure M-15 – Boxplot of Second-by-second Readings of RPM over different LOS (Tryon Rd WB – Site 4)

APPENDIX O - BOXPLOT OF SECOND-BY-SECOND READINGS OF THROTTLE POSITION (%) OVER DIFFERENT LOS

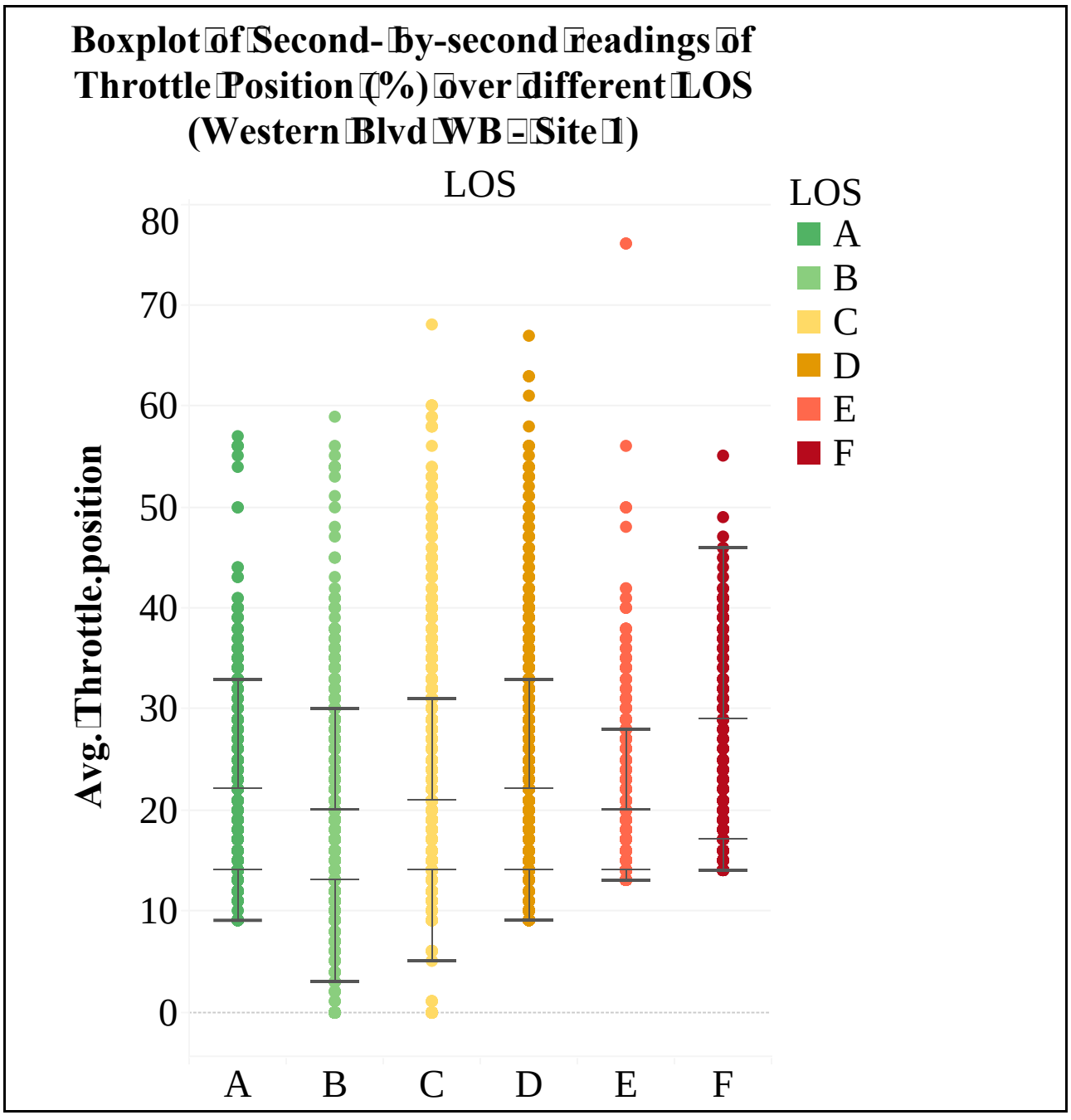

Figure N-1 – Boxplot of Second-by-second readings of Throttle Position (%) over different LOS (Western Blvd WB – Site 1)

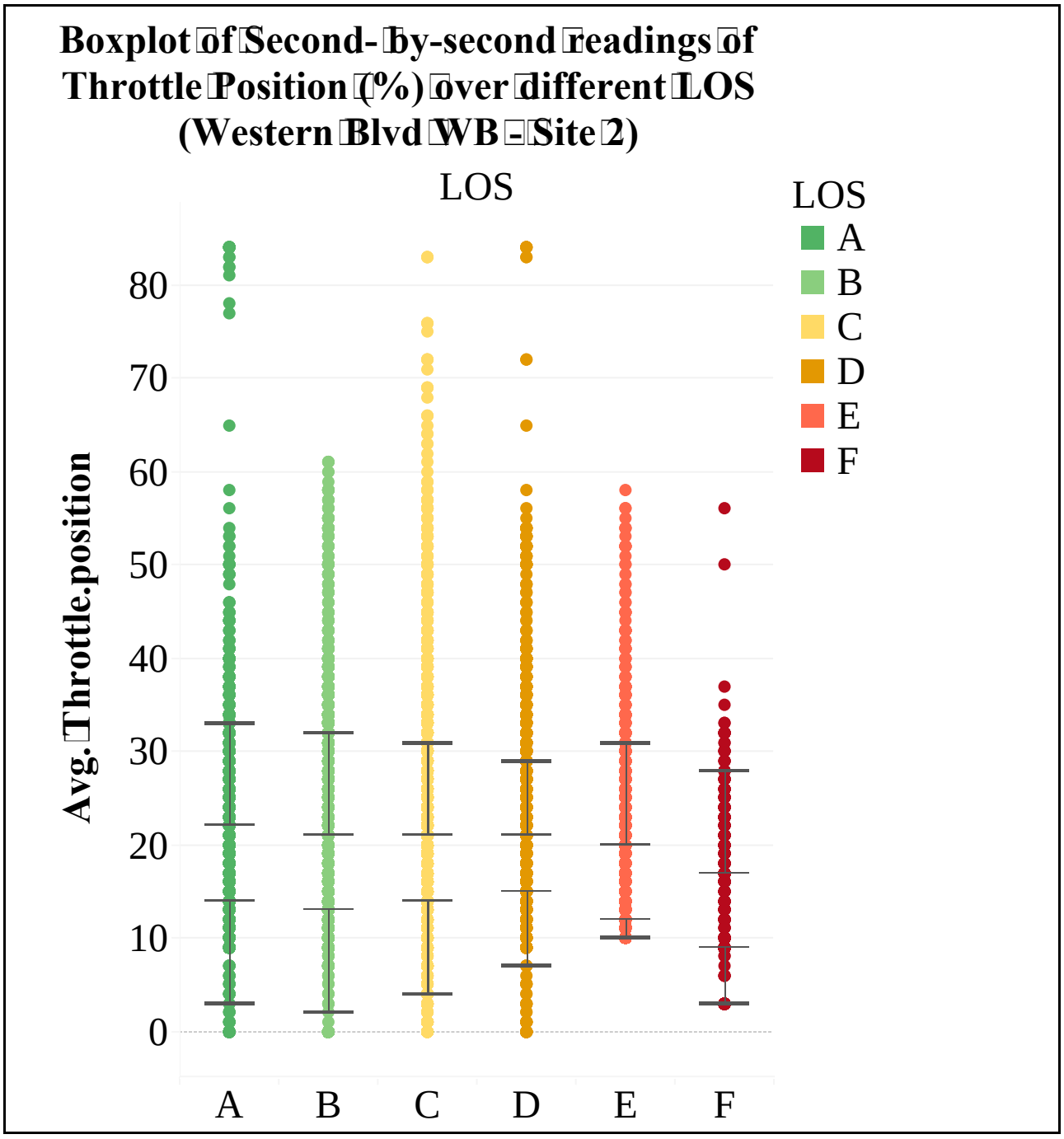

Figure N-2 – Boxplot of Second-by-second readings of Throttle Position (%) over different LOS (Western Blvd WB – Site 2)

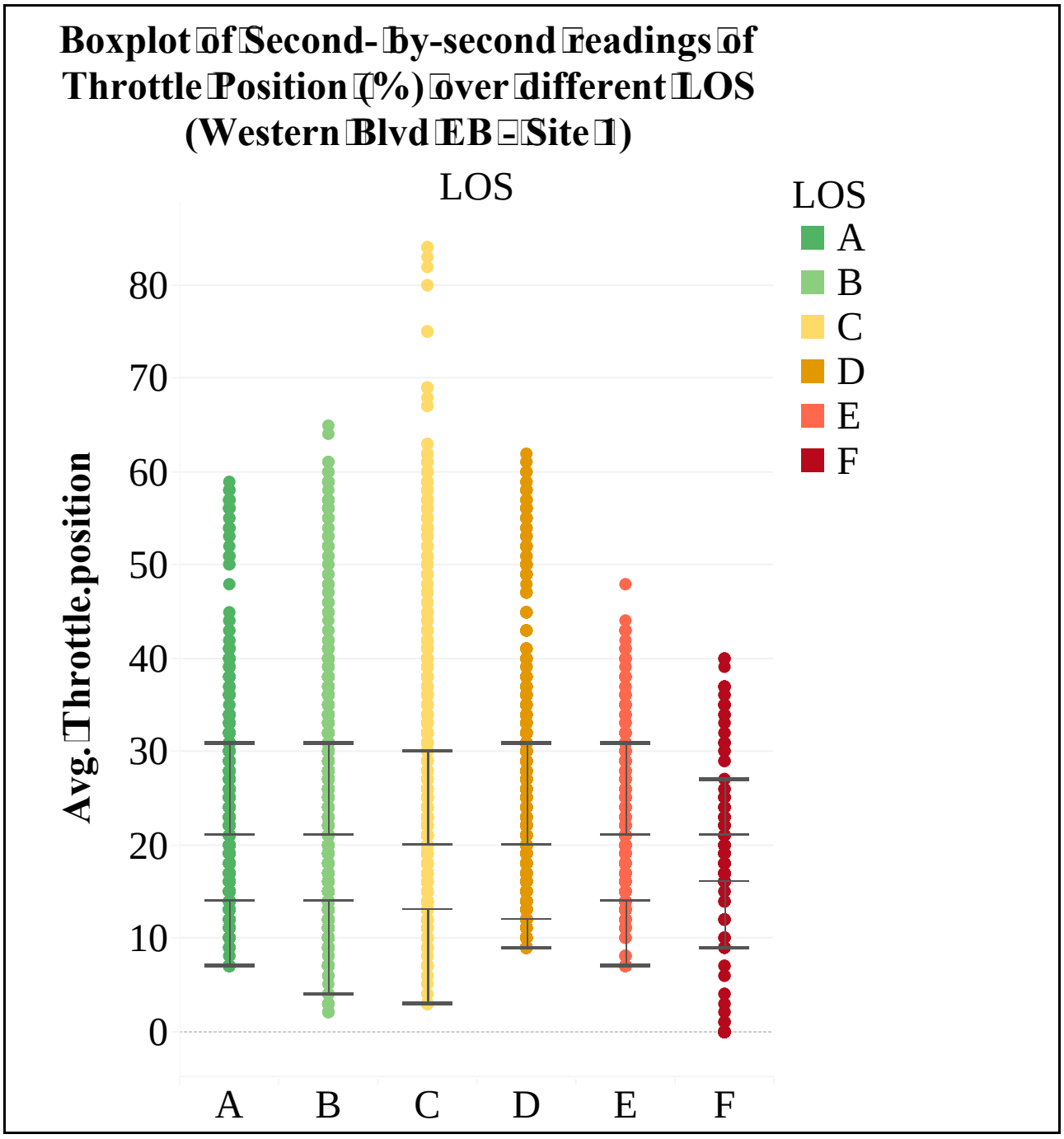

Figure N-3 – Boxplot of Second-by-second readings of Throttle Position (%) over different LOS (Western Blvd EB – Site 1)

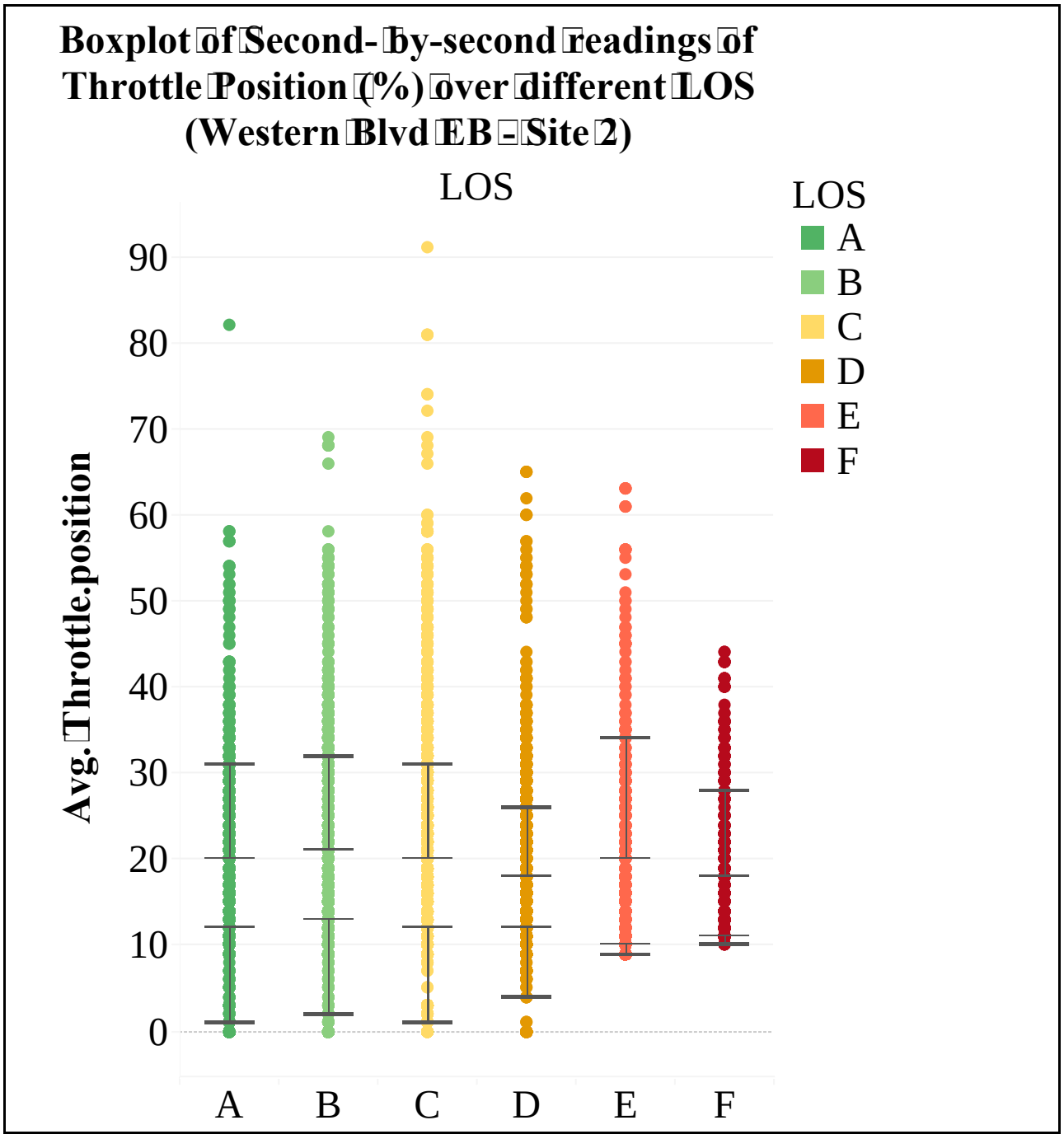

Figure N-4 – Boxplot of Second-by-second readings of Throttle Position (%) over different LOS (Western Blvd EB – Site 2)

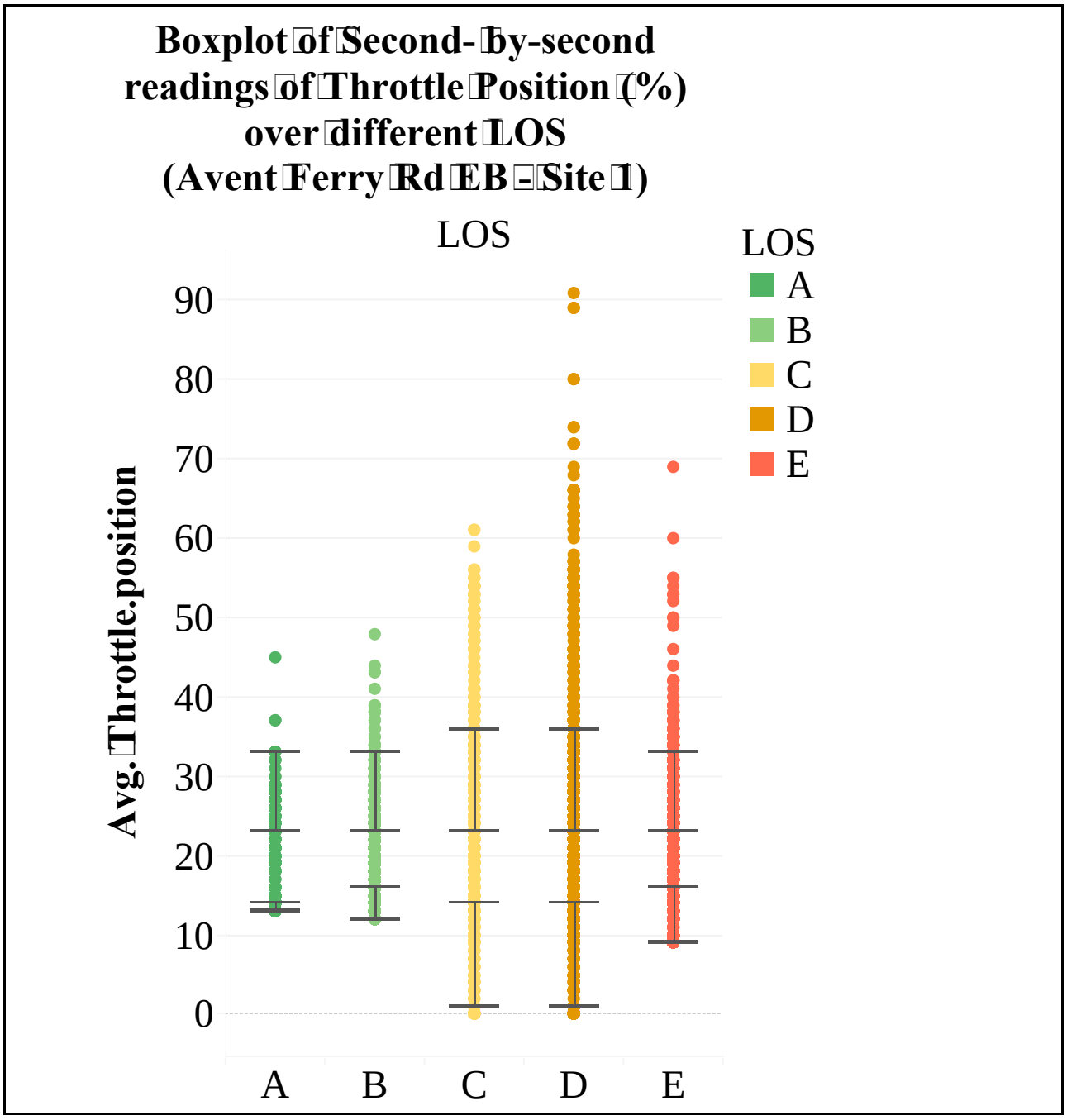

Figure N-5 – Boxplot of Second-by-second readings of Throttle Position (%) over different LOS (Avent Ferry Rd EB – Site 1)

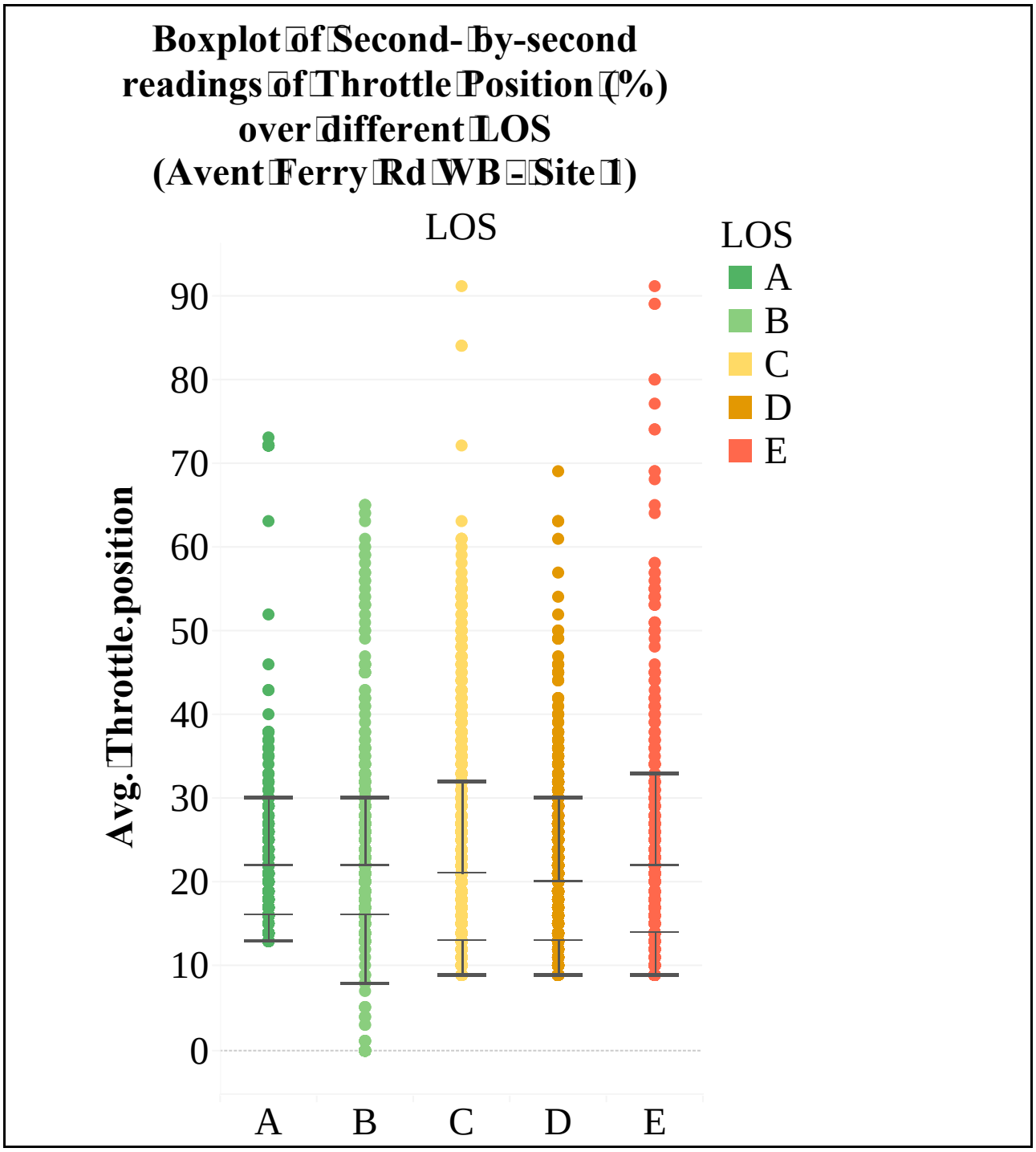

Figure N-6 – Boxplot of Second-by-second readings of Throttle Position (%) over different LOS (Avent Ferry Rd WB – Site 1)

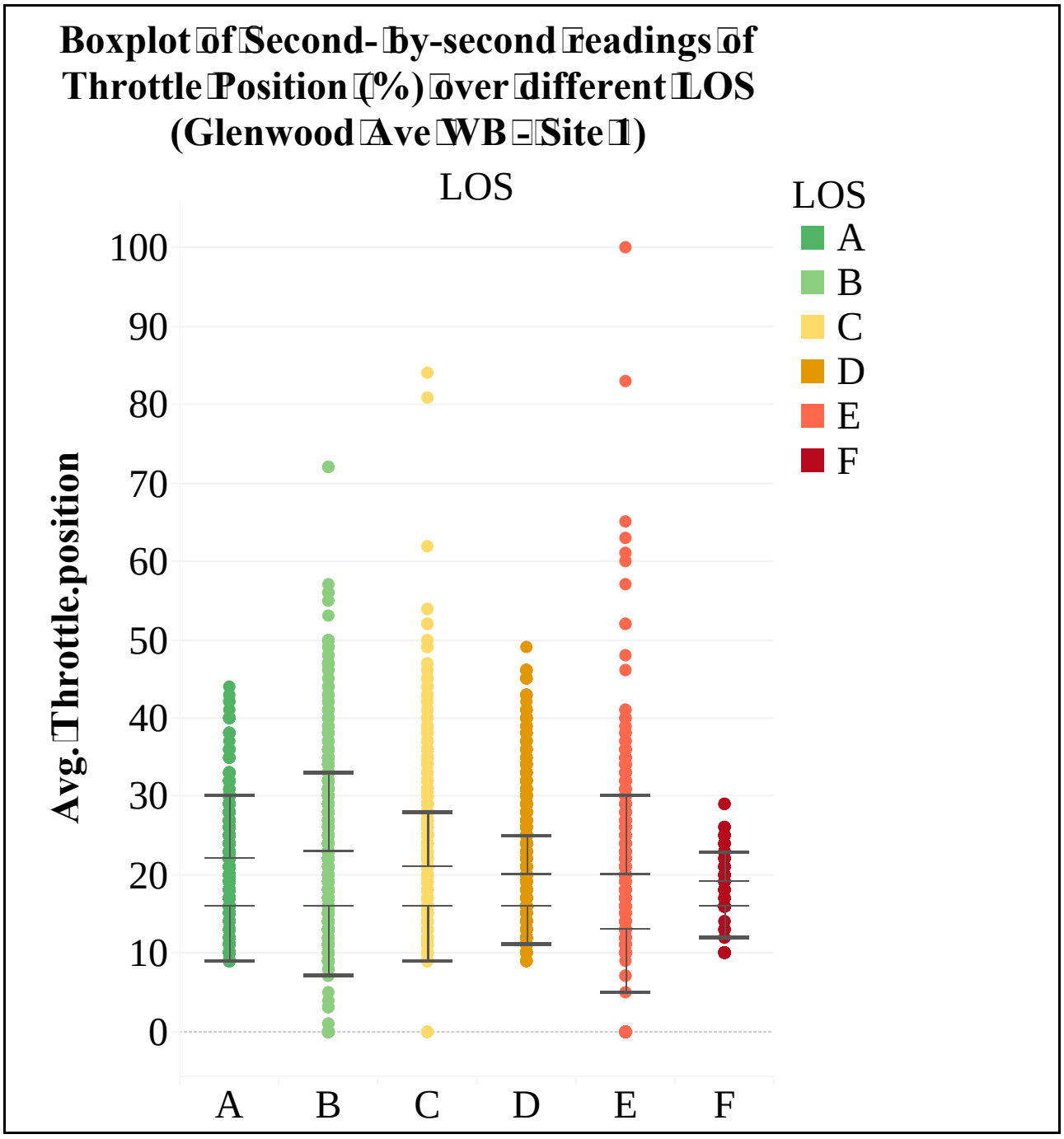

Figure N-7 – Boxplot of Second-by-second readings of Throttle Position (%) over different LOS (Glenwood Ave WB – Site 1)

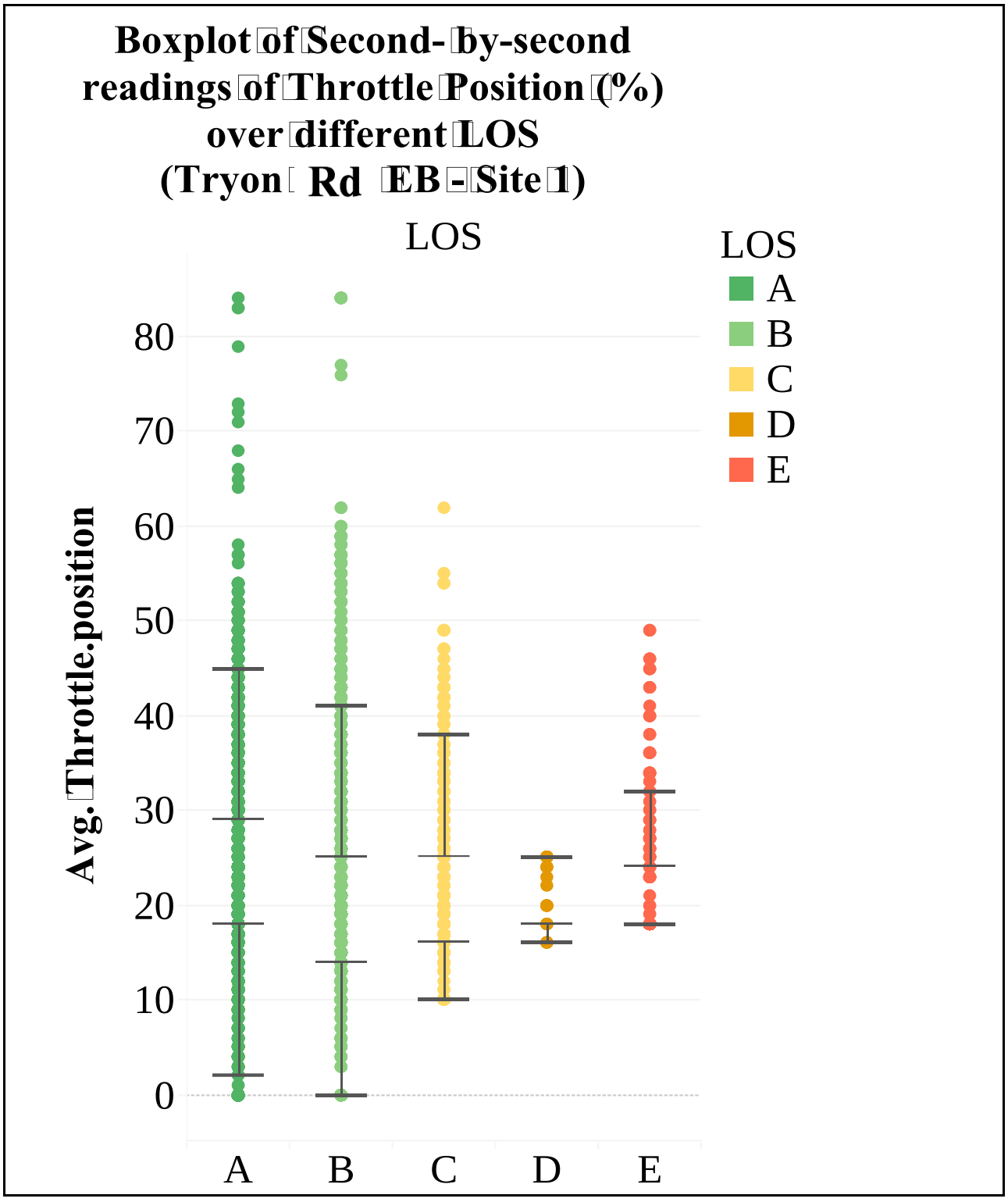

Figure N-8 – Boxplot of Second-by-second readings of Throttle Position (%) over different LOS (Tryon Rd EB – Site 1)

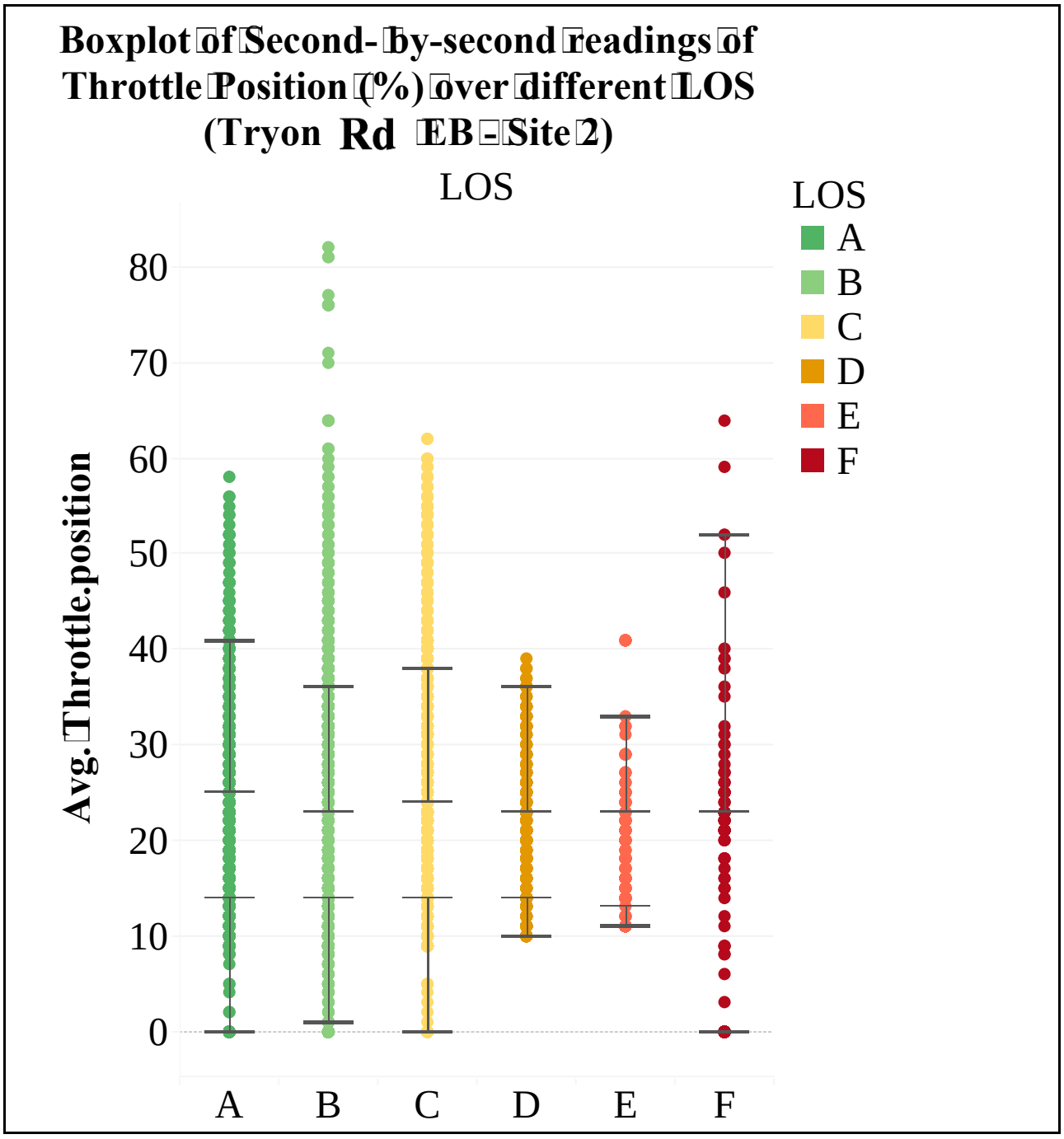

Figure N-9 – Boxplot of Second-by-second readings of Throttle Position (%) over different LOS (Tryon Rd EB – Site 2)

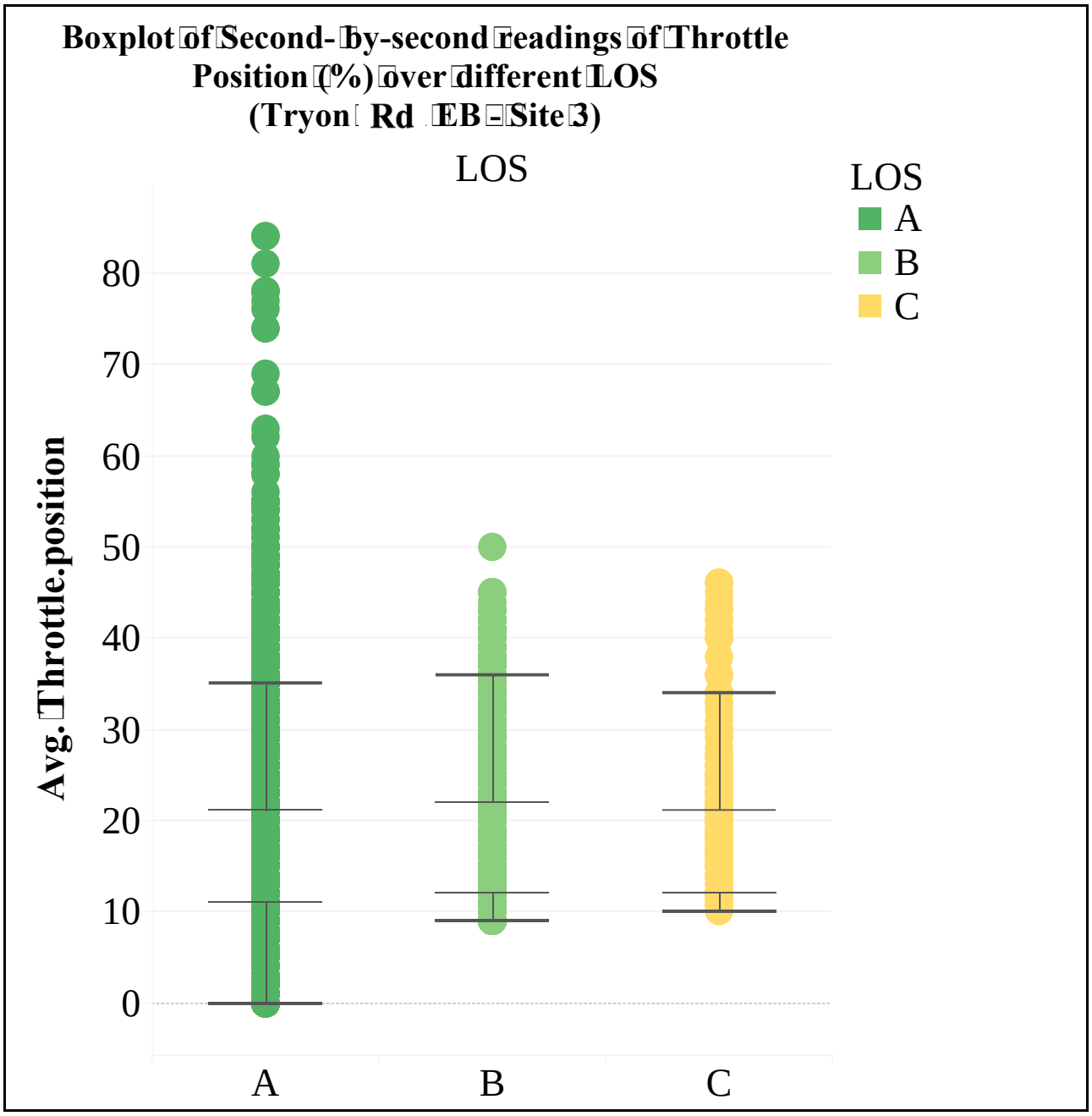

Figure N-10 – Boxplot of Second-by-second readings of Throttle Position (%) over different LOS (Tryon Rd EB – Site 3)

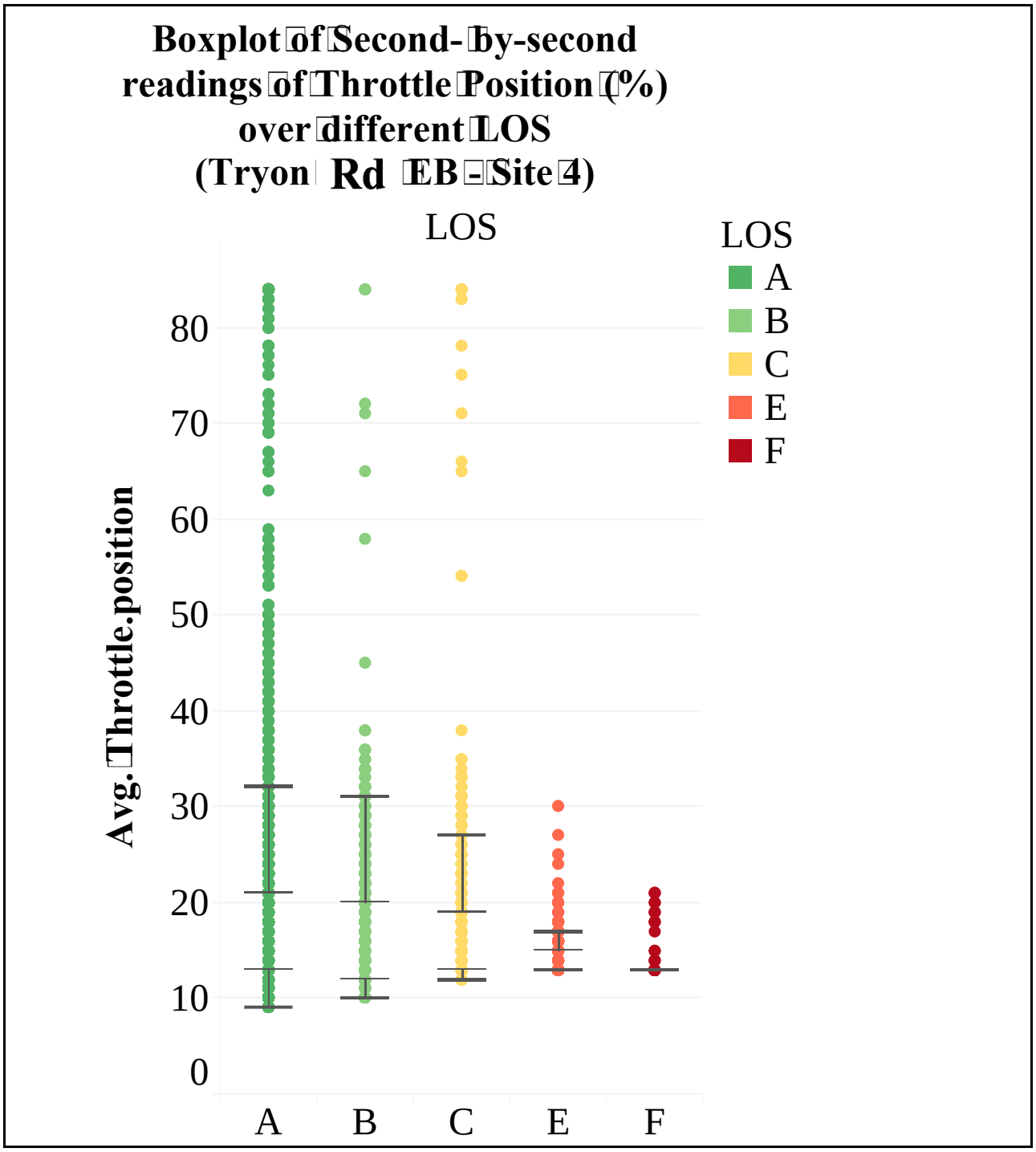

Figure N-11 – Boxplot of Second-by-second readings of Throttle Position (%) over different LOS (Tryon Rd EB – Site 4)

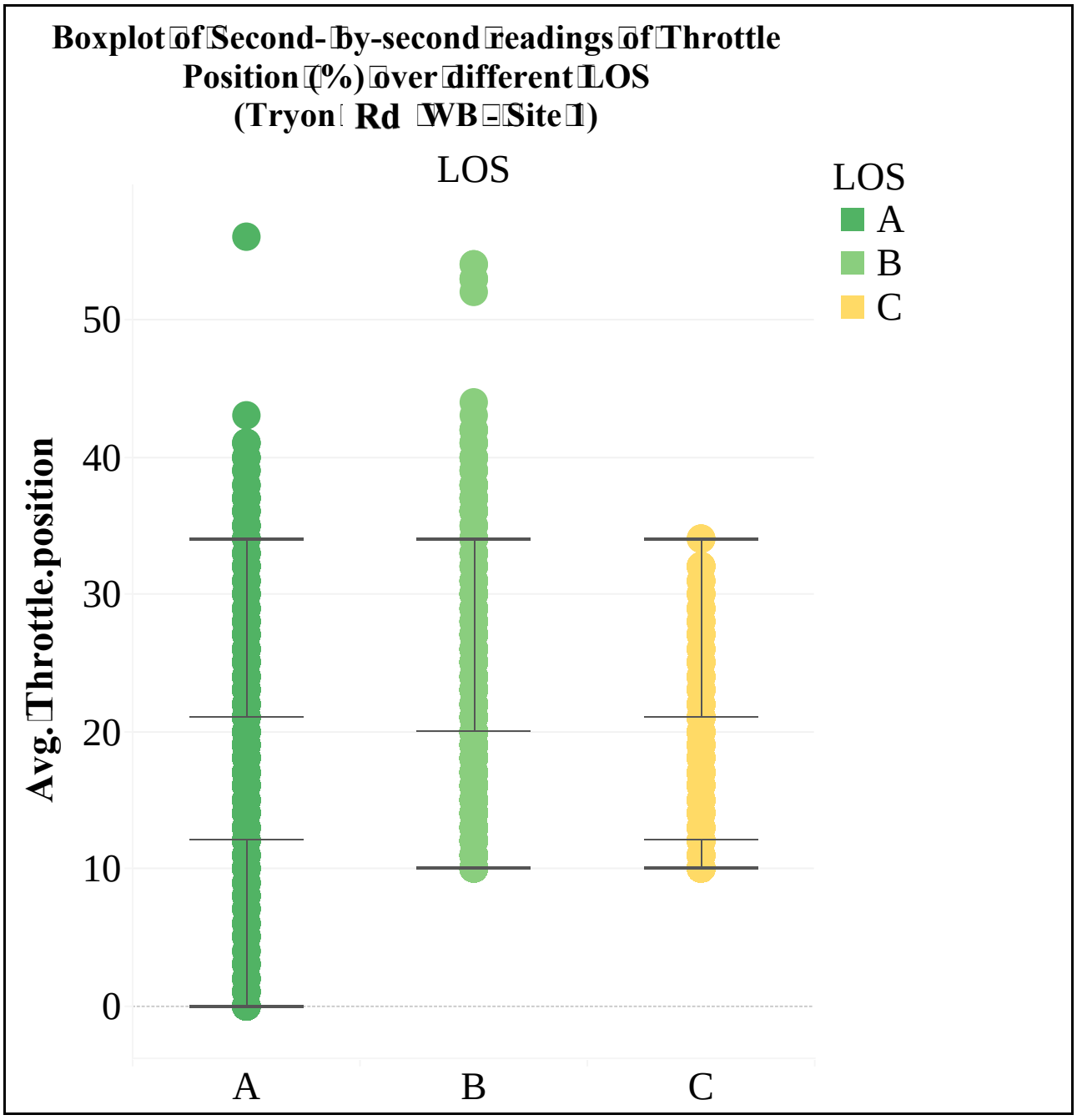

Figure N-12 – Boxplot of Second-by-second readings of Throttle Position (%) over different LOS (Tryon Rd WB – Site 1)

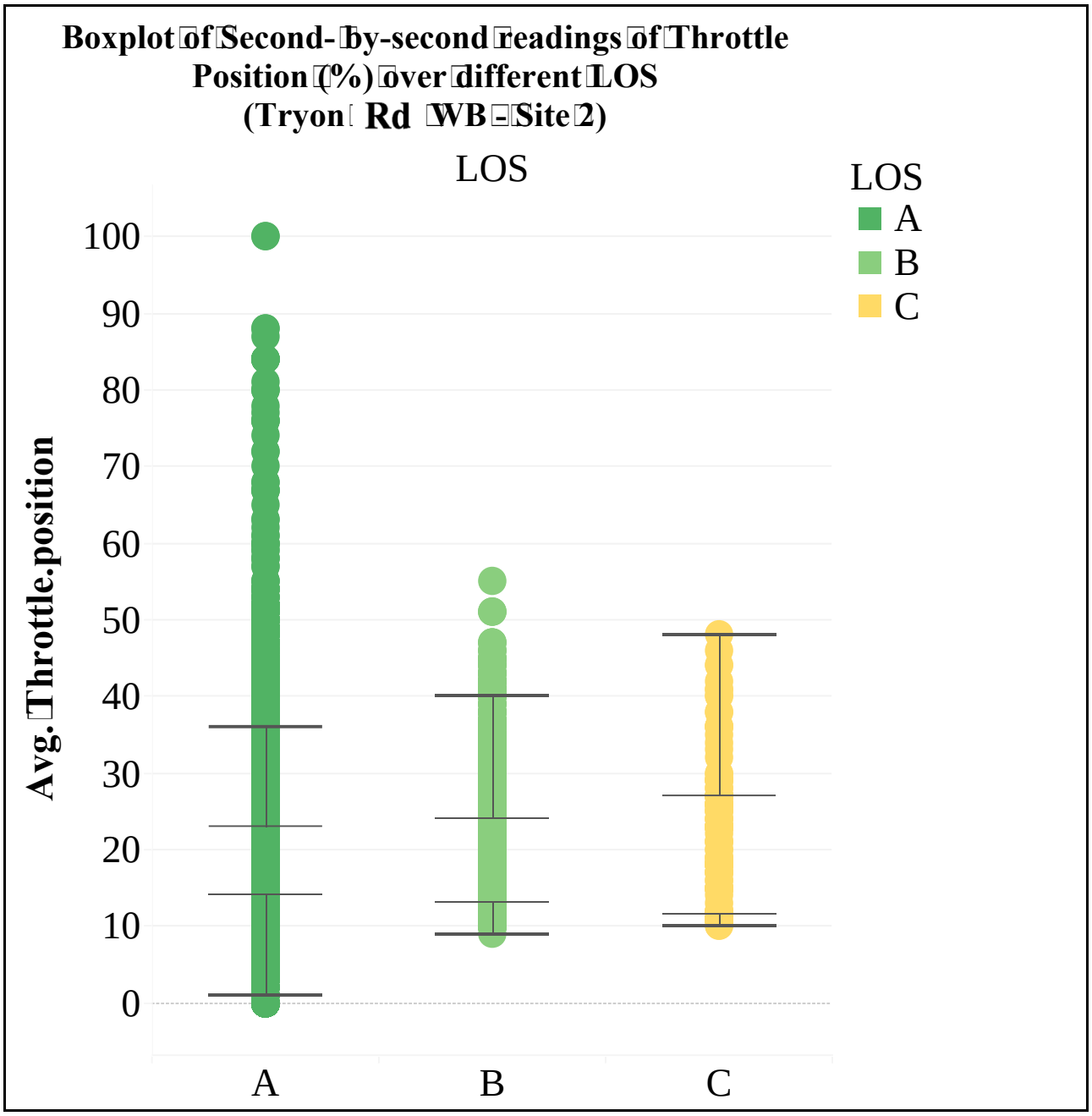

Figure N-13 – Boxplot of Second-by-second readings of Throttle Position (%) over different LOS (Tryon Rd WB – Site 2)

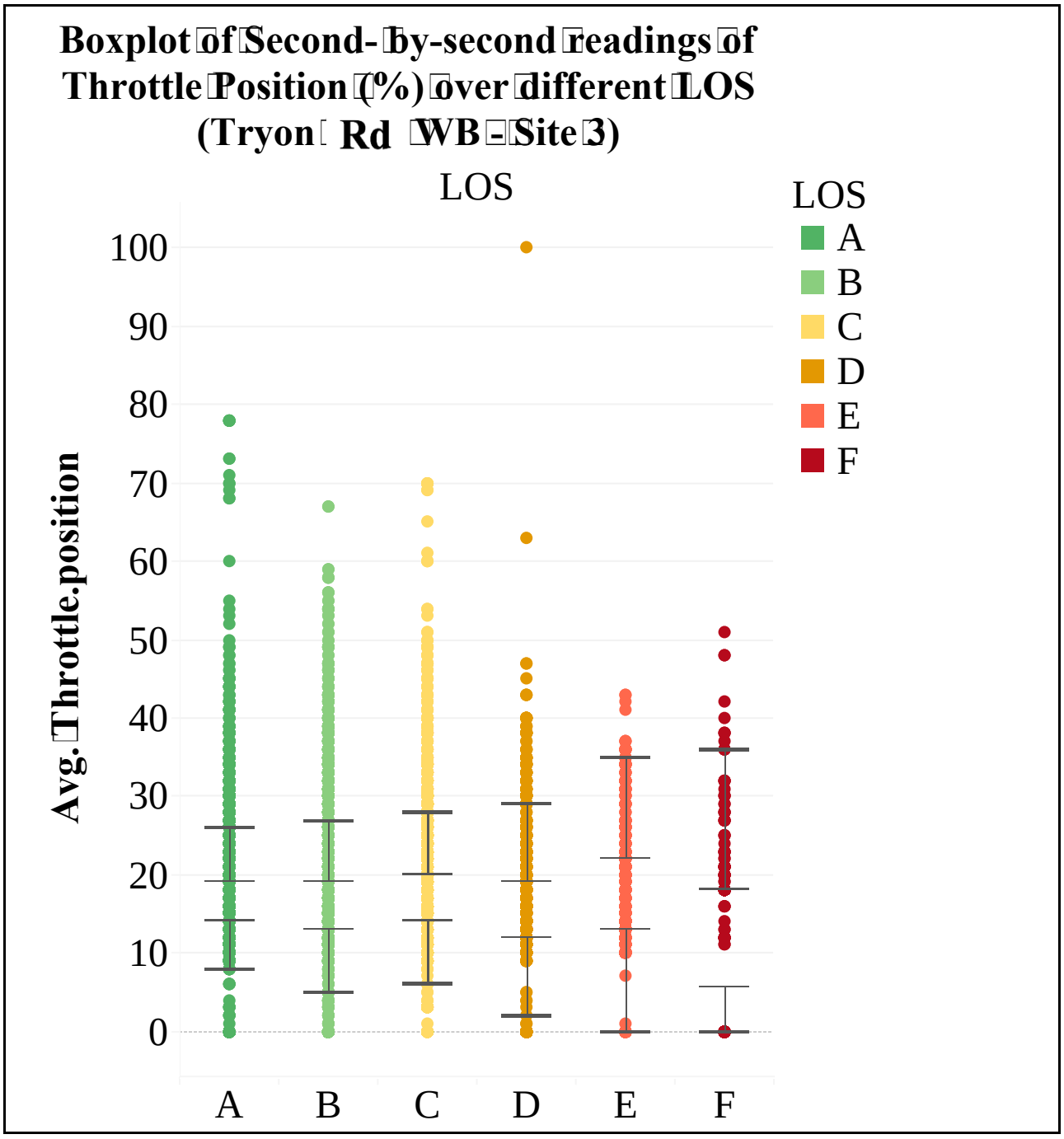

Figure N-14 – Boxplot of Second-by-second readings of Throttle Position (%) over different LOS (Tryon Rd WB – Site 3)

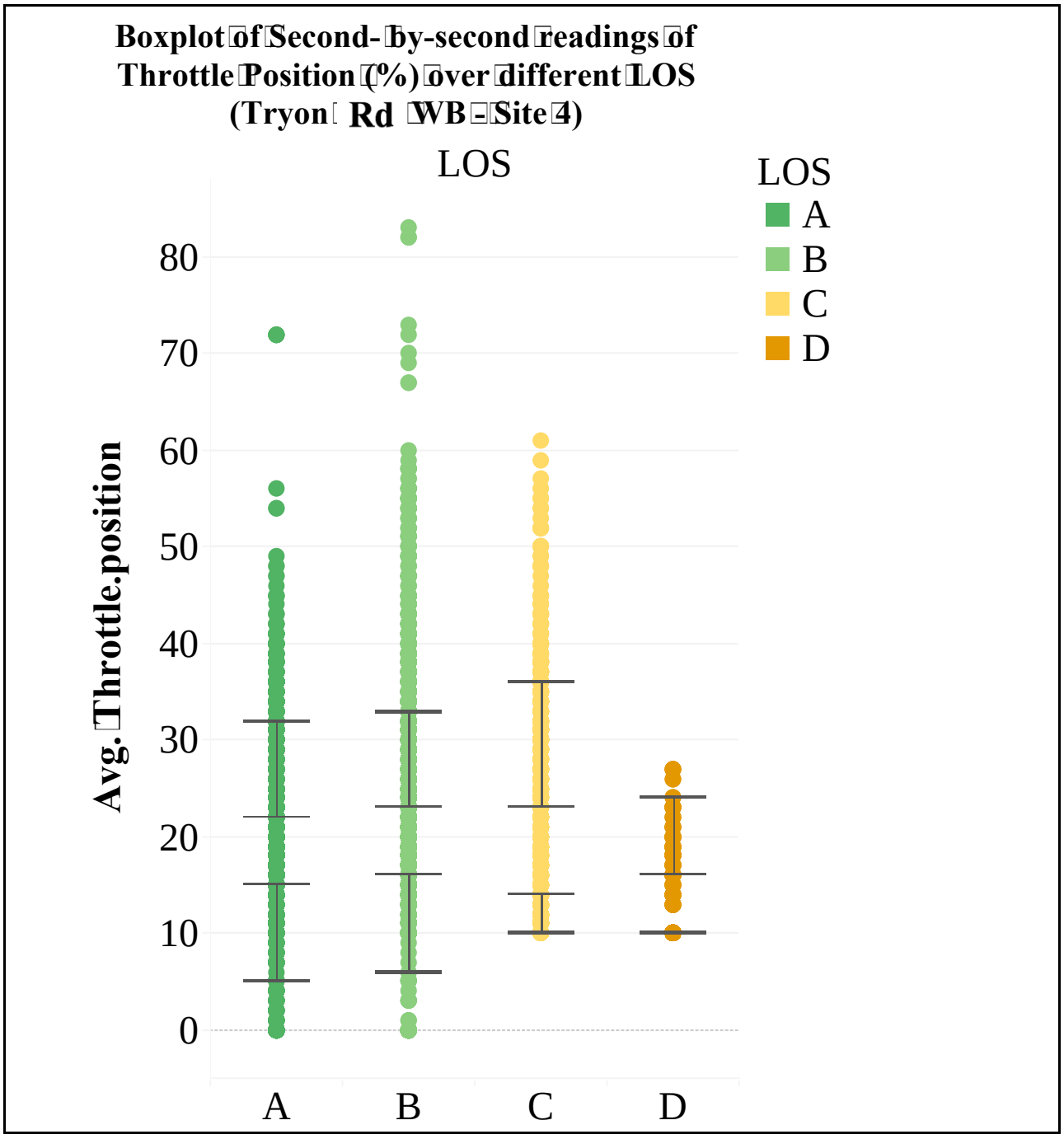

Figure N-15 – Boxplot of Second-by-second readings of Throttle Position (%) over different LOS (Tryon Rd WB – Site 4)